Wales, Craig (2013) Multi-component crystallisation approaches to controlling crystalline forms of active pharmaceutical ingredients. PhD thesis

http://theses.gla.ac.uk/3941/

Copyright and moral rights for this thesis are retained by the author

A copy can be downloaded for personal non-commercial research or study, without prior permission or charge

This thesis cannot be reproduced or quoted extensively from without first obtaining permission in writing from the Author

The content must not be changed in any way or sold commercially in any format or medium without the formal permission of the Author

When referring to this work, full bibliographic details including the author, title, awarding institution and date of the thesis must be given.

Glasgow Theses Service
http://theses.gla.ac.uk/
theses@gla.ac.uk

Multi-Component Crystallisation Approaches to Controlling Crystalline Forms of Active Pharmaceutical Ingredients

Craig Wales

Thesis submitted to the University of Glasgow for the degree of Doctor of Philosophy

School of Chemistry

College of Science and Engineering

Supervisor: Prof. Chick C. Wilson

Submitted September 2012

Declaration

This thesis has been written in accordance with the University of Glasgow regulations and all work presented is original and performed by the author unless otherwise stated and referenced in text.

Craig Wales, September 2012

© Craig Wales

Abstract

Multi-component crystallisation is investigated as a route to controlling crystalline forms of selected materials that possess pharmaceutical properties. This includes investigating the use of co-crystallisation methodology to selectively crystallise metastable polymorphs and solvated forms of these materials. This differs from the conventional use of co-crystallisation, as the aim of this aspect of the investigation is not to obtain a molecular complex of the two components, but instead for them to crystallise independently, while one component perturbs the solution environment to direct the crystallisation of the second component towards a different, often metastable, polymorph (or solvate). This co-crystallisation methodology is used as a route to crystallising new or elusive polymorphs (or solvates) of the active pharmaceutical ingredients paracetamol, piroxicam, gallic acid monohydrate and piracetam. It is also demonstrated that the use of this method can lead to crystal forms with otherwise unobtainable structural features.

Co-crystallisation is also investigated as a route to controlling the ionisation state of piroxicam in the formation of molecular complexes. Molecular complexes were formed with a number of mono-substituted benzoic acids as well as with nitrogen-heterocycles and strong acids. In the molecular complexes formed, piroxicam was found to adopt the non-ionised, zwitterionic, anionic or cationic form, depending on the co-former used. Attempts are made to rationalise the occurrence of each ionisation state by consideration of the relative pKa values of piroxicam and the co-formers. The hydrogen bonded supramolecular synthons in these molecular complexes are also investigated.

Co-crystallisation is also used as a route to obtaining molecular complexes of paracetamol and its derivative, 4-acetamidobenzoic acid, with nitrogen-heterocycles as co-formers. Molecular complexes of the two, with similar co-formers, are compared in terms of their hydrogen bonded supramolecular synthons. Despite having otherwise similar structural features, the phenolic hydroxyl group in paracetamol and carboxylic acid group in 4-acetamidobenzoic acid result in the formation of very different synthons and in some cases different component ratios. The susceptibility of 4-acetamidobenzoic acid to deprotonation is found to play a major role in the differences observed.

Molecular complexes of paracetamol with co-formers containing multiple carboxylic acid groups are also investigated, with a view towards further crystal engineering approaches for molecular complexes of paracetamol. Piracetam complexes with carboxylic acids are investigated in a similar manner.

The potential for transfer of a range of these multi-component crystallisations into a non-evaporative environment, with a view to implementing continuous crystallisation approaches, is also investigated. This transfer is found to be challenging for the systems investigated.

Acknowledgements

First of all I would like to thank Chick for giving me this opportunity and for all the help and guidance during the course of my research. It has been a pleasure to be part of the group.

I would also like to thank the rest of The Wilson Group (past and present) for all their help throughout the different stages of my PhD. I should especially mention the upstairs office people (Wilson and Gilmore group): Big Craig ("this is the last time we'll all be together as a group"), Bryan (football pundit), Ioana ("ham ham"), Alan ("Craig have you seen this?") and wee Gordon (IT assistant). Not forgetting the Bath office people: Kate ("8-azaguaniiine", Louise ("it's my turn to empty the bin") and Alan (again).

I would also like to thank Andrew for his help with the neutron data as well as Davinder for the work he put in during his final year project.

A special mention should go to Lynne who has given up a lot of time and had a lot of patience over the last four years to help me get to this stage. The contribution to my knowledge and my research has been very much appreciated.

I would like to thank all the people at NiTech/CMAC for their help with the continuous crystallisation work, in particular, Lihua, who was always willing to give her time, and Craig, who was a big help in the lab.

I would also like to thank my mum and dad for all their support over my eight long years at Uni and for putting me up! I should also thank my brother who has been a big help with stuff at home since I moved to Bath.

Last, but definitely not least, I would like to thank Jennifer for all her support throughout my time at Uni and especially my PhD. She has had to put up with us putting our plans together on hold while I worked in Bath for a year and her patience and support has helped me throughout my time at Uni and has especially helped me through the last year.

List of Figures

List of Tables

List of Abbreviations

Below is a list of common abbreviations used throughout this thesis.

Abbreviation	Meaning	Abbreviation	Meaning
PA	Paracetamol	BA	Benzoic Acid
PX	Piroxicam	FBA	Fluorobenzoic acid
PXZ	Piroxicam (zwitterionic tautomer)	CLBA	Chlorobenzoic acid
PXN	Piroxicam (non-ionised tautomer)	BRBA	Bromobenzoic acid
GA	Gallic acid (anhydrous)	HBA	Hydroxybenzoic acid
GAM	Gallic acid monohydrate	IM	Imidazole
PGAM	Gallic acid (porous hydrate)	2MIM	2-methylimidazole
PTM	Piracetam	4MIM	4-methylimidazole
TZ	1,2,4-triazole	BZ	Benzimidazole
PZN	Pyrazine	CA	Chloranilic acid
PIC	Picoline	BRA	Bromanilic acid
BP	4,4’-bipyridine	4ABA	4-acetamidobenzoic acid

1. Introduction

1.1 Co-crystallisation

Co-crystallisation is described as a deliberate attempt to bring together different molecular species within one periodic crystalline lattice without making or breaking covalent bonds[1]. The intent is to obtain a hetero-molecular crystal product with discrete molecules held together by intermolecular interactions, distinguishing it from recrystallisation, where a homo-molecular product is obtained[1]. Although the meaning of co-crystallisation is generally agreed upon, the exact definition of the term "co-crystal" is cause for much debate[2-6] as the term could be interpreted to imply a relationship is present between the crystal structure of the co-crystal and those of its components. The one broad commonality in this debate is that a co-crystal comprises at least two different components, although further ambiguity arises as to whether or not both components are required to be solid at room temperature[4] and whether a distinction should be made between multi-component ionic solids (salts) and multi-component solids containing neutral molecules (neutral molecular complexes)[1, 4, 5].

The use of the term co-crystal will therefore be avoided in this work and the term "multi-component molecular complex" will be used in the broadest sense to describe crystals comprising two or more components, i.e. with neutral molecular complexes, molecular complexes where hydrogen transfer has taken place (generating charged molecular species), and solvates being subsets. For the purpose of this section, discrimination will be made between pharmaceutical salts produced using traditional counter-ions and molecular complexes between two (or more) neutral starting components where hydrogen transfer has taken place (although both are generally considered as salts).

1.2 Molecular Complexes as Functional Materials

The consensus is that co-crystallisation, like crystallisation in general, is not a well understood process in that it is not currently possible to predict with any reasonable level of confidence the crystal structure of an organic material[7]. However, molecular complexes from co-crystallisation are considered to have a lot to offer the pharmaceutical

industry, as not only can they be patented as new compounds[8, 9] but they can also have very different properties from their component materials[9-11] (Table 1.1). They offer multiple opportunities to modify the chemical and/or physical properties of active pharmaceutical ingredients (APIs) without making or breaking covalent bonds[10] and pharmaceutical companies routinely screen for and patent such complexes[12]. This derivatisation of APIs (or indeed materials in general) through non-covalent interactions is considered a greener approach than making and breaking covalent bonds as it minimises the formation of by products[13]. In addition, the potential number of molecular complexes for a given API far exceeds that of traditional pharmaceutical salts due to the relatively low number of acceptable counter-ions when compared with the large number of counter-molecules that would be acceptable in a molecular complex[8]. Molecular complex formation also provides a potential route to optimising the properties of APIs which are not acidic or basic enough to form a salt[10]. Given that in the chemical industry "few compounds reach development and even fewer are marketed"[14], the potential benefits of such a flexible approach are obvious. It is somewhat surprising, therefore, that salt-formation is one of the most common methods of altering the solid state properties of a drug and that over half of medicines on the market are administered as salts, whereas there are no drugs on the market which are molecular complexes[9].

The practical use of molecular complexes to optimise properties of APIs has been demonstrated in several recent studies. These have shown that complexes of APIs can have favourable properties such as: resistance to relative humidity stress[15, 16], improved compaction properties (for tabletting)[17, 18], improved solubility[15, 19, 20], improved dissolution rate[15, 21 22] and improved bioavailability[15, 23]. In addition to patent space expansion and property optimisation, another potential application is that of combination drugs, where two APIs are included in a single molecular complex[6, 24, 25]. Molecular complex formation also offers a method of preferentially crystallising a particular tautomer of a material depending on the co-former used. This has previously been carried out by exploiting the preferential hydrogen bond interactions of the different functional groups present in different tautomers[26]. Other studies have shown that varying the co-former used to co-crystallise the APIs piroxicam[27], sulfamethazine[28] and norfloxacin[29] will result in a different tautomer in the molecular complex formed - although in these cases this outcome has to date been serendipitous rather than the result of rational design.

Molecular complexes of APIs therefore represent a broad patent space and have broad scope for non-covalent derivatisation[13] through the formation of freely reversible

interactions that do not compromise the structural integrity of the API, thus allowing it to retain its bioactivity.

Although a large portion of the literature is devoted to the co-crystallisation of APIs, the applications of multi-component molecular complexes are much further reaching. Molecular complex formation has previously been investigated as a means of altering the properties of other functional materials such as agrochemicals[30] and coloured materials[31, 32]. It has also been shown to be useful in generating non-centrosymmetric complexes with non-linear optical (NLO) properties[33-35] as well as porous materials with gas or small molecule storage applications[36, 37].

Table 1.1[38] *Examples of physical and chemical properties that can differ among different crystal forms (polymorphs and multi-component complexes).*

Physical and chemical properties	Density and refractive index, thermal and electrical conductivity, hygroscopicity, free energy and chemical potential, melting points, heat capacity, vapour pressure, solubility, thermal stability
Spectroscopic properties	Electronic, vibrational and rotational properties, nuclear magnetic resonance spectral features
Kinetic properties	Rate of dissolution, kinetics of solid state reactions, stability
Surface properties	Surface free energy, crystal habit, surface area, particle size distribution
Mechanical properties	Hardness, compression, thermal expansion
Chemical properties	Chemical and photochemical reactivity

1.3 Polymorphism

Another crucial aspect with regards to the properties of materials such as APIs during their development for application is polymorphism, as different polymorphs of a material can also possess very different properties (Table 1.1), effectively behaving as different

materials in terms of their physical properties[38]. Polymorphism is defined as "the ability of a substance to exist as two or more crystalline phases that have different arrangements and/or conformations of the molecules in the crystal lattice"[39]. Like multi-component complexes, different polymorphs of a drug can also be patented as discrete materials[40] and it is commonplace to search for polymorphs in solid-state pharmaceutics[9]. Polymorphism has long been known to be a very common occurrence[41] and it has been suggested that "every compound has different polymorphic forms and that, in general, the number of forms known for a given compound is proportional to the time and money spent in research on that compound"[42]. Although caution should be exercised with regards to the accuracy of this statement[43], it is clear that polymorphism further broadens the range of non-covalent derivatives that can be generated for a given material (Figure 1.1). Combining the potential of the two types of materials discussed to date, polymorphs of molecular complexes could offer even further opportunities to modify the properties of organic materials. Several examples of polymorphic molecular complexes of APIs, including carbamazepine[44], piroxicam[27] and chlorzoxazone[45], have been published in recent years.

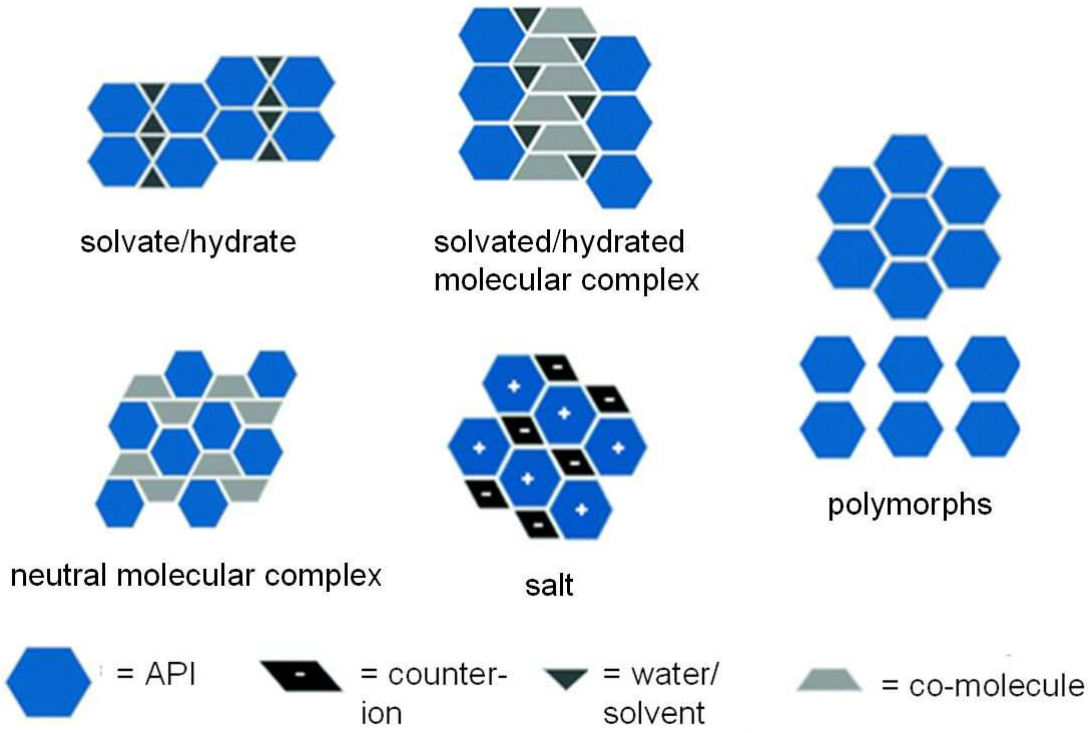

Figure 1.1[9] *An illustration of some of the possible crystal forms that can result from non-covalent derivatisation of materials such as APIs.*

1.3.1 Polymorphism in Functional Materials

Polymorph screening is a routine part of solid form selection of functional materials such as APIs. In the vast majority of cases, the most stable polymorph is selected for processing, scale-up, formulation and storage as it minimises the chance of conversion to another form[46]. However, the most stable form of a material generally has the lowest solubility at any given temperature and a metastable form of an API may be selected if it offers a significant improvement in solubility or indeed other properties such as dissolution rate or bioavailability[46]. A prominent example of a metastable polymorph of an API with potentially improved properties over the commercial form is paracetamol form II[47]. Studies of the properties of paracetamol form II have concluded it has both improved dissolution rate[48] and compaction properties[49] compared with those of form I. Its potential for large scale use has been limited, however, by the inability to produce this metastable solid form in large quantities and its poor stability over time[50].

The importance of solid form selection and properties has perhaps been most dramatically illustrated by the case of the anti-HIV drug ritonavir[51, 52], where the sudden appearance and subsequent prevalence of an unknown, more stable polymorph, prevented formulation of the marketed product. It became clear that the marketed product utilised a metastable polymorph of ritonavir and the significantly altered dissolution rate of the new form precluded formulation. This illustrates the need to identify the most stable form prior to taking a product to market in order to be aware of the potential for such difficulties arising and to take steps to mitigate this. It also highlights the importance of being able to selectively crystallise and maintain a metastable form if it has favourable properties.

The case of ritonavir also raises the subject of “disappearing polymorphs”, where the (often serendipitous) crystallisation of a more stable polymorph is believed to subsequently nucleate the crystallisation of that polymorph through undetectable seeds - precluding crystallisation of the less stable form thereafter[53]. Several other examples of this have been reported[54-56]. The general consensus is that re-obtaining the metastable forms is always possible by manipulating the crystallisation conditions - although identifying the conditions required may not be a trivial task[54, 57].

As is the case for molecular complexes, polymorphism can also be exploited for functional materials other than APIs. Polymorphic porous materials have been shown to have gas absorption properties and have also been shown to have the potential to turn

the porosity "on and off" by converting between porous and non-porous polymorphs[58]. Different polymorphs of materials can also exhibit different NLO properties[35, 59], affect the colour of pigments[43, 60] and affect the properties of high energy materials[43].

1.3.2 Tautomeric Polymorphism

Tautomeric polymorphism - more strictly termed desmotropy, although arguments have been made for use of both terms[61-63] - is the existence of two or more crystal structures of the same chemical composition, but with different tautomers in each. In some cases, polymorphs are also known to have both tautomers co-existing in the same crystal structure[12, 64]. A recent study[62] of the Cambridge Structural Database (CSD)[65] showed that tautomeric polymorphism is a very rare phenomenon; only 16 pairs of tautomers were found in the CSD, representing just 0.5% of molecules that are known to have different tautomeric forms. A handful of materials exhibiting tautomeric polymorphism have been found since, including triclabendazole[12] and 2-(p-tolylamino)nicotinic acid[66].

Cases of tautomeric polymorphism have been reported with one polymorph comprising a neutral form and another comprising a zwitterionic form[27, 64, 66], as well as cases where both polymorphs comprise only neutral tautomers[12, 67]. In addition to pure compounds, tautomeric polymorphism has also been reported to occur in a molecular complex[27].

1.4 Controlling and Predicting Crystal Forms

1.4.1 Crystal Engineering

As stated above, co-crystallisation is not a well understood process and there is no guaranteed method of predicting the interactions that will occur in a molecular complex or whether or not a co-crystallisation experiment will even be successful in producing a molecular complex[9]. A commonly used method of increasing the probability of forming a molecular complex, however, is using the "supramolecular synthon[68]" approach. A supramolecular synthon describes recognition events when molecules assemble into supermolecules[1]. These transferrable connectors can be identified by empirical methods[69], such as systematic co-crystallisation experiments and/or analysis of the CSD,

to map out the common molecular associations in which functional groups engage. These molecular recognition events can be with other identical functional groups (homosynthons) or with different but complementary functional groups (heterosynthons)[70] (Figure 1.2). Although recent studies have suggested that π···π interactions[71, 72], CH···π interactions[73, 74] and halogen bonds[75-78] may have the potential for use in crystal engineering, the majority of organic molecular complexes are assembled via conventional (stronger) hydrogen bonds, with other intermolecular interactions having not been found to be as robust[1]. Accordingly, crystal engineering of molecular complexes usually involves identifying hydrogen bonding synthons and using them to determine suitable co-formers for a material based on the complementarities of the functional groups. This approach, in theory, should lead to heteromeric interactions being favoured over homomeric interactions. The nature of APIs means that they inherently contain functional groups that engage in molecular recognition, making co-crystallisation much more probable[79] although still impossible to guarantee.

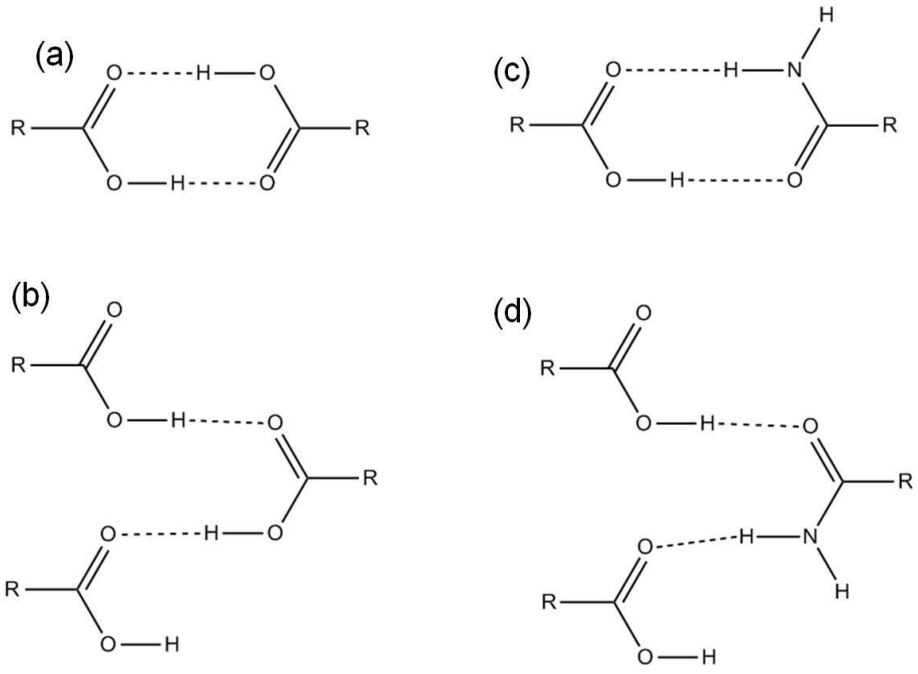

Figure 1.2 *Examples of hydrogen bonded homosynthons and heterosynthons that can be formed by a carboxylic acid group. (a) carboxylic acid dimer homosynthon; (b) carboxylic acid catemer homosynthon; (c) carboxylic acid : amide dimer heterosynthon; (d) carboxylic acid : amide catemer heterosynthon.*

To aid in the identification of common hydrogen bonding motifs, they are commonly classified using graph set notation[80]. Graph set notation is written in the form $X_D^A(Y)$. X is

a letter describing the hydrogen bonding in a motif (C = chains, D = dimers, R = rings, S = intramolecular hydrogen bonds). A and D are numbers denoting the number of hydrogen bond donors (subscript D) and acceptors (superscript A). A third number in parentheses (Y) denotes the size or degree of the motif (number of atoms in the repeat unit) (Figure 1.3).

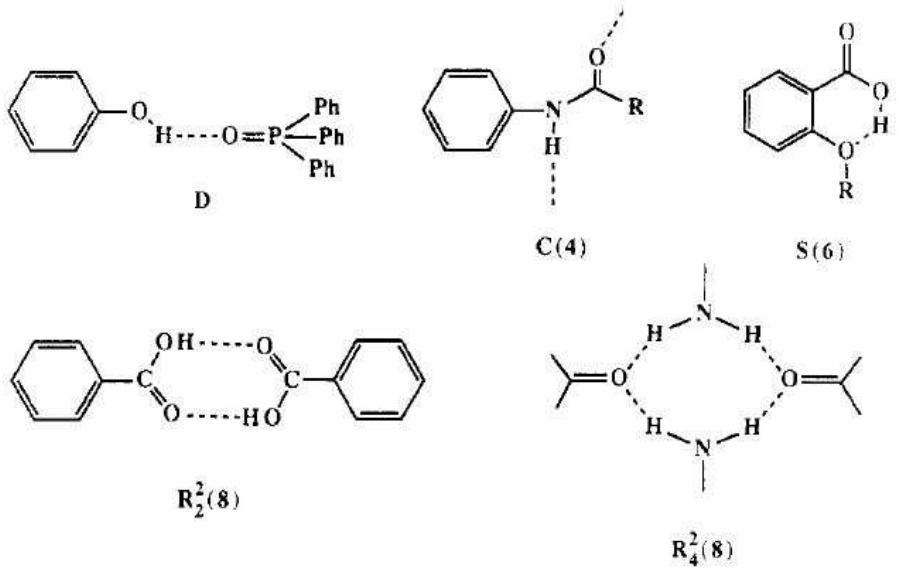

Figure 1.3[80] *Examples of graph set assignments for some hydrogen bonding motifs.*

Various studies of known crystal structures have been carried out investigating the hierarchy of hydrogen bonds and statistical probabilities of certain supramolecular synthons occurring[69, 79, 81-85]. These studies can be used to increase the probability that a co-crystallisation experiment will be successful. Early empirical studies of the hierarchy of hydrogen bonds resulted in a general set of guidelines being devised for the design of molecular solids[80]. These guidelines are as follows:

1. All good proton donors and acceptors are involved in hydrogen bonding;
2. Six-membered ring intramolecular hydrogen bonds form in preference to intermolecular hydrogen bonds;
3. The best proton donor and acceptor remaining after intramolecular hydrogen bond formation will form intermolecular hydrogen bonds.

The empirical method of determining transferrable synthons has proved to be highly useful in some cases. For example, the carboxylic acid - pyridine OH···N hydrogen bonding

motif has been demonstrated to be a highly robust synthon in co-crystallisation experiments. A recent CSD study showed it is present in 98% of complexes with no other competing functional groups present and 77% of complexes where competing functional groups are present[86].

Another transferrable synthon commonly used in the crystal engineering of molecular complexes is the carboxylic acid - primary amide heterodimer (illustrated in Figure 1.2c) [40, 87-91]. However, this synthon is far less predictable, with a 2004 CSD study[85] showing that only 47% of molecular complexes containing both functional groups exhibit this heteromeric hydrogen bonding motif. Of these, 28% also exhibited either homomeric acid-acid synthons or amide-amide synthons. It has also been shown that in the presence of other competing functional groups, the occurrence of this hydrogen bonding motif becomes even less likely[88, 91, 92]. This example illustrates the difficulty in using non-covalent interactions as synthetic tools with an incomplete understanding of the forces involved. Further complications in the design of molecular complexes arise with the possibility of solvated or hydrated molecular complexes, as they interfere with the formation of hydrogen bonded synthons and their formation is generally not considered predictable in a co-crystallisation experiment[93]. Even in cases where the predicted primary hydrogen bonding synthon is consistently observed, progression from this to prediction of the structure as a whole is not possible - even for molecular complexes comprising structurally similar components[94].

In order to achieve the ultimate goal of crystal engineering - the design of molecular solids with specific interactions to obtain specific properties - a complete understanding of the interrelated strong and weak interactions, close packing effects and nucleation kinetics is required. The need for a complete understanding of these factors has long been stressed by various authors[95-100]. Progress in crystal structure prediction of molecular complexes is being made using computational methods, although these too require a fuller understanding of the kinetic aspects of crystallisation[100-104].

Despite the relative success of the supramolecular synthon approach, it is not yet possible to predict if a co-crystallisation experiment will be successful. Knowledge of the common synthons is not always enough, as compounds with the same functional groups can exhibit different reactivity towards molecular complex formation and molecules may form molecular complexes without any obvious synthons connecting them[84]. For this reason a high-throughput (trial and error) screening strategy can be used to maximise the

potential number of hits, from which a more designed synthon based strategy may evolve based specifically on the target molecule[19, 105, 106].

It has been suggested that a more careful consideration of the component solubilities is required to predict if a co-crystallisation experiment will be successful; ternary phases diagrams can be used in this respect to determine the mole fraction of each component that is required at a given temperature to crystallise the molecular complex [107, 108]. The mole fraction of each component required will be dependent on the solubility curve of the two components and of the molecular complex in that particular solvent. Using solvents which result in similar solubilities of the two components is more likely to result in crystallisation of the 1:1 stoichiometric complex. Where there is a large difference in the solubility of the component materials, different solution stoichiometries may be required for successful co-crystallisation. Recent work has also suggested that it may be possible to predict the successful formation of molecular complexes by theoretical prediction of the solid state miscibility of the components[109] or by comparison of the global lattice energies of the component crystal structures with that of the molecular complex using computational methods[110].

1.4.2 Intermolecular and Intramolecular Hydrogen Transfer in Molecular Complexes

An important consideration when co-crystallising two (or more) materials is whether or not intermolecular hydrogen transfer will take place between them. When intermolecular hydrogen transfer is complete the complex is a salt and when no hydrogen transfer occurs it is a neutral molecular complex. Predicting the occurrence of hydrogen transfer for a particular system is generally done using the "pKa rule", which states the approximation that ΔpKa = pKa[protonated base] – pKa[acid] ≥ 3 for salt formation[111]. In general, when ΔpKa is less than 0, no intermolecular hydrogen transfer will take place[112]. When ΔpKa lies between 0 and 3, however, hydrogen transfer may or may not occur depending on the particular system[113]. Predicting if hydrogen transfer will occur can be critical when using the supramolecular synthon approach as it can have consequences for the primary interactions between the molecules, as well as the stoichiometry of the complex[114, 115]. The pKa rule has been shown to be a useful tool for successfully predicting hydrogen transfer in various molecular complex systems[111, 116, 117]. Its utility has, however, been shown to be system-dependent and the ΔpKa boundaries for hydrogen transfer may need to be adjusted depending on the system being investigated[112, 118]. The lack of

ubiquity in transferring the pKa rule between systems comes as little surprise. pKa values describe solution processes and thus a rule based on pKa values to describe solid state processes cannot be expected to be a hard and fast one. The pKa "rule" can therefore be seen as more of a guideline when predicting the possible occurrence of intermolecular hydrogen transfer for a molecular complex system.

Classifying a molecular complex as a salt or neutral molecular complex is not always a trivial procedure[5, 6, 119]. Issues arise in the identification of the exact position of the proton, as illustrated by examples where the proton position is temperature dependent[120, 121]. The 4-methylpyridine : pentachlorophenol complex[120], for example, exhibits a short strong intermolecular O···H···N hydrogen bond where the proton lies on the oxygen at room temperature, on the nitrogen at low temperature and is exactly centred at 90K (Figure 1.4). Hydrogen bonds in molecular complexes are therefore said to lie on a continuum[113], with complete hydrogen transfer at one extreme and no hydrogen transfer at the other. Further ambiguity may arise in 2:1 molecular complexes where hydrogen transfer occurs, for example, in the anilinium fumarate-fumaric acid complex[122]. This complex features a deprotonated fumaric acid molecule, a protonated aniline molecule and a neutral fumaric acid molecule in the asymmetric unit making the term "salt" an inadequate descriptor.

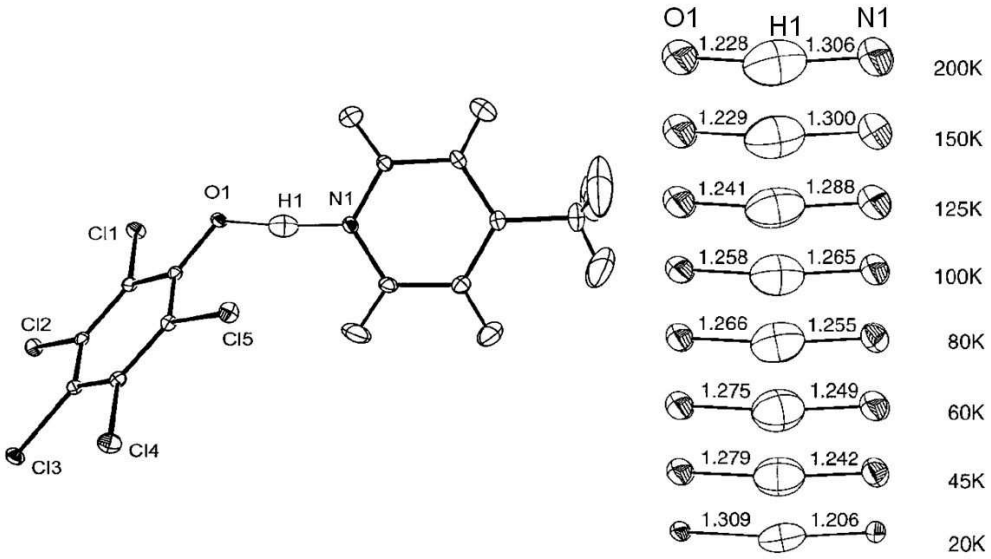

Figure 1.4 *Thermally induced proton migration in the O···H···N hydrogen bond in the 4-methylpyridine : pentachlorophenol molecular complex, as observed by neutron diffraction studies*[120].

The pKa rule can be used for predicting *inter*molecular hydrogen transfer in molecular complexes; however, no such guidelines exist for predicting *intra*molecular hydrogen transfer in a co-crystallisation experiment. Tautomeric materials have been observed to form molecular complexes with the tautomer present in the complex dependent on the co-former used[12, 27, 28]. Only one study has been carried out investigating the influence of the co-former on the tautomeric preference of a material[12]. Another study also suggested that using crystal engineering principles, certain zwitterionic materials can be induced into crystallising as the zwitterion by exploiting the preferential hydrogen bonding synthon of the zwitterionic tautomer with weakly acidic co-formers[26]. As yet, no attempt has been made to rationalise intramolecular hydrogen transfer, in terms of the properties of the co-formers, to facilitate the prediction of which tautomer will be present in a given molecular complex system.

1.4.3 Crystallisation Methods for Controlling Polymorph and Molecular Complex Formation

1.4.3.1 The Rule of Stages

Crystallisation follows the Rule of Stages as postulated by Ostwald[123]. The rule states that crystallisation follows the quickest path to the lowest free energy state through a number of metastable states, with minimal changes in free energy between each step[124]. In practical terms this means that in a given crystallisation, the least stable polymorph will form first, followed by sequential recrystallisations to thermodynamically more stable polymorphs. The free energy barrier for this change dictates how rapid this transformation is and it is accelerated when the system is in contact with solution, which can make obtaining metastable polymorphs difficult[125]. When the free energy barrier is low enough, polymorphs of materials can be obtained through solid-solid transformations of single crystals which can occur over time[125-127]. Solid-solid transformations can also be induced to higher or lower energy states by altering the environment of the crystal, for example by increasing/decreasing temperature[128, 129], humidity[128] or pressure[128, 130].

1.4.3.2 Common Crystallisation Techniques for Isolation of Polymorphs and Molecular Complexes

Screening of polymorphs and molecular complexes is frequently carried out via crystallisation from solution, often in an evaporative environment. Polymorph selectivity can be achieved through varying the solvent used[131, 132] and the success of a co-crystallisation experiment is also often dependent on the solvent used[107, 133]. The rate of solvent extraction can also affect the solid phase obtained, with rapid evaporation generally resulting in metastable forms and slow evaporation producing thermodynamically stable forms[134]. Similarly, cooling crystallisation can be used to obtain different crystal forms by varying the solvent used[135] or by varying the cooling rate[136].

Crystallisation / co-crystallisation at high pressure has recently emerged as a route to novel and otherwise unobtainable polymorphs and molecular complexes. This technique has been used to produce a new dihydrate of piracetam[130] as well as a dihydrate[137], a trihydrate[138] and a methanol solvate of paracetamol[139]. In recent years there has also been an increase in research focused on "solvent free" co-crystallisation[140-142]. This is viewed as an environmentally friendly process compared with other methods, as it involves the co-grinding of two components in little or no solvent to induce molecular complex formation. It has proved of great interest in co-crystallisation as it has been shown to facilitate synthesis of new multi-component complexes[32, 140] and can also be used to obtain different polymorphs of materials[40, 142].

1.4.3.3 Seeding, Additives and Co-Crystallisation in Controlling Polymorph Selection

A common method of promoting the growth of a particular polymorph of a material is to seed a saturated solution with crystals of the desired polymorph[143, 144]. Under cooling or evaporation to supersaturation, nucleation should occur preferentially at the surface of the seed, promoting crystallisation of that form. As well as homonucleation it has also been observed that heteronucleation is possible, where seeds of one polymorph can cross-nucleate the crystallisation of another[145].

Additives have been widely used to direct and control the formation of metastable polymorphs; these are normally used in trace quantities[146, 147] or are engineered so that a structural relationship is present between the additive and the desired polymorph, thus facilitating epitaxial growth on the substrate surface[148-150] or inhibiting the growth of the

more stable form[151]. Co-crystallisation from multi-component environments, however, is relatively rare as a route to polymorph selection. This method differs from the conventional co-crystallisation method, as the two components do not form a complex, instead crystallising independently, whilst one component perturbs the solution environment to direct crystallisation of the second component towards a particular, often metastable, polymorph. In contrast to the use of additives, co-crystallisation utilises molar quantities of the two components. Although rare, discovery of new and elusive polymorphs resulting from co-crystallisation experiments has been known to occur, mainly as the serendipitous outcome from experiments aimed at molecular complex formation.[56, 66, 132, 152, 153]

1.4.3.4 Continuous Crystallisation

In industry, large scale crystallisation of materials is generally performed in stirred-tank batch crystallisers. Stirred tank reactors have operated on the same basic principles for hundreds of years however, and are seen as being inefficient due to the large vessels required and limited control over temperature and mixing when scaled up. This can result in inconsistent products being obtained and a greater amount of wastage and cost[154].

In recent years there has been an increase in research focused on large scale continuous flow crystallisation with a view to improving the efficiency of crystallisation processes[154]. Of particular interest is the continuous oscillatory baffled crystalliser (COBC)[155-158]. The COBC consists of a continuous cylindrical tube or column with baffles periodically spaced along the inside walls, with the sharp edges of these baffles positioned transverse to the flow (Figure 1.5). The solution is oscillated axially by means of a diaphragm, bellows or pistons at one or both ends of the column. The oscillating flow forces the liquid through the baffles on the upstroke, generating vortex rings, which are then unravelled on the downstroke (also Figure 1.5).

The generation of these vortex rings in the cell means that mixing is uniform throughout the column, which facilitates uniform control over the temperature. Plug flow of the solution through the column can be achieved in the COBC even at low flow rates, i.e. radial mixing is uniform and axial dispersion is at a minimum. This also allows for very precise cooling profiles along the length of the reactor. Being able to exercise such precise control over crystal growth conditions therefore allows for the development of processes capable of producing very consistent products in terms of crystal morphology and quality.

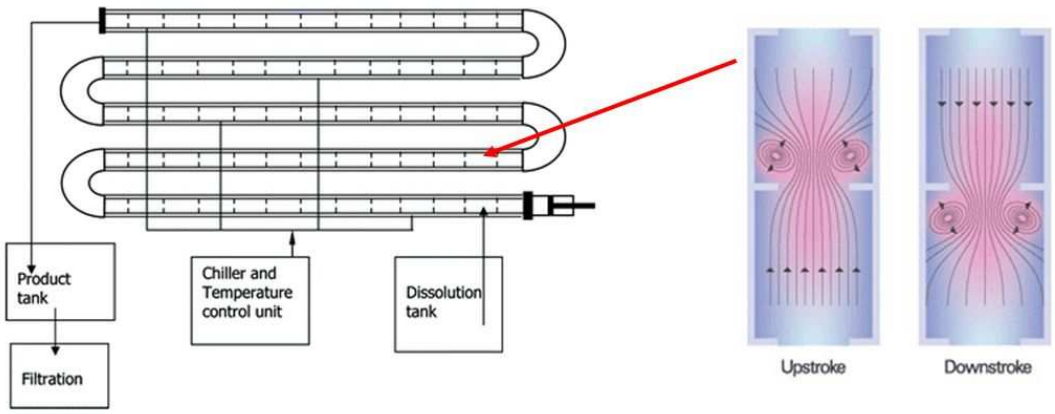

Figure 1.5 *Schematic of an OBC. The typical set up of an OBC[155] (LHS) and the mixing mechanism within a cell (RHS)[159].*

In a study of the crystallisation of L-glutamic acid in a COBC, it has been demonstrated that selective polymorph formation can be achieved by altering the solution concentration and the crystal size can also be varied by altering the cooling rate[157]. A study of this technology using paracetamol showed that the product recrystallised from an OBC is of much better consistency in terms of particle size and surface characteristics than from conventional methods[156]. These studies emphasise the value of the technology in developing processes for precise control of the crystallisation of materials such as APIs.

1.5 Intermolecular Interactions

1.5.1 The Hydrogen Bond

The hydrogen bond is considered the most important of all directional intermolecular interactions[160]. It is the main force responsible for molecular recognition and it can be strong enough and directional enough so that this recognition is orientationally specific[161]. Hydrogen bonds are responsible for biological processes such as protein folding and enzyme-substrate recognition and they are the primary influence in the crystal packing of solids, causing deviations from the principles of close packing as defined by Kitajgorodskij[162]. The importance of the hydrogen bond in crystal engineering is highlighted in Section 1.4.1.

The IUPAC recommends that a hydrogen bond is defined as "an attractive interaction between a hydrogen atom from a molecule or a molecular fragment X–H in which X is more electronegative than H, and an atom or a group of atoms in the same or a different molecule, in which there is evidence of bond formation"[163] (X will from here forward be referred to as the donor atom (D)). Hydrogen bonds, $D^{\delta-}$-$H^{\delta+}\cdots A^{\delta-}$ (where A is the acceptor), could be viewed as an extreme case of a dipole-dipole interaction, however, the unique characteristics of hydrogen bonds indicate that this is an over-simplification. The distance between D and A atoms is often less than the sum of the van der Waals (vdW) radii and the DHA angle is typically very linear (although a significant degree of variation in the DHA angle can occur in weaker hydrogen bonds). Hydrogen bond energies range from 2-170 kJ mol^{-1}; the strongest hydrogen bonds are stronger than the weakest covalent bonds and the weakest hydrogen bonds are weaker than vdW interactions. The characteristics outlined above distinguish hydrogen bonds from both vdW interactions and covalent bonds[161].

Classification of hydrogen bonds can be generally broken down into three categories as defined by Jeffrey[164]: strong, moderate and weak (Table 1.2). Strong hydrogen bonds generally occur when there is an electron deficiency in the donor atom, which deshields the proton and thus induces a greater electropositive charge upon it. They also occur when there is an excess in electron density on the acceptor atom, which increases the dipole-dipole interaction potential between the proton and the acceptor atom. These types of hydrogen bonds are usually referred to as ionic or charge assisted hydrogen bonds. Strong hydrogen bonds can also occur when the conformation of a molecule forces the hydrogen bond donors and acceptors into being closer than would normally be expected.

Moderately strong hydrogen bonds (also Table 1.2) are the most commonly occurring and generally involve an electronegative donor atom and an acceptor atom which has lone-pair unshared electrons. The term "conventional hydrogen bonds" normally comprises both moderate and strong hydrogen bonds. The supramolecular synthon approach to crystal engineering normally utilises these conventional hydrogen bonds, as they are the most robust and transferrable intermolecular interactions.

Weak hydrogen bonds typically involve a carbon as the donor atom, which is relatively electroneutral - reducing the electropositive charge on the hydrogen. Acceptor groups are typically those with polarisable π electrons such as double bonds, triple bonds or aromatic rings. Halogen atoms are also common acceptors in weak hydrogen bonds.

These three classifications of hydrogen bond are mainly for convenience and there can be significant overlap between the characteristics and the functional groups involved.

Table 1.2 *Classification of hydrogen bonds into strong, moderate and weak*[164].

	Strong	Moderate	Weak
D-H···A interaction	mostly covalent	mostly electrostatic	electrostatic
Bond lengths	D-H ≈ H···A	D-H < H···A	D-H << H···A
H···A (Å)	1.2-1.5	1.5–2.2	2.2-3.2
D···A (Å)	2.2-2.5	2.5-3.2	3.2-4.0
Bond angles (°)	175-180	130-180	90-150
Bond energy (kJ mol^{-1})	>60	18-60	2-18

Hydrogen bonds can involve two hydrogen atoms (and hence two donors) or two acceptors, and hydrogen bonds of this type are referred to as bifurcated hydrogen bonds (Figure 1.6). Bifurcated hydrogen bonds, where two acceptors are present also have constraints, in that the hydrogen atom should lie approximately in the plane of the donor atom and the two acceptor atoms. Where two donor hydrogen atoms are present the interaction is usually asymmetric, with one component forming a stronger interaction than the other.

Figure 1.6 *An illustration of a bifurcated hydrogen bond with two acceptor atoms (LHS) and an asymmetric bifurcated hydrogen bond with two donor hydrogen atoms (RHS).*

1.5.2 Other Intermolecular Interactions

1.5.2.1 π···π Interactions

Although hydrogen bonds are considered the dominant interactions in the relative arrangement of molecules in the solid state, other weaker interactions such as π interactions also play an important role. π···π interactions typically involve the interaction of aromatic rings. Aromatic ring systems are composed of a σ-framework sandwiched between two π-electron clouds. In π···π interactions, aromatic rings align themselves to maximise the attractive electrostatic interaction of the orbitals and to minimise electrostatic repulsion[71] (Figure 1.7). The relative orientation of the aromatic rings is therefore important in determining how attractive or repulsive the interaction is, as are the electron donating/withdrawing characteristics of any substituents, as these influence how electron rich/poor the π system is. π systems can also form interactions with anions or cations, depending on how electron deficient or rich the system is.

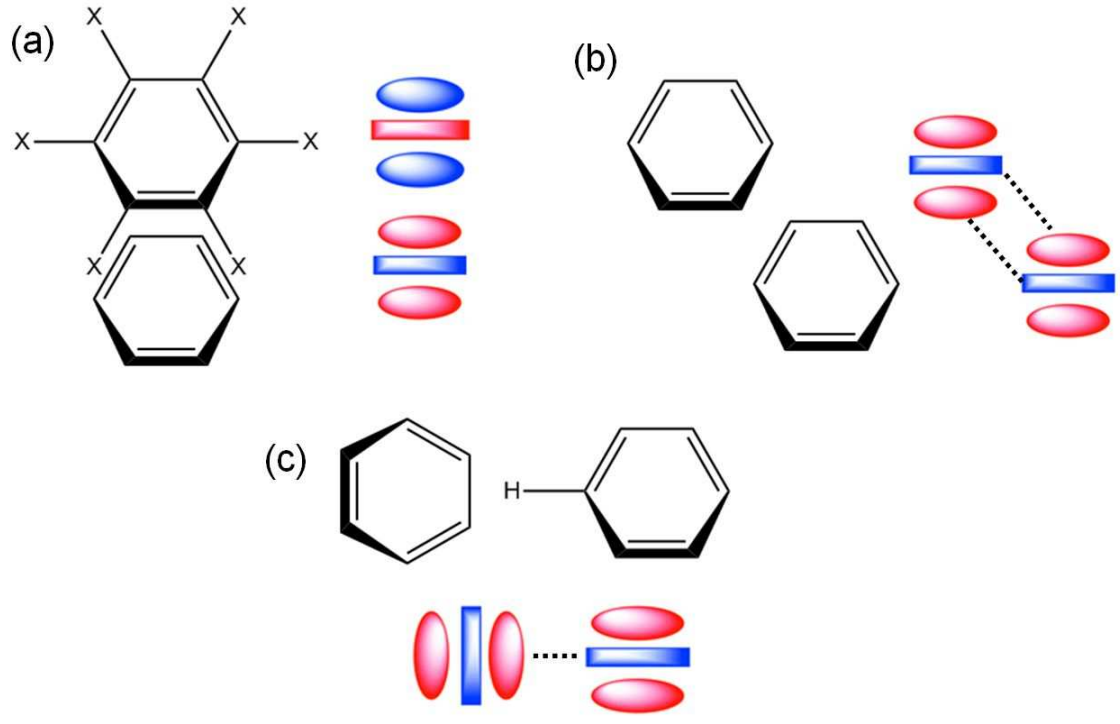

Figure 1.7 *π···π interactions between electron rich and electron deficient aromatic rings, showing how the orbitals align relative to each other. (a) Face to face stacking (b) Offset stacking (c) edge to face interactions/CH···π interactions.*

1.5.2.2 Halogen Bonds

Halogen bonding is an interaction of the form D···X-Y, where a halogen atom (X) acts as an electron density acceptor from an electron rich donor (D) such as oxygen, nitrogen, sulfur or π systems (Y = C, N, X etc that is covalently bonded to X). All halogens are capable of forming halogen bonds, with their tendency to form these interactions and the strength of the interactions generally increasing with decreasing electronegativity. The strength of the halogen interaction is also dependent on the donor; nitrogen as an electron donor generally forms stronger halogen bonds than oxygen and sulfur, with π systems generally being weaker halogen bond acceptors than electron rich atoms[77]. Accordingly, N···I interactions have been shown to be particularly useful in the design of molecular complexes[36, 78, 165, 166]. The donor atom can also be another halogen atom and these halogen-halogen bonds have also been used in crystal engineering[75]. There are two classifications of halogen-halogen bonds based on the geometry of the interaction (Figure 1.8). Geometries which fall outwith the ranges set in these classifications are electrostatically repulsive in nature, although can still be attractive due to dispersion forces[75]. An analogy is often made between halogen bonds and hydrogen bonds[77], as both have an electron density donor/acceptor relationship, both are generally highly directional and both are hierarchical - giving rise to robust reproducible supramolecular synthons that can be used in crystal engineering. The energy of halogen bonds also spans a wide range (5-180 kJ mol^{-1}) and strong halogen bonds have been known to be effective in breaking the tendency for hydrogen bond formation by the preferential formation of halogen bonds[77].

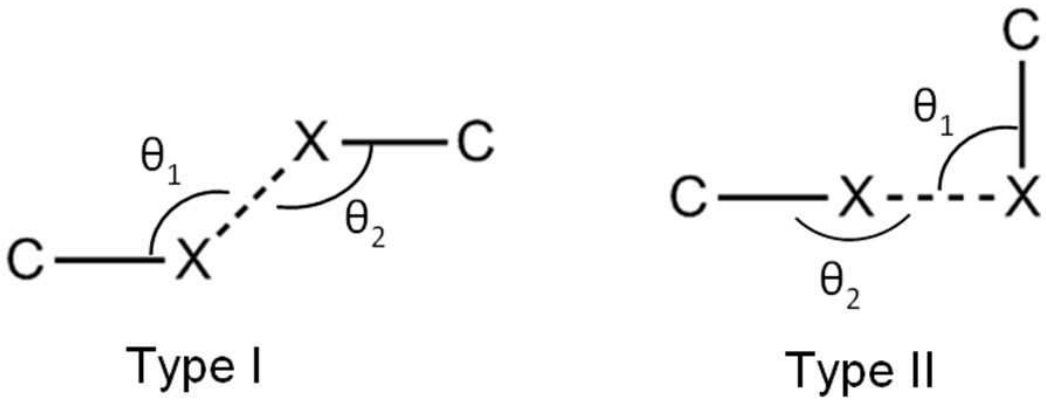

Figure 1.8 *The geometry of the two types of halogen-halogen bonds. In type I, 140° < $\theta_1 \approx \theta_2$ < 160°. In type II, $\theta_1 \approx 90°$ and $\theta_2 \approx 180°$.*

2. Characterisation of Materials

2.1 X-Ray Diffraction

Perfect crystalline solids are composed of many molecules, atoms or ions, arranged in a regular way, repeating in three dimensions to give a highly ordered structure[167]. Diffraction from such regular arrays allows access to objects that are of similar dimension to the wavelength of the incident radiation; the wavelength of X-rays is of comparable magnitude to interatomic distances in crystalline solids and this property of X-rays is exploited in X-ray diffraction. When a beam of monochromatic X-rays is passed through a single crystal, the beam is scattered by the electrons of the atoms in definite directions with varying intensities. This process is called diffraction and the scattered rays can be recorded with a detector giving a pattern consisting of a regular array of spots with a definite geometry and a degree of symmetry in the positions and intensities of the spots. It is from this pattern that crystal structures can be determined, as the symmetry of the pattern is related to the symmetry of the solid state arrangement of the molecules, while the intensities are related to the positions of atoms of different scattering powers in the crystal structure[168].

2.1.1 The Crystal Lattice and Unit Cell

All crystalline solids contain translational symmetry, regardless of whether other types of symmetry are present. The complete crystal structure can be described by the contents of the unit cell and translations of this in all three dimensions. To define the symmetry of a crystal structure, the lattice is initially obtained by taking a point in the structure and all other points identical to this (i.e. identical surroundings and same orientation). What is left is a regular pattern of equivalent points all related to each other by translational symmetry – this is called the crystal lattice. The lattice defines the repeating nature of the structure but not the contents of the unit cell. The vectors between lattice points define the unit cell, which is represented by three vector lengths (a, b and c) and three angles (α, β and γ), such that α lies between b and c, β between a and c, and γ between a and b (Figure 2.1). These six values are the unit cell (or lattice) parameters.

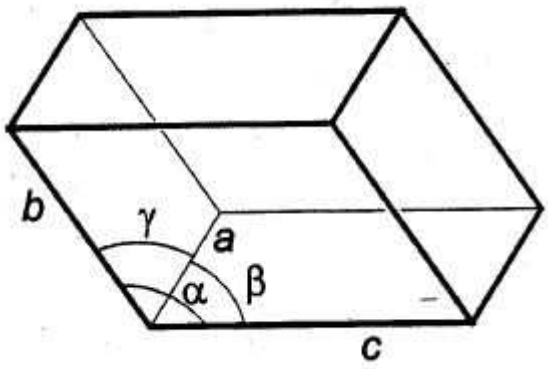

Figure 2.1 *Illustration of a 3-D unit cell*[167].

There are many choices of unit cell, however in the absence of any internal symmetry, convention states that the three sides should be as short as possible and the three angles as close to 90° as possible. The presence of internal symmetry in the unit cell imposes restrictions on values that can be taken by the unit cell parameters. These restrictions divide the crystal symmetry into seven different types called the seven crystal systems. Table 2.1 shows the unit cell restrictions on each of these crystal systems. Unit cells with only one lattice point are referred to as primitive (P). For some structures it is convenient to select a unit cell that contains more than one lattice point for the purpose of adding symmetry to the cell. Different kinds of centering are possible involving unit cells with lattice points at the centre of opposite pairs of faces (A, B or C depending on which faces are centred), at the centre of all faces (F), or body centred (I). The combination of crystal systems with cell centring choices (Table 2.1) gives fourteen possible lattices – the Bravais lattices (Figure 2.2).

In the solid state, there are symmetry elements such as rotation axes, mirror planes and inversion centres, together with combinations of these with internal translations, creating screw axes and glide planes; the total number of possible arrangements of these symmetry elements within the lattices is 230. These are the 230 so-called space groups to which every crystal structure belongs.

Table 2.1 *Unit cell restrictions on each of the seven crystal systems*

Crystal System	**Unit Cell Restrictions**	**Cell Types**
Triclinic	None	P
Monoclinic	$\alpha = \gamma = 90°$	P, C
Orthorhombic	$\alpha = \beta = \gamma = 90°$	P, C, I, F
Tetragonal	$a = b$; $\alpha = \beta = \gamma = 90°$	P, I
Trigonal / Rhombohedral	$a = b$; $\alpha = \beta = 90°$, $\gamma = 120°$	P
Hexagonal	$a = b$; $\alpha = \beta = 90°$, $\gamma = 120°$	P
Cubic	$a = b = c$; $\alpha = \beta = \gamma = 90°$	P, I, F

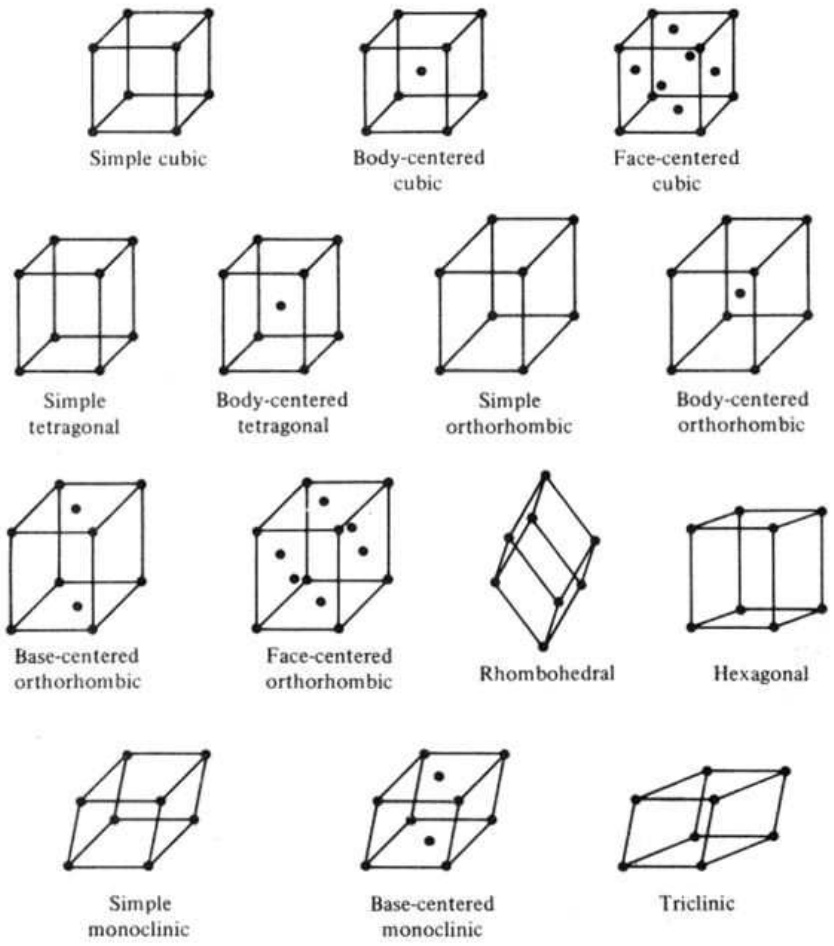

Figure 2.2 *The fourteen Bravais Lattices*[169]

2.1.2 Bragg's Law and the Ewald Construction

When an X-ray beam passes through a crystal, each atom scatters the incident beam in all directions and these scattered rays interact via constructive and destructive interference. For a set of lattice planes, the path differences of the radiation scattered by a lattice plane and that of the lattice plane(s) below must be a whole number of wavelengths for interference to be completely constructive. The directions in which this interference is completely constructive are defined by Bragg's law (Equation 2.1). Bragg's law is derived from the construction that every diffracted beam that can be produced by the crystal in an appropriate orientation can be treated as if it were a reflection from a set of parallel planes within the crystal[168]. Figure 2.3 shows a two-dimensional illustration of Bragg's law. The three Miller indices, *h*, *k* and *l*, are used to define the orientation of the plane within the crystal with respect to the unit cell edges, such that the plane intercepts the cell axes at a/*h*, b/*k* and c/*l*.

Equation 2.1 Braggs Law: $\lambda = 2\, d_{hkl} \sin\theta$ $\therefore$ $\sin\theta = (\lambda/2) \times (1/d_{hkl})$

where λ = wavelength of incident beam

d_{hkl} = spacing between planes with Miller indices *hkl*

θ = angle of incidence (Bragg angle)

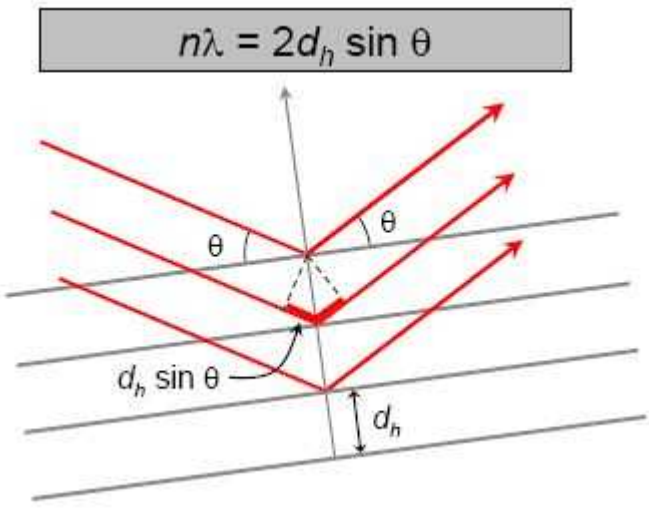

Figure 2.3 *The geometry of diffraction for a two-dimensional set of parallel planes, used to derive Bragg's Law*[168].

Every reflection therefore represents a set of lattice planes. This allows construction of a reciprocal lattice that is used in the interpretation of a diffraction experiment; the reciprocal lattice point associated with each plane is defined with both a direction (perpendicular to the plane) and a magnitude ($1/d_{hkl}$). This construction can be used to predict the orientation that the reciprocal lattice (and therefore the direct crystal lattice) must lie in relative to the incident X-ray beam for a particular reflection to be observed. The Ewald sphere is one construction used to derive the relative lattice orientation required to observe a particular reflection (Fig 2.4).

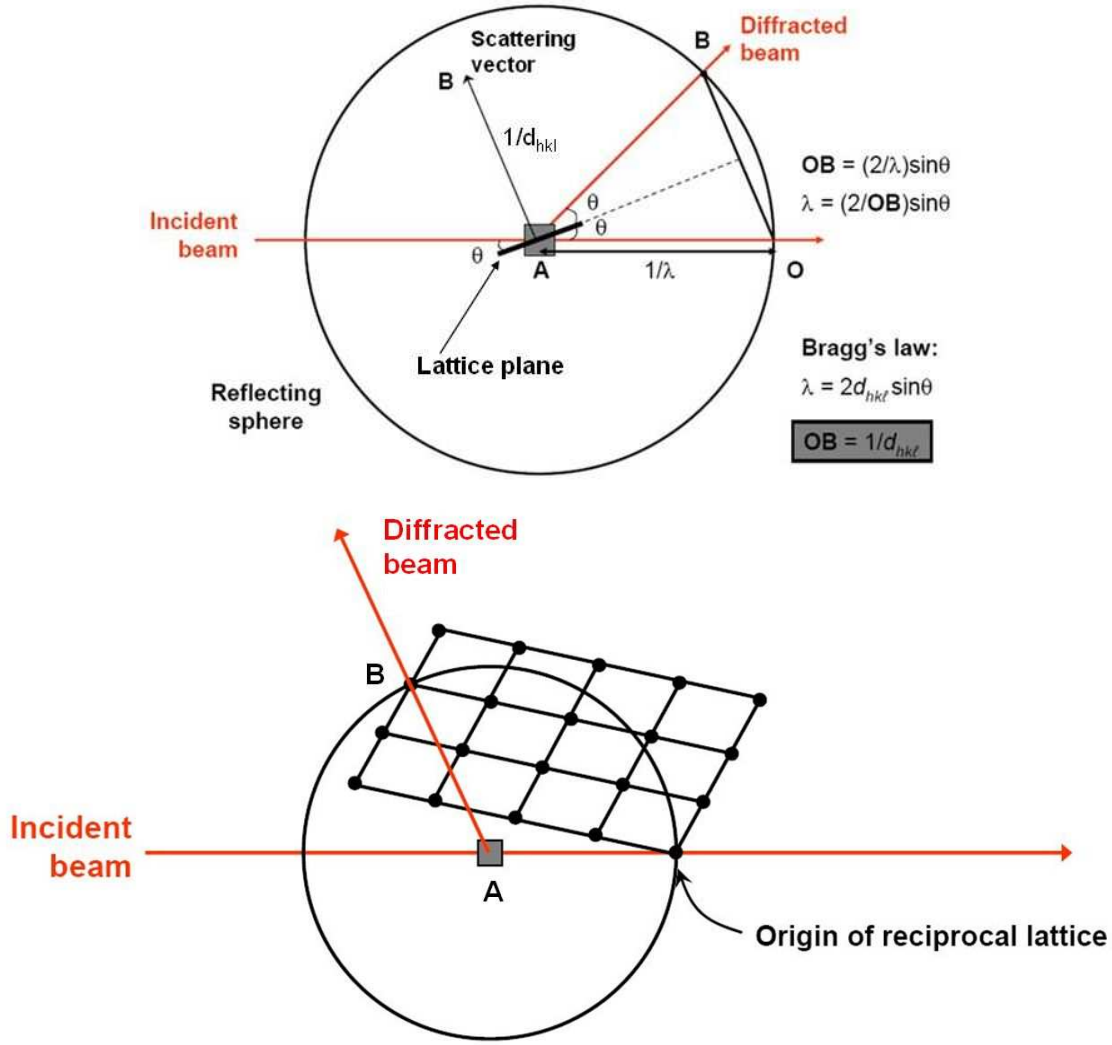

Figure 2.4[168] *A 2D representation of the Ewald construction showing (top) the geometry of the Ewald sphere and (bottom) a visualisation of the reciprocal lattice placed on the sphere (with the origin placed at point O). With the lattice in this orientation only one reflection is observed (point B) as only one reciprocal lattice point intersects the sphere. Rotation of the lattice about the origin brings other reciprocal lattice points into contact with the sphere.*

The Ewald construction consists of a sphere of radius 1/λ, centred on the crystal position, A. The reciprocal lattice is placed with its origin lying on the edge of the sphere (O) and a reflection is observed when the reciprocal lattice point for reflecting planes *hkl* intersects the surface of the sphere (B). The vector AB gives the direction of this diffracted beam. If a lattice point does not lie on the sphere then Bragg's law is not satisfied. Rotation of the reciprocal lattice around the origin brings other lattice points into contact with the sphere allowing the conditions to be specified under which Bragg's law will be satisfied for those reflections. Reflections which cannot be brought into contact with the sphere cannot be observed, limiting the maximum number of reflections that can be accessed for a given incident wavelength (which defines the radius of the Ewald sphere).

2.1.3 The Fourier Transform and the Phase Problem

From the diffraction pattern an image of electron density must be obtained, where areas of concentrated electron density generally represent individual atoms. The intensities of the diffraction pattern and the arrangement of atoms in the unit cell are related to each other by Fourier transformation. The diffraction pattern is the Fourier transform of the crystal structure (Eq. 2.2a), and is defined in terms of the structure factor F_{hkl}, which represents the diffraction pattern measured at the reciprocal lattice point *hkl*. The crystal structure expressed in terms of the electron density is thus the inverse Fourier transform of the diffraction pattern (Eq. 2.2b).

The structure factor associated with each reflection is a complex number that describes both the phase (Φ_{hkl}) and the amplitude ($|F_{hkl}|$) of the diffracted wave. The intensity of the beam reflected from the lattice planes can be measured and from this the wave amplitude $|F_{hkl}|$ can be calculated (Eq. 2.3). The phase information is lost, however, and this is known as "the phase problem"; evaluating the Fourier transform requires the phases of the different reflections to be known to allow the calculation of the electron density (Eq. 2.2b). The task of solving a crystal structure involves recovery of these lost phases, at least as approximate values so that the inverse Fourier transformation can be carried out.

Equation 2.2 (a) The Structure Factor as Fourier Transform of the electron density:

$$F_{hkl} = \int_{cell} \rho(xyz) \, . \, \exp\,[2\pi i(hx + ky + lz)]dV$$

Equation 2.2 (b) The electron density as inverse Fourier Transform of the structure factors:

$\rho(xyz) = 1/V \sum_{h,k,l} F_{hkl} . \exp[-2\pi i(hx + ky + lz)]$, or

$\rho(xyz) = 1/V \sum_{h,k,l} |F_{hkl}| .\exp[i\Phi_{hkl}].\exp[-2\pi i(hx + ky + lz)]$

where $F_{hkl} = |F_{hkl}| .\exp[i\Phi_{hkl}]$ is the Structure Factor

$\rho(xyz)$ = the electron density

$|F_{hkl}|$ = magnitude of reflection *hkl*

Φ_{hkl} = phase of reflection *hkl*

V = Volume of unit cell

x, y, z = coordinates of the position within the unit cell

Equation 2.3: $|F^{o}_{hkl}| = c\, I_{hkl}^{1/2}$

$|F^{o}_{hkl}|$ = observed structural amplitude

I_{hkl} = Intensity of reflection *hkl*

c = experimental constant

Eq. 2.2a can be used at any point during structure determination to calculate the diffraction pattern for a known structure even if it is incomplete. This results in the calculated structure factor, F^{c}_{hkl}. The experiment only gives us the amplitudes and not the phases so the observed structure factors are the structure factor amplitudes $|F^{o}_{hkl}|$.

2.1.4 Structure Solution

As previously stated, structure solution involves the regeneration of the phase information lost during the diffraction experiment. The two most common methods of doing this are outlined in the following.

2.1.4.1 Patterson Methods

In Patterson methods the intensities are used as the Fourier coefficients in Eq. 2.2b rather than the structure factors. As the intensity is the product of the structure factor and its complex conjugate, this effectively results in the observed amplitudes ($\left| F^{o}_{hkl} \right|$) in Eq. 2.2b being replaced by their squares ($\left| F^{o}_{hkl} \right|^2$) and the phases being set to 0 (Eq. 2.4). The result of this equation is a Patterson map which is no longer a map of electron density but instead represents vectors between individual atoms; every pair of atoms in a structure will have a vector represented in the Patterson map. This shows where atoms lie relative to each other but not where they lie relative to the unit cell origin. The peak magnitudes are proportional to the product of the atomic numbers of the two atoms concerned and therefore their number of electrons. If the structure consists of a small number of heavy atoms with a majority of lighter atoms then the heavy atom – heavy atom vectors will be the largest peaks on the map. This allows a set of positions to be deduced for the heavy atoms from which approximate phases can be calculated and the reverse Fourier synthesis carried out, as the electron density of these heavy atoms will dominate the overall electron density. The map of electron density produced will allow more atomic positions to be determined and a better estimate of the phases can be used to repeat the reverse Fourier transform calculation.

Equation 2.4 The Patterson Function:

$$I = \left| F_{hkl} \right| \exp(i\Phi_{hkl}) \cdot \left| F_{hkl} \right| \exp(-i\Phi_{hkl}) = \left| F_{hkl} \right|^2$$

(since: $\exp(i\Phi_{hkl}) \cdot \exp(-i\Phi_{hkl}) = \exp(0) = 1$)

Therefore: $$P(uvw) = 1/V \sum_{h,k,l} \left| F_{hkl} \right|^2 \cdot \exp[-2\pi i(hu + kv + lw)]$$

u, v, w = coordinates of vectors between pairs of atoms in the structure

2.1.4.2 Direct Methods

Direct methods are methods which attempt to derive the structure factor phases, and hence the electron density and atomic coordinates by mathematical means from a single set of X-ray intensities with no other information of the crystal structure, i.e. it is a direct solution to the phase problem. They are statistical methods and do not depend on the presence of heavy atoms meaning it is possible to solve most structures by direct methods. The discrete atomic nature of matter and its implications for diffraction allows constraints and probability relationships to be set up to generate the phases. Constraints, such as atoms being discrete and the impossibility of negative electron density, put restrictions on the possible values for phases and probability relationships are set up between the phases of the most important reflections (those which contribute most to the Fourier transform).

The probability relationships used in direct methods make use of the Sayre equation which is based on the above constraints that electron density must be positive and that atoms are discrete, i.e. the electron density is concentrated in well-defined maxima. The Sayre equation states that the structure factor of a reflection can be calculated as the sum of the products of all pairs of reflections whose indices sum to it[170]. For centrosymmetric structures, where the solution to the phase problem is a case of assigning positive or negative values, reflections that are weak have little contribution to the magnitude of the structure factor and are ignored initially which allows triplet relationships to be set up (Eq. 2.5 illustrates a triplet relationship for reflection (3,2,1)). Triplet relationships allow the calculation of structure factors using three strong reflections. The structure factors are normalised to an expectation value, $E_{hkl,}$ to allow for intensity fall off (and therefore fall off in the magnitude of the structure factor) with increasing scattering angle.

Equation 2.5[170] $E_{321} \approx E_{100} \cdot E_{221}$

E_{hkl} = normalised structure factor

The phase of E_{321} in Eq. 2.5 is now assumed to be approximately the product of the phases of E_{100} and $E_{221.}$ Therefore, if E_{100} and E_{221} have the same sign, then E_{321} is probably positive and if they have different signs then E_{321} is probably negative. A number of similar

relationships are set up and starting with random phases, different possible phases are tried in order to see which will satisfy the probability relationships best. The stronger the reflections used in these relationships, the more likely the relationships are to be accurate. Fourier transforms are then calculated for the best set of phases and observed amplitudes and an electron density map is generated which can then be analysed for recognisable molecular fragments[167].

For the case of non-centrosymmetric structures, the same principle applies, except that the values of the phase can now assume all values not just positive and negative. In practice a multi-solution approach is usually adopted in the application of direct methods, in which sets of reflections are assigned a range of potential initial phases, which are permuted until a plausible set can be obtained.

2.1.5 Structure Completion and Refinement

When all non-hydrogen atoms have been found, the model has to be refined to reach the best agreement between the calculated diffraction data of the model structure and the diffraction data from the experiment. A measure of the agreement is usually obtained using the residual factor or R-factor. Using the Fourier transform, the diffraction data resulting from the current model can be constructed, and a set of calculated structure factors is determined. The calculated structure factors contain values for both amplitudes and phases, but since the observed structure factors only have a value for amplitude, the calculated structural amplitudes are compared to the observed amplitudes to give the R-factor (Eq. 2.6a). The closer this value is to zero, the better the model. There are variations on this equation using F^2 values instead of $|F|$ and weighted R-factors can also be calculated (Eq. 2.6b) where the structure factors of the reflections are multiplied by factors depending on the reliability of the measurement[167].

Equation 2.6 Calculating R-factors:

(a)

$$R = \frac{\sum_{h,k,l} \left\| F_{obs} \right| - \left| F_{calc} \right\|}{\sum_{h,k,l} \left| F_{obs} \right|}$$

(b)

$$wR2 = \sqrt{\left(\frac{\sum_{h,k,l} w({F_{obs}}^2 - {F_{calc}}^2)^2}{\sum_{h,k,l} w(F_{obs}^2)^2} \right)}$$

The calculated phases, Φ_c (from the model structure), and the observed amplitudes, $|F_o|$, are used to calculate a new electron density map for the structure which will show the molecular fragments already found as well as regions of electron density that may represent atoms yet to be assigned. When only a partial structure model is obtained from initial structure determination, this process is repeated until all non-hydrogen atoms are found. Each time a new set of improved structure factors (and therefore Φ_c) are determined until the difference in F_c and F_o give as low an R-factor as possible. During this process, least squares optimisation of atom positions and thermal parameters are carried out to further improve the R-factor. Fourier difference maps can also be used to find atoms not yet found and can indicate incorrect atom assignments. Fourier difference maps are generated via replacing $|F_o|$ in Eq. 2.2b with $|F_o| - |F_c|$.

With all non hydrogen atoms found and assigned, the difference in F_c and F_o must be minimised by further least-squares refinement of the atomic coordinates and the vibrational parameters of the atoms. The vibration of the atoms is initially represented by a single value as the atoms are represented as spheres vibrating by the same amount in all directions. This value is the isotropic thermal parameter. A more realistic representation is given by refining the atoms anisotropically, where the atoms vibrate by different amounts in different directions. This then becomes six values, representing the magnitude and directions of the vibrations, known as the anisotropic thermal displacement parameters. Hydrogen atoms identified from the electron density map or difference map should not be refined anisotropically against X-ray data as they contribute relatively little to the scattering due to only having one electron. The fact hydrogen has only one electron also means that covalent bonds involving hydrogen will be observed as being shortened due to displacement of the bonding electron towards the heavier atom to which the hydrogen is bonded. This has the effect of producing systematic errors in hydrogen bond lengths. As it may not be possible to locate hydrogen atoms accurately, in some cases they should be constrained to have fixed bond lengths and their vibrations tied to the atoms to which they are bonded. As a consequence of these factors, hydrogen bond lengths from X-ray data are often expressed in terms of the distance from the donor atom to the acceptor atom.

2.1.6 Powder X-ray Diffraction

As well as using single crystal X-ray diffraction for structure determination, powder X-ray diffraction (PXRD) is also used in this work. PXRD is primarily used for identification and quantification of new co-crystals and/or phases although structure determination is possible in some cases using, where appropriate, structure determination from powder diffraction (SDPD) methods, and Rietveld refinement techniques[171]. In PXRD, instead of using a single crystal, the sample is extracted or ground to a polycrystalline powder and packed into a capillary for data collection; one advantage of this technique is that it negates the need to find good quality single crystals as required for single-crystal XRD. The capillary is placed in an X-ray beam and rotated to minimise preferred orientation effects. Instead of a pattern of spots, as is produced with a single crystal, a pattern of concentric rings is produced. As the powder contains randomly orientated polycrystallites, each individual crystal generates a limited set of Bragg reflections depending on its orientation. The resultant pattern from all of the many randomly oriented crystallites generates the full set of Bragg reflections, characterised only by the Bragg angle 2θ. A detector measures the diffracted beams and intensity is recorded as a function of angle for each reflection i.e. a cross section through the diffraction rings. As with single crystal XRD, the peak positions are related to the unit cell geometry and intensities are related to atom positions within the cell. Different crystal structures thus produce their own unique diffraction pattern. Figure 2.5 shows how the powder diffraction pattern is built up from a large number of crystallites.

Where a heterogeneous sample is being analysed, the technique can be used to probe the bulk, resulting in a pattern showing a superposition of the PXRD patterns of all components of the mixture. This allows for fairly high-throughput analysis of whole samples to identify the composition of multi-phase samples and determine if a new phase has been produced in co-crystallisation experiments. Tentative quantitative analysis of the mixture can also be carried out by comparing relative peak heights. The relative peak heights are affected by the scattering strength of the material and therefore factors such as different chemical composition can prevent accurate phase quantification using this method. Quantitative analysis is further complicated by preferred orientation effects as well as peak overlap in some cases, although these issues can be taken into account using Rietveld refinement[172]. As previously stated, structure solution from powder data can be carried out for samples containing a single phase but is made difficult as the three-

dimensional information from the diffraction pattern is compressed into a one-dimensional pattern. This method will thus only be used in this work for identification of new phases (both new molecular complexes and new polymorphs) and quantitative analysis of mixtures of polymorphs.

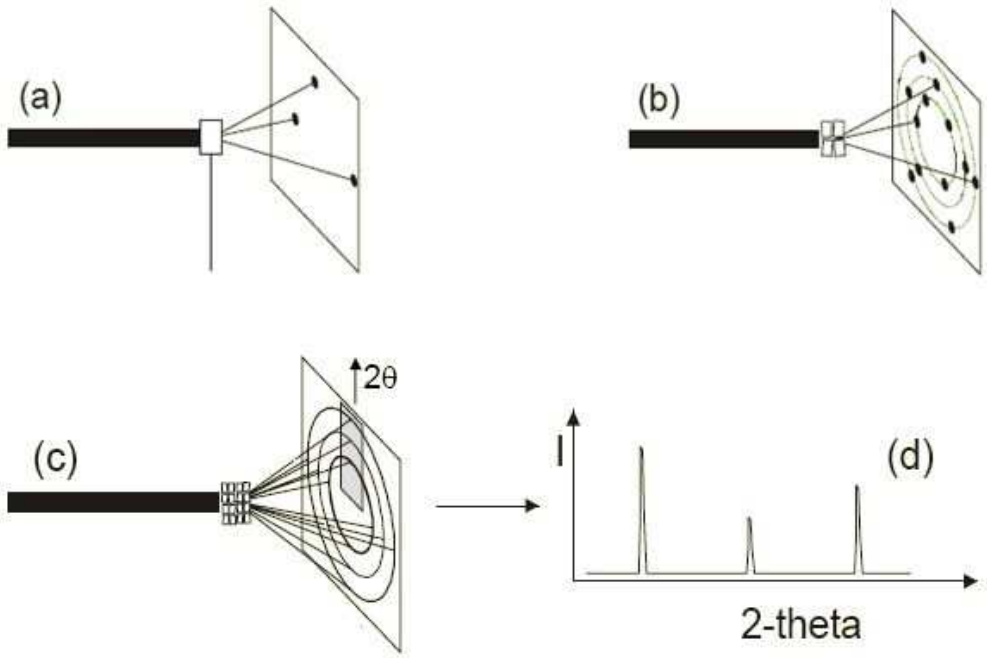

Figure 2.5[168] *Illustration of how a diffraction pattern is built up showing: (a) spots from a single crystal; (b) spots from 4 single crystals in different orientations; (c) rings from polycrystalline powder; (d) diffraction pattern of intensity vs. 2theta.*

2.1.7 Single Crystal Neutron Diffraction

As mentioned previously, locating hydrogen atoms via X-ray diffraction is difficult and results in inaccuracies due to hydrogen atoms possessing only one electron that is inherently involved in a covalent bond. To this end, neutron diffraction can be used as an alternative to X-ray diffraction as a means of locating and modelling the parameters of hydrogen atoms more accurately. Neutrons are scattered by atomic nuclei rather than the electrons and thus all atoms in a crystal structure are measured at a similar level of precision[173] with scattering lengths varying irregularly with Z across a smaller range of values (Figure 2.6). Hydrogen has a relatively large negative neutron scattering length allowing hydrogen atom coordinates and amplitudes of vibration to be measured to a precision that is similar to that obtained for heavier (C, N, O) atoms in X-ray experiments, in which hydrogen atoms can only be measured to an order of magnitude less in precision[173]. This makes neutron diffraction an ideal technique in cases where accurate modelling of hydrogen atoms is required. Another advantage of neutron diffraction is that the intensity fall-off with increasing scattering angle is far less pronounced than in X-ray diffraction (Figure 2.7), allowing access to high-resolution and therefore more precise data. A less pronounced fall-off does occur due to thermal vibration of the atoms about their equilibrium position which is described, as in the case of X-rays, by the Debye-Waller factor[173].

Due to the limited access to neutron diffraction sources, materials suitable for study are usually characterised by X-ray diffraction initially. Materials where hydrogen atoms exhibit interesting behaviour may then be selected for study via neutron diffraction, for example, materials where hydrogen atoms appear to be disordered (to verify/quantify the disorder) or involved in very short strong hydrogen bonds (to identify the accurate position of the hydrogen). X-ray diffraction data also provides initial heavy atom coordinates to simplify the process of refining the structure against the neutron data. Variable temperature neutron diffraction studies are frequently carried out in examining those structures where the neutron data can provide key information, allowing the study of the evolution of hydrogen parameters with increasing temperature. This has previously been used to study phenomena such as proton migration[174] or libration of functional groups[175].

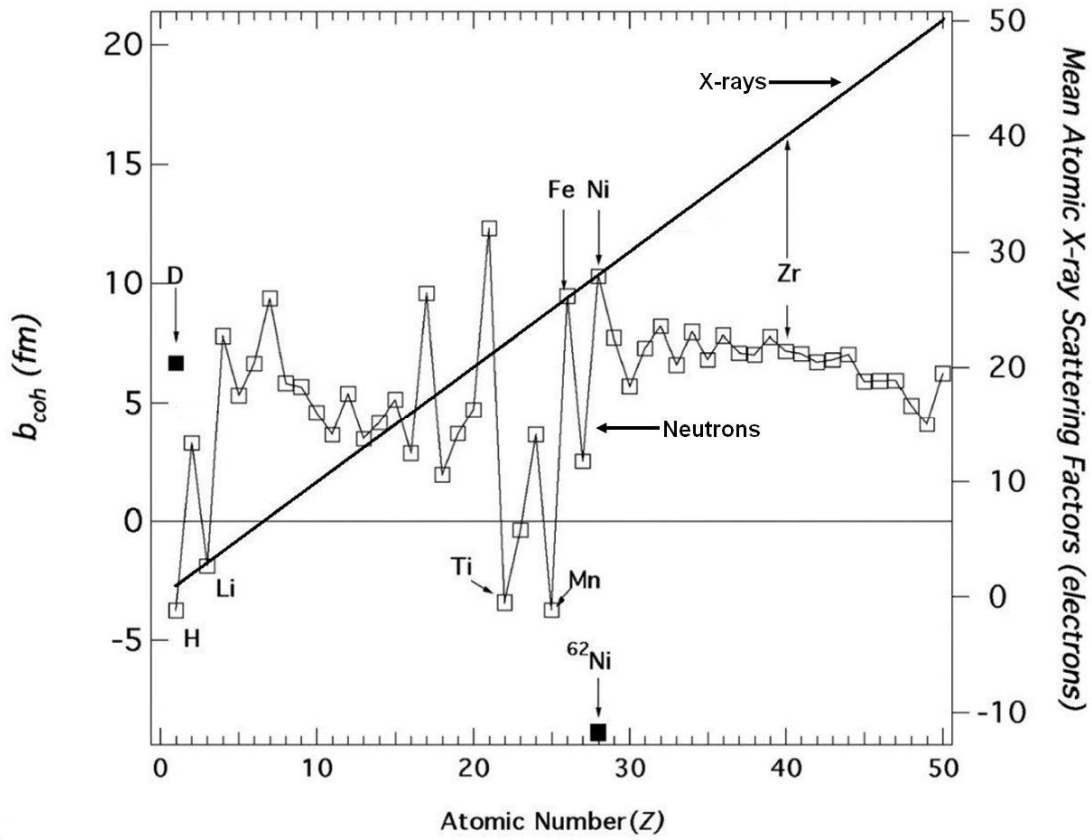

Figure 2.6 *Variation of X-ray scattering factors and neutron scattering lengths with increasing Z*[176]

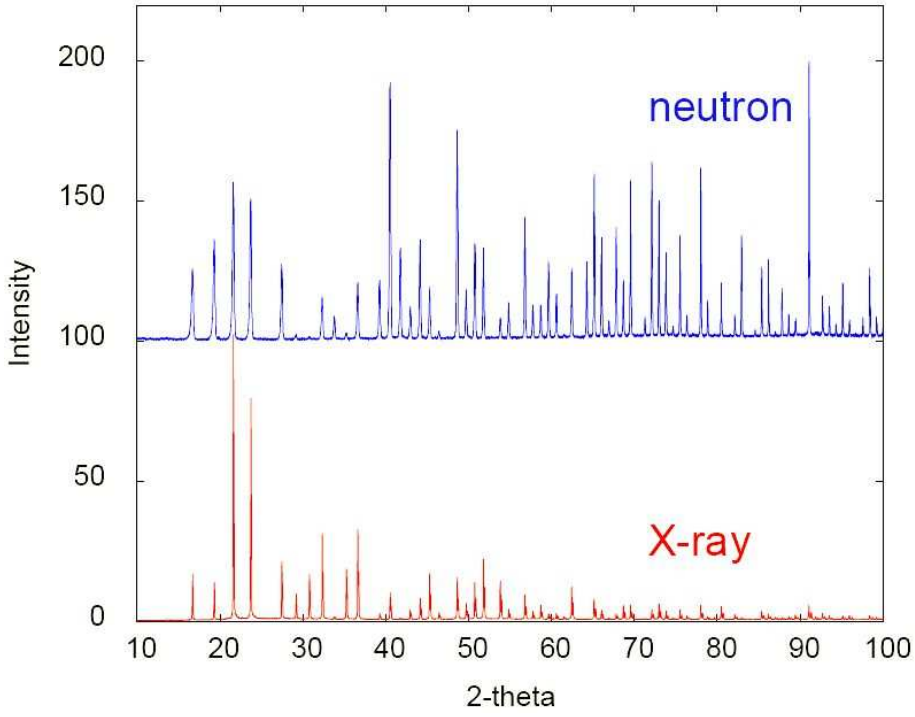

Figure 2.7 *Powder diffraction patterns emphasising the fall-off in X-ray intensity with scattering angle compared with neutrons, where the fall-off in intensity is far less pronounced*[168].

2.2 Thermal Analysis

2.2.1 Differential Scanning Calorimetry (DSC)

Differential scanning calorimetry is a thermoanalytical technique which is routinely used in the identification and characterisation of co-crystals and polymorphs of materials. The method is based on the principle that a change in the physical state of a material is accompanied by the liberation or absorption of heat[177]. In practice it is used to measure the heat energy necessary to establish a near zero temperature difference between a substance and a reference material, as the two specimens are subjected to identical temperature regimes in an environment where they are heated or cooled at a controlled rate[178].

In the analyses carried out as part of this work, the DSC method used is heat flux DSC. In heat flux DSC the sample and reference are enclosed in a single furnace and connected by a low-resistance heat-flow path (Figure 2.8) with a purge gas flow for efficient heat transfer and removal of volatiles.

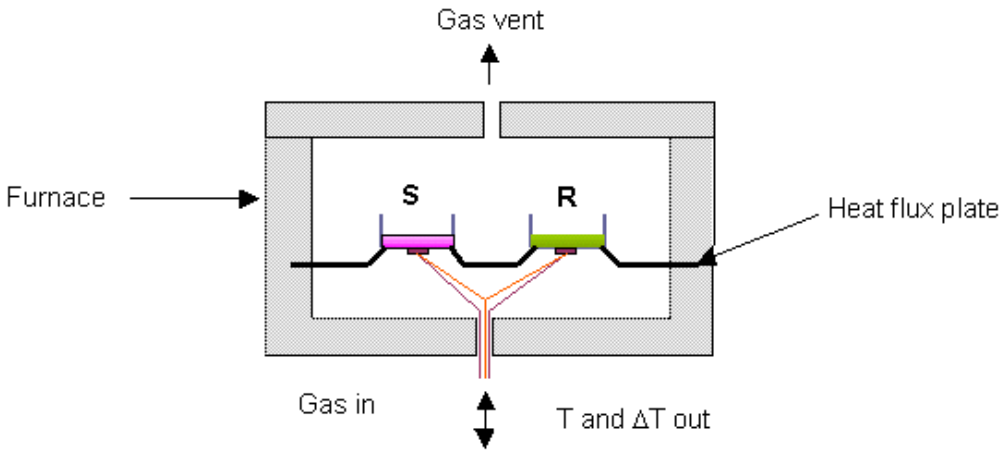

Figure 2.8 *Schematic of Heat Flux DSC Set-up*[179].

As the temperature is changed in a linear manner, any heat changes in the sample will result in a difference in the energy needed to maintain the sample and reference at the same temperature. As they are in good thermal contact any excess heat energy will flow into the metallic disc and this heat flow is measured as it is directly proportional to the small temperature difference between the sample and the reference. This technique can therefore be used to observe phase transitions in materials as they undergo heating or

cooling, as endothermic processes such as melting will result in a negative heat flow, whereas exothermic processes such as crystallisation will result in a positive heat flow (Figure 2.9). Glass transitions, where a change in heat capacity occurs in the sample, can also be observed using DSC (also Figure 2.9).

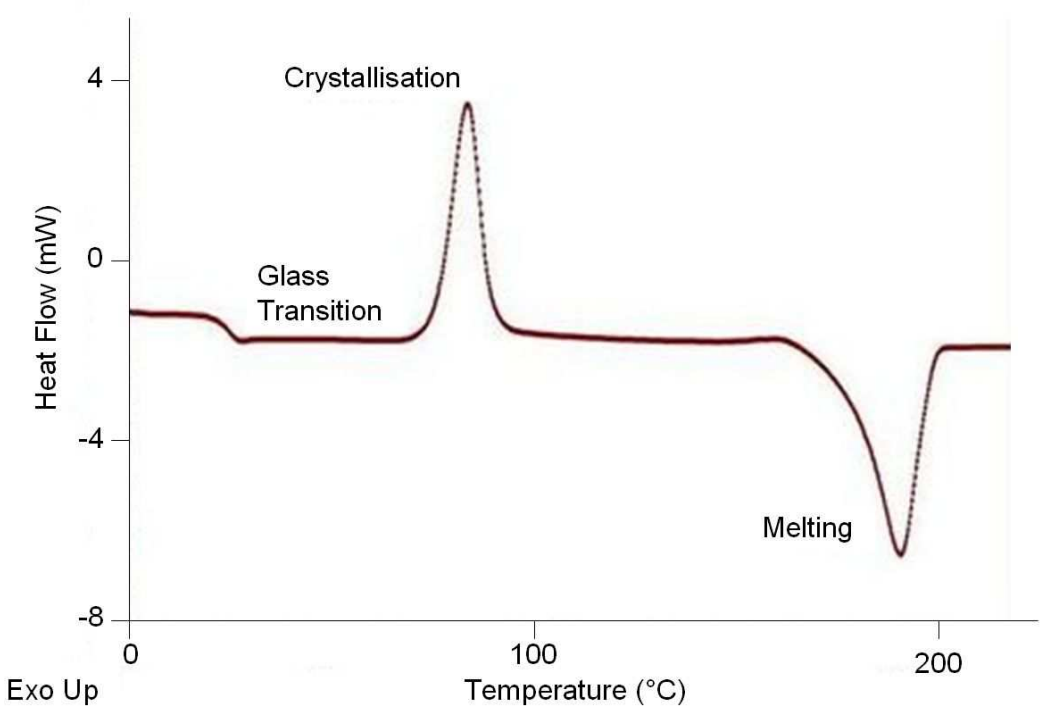

Figure 2.9 *Example of a DSC trace exhibiting endothermic (melting) and exothermic (crystallisation) processes, as well as a glass transition, where a change in heat capacity occurs*[180].

This technique will be used in the initial analysis of the products of the attempted co-crystallisations to ascertain which, if any, have formed new phases. Comparing the melting point of the product to that of a reference of the starting materials gives an indication of whether they are the same or not. A co-crystal would be expected to have a unique melting point, different from that of its components, while a new polymorph of one (or both) of the components would also be expected to have a unique melting point. Should the results indicate the presence of a potentially new phase, this preliminary analysis would have to be followed up by X-ray diffraction techniques to ascertain the exact nature of the new phase. In cases where polymorphic materials are discovered in this work, DSC will be used to ascertain the relative thermal stability of the polymorphs, as the more stable polymorphs should have higher melting points.

2.2.2 Thermogravimetric Analysis

Thermogravimetric analysis (TGA) is a technique used to measure the change in weight of a sample as a function of temperature, providing information on the composition of the sample. The sample is loaded in an inert pan (normally platinum) which is placed on a balance and the sample weight recorded accurately. The pan is then heated until vaporisation of one of the sample components occurs causing it to leave the pan with the weight being recorded throughout. A plot of % weight versus temperature is produced (Figure 2.10), where the % weight loss can be used to infer information on the process that has taken place. A derivative weight loss curve can also be produced to aid interpretation, emphasising areas where weight loss is more pronounced (also Figure 2.10). TGA is often used to assess sample purity as well as investigate the decomposition/stability of samples. It is also used in studies of porous materials to investigate the evolution of gases stored in the pores[181].

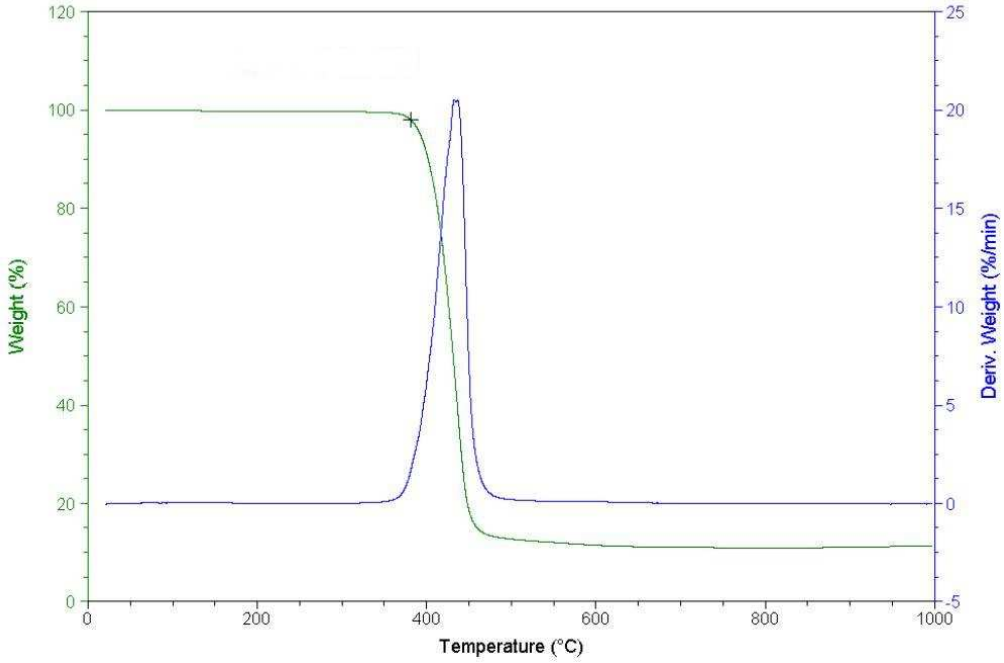

Figure 2.10 *Example of typical weight loss TGA plot (green) and the corresponding derivative weight loss TGA plot (blue). The drop in weight between 375°C and 450°C indicates vaporisation of one of the sample components has occurred.*

3. Techniques and Instrumentation

This chapter will outline the general experimental techniques used to gather data for this work and will detail the instrumentation used for analysis. Where appropriate, more specific details will be given throughout the chapters describing the materials studied, or in the relevant appendices.

3.1 Crystallisation Techniques

3.1.1 General Evaporative Method for Co-Crystallisation Screening

Obtaining good quality crystalline samples of the molecular complexes or polymorphs under investigation is the first step of the studies presented herein. As discussed in Chapter 1, various crystallisation methods can be used to screen for co-crystals. In this work, a medium-to-high throughput evaporation method was selected. The simplicity of the evaporation method offers the opportunity to set up numerous experiments simultaneously under various conditions to maximise the chances of obtaining good quality crystals of the desired molecular complex.

The general evaporative co-crystallisation screening method used in this work is outlined below:

1. Target molecule and co-former were dissolved in a 1:1 molar ratio (between 10-100 mg) in an excess quantity of an appropriate solvent (generally 2-6 ml). Samples were sometimes heated gently to facilitate dissolution of the materials. The vials used were made of glass and had a maximum volume of 7 ml.

2. The plastic lid of the vial was perforated to allow the solvent to evaporate slowly over time. The solvent was allowed to evaporate completely at a fixed temperature (or at ambient temperature) and crystallisation occurs at the point where the solution becomes supersaturated.

3. Iterations of each co-crystallisation were set up under various conditions to maximise the chances of obtaining the desired molecular complex and good quality crystals thereof. The use of different crystallisation conditions may also result in different polymorphs of the complex. The main variables altered in this screen were the solvent used and the temperature of evaporation. The solvents generally used were methanol, ethanol, acetone, isopropanol and acetonitrile. The poor solubility of piroxicam in most solvents meant that acetonitrile was used initially (see Chapters 4, 5 and 6). If this failed to yield a molecular complex, methanol or acetonitrile/methanol mixtures were used as solvent. The temperature of evaporation was controlled using an Asynt hot-plate with jacketed vessels (Figure 3.1).

4. If varying the solvent and/or the evaporation temperature failed to yield a molecular complex, the relative quantities of the components in solution could be varied.

Figure 3.1 *A temperature controlled hot-plate with jacketed vessels used for controlling the temperature of evaporation of the co-crystallisation experiments. The glass vials were kept in the jacketed vessels during the evaporation process to maintain a constant temperature during crystallisation.*

3.1.2 Scale-up for Co-Crystallisation in an Oscillating Baffled Crystalliser (OBC)

3.1.2.1 General Viability Screening Method for Co-Crystallisation in an OBC

After full structural characterisation, certain phases that have potential pharmaceutical relevance were selected to be trialled for scaled-up crystallisation in an OBC. This required conversion from an evaporation co-crystallisation technique to a cooling or anti-solvent addition technique, as evaporation crystallisation is not possible in an OBC.

Small scale trials were carried out to assess the viability for scale-up to a cooling co-crystallisation method. These initially involved dissolving the two components in the same solvent and molar ratio used in the corresponding successful evaporation co-crystallisation. The components were dissolved at high temperature (60-75°C) to generate a saturated solution and the solution was allowed to cool to induce crystallisation. The crystalline product was then isolated by filtration and the sample analysed by PXRD. Several co-crystallisations were set up at varying degrees of supersaturation and cooled to different temperatures (either room temperature or 0°C). If these initial trials failed to produce the desired crystalline phase, different conditions were trialled, i.e. using different solvents or different component ratios. If the PXRD indicated that one component precipitated preferentially ("crashed") out of solution while the second component remained in solution, the relative molar quantity of the second component could be increased in an attempt to encourage molecular complex formation upon crystallisation. Anti-solvent crystallisation could also be trialled, with the anti-solvent used dependent on the solubilities of the component materials.

3.1.2.2 The Batch OBC (BOBC) and Continuous OBC (COBC)

When a viable co-crystallisation system had been identified for scale-up, initial scaled-up trials were to be carried out in a BOBC (Figure 3.2). The BOBC is a round bottom jacketed vessel (typically of volume 250 ml – 500 ml), in which the baffles are oscillated through the solution by a linear motor - as opposed to oscillation of the solution through the baffles by bellows, as is the case in the COBC. A programmable temperature controlled oil circulator unit is attached to the jacket to control the cooling profile and a thermocouple inserted from the top to monitor the solution temperature. Probes can also be attached to the side of the vessel to monitor particle size of the product. The BOBC is used to

determine an initial set of parameters for crystallisation in the COBC, such as optimal cooling rate, optimal oscillation amplitude and optimal oscillation frequency. Solution concentration may have to be significantly altered at this stage as solubility does not scale-up linearly.

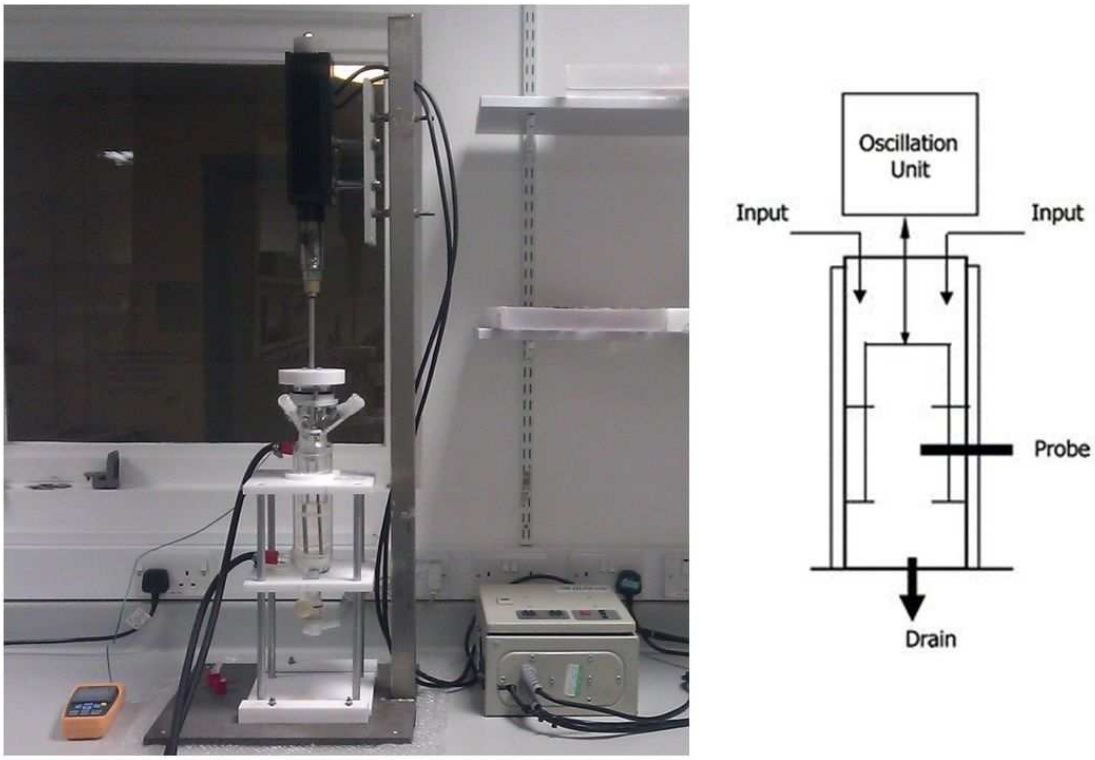

Figure 3.2 *Photograph of the 250 ml batch oscillatory baffled crystalliser (BOBC) in the laboratory, with a linear motor and control box attached (LHS) and a schematic of a BOBC*[155] *(RHS). The probe indicated on the schematic is optional.*

When initial parameters have been determined from the BOBC, scale-up trials move to the COBC (Figure 3.3). Although the set-up in the COBC is based on the parameters from the BOBC trials, the solution concentration must again be optimised due to the larger volume used. Differences in the parameters should also be anticipated due to the different oscillation mechanism and the fact that the solution is flowing through the column. In the COBC at the University of Bath, the column is constructed from twenty 125 ml jacketed glass tubes. The temperature in each tube can be controlled individually by attaching separate temperature controlled oil circulator units. A 5 L – 20 L solution is initially dissolved in a stirred tank and fed into the COBC, where it is oscillated with a positive net flow. As the temperature decreases along the length of the column, crystallisation occurs. The slurry is collected at the end of the column and filtered. For

anti-solvent crystallisation, inlets can be introduced along the length of the column to add the anti-solvent.

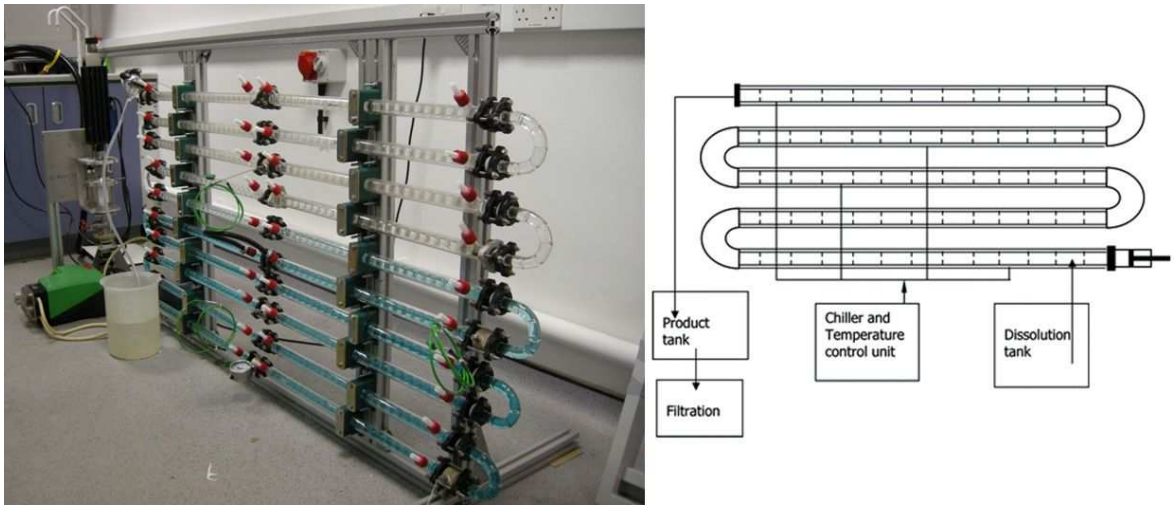

Figure 3.3 *Photograph of the continuous oscillatory baffled reactor (COBC) installed in the laboratory (LHS), with a coloured sample solution being pumped through – this has reached around halfway up the COBC in this picture. A schematic of the COBC*[155] *is also shown (right).*

3.2 Single-crystal X-ray Diffraction

3.2.1 Sample Selection

When performing a single crystal X-ray diffraction experiment, selection of a suitable sample is critical to the success of the experiment and the quality of the data obtained. A number of crystals are selected from the crystallisation vessel and placed under the microscope for initial inspection. The difficulty in selecting a single crystal can vary immensely depending on the sample under investigation. Generally a single crystal will have clear, well defined faces and edges with few or no fault lines visible. Visual analysis using plane polarised light is a key method in identifying if crystals are single or not. A single crystal should extinguish uniformly when rotated 90° under plane-polarised light. Two or more extinctions would suggest the crystal is not single. Ideally the crystal should be approximately 0.2 mm - 0.5 mm in at least two dimensions, although smaller crystals can be used. Significantly larger crystals may be cut down to a more suitable size.

3.2.2 Laboratory Source Diffractometers

Three different laboratory diffractometers were used during the course of this work. The Bruker Apex II and Bruker-Nonius Kappa diffractometers were equipped with charge-coupled-device (CCD) detectors and the Rigaku R-axis/RAPID diffractometer was equipped with an image-plate detector (Figure 3.4). All three diffractometers were equipped with graphite monochromated Mo-Kα radiation (λ = 0.71073 Å). Data for all samples were collected at 100 K. Samples on the Kappa and RAPID diffractometers were cooled by Oxford Cryosystems cryostream low temperature devices, while the Apex used an Oxford Cryosystems Helix, all of which which direct gaseous nitrogen onto the sample from above (Figure 3.4). The cryostream is fed by a liquid nitrogen cylinder, while the Helix uses a nitrogen recovery unit.

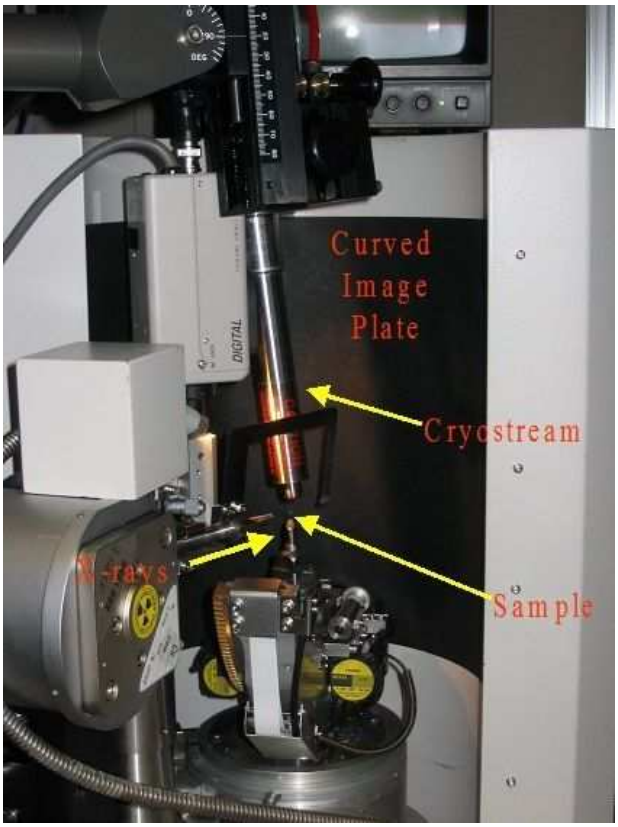

Figure 3.4 *The setup of the Rigaku R-axis RAPID diffractometer. The sample is kept at low temperature during the experiment by the cryostream positioned above it.*

3.2.3 General Procedure of a Diffraction Experiment

Although there are slight differences between the three diffractometers, the general procedure of the diffraction experiment is the same. The sample is mounted on a glass fibre on a goniometer and centred in the X-ray beam to ensure it remains in the beam in all orientations. A preliminary set of X-ray images is taken from different regions of reciprocal space. The number of images is dependent on the diffractometer and the detector type. The Rigaku diffractometer generally requires only four images in this initial scan as the image plate measures a much a larger area of reciprocal space in a single image whereas the Apex II and Kappa diffractometers require more images (between ten and thirty) as the CCD detector measures a relatively small area of reciprocal space in a single image. Exposure time for each image is dependent on the X-ray intensity from the diffractometer as well as the sample size and composition. A tentative unit cell is determined from the spot positions in this set of initial images and this unit cell is compared to the unit cell parameters of the starting materials. If a different unit cell from those of the the starting materials is determined, this is likely to indicate that a molecular complex has been formed, or possibly a new polymorph of one of the starting materials. This unit cell screening procedure can also be useful when identifying phases in complex mixtures, which can be difficult to interpret using PXRD. During the unit cell screening stage a better assessment of the crystal quality can be made, as when a single crystal diffracts it should produce a pattern of well defined peaks. Split peaks or streaks on the diffraction pattern indicate that the crystal may be twinned or have poor mosaicity or have intergrown crystallites.

When a possible new material is identified, a data collection strategy is determined by the diffractometer software based on the Bravais lattice of the unit cell. The data collection should ideally have a d-spacing resolution of approximately 0.75 Å - 0.80 Å with a minimum redundancy of three or four. After all images are collected, the data have to be integrated to obtain a set of peak intensities. At this point background intensity is accounted for in each individual peak. In this work absorption corrections are applied using the multi-scan correction method[182]. The multi-scan correction method also corrects for any other systematic errors such as poor crystal centring. After integration, a reflection data file (*.hkl* file) is generated comprising the Miller indices of the reflections and their corresponding intensities. This file is then used in the structure solution programme. In this work, all structures were solved by direct methods using SHELXS-

97[183], SHELXS-86[183], or SIR-92[184]. Full-matrix least-squares refinement on F^2 was carried out using SHELXL-97[183] within the WinGX program suite[185]. The data processing software used for each diffractometer is summarised in Table 3.1.

Table 3.1 *The data processing software used for each diffractometer.*

Diffractometer	Data Processing Software	Absorption Correction
Bruker Apex II	Bruker APEX2[186]	SADABS[187]
Bruker-Nonius Kappa	Collect[188] HKL Denzo and Scalepack[189]	SADABS[187]
Rigaku R-Axis RAPID	CrystalClear v1.4.0 [190]	ABSCOR[191]

3.2.4 Synchrotron X-ray Source (Diamond Light Source)

Crystals that were too small for X-ray diffraction studies using a lab source were analysed at Beamline I19 (experimental hutch 1) at the Diamond Light Source synchrotron facility (Figure 3.5). The synchrotron exploits the relativistic effects of moving charged electrons at close to the speed of light to produce a high flux and high brilliance X-ray beam with tuneable wavelengths. Electrons are initially produced by an electron gun, in which a cathode is heated to incandescence resulting in the ejection of electrons from the surface. These electrons are accelerated by the high voltage into the linear accelerator (Linac), which further accelerates the electrons through a series of potential differences into the booster ring. In the booster ring, electrons are accelerated to approximately 99.9% of the speed of light before being injected into the storage ring. Bending magnets in the rings control the path of the electrons. When the electrons travel in a straight line no radiation is emitted; when the path of the electron is changed (i.e. they are accelerated), high intensity radiation is emitted tangentially to the storage ring. The X-rays produced from this process can be used for diffraction experiments. Greater intensity can be achieved by the use of insertion devices called wigglers and undulators, positioned in the straight sections of the storage ring. These induce oscillations in the path of the electrons, with each oscillation resulting in more radiation being emitted.

Focusing magnets are also used to keep the electron beam narrow and well defined which results in higher intensity X-rays being produced.

The experiments using synchrotron radiation in this work utilised silicon (111) monochromated radiation (λ = 0.6889 A°) with a Rigaku Saturn CCD detector. Data were processed using CrystalClear-SM Expert 2.0 r5[192] and absorption corrections were carried out using ABSCOR[191].

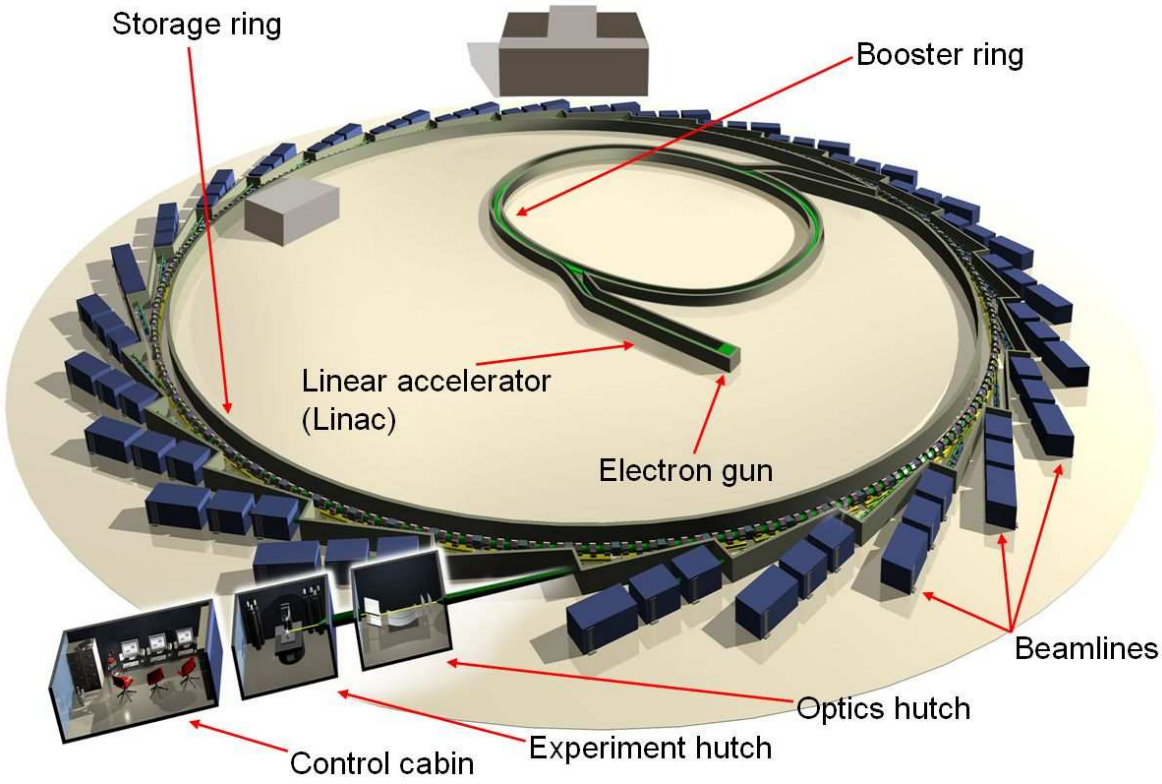

Figure 3.5 *A 3D schematic of the synchrotron at the Diamond Light Source*[193].

3.3 Single Crystal Neutron Diffraction

Single crystal neutron diffraction for this work was carried out at the Institut Laue Langevin (ILL) facility in Grenoble, France. The ILL facility is a steady state neutron source where neutrons are produced by nuclear fission, similar to a nuclear power station. It provides the most intense continuous neutron source in the world, providing neutrons with tuneable wavelengths for more than forty instruments.

3.3.1 VIVALDI at ILL

The instrument used for the neutron diffraction experiments was VIVALDI (very intense vertical axis Laue diffractometer)[194]. VIVALDI is a Laue diffractometer that utilises a high intensity (quasi-) white beam, with a wavelength range of 0.8 Å - 5.2 Å used for the diffraction studies presented in this work. The use of white beam radiation allows faster data collection and also facilitates the use of smaller sample sizes (< 1 mm^3) than are typically required for neutron diffraction (although still requiring larger crystals than are typically used in X-ray diffraction). Data collection time is also reduced as the instrument is equipped with large image plates which cover a large area of reciprocal space. A helium cryostat allows data collection to be carried out at temperatures as low as 30 K. As the experiments use white beam radiation and VIVALDI is one of only two instruments of its type in the world, the data are difficult to process and processing was therefore carried out by the beamline scientists at ILL, subsequent to the experiments being carried out at the ILL by the author. Reflection data files containing processed structure factor data suitable for structural refinement in a program such as SHELXL-97 were provided to the author by the beamline scientists.

3.4 Powder X-ray diffraction (PXRD)

3.4.1 Sample preparation

Samples for PXRD were prepared by gently grinding the sample in a mortar and pestle to obtain a larger number of small crystallites which will reduce preferred orientation effects. The ground sample is then packed into a capillary. Unlike single crystal diffraction, PXRD is used to probe the crystalline properties of the bulk product and so a sample representative of the entire contents of the crystallisation vessel is taken. Capillaries of 0.5 mm - 1.0 mm diameter were used in this work depending on the sample quantity and ease of filling the capillary. Samples were mounted on the diffractometer and centred to ensure they remained in the beam when rotated. Samples were rotated in the beam to minimise preferred orientation effects.

3.4.2 X-ray Powder Diffractometers

The X-ray powder diffractometers used in this work were a Bruker D8 Advance and a PANalytical X'pert Pro. Both machines were equipped with graphite monchromated Cu-Kα radiation and a capillary holder using transmission geometry (Figure 3.6). In this configuration the incident X-ray beam is kept stationary. The sample holder is kept stationary relative to the path of the incident beam while the centred capillary is rotated around an axis perpendicular to the incident beam path - such that the capillary remains in the beam at all times. The detector is attached to an arm and moved through a user-defined 2θ range throughout the experiment. Measurements in this work were carried out between a 2θ range of 5° and 50°. Scan speeds were typically 1° per minute, although slower speeds were used for weakly scattering samples and to obtain patterns with lower background relative to the peaks, for quantitative analysis.

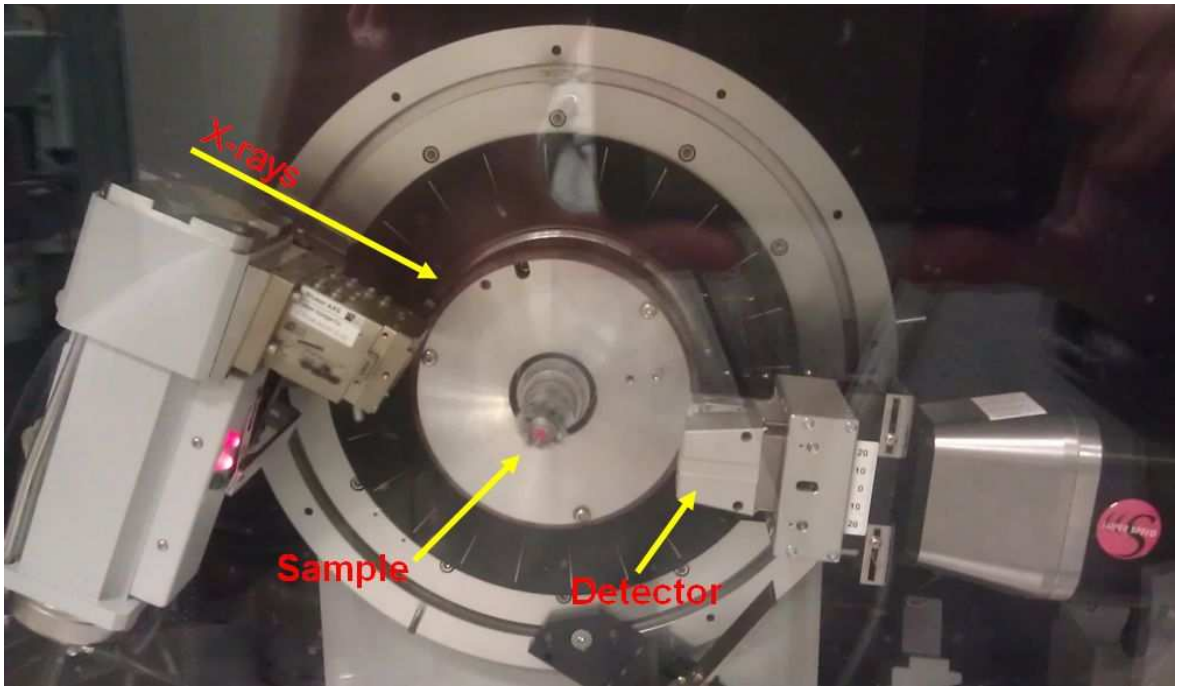

Figure 3.6 *The setup of the Bruker D8 Advance powder diffractometer in transmission mode.*

3.4.3 PolySNAP - Phase Identification and Quantitative Analysis

The PolySNAP software package[195] was used to assist in the interpretation of the PXRD results. This software can be used to match powder patterns in terms of similarity and for

quantitative analysis of mixtures. PolySNAP performs cluster analysis and uses full profile powder pattern matching as opposed to some older methods which only use the 2θ and intensity values of the strongest peaks[196]. Background can also be removed and the data smoothed before peak finding, although this is optional processing. The PXRD patterns can be imported in various formats; the Bruker raw data format is used in this work. Once the powder patterns are imported, various statistical correlation calculations (full pattern and optional individual peak methods) are carried out and a weighted mean of the correlation coefficients is used as an overall measure of the correlation between patterns. Each pattern imported is matched against every other imported pattern and each correlation value for a pair of patterns is used to give a numerical value of similarity between the two patterns. The patterns are then partitioned into related clusters or sets and this partitioning can be presented numerically or in various graphical forms.

A database of pure phases can also be imported by the user to carry out pattern matching relative to an individual input pattern. In this case the input sample is checked against the database for similarity to any of the known phases. Quantitative analysis of mixtures can also be carried out for an individual pattern, using the database to determine a percentage composition of known phases.

In this work, the basic pattern-matching operation was used to compare the products of the co-crystallisations to the starting materials (and known polymorphs thereof) and assist in identifying any interesting or new phases. As mixtures of phases may be difficult to interpret, the quantitative analysis function was used in conjunction with pattern matching to determine if the co-crystallisation had resulted in a new phase or if the sample contained a mixture of the starting materials. Using this method enabled rapid identification of samples which required further analysis. In cases where more than one polymorph of a material had been produced, quantitative analysis allowed quick and easy deduction of the relative ratios of the polymorphs.

3.5 Thermal Analysis

3.5.1 DSC – differential scanning calorimetry

Heat flux DSC measurements were carried out using a TA Instruments Q100 DSC system. Crystals were gently ground and 1–3 mg of sample placed in a hermetically sealed

aluminum pan. Where molecular complexes were analysed, the sample was heated from ambient temperature to typically 10°C or 20°C above the melting point of the highest melting component of the molecular complex. DSC measurements on new polymorphs of materials were carried out to 10°C or 20°C above the melting point of the most stable known polymorph. Samples were heated at either 5°C min^{-1}or 10°C min^{-1}. Melting points were derived from the onset point of the peak using the TA Universal Analysis software from TA instruments.

4. Multi-Component Crystallisation Routes to New and Elusive Polymorphs

This chapter will focus on the use of the co-crystallisation approach to direct the assembly of rare or new metastable polymorphs of one of the components (as discussed in Chapter 1, Section 1.4.3.3). The co-crystallisation experiments discussed herein do not result in molecular complex formation between the API and the co-molecule; they instead crystallise independently, with the co-molecule perturbing the crystallisation environment in such a way as to direct the formation of a metastable polymorph of the API (or in some cases, a solvate). This technique is investigated as an alternative method of polymorph control for four different materials with pharmaceutical properties: paracetamol, piroxicam, piracetam and gallic acid.

4.1 Introduction to Paracetamol Crystal Forms

Paracetamol (acetaminophen, p-hydroxyacetanilide; Scheme 4-1) is an important bioactive compound and active pharmaceutical ingredient (API), previously studied intensively in the crystalline state[47-50, 175, 197-199]. There are currently three known polymorphs of paracetamol (PA); the crystal structures of all three have been determined previously, although the structure of form III has only been determined relatively recently from powder X-ray diffraction data[200]. The metastable orthorhombic form II polymorph (PA II) has been shown to be more soluble[48] and more readily compressible into tablets than the commercially available form I[49,50], due to the layered nature of its packing in the solid state. PA molecules in form I (PA I) are arranged in a herringbone fashion resulting in an interlocked structure with poor compression properties[50] (Figure 4.1). The layered arrangement of the molecules in form II results in slip layers which facilitate direct compression for tabletting without the need for binding agents[49,50]. These physical characteristics make form II far more attractive in formulation. However, existing routes to selective crystallisation of this phase are complex, and solid form II products from these tend to convert into form I over time[50]; form II is a metastable polymorph. Previous crystallisation routes to this polymorph include carefully controlled heating, cooling and filtering cycles over periods of days[201], rapid removal and drying of crystals grown by seeding using crystals from the melt[50], heteronucleation involving heating and cooling

cycles[202], high pressure crystallisation[197] and using porous membrane crystallisers[203]. The favourable physical properties of form II make it desirable to find a facile route to selective crystallisation of this polymorph that would lend itself to production on an industrial scale but as yet no straightforward, reliable method is known.

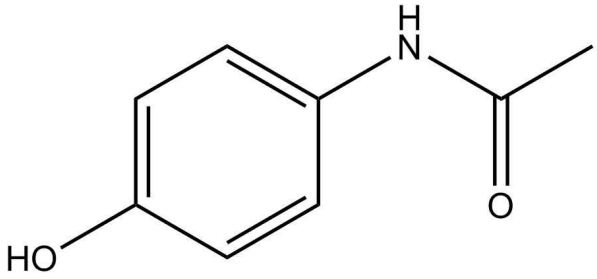

Scheme 4-1 *Molecular structure of paracetamol*

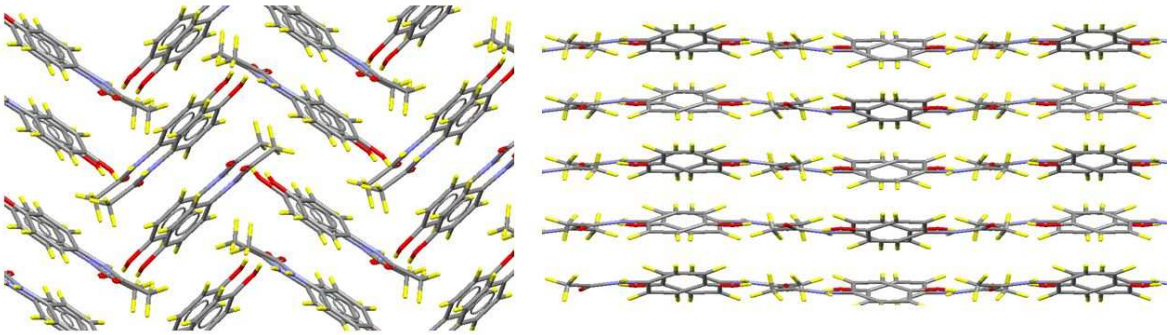

Figure 4.1 *The crystal packing in paracetamol form I (LHS) and form II (RHS). The molecules in paracetamol form I are packed in a herringbone arrangement whereas the molecules in form II are arranged in layers.*

4.2 Multi-Component Crystallisation Routes to Paracetamol Form II: Co-crystallisation with Carboxylic Acids

A medium to high throughput co-crystallisation screen of paracetamol was initially carried out with a view to molecular complex formation. The discovery that co-crystallisation with certain mono-substituted benzoic acids resulted in the concomitant recrystallisation of the mono-substituted benzoic acid with metastable PA II - as opposed to the stable PA I - led to the possibility of polymorph control via co-crystallisation being investigated.

4.2.1 Crystallisation Conditions

4.2.1.1 Evaporation Co-crystallisations

Co-crystallisations were carried out according to the procedure outlined in Chapter 3 unless otherwise stated. Systematic 1:1 evaporative co-crystallisations of paracetamol were carried out with a range of mono-substituted benzoic acids in a range of different solvents at room temperature. In some cases other temperatures were used for the crystallisation in attempts to induce molecular complex formation. Co-crystallisations of 4-bromobenzoic acid and 4-chlorobenzoic acid were also carried out in 2:1 molar ratios (PA:BA) and in the case of 4-bromobenzoic acid, 4:1 ratios were also used, to assess the affects of altering the component ratios. Other molecules containing carboxylic acid groups were also used as co-molecules in crystallisation attempts. Relevant results from co-crystallisations with co-molecules that do not possess carboxylic acid groups are also presented in this chapter. Table 4.1 shows a summary of all the relevant co-molecules and solvents explored in the co-crystallisation experiments.

Table 4.1 *Summary of the relevant co-molecules and the main solvents used in the co-crystallisation experiments with paracetamol. Only one co-molecule from either column A or B was used with one solvent from column C.*

Note: In the case of taurine, water was used as the solvent as it is poorly soluble in most solvents.

(A) Carboxylic Acid Co-molecules	(B) Other Co-molecules	(C) Solvents
Benzoic acid (BA)	Benzamide	Methanol(MeOH)
2-, 3-, and 4-fluorobenzoic acid (FBA)	Erythritol	Ethanol (EtOH)
2-, 3-, and 4-chlorobenzoic acid (CLBA)	Taurine*	Acetone (ACE)
2-, 3-, and 4-bromobenzoic acid (BRBA)	Resorcinol	Isopropanol (IPA)
Succinic acid	Creatinine	Acetonitrile (ACN)
Nicotinic acid	Urea	Water*
Creatine	Pyrazole	
Fumaric acid	3,5-dimethylpyrazole	
Maleic acid	Pyrazine	
Citraconic acid		
Oxalic acid		
Malonic acid		

4.2.1.2 Recrystallisations of Paracetamol Using Acetic Acid

Recrystallisation of paracetamol was carried out by dissolving paracetamol (approx. 80 mg) in excess acetic acid (5-7 ml) and allowing the solvent to evaporate at room temperature. Further evaporative experiments were carried out using supersaturated solutions generated through heating, which were then allowed to evaporate at room temperature.

Recrystallisations were also carried out using acetic acid as an additive in varying molar quantities. Acetic acid was added to paracetamol (between 40 mg and 80 mg) in 20:1, 10:1 and 1:1 (acetic acid: paracetamol) molar ratios with excess solvent (methanol, ethanol, acetone, acetonitrile or IPA). The solvent was then allowed to evaporate at room temperature.

4.2.1.3 Co-Grinding

Co-grinding experiments were carried out by grinding the two components in a 1:1 molar ratio using a mortar and pestle for approximately ten minutes. Experiments were carried out both in the absence of solvent and with 4-5 drops of methanol from a pipette.

4.2.2 Co-crystallisation Routes to Paracetamol Form II

In experiments initially targeted at the formation of molecular complexes, it was found that co-crystallisation of PA with mono-substituted benzoic acids (BAs) could be used as a facile and reliable evaporative route to produce PA II[204]. After a period of days to weeks, depending on the volatility of the solvent used, distinct crystals of both PA II and the pure benzoic acid were formed, which could be easily separated and identified by the crystal habit and the pink hue characteristic of the PA II crystals. Samples were analysed by PXRD (Appendix B4a) to ascertain which PA polymorphs were present. No molecular complex was formed, with the BA crystallising concomitantly with PA I or II (or a mixture) in all cases. Repeat experiments show consistency in the yields obtained, and recrystallisations on the 100 mg scale have been successfully performed to date. Single crystals of form II have also been produced, verified by full redetermination of the previously reported crystal structure (Appendix A4). Moreover, very large (mm-sized) single crystals of good quality have been obtained, representing a significant advance in the production of this previously elusive material in large quantities.

By systematically tuning the BA co-molecule and solvent used in the co-crystallisation (Scheme 4-2), 100% yields of PA II can be obtained (Figure 4.2). Table 4.2 shows a summary of the PA polymorphs obtained from the co-crystallisation experiments. Both the solvent and the BA used appear to play a role in controlling the crystallisation outcome, possibly through solution-mediated templating processes. The 4-substituted BAs produce PA II most reliably, with 100% yields obtained reproducibly from 1:1 crystallisations (Figure 4.2). The three 4-substituted BAs could all be used to produce 100% form II and resulted in products that, at the least, comprised mixtures of both forms from all five solvents used. MeOH and IPA were the most reliable solvents yielding 100% PA II using the 4-substituted BAs. Use of the other halo-substituted BAs as co-molecules can also give up to 100% form II yields, but less reliably and predictably than in the 4-substituted cases, with the yield again being solvent dependent. Interestingly, using

unsubstituted BA as the structure-directing co-molecule did not lead to the production of 100% PA II, with a mixture of PA I and II formed when co-crystallised in methanol and only PA I formed when co-crystallised in the remaining four solvents used.

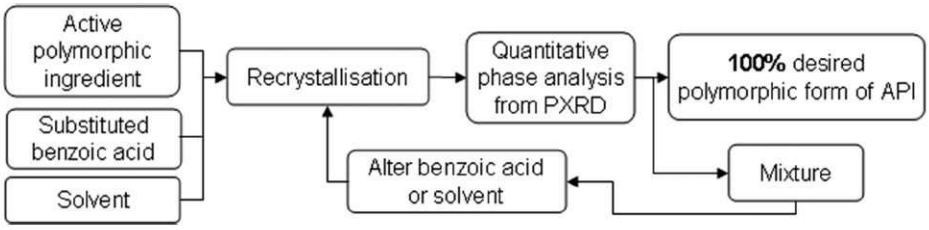

Scheme 4-2 *Methodology for templated selective crystallisation of paracetamol form II from multi-component solutions.*

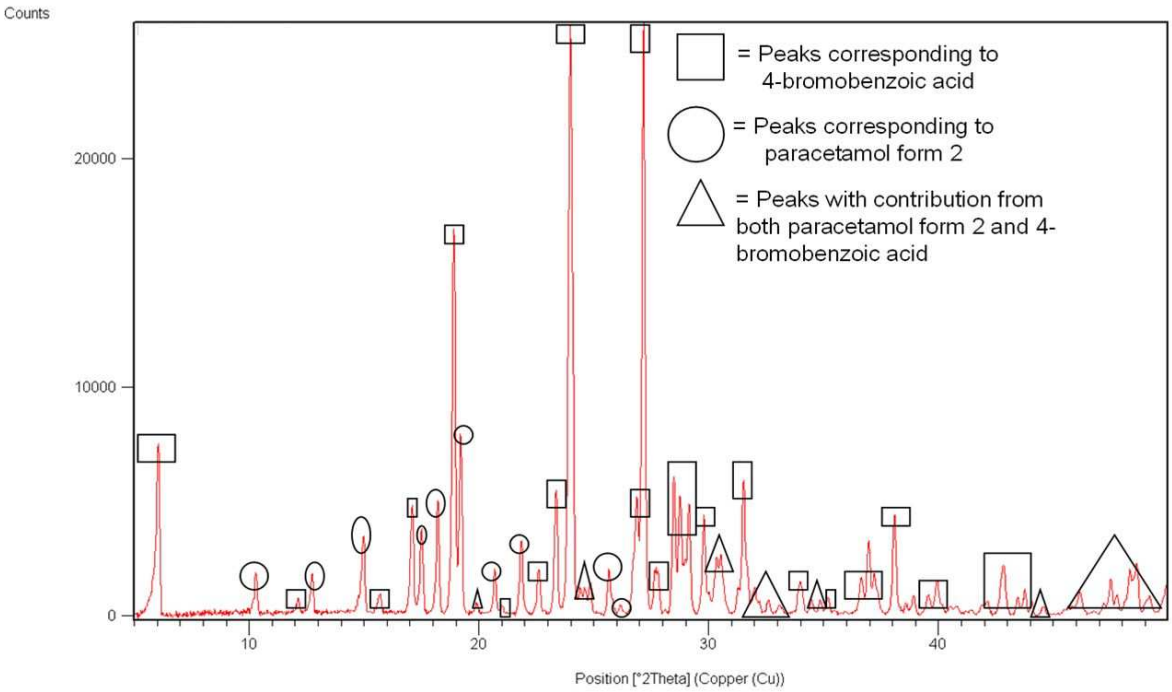

Figure 4.2 *PXRD of the paracetamol co-crystallisation with 4-bromobenzoic acid in methanol. All peaks correspond to either paracetamol form II or 4-bromobenzoic acid indicating that paracetamol form II is obtained in 100% yield.*

The molar ratio of the benzoic acid used in the multi-component crystallisations is also important to the yield of PA II obtained. Using the co-crystallisation with 4BRBA in MeOH as a model system, the quantity of BA required to produce 100% form II was tested. 100% PA II could be produced from a 2:1 molar ratio (PA:4BRBA); using a 4:1 ratio, however, resulted in a mixture of PA I and PA II, suggesting that high concentrations of the BA are

required to obtain 100% PA II. Similarly, 2:1 co-crystallisations with 4CLBA in MeOH also resulted in 100% PA II.

Table 4.2 *PXRD quantitative analysis of paracetamol polymorphs from 1:1 co-crystallisations with various benzoic acid derivatives in various solvents. PXRD patterns can be found in Appendices B4a-1 to B4a-10.*

Co-molecule	Solvent	Form produced	Comment
4BRBA	Methanol	100% Form II	Stable for >1 year
	Ethanol	Mixture	Some batches 100% II
	Acetone	Mixture	Converts to I with time
	Acetonitrile	100% Form II	
	Isopropanol	100% Form II	
4ClBA	Methanol	Majority Form II	Some batches 100% II
	Ethanol	Mixture	
	Acetone	100% Form II	
	Acetonitrile	Mixture	Some batches 100% I
	Isopropanol	100% Form II	
4FBA	Methanol	Mixture	Some batches 100% II
	Ethanol	Mixture	
	Acetone	100% Form II	
	Acetonitrile	Mixture	
	Isopropanol	100% Form II	
3BRBA	Methanol	100% Form I	
	Ethanol	100% Form I	
	Acetone	100% Form II	
	Acetonitrile	100% Form I	
	Isopropanol	Mixture	Converts to I with time
3ClBA	Methanol	100% Form I	
	Acetone	100% Form I	
3FBA	Acetone	100% Form I	
	Isopropanol	100% Form II	
2BRBA	Methanol	100% Form I	
	Ethanol	100% Form II	
	Acetone	Mixture	
2ClBA	Ethanol	100% Form II	
	Acetone	Mixture	
	Acetonitrile	100% Form I	
	Isopropanol	100% Form II	
2FBA	Methanol	100% Form I	
	Ethanol	Mixture	
BA	Methanol	Mixture	Majority Form I
	Ethanol	100% Form I	
	Acetone	100% Form I	
	Acetonitrile	100% Form I	
	Isopropanol	100% Form I	

The co-crystallisation route to producing PA II was found to be possible using co-molecules other than mono-substituted BAs. Tables 4.3 and 4.4 show a summary of other co-molecules that could be used to obtain paracetamol form II and the outcomes of the quantitative analysis of PA polymorphs from PXRD. The results again show that the polymorph obtained is very much dependent on the co-molecule and the solvent used, with methanol being the most reliable solvent in most cases.

Although very different molecules are used in these co-crystallisation experiments, the most common feature is the presence of a carboxylic acid group. As well as the mono-substituted BAs, four of the other co-molecules used (Table 4.3) contain carboxylic acid groups. This suggested the investigation of a "single component" crystallisation using a solvent containing a carboxylic acid group. By using excess quantities of acetic acid as a solvent for direct recrystallisation of dissolved PA I (i.e. with no co-molecule), large yields of PA II were obtained, although small quantities of PA I remained in the samples (Figure 4.3). The sensitivity of these crystallisations to the precise conditions is emphasised by the fact that in carrying out these experiments, crystallisation from supersaturated solutions of paracetamol in acetic acid - generated by heating and with a far lower excess of acetic acid - result instead in the production of pure form I, probably due to undissolved paracetamol form I seeding the solution.

Table 4.3 *PXRD quantitative analysis of paracetamol polymorphs from 1:1 co-crystallisations with various co-molecules containing carboxylic acid groups. Crystallisations were carried out at room temperature (RT) unless otherwise stated. PXRD patterns can be found in Appendices B4a-12 to B4a-15.*

Co-molecule	Solvent	Form produced	Comment
Nicotinic Acid	Methanol	Almost 100% Form II	Small amount of PA I
	Ethanol	Form I	
	Acetone	Form I	
	Acetonitrile	Form I	
	Isopropanol	Form I	
Fumaric Acid	Methanol	100% Form II	
	Ethanol	Mixture	
	Acetone	Mixture	
Succinic Acid	Methanol	100% Form II	
	Acetone	100% Form II	
Creatine	Methanol	100% Form II	
	Ethanol	100% Form II	
	Dichloromethane	Form I	Crystallised at 40°C*

***** Other temperatures were used but the products not analysed at the time of writing.

Table 4.4 *PXRD quantitative analysis of paracetamol polymorphs from 1:1 co-crystallisations with various co-molecules not containing carboxylic acid groups. Crystallisations were carried out at room temperature (RT) unless otherwise stated. PXRD patterns can be found in Appendices B4a-16 to B4a-24. In all cases other temperatures were studied but the products had not been analysed at the time of writing.*

Co-molecule	Solvent	Form produced	Comment
Taurine	Water	100% Form II	30°C
	Water	Form I	50°
Creatinine	Methanol	Mixture	50°
	Ethanol	Form I	50°
	Acetone	Form I	50°
	Methanol/Acetonitrile	100% Form II	50°
Erythritol	Methanol/Ethanol	100% Form II	40°C
	Methanol/Acetone	Form I	30°C
	Methanol/Acetonitrile	100% Form II	30°C
Resorcinol	Methanol	Form I	
	Acetonitrile	Mixture	Majority form I
Urea	Methanol	Mixture	
	Ethanol	Form I	
Benzamide	Methanol	100% Form II	
	Ethanol	Mixture	
Pyrazole	Methanol	Form I	RT or 40°C
	Methanol	100% Form II	50°
	Acetone	Form I	RT or 50°C
3,5-dimethylpyrazole	Methanol	Mixture	50°C
	Acetone	Mixture	
Pyrazine	Methanol	Form I	RT or 40°C
	Methanol	100% Form II	50°C
	Acetone	Form I	50°C

Although the use of co-molecules containing carboxylic acid groups in multi-component crystallisations with paracetamol has been demonstrated as a general route to PA II, it was found not to be a universal rule. It has been noted above that it was not possible to produce PA II using BA and some 2- and 3- substituted BAs. In addition, co-crystallisations of PA I with oxalic acid or malonic acid resulted in neither molecular complex formation nor generation of PA II. Co-crystallisation with maleic acid resulted in a mixture of PA I, maleic acid and a 1:1 PA: maleic acid molecular complex (see Chapter 8). Similarly, co-crystallisation with citraconic acid also resulted in formation of a 1:1 molecular complex with PA - isostructural to that formed with maleic acid (also Chapter 8).

As mentioned above, co-molecules that do not contain carboxylic acid groups were also used in the PA multi-component crystallisation attempts. Three nitrogen-heterocycle co-molecules were found to produce PA II in these experiments: pyrazole, 3,5-dimethylpyrazole and pyrazine (Table 4.4).

The use of co-grinding to produce PA II was also investigated. PA I was ground with succinic acid, 4-fluorobenzoic acid or 4-bromobenzoic acid both in a solvent-free environment and in the presence of a "catalytic" amount of solvent. PXRD analysis of the resulting samples indicated that no PA II had been formed and only PA I and the co-molecule were found to be present.

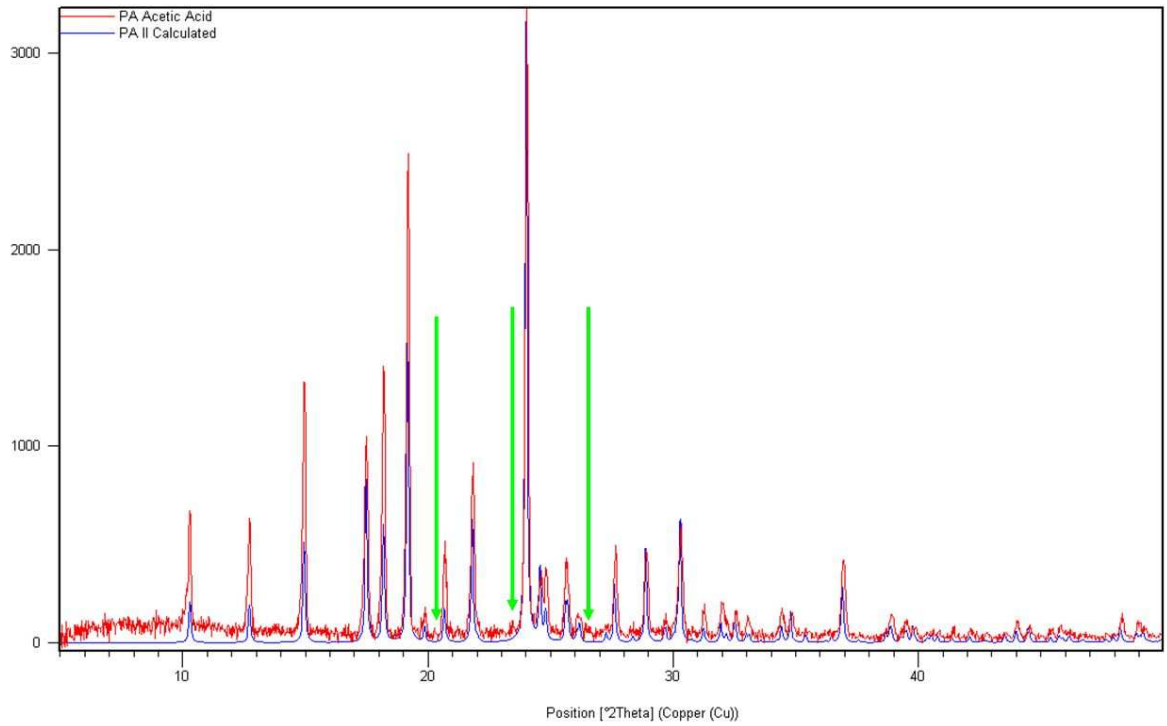

Figure 4.3 *PXRD analysis of the recrystallisation of paracetamol from excess acetic acid (red). The calculated PXRD pattern for PA II is shown in blue. The yield of PA II is close to 100% although trace quantities of PA I are present (small peaks indicated by green arrows). A large version of this PXRD pattern can be found in Appendix B4a-11.*

Samples in which 100% PA II was formed were found to be stable for periods of greater than three years. The critical importance of generating form II at 100% yield is emphasised by the fact that the presence of small quantities of form I in the final product encourages the conversion of the metastable form II into the more stable form I over a

period of weeks to months. This can be seen from PXRD analysis as a significant increase in the relative intensity of the PA I peaks with respect to the PA II peaks (Figure 4.4).

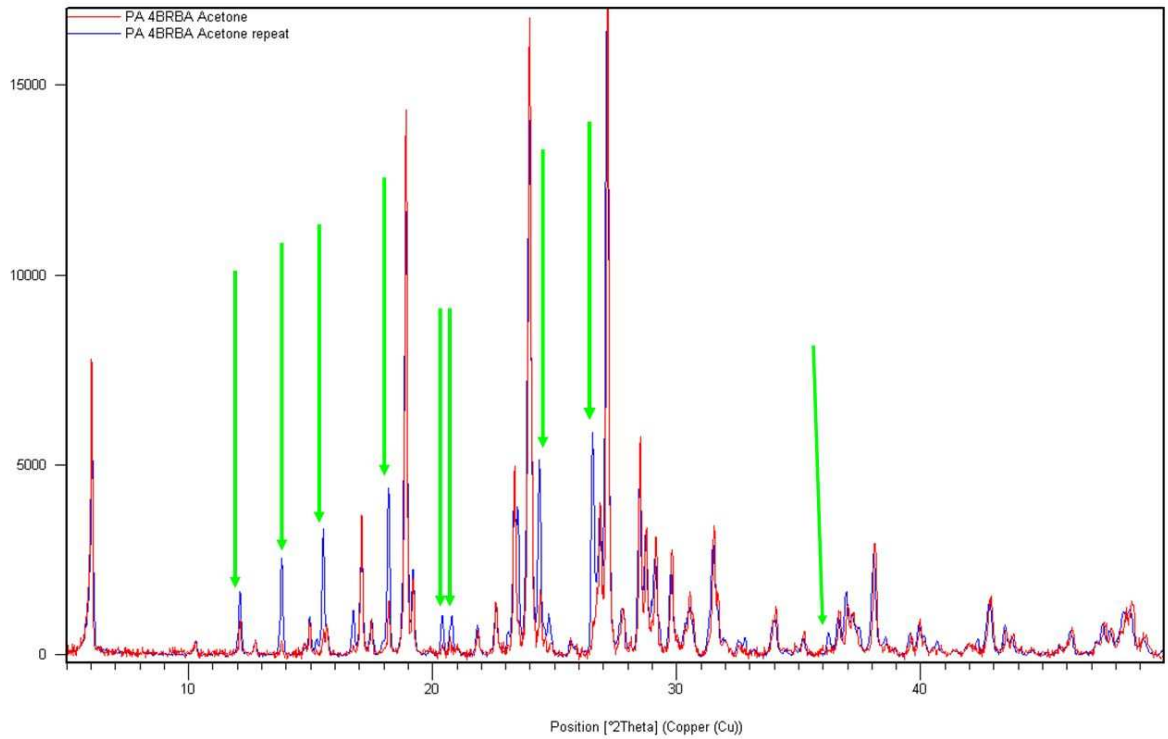

Figure 4.4 *PXRD analysis of the products from a paracetamol co-crystallisation with 4-bromobenzoic acid from acetone. Initial analysis (red) shows a mixture of PA I, PA II and 4BRBA. Analysis of the same sample (same capillary) one month later (blue) shows a significant increase in the intensity of the PA I peaks relative to the PA II peaks, reflecting the conversion from metastable form II to the more stable form I, which occurs in the presence of form I. PA I peaks which have increased significantly in intensity are highlighted by green arrows.*

4.2.3 Paracetamol Form II: Scale up for Continuous Crystallisation in an Oscillatory Baffled Crystalliser

Initial attempts were made to scale up the production of PA II into a non-evaporative environment within the COBC using the co-crystallisation method presented in this chapter. To this end, attempts were made to convert the evaporative co-crystallisation method employed in producing PA II to a cooling crystallisation method. 1:1 molar ratio

solutions of paracetamol and the co-molecule, at various degrees of supersaturation, were therefore generated through heating and the solutions cooled to either 4°C or ambient temperature to induce crystallisation. In some cases 2:1 molar ratios were also trialled. A summary of the conditions studied is presented in Table 4.5. Cooling crystallisations were also carried out using acetic acid as the solvent with no co-molecule present.

Table 4.5 *Summary of trial conditions for cooling co-crystallisations to produce paracetamol form II.*

Co-molecule	**Molar Ratios (Paracetamol:Co-Molecule)**	**Solvents Used**
4BRBA	1:1	MeOH
4CLBA	1:1	MeOH, EtOH
Succinic Acid	1:1, 2:1	EtOH, IPA, EtOH/Water (50/50, V/V)
Fumaric Acid	1:1, 2:1	MeOH, EtOH, ACE
Urea	1:1, 2:1	EtOH, IPA
N/A	N/A	Acetic Acid

Under the conditions studied, only PA I could be obtained. Using 4BRBA, 4CLBA or succinic acid as the co-molecule resulted mainly in recrystallisation of the co-molecule with the PA still in solution due to the large difference in solubility between the two in the solvents used. Given that these co-molecules have proven consistent in yielding 100% PA II in the evaporation experiments, a more thorough investigation of the conditions may be appropriate.

4.2.4 Variable Temperature Neutron Diffraction Study of Paracetamol Form II

As stated above, large single crystals (>1 mm^3) of PA II were grown using the co-crystallisation method described. Large crystals, grown by co-crystallising with 4BRBA in methanol, were suitable for single crystal neutron diffraction. A variable temperature study was carried out in order to investigate the evolution of the hydrogen parameters as

a function of temperature. Full refinement details can be found in (Appendix A4, Table A-4a).

As unit cell parameters cannot be calculated accurately from Laue diffraction, unit cell parameters were fixed to those observed in X-ray structure determinations at the corresponding temperatures. Unit cell parameters for the 100K neutron data were taken from the 100K single crystal X-ray re-determination carried out as part of this work. Unit cell parameters for the 200K and 300K neutron data were taken from X-ray diffraction data found in the CSD at the corresponding temperatures[205]. Structure determination using X-rays at 30K has yet to be carried out; the unit cell parameters were therefore extrapolated from the difference between 200K and 100K unit cell parameters and may not be accurate.

Comparison between the parameters obtained from the X-ray and neutron diffraction data for the hydrogen bonds found in PA II (Table 4.6) shows good correlation between the D···A distances and D-H···A angles at all temperatures, with both sets of data showing a gradual increase in D···A distances with increasing temperature. As expected, a shortening of the D-H distances (and therefore lengthening of H···A distances) is observed from the X-ray data when compared with the neutron values. The X-ray data show very little change in D-H and H···A values over the temperature range, however, the neutron data shows this to be inaccurate with the H···A distance generally showing a small increase with increasing temperature. A slight decrease in the D-H distances is seen between 200K and 300K, likely due to the decreased interaction of the hydrogen with the acceptor oxygen, which is supported by the increase in H···A distances.

The methyl group hydrogen atoms show a significant increase in librational motion with increasing temperature (Figure 4.5), similar to that seen in variable temperature neutron diffraction studies of PA I[199].

Table 4.6 *Hydrogen bond distances and angles for paracetamol form II from variable temperature X-ray and neutron diffraction data. Note that there is currently no X-ray diffraction data at 30K for comparison to the neutron data.*

Data / Temp. (K)	H-Bond	D-H	H···A	D···A	∠ D-H···A
Neutron 30K	O-H···O	0.987(2)	1.725(2)	2.706(2)	171.9(2)
	N-H···O	1.022(2)	1.940(2)	2.932(2)	162.9(2)
X-ray 100K	O-H···O	0.87(3)	1.85(3)	2.709(1)	171(2)
	N-H···O	0.88(2)	2.09(2)	2.939(2)	162(2)
Neutron 100K	O-H···O	0.987(2)	1.728(2)	2.708(2)	171.5 (2)
	N-H···O	1.022(2)	1.948(2)	2.941(2)	162.9(1)
X-ray 200K[205]	O-H···O	0.88(2)	1.85(2)	2.717(2)	170(2)
	N-H···O	0.88(2)	2.09(2)	2.955(3)	166(2)
Neutron 200K	O-H···O	0.987(3)	1.739(3)	2.719(3)	171.5(3)
	N-H···O	1.022(2)	1.962(3)	2.956(2)	163.2(3)
X-ray 300K[205]	O-H···O	0.89(3)	1.84(3)	2.725(2)	173(3)
	N-H···O	0.88(4)	2.12(4)	2.971(3)	165(3)
Neutron 300K	O-H···O	0.981(4)	1.751(4)	2.726(3)	171.8(4)
	N-H···O	1.015(3)	1.989(3)	2.976(3)	163.7(3)

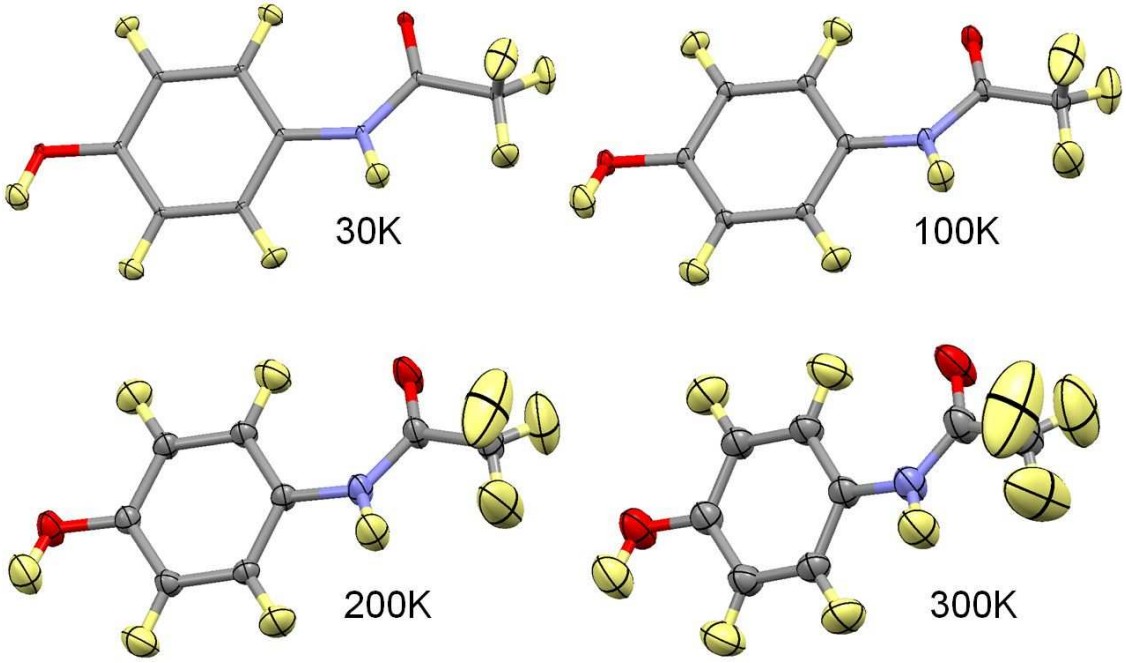

Figure 4.5 *The evolution of the anisotropic displacement parameters of paracetamol form II at 30K, 100K, 200K and 300K as determined from single crystal neutron diffraction. A significant increase in the libration of the methyl group is observed with increasing temperature with significant residual motion seen at 30K.*

4.3 Discussion

4.3.1 Paracetamol Form II

A facile and reliable new route to the production of the pharmaceutically relevant PA II has been demonstrated using co-crystallisation methodology. By introducing a benign second component into the solution environment, PA II can be selectively grown in 100% yields. The technique not only offers access to larger quantities of PA II than were previously possible (at the 100 mg level to date), but also large single crystals which have enabled a neutron diffraction study of PA II to be carried out. The simplicity and flexibility of this solution based crystallisation route may have the potential for scale up to a bulk process although initial attempts to convert this evaporation crystallisation method to a cooling method have to date been unsuccessful.

Co-molecule and Solvent Dependency

The co-crystallisation technique employed has been shown to be co-molecule and solvent dependent with regards to the yield of PA II obtained. The substitution position of the BA clearly had a significant effect; 4-substituted BAs were the most reliable co-molecules of the mono-substituted BAs used, with 100% yields of PA II obtained consistently. 4BRBA was found to be particularly reliable in producing 100% PA II with large single crystals. It is unclear why the 2- and 3-substituted BAs were less reliable. It is also interesting that non-substituted BA worked poorly with only small amounts of PA II produced when co-crystallised from methanol.

Although much of this study was focused on the use of mono-substituted BAs, a number of other structure-directing co-molecules were found. Four others contain a carboxylic acid group which in addition to the BAs suggests a relationship may be present in terms of the mechanism that leads to the formation of PA II. However, a number of co-molecules that do not contain carboxylic acid groups were also found to facilitate the crystallisation of PA II in 100% yields and it is unclear what relationship, if any, they have to the carboxylic acid containing molecules. Three of these molecules - pyrazole, 3,5-dimethylpyrazole and pyrazine - are NHCs which have also been shown to act as structure directing co-molecules for elusive polymorphs of PX (PX III and PX IV – see section 4.5) which again may suggest a related mechanism may be responsible. Indazole, another

NHC, was also found to direct the formation of a previously unknown phase of PX although co-crystallisation experiments of indazole with PA have yet to be carried out.

The high selectivity achieved through the use of co-molecules containing carboxylic acid groups led to the investigation of acetic acid as a solvent for direct recrystallisation of PA I to form PA II. Although close to 100% yields were obtained from a solution of excess acetic acid, some PA I remained in the samples. As it has been demonstrated that the presence of form I facilitates the PA II→PA I solid-solid conversion, 100% yields of PA II are vital if the latter is to be stable and optimising of this method is therefore required.

The co-crystallisation experiments indicate methanol is the most reliable solvent for production of PA II, with 100% yields possible using all three 4-substituted BAs studied (and various other co-molecules). Varying yields of PA II could also be produced from methanol solution using co-molecules which otherwise produce only form I (nicotinic acid and benzoic acid).

Neutron Diffraction Study of Paracetamol form II

The large single crystals of PA II obtained using the co-crystallisation method enabled the first neutron diffraction study of this material to be carried out. The improvement in detail of the hydrogen bonds is illustrated by the increasing H···A distances from 200 K to 300 K which cannot be seen from X-ray diffraction data. The data also shows similar libration of the methyl group to that seen in form I. The data may have useful future applications in lattice energy calculations of PA II.

4.4 Introduction to Known Piroxicam Crystal Forms

Piroxicam (PX) is a non-steroidal anti-inflammatory drug that has been studied extensively in the solid state[206-210], but the literature on PX polymorphism is largely conflicting in terms of the number and nomenclature of polymorphs. There are currently three known polymorphs of piroxicam[209], although the crystal structure of form III has yet to be determined and has only been characterised by powder XRD and thermal analysis[208, 209]. Forms I and II of PX are easily obtained through simply varying the solvent used or the temperature of crystallisation[208]. Crystallisation of form III has previously involved more

complex routes, including cryo-grinding to obtain an amorphous phase followed by heating[209] or spraying a saturated ethanol solution on dry ice[208]. Both of these methods result in powder products, unsuitable for structure determination using single crystal X-ray diffraction, and thus, this phase has to date only been characterised by PXRD and DSC. In the three known polymorphs of PX, it is present as the non-ionised tautomer only, although a zwitterionic tautomer has been observed in the solid state[27, 211] (Scheme 4-3). A monohydrate of PX is known where PX is in the zwitterionic form[211], as well as several other multi-component complexes where PX is present as the zwitterionic tautomer[27]. Multi-component complexes where PX is present as the non-ionised tautomer are also known[27]. The tautomer obtained in these complexes can be inferred visually from the yellow colour of the zwitterionic complexes and the colourless nature of those that are non-ionised. PX is poorly water soluble which affects its bioavailability[212]; new crystalline phases of PX with improved solubility may therefore be desirable.

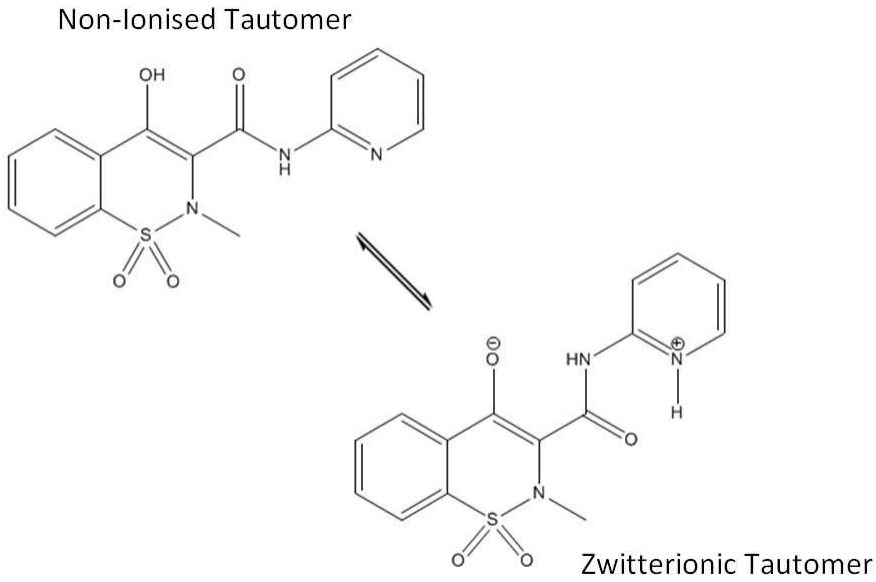

Scheme 4-3 *The two known tautomers of piroxicam.*

4.5 Multi-Component Crystallisation Routes to Piroxicam Form III, Form IV and a Methanol Solvate: Co-Crystallisation with Nitrogen-Heterocycles

4.5.1 Crystallisation Conditions

A series of co-crystallisations of PX were carried out with nitrogen-heterocycles (NHCs) using the procedure outlined in Chapter 3. Table 4.7 shows a summary of the co-

Table 4.7 *Experimental conditions for co-crystallisations of piroxicam with nitrogen-heterocycles. Co-molecules marked with * resulted in formation of new or elusive phases of piroxicam which do not incorporate the co-molecule. Co-molecules marked with # resulted in molecular complexes (discussed in Chapter 6). The remaining co-molecules resulted in neither a new phase of piroxicam nor a molecular complex. Note: The formation of molecular complexes and new phases did not occur under all the conditions investigated.*

Co-Molecule	**Quantity of Co-molecule**	**Solvent(s)**	**Temp(s) (°C)**
Pyrazole*	Excess (2:1 and 4:1 mass ratios)	MeOH, ACN	RT, 40, 50
3,5-dimethylpyrazole*	Excess (2:1 mass ratio)	MeOH, ACN	RT, 40, 50
Pyrazine*#	1:1 molar, Excess (2:1 molar)	ACN	RT, 40, 50
Indazole*	1:1 molar	ACN, MeOH, MeOH/ACN	RT, 40, 50
Imidazole#	1:1 molar	MeOH,ACN	RT, 40, 50
2-methylimidazole#	1:1 molar	ACN	RT, 40, 50
Benzimidazole#	1:1 molar	MeOH/ACN	RT, 40, 50
Benzotriazole#	1:1 molar	ACN	RT, 40, 50
1,2,4-triazole#	Excess (2:1 mass ratio)	ACN	RT, 40, 50
2,2-bipyridine	1:1 molar	ACN, MeOH	RT, 40, 50
4,4-bipyridine	1:1 molar	MeOH, ACN	RT, 40, 50
s-triazine	Excess (2:1 mass ratio)	ACN	RT, 30, 40 50
Quinoxaline	Excess (2: 1 mass ratio)	MeOH, ACN	RT, 40, 50
1,2,3-triazole (l)	Excess (used as solvent)	N/A	RT, 6
Pyridazine (l)	Excess (used as solvent)	N/A	RT, 40

RT = Room Temperature, l = liquid at RT

molecules used in these experiments. Six of the NHC co-molecules used resulted in molecular complex formation (marked with # in Table 4.7 and discussed in detail in Chapter 6). Four of the co-molecules resulted in the formation of a new or previously elusive PX phase not incorporating the co-molecule (Scheme 4-4; marked with * in Table 4.7); the details of the latter are discussed below.

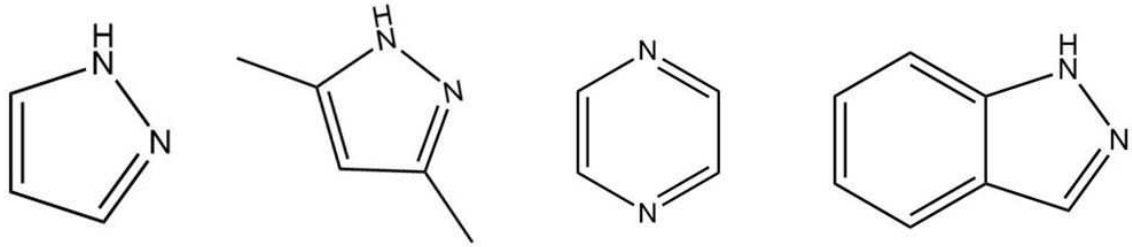

Scheme 4-4 *The molecular structures of the NHCs which were used to obtain new or previously unknown phases of piroxicam.*

4.5.2 Co-crystallisation Routes to Piroxicam Form III, Form IV and a Piroxicam Methanol Solvate

In initial experiments aimed at molecular complex formation, unit cell screening of the resultant crystals found that co-crystallisation of PX with pyrazole from ACN at 50°C resulted in the formation of PX form III (PX III). Large (~0.4 mm^3) single crystals of PX III were formed on the side of the crystallisation vessel, along with significant quantities of PX monohydrate and PX II. Full structure determination was carried out (see Section 4.4.3.1 below) and the calculated PXRD pattern for this structure was then compared to the experimental PXRD pattern from previous studies[208, 209] to verify that it was indeed form III (Figure 4.6). An excess of pyrazole was used in the co-crystallisation experiments as pyrazole has a relatively low melting point (69°C) and previous work using 1:1 ratios had indicated that pyrazole evaporates from the solution - particularly at high temperature. Unit cell screens of repeat co-crystallisations showed that crystallisation of form III could be reproduced, albeit still in relatively small quantities. In some cases it was also found to crystallise at 40°C although it has not been observed to crystallise at room temperature. Subsequently, co-crystallisation experiments were carried out using excess 3,5-dimethylpyrazole to assess the transferability of the method between similar co-molecules. Co-crystallisation with excess 3,5-dimethylpyrazole (1:2 mass ratio) using ACN or MeOH as the solvent at 50°C resulted in the formation of PX III in similar quantities to that in the initial preparation. PX III was not observed to crystallise from MeOH when pyrazole was used as the co-molecule.

In the majority of cases, PXRD was not found to be a useful method of analysis in this case as PX III often could not be detected despite being confirmed by unit cell screens (Appendices B4b-1 to B4b-3). This may be due to the low quantities of PX III present

relative to those of the other components of the phase mixture (PX I and/or II and/or the monohydrate) or possibly due to a PX III→PX I phase transformation induced by the grinding procedure used in preparation for PXRD analysis. PXRD analysis also showed that despite the high concentrations of co-molecule, the majority of both pyrazole and 3,5-dimethylpyrazole were not present in the final product from the 50°C crystallisations. This suggests that these components evaporated from the solution at 50°C although they may have been crystallised on the lid of the crystallisation vessel. This was particularly unexpected in the case of 3,5-dimethylpyrazole given its melting point is approximately 105°C, although the melting point and sublimation point are not necessarily related.

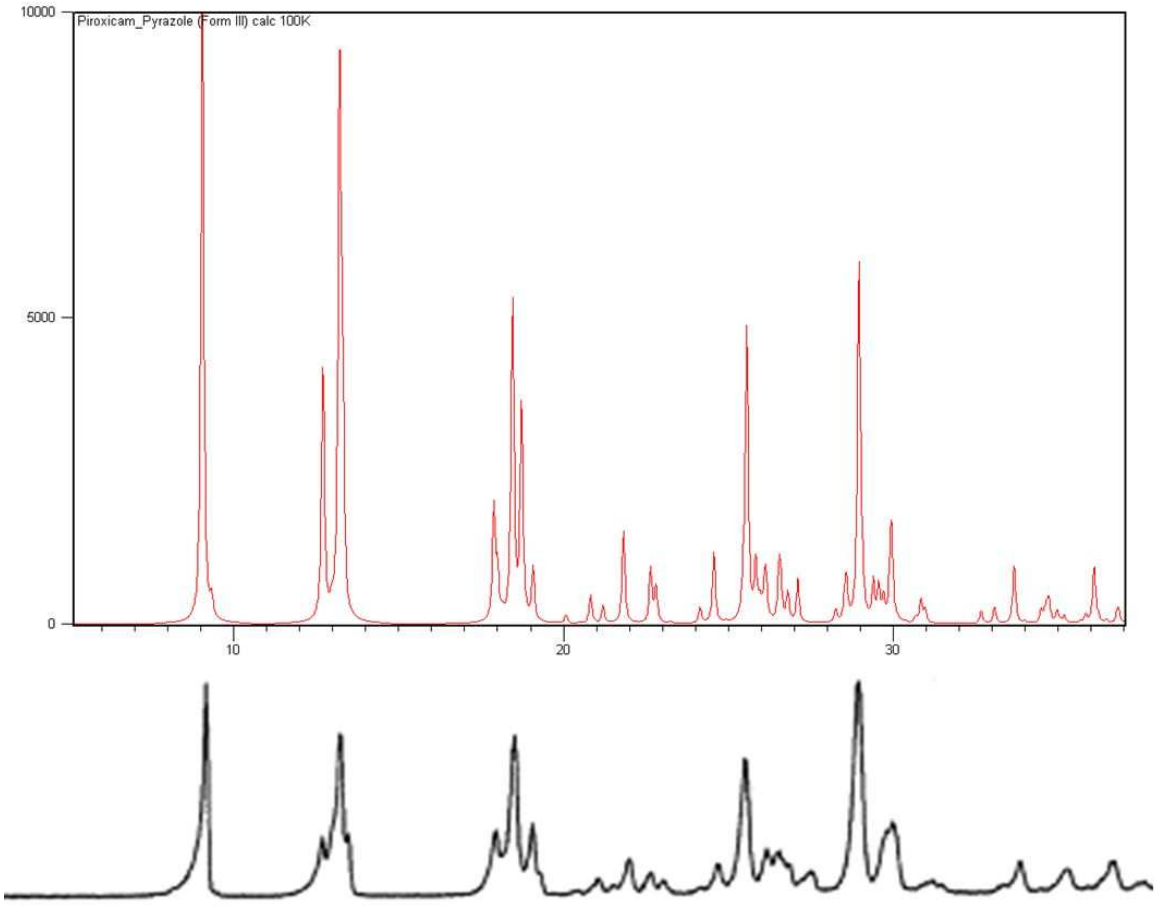

Figure 4.6 *The calculated PXRD pattern for piroxicam form III (red) and the experimental PXRD pattern from a previous study*[208] *(bottom).*

Co-crystallisation of PX with pyrazine as the benign co-component (2:1 mass ratio, pyrazine:PX) resulted in a similar phenomenon: using acetonitrile as the solvent and a crystallisation temperature of 50°C (also at 40°C although less reliably), a new form of

piroxicam is templated – designated form IV (PX IV). The crystal structure of PX IV is unique as it is the only known polymorph where piroxicam molecules are present in both the non-ionised and zwitterionic tautomers; furthermore, this has a surprisingly large asymmetric unit, with four neutral and one zwitterionic molecule contained within it (discussed in detail in section 4.4.3.2). The small needle-shaped crystals of PX IV could be distinguished from form I, II and III (all colourless) by the yellow colouring of the crystals – which is also seen in molecular complexes of PX containing the zwitterionic tautomer[27]. Relatively high yields of form IV were obtained (Appendix B4b-4), although repeat experiments were unpredictable; a previously unknown PX : pyrazine molecular complex occasionally formed (see Chapter 6) and/or PX form I, form II or PX monohydrate. This indicates the subtle balance that can exist in product formation in these multi-component crystallisation experiments. A combination of unit cell screening and visual analysis indicated that experiments using 1:1 molar ratios of the co-molecule or crystallisation at lower temperatures resulted in formation of PX I or II only (Appendix B4b-5).

Crystallisation of PX with indazole was carried out in a 1:1 molar ratio due to indazole having a significantly higher melting point than pyrazole and pyrazine (approx. 148°C), making it unlikely to evaporate during the crystallisation process. When crystallised from MeOH at 60°C a new PX : MeOH solvate was formed. As in PX IV, the crystal structure was found to contain a mixture of both tautomers, zwitterionic and neutral (see section 4.4.3.3). PXRD of the products of the co-crystallisation experiment showed that the PX : MeOH solvate was crystallised concomitantly with PX I (PXRD Appendix B4b-6). The solvate was not observed to crystallise in experiments carried out without the co-molecule under the same conditions (PXRD Appendix B4b-7).

4.5.3 Crystal Structures of the New and Elusive Piroxicam Crystalline Phases

The crystal structures of the two new polymorphs of PX and the methanol solvate are described below. Crystallographic data and full refinement details can be found in (Appendix A4, Table A-4b).

4.5.3.1 Piroxicam Form III (PX III)

The crystal structure of PX form III consists of a single molecule in the asymmetric unit which forms the same PX dimers that are found in PX form I[206]. These dimers are formed via NH···O hydrogen bonds between the amide NH and the sulfonyl oxygen atoms (Figure 4.7). The NH···O hydrogen bond length in this dimer is similar to that found in form I, although a slightly longer donor-acceptor distance is observed despite the structure being determined at lower temperature (100K c.f. 300K for form I) (Table 4.8). The structure of form III is also layered in a similar fashion to form I (Figure 4.8a), with the methyl and sulfonyl groups bridging between the layers. The differences between form I and form III are seen in the extended packing and the weaker hydrogen bonds. PX molecules in form III link to PX molecules above, via CH···O hydrogen bonds between the pyridine aromatic CH groups and the second sulfonyl oxygen atom (Figure 4.8b). The second sulfonyl oxygen in PX I forms hydrogen bonds to the benzene CH group of a PX molecule above (Figure 4.8c), resulting in very different relative positions of PX molecules in different layers (Figure 4.8d).

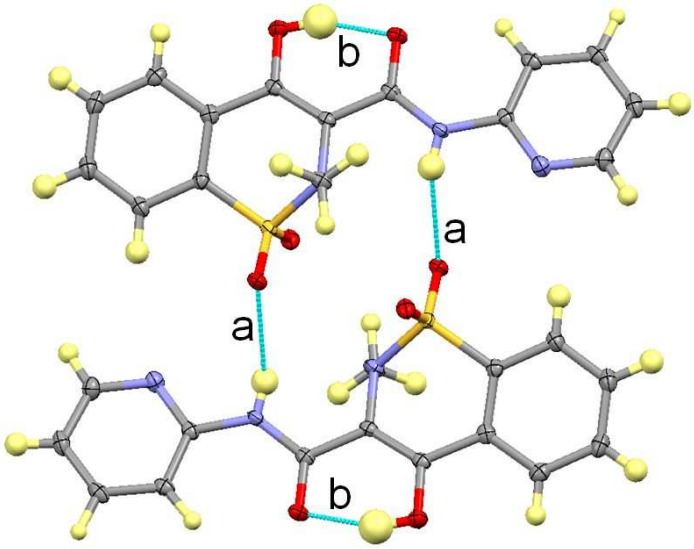

Figure 4.7 *The hydrogen bonded PX dimers formed in piroxicam form III.*

Table 4.8 *Hydrogen bond distances and angles in the piroxicam dimers in PX form I[206] and form III (refer to Figure 4.7 for key).*

Polymorph	Temp (K)	H-Bond	D-H (Å)	H···A (Å)	D···A (Å)	∠D-H···A (°)
III	100	a	0.80(2)	2.41(2)	3.059(2)	139(2)
		b	0.89(3)	1.70(3)	2.544(2)	157(2)
I[206]	300	a	0.84(3)	2.44(3)	3.053(3)	130(3)
		b	0.81(3)	1.79(3)	2.561(3)	156(4)

A second CH group of the pyridine ring forms CH···O hydrogen bonds with the hydroxyl oxygen of a PX molecule below (C···O = 3.384(2) Å) (Figure 4.9). Molecules above and below each other are further linked by weak hydrogen bonds between the methyl CH groups and the amide carbonyl oxygen (C···O = 3.363(2) Å) as well as well as π···π interactions between the amide carbonyl double bonds, with approximately 3.049 Å between the centroids of the π bonds (Figure 4.10).

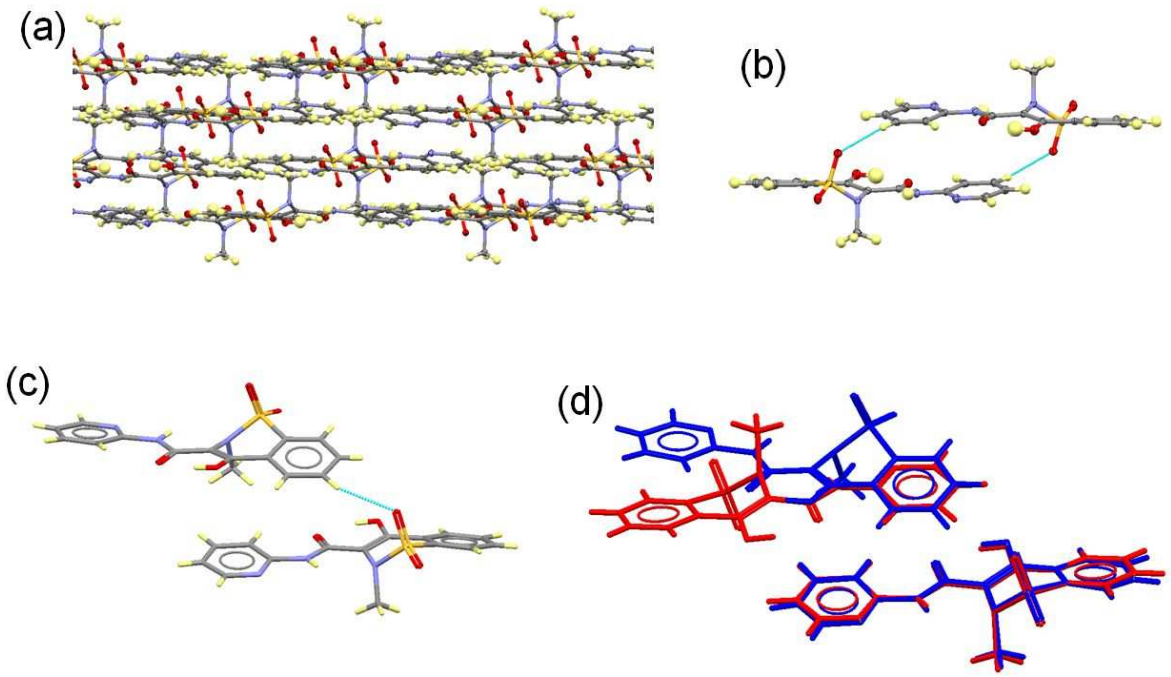

Figure 4.8 *Crystal packing in piroxicam form III. (a) The layered arrangement of molecules. (b) CH···O hydrogen bonds between a pyridine CH and the sulfonyl O of PX molecules above and below each other. (c) The similar CH···O hydrogen bonds in PX form I, where the sulfonyl oxygen instead forms hydrogen bonds with the benzene CH of the PX molecule above. (d) An overlay of the crystal structures of PX I and III, showing the difference in the relative arrangement of the PX molecules above each other.*

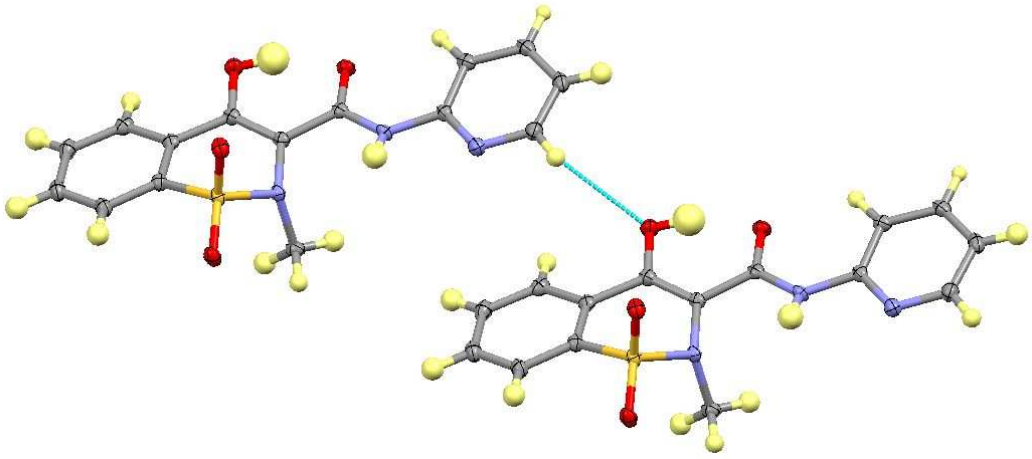

Figure 4.9 *CH···O interactions between a pyridine CH group and the hydroxyl oxygen in piroxicam form III.*

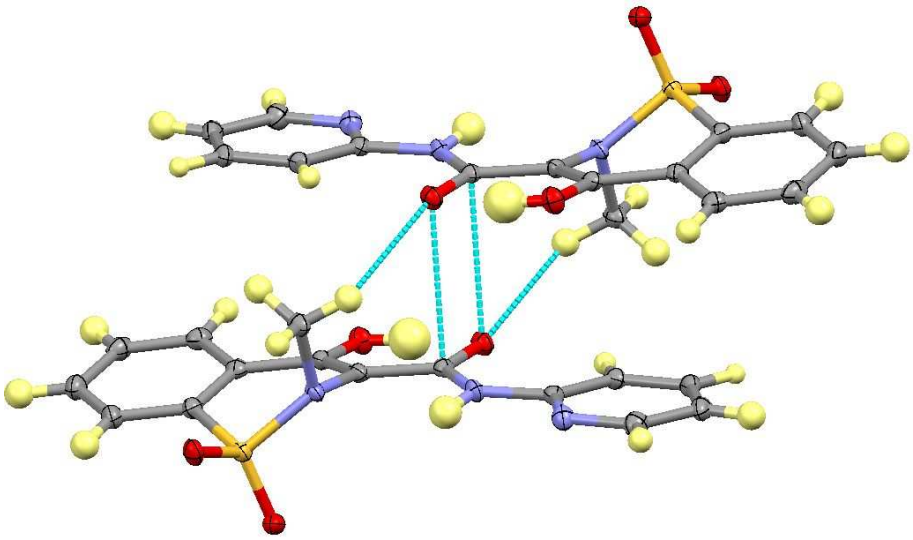

Figure 4.10 *CH···O and π···π interactions involving the amide oxygen in piroxicam form III.*

4.5.3.2 Piroxicam Form IV (PX IV)

As noted above, piroxicam form IV features five molecules in the asymmetric unit and is unusual in that four of the molecules are present as the non-ionised tautomer (PXN) and the other as the zwitterionic tautomer (PXZ). As before, in addition to the different distribution of hydrogen atoms within the tautomers, there is a substantial conformational difference between the neutral and zwitterionic forms, offering unambiguous conclusion to be drawn regarding the tautomers present from the X-ray data. The PXN molecules dimerise with non-equivalent PXN molecules through two NH···N hydrogen bonds (Figure 4.11), with two symmetry independent dimers formed in this way. The hydrogen bonding in this dimer is unique from that seen in any of the other

three polymorphs of PX. The NH···N hydrogen bonds in one dimer are slightly stronger than in the other, with the PXN molecules in the weaker dimer possessing stronger intramolecular OH···O hydrogen bonds (Table 4.9).

Equivalent PXZ molecules also dimerise, although the presence of the different tautomer results in a completely different type of dimer to that formed by the PXN molecules. The dimer is formed by two moderately strong charge-assisted bifurcated DHAA N^{+}-H···O hydrogen bonds between the protonated pyridinal nitrogen and the amide carbonyl oxygen (also Figure 4.11). This type of dimer is formed by PXZ molecules in all previously reported complexes containing PXZ[27, 211].

The PXZ dimers are linked to PXN molecules through a number of weak CH···O hydrogen bonds (Figure 4.12). Pyridine CH groups of PXN molecules form charge assisted hydrogen bonds to the enolate oxygen of the PXZ molecules (C···O = 3.440 (7)Å) (Figure 4.12a). Benzene and pyridine CH groups of PXZ molecules also form hydrogen bonds to the sulfonyl oxygen atoms of PXN molecules (C···O = 3.445(7) Å and 3.398(9) Å respectively) (also Figure 4.12a). Similar hydrogen bonds are formed from the benzene and pyridine CH groups of PXN molecules to the sulfonyl oxygen atoms of PXZ molecules (C···O = 3.480(8) Å and 3.264(8) Å) (Figure 4.12b).

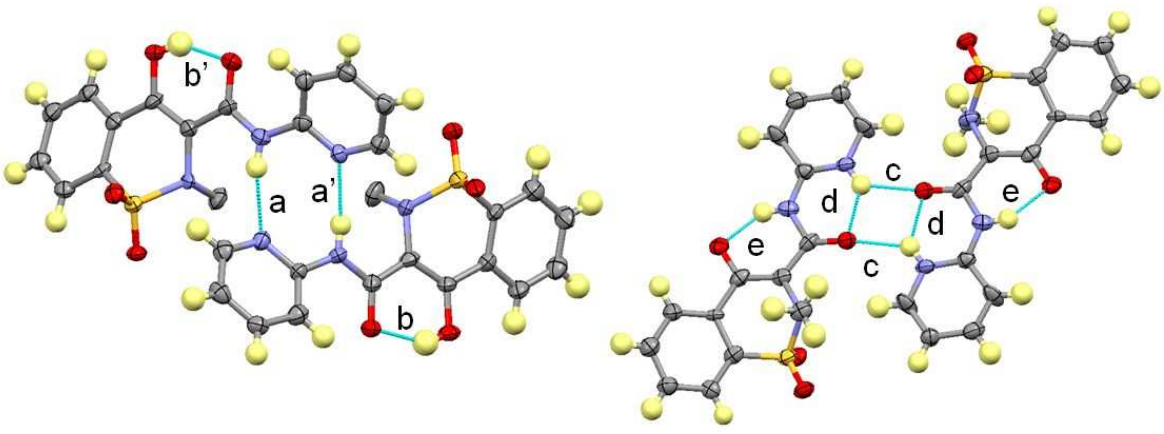

Figure 4.11 *The dimers formed in piroxicam form IV. Non-ionised molecules dimerise through NH···N hydrogen bonds (LHS - methyl hydrogen atoms omitted), whilst the zwitterionic molecules dimerise via charge-assisted bifurcated DHAA N^{+}- H···O hydrogen bonds (RHS).*

Table 4.9 *Hydrogen bond distances and angles in piroxicam form IV (refer to Figure 4.11 for key). Note that the numbers 1 and 2 refer to the symmetry independent dimers of PXN molecules. Hydrogen atoms were placed on calculated positions due to the poor quality of the data (see Appendix A4, Table A-4b).*

H-Bond	D-H (Å)	H···A (Å)	D···A (Å)	∠D-H···A (°)
a1	0.86	2.16	2.934(7)	149
a1’	0.86	2.14	2.933(8)	153
a2	0.86	2.18	2.985(7)	155
a2’	0.86	2.14	2.953(7)	158
b1	0.82	1.79	2.518(7)	148
b1’	0.82	1.81	2.531(6)	146
b2	0.82	1.78	2.509(8)	148
b2’	0.82	1.77	2.498(6)	147
c	0.86	2.25	2.930(7)	136
d	0.86	1.99	2.638(7)	131
e	0.86	1.80	2.533(7)	141

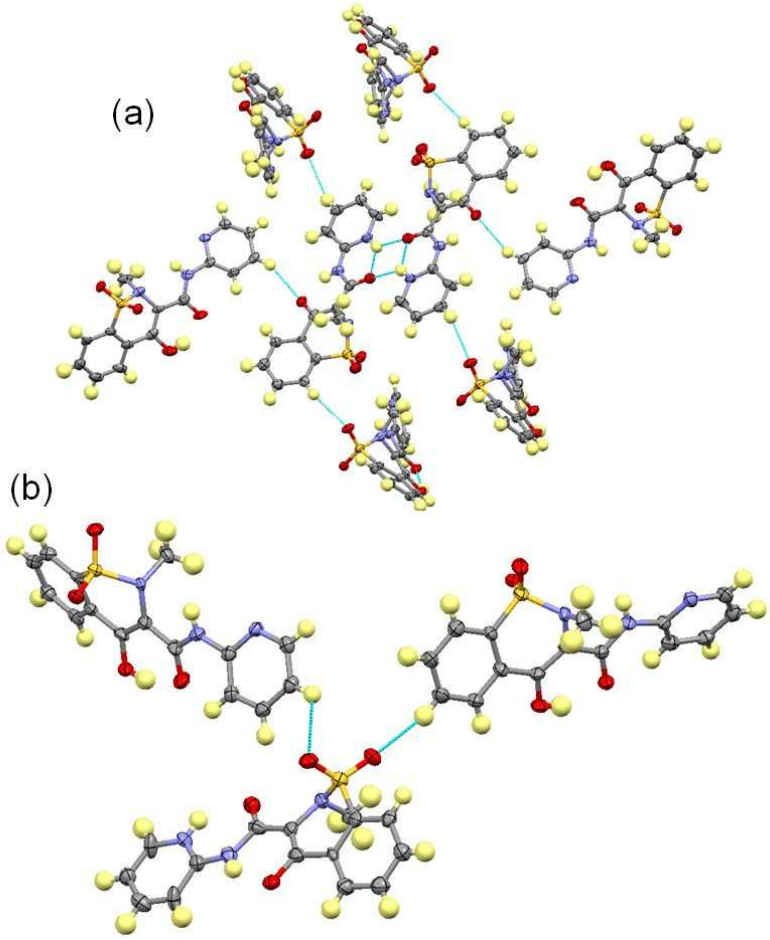

Figure 4.12 *Weak CH···O hydrogen bonds linking PXZ dimers to PXN molecules in piroxicam form IV. (a) CH···O hydrogen bonds from the PXZ pyridine and benzene ring CH groups to the PXN sulfonyl oxygen atoms and from the PXN pyridine ring Ch group to the PXZ enolate oxygen. (b) CH···O hydrogen bonds involving the PXZ sulfonyl oxygen atoms.*

The pairs of PXN molecules in both of the symmetry independent PXN dimers do not lie co-planar and these dimers are linked to each other through further moderate to weak strength CH···O hydrogen bonds (Figure 4.13) between benzene CH groups and sulfonyl oxygen atoms (C···O = 3.079(9) Å, 3.218(9) and 3.112(9) Å). The staggered nature of the dimers results in a non-layered structure unlike PX I and PX II. Further CH···O hydrogen bonds between PXN molecules are present involving the methyl group and hydroxyl oxygen groups (C···O = 3.266(7) Å) and π···π interactions are also present between benzene rings, with approximately 3.309 Å between the planes of the rings (Figure 4.14)

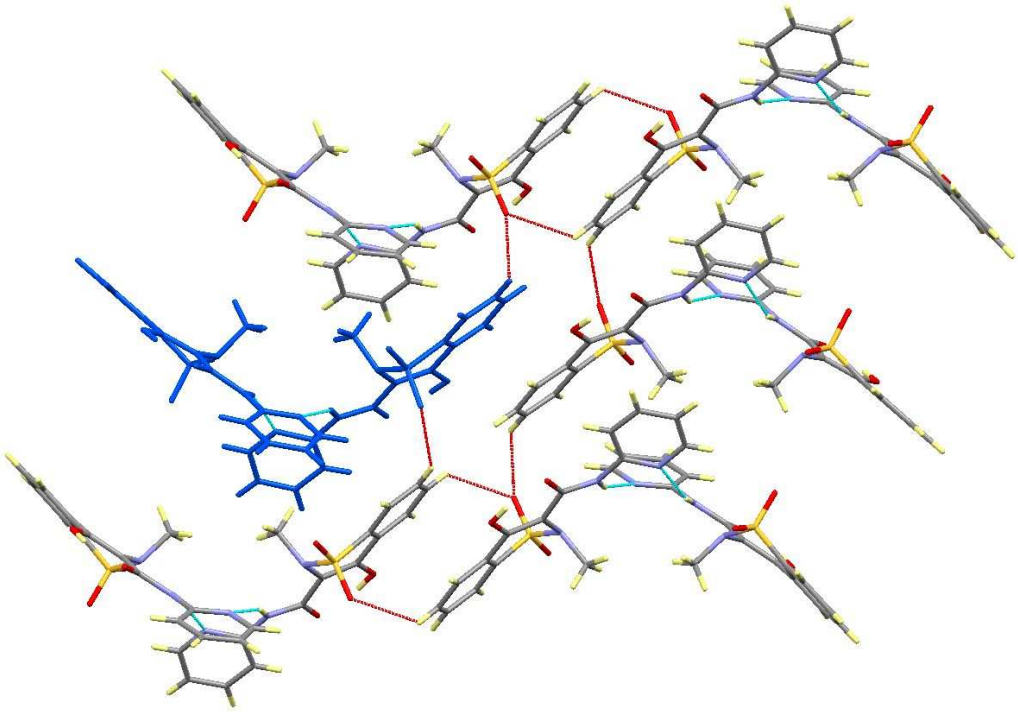

Figure 4.13 *Weak CH···O hydrogen bonds (red dashed lines) linking PXN dimers in piroxicam form III. The diagram also shows the staggered nature of the PXN dimers (one dimer highlighted in blue).*

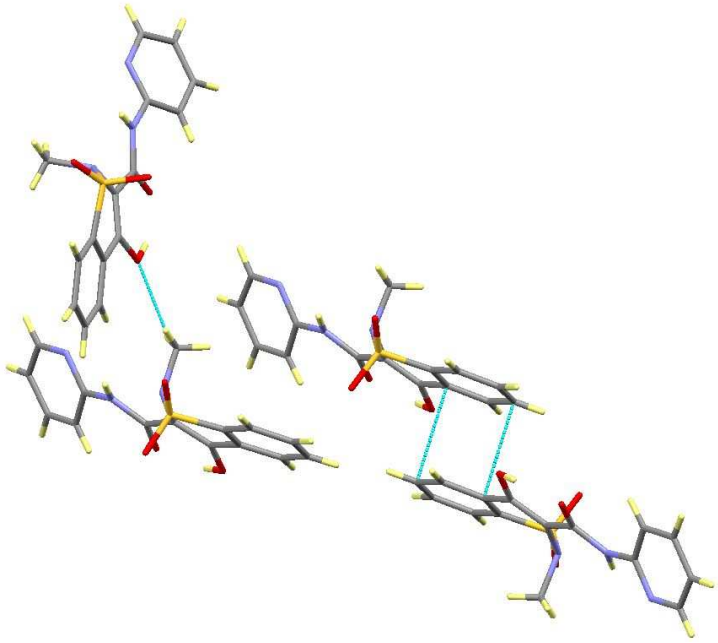

Figure 4.14 *Further weak interactions between PXN molecules showing the CH···O hydrogen bond between the methyl and hydroxyl groups and π···π interactions between the benzene rings.*

4.5.3.3 Piroxicam : Methanol Solvate (3:1) (PX:MeOH)

Crystals of the piroxicam : methanol solvate were particularly small and of poor quality and as a result the data is also poor (R_{int} = 23.6%). Anisotropic refinement of the heavy atoms resulted in implausible thermal parameters for a number of atoms and the structure was therefore refined isotropically for the final refinement cycles (see Appendix A4 for further details).

The PX:MeOH solvate crystallises in a 3:1 molar ratio. The crystal structure is again unusual in that piroxicam molecules are again present in mixed tautomeric states - with two zwitterionic molecules and one non-ionised molecule in the asymmetric unit. The symmetry independent PXZ molecules again dimerise in the same way as is seen in form IV, with two moderately strong charge-assisted bifurcated DHAA N^{+}-H···O hydrogen bonds formed between them (Figure 4.15). The MeOH molecule lies below the plane of the dimer and links to one of the PXZ molecules through a further moderately strong, charge assisted OH···O hydrogen bond (also Figure 4.15). Hydrogen bond lengths and angles for these interactions are provided in Table 4.10.

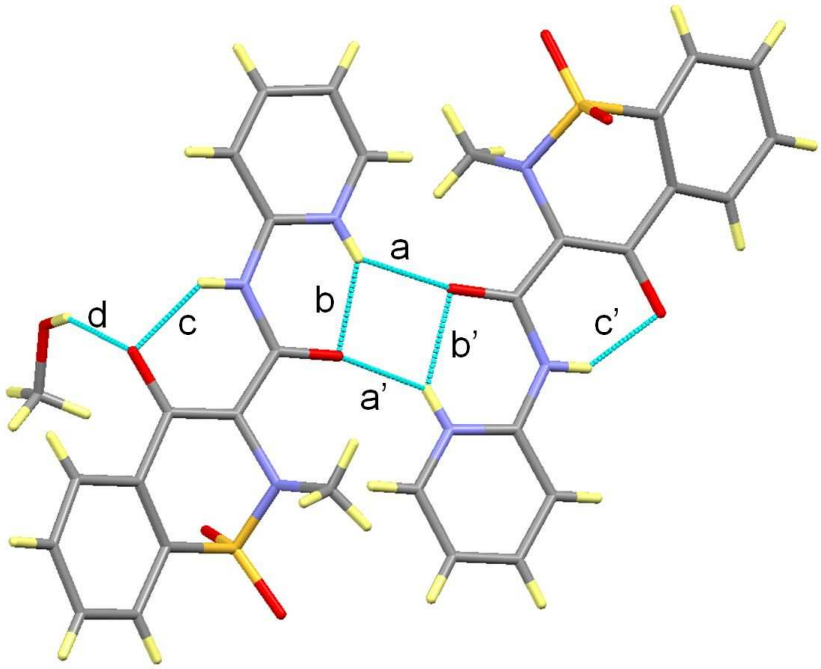

Figure 4.15 *The PXZ dimer in the piroxicam: methanol solvate and the methanol molecule hydrogen bonded to the enolate oxygen through an OH···O hydrogen bond.*

Table 4.10 *Hydrogen bond distances and angles in the PXZ dimer in the piroxicam : methanol solvate (refer to Figure 4.15 for key). Values with no errors are due to hydrogen atoms being placed on calculated positions. Note: Due to the poor quality data, heavy atoms were refined anisotropically resulting in the poor precision of the D···A values.*

H-Bond	D-H (Å)	H···A (Å)	D···A (Å)	∠D-H···A (°)
a	0.86	2.20	2.86(2)	134
a’	0.86	2.20	2.83(3)	130
b	0.86	1.92	2.58(3)	132
b’	0.86	1.97	2.64(3)	134
c	0.86	1.94	2.64(3)	137
c’	0.86	1.81	2.55(3)	143
d	0.90(7)	2.05(10)	2.88(2)	151(19)

The PXN molecule links PXZ dimers through weak CH···O hydrogen bonds with the enolate oxygen of both PXZ molecules (pyridine C···O = 3.31(4) Å and benzene C···O = 3.48(3) Å) (Figure 4.16). The PXN molecule also links to the MeOH molecule through a moderately strong NH···O hydrogen bond (N···O = 3.04 (3)Å) with the hydroxyl oxygen acting as acceptor (also Figure 4.16). A weak hydrogen bond also occurs between the MeOH methyl CH and the pyridine nitrogen (C···N = 3.24(4) Å). The PXZ molecules also link to the PXN molecules through CH···O hydrogen bonds between the benzene ring CH groups and both the amide oxygen (C···O = 3.38(3) Å) and the sulfonyl oxygen (C···O = 3.22(4) Å)

(Figure 4.17). The intramolecular hydrogen bond of the PXN molecule is strong with an O···O distance of 2.50(2) Å.

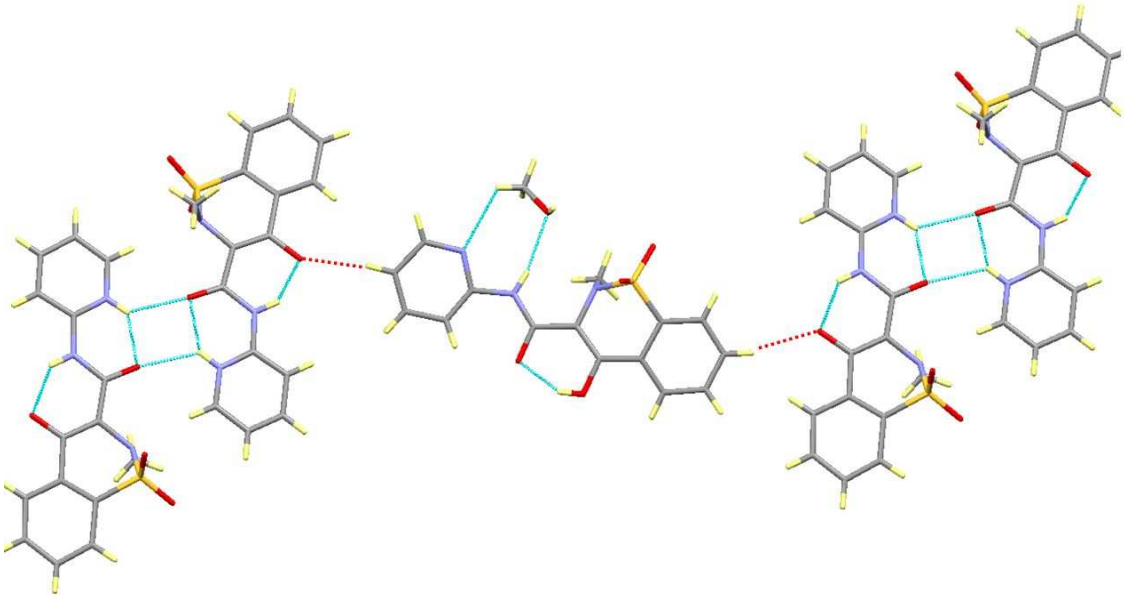

Figure 4.16 *The PXN molecule linking PXZ dimers through weak CH···O hydrogen bonds involving the enolate oxygen atoms (red dashed lines) in the piroxicam : methanol solvate.*

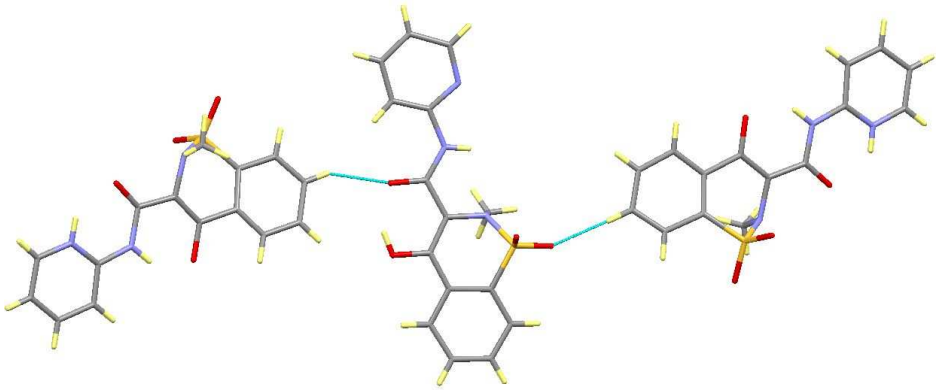

Figure 4.17 *Weak CH···O hydrogen bonds involving the benzene CH groups of PXZ molecules and the amide and sulfonyl oxygen atoms of the PXN molecules in the piroxicam : methanol solvate.*

The structure is layered (Figure 4.18) with the MeOH molecule linking the PXN molecules to PXZ molecules above. Further weak CH···O hydrogen bonds occur between the PXN molecules with other PXN molecules and PXZ molecules in the layer above involving the sulfonyl oxygen atoms (Figure 4.19a). Similar interactions are also present between PXZ molecules - both with adjacent PXZ molecules and PXZ molecules above the plane of the PXZ molecule (Figure 4.19b).

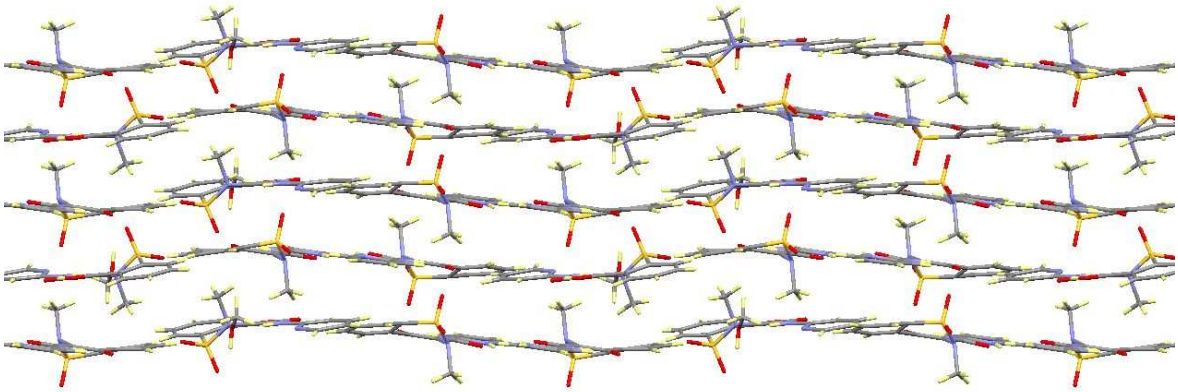

Figure 4.18 *Layers in the piroxicam : methanol solvate.*

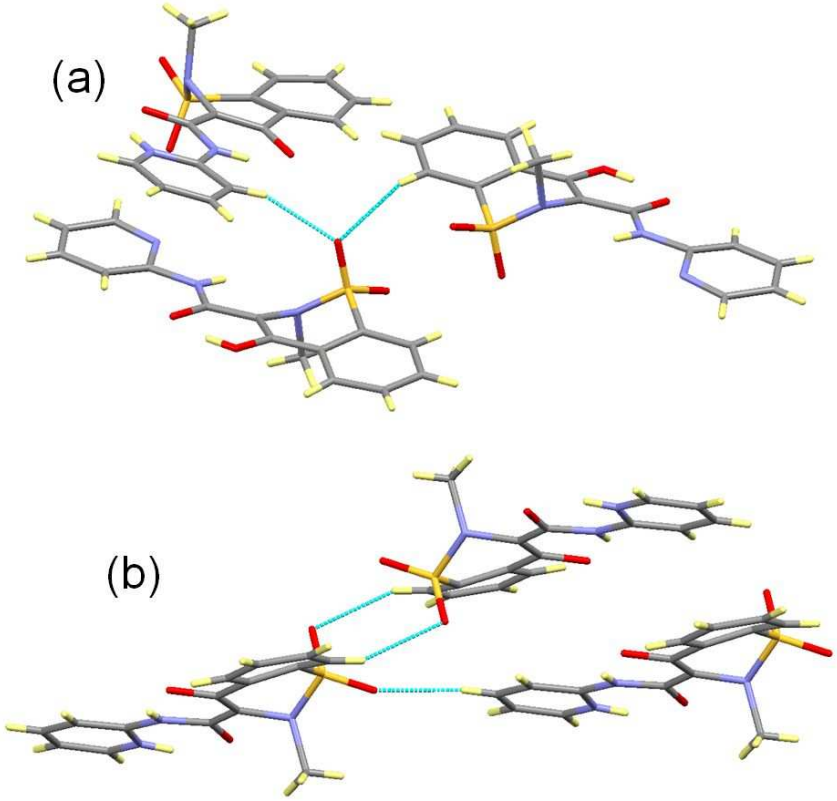

Figure 4.19 CH···O *hydrogen bonds in the piroxicam : methanol solvate involving the sulfonyl oxygen atoms between (a) the PXN molecule and the PXN and PXZ molecules above and (b) PXZ molecules with other PXZ molecules above and adjacent to them.*

4.6 Introduction to Gallic Acid Crystal Forms

Gallic acid (3, 4, 5 - trihydroxybenzoic acid, Scheme 4-5) is a naturally occurring substance which is known to have pharmaceutical properties[213]. In the solid state, anhydrous gallic acid (GA) is known to have only one crystal form[214]. However, gallic acid monohydrate

(GAM) forms readily and is the only known tetramorphic hydrate for which all four crystal structures have been determined[215].

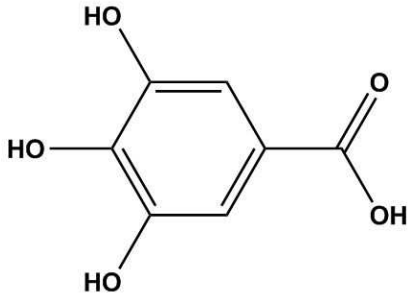

Scheme 4-5 *Structure of gallic acid*

4.7 A Multi-Component Crystallisation Route to a New Porous Form of Gallic Acid Monohydrate

4.7.1 Crystallisation Conditions

Co-crystallisations of GA with piracetam (PTM) were carried out according to the evaporation procedure outlined in Chapter 3 using a 1:1 molar ratio at room temperature. The co-crystallisation screen involved varying the solvent - selected from the following: methanol, ethanol, acetone, acetonitrile and ethyl acetate.

4.7.2 A Co-crystallisation Route to a New Porous Form of Gallic Acid Monohydrate

A screen for molecular complexes of GA and PTM resulted in the discovery of a new form of GAM (PGAM). This form of GAM is unique from the four published polymorphs in that it is porous, with large channels containing disordered solvent molecules running through the crystal structure (see Section 4.6.2.1 for structural details). Structure determination was carried out from single crystals obtained using methanol as the solvent. Unit cell screens showed that PGAM was also formed in crystallisations from ethanol, acetone and acetonitrile. On the other hand PXRD of the crystallisation product from methanol (as opposed to single crystals isolated from this product) showed no trace of PGAM and did not correspond to anhydrous GA or any of the other GAM or PTM polymorphs. Instead, the PXRD pattern corresponds to almost 100% of a previously unknown GA : PTM molecular complex - later also isolated via co-crystallisation from ethyl acetate (the GA : PTM complex is described in detail in Chapter 8) (Appendix B4c-1). This would suggest

that PGAM breaks down under mechanical stress during grinding in preparation for PXRD analysis. However, PXRD of the product of co-crystallisation from ethanol showed a mixture of both PGAM and the GA : PTM molecular complex (Appendix B4c-2). Unit cell screening and PXRD analysis of GA recrystallised from methanol without the presence of PTM showed that no PGAM was formed with only GAM forms I and II present (Appendix B4c-3).

4.7.2.1 Crystal Structure of Porous Gallic Acid Monohydrate (PGAM)

The porous gallic acid monohydrate form has a single GA molecule and a single water molecule in the asymmetric unit. The GA molecules dimerise through the typical carboxylic acid dimer formed by moderately strong OH···O hydrogen bonds (a in Figure 4.20). Weaker OH···O hydrogen bonds between the hydroxyl groups (b and c in Figure 4.20) link the GA molecules into large rings forming the structural frame of the channels. The oxygen of the water molecule has large, elongated anisotropic displacement parameters (Figure 4.21), suggesting it possibly has a large degree of freedom. As a consequence, no water hydrogen atoms could be located (all other hydrogen atoms were located using the difference Fourier synthesis). The hydroxyl OH of one GA molecule forms a moderately strong OH···O hydrogen bond to the water oxygen (d in Figure 4.20). Although hydrogen atoms were not located, the hydrogen bonding of the water molecule is inferred from the neighbouring atoms. The water appears to form another moderately strong OH···O hydrogen bond to the hydroxyl oxygen of another GA molecule (e in Figure 4.20). Hydrogen bond distances and angles for these interactions are presented in Table 4.11.

Table 4.11 *Hydrogen bond distances and angles in the porous gallic acid monohydrate (refer to Figure 4.20 for key). Note: Hydrogen bond e is a proposed hydrogen bond between the GA molecules and the disordered water molecule; water hydrogen atoms could not be located.*

H-Bond	D-H (Å)	H···A (Å)	D···A (Å)	∠D-H···A (°)
a	1.22(4)	1.48(4)	2.619(3)	152(3)
b	0.84(3)	1.97(3)	2.783(3)	164(3)
c	0.98(4)	2.00(3)	2.838(3)	143(3)
d	0.93(4)	1.76(4)	2.668(3)	166(3)
e	-	-	3.008(3)	-

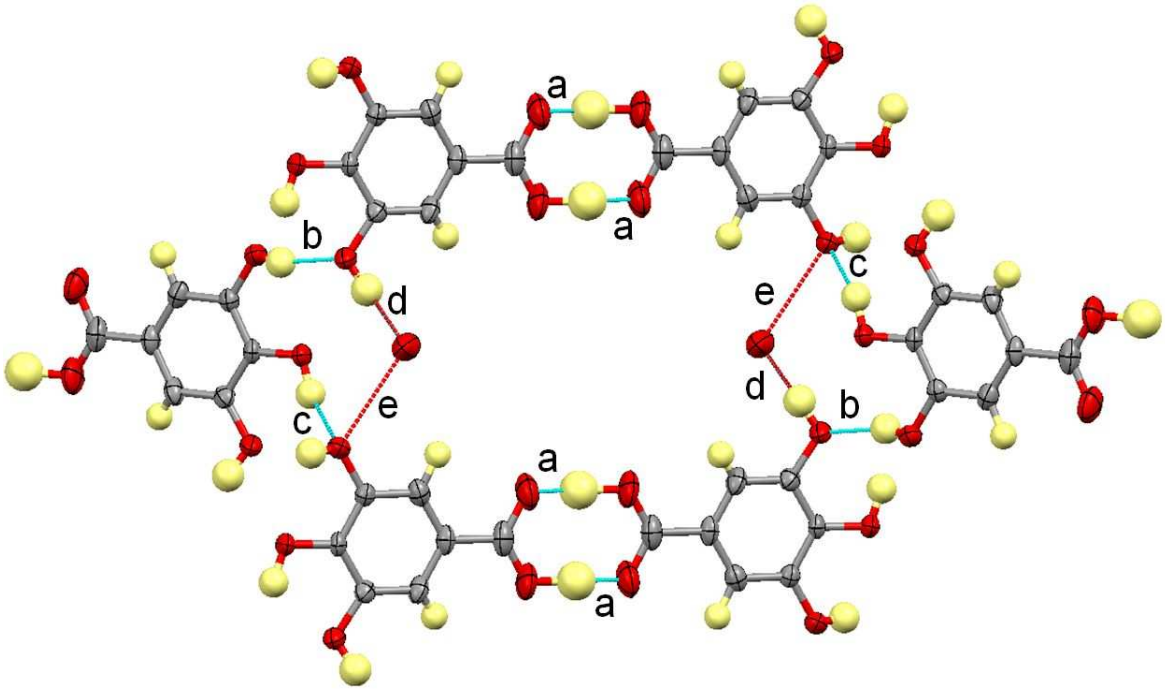

Figure 4.20 *Hydrogen bonding forming the pore in the porous gallic acid monohydrate crystal structure.*

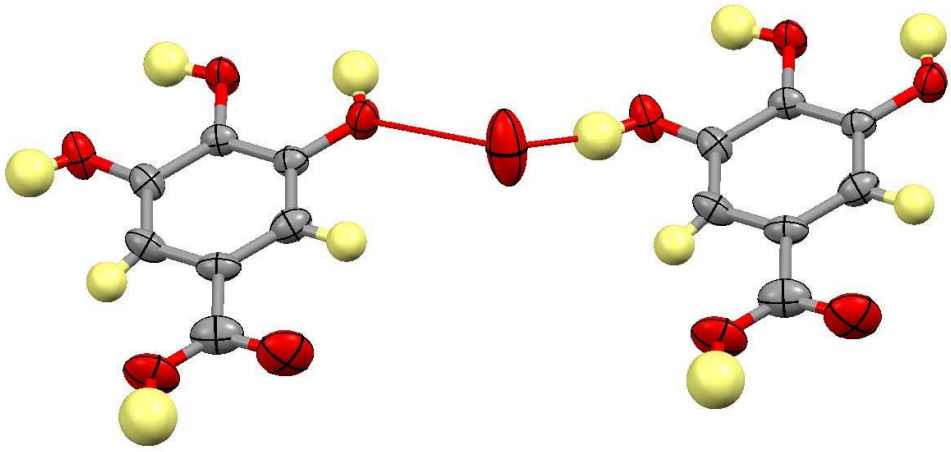

Figure 4.21 *The elongated anisotropic displacement parameters of the water oxygen atom relative to the two GA molecules to which it forms hydrogen bonds.*

The hydrogen bonding between the hydroxyl groups (b and c in Figure 4.20) links rings parallel to each other to form the channels (Figure 4.22), with each GA molecule forming hydrogen bonds to two other GA molecules through these interactions. The channels account for a significant proportion of the unit cell volume (Figure 4.23), with approximately 5.0% of the unit cell volume (47.60 $Å^3$) accessible to solvent water molecules (using a probe with a van der Waals radius of 1.4 Å). The channels contain

disordered solvent molecules which could not be resolved. The SQUEEZE procedure[216] was therefore used to remove and estimate the electron density from the channel prior to the final refinement cycle. An estimate of 69 electrons per unit cell was given which could be accounted for by roughly ten water molecules or 4 methanol molecules although a definite conclusion could not be reached.

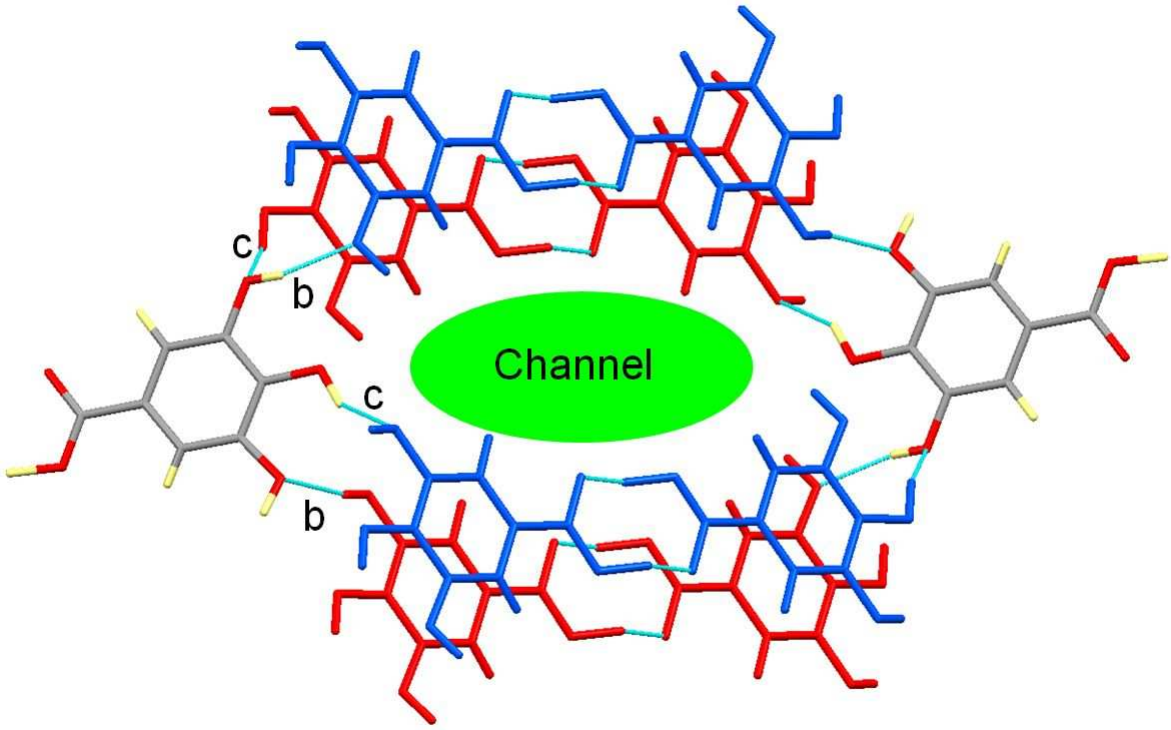

Figure 4.22 *Formation of the channels in the porous form of gallic acid monohydrate (PGAM). The hydrogen bonding between hydroxyl groups links the large rings parallel to each other to form the channel. The blue GA dimers lie in front of the red dimers, parallel to their plane.*

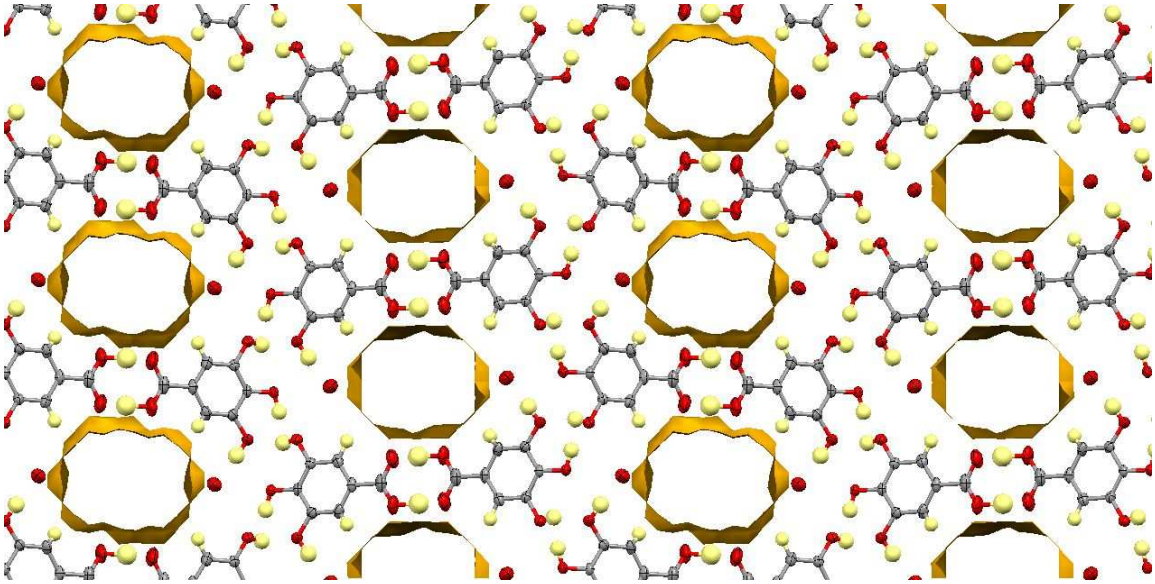

Figure 4.23 *Relative arrangement of the channels in the porous gallic acid monohydrate.*

4.8 Introduction to Piracetam Crystal Forms

The API piracetam (PTM) (Scheme 4-6) has five known polymorphs, the structures of which have all been previously determined. Two of the polymorphs can only be isolated using high pressure[130, 217]. Forms II and III are the most stable at ambient temperature and are the forms generally produced from evaporation crystallisation experiments[218]. The structure of form I had until recently[217] only been determined by PXRD methods[217, 219] as the generation of single crystals is difficult and unpredictable. Forms II and III are reported to undergo a solid-solid phase transformation to the metastable form I above 400K (127°C)[217].

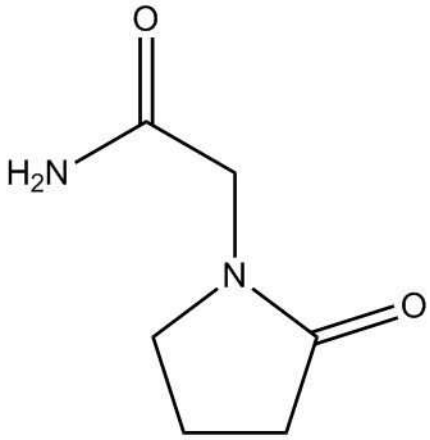

Scheme 4-6 Structure of piracetam

4.9 A Multi-Component Crystallisation Route to Piracetam form I

4.9.1 Crystallisation Conditions

Following the results of experiments using pyrazole as a structure-directing co-molecule to produce PA form II and PX form III, similar co-crystallisation experiments were carried out using PTM and pyrazole. Crystallisation conditions were chosen based on the PX experiments to produce PX III, with pyrazole in excess (2:1 mass ratio) using methanol as the solvent at 50°C. Control crystallisation experiments were also set up around one month after these experiments under the same conditions in the absence of pyrazole.

4.9.2 A Possible Co-Crystallisation Route to Piracetam Form I

Unit cell screening and PXRD (Appendix B4d-1) of the products of the co-crystallisation experiments showed that the co-crystallisation had produced a mixture of PTM form I and II with repeat experiments showing this to be highly reproducible. PXRD analysis of the control experiments in the absence of pyrazole (carried out *after* the initial co-crystallisations), however, also showed the same results (Appendix B4d-2). It is unclear whether high temperature recrystallisation from methanol is sufficient to produce PTM form I or if the initial co-crystallisation experiments have resulted in seeding of the laboratory, facilitating the production of PTM I in subsequent experiments in the absence of pyrazole.

Detection of pyrazole was made difficult as the major peaks in the pyrazole PXRD pattern overlap with those of PTM II, although the evidence suggests that at least the majority of it is not present in the product. The non-overlapping pyrazole peaks are significantly weaker then the major peaks making it difficult to see them even if they were there. PXRD of PTM I samples left at room temperature for over a week shows that PTM I gradually transforms into the more stable form II as is consistent with previous reports[217].

4.10 Discussion

4.10.1 New and Elusive Phases of Piroxicam

The elusive piroxicam form III and a new polymorph, designated form IV, as well as a new PX methanol solvate were crystallised using nitrogen heterocycles as structure-directing co-molecules in solution.

By crystallising piroxicam in the presence of pyrazole or dimethylpyrazole, piroxicam form III has been successfully isolated and its crystal structure determined for the first time. Although 100% yields could not be obtained, large crystals suitable for single crystal X-ray diffraction were produced for the first time. Similarly, by crystallising PX in the presence of pyrazine, a new polymorph of piroxicam has been discovered - form IV. The methanol solvate was crystallised using indazole as a co-molecule. Both PX IV and the methanol solvate contain a mixture of both the non-ionised and the zwitterionic PX tautomers. All other polymorphs of PX contain the PXN tautomer only and only one molecular complex of PX was known previously that had a mixture of both tautomers[27]. This illustrates the potential of this co-crystallisation method in accessing crystalline phases possessing otherwise unobtainable structural features.

Relative Stability of Piroxicam Polymorphs

As previously stated, the reproducibility of the formation of PX IV was poor using this co-crystallisation method. The yield of PX III obtained was also low, with PX I or the monohydrate crystallising concomitantly in larger quantities. DSC of all polymorphs was carried out to determine their relative thermodynamic stability, which could provide a rationale behind these observations. The melting points are reported in Table 4.12 along with previously reported values for forms I, II and III. The DCS traces for all four forms can be found in Appendix C4.

Table 4.12 *Melting points (in °C) of the four polymorphs of piroxicam from DSC measurements.*

Polymorph	I	II	III	IV
This work	200.4	196.15	197.98	195.7
Literature	202.6[208]	199.7[208]	178.4[207]*	No data

** In a later publication[208], the same author also reported that form III converts to the more stable form II then to form I upon heating - conflicting with their previous data and the experimental data obtained in the present study. In the previous reports, form III was also prepared from the melt which is not an optimal method as melting of PX is accompanied by chemical degradation[209].*

Being the dominant form to crystallize under most crystallization conditions, form I is unsurprisingly the most stable form. Given the difficulty in crystallizing form III, it may be somewhat surprising to see it is the second most stable form according to the DSC measurements. This may be explained, however, by the similarity of the crystal structure to that of form I, as they both feature the same hydrogen bonding in their piroxicam dimers, with the differences lying in the extended packing. The difficulty in obtaining form III may therefore arise due to the energetic similarities to form I, with the most stable form of the two prevailing under most conditions due to two close lying energy minima. Form IV was found to be the least stable form, explaining its late discovery despite the extensive previous research into piroxicam polymorphism. The crystallisation of these metastable polymorphs is likely to be highly sensitive to perturbations in the crystallisation conditions which would explain the difficulty in obtaining consistent yields. Examples in the literature report similar issues when using co-crystallisation to produce elusive, metastable polymorphs[66]. It could, however, be possible to optimise yields to 100% by varying conditions such as the solvent used, the co-molecule used or the crystallisation temperature - as has been demonstrated with PA II.

Nitrogen-Heterocycles as Structure Directing Co-molecules: Implications for Polymorph Screening

The systematic co-crystallisation experiments of PX with NHCs have led to the discovery of two new phases of PX as well as a new route to a previously elusive phase. The systematic methodology has been shown to be a critical part of the process, as the initial discovery of one of these phases led to further experiments using NHCs as structure directing co-molecules - not only with PX, but also with PA and PTM resulting in new routes to PA II and PTM I. Polymorph screens of materials generally do not include co-crystallisation experiments, however, the work presented here indicates there may be a case for including co-crystallisation with certain co-molecules as part of systematic polymorph screens.

4.10.2 New Form of Gallic Acid Monohydrate

A new porous monohydrate of GA (PGAM) was obtained via co-crystallisation with PTM from methanol, ethanol, acetone or acetonitrile. The new form has not been termed

“form V” GAM due to the unidentified disordered solvent/water in the pore meaning it may not strictly exist as a monohydrate.

PXRD of the co-crystallisation from ethanol showed that PGAM may crystallise concomitantly with a molecular complex of GA with PTM (see Chapter 8). The PXRD of the product of the co-crystallisation from methanol showed only the GA : PTM molecular complex. This is despite the fact that unit cell screening of single crystals from the same preparation found only PGAM and the structure was subsequently determined from a crystal from the same crystallisation batch. It is unclear at present whether the GA : PTM complex has formed under the mechanical stress of grinding or if the storage conditions have resulted in it forming over time. PXRD analysis of the products of the co-crystallisation from ethanol showed a mixture of both PGAM and the GA : PTM complex suggesting that PGAM does not break down under grinding. Structure determination of PGAM has not been carried out from samples recrystallized from solvents other than methanol, although it is possible that the disordered solvent/water contained in the pore may differ depending on the solvent used, which may affect the stability. Possible structure determination of PGAM samples from a range of solvents as well as using other analysis methods such as TGA to characterise the disordered solvent in the pores could be important steps in understanding the nature of PGAM. The ability to incorporate the small solvent molecules into the pores indicates the potential for applications as a lightweight organic material for gas storage.

4.10.3 Piracetam Form I: A multi-component crystallisation route or a high temperature crystallisation route?

PTM I was initially obtained from co-crystallisation of PTM with pyrazole at 50°C from methanol and later obtained from the same conditions in the absence of pyrazole. It is unclear if the initial co-crystallisation experiments used to obtain PTM I have resulted in seeding of the laboratory environment, thereafter enabling more facile production of this metastable form even from single component crystallisations. The possibility remains that crystallisation of PTM at 50°C from methanol would have resulted in PTM I regardless of this initial co-crystallisation having been carried out. To clarify this, independent crystallisations of PTM at 50°C from methanol need to be carried out in another laboratory in which PTM I has not previously been obtained.

Nevertheless a facile route to obtaining PTM I has been discovered through the systematic co-crystallisation methodology employed. The solid-solid phase transformations of II and III to form I have been reported to occur above 127°C[217], which is significantly higher than the temperatures used in the solution method presented here. The evaporation method described above also results in good quality single crystals, suitable for single crystal X-ray diffraction.

4.10.4 General Comments on Co-crystallisation as a Route to New and Elusive Phases

Potential of Co-crystallisation as a Route to New and Elusive Polymorphs

Co-crystallisation is a relatively unexplored route to obtaining new polymorphs of materials and its importance is highlighted in the work presented above. It has been shown to offer simple routes to obtaining new and elusive crystal forms of materials with otherwise unobtainable characteristics, i.e. larger crystals and yields (PA II and PX III), mixed tautomers (PX IV and the PX methanol solvate) and porous structures of extensively studied materials (PGAM).

Systematic identification of a certain classes of co-molecule which direct the formation of metastable forms of a material may have applications in having the same effect for other materials. This is seen with the NHCs which have been used to direct the formation of both PA II and three new PX crystal forms. It is interesting also to note that multicomponent crystallisations using a variety of NHCs have previously been used to produce a new zwitterionic polymorph of 2-(p-tolylamino)nicotinic acid[66]. The systematic approach to the crystallisation conditions also resulted in a method of obtaining PTM I, although the exact conditions required remain unclear.

Challenges in using this method of polymorph selection do however remain, with removal of the co-molecule from the final product a problem in some cases. PXRD analysis showed that certain co-molecules in this work were not present in the final product (e.g. pyrazole, pyrazine); selection of co-molecules such as these may overcome this problem. The metastable polymorphs produced can also be difficult to reproduce (PX IV) or difficult to obtain in 100% yields (PX III, PGAM). Significant tuning may therefore be required to obtain 100% yields; this has however been successfully achieved with PA II.

The scale up of this method to an industrial level may also prove problematic. The preliminary work carried out with PA II showed that conversion of this evaporation

method to a cooling method may not necessarily be straightforward although further work is required to assess if it is possible.

Mechanism

The mechanism by which certain co-molecules direct the formation of a particular crystal form of another material remains unclear. The evidence gathered in this study suggests a solution-based mechanism rather than epitaxy, as no intergrowths of crystals with the co-molecule were observed. Also, when using pyrazole, 3,5-dimethylpyrazole and pyrazine as co-molecules, very little or no co-molecule was found in the final product isolated in the crystallisation vessel. Further evidence of a solution based mechanism was provided by the systematic approach using co-crystallisation of PA with carboxylic acids to produce PA II, which led to the use of acetic acid as a solvent to obtain yields of approaching 100% PA II in a single component preparation. A solution-based mechanism could also offer a partial explanation for the failed attempts at using co-grinding to produce PA II. The ability to use NHCs to produce a number of different crystal forms of PX and PA also indicates a related mechanism may be involved. The mechanism of nucleation in general is not well understood and thus the nature of a possible solution based mechanism is not obvious. Possibilities include co-molecule assisted stabilisation of pre-nucleation aggregates of the metastable forms or the co-molecule possibly inhibiting nucleation of the more stable form. Another interesting point is that high temperature conditions (*ca.* 50°C) are a required condition for the crystallisation of all three PX crystal forms reported here, for the crystallisation of PTM I, and also play an important part in the crystallisation of PA II when using NHC co-molecules. In some cases an excess quantity of the co-molecule is required to produce the desired polymorph; this may also have implications as to the mechanism.

The role of impurities in these co-crystallisation experiments also warrants investigation. As many of the compounds used as structure directing co-molecules are of similar chemical identity and were obtained from the same supplier, it is conceivable that the same or similar impurities are present alongside the different compounds. It could therefore be the case that these trace impurities are having a structure directing effect towards the crystallisation of the metastable forms obtained. The presence of impurities may also provide an explanation for the pink hue observed in some of the PA II crystals obtained. Another factor worthy of investigation is the role of the crystallisation vessel

surface, as the co-molecules may be interacting with the vessel in such a way as to provide nucleation points favourable to nucleation of metastable forms.

Conclusions

In summary, it has been shown that the systematic investigation of co-crystallisation conditions can lead to new and potentially useful crystal forms of various APIs as well as new routes to metastable forms. The method facilitates access to a range of crystal forms with otherwise unobtainable structural features as demonstrated by the ability to produce crystal forms of PX containing mixed tautomeric states as well as a porous form of GAM. It remains unclear whether PTM I is formed due to the structure directing effect of the co-molecule or whether its formation is solely due to the use elevated temperature conditions.

Selected NHCs have the ability to direct the crystallisation of both paracetamol and piroxicam towards elusive polymorphs. In the cases of PX III and PA II, these otherwise difficult to obtain polymorphs can be crystallised in significant quantities from simple evaporation and in the case of PX IV and the PX methanol solvate, previously undiscovered forms are crystallised. The crystallisation of PX III and IV is more sensitive to the crystallisation environment than that of PA II, possibly due to the increased competition incurred by the existence of the more stable forms I and II as well as the monohydrate. The fact that the similar co-molecules can induce polymorph formation in different materials also indicates a related mechanism may be responsible for the formation of these elusive polymorphs. The evidence from these experiments also indicates that the mechanism is indeed solution based rather than epitaxial. An understanding of this mechanism is, however, still elusive.

5. Tautomerism in Multi-Component Complexes of Piroxicam with Mono-substituted Benzoic Acids

5.1 Known Molecular Complexes of Piroxicam

Various molecular complexes of piroxicam (PX) are known. In these, PX is found to adopt a range of forms, including being present as a salt in which it is in the anionic form[220], in five molecular complexes in which it is in the non-ionised form[27] and in five molecular complexes in which it is in the zwitterionic form[27,221]. Prior to the discovery of PX form IV (see Chapter 4), molecular complex formation (taken here to include the known solvate, piroxicam monohydrate[211]) was the only reported route to obtaining the zwitterionic tautomer of piroxicam in the solid state. A recent study of the molecular complex formation of PX with carboxylic acids[27] indicated some interesting behaviour, dependent on the carboxylic acid used for co-crystallisation. Whereas co-crystallisation with four of the co-molecules (succinic acid, 1-hydroxy-2-napthoic acid, caprylic acid and malonic acid) resulted in molecular complexes with the non-ionised tautomer of PX (PXN), use of benzoic acid as co-molecule resulted in a complex with the zwitterionic tautomer (PXZ), while the use of fumaric acid resulted in a complex containing both PX tautomers in a 1:1 ratio. Of particular interest was the molecular complex of PX with 4-hydroxybenzoic acid (4HBA) which exhibited the rare phenomenon of tautomeric polymorphism. This is the only previously reported complex of piroxicam to exhibit this type of polymorphism.

Further studies of tautomerisation in the solid state have potential value in the development of APIs for applications, as the ionisation state can have a profound effect on the properties of the target API. Most zwitterionic APIs such as PX have issues with solubility in polar and non-polar media and studies have shown this can be improved through ion-pairing[212]. Co-crystallisation could offer a more flexible alternative to this, given the number of potential co-formers available. It is also important to establish which tautomeric form of an API is the most stable upon co-crystallising with a particular co-former candidate, to ensure that form can be further developed with minimal risk of conversion to another form. The ability to predict which tautomeric form is favoured in a given multi-component system is therefore a desirable goal, yet to-date we know of only one study investigating this[12]. Whereas salt formation can be anticipated to a certain degree using pKa matching[111], this rule does not extend to cases such as PX complexes

which involve intra- rather than intermolecular H-transfer. It has been demonstrated that in some cases where the tautomerism involves formation of a carboxylate, complexes containing the zwitterionic form only can be crystallised preferentially by using weakly acidic alcohols and exploiting the preferential formation of the $COO^{-}\cdots O\text{-}H$ heterosynthon[26]. Previous studies have also indicated that the predominant form present in solution is not always the form seen in the solid state[62].

In this chapter the molecular complex formation of PX and mono-substituted benzoic acids is investigated[222]. The systematic co-crystallisation of PX with a group of closely related carboxylic acids is used to establish if a relationship exists between the properties of the benzoic acid co-molecules and the PX tautomer present in the resultant molecular complex. Identification of such a relationship will hopefully enable us to predict which tautomer is preferred in molecular complex formation with a particular co-molecule. Systematic identification of the most stable polymorphs in systems exhibiting tautomeric polymorphism would also be a further tentative step along the road to understanding the preference of tautomeric materials such as piroxicam to co-crystallise as one tautomer or another depending on the co-former used.

5.2 Tautomeric Polymorphism in Molecular Complexes of Piroxicam with Mono-Substituted Benzoic Acids

Of the sixteen co-molecules found to form molecular complexes with piroxicam in this study, three were found to exhibit tautomeric polymorphism. Crystallographic data and refinement details for all six of these complexes can be found in (Appendix A5).

5.2.1 Crystallisation of Polymorphs

Piroxicam : 2-Fluorobenzoic Acid

Initial co-crystallisation of the PX:2FBA polymorphic pair was carried out in a 50/50 v/v mixture of methanol and acetonitrile by varying the temperature, with the zwitterionic polymorph (PXZ:2FBA) crystallising at 40°C and the non-ionised polymorph (PXN:2FBA) crystallising at 50°C. Repeat experiments proved unpredictable with recrystallisation of the starting materials and/or PX monohydrate often the result.

Piroxicam : 3-Fluorobenzoic Acid

The PX:3FBA polymorphic pair were crystallised from pure acetonitrile with large crystals of the non-ionised complex (PXN:3FBA) forming at 40°C and small needle-like crystals of the zwitterionic complex (PXZ:3FBA) forming at 50°C. In both cases small quantities of the other polymorph were also found in the resulting solid product.

Piroxicam : 4-Fluorobenzoic Acid

The polymorphic piroxicam : 4-fluorobenzoic acid complexes were also crystallised from acetonitrile with the zwitterionic complex (PXZ:4FBA) initially crystallising with 100% yield at 50°C and the non-ionised complex (PXN:4FBA) crystallising with 100% yield at 40°C. 100% yields of each polymorph were verified using PXRD, however, PXRD of repeat crystallisations were erratic with mixtures of both forms found at 50°C and 100% yield of the zwitterionic form also found at 40°C in some experiments (see Appendix B5).

5.2.2 Crystal Structures of Piroxicam Complexes Exhibiting Tautomeric Polymorphism

5.2.2.1 Piroxicam : 2-Fluorobenzoic Acid (Zwitterionic Piroxicam) (PXZ:2FBA)

The zwitterionic PXZ:2FBA complex crystallises with one PXZ molecule and one 2FBA molecule in the asymmetric unit. It features a tetramer-like building block with a BZZB (B = benzoic acid, Z = zwitterionic piroxicam) configuration (Figure 5.1) with an inversion centre lying in the middle of the PXZ dimer. The dimer is formed by charge-assisted, DHAA bifurcated intra- and intermolecular N^+-H···O hydrogen bonds between the protonated PXZ pyridinal NH and the amide carbonyl oxygen atoms forming an $R_2^2(12)$ hydrogen bonded ring (Figure 5.1). The hydrogen bonds are moderately strong with N···O distances of 2.611(4) Å and 2.920(3) Å respectively (see Table 5.1).

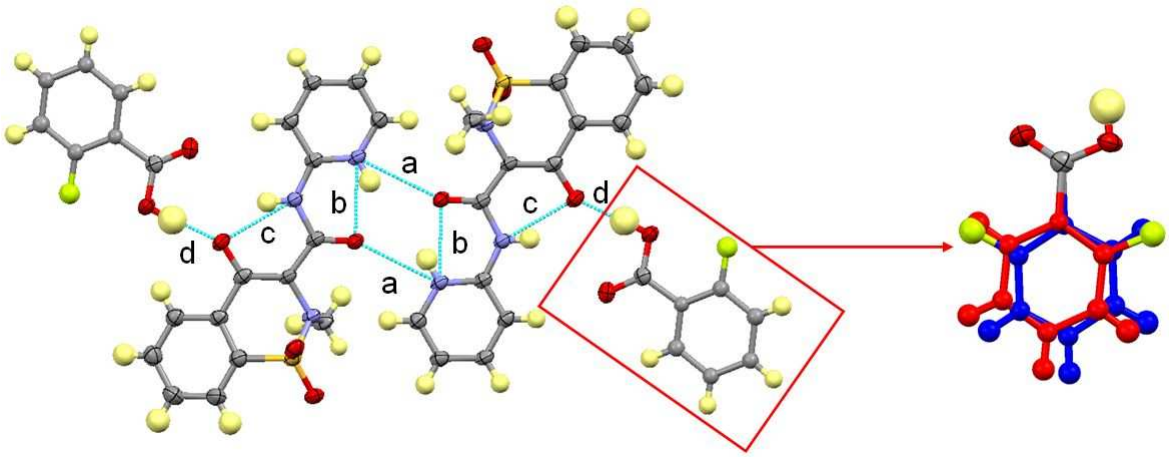

Figure 5.1 *Tetramer in the PXZ:2FBA complex with the major positions of the 2FBA molecules shown (left). The 2FBA molecules are disordered with the major position (60%) shown in red and minor position (40%) in blue (right).*

The 2FBA molecule (red box in Figure 5.1) is orientationally disordered over two positions. The relative occupancies of these two positions were refined to approximately 60/40, with the major component oriented with the fluorine on the same side of the ring as the carboxylic acid hydroxyl group. The carboxylic acid OH of the 2FBA molecule forms a charge-assisted O-H···O^- hydrogen bond (O···O = 2.568(3) Å) to the deprotonated PXZ oxygen atom to form the tetramer. A weak hydrogen bond is also formed between the 2FBA carbonyl O and the aromatic CH of PXZ (C···O = 3.233(4) Å). π-π interactions of the pyridine ring of PXZ with the enolate oxygen and benzene ring of the PXZ molecule hold tetramers above and below each other such that the molecules lie head to tail (Figure 5.2). These PXZ molecules further interact via weak bifurcated DDHHA CH···O interactions between the aromatic CH groups of the pyridine ring and the sulfonyl oxygen (C···O = 3.217(3) Å and 3.405(3) Å, ∠DHA = 124.7(2)° and 109.6(2)° respectively) (also shown in Figure 5.2).

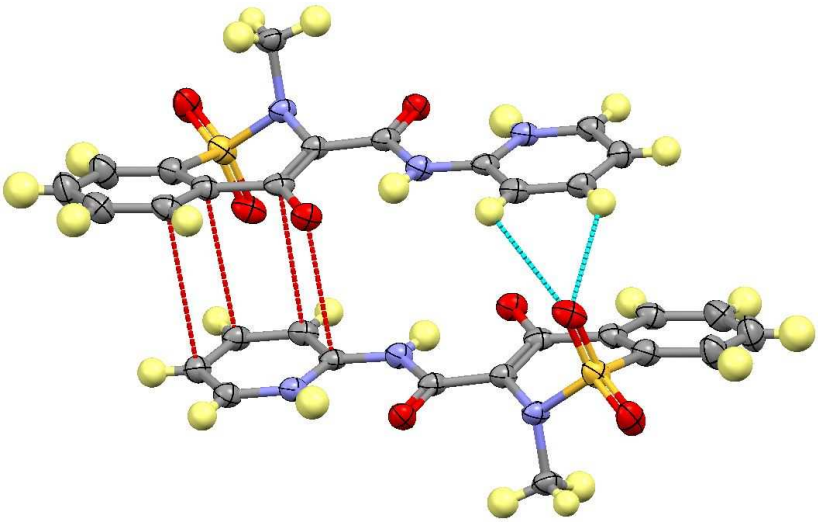

Figure 5.2 *Piroxicam molecules in the PXZ:2FBA complex lying head to tail relative to each other, held together by π-π interactions (red dashed line) and weak CH···O hydrogen bonds (blue dashed line).*

There are further interactions of the sulfonyl oxygen with the disordered fluorine atoms of the 2FBA in the minor position (O···F = 2.851(6) Å, c.f. sum of vdW radii = 2.99 Å), as well as weak methyl CH···F (C···F = 2.948(5) Å) hydrogen bonds when the fluorine is in the major position (Fig 5.3). The tetramers are arranged in stacks forming a herringbone structure as shown in Figure 5.4, with CH···π interactions between 2FBA molecules holding different stacks together.

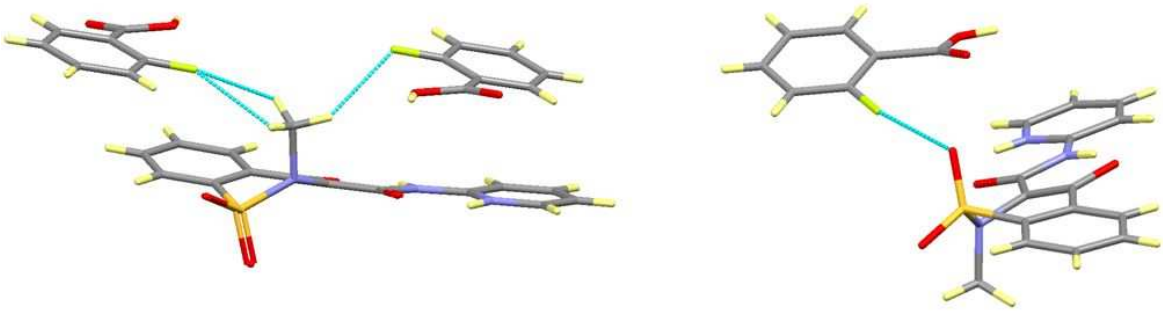

Figure 5.3 *Weak methyl CH···F hydrogen bonds when fluorine is in the major position (left) and weak interactions of the sulfonyl oxygen with fluorine in the minor position (right) in the PXZ:2FBA complex.*

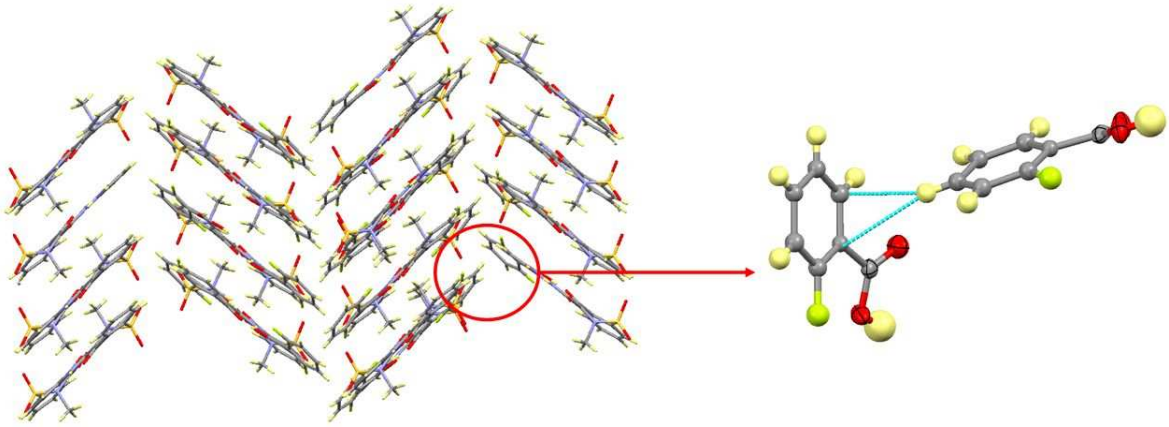

Figure 5.4 *Herringbone structure of the PXZ:2FBA complex and the CH···π interactions between 2FBA molecules in different stacks (major component shown only).*

Table 5.1 *Hydrogen bond lengths and angles in the BZZB tetramer formed in zwitterionic piroxicam complexes with fluorobenzoic acids (see Figure 5.1 for key).*

Complex	H-Bond	D-H (Å)	H···A (Å)	D···A (Å)	∠ D-H···A (°)
PXZ: 2FBA	a	0.84(4)	2.29(4)	2.920(3)	132(3)
	b	0.84(4)	1.94(3)	2.611(4)	137(3)
	c	0.85(4)	1.89(4)	2.621(4)	144(3)
	d	0.90(5)	1.67(5)	2.568(3)	176(4)
PXZ: 3FBA	a	0.89(5)	2.21(5)	2.913(6)	135(4)
	b	0.89(5)	1.94(5)	2.604(5)	130(4)
	c	0.88(5)	1.90(5)	2.599(6)	136(4)
	d	1.18(7)	1.40(6)	2.578(5)	171(5)
PXZ: 4FBA	a	0.91(2)	2.15(2)	2.8518(14)	132.6(15)
	b	0.91(2)	1.94(2)	2.6348(14)	131.9(14)
	c	0.88(2)	1.81(2)	2.5635(14)	142(2)
	d	0.86(2)	1.75(2)	2.5985(13)	175(2)

5.2.2.2 Piroxicam: 3-Fluorobenzoic Acid (Zwitterionic Piroxicam) (PXZ:3FBA)

The zwitterionic PXZ:3FBA complex is isomorphous to the PXZ:2FBA structure; the change in substituent position therefore has no significant effect on the crystal packing. The complex features the same BZZB tetrameric building block (Figure 5.5), but in this case, the 3FBA molecule is not disordered. The F atom lies solely on the hydroxyl side of the ring, and forms weaker aromatic CH···F hydrogen bonds (C···F = 3.171(7) Å) with a neighbouring PXZ molecule (Figure 5.6). A hydrogen bond with the methyl group is still

possible but is much weaker with a C···F distance of 3.553(2) Å (also Figure 5.6). The different position of the F atom on the ring and different CH···F hydrogen bonds result in only very slight changes in the packing (Figure 5.7), hence the hydrogen bond distances in the tetramer are very similar (see Table 5.1). Although similar, all the hydrogen bond distances are slightly stronger with the exception of the intermolecular OH···O interaction between the 3FBA molecule and the PXZ molecule, which is slightly weaker.

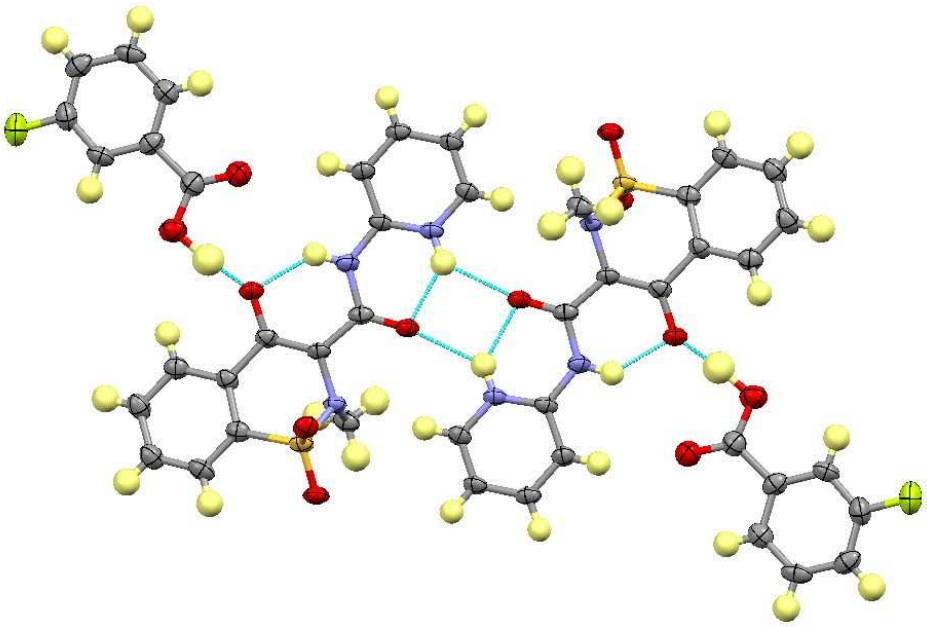

Figure 5.5 *BZZB tetramer in the PXZ:3FBA complex.*

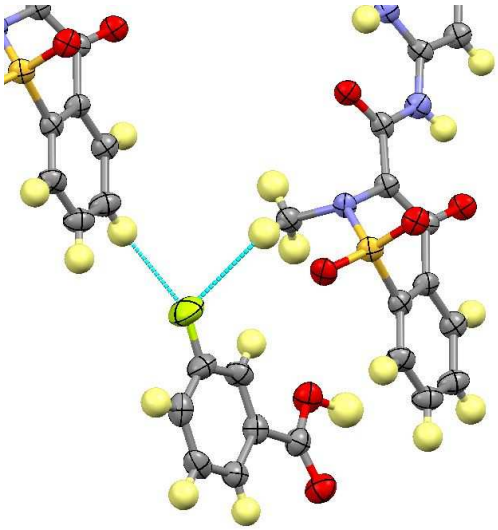

Figure 5.6 *Weak CH···F hydrogen bonds in the PXZ:3FBA complex.*

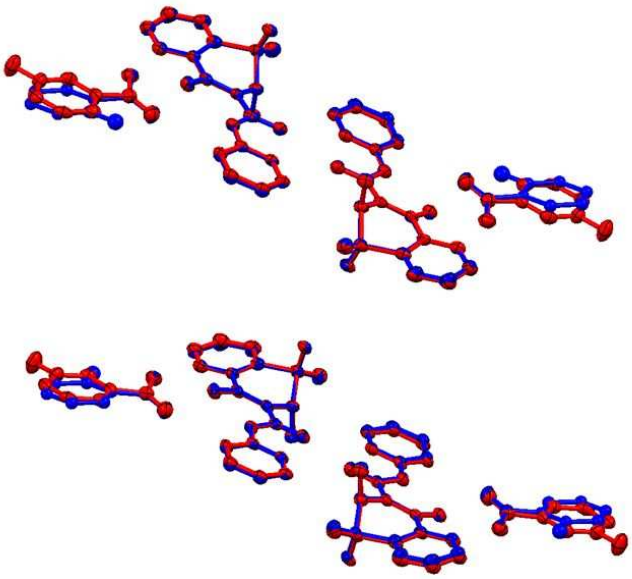

Figure 5.7 *Overlay showing the slight differences in crystal packing of PXZ:3FBA (red) with the major component (top) and minor component (bottom) of PXZ:2FBA (blue). Hydrogen atoms are omitted for clarity.*

5.2.2.3 Piroxicam: 4-Fluorobenzoic Acid (Zwitterionic) (PXZ:4FBA)

The zwitterionic PXZ: 4FBA complex features the same BZZB tetramer-like building block (Figure 5.8), lying on an inversion centre, as the other FBA complexes, but is not isomorphous to these. The N^{+}-H···O interactions in the PXZ dimer have slightly different N···O distances, with a weaker intramolecular hydrogen bond (2.6348(14) Å) but a stronger intermolecular hydrogen bond (2.8518(14) Å).

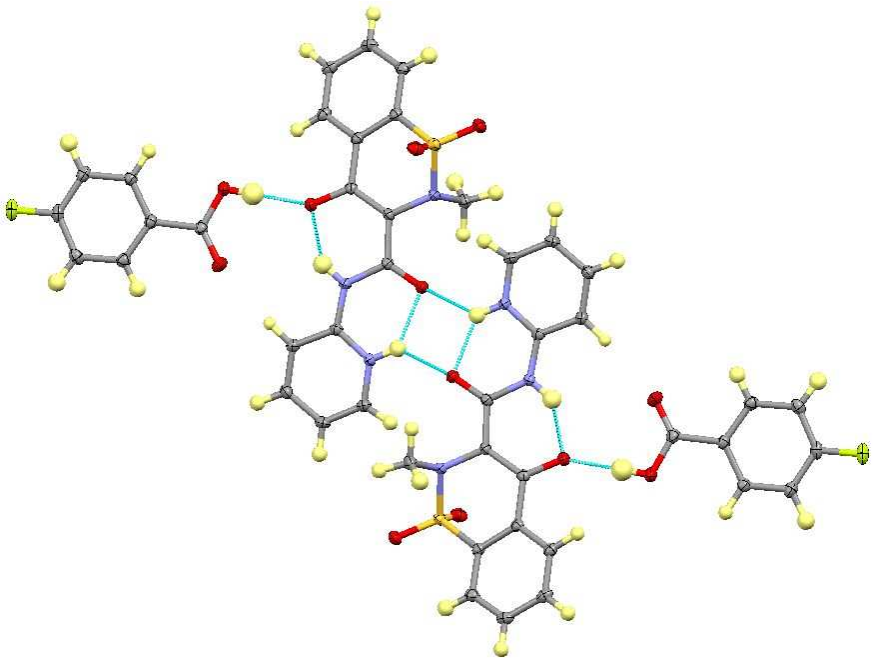

Figure 5.8 *Tetramer in the PXZ:4FBA complex.*

The tetramer differs from that of the other FBA complexes, with the 4FBA molecules lying much further out of plane of the piroxicam molecules (Figure 5.9a). The OH···O hydrogen bond between the PXZ molecule and the 4FBA molecule is weaker than in the 2- and 3FBA complexes and there is a stronger intramolecular NH···O hydrogen bond. Further differences are seen in the relative arrangement of molecules above and below each other. The PXZ molecules interact via π···π interactions and lie head to tail almost directly above each other in the 2FBA and 3FBA complexes, with the pyridine ring forming further π-interactions with the BA molecule (Figure 5.9b). In the 4FBA complex, the PXZ molecules are more staggered relative to each other with only the benzene rings overlapping - forming π···π interactions - and no π···π interactions are formed with 4FBA (also Figure 5.9b). The PXZ molecules arrange into planar layers with the out of plane 4FBA molecules intersecting the layers diagonally (Figure 5.9c). The F atom also forms weak hydrogen bonds between layers. These hydrogen bonds are formed with the aromatic CH of another 4FBA molecule (C···F = 3.280(2) Å) as well as the methyl CH of a PXZ molecule (C···F = 3.464(2) Å) (Figure 5.10). A bifurcated hydrogen bond is also formed with the pyridine ring NH and CH groups of another PXZ molecule (N···F = 2.9187(13) Å, C···F = 3.049(2) Å) (also Figure 5.10).

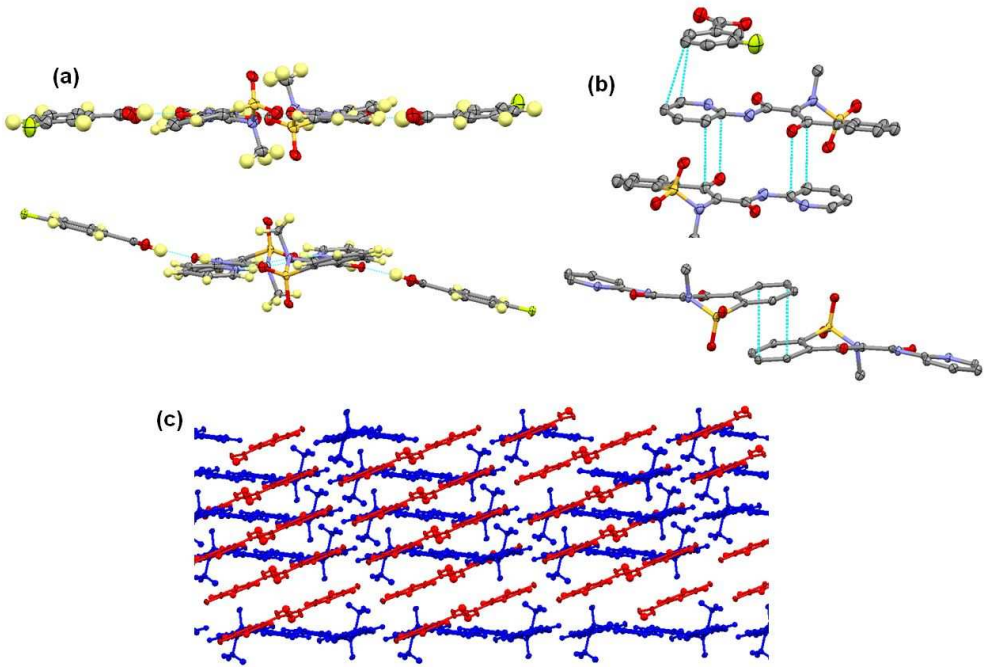

Figure 5.9 *(a) Top, planar tetramers in PXZ:3FBA complex (identical to PXZ:2FBA, not shown) and bottom, non-planar tetramers in PXZ:4FBA. (b) Top, relative arrangement of π-stacked molecules in PXZ:3FBA (identical to PXZ:2FBA, not shown) and bottom, PXZ:4FBA with H-atoms omitted for clarity. (c) Layered structure of PXZ:4FBA, PXZ in blue, 4FBA in red.*

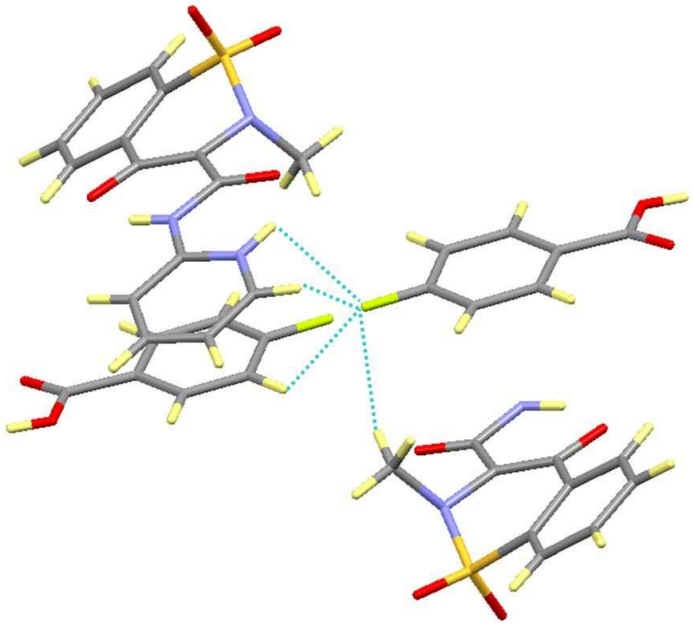

Figure 5.10 *Weak hydrogen bonds involving the fluorine atom in the PXZ:4FBA complex.*

5.2.2.4 Piroxicam: 2-Fluorobenzoic Acid (Non-Ionised Piroxicam) (PXN:2FBA)

The PXN molecules in this complex dimerise but due to the lack of intramolecular H-transfer and the different conformation adopted by non-ionised PXN molecules, the dimer formed is completely different to that seen in the zwitterionic PXZ complexes. The dimer (Figure 5.11), is formed via two equivalent moderately strong hydrogen bonds between the hydroxyl groups and the sulfonyl oxygen atoms (hydrogen bond lengths in Table 5.2), with the two piroxicam molecules lying in different planes related by an inversion centre. The hydrogen bond is bifurcated with a shorter intramolecular hydrogen bond between the OH and the amide carbonyl.

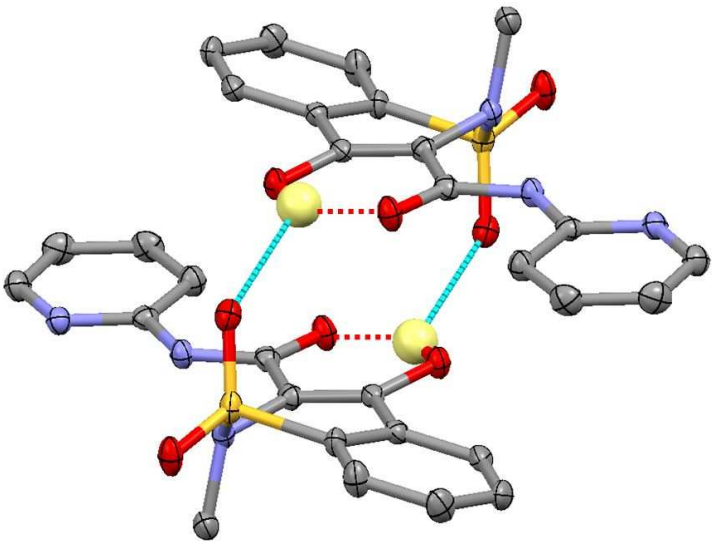

Figure 5.11 *Piroxicam dimer in the PXN:2FBA complex with intermolecular hydrogen bonds shown as blue dashed lines and intramolecular hydrogen bonds shown as red dashed lines. Hydrogen atoms not involved in the hydrogen bonds have been omitted for clarity.*

Table 5.2 *Hydrogen bond lengths and angles in the BNNB tetramer found in non-ionised piroxicam complexes with 2-fluorobenzoic acid and 3-fluorobenzoic acid (refer to Figure 5.12 for key).*

Complex	H-Bond	D-H (Å)	H···A (Å)	D···A (Å)	∠D-H···A (°)
PXN: 2FBA	a	0.89(2)	2.40(2)	2.961(2)	121(2)
	b	0.89(2)	1.79(3)	2.587(2)	149(2)
	c	0.77(2)	2.24(2)	2.997(2)	168(2)
	d	0.89(2)	1.80(2)	2.676(2)	171(2)
PXN: 3FBA	a	0.86(2)	2.44(2)	2.931(2)	117(2)
	b	0.86(2)	1.80(3)	2.591(2)	150(2)
	c	0.86(2)	2.13(2)	2.974(2)	167(2)
	d	0.92(2)	1.77(2)	2.676(2)	169(2)

The 2FBA molecules link to each PXN molecule in the dimer via moderately strong N-H···O hydrogen bonds to form a hydrogen bonded ring, which can be described by graph-set notation $R_2^2(8)$ (Figure 5.12a). This again forms a tetramer-like building block with a BNNB (B = benzoic acid, N = non-ionised piroxicam) configuration (Figure 5.12b), where the PXN-2FBA pair lies relatively coplanar and the inverted pair is staggered relative to the first.

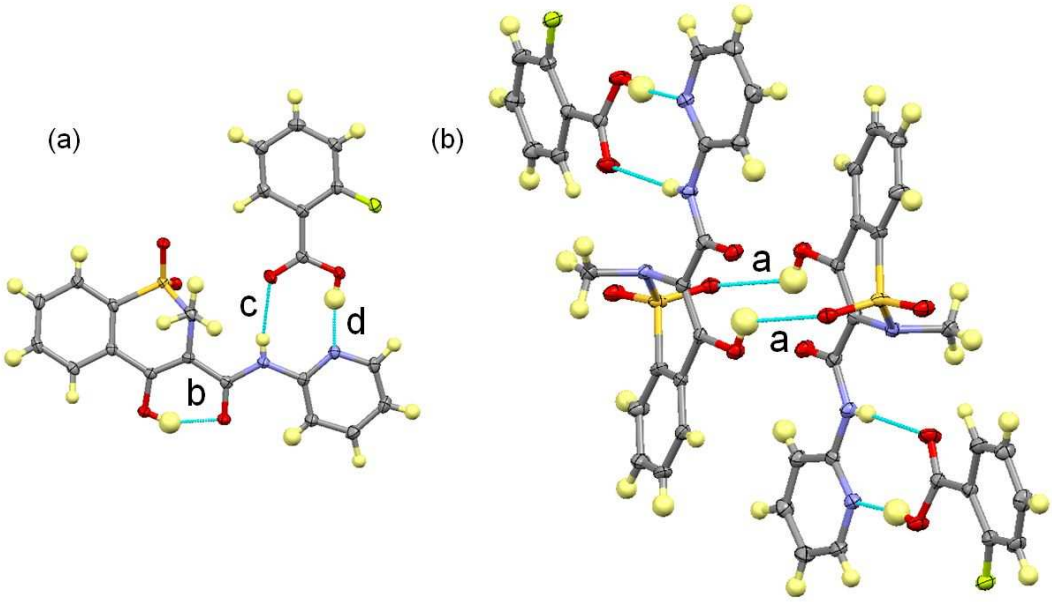

Figure 5.12 *Non-ionised piroxicam complex with 2-fluorobenzoic acid, (a) $R^2_2(8)$ hydrogen bonded ring linking the 2FBA molecule to the PXN molecule and (b) the hydrogen bonded tetramer formed.*

The sulfonyl oxygen involved in the PXN dimer also forms weak CH···O hydrogen bonds with aromatic CH groups of the PXN and 2FBA molecules below (Figure 5.13). The CH group of PXN forms a weak hydrogen bond with the sulfonyl oxygen (C···O = 3.343(2) Å, ∠CHO = 155.7(17)°), whereas the 2FBA CH lies closer (C···O = 3.055(3) Å) but the hydrogen bond is less linear (∠CHO = 108(1)°). The methyl groups, which lie out of the plane of the PXN molecule, also form weak hydrogen bonds to the fluorine (C···F = 3.098(2) Å) and hydroxyl oxygen atoms (C···O = 3.437(2) Å and 3.419(3) Å) of other 2FBA molecules (Figure 5.14). This creates a layered structure, with the methyl groups and sulfonyl oxygen atoms acting as bridges between layers (Figure 5.15).

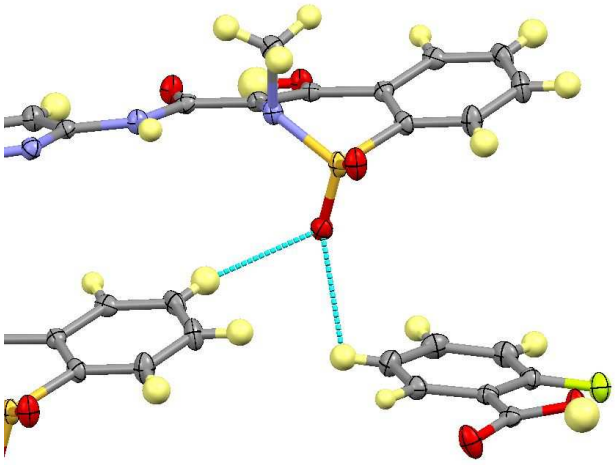

Figure 5.13 *Weak CH···O hydrogen bonds involving the sulfonyl oxygen lying out of the plane in the PXN:2FBA complex.*

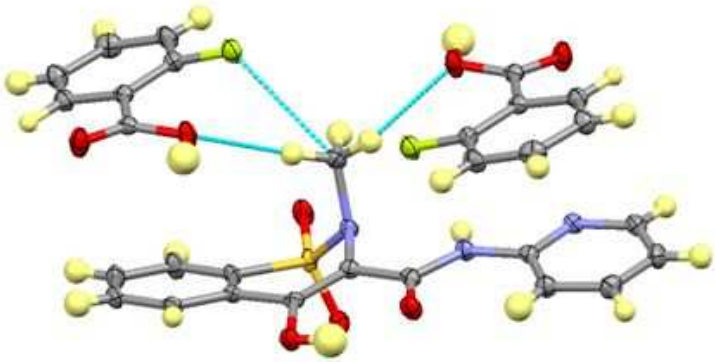

Figure 5.14 *Weak hydrogen bonds involving the methyl group of piroxicam in the PXN:2FBA complex.*

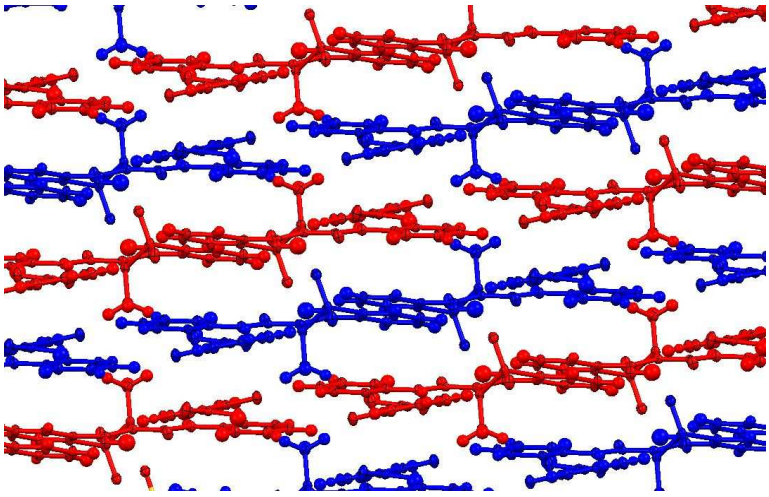

Figure 5.15 *Layered arrangement of the molecules in the PXN:2FBA complex with sulfonyl oxygen and methyl groups bridging the layers (alternate layers shown in different colours).*

5.2.2.5 Piroxicam: 3-Fluorobenzoic Acid (Non-Ionised) (PXN:3FBA)

As in the case of the zwitterionic complexes, the PXN:3FBA complex is isomorphous to the PXN:2FBA complex. The tetramer (Figure 5.16) features a slightly stronger OH···O hydrogen bond between PXN molecules (see Table 5.2) and a slightly stronger NH···O hydrogen bond between the PXN and 3FBA molecules. The intramolecular hydrogen bond in the PXN molecule is slightly weaker, however. The methyl CH···F hydrogen bonds between planes in PXN:2FBA are replaced by weaker aromatic CH···F hydrogen bonds within the planes (C···F = 3.405(2) Å) due to the different fluorine position (Figure 5.17). Consequently, only very slight changes in the packing are seen in the PXN:3FBA complex when compared with the PXN:2FBA complex (Figure 5.18).

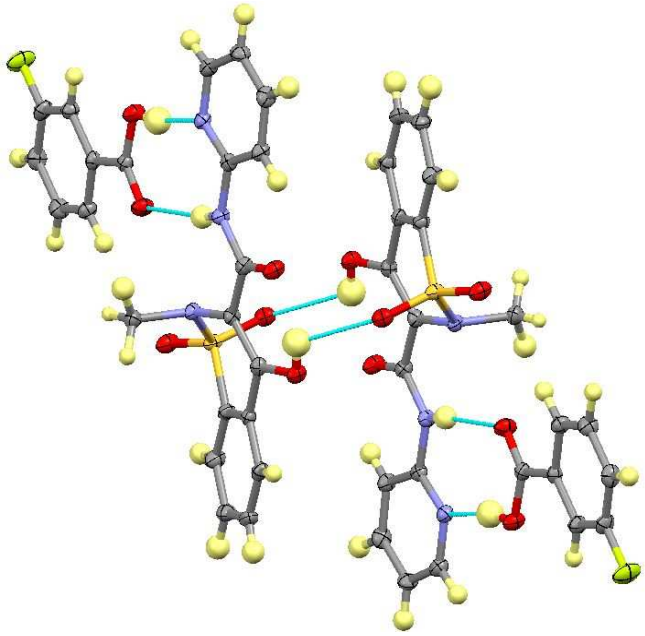

Figure 5.16 *The BNNB tetramer in the PXN:3FBA complex.*

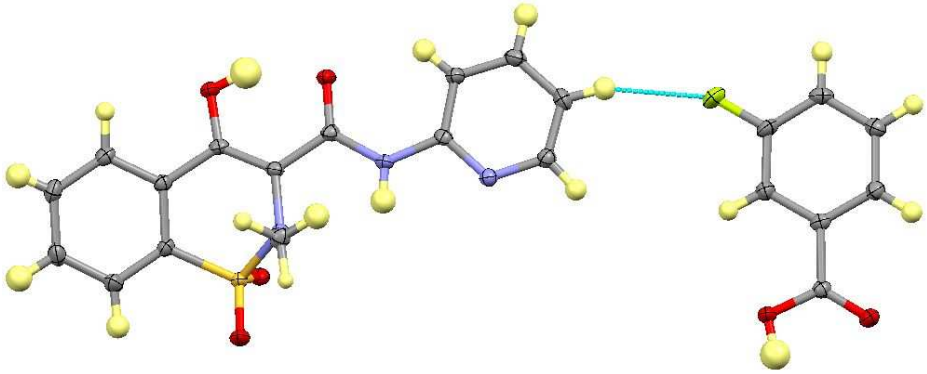

Figure 5.17 *Weak CH···F hydrogen bonds between the co-planar 3FBA and PXN pyridine ring in the PXN:3FBA complex.*

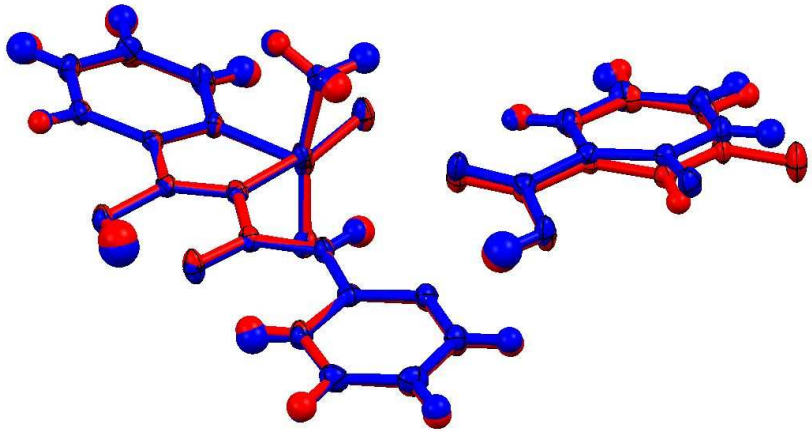

Figure 5.18 *Overlay of the crystal packing of PXN:2FBA (blue) and PXN:3FBA (red) showing the slightly offset position of the FBA molecules relative to the PXN molecules.*

5.2.2.6 Piroxicam: 4-Fluorobenzoic Acid (Non-Ionised) (PXN:4FBA)

Like the zwitterionic structures, the PXN:4FBA complex is not isostructural to the 2- and 3FBA complexes. Once again, the primary building block is a BNNB tetramer-like structure. However, the interactions between PXN molecules are very different (Figure 5.19a).

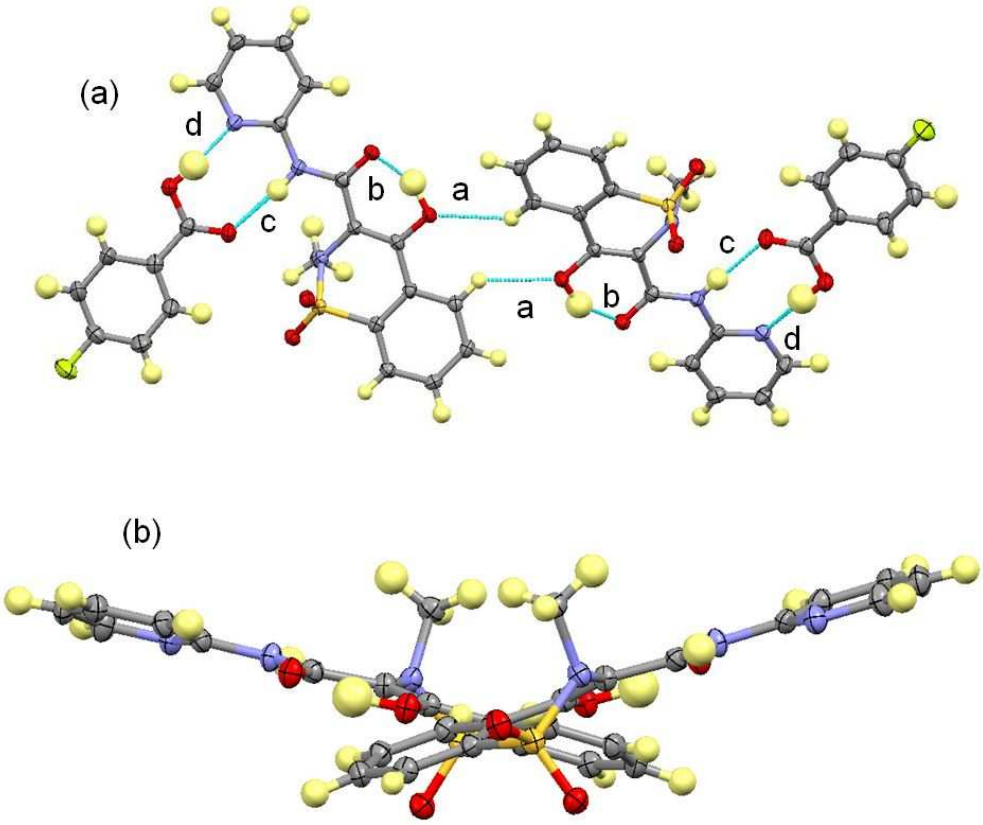

Figure 5.19 (a) the *BNNB tetramer in the PXN:4FBA complex, (b) the relative planes of the PXN molecules in the PXN dimer.*

Table 5.3 *Hydrogen bond lengths and angles in the PXN:4FBA complex (refer to Figures 5.19a and 5.20 for key). Corresponding hydrogen bond distances for the PXN:2FBA and PXN:3FBA complexes are shown where relevant.*

Complex	H-Bond	D-H (Å)	H···A (Å)	D···A (Å)	∠ D-H···A (°)
PXN: 4FBA	a	0.97(2)	2.44(2)	3.207(2)	135.8(14)
	b	1.07(2)	1.52(2)	2.508(2)	150(2)
	c	0.94(2)	1.98(2)	2.905(2)	173(2)
	d	0.969(3)	1.76(3)	2.715(2)	175(3)
	e	0.95(2)	2.54(2)	3.445(3)	159(2)
PXN: 2FBA	b	0.89(2)	1.79(3)	2.587(2)	149(2)
	c	0.77(2)	2.24(2)	2.997(2)	168(2)
	d	0.89(2)	1.80(2)	2.676(2)	171(2)
PXN: 3FBA	b	0.86(2)	1.80(3)	2.591(2)	150(2)
	c	0.86(2)	2.13(2)	2.974(2)	167(2)
	d	0.92(2)	1.77(2)	2.676(2)	169(2)

The 4FBA molecules link to the PXN molecules in the same way as the 2- and 3FBA complexes by forming the hydrogen bonded $R_2^2(8)$ ring, but in this case the O-H···O interactions between PXN molecules are replaced by weak CH···O interactions between aromatic CH groups and the hydroxyl oxygen atoms (hydrogen bond distances in Table 5.3). The PXN dimers lie diagonal relative to each other (Figure 5.19b) and the CH···O hydrogen bonds are considerably weaker (Table 5.3) than the OH···O hydrogen bonds in the 2FBA and 3FBA complexes. The $R_2^2(8)$ ring consists of a stronger NH···O interaction and a weaker OH···N interaction than the aforementioned complexes. The intramolecular OH···O hydrogen bond in PXN is significantly stronger in the 4FBA complex, presumably due to the lack of a second donor pulling the hydrogen atom towards it - which is the case in the 2FBA and 3FBA complexes. Dimers are also formed between 4FBA molecules by weak CH···F hydrogen bonds (Figure 5.20). PXN molecules above and below each other interact via further weak hydrogen bonds to the sulfonyl oxygen atom formed by the methyl group (C···O = 3.184(3) Å) and CH group (C···O = 3.308(2) Å) of two other PXN molecules above (Figure 5.21).

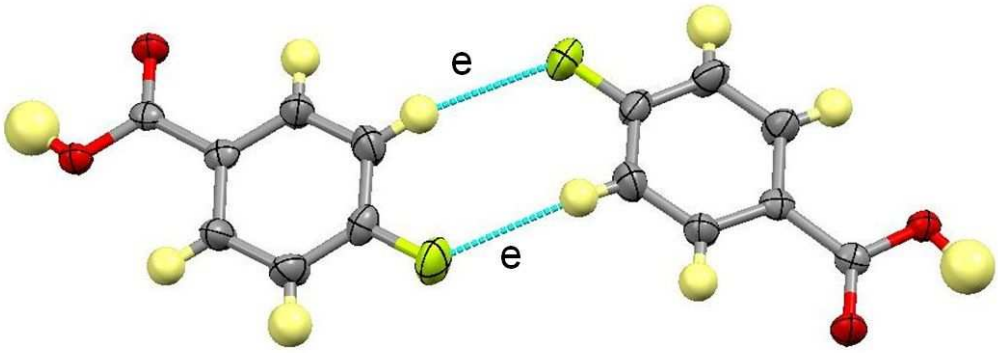

Figure 5.20 *CH···F dimers between 4FBA molecules in the PXN:4FBA complex.*

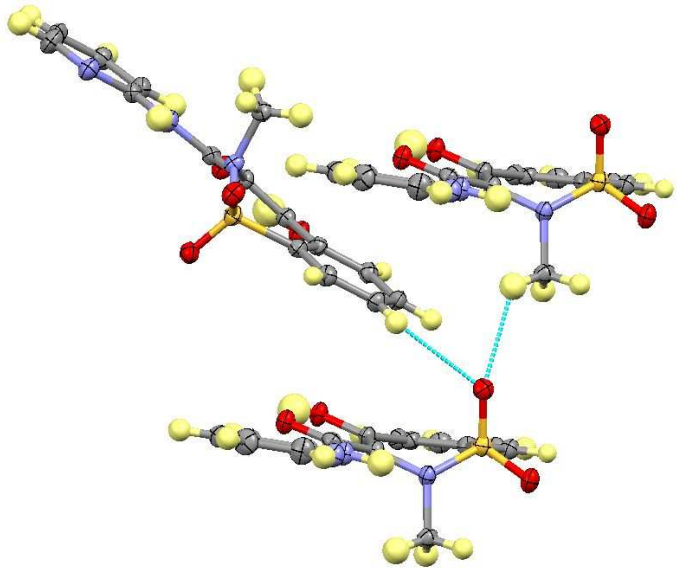

Figure 5.21 *CH···O interactions between the sulfonyl oxygen and the methyl and aromatic CH groups of PXN molecules above in the PXN:4FBA complex.*

Due to the PXN dimers lying out of plane with each other, the overall structure is built up of zigzagging bilayers (Figure 5.22), with the CH···O interactions in Figure 5.21 bridging across the interface of the bilayers.

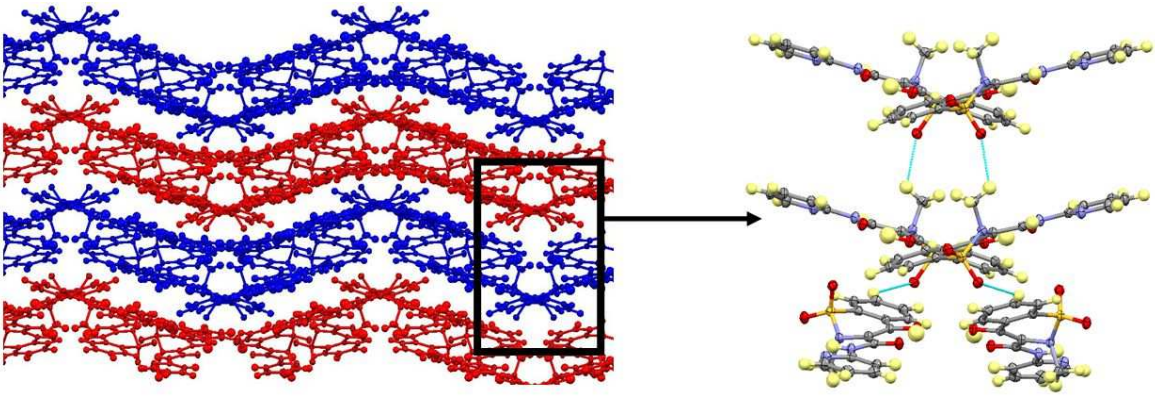

Figure 5.22 *Bilayers in the PXN:4FBA complex with alternate bilayers shown in different colours and the arrangement of the weak hydrogen bonds at the interface of the bilayers.*

5.3 Tautomerism in other Complexes of Piroxicam with Mono-substituted Benzoic Acids

Of the twenty molecular complexes crystallised, polymorphism was not observed in the remaining fourteen. The tautomer present in each of these complexes varied, however, depending on the particular mono-substituted benzoic acid present in the complex.

5.3.1 Crystallisation Conditions

Crystallisations were carried out according to the procedure outlined in Chapter 3. Table 5.4 below outlines the solvent and temperature systems under which each molecular complex described in this section was observed to crystallise. Crystallographic data and full refinement details can be found in (Appendix A5).

Table 5.4 *Crystallisation conditions for molecular complexes of piroxicam with mono-substituted benzoic acids.*

Piroxicam Molecular Complex	Solvent	Temp (°C)
2-Chlorobenzoic Acid	Acetonitrile	RT/40/50
3-Chlorobenzoic Acid	Acetonitrile	40/50
2-Bromobenzoic Acid	Acetonitrile	40/50
3-Bromobenzoic Acid	Acetonitrile	40/50
2-Hydroxybenzoic Acid	Acetonitrile	RT/40/50
3-Hydroxybenzoic Acid Monohydrate	Acetonitrile	RT
2-Nitrobenzoic Acid	Acetonitrile	50
3-Nitrobenzoic Acid	Acetonitrile/Methanol 2:1 V/V	50
4-Nitrobenzoic Acid (Hydrate)	Acetonitrile	50
2-Methylbenzoic Acid	Acetonitrile	50
3-Methylbenzoic Acid	Acetonitrile	40/50
3-Methylbenzoic Acid: Acetonitrile Solvate	Acetonitrile	RT
4-Methylbenzoic Acid	Acetonitrile	40/50
2-Aminobenzoic Acid	Acetonitrile	40/50

RT = Room Temperature

5.3.1.1 Piroxicam: 2-Chlorobenzoic Acid (Zwitterionic) (PXZ:2CLBA)

PX in this complex is present as the zwitterionic tautomer, and the structure is built up from the BZZB unit that is present in the PXZ:FBA complexes (Figure 5.23). The structure consists of relatively flat layers, with the methyl and sulfonyl groups bridging between layers (Figure 5.24). Unlike the previous zwitterionic complexes described, the

asymmetric unit consists of two PXZ molecules and two 2CLBA molecules and the BZZB tetramer is made up of two independent molecules of both the PXZ and the 2CLBA. Hydrogen bond lengths in the tetramer are shown in Table 5.5. One 2CLBA molecule has a twisted conformation, with the carboxylic group out of plane with the benzene ring. The molecule has a torsion angle of approximately 98° between the carboxylic acid carbonyl oxygen, the carbon of the carboxylic acid and the aromatic carbons in the 1- and 4-positions (c.f. 174° for the symmetry independent 2CLBA molecule).

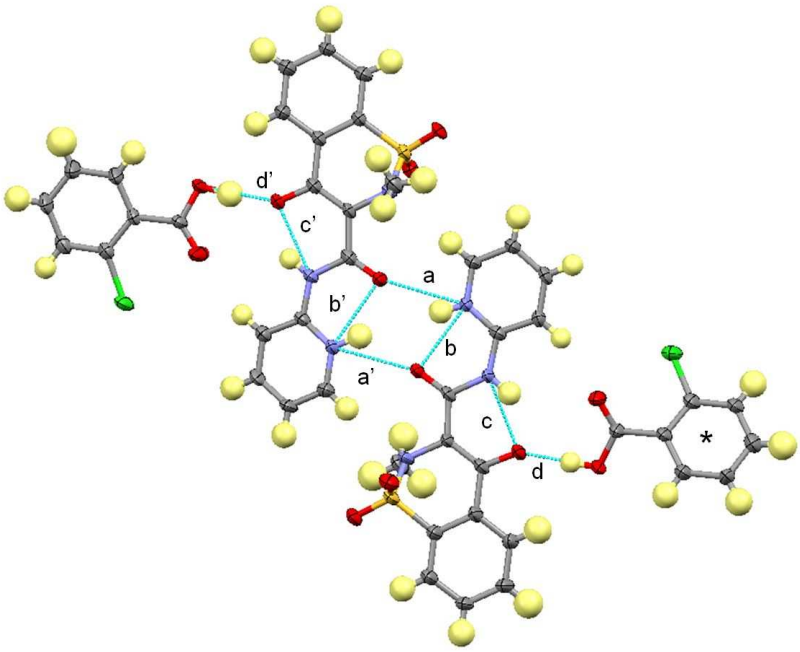

Figure 5.23 *The BZZB tetramer in the PXZ:2CLBA molecular complex. * indicates the twisted 2CLBA molecule.*

Table 5.5 *Hydrogen bond lengths and angles in the PXZ:2CLBA tetramer (refer to Figure 5.23 for key).*

Complex	H-Bond	D-H (Å)	H···A (Å)	D···A (Å)	∠ D-H···A (°)
PXZ: 2CLBA	a	0.84(6)	2.17(6)	2.842(6)	137(5)
	a’	0.94(6)	2.11(6)	2.791(6)	128(5)
	b	0.84(6)	2.00(6)	2.597(6)	127(5)
	b’	0.94(6)	1.91(6)	2.623(6)	131(5)
	c	0.86	1.88	2.593(6)	139
	c’	0.86	1.83	2.557(6)	141
	d	0.90(6)	1.66(6)	2.550(6)	179(8)
	d’	0.97(9)	1.61(9)	2.566(6)	168(5)

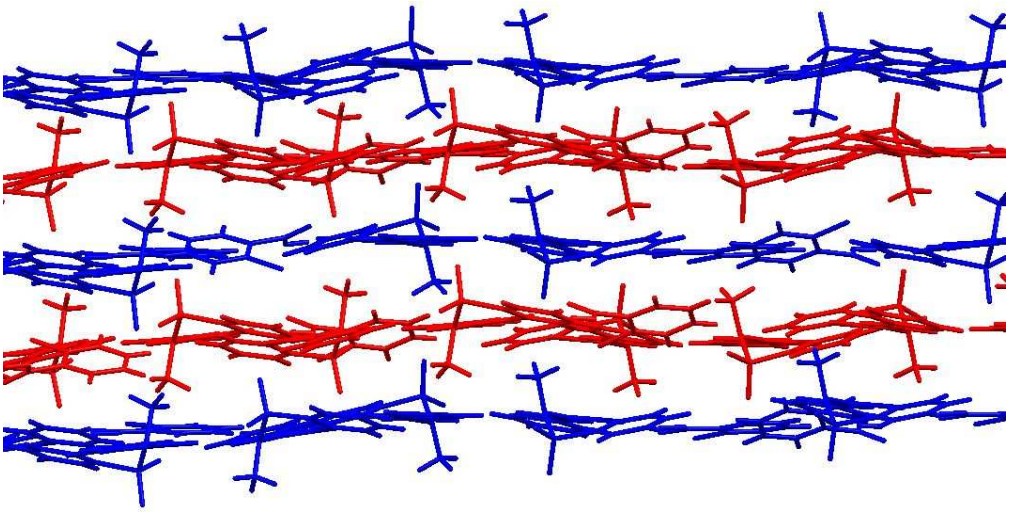

Figure 5.24 *Layered structure in the PXZ:2CLBA complex with methyl groups and sulfonyl oxygen atoms bridging between layers (alternate layers shown in different colours).*

The BZZB units are linked within the layers by weak CH···O=S hydrogen bonds (C···O = 3.346(3) Å and 3.468(3) Å) on both sides of the tetramer (Figure 5.25). Benzene ring CH groups of the PX molecule above form a weak hydrogen bond to the twisted carbonyl O (C···O = 3.460(9) Å) as well as a weak CH···π interaction with the aromatic π cloud (approx. 3.308 Å between the carbon and the plane of the benzene ring (Figure 5.26a). The more planar 2CLBA molecule forms π···π interactions with the pyridine rings of PXZ molecules above and below it (approx. 3.472 Å (PXZ above) and 3.423 Å (PXZ below) between the two closest aromatic C-C bonds, as shown in Figure 5.26b)**.** The bridging methyl groups and sulfonyl oxygen atoms interact via weak hydrogen bonds (C···O = 3.186(3) Å) (Figure 5.27) with the methyl group also forming weak interactions with the chlorine of the 2CLBA in the next layer (3.576(2) Å) (also figure 5.27).

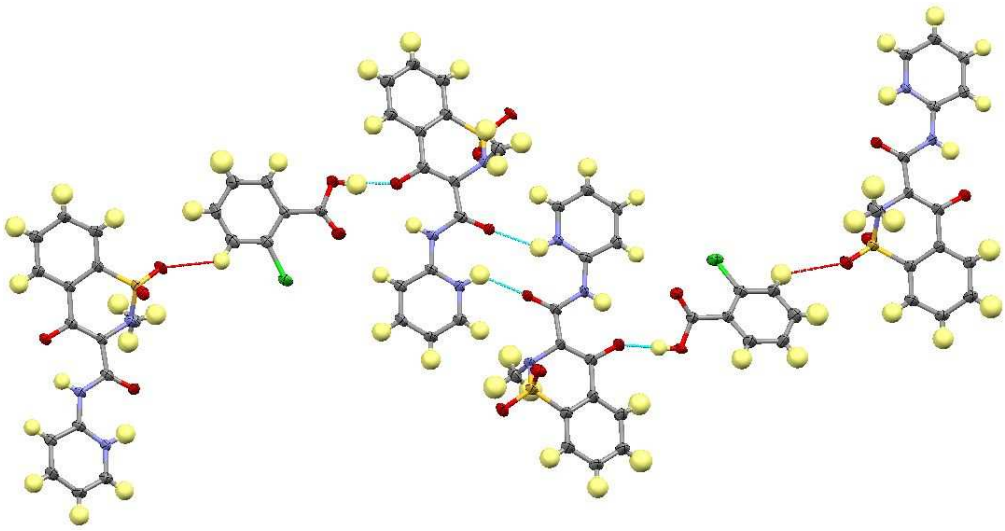

Figure 5.25 *The weak CH···O interactions (red dashed) linking tetramers within the layers in the PXZ:2CLBA complex.*

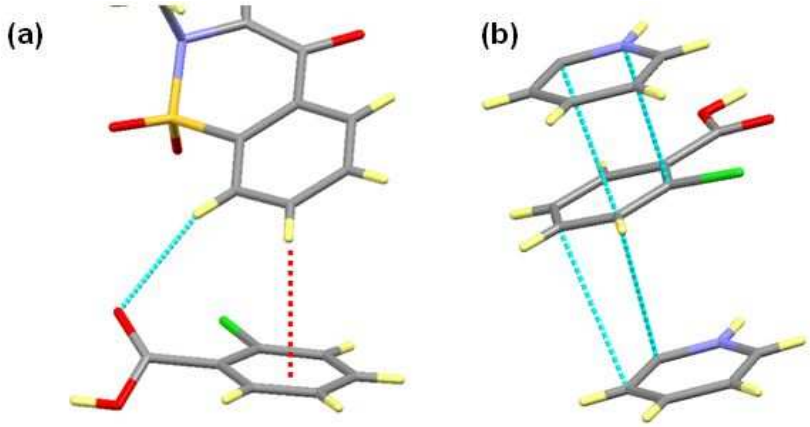

Figure 5.26 *Differing weak interactions formed by symmetry independent 2CLBA molecules in the PXZ:2CLBA complex. (a) CH···O hydrogen bond (blue dashed line) and CH···π interactions (red dashed) in twisted 2CLBA molecule. (b) π···π interactions in planar 2CLBA.*

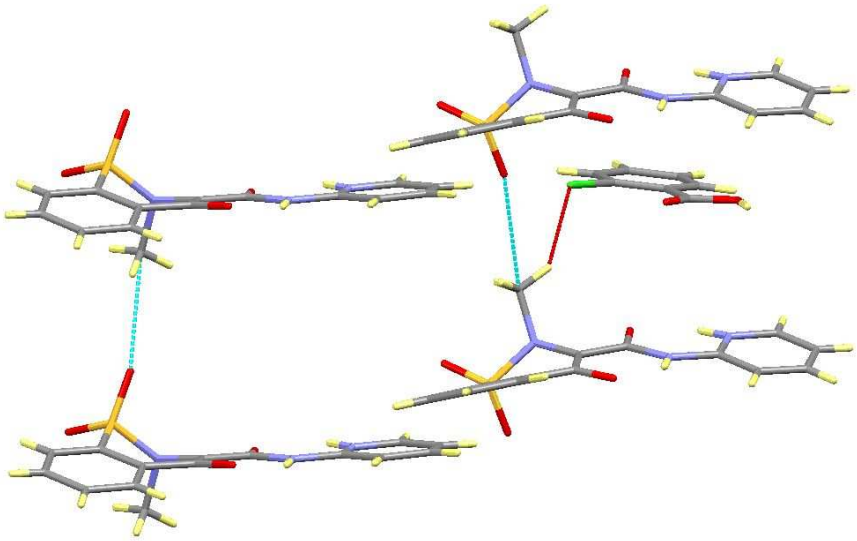

Figure 5.27 *Weak methyl CH···O hydrogen bonds (blue dashed lines) and methyl CH···Cl interactions (red dashed lines) bridging layers in PXZ:2CLBA.*

5.3.1.2 Piroxicam : 3-Chlorobenzoic Acid (Non-Ionised) (PXN:3CLBA)

In the PXN:3CLBA complex, non-ionised PXN molecules dimerise, forming a new synthon, different to any of the non-ionised PXN : fluorobenzoic acid complexes (Figure 5.28). The dimers consist of bifurcated DHAA intra- and intermolecular OH···O=C hydrogen bonds with an $R_2^2(6)$ hydrogen bonded ring formed lying on an inversion centre. The intramolecular interaction is considerably shorter than the intermolecular interaction (see Table 5.6). The 3CLBA molecule is linked to both sides of the dimer via the same $R_2^2(8)$ hydrogen bonding seen in the PXN:FBA complexes, forming a new type of BNNB tetramer.

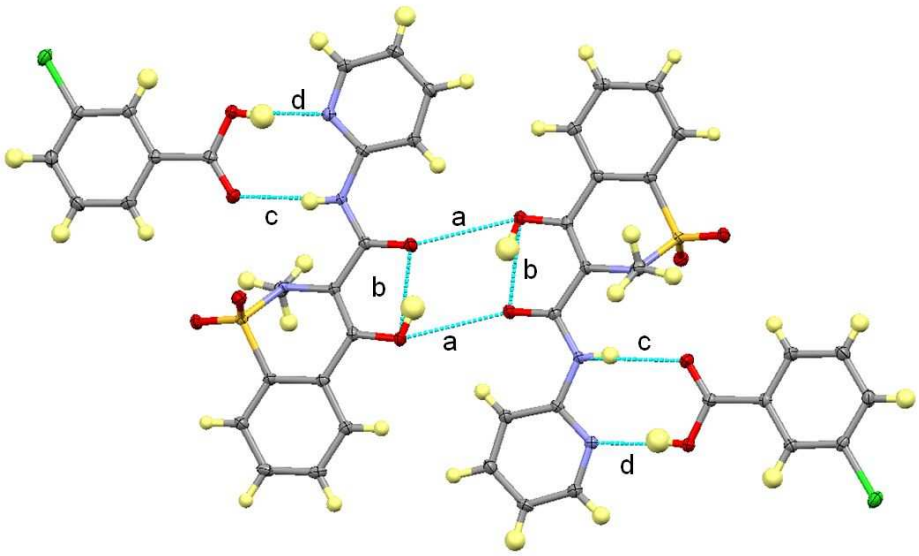

Figure 5.28 *The BNNB tetramer in the PXN:3CLBA molecular complex.*

Table 5.6 *Hydrogen bond lengths and angles in the BNNB tetramer for complexes featuring the OH···O=C PXN homodimer (refer to Figure 5.28 for key).*

Complex	H-Bond	D-H (Å)	H···A (Å)	D···A (Å)	∠ D-H···A (°)
PXN: 3CLBA	a	0.90(2)	2.56(2)	2.9818(15)	109(2)
	b	0.90(2)	1.74(3)	2.5793(16)	155(2)
	c	0.84(2)	2.14(2)	2.965(2)	167(2)
	d	0.83(2)	1.82(2)	2.648(2)	171(3)
PXN: 3BRBA	a	0.84(3)	2.49(3)	2.992(3)	120(3)
	b	0.84(3)	1.84(3)	2.578(3)	146(3)
	c	0.86(2)	2.12(2)	2.968(3)	167(2)
	d	0.88(4)	1.79(4)	2.660(3)	169(4)
PXN: 3NBA	a	0.89(2)	2.52(2)	3.011(2)	115(2)
	b	0.89(2)	1.78(3)	2.573(2)	148(2)
	c	0.85(2)	2.12(2)	2.970(2)	172(2)
	d	0.88(2)	1.75(2)	2.618(2)	171(3)
PXN: 4NBA	a	0.89(3)	2.51(3)	3.075(2)	122(2)
	a’	0.89(3)	2.53(3)	3.128(2)	125(2)
	b	0.89(3)	1.78(3)	2.592(2)	151(3)
	b’	0.89(3)	1.80(3)	2.609(2)	150(3)
	c	0.92(3)	2.08(3)	2.982(3)	167(2)
	c’	0.92(2)	2.09(2)	2.998(2)	171(2)
	d	0.93(3)	1.70(3)	2.626(3)	172(3)
	d’	0.97(3)	1.64(3)	2.598(2)	170(3)

Once again the structure consists of relatively planar layers (Figure 5.29) with the methyl group and sulfonyl oxygen bridging the layers. The methyl group forms a weak hydrogen bond to the 3CLBA hydroxyl oxygen atom (C···O = 3.330(2) Å) as well as a very weak hydrogen bond to the chlorine atom (C···Cl = 3.857(2) Å) (Figure 5.30a). PXN molecules

above and below each other are also linked through weak hydrogen bonds between the aromatic CH groups and the sulfonyl oxygen atoms (C···O = 3.222(2) Å and 3.287(2) Å) (Figure 5.30b). The tetramer building blocks are held together in the layers via weak hydrogen bonds between the aromatic CH groups of the 3CLBA and the co-planar sulfonyl oxygen of PXN (C···O = 3.215(2) Å) (Figure 5.31).

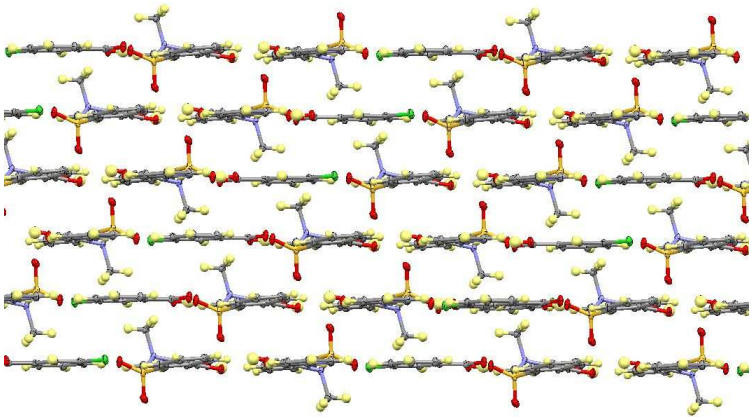

Figure 5.29 *Layered arrangement of the molecule in PXN:3CLBA.*

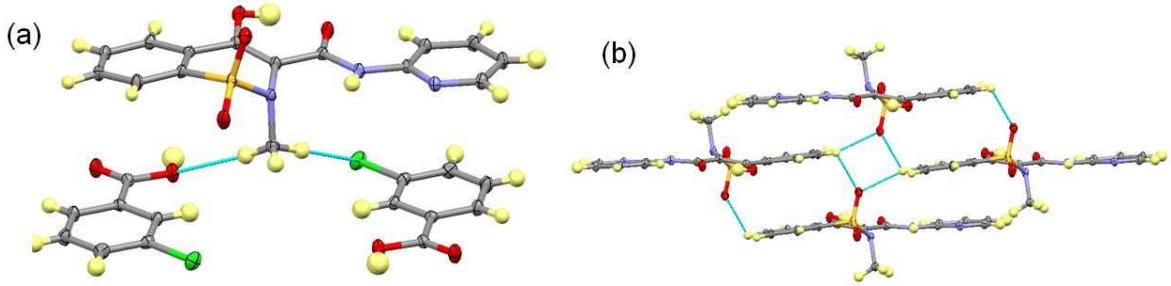

Figure 5.30 *Weak hydrogen bonds in the PXN:3CLBA complex. (a) Weak CH···O and CH···Cl hydrogen bonds between layers involving the methyl group, (b) weak aromatic CH···O hydrogen bonds between layers involving the sulfonyl oxygen***.**

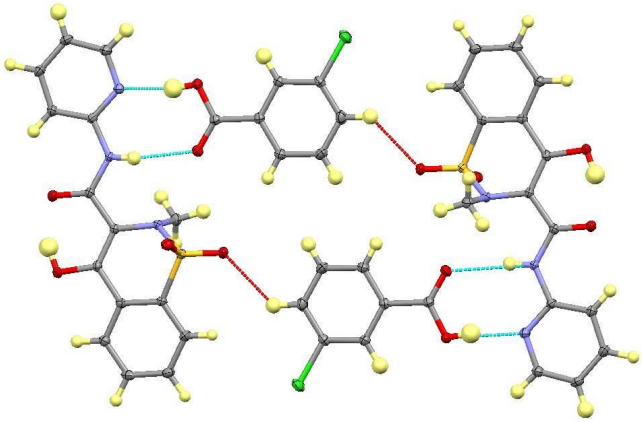

Figure 5.31 *Weak CH···O hydrogen bonds linking tetramers within layers involving the aromatic CH group of 3CLBA and the co-planar sulfonyl oxygen of PXN in the PXN:3CLBA complex.*

5.3.1.3 Piroxicam: 2-Bromobenzoic Acid (Zwitterionic) (PXZ:2BRBA)

The zwitterionic PXZ:2BRBA complex again features the BZZB tetramer (Figure 5.32). The hydrogen bonds in the tetramer are similar in strength to those in the FBA complexes (see Table 5.7).

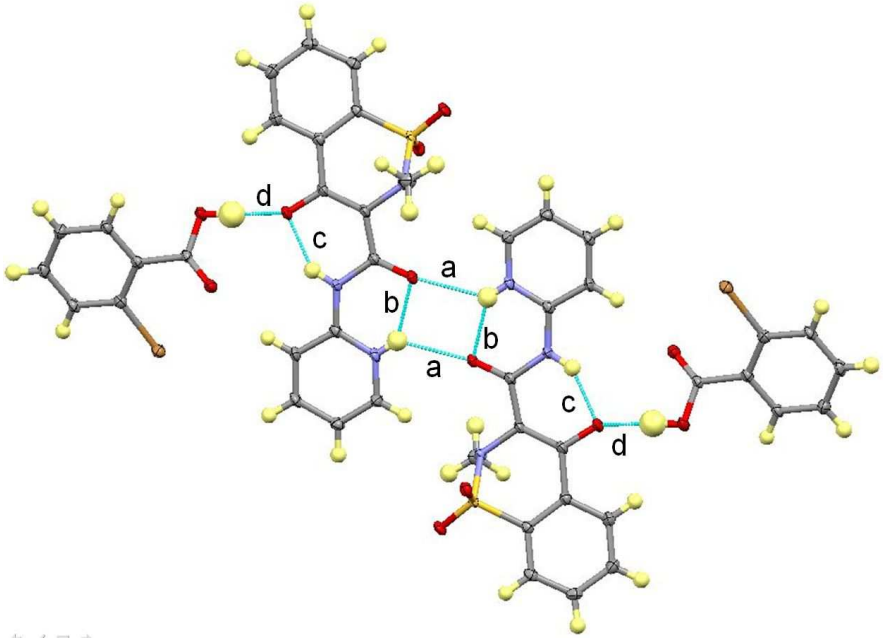

Figure 5.32 *BZZB tetramer in the PXZ:2BRBA complex*

The structure is layered (Figure 5.33), with the BZZB units in the layers held together by weak bifurcated DDHHA CH···O hydrogen bonds (C···O = 3.252(3) Å and 3.273(3) Å) between the aromatic CH groups of the 2BRBA and the sulfonyl O of PXZ similar to the

2CLBA complex (Figure 5.34). PXZ molecules above and below each other are staggered, with the other sulfonyl bridging between layers, forming weak aromatic CH···O=S hydrogen bonds (Figure 5.35a). There are also short contacts between this sulfonyl oxygen and the bromine atom of the 2BRBA (O···Br = 2.993(2) Å, c.f. sum of vdW radii = 3.037 Å). The carboxylic acid group of 2BRBA twists out of the plane of the benzene ring, a consequence of the larger bromine atom positioned adjacent to it. The molecule has a torsion angle of approximately 120° between the carboxylic acid carbonyl oxygen, the carbon of the carboxylic acid and the aromatic carbons in the 1- and 4-positions. The PXZ methyl group also bridges between layers, forming a weak CH···O hydrogen bond (C···O = 3.372(4) Å) to the hydroxyl O of the carboxylic group (Figure 5.35b).

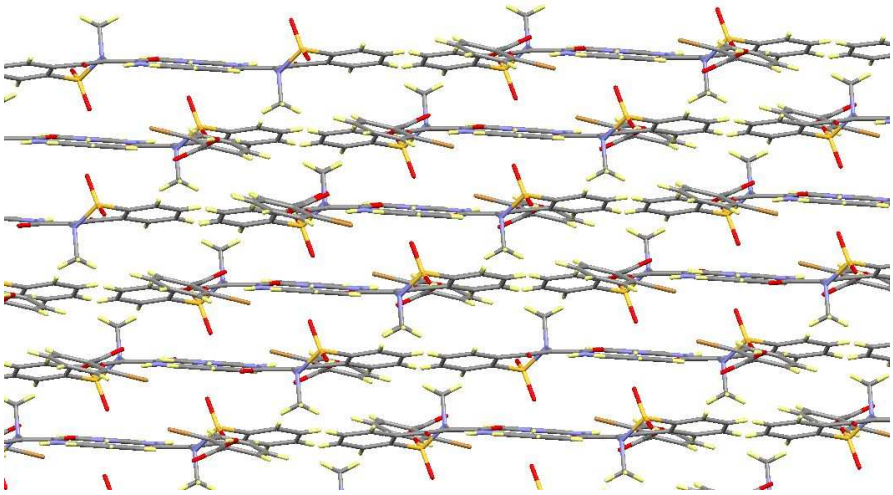

Figure 5.33 *The layered structure of the PXZ:2BRBA complex.*

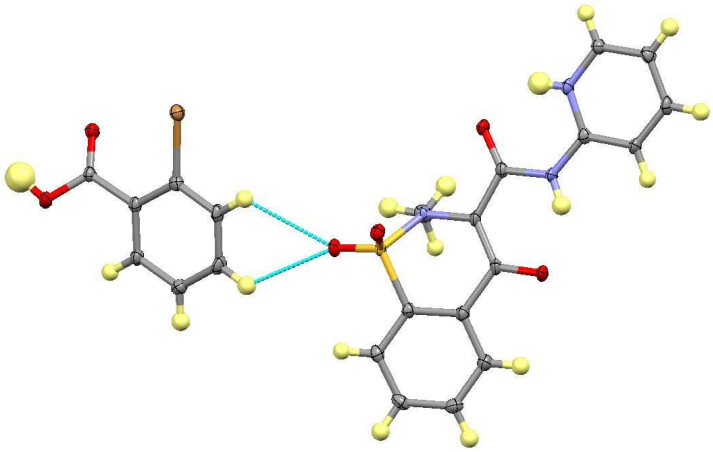

Figure 5.34 *Bifurcated CH···O hydrogen bonds between the 2BRBA aromatic CH groups and the sulfonyl oxygen atoms of the PXZ molecule in PXZ:2BRBA.*

Table 5.7 *Hydrogen bond lengths and angles in the BZZB tetramer of the molecular complexes featuring piroxicam in the zwitterionic form (see Figure 5.23 for key).*

Note: * indicates two independent molecules of each component in asymmetric unit

Complex	H-Bond	D-H (Å)	H···A (Å)	D···A (Å)	∠ D-H···A (°)
PXZ: 2CLBA*	a	0.84(6)	2.17(6)	2.842(6)	137(5)
	a’	0.94(6)	2.11(6)	2.791(6)	128(5)
	b	0.84(6)	2.00(6)	2.597(6)	127(5)
	b’	0.94(6)	1.91(6)	2.623(6)	131(5)
	c	0.86	1.88	2.593(6)	139
	c’	0.86	1.83	2.557(6)	141
	d	0.90(6)	1.66(6)	2.550(6)	179(8)
	d’	0.97(9)	1.61(9)	2.566(6)	168(5)
PXZ: 2BRBA	a	0.80(4)	2.29(4)	2.874(3)	131(3)
	b	0.80(4)	2.02(4)	2.660(3)	138(3)
	c	0.85(3)	1.85(3)	2.575(3)	144(3)
	d	0.91(5)	1.65(5)	2.558(3)	176(3)
PXZ: 2HBA	a	0.86(3)	2.27(3)	2.929(3)	133(3)
	b	0.86(3)	1.97(3)	2.655(3)	136(3)
	c	0.88(3)	1.80(3)	2.573(3)	146(2)
	d	0.99(4)	1.55(4)	2.533(3)	171(4)
PXZ: 3HBA (Monohydrate)	a	0.99(4)	2.12(4)	2.907(4)	135(3)
	b	0.99(4)	1.88(4)	2.629(4)	131(3)
	c	0.86	1.91	2.622(4)	139
	d	1.03(5)	1.57(5)	2.587(4)	168(5)
PXZ: 2NBA	a	0.88(2)	2.29(3)	2.896(2)	126(2)
	b	0.88(2)	1.98(2)	2.643(2)	131(2)
	c	0.88(3)	1.83(3)	2.590(2)	144(3)
	d	0.89(3)	1.69(3)	2.584(2)	176(3)
PXZ: 3MBA	a	0.88(4)	2.18(4)	2.865(3)	135(3)
	b	0.88(4)	1.96(3)	2.625(3)	131(3)
	c	0.88(4)	1.85(3)	2.607(3)	143(3)
	d	0.90(4)	1.68(4)	2.581(3)	179(5)
PXZ: 3MBA (ACN Solvate)	a	0.95(4)	2.15(4)	2.862(3)	132(3)
	b	0.95(4)	1.92(4)	2.625(3)	129(3)
	c	0.88(4)	1.83(4)	2.596(3)	145(3)
	d	0.81(10)	1.80(11)	2.597(7)	171(8)
PXZ: 4MBA	a	0.95(4)	2.12(4)	2.859(4)	133(3)
	b	0.95(4)	1.92(3)	2.658(3)	133(3)
	c	0.90(4)	1.79(4)	2.577(3)	145(3)
	d	0.98(5)	1.65(5)	2.582(3)	157(5)
PXZ: 2ABA	a	0.93(3)	2.16(3)	2.843(3)	130(3)
	b	0.93(3)	1.94(3)	2.651(3)	132(3)
	c	0.89(3)	1.74(2)	2.548(3)	149(2)
	d	0.86(4)	1.73(4)	2.594(2)	173(3)

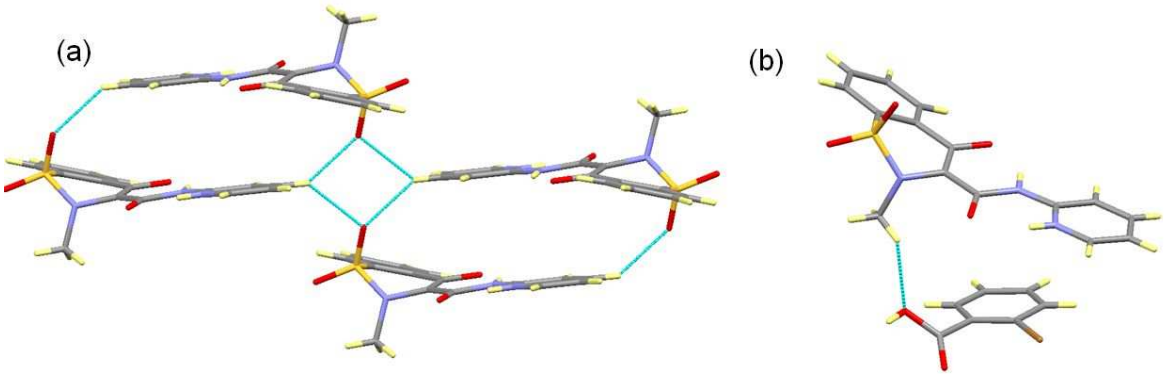

Figure 5.35 *Weak hydrogen bonds involving bridging sulfonyl oxygen atoms (a) and methyl groups (b).*

5.3.1.4 Piroxicam: 3-Bromobenzoic Acid (Non-Ionised) (PXN: 3BRBA)

PX in this complex is in the non-ionised tautomeric form and the structure is isomorphous to that of the PXN:3CLBA complex, featuring the same BNNB tetramer with the CH···O=C dimer at the centre. The PX dimer has a slightly weaker intermolecular interaction and a slightly stronger intramolecular interaction than the isomorphic 3CLBA complex (see Table 5.6). The interactions in the $R_2^2(6)$ ring between PXN molecules and 3BRBA molecules are both slightly weaker than in the 3CLBA complex. The difference in these interactions is very slight and an overlay of the 3BRBA and 3CLBA structures (Figure 5.37) shows them to be almost identical in the relative positions of the molecules.

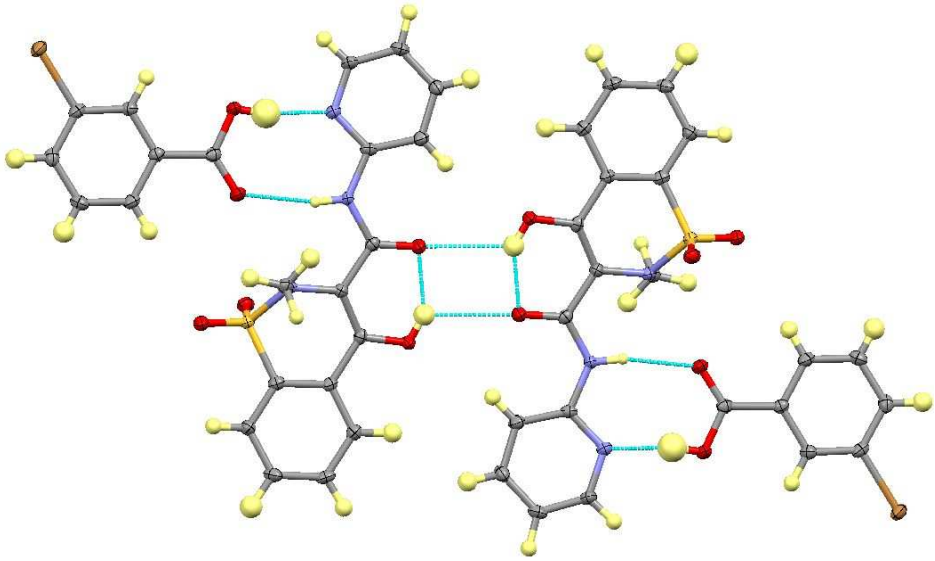

Figure 5.36 *The BNNB tetramer in the PXN:3BRBA complex.*

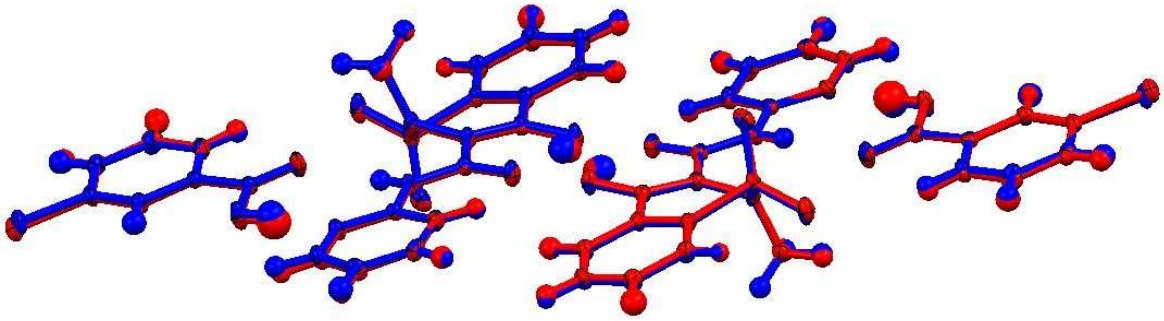

Figure 5.37 *An overlay of the isomorphous PXN:3BRBA (red) and PXN:3CLBA (blue) complexes.*

5.3.1.5 Piroxicam: 2-Hydroxybenzoic Acid (Zwitterionic) (PXZ:2HBA)

The PXZ:2HBA complex contains zwitterionic PXZ molecules with the BZZB tetramer again the structural unit (Figure 5.38a). The interactions in the BZZB tetramer are interesting when compared to the others, as the NH···O interactions between PXZ molecules are the weakest of all the zwitterionic complexes but the OH···O interactions between the PXZ and 2HBA molecules are the strongest (Table 5.7). The OH group of 2HBA does not form any intermolecular hydrogen bonds with the only interaction involving this group being a moderately strong intramolecular hydrogen bond with the carbonyl O (O···O = 2.624(3) Å). The 2HBA molecule is twisted relative to the PXZ molecule (Figure 5.38b) and is involved in a number of weak hydrogen bonds.

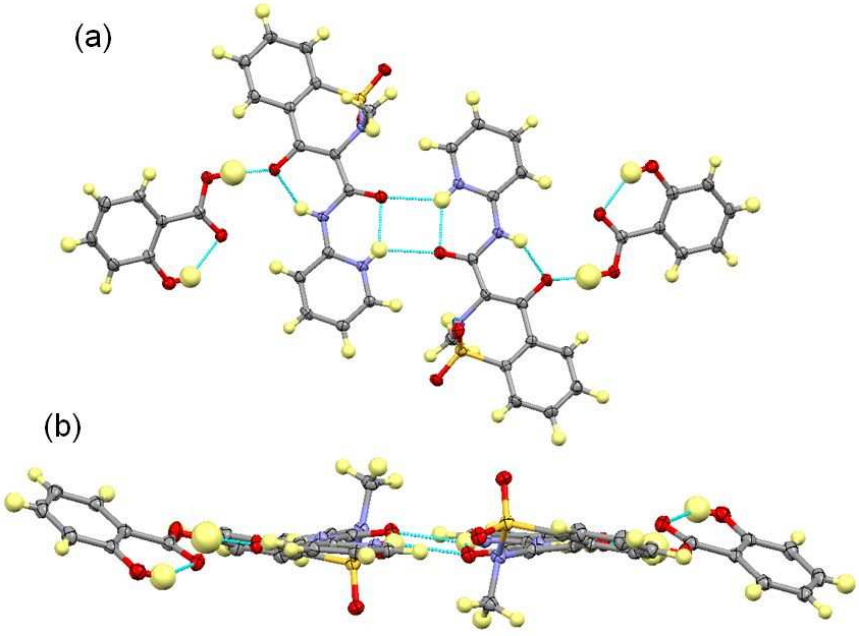

Figure 5.38 *(a) The PXZ:2HBA tetramer, (b) the tetramer rotated 90° showing the twisted 2HBA molecules relative to the plane of the PXZ molecules .*

The aromatic CH groups of 2HBA form weak hydrogen bonds to the sulfonyl oxygen atoms of two PXZ molecules (C···O = 3.319(3) Å and 3.437(3) Å) as well as the hydroxyl O of a neighbouring 2HBA molecule (C···O = 3.503(3) Å) (Figure 5.39a). PXZ molecules above and below each other are linked by further weak hydrogen bonds between the pyridinal CH groups and the sulfonyl oxygen atoms (C···O = 3.317(3) Å) (Figure 5.39b). This gives the PXZ dimers a step-like arrangement relative to each other (Figure 5.40a), with the twisted 2HBA molecules running diagonal to the plane (Figure 5.40b).

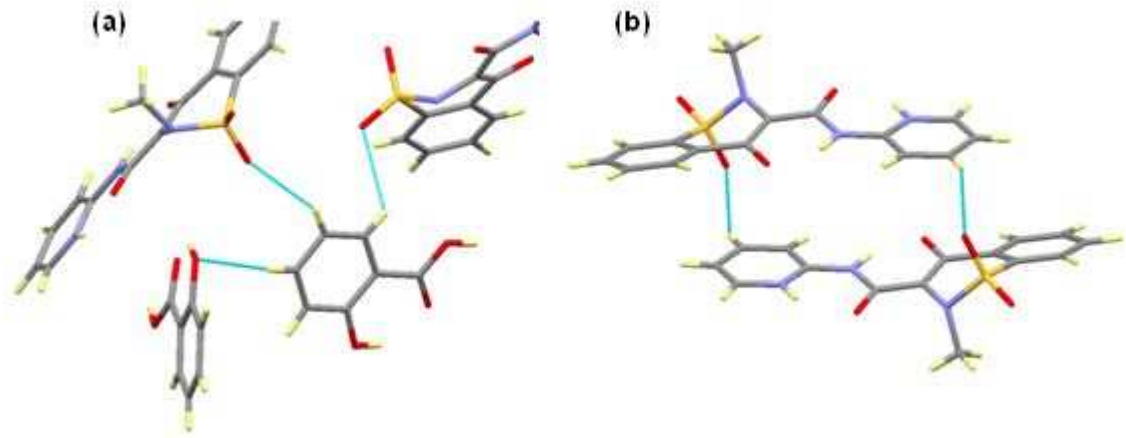

Figure 5.39 *(a) Weak CH···O hydrogen bonds involving 2HBA in PXZ:2HBA (b) weak CH···O hydrogen bonds between PX molecules in PXZ:2HBA.*

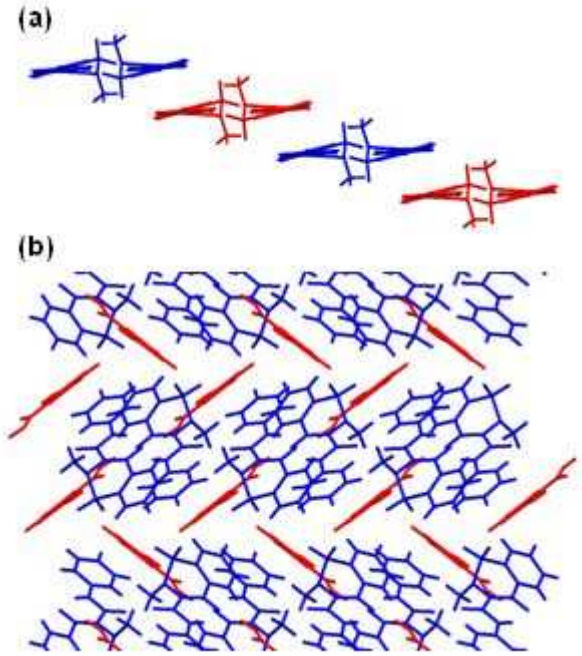

Figure 5.40 *Structure of PXZ:2HBA showing (a) the step-like arrangement of the PXZ dimers (alternate dimers shown in different colours) and (b) the 2HBA molecules (red) running diagonal to the plane of the PXZ molecules (blue).*

5.3.1.6 Piroxicam: 3-Hydroxybenzoic Acid Monohydrate (Zwitterionic) (PXZ: 3HBA.H_2O)

The PXZ:3HBA.H_2O complex features the BZZB tetramer (Figure 5.41) with PXZ in the zwitterionic form and similar hydrogen bond lengths to the PXZ:2HBA complex (Table 5.7). Two water molecules act as linkers between tetramers, forming an $R_4^4(8)$ hydrogen bonded ring with two 3HBA molecules (Figure 5.42a). The water oxygen is acceptor to the hydroxyl OH of one 3HBA molecule (O···O = 2.708(4) Å) and donor to the hydroxyl oxygen of the other (O···O = 3.033(5) Å, ∠DHA = 126(3)°).

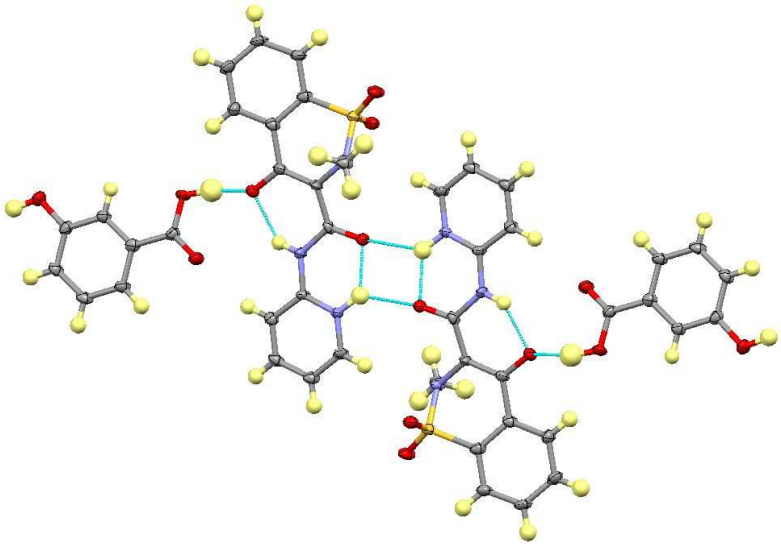

Figure 5.41 *The PXZ: 3HBA tetramer in the PXZ:3HBA.H_2O complex.*

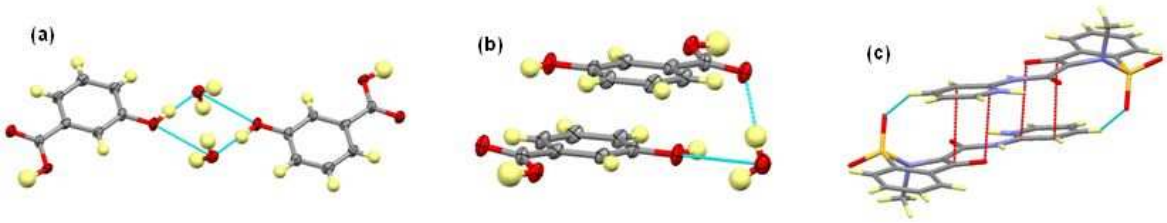

Figure 5.42 *Intermolecular interactions in PXZ:3HBA.H_2O (a) $R_4^4(8)$ rings, (b) hydrogen bonding between layers via water molecules, (c) π···π interactions between PXZ molecules (red dashed lines) and weak CH···O hydrogen bonds between the aromatic CH and sulfonyl O atoms.*

The BZZB tetramers connected by the $R_4^4(8)$ ring are almost co-planar with one another, forming layers (Figure 5.43). The water molecule forms another hydrogen bond to the carboxylic carbonyl oxygen (O···O = 2.812(5) Å) of the 3HBA molecule lying above/below (Figure 5.42b) which links the layers together. Further interactions between layers occur

between PXZ molecules, with weak CH···O hydrogen bonds (C···O = 3.271(1) Å) between the aromatic CH and sulfonyl O (Figure 5.42c) as well as π···π interactions between the pyridine ring and the delocalised enolate π-bond with a distance of approximately 3.241Å between the centre of the two bonds (also Figure 5.42c).

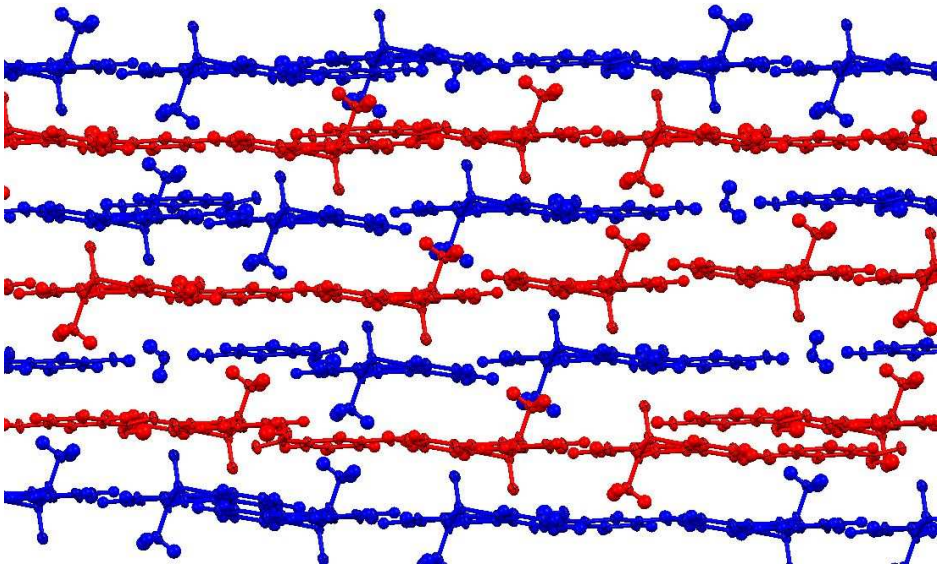

Figure 5.43 *Layered structure of PXZ:3HBA.H_2O.*

5.3.1.7 Piroxicam : 2-Nitrobenzoic Acid (Zwitterionic) (PXZ:2NBA)

The PXZ:2NBA complex contains PX as the zwitterionic tautomer within the BZZB tetramer building block (Figure 5.44). The tetramer building blocks are linked by weak CH···O hydrogen bonds between the aromatic CH of the 2NBA molecule and the PXZ sulfonyl O (C···O = 3.201(3) Å), along with further weak hydrogen bonds of the aromatic CH of the PXZ pyridine ring with the nitro group O (C···O = 3.248(3) Å) (Figure 5.45a). This links the tetramers into layers (Figure 5.45b) with the methyl group and one sulfonyl oxygen atom bridging the layers.

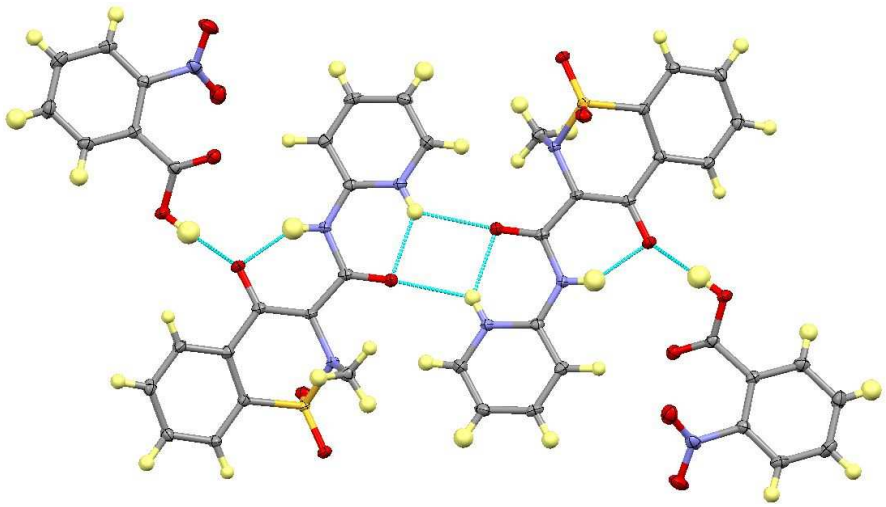

Figure 5.44 *Tetramer in the PXZ:2NBA complex.*

The nitro- and carboxylic acid group of 2NBA are twisted relative to the benzene ring due to steric effects. The twisted carboxylic acid group allows a weak hydrogen bond to be formed between the protonated pyridinal NH of the PXZ molecule above with the carbonyl oxygen (N···O = 2.962(2) Å)(Figure 5.45c). The twisted nitro group forms a weak interaction with the methyl CH of the same PXZ molecule (C···O = 3.320(3) Å). A weak CH···O hydrogen bond is also formed between the bridging sulfonyl oxygen of PXZ and the aromatic CH of the 2NBA molecule below (C···O = 3.296(3) Å) (also Figure 5.45c). The hydrogen bonds in the BZZB tetramer are of similar strength to the other complexes exhibiting this synthon (Table 5.7), despite the twisting of the carboxylic group.

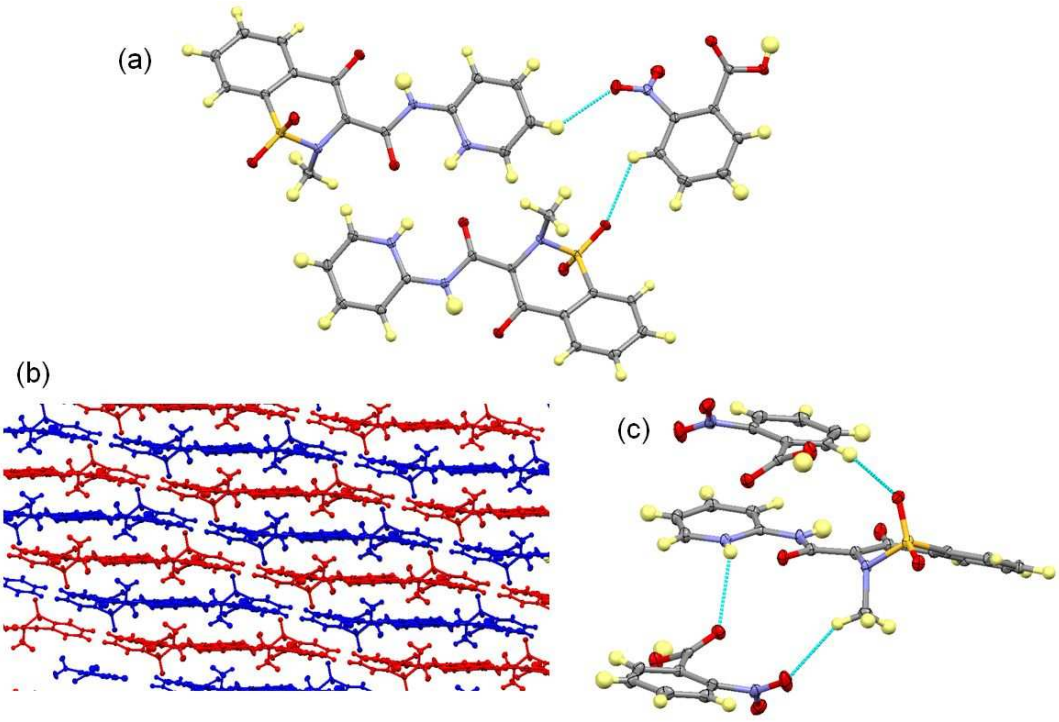

Figure 5.45 *Crystal Structure of PXZ:2NBA. (a) Weak interactions within layers, (b) layered arrangement of molecules, (c) weak interactions between layers.*

5.3.1.8 Piroxicam: 3-Nitrobenzoic Acid (Non-Ionised) (PXN:3NBA)

PX in this complex is in the non-ionised tautomeric form and is isomorphous to the layered PXN:3ClBA complex, again comprising of the BNNB tetramer with a CH···O=C PXN dimer (Figure 5.46). Interactions in the tetramer are largely similar to those in the PXN:3CLBA complex (Table 5.6). Slightly weaker interactions occur between PXN molecules and slight differences are observed in the $R_2^2(6)$ ring formed between the PXN and 3NBA molecules, with the OH···N hydrogen bond being slightly stronger and the NH···O interaction being slightly weaker. The nitro group occupies the corresponding space that the chlorine atom occupies in the 3ClBA complex; the weak methyl CH···Cl hydrogen bonds between layers are replaced with CH···O hydrogen bonds (C···O = 3.269(3) Å) (Figure 5.47). The nitro group oxygen also forms weak hydrogen bonds within the layers with the aromatic CH groups of the two neighbouring PXN molecules (C···O = 3.209(2) Å and 3.535(2) Å) (Figure 5.48).

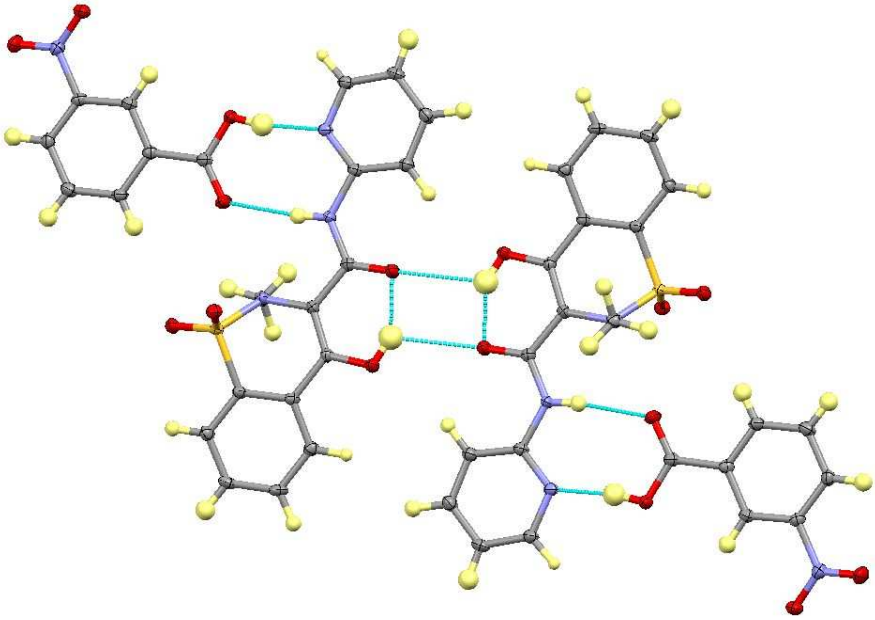

Figure 5.46 *The BZZB tetramer in the PXN:3NBA complex.*

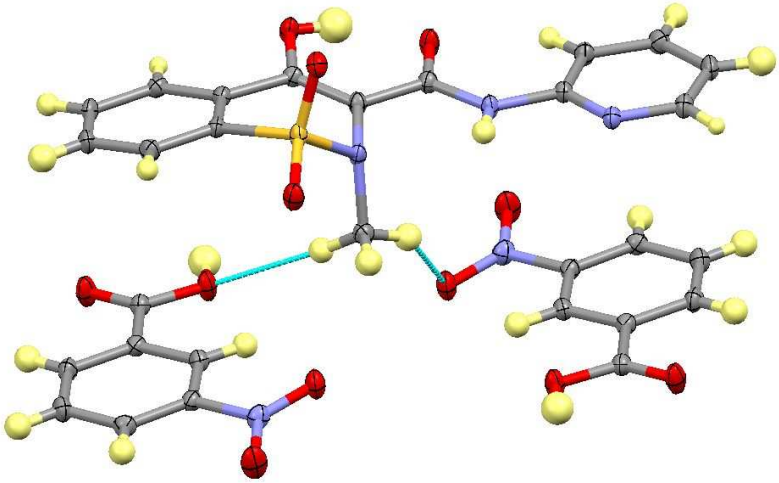

Figure 5.47 *PXN methyl interactions with the nitro group and hydroxyl oxygen in PXN:3NBA molecular complex.*

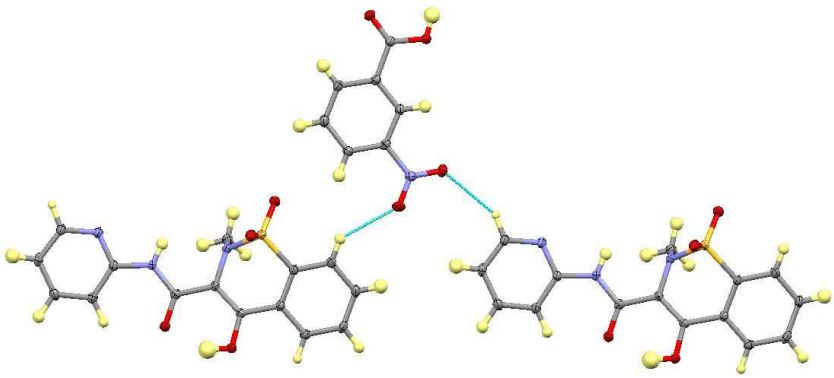

Figure 5.48 *Weak CH···O interactions within layers in PXN:3NBA.*

5.3.1.9 Piroxicam : 4-Nitrobenzoic Acid Hydrate (Non-Ionised) (PXN:4NBA.H_2O)

The complex has two non-ionised PXN molecules and two 4NBA molecules in the asymmetric unit. A large peak on the Fourier difference synthesis also indicated the presence of a single heavy atom not bonded to any other heavy atom - suggesting that the atom was the oxygen of a water molecule. Before assignment of the water molecule, the excess electron density was estimated using the SQUEEZE procedure[216]. This estimated that 16 excess electrons were present in the unit cell, representing an average of less than half a water molecule per asymmetric unit. The poor quality data (R_{int} = 14.40%) makes this estimate unreliable. For the final refinement cycle the SQUEEZED structure was not used. Instead, the oxygen was fixed at 30% occupancy to obtain a reasonable sized thermal parameter, although this may not be an accurate occupancy value. Due to the large void in which the water molecule resides, it is likely that it has a significant degree of freedom, with the modelled position being the major position. This is further supported by various small satellite peaks observed in the Fourier difference map (of height <0.25 eÅ^{-3}) surrounding the oxygen atom (see Appendix A5 for full refinement details). The water hydrogen atoms could not be located using Fourier difference synthesis.

The non-ionised PXN molecules dimerise via the OH···O=C dimer, with the 4NBA molecule hydrogen bonded via the $R_2^2(8)$ ring forming the tetramer that has previously been seen in PXN complexes with 3CLBA, 3BRBA and 3NBA, although with non-equivalent molecules in the tetramer (Figure 5.49). Hydrogen bond lengths in the tetramer can be found in Table 5.6.

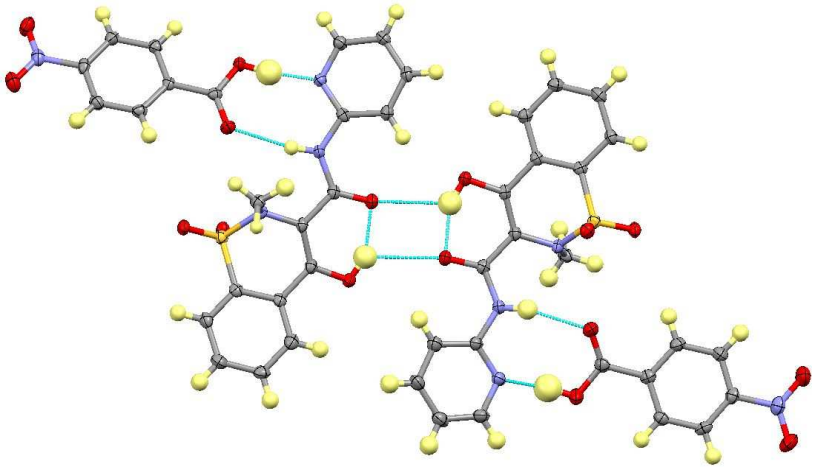

Figure 5.49 *The BNNB tetramer in the PXN:4NBA.H_2O complex.*

The structure consists of wave-like layers (Figure 5.50) with the methyl groups and sulfonyl oxygen atoms bridging between layers. Weak CH···O hydrogen bonds between the methyl and sulfonyl oxygen atoms (C···O = 3.312(3) Å and 3.306(3) Å) are formed between every third layer (Figure 5.51a) with the sulfonyl oxygen also involved in weak aromatic CH···O hydrogen bonds with PXN molecules in alternate layers (Figure 5.51b). The single hydrogen bonds in Figure 5.51b have a C···O distance of 3.548(3) Å, while the bifurcated hydrogen bonds have C···O distances of 3.312(3) Å and 3.306(3) Å. A weak bifurcated hydrogen bond (Figure 5.51b) is also present between the aromatic CH groups of the pyridine ring and the nitro group oxygen atom (C···O = 3.206(3) Å and 3.224(3) Å). Aromatic CH groups of two PXN molecules form weak hydrogen bonds to the water molecule oxygen (C···O = 3.254(3) Å and 3.262(3) Å) (Figure 5.52). Possible hydrogen bonds from the water OH groups are indicated by the proximity to both a PXN sulfonyl oxygen and a 4NBA nitro oxygen (O···O = 3.110(6) Å and 2.821(6) Å) (also shown in Figure 5.52).

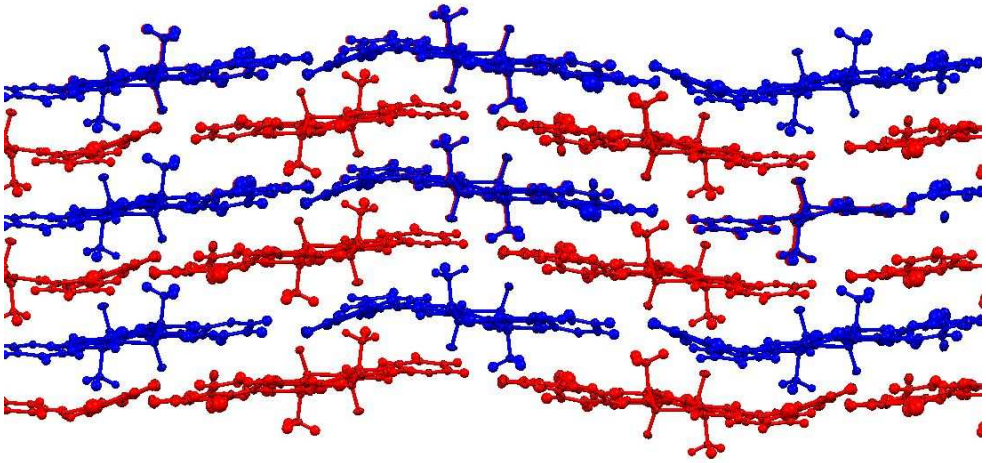

Figure 5.50 *Wave-like layers in PXN:4NBA with methyl and sulfonyl groups bridging the layers.*

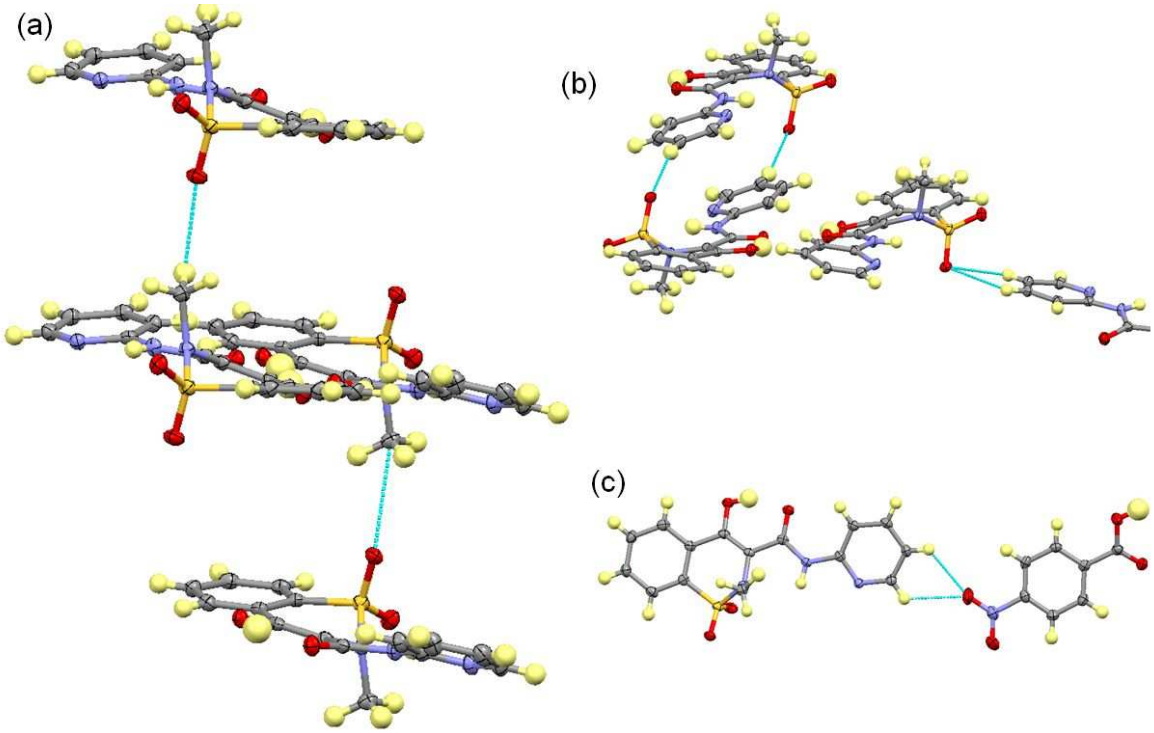

Figure 5.51 *Weak interactions in the PXN:4NBA complex (a) methyl CH hydrogen bonds with the sulfonyl oxygen atoms (b) aromatic CH hydrogen bonds with the sulfonyl oxygen atoms (c) bifurcated DDHHA hydrogen bond between the pyridine ring and the nitro oxygen.*

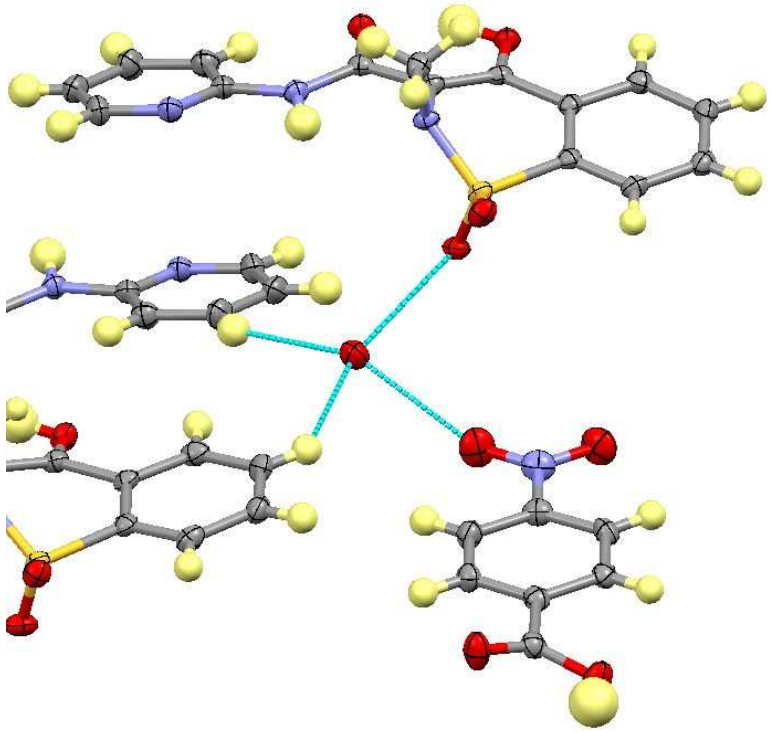

Figure 5.52 *The major position of the water oxygen atom and hydrogen bond interactions in the PXN:4NBA hydrate complex. The 4NBA molecule and bottom two PXN molecules lie in the same plane as the water oxygen with the top PXN molecule in the layer above.*

5.3.1.10 Piroxicam : 2-Methylbenzoic Acid (Non-Ionised) (PXN:2MBA)

The non-ionised PXN molecules dimerise through the S=O···H-O dimer seen in the non-ionised PXN complexes with 2- and 3FBA (Figure 5.53a). The 2MBA molecules are then hydrogen bonded to the PXN molecules through the $R_2^2(8)$ ring (Figure 5.53b). The sulfonyl oxygen atom forms weak hydrogen bonds with the aromatic CH groups of two neighbouring PXN molecules with approximate C···O lengths of 3.203(2) Å and 3.485(2) Å (Figure 5.54a). The other sulfonyl oxygen atom also forms weak hydrogen bonds with the aromatic CH of the adjacent 2MBA molecule, as well as with the methyl group of the 2MBA molecule that is hydrogen bonded to that PXN molecule via the $R_2^2(8)$ ring hydrogen bond motif (approximate C···O = 3.361(3) Å and 3.542(2) Å respectively) (Figure 5.54b). There are also π···π interactions between these two 2MBA molecules (Figure 5.54b), with a distance of approximately 3.578 Å between the centroids of the two π bonds. The non-planar arrangement of the 2MBA molecules relative to the PXN molecules in the tetramer results in layers of approximately planar regions of PXN molecules intersected by 2MBA molecules running diagonal to the plane of the PXN molecules (Figure 5.54c).

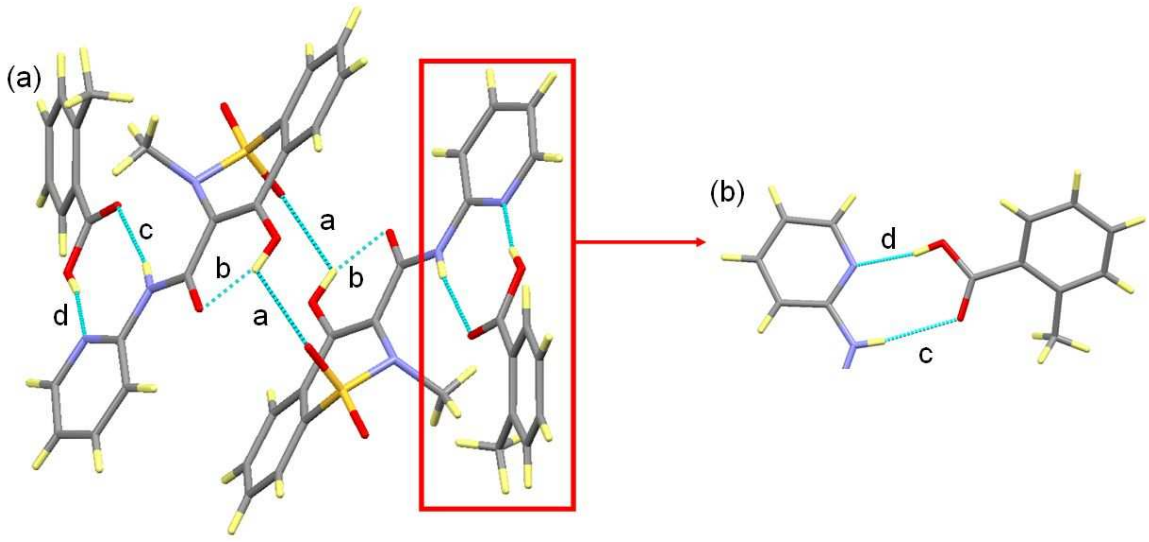

Figure 5.53 *(a) The tetramer in the PXN:2MBA complex, (b) the* $R_2^2(8)$ *ring.*

Table 5.8 *Hydrogen bond lengths and angles in the PXN:2MBA tetramer and the other complexes which exhibit this hydrogen bonding synthon (see Figure 5.53 for key).*

Complex	H-Bond	D-H (Å)	H···A (Å)	D···A (Å)	∠ D-H···A (°)
PXN: 2MBA	a	0.89(3)	2.54(3)	2.938(2)	108(2)
	b	0.89(3)	1.82(3)	2.617(2)	149(3)
	c	0.84(2)	2.36(2)	3.187(2)	170(2)
	d	0.84(3)	1.87(3)	2.700(2)	170(3)
PXN: 2FBA	a	0.89(2)	2.40(2)	2.961(2)	121(2)
	b	0.89(2)	1.79(3)	2.587(2)	149(2)
	c	0.77(2)	2.24(2)	2.997(2)	168(2)
	d	0.89(2)	1.80(2)	2.676(2)	171(2)
PXN: 3FBA	a	0.86(2)	2.44(2)	2.931(2)	117(2)
	b	0.86(2)	1.80(3)	2.591(2)	150(2)
	c	0.86(2)	2.13(2)	2.974(2)	167(2)
	d	0.92(2)	1.77(2)	2.676(2)	169(2)

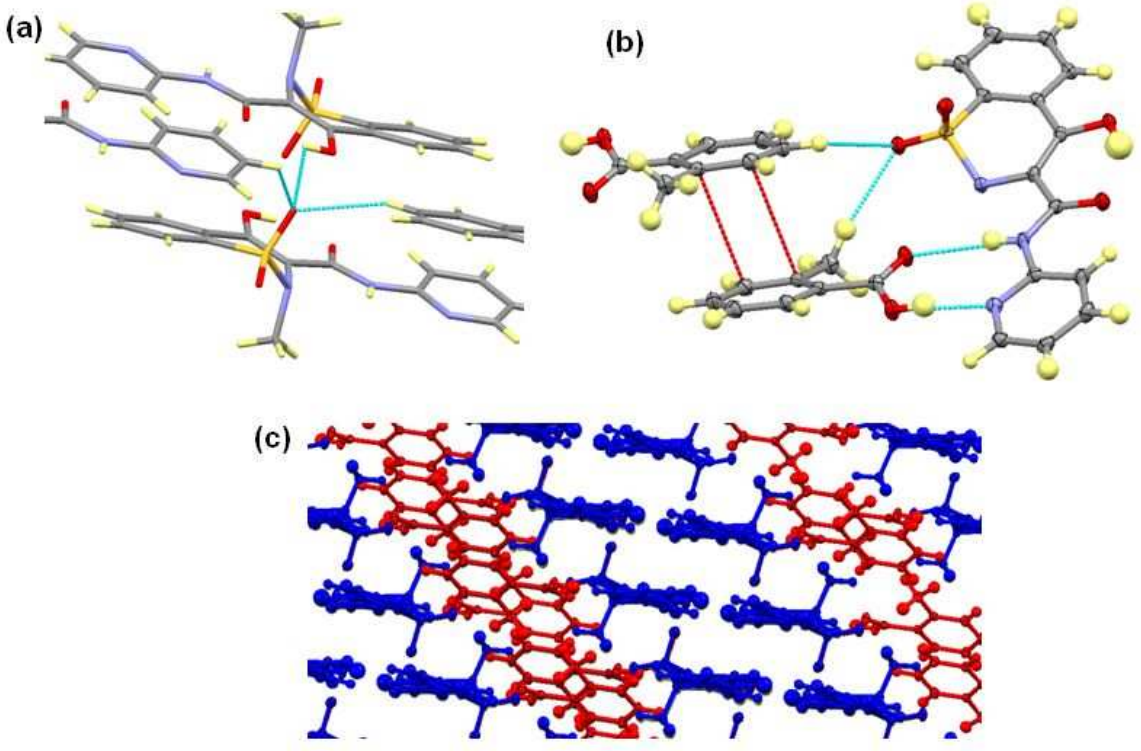

Figure 5.54 *(a) Crystal structure of PXN:2MBA. (a) Weak CH···O hydrogen bonds between sulfonyl O and CH of PXN molecules, (b) weak CH···O hydrogen bonds between sulfonyl O and 2MBA molecules (blue dashed lines) and π···π interactions between 2MBA molecules (red dashed lines), (c) 2MBA molecules (red) running diagonal to planes of PXN molecules (blue).*

5.3.1.11 Piroxicam : 3-Methylbenzoic Acid (Zwitterionic) (PXZ:3MBA)

The structure consists of the zwitterionic PXZ:3MBA BZZB tetramers (Figure 5.55, see Table 5.7 for bond lengths). The PXZ molecules are stacked upon each other through π···π interactions of the pyridine ring with both the benzene ring and the delocalised π bond of the deprotonated oxygen (Figure 5.56a). The same two molecules are further linked by weak aromatic CH···O=S (C···O = 3.405(4) Å) hydrogen bonds (also Figure 5.56a). Further π···π interactions occur between the pyridine ring of the PXZ molecules and the aromatic ring of the 3MBA molecules (Figure 5.56b) resulting in stacks of the tetramers. The stacks run alternately in different planes (Figure 5.57a). Interactions between stacks in different planes are relatively weak with CH···O hydrogen bonds (C···O = 3.450(4) Å) as well as CH···π interactions (Figure 5.57b).

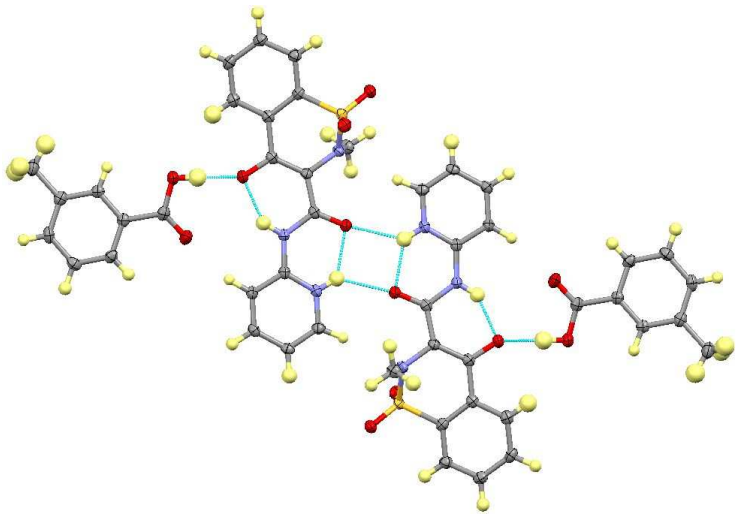

Figure 5.55 *BZZN tetramer in the PXZ:3MBA complex.*

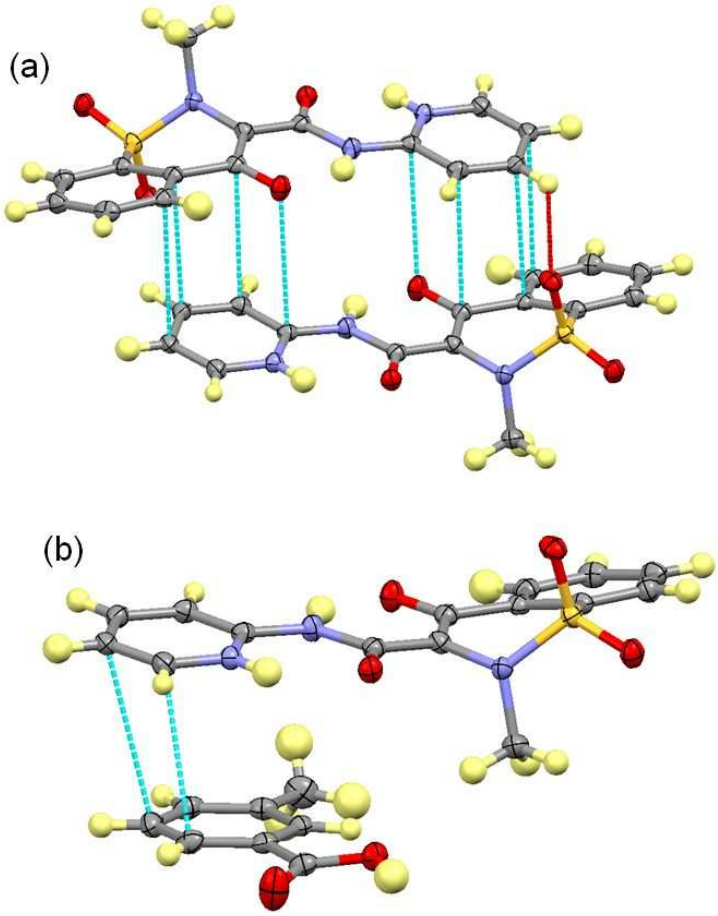

Figure 5.56 *π···π interactions in the PXZ:3MBA complex between (a) PXZ molecules and (b) PXZ and 3MBA molecules.*

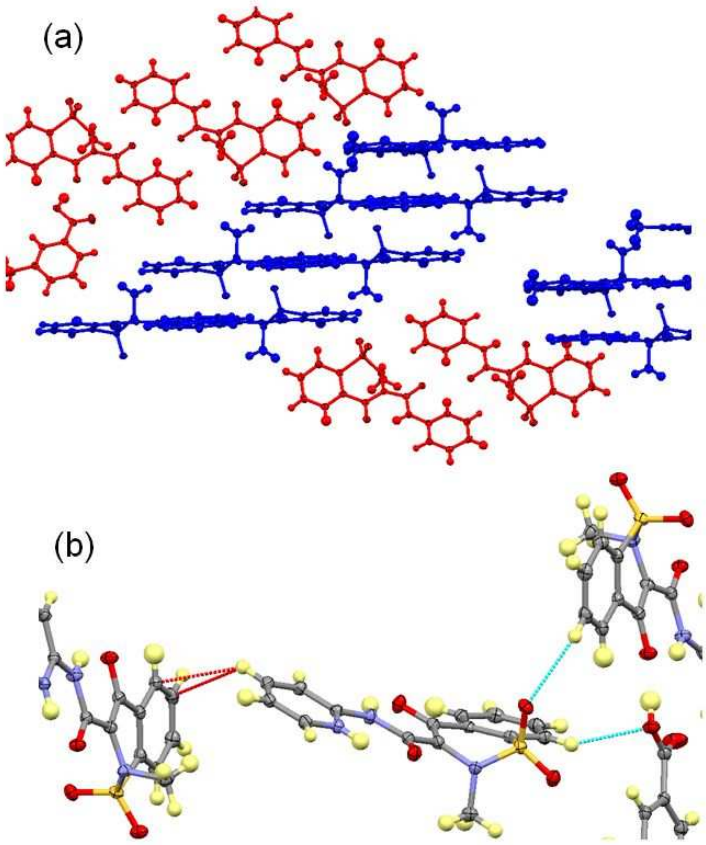

Figure 5.57 *Crystal packing in the PXZ:3MBA complex. (a) Regions of stacks lying in different planes with 3MBA in red and PXZ in blue; (b) weak interactions between molecules lying in different planes.*

5.3.1.12 Piroxicam: 3-Methylbenzoic Acid Acetonitrile Solvate (Zwitterionic) (PXZ:3MBA.ACN)

The PXZ:3MBA.ACN complex crystallises in a 2:1:1 ratio, with the PX molecules in the zwitterionic form. Although the BZZB tetramer is present, the 3MBA and acetonitrile (ACN) molecules are disordered over two positions related by an inversion centre (Figure 5.58). This results in three possible tetramer configurations (Figure 5.59) on a local-level when the disorder is removed. The first is the standard BZZB tetramer with two PXZ molecules sandwiched by two 3MBA molecules (BZZB),the second is the PXZ dimer flanked by two ACN molecules ((ACN):Z:Z:(ACN)), while the third is a combination of the two, an (ACN):Z:Z:B. It is not possible to resolve the combination of these which contribute to the average disordered structure from this analysis. Table 5.7 shows that the NH···O hydrogen bonds between PXZ molecules and OH···O hydrogen bonds between

PXZ and 3MBA molecules in the BZZB tetramer (Figure 5.59a) are of comparable strength to those in the other zwitterionic piroxicam complexes, despite the presence of the solvent molecule.

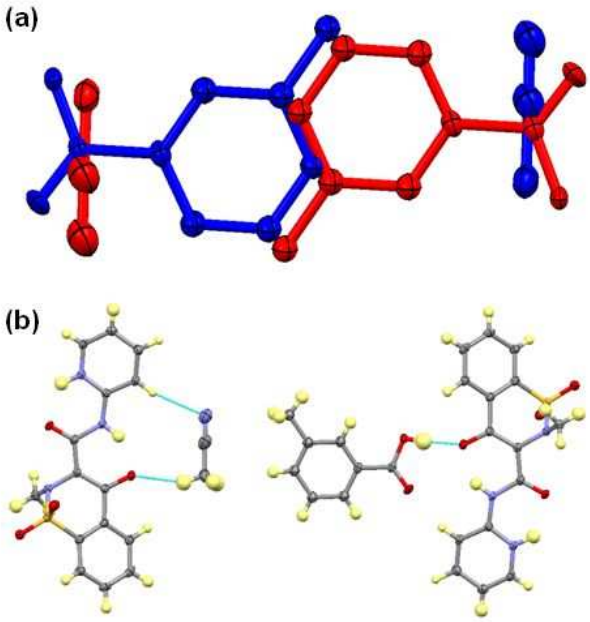

Figure 5.58 *(a) Disordered positions of 3MBA molecules and ACN molecules in the PXZ:3MBA.ACN complex, with the hydrogen atoms omitted for clarity. (b) The hydrogen bonding arrangements of PXZ with acetonitrile (left) and 3MBA (right). These occur in equal proportions.*

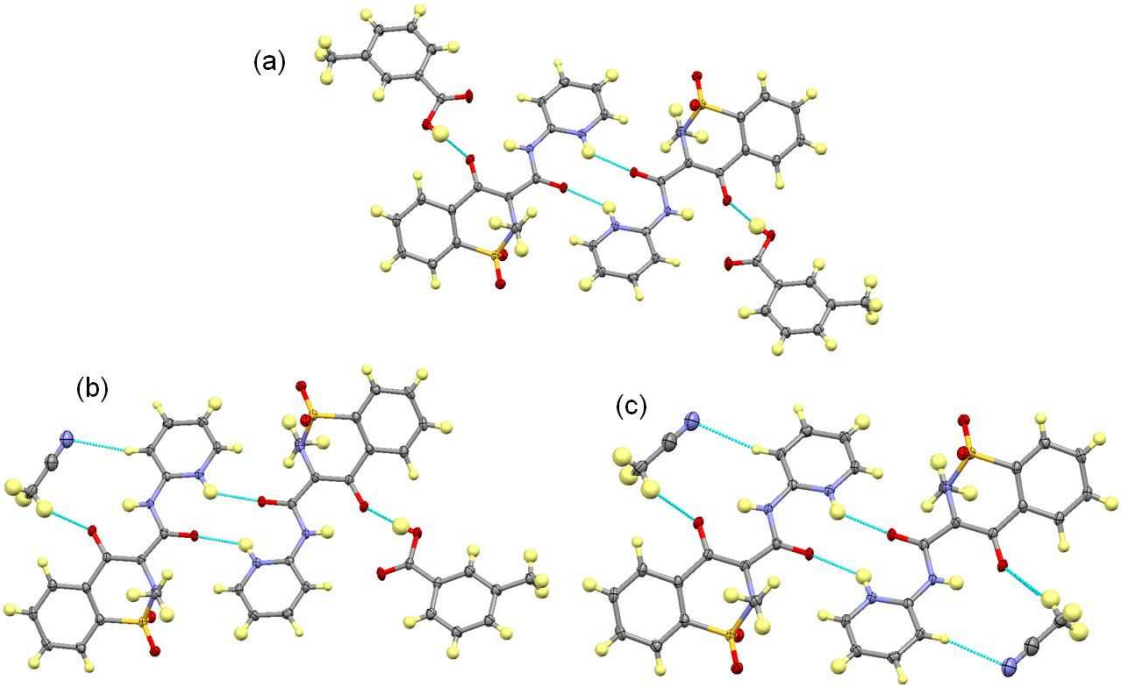

Figure 5.59 *The three possible permutations of the tetramer in the disordered PXZ:3MBA.ACN complex (a) BZZB (b) (ACN):Z:Z:B (c) (ACN):Z:Z:(ACN).*

The ACN molecule is hydrogen bonded to the PXZ molecule via weak CH···O interactions between the methyl group and the PX enolate O atom (C···O = 3.191(9) Å) as well as weak CH···N interactions between aromatic PXZ CH groups and the ACN N (C···N = 3.443(8) Å) (Figure 5.59b and c). The disordered tetramers are once again arranged in layers with the methyl group and sulfonyl oxygen pointing outward from the layers (Figure 5.60).

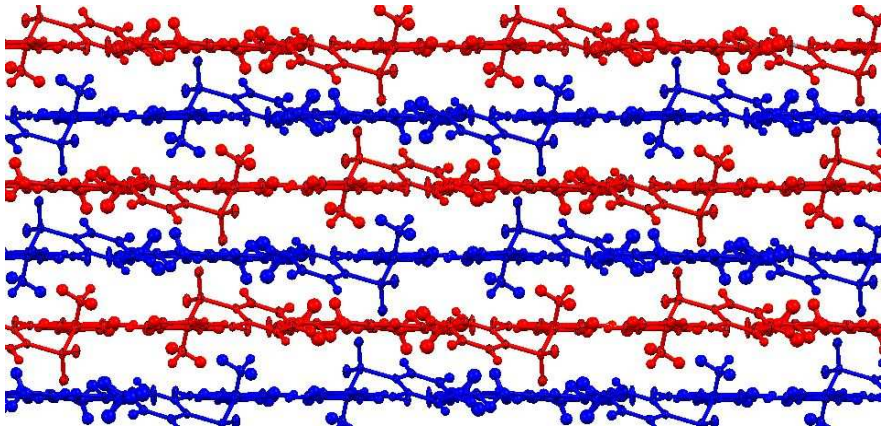

Figure 5.60 *Layered structure of PXZ:3MBA.ACN with alternate layers in different colours.*

The layers are linked by weak hydrogen bonds, mainly involving the sulfonyl oxygen atom. CH···O interactions are formed between the aromatic benzene CH groups of the PXZ molecules below (C···O = 3.366(3) Å) as well as the 3MBA molecule below (C···O = 3.398(6) Å) (Figure 5.61). A further weak CH···O hydrogen bond is formed between the methyl group of 3MBA and the enolate oxygen (C···O = 3.378(9) Å) (Figure 5.62). The ACN molecule is also involved in weak hydrogen bonds between layers with ACN dimers formed between layers through CH···N interactions (approximate C···N = 3.534(11) Å) as well as CH interactions with the PXZ molecules through the enolate oxygen (C···O = 3.455(9) Å) (Figure 5.63). The main interaction linking tetramers within the layers is the bifurcated CH···O interactions involving the sulfonyl oxygen and the pyridinal CH groups of PXZ (C···O = 3.204(3) Å and 3.290(3) Å) (Figure 5.64).

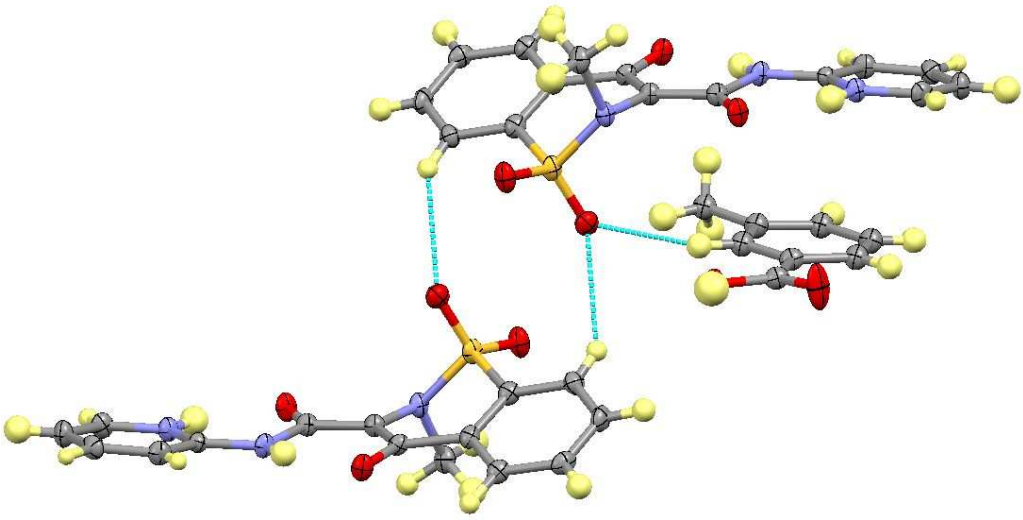

Figure 5.61 *Weak CH···O interactions between layers involving the sulfonyl oxygen atom in the PXZ:3MBA.ACN complex.*

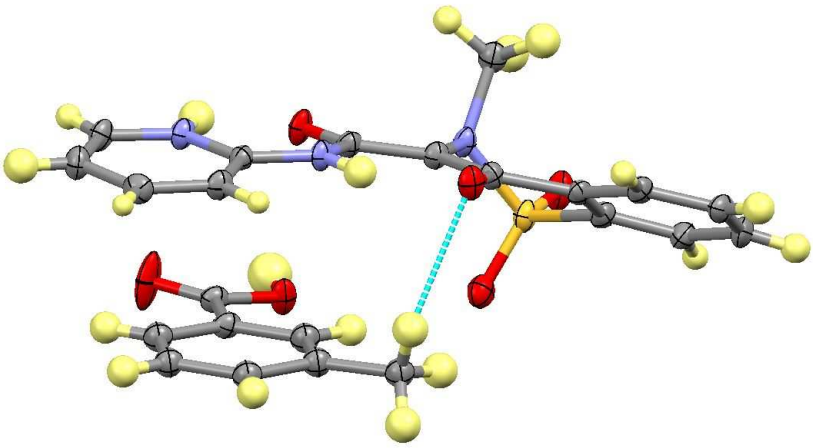

Figure 5.62 *Weak CH···O hydrogen bonds between the 3MBA methyl group and the enolate oxygen of PXZ in the PXZ:3MBA.ACN complex.*

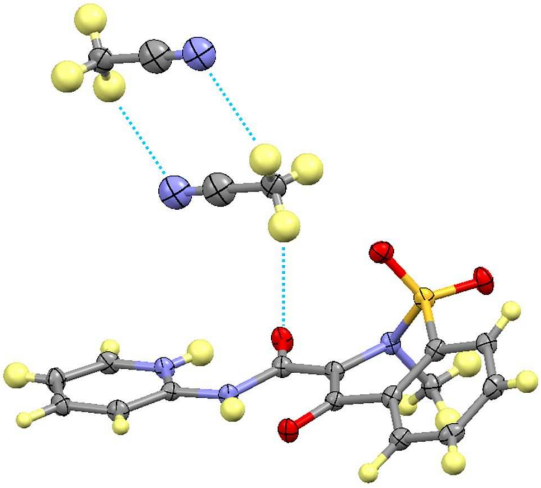

Figure 5.63 *Weak hydrogen bonds between layers involving the acetonitrile molecule in the PXZ:3MBA.ACN complex.*

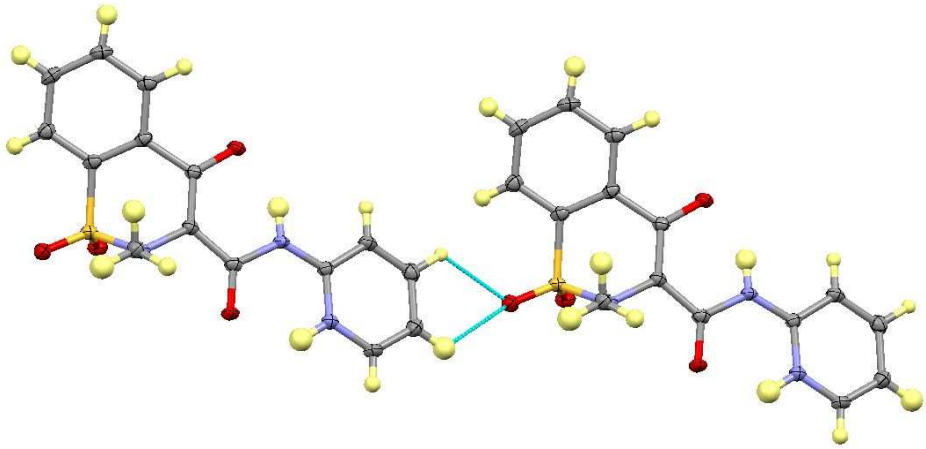

Figure 5.64 *Bifurcated CH···O interactions between neighbouring PXZ molecules in the layers in the PXZ:3MBA.ACN complex.*

5.3.1.13 Piroxicam : 4-Methylbenzoic Acid (Zwitterionic) (PXZ:4MBA)

The PX molecules are in the zwitterionic form with the BZZB tetramer again the hydrogen bonded building block (Figure 5.65). The BZZB building block differs from the others with the 4MBA molecule forming hydrogen bonds to the same deprotonated hydroxyl oxygen atom. However, the CH···O hydrogen bond is formed between the carbonyl and the aromatic H atom of the benzene ring (C···O = 3.139(4) Å), instead of the pyridinal CH of the PXZ molecule. The hydrogen bonded dimer between PXZ molecules, however, is the same as in the other PXZ complexes, with the remaining hydrogen bonds of similar strength as in those other complexes (Table 5.7).

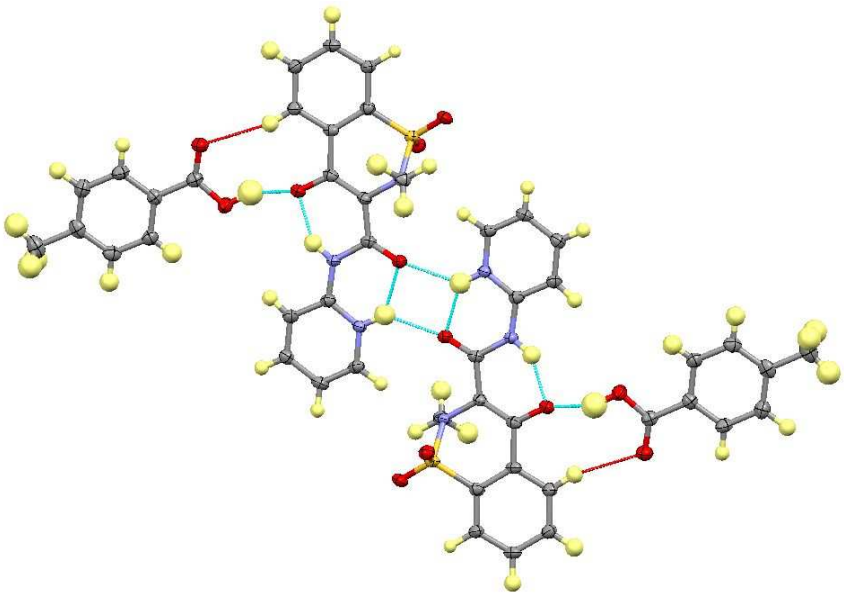

Figure 5.65 *The BZZB tetramer in the PXZ:4MBA molecular complex. Hydrogen bonds common to all PXZ tetramers are shown as blue dashed lines with the unique CH···O interactions shown as red dashed lines.*

Weak aromatic CH···O=S hydrogen bonds (C···O = 3.230(4) Å) (Figure 5.66a) link PXZ molecules together in layers (Figure 5.66b). The sulfonyl oxygen atoms form further weak CH···O hydrogen bonds with the aromatic CH groups of PXZ molecules in the layers above (C···O = 3.257(4) Å and 3.484(4) Å) as well as the methyl CH groups of 4MBA molecules in the alternate layer (C···O = 3.649(5) Å) (Figure 5.67a). Further weak hydrogen bonds occur between the PXZ methyl group and the carbonyl oxygen of 4MBA (C···O = 3.547(4) Å) accompanied by π···π interactions between the two molecules (Figure 5.67b). This again results in layers where the weak hydrogen bonds involving the non-coplanar methyl groups and a sulfonyl oxygen connect the layers.

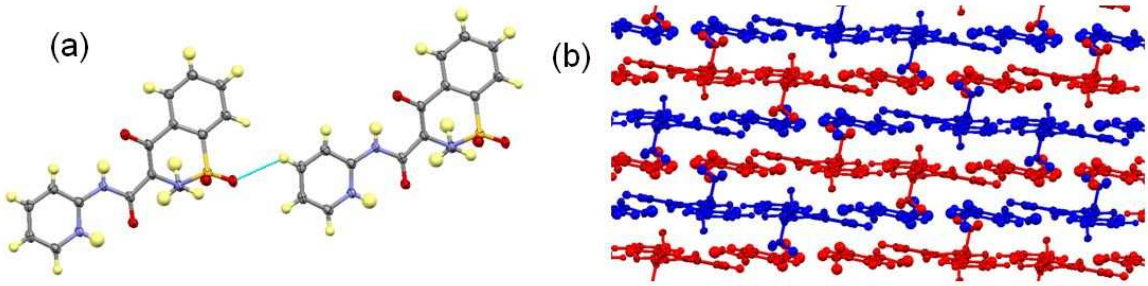

Figure 5.66 (a) *Weak hydrogen bonds within layers of the PXZ:4MBA complex; (b) layered arrangement of the structure with alternate layers in different colours.*

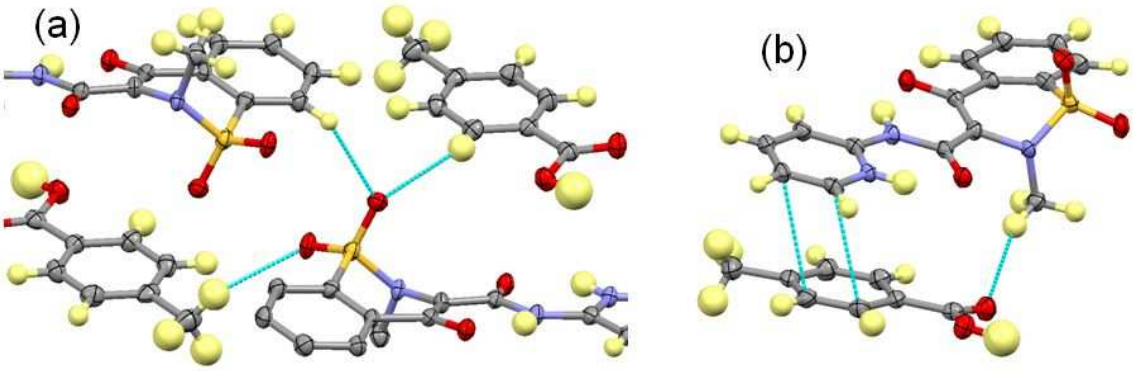

Figure 5.67 *Weak interactions between layers. (a) CH···O hydrogen bonds involving the sulfonyl oxygen (b) π···π interaction and CH···O hydrogen bond between PXZ and 4MBA.*

5.3.1.14 Piroxicam : 2-Aminobenzoic Acid (Zwitterionic) (PXZ:2ABA)

The PXZ molecules are in the zwitterionic form and despite the added competition for hydrogen bonding due to the amino group, the structure is isomorphous to PXZ:4FBA with the BZZB tetramer (Figure 5.68) remaining the main building block. The PXZ dimer has N···O distances of 2.651(3) Å (intramolecular) and 2.843(3) Å (intermolecular), while the OH···O hydrogen bond between PXZ and 2ABA has an O···O distance of 2.594(2) Å. The 2ABA molecules lie diagonal to the plane of the PXZ dimer as in PXZ:4FBA, with the formation of a moderately strong hydrogen bond between the amino NH and the sulfonyl oxygen of the PXZ molecule below (N···O = 3.137(3) Å) (Figure 5.69). The other NH of the amino group forms an intramolecular hydrogen bond with the carbonyl oxygen (N···O = 2.730(3) Å) (also Figure 5.69).

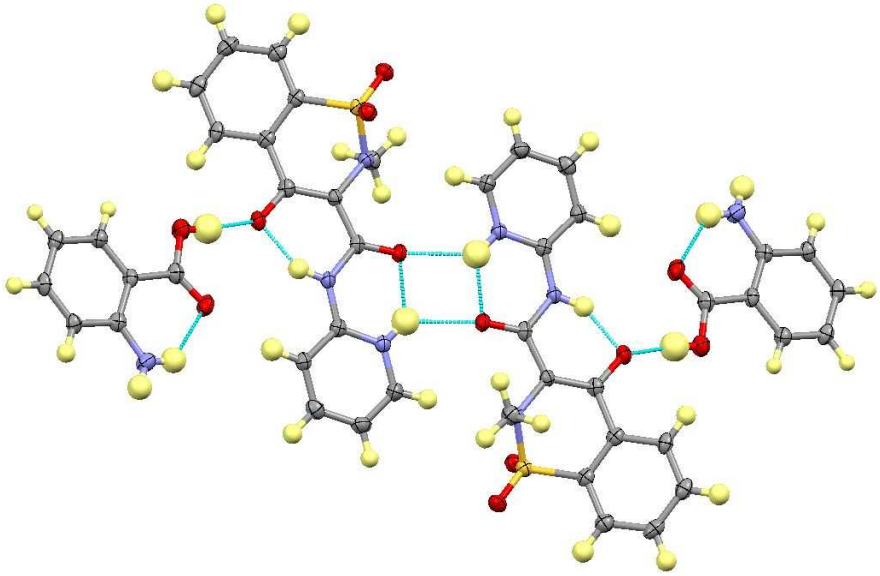

Figure 5.68 *The BZZB tetramer in the PXZ:2ABA complex.*

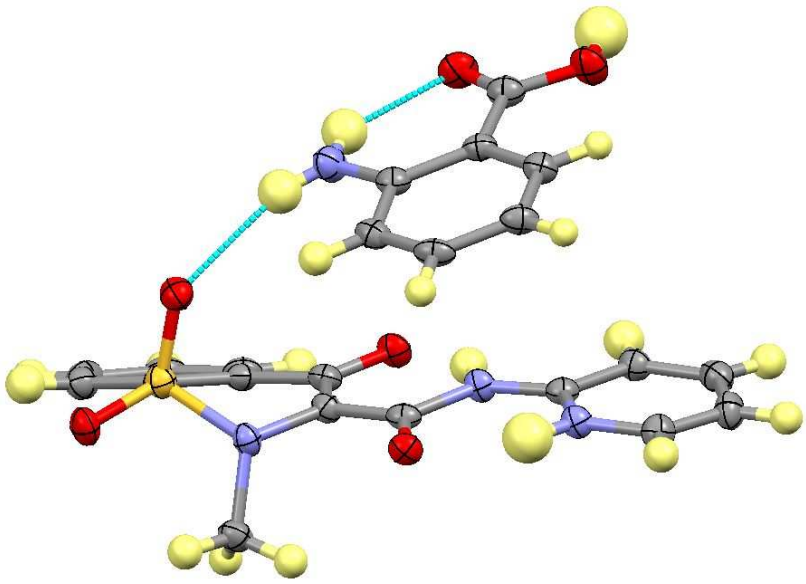

Figure 5.69 *Intramolecular and intermolecular hydrogen bonding involving the amino group in the PXZ:2ABA complex.*

5.4 Discussion

5.4.1 Supramolecular Synthons

Twenty molecular complexes of piroxicam with mono-substituted benzoic acids have been obtained in this study. Of these molecular complexes, twelve are found to incorporate the zwitterionic form of piroxicam and eight the non-ionised form. This adds to the non-ionised molecular complex with 4-hydroxybenzoic acid and the two zwitterionic molecular complexes with benzoic acid and 4-hydroxybenzoic acid already reported[27]. A significant conformational change of the piroxicam molecule accompanies the intramolecular hydrogen transfer to form the zwitterion (Figure 5.70) and therefore the supramolecular units obtained are quite different between the zwitterionic structures and the non-ionised structures. This also provides a clear identification of the tautomeric form without having to rely on sometimes inaccurate H atom positions. The tautomeric form obtained can also be inferred visually from the yellow colour of the zwitterionic complexes and the colourlessness of those that are non-ionised. Tautomeric polymorphs have been obtained for the molecular complexes with the fluoro-substituted benzoic acids. There is a strong tendency for a four molecule tetrameric unit to be formed in all cases with two piroxicam molecules dimerising in the centre, flanked by two benzoic acid molecules.

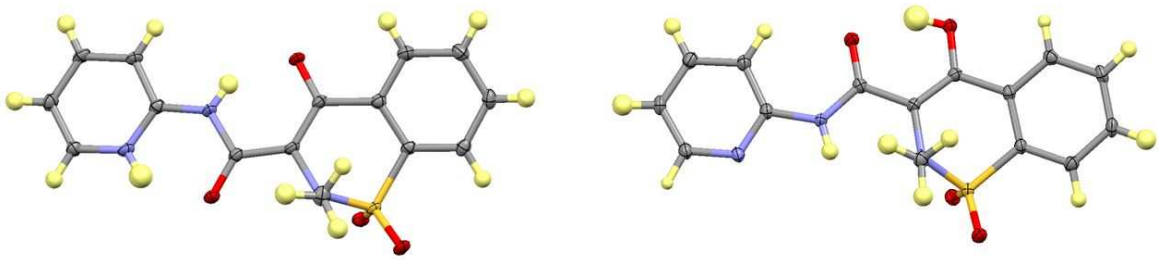

Figure 5.70 *The different conformations adopted by piroxicam molecules in the zwitterionic and non-ionised forms.*

The hydrogen bonded BZZB tetramer of the zwitterionic complexes is recurrent in all of the molecular complexes reported here. The piroxicam dimers are approximately planar (with the exception of the methyl and sulfonyl groups) and are held together by two

charge-assisted bifurcated DHAA N^+-H···O hydrogen bonds between the protonated pyridinal nitrogen and the carbonyl oxygen. An inversion centre is located in the middle of the resultant $R_2^2(12)$ ring. The benzoic acid molecule is then connected to this dimer on either side through an O-H···O^- charge-assisted hydrogen bond to the deprotonated hydroxyl group of the piroxicam molecule. A second, weaker CH···O hydrogen bond is formed between an aromatic CH group of the pyridine ring of the piroxicam and the carbonyl oxygen of the carboxylic acid group of the benzoic acid. One exception occurs in the complex PXZ:4MBA where the carboxylic acid group is rotated relative to the PXZ molecule and the weak hydrogen bond is instead formed between the aromatic CH of the benzene ring. In both cases these interactions tend to result in the carboxylic acid group and the piroxicam molecules being approximately co-planar with each other. Substituent effects cause the carboxylic acid group to deviate from the plane of the benzene ring in benzoic acid molecules; this has the effect of the benzene ring lying out of the plane of the rings in the PX molecules. This is particularly found in the cases where there is a large atom at the 2-position although in the PXZ:4FBA complex a large deviation from the plane also occurs despite the fluorine being in the 4-position.

Analysis of previously reported zwitterionic PXZ complexes with benzoic acids shows that this unit is also present in the PXZ:benzoic acid complex[27]. The 4-hydroxybenzoic acid (4HBA) molecular complex[27] is an exception, however, and does not feature the same tetrameric building block. The piroxicam dimer is identical in terms of the types of hydrogen bonds formed, but the 4HBA molecule instead coordinates to it through a charge-assisted O-H···O^- hydrogen bond from the phenolic hydroxy group (Figure 5.71, LHS). The carboxylic acid OH then forms an O-H···O hydrogen bond to the sulfonyl oxygen of PXZ, with the carbonyl oxygen accepting a hydrogen bond from the pyridinal N^+-H of a neighbouring PXZ molecule (Figure 5.71, RHS). As highlighted in the original publication[27], the expected hydrogen bond interaction, based on the strongest donor - strongest acceptor rule, is therefore replaced by weaker hydrogen bonds, although the OH···O hydrogen bonds are maintained for both the donor and acceptor. This deviation from the expected hydrogen bonding may be partly rationalised by the fact that the NH···O interaction formed to the carbonyl O is considerably stronger than the CH···O interactions that are typically formed in the BZZB tetramer. The PXZ complexes with 2- and 3HBA maintain the BZZB synthon; this is not surprising in the case of 2HBA as

the hydroxyl group participates in an intramolecular hydrogen bond and therefore is not available to provide a different coordination pathway to the piroxicam dimer.

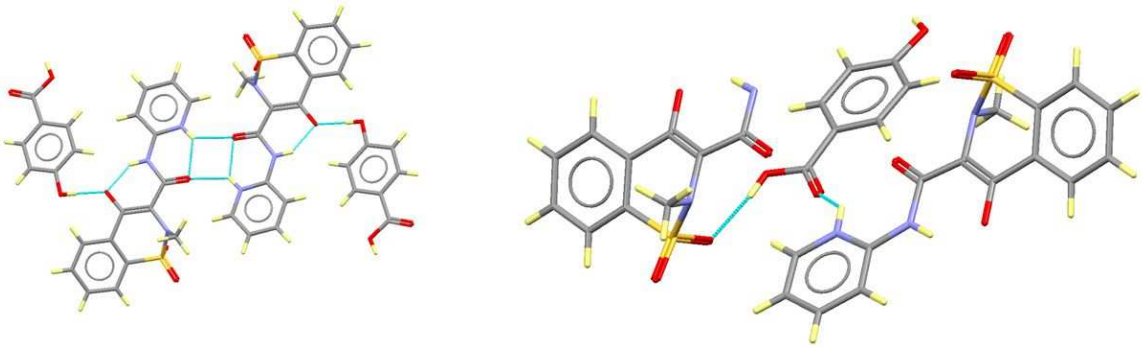

Figure 5.71 *The hydrogen bonding in the PXZ:4HBA complex[27], showing the different tetramer formed by the PXZ molecules and the 4HBA molecules (LHS) and the hydrogen bonding involving the 4HBA carboxylic acid group (with one PXZ molecule partially omitted for clarity) (RHS).*

On consideration of the strongest donor and strongest acceptor, it may be surprising that there are no occurrences of the positively charged NH group of PXZ forming a hydrogen bond with the negatively charged O atom of another PXZ molecule. This interaction, however, is most likely inhibited by crystal packing and steric effects due to the conformation adopted by PX when it is in the zwitterionic form preventing sufficiently close interaction of these groups. Although the BZZB tetramer is the building block of all but one of the structures, the extended packing is very different in the majority of these. This is due to the lack of any other strong recurring interactions. The weak CH···O=S hydrogen bonds occur frequently with either methyl or aromatic H-donors, although these interactions are not robust enough to form a reliable synthon and vary in their nature from system to system.

The complexes featuring non-ionised PXN molecules are less predictable in terms of hydrogen bonding patterns, although BNNB tetramers and three recurring synthons are observed (see Figures 5.12 and 5.28). One common synthon found in all non-ionised PX complexes reported here is a $R_2^2(8)$ ring (see Figure 5.12a) comprising an NH···O and an O-H···N hydrogen bond between BA and PXN molecules. The non-ionised PXN:4HBA complex[27] is, once again, the exception to this, with the hydroxyl group interacting with the piroxicam pyridinal N and amide NH rather than the carboxylic acid group, breaking the $R_2^2(8)$ ring and instead forming an $R_2^2(6)$ ring (Figure 5.72). The carboxylic acid

groups then form homodimers with a second 4HBA molecule. The second and third recurring synthons are the PXN dimers held together by O-H···O=S hydrogen bonds (Figure 5.12) in complexes with 2FBA, 3FBA and 2MBA ,and O-H···O=C hydrogen bonds (Figure 5.28) in complexes with 3CLBA, 3BRBA, 3NBA and 4NBA. The former occur in complexes with fluorine in the 2- and 3-position and the methyl in the 2-position. The small fluorine groups and the position of the methyl in the 2-position mean they are less likely to affect the crystal packing whereas the latter three complexes possess benzoic acids with bulky groups in the 3-position or 4-position.

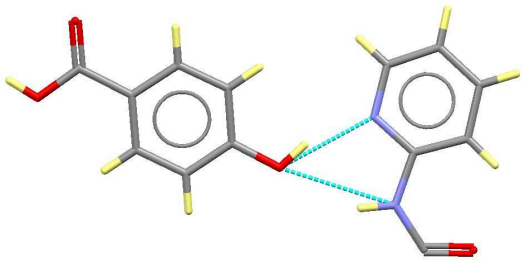

Figure 5.72 $R_2^2(6)$ *hydrogen bonded ring in the PXN:4HBA complex*[27] *(Only part of the PXN molecule is shown for clarity).*

The interactions occurring between PXN molecules in the PXN:4FBA complex and the previously reported PXN:4HBA complex are unique in this series. The former features weaker CH···O hydrogen bonds rather than moderately strong O-H···O hydrogen bonds between PXN molecules (Figure 5.19a). As there is an intramolecular O-H···O hydrogen bond in both cases, the energetic difference between the O-H···O and the CH···O interactions may be relatively small. In addition to the interactions between PXN molecules, the 4FBA molecules form dimers connected by pairs of CH···F weak hydrogen bonds (Figure 5.20). The PXN:4HBA complex also shows only weak CH···O hydrogen bonds between PXN molecules (Figure 5.73) but the relative arrangement of these is different to that seen in the 4FBA complex.

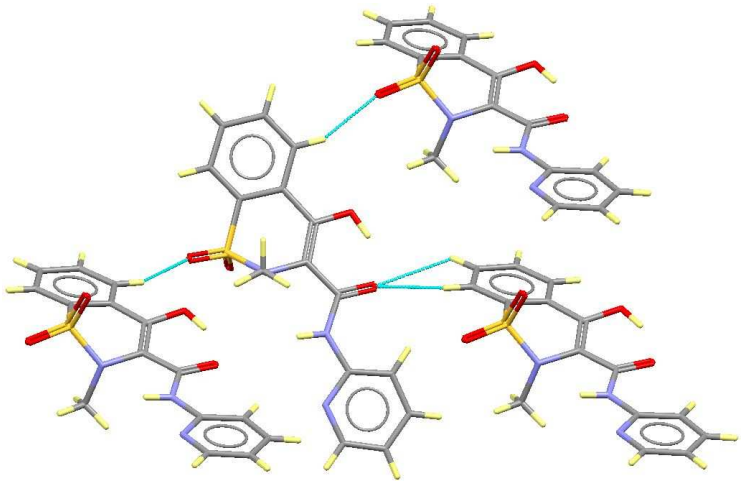

Figure 5.73 *The weak CH···O hydrogen bonds in the PXN:4HBA molecular complex*[27]

The OH···O hydrogen bond strengths between PXZ and the benzoic acid in the recurring zwitterionic PXZ BZZB synthon vary within a fairly narrow range, between 2.533(3) Å (PXZ:2HBA) and 2.5985(13) Å (PXZ:4FBA). The NH···O hydrogen bonds between PXZ molecules in the BZZB tetramer vary over a larger range of 2.791(6) Å (PXZ:2CLBA) to 2.929(3) Å (PXZ:2HBA).

Some trends are observed in the recurring synthons of the non-ionised PXN complexes. The OH···O hydrogen bonds between PXN molecules are stronger in the complexes featuring the OH···O=S PXN dimer (O···O = 2.938(2) Å - 2.961(2) Å) than in the complexes featuring the OH···O=C PXN dimer (O···O = 2.9818 (15) - 3.128(2) Å). The CH···O hydrogen bond (C···O = 3.207(2) Å) between PXN molecules in PXN:4FBA is weaker than the OH···O hydrogen bonds in both the OH···O=S and the OH···O=C dimers as expected. Other trends are also present with regards to the hydrogen bonding between the PXN and the benzoic acid molecule in the non-ionised PXN complexes. The NH···O interaction in the $R_2^2(8)$ ring (Table 5.9) is strongest in the PXN:4FBA complex featuring the CH···O PXN dimer whilst the OH···N interaction in this complex is the weakest. The N-H···O interaction is generally stronger in the complexes featuring the OH···O=C dimer than those with the OH···O=S dimer with the PXN:4NBA hydrate the only exception. Similarly, the OH···N interaction of the $R_2^2(8)$ ring is also stronger in the complexes featuring the OH···O=C dimer than those with the OH···O=S dimer. In the complexes featuring the OH···O=S dimer, all interactions in the $R_2^2(8)$ ring are stronger in the fluorobenzoic acid complexes than in the PXN:2MBA complex. In the four complexes featuring the OH···O=C dimer, the two nitro complexes feature weaker interactions between PXN molecules than the two halo-substituted complexes (Table 5.6).

Table 5.9 *Hydrogen bond distances and angles in the* $R_2^2(8)$ *hydrogen bonded ring between PXN and mono-substituted benzoic acids (c = NH···O; d = OH···N).*

Complex	PXN Dimer	H-Bond	D···A (Å)	∠ D-H···A (°)
PXN:2FBA	OH···O=S	c	2.997(2)	168(2)
		d	2.676(2)	171(2)
PXN:3FBA	OH···O=S	c	2.974(2)	167(2)
		d	2.676(2)	169(2)
PXN:2MBA	OH···O=S	c	3.187(2)	170(2)
		d	2.700(2)	170(3)
PXN:4FBA	CH···O	c	2.905(2)	173(2)
		d	2.715(2)	175(3)
PXN:3CLBA	OH···O=C	c	2.965 (2)	167(2)
		d	2.648(2)	171(3)
PXN:3BRBA	OH···O=C	c	2.968(3)	167(2)
		d	2.660(3)	169(4)
PXN:3NBA	OH···O=C	c	2.970(2)	172(2)
		d	2.618(2)	171(3)
PXN:4NBA	OH···O=C	c	2.982(3)	167(2)
		c’	2.998(2)	171(2)
		d	2.626(3)	172(3)
		d’	2.598(2)	170(3)

There are several isomorphous complexes although no more than three complexes share the same crystal packing. The 3-substituted chloro-, bromo- and nitrobenzoic acid complexes with PX in the non-ionised tautomeric form all share the same crystal packing which may be expected as they all have groups of a similar physical size in the 3-position. These groups are therefore not involved in structure directing interactions. The complexes PXZ:2FBA and PXZ:3FBA are isomorphous despite having a different substitution position for the fluorine atom. However, the fluorine atom is able to participate in CH···F weak hydrogen bonds to the piroxicam molecule without changing the crystal packing. When the fluorine is in the 4-position there is less steric hindrance and several weak hydrogen bonds are formed to surrounding CH groups and the pyridinal NH (Figure 5.10). The same argument can be made for isomorphous PXN:2FBA and PXN:3FBA. The fluorine in PXN:4FBA is again more freely available than in the PXN:2FBA and PXN:3FBA complexes, forming CH···F dimers between 4FBA molecules. The complexes PXZ:4FBA and PXZ:2ABA are also isomorphous, however, which is unusual given that 4FBA has a hydrogen bond acceptor (fluorine) in the 4 position and 2ABA has a donor (NH_2) in the 2 position.

5.4.2 Disorder

Two of the molecular complexes reported exhibit disorder of the co-component. In the PXZ:2FBA complex, the 2FBA molecules are disordered over two positions. The volume of space required to accommodate such a conformational change is small and the fluorine atom forms either weak F···O interactions with the sulfonyl oxygen atom (40% occupancy) or weak CH···F hydrogen bonds to the methyl group of the PXZ molecule (60% occupancy). This does not, therefore, disrupt the main interactions comprising the BZZB supramolecular unit.

The PXZ:3MBA.ACN complex is the only example where, at least some of the time, the reliable and predictable BZZB unit is broken, at least on a local scale. The 2:1:1 stoichiometry of the complex allows three possible short length scale units to be formed, BZZB, (ACN):Z:Z:B and (ACN):Z:Z:(ACN). Consideration of the close positions of the two disordered, symmetry related positions for the 3MBA or ACN molecules implies that it is not possible to have neighbouring units of BZZB adjacent to one another essentially forming BZZB:BZZB units. However, it is possible to form BZZB:(ACN):Z:Z:B or BZZB:(ACN):Z:Z:(ACN) units. The formation of this solvated complex is crystallisation condition dependent and it is only produced at room temperature, with the 1: 1 complex of PXZ:3MBA formed at 40°C or above.

5.4.3 Tautomeric polymorphism

Three of the systems reported exhibit the rare phenomenon of tautomeric polymorphism, those of the 2FBA, 3FBA and 4FBA complexes. Thermal analysis of all polymorphic samples was carried out to determine the most thermodynamically stable polymorph of each complex (Table 5.10; DSC traces can be found in Appendix C5).

Table 5.10 *Onset point of melting (in °C) from DSC of tautomeric polymorphs. PXN represents the polymorph featuring non-ionised piroxicam and PXZ represents the polymorph featuring zwitterionic piroxicam. DSC traces for all six complexes can be found in Appendix C5.*

	PX:2FBA	**PX:3FBA**	**PX:4FBA**
PXN	151.4	158.9	166.6
PXZ	Converts to non-ionised form at ~140	164.5	167.5

The DSC patterns of the PX:2FBA polymorphs show the zwitterionic polymorph to be the least stable of an enantiotropic pair, with the small broad endotherm at approximately 139.9°C indicating a solid-solid transformation before melting at approximately 150-151°C. This is supported by hot-stage microscopy which showed that a distinct change in colour (yellow to colourless) occurs upon heating single crystals of PXZ:2FBA to 140°C and holding the sample isothermally for 20 minutes. PXRD analysis of the sample after the colour change confirmed conversion to the PXN polymorph was occurring (Appendix B5). Analysis using PolySNAP[195] indicated an increase in the pattern matching coefficient between the sample after heating and the calculated PXRD pattern for PXN:2FBA, as well as a decreased pattern matching rank between the post-heating regime sample and the calculated PXRD pattern for PXZ:2FBA (Table 5.11).

Table 5.11 *PolySNAP pattern matching coefficients between calculated PXRD patterns of both tautomeric polymorphs of PX:2FBA and of pure PXZ:2FBA (calculated directly from the single crystal structure) before and after undergoing the heating regime. The values indicate a solid to solid transformation has occurred after heating as the pattern matching rank increases with respect to PXN:2FBA and decreases with respect to PXZ:2FBA.*

PXRD Pattern	Calculated PXZ:2FBA	Calculated PXN:2FBA
PXZ:2FBA prior to heating regime	0.3302	0.1440
PXZ:2FBA post heating regime	0.0782	0.1807

Note: The PXRD patterns were of poor quality due to the poor crystallinity of the samples, thus comparison of correlation values is made relative to the starting values only.

Analysis of the PX:4FBA polymorphs show very similar melting points, with the non-ionised form being the least stable. As highlighted in the previous section, the PXN:4FBA complex has only weak CH···O hydrogen bonds between PXN molecules, which is the likely reason it is less stable than its zwitterionic counterpart where charge-assisted hydrogen-bonds link the two PXZ molecules.

DSC of the PXZ:3FBA complex shows a considerably higher melting point than the PXZ:2FBA complex despite the two being isomorphous and the similar melting points of 2- and 3FBA. This is possibly due to the disorder present in the PXZ:2FBA complex as the CH···F hydrogen bonds are broken when the fluorine is in the minor position which has significant occupancy (40%). DSC of the sample containing the PXN:3FBA complex indicates a major endotherm occurring at 158.9°C and a separate minor endotherm at 170.6°C. The major endotherm is assumed to be the melting point of the PXN:3FBA complex indicating that this complex is also more stable than the isomorphous PXN:2FBA complex but less stable than the PXZ:3FBA polymorph. As yet the minor endothermic peak has not been assigned as it does not fit with the melting point of any known PX or 3FBA polymorph or PX monohydrate. This small endotherm may indicate a third polymorph is present in very small quantities.

In both the PX:3FBA and PX:4FBA systems, the zwitterionic polymorph is the most stable as may be expected due to the presence of charge-assisted hydrogen bonds. In the PX:2FBA system, however, the opposite is true despite these complexes being isomorphous with the PX:3FBA complexes. This, again, may be due to the disorder in the PXZ:2FBA complex disrupting the hydrogen bonding of the fluorine causing a loss of stability that is not seen in the PXZ:3FBA complex as it is not disordered.

5.4.4 Factors Influencing Tautomeric form of Piroxicam

Neither the substitution position or substituent type appears to be the main influence on the piroxicam tautomer found in the resultant molecular complex. However, an empirical observation can be made when considering the pKa values of the co-formers (Table 5.12). The groups of co-formers with the lowest and highest pKa values result in complexes where the zwitterionic tautomer is found. The non-ionised tautomer of piroxicam is only found in the middle range of pKa values (~3.4-4, blue in Table 5.12). One rationale for the presence of different tautomers would be that the acidity of the co-former is influencing

the solution environment (eq. 5.1) thus promoting one tautomer over another but this is not consistent with an observation reported here with two boundary conditions. Solvent and temperature effects were also considered, however, in a number of the co-crystallisations the same solvent and/or temperature systems were used but produced different tautomers in the resultant complexes.

Equation 5.1 The Henderson-Hasselbalch Equation: $pH = pKa + \log([A^-] / [HA])$

The systems exhibiting tautomeric polymorphism are of course exceptions to the empirical observation of the effect of pKa on the PX tautomer. It is as yet unclear whether these polymorphic complexes are a result of exceptional cases where the energy difference between polymorphs is small or if all the complexes are capable of exhibiting this phenomenon given the correct crystallisation conditions. It is interesting to note the relative pKa values of the benzoic acids which form tautomeric polymorphs with PX - the fluorobenzoic acids all lie close to the boundary regions and 4-hydroxybenzoic acid is at the extreme as the least acidic of those studied.

Table 5.12 *pKa values of benzoic acids and the tautomer observed in their molecular complexes with piroxicam. The region where the non-ionised tautomer is present is highlighted in blue. In cases where tautomeric polymorphism occurs, the more stable polymorph (if known) is signified by *.*

Substituent	pKa	PXZ	PXN
2-Amino	2.11	X	
2-Nitro	2.19	X	
2-Bromo	2.84	X	
2-Chloro	2.94	X	
2-Hydroxy	2.98	X	
2-Fluoro	3.27	X	X*
4-Nitro	3.44		X
3-Nitro	3.47		X
3-Bromo	3.81		X
3-Chloro	3.82		X
3-Fluoro	3.86	X*	X
2-Methyl	3.91		X
3-Hydroxy	4.08	X	
4-Fluoro	4.15	X*	X
No Substituent	4.19	X	
3-Methyl	4.27	X	
4-Methyl	4.36	X	
4-Hydroxy	4.58	X	X

5.4.5 Summary and Conclusions

Piroxicam readily crystallises with a variety of mono-substituted benzoic acids in both the zwitterionic and non-ionised forms. A related series of piroxicam complexes exhibiting tautomeric polymorphism has also been obtained. An empirical relationship between the pKa of the benzoic acid co-former and the preferred PX tautomer in the resultant complex has been identified with a pKa region with two boundaries where the non-

ionised tautomer is favoured. Although a relationship between the pKa of the co-former and the PX tautomer might be expected, it is not clear why benzoic acids with relatively high and low pKa values would favour one tautomer whereas the benzoic acids with pKa values in a middle region would favour the other. More data is required on this system and other similar tautomeric systems to ascertain the reliability and rationale for this relationship.

DSC analysis of the tautomeric polymorphs shows that the PX tautomer adopted in each complex is not always the critical factor in determining the relative stability of the polymorphic complexes. This is illustrated by the PX:2FBA system in which the non-ionised polymorph is the most stable despite the lack of charge-assisted hydrogen bonds. It is not yet known whether the tautomeric form results in different physical properties.

Analysis of the crystal structures has revealed a predominant hydrogen bonding pattern in the zwitterionic PXZ complexes with mono-substituted benzoic acids. In all but one of the crystal structures (both reported here and in the literature), the BZZB moiety corresponding to Figure 5.1 is found with the only exception being the case of 4-hydroxybenzoic acid. The PX homo-dimerisation that occurs at the centre of the BZZB tetramer is however, found in every known zwitterionic piroxicam complex. The non-ionised PXN complexes have less predictable interactions between PXN molecules although two recurring synthons were found. The $R_2^2(8)$ hydrogen bonded ring synthon between PX and the carboxylic acid group of the benzoic acids appears to be fairly robust with only one complex not exhibiting this synthon. The hydrogen bond strengths in this motif were found to depend on the type of PXN dimer formed at the centre of the tetramer, with the complexes exhibiting the OH···O=C dimer generally possessing stronger hydrogen bonds between the BA and the PXN molecules.

6. Intermolecular Hydrogen Transfer in Multi-Component Complexes of Piroxicam

6.1 Introduction to Intermolecular Hydrogen Transfer in Piroxicam Complexes

In the solid state, piroxicam has previously been known to exist in two ionisation states when not in its neutral form. As discussed in Chapters 4 and 5, intramolecular hydrogen-transfer has been observed in polymorphs and molecular complexes of piroxicam resulting in the formation of the zwitterion[220]. Similarly, intermolecular hydrogen transfer has been observed previously in a piroxicam complex, forming a salt with a piroxicam anion (PX^-), although only one example of this exists[212]. The complex is a 1:1 salt with ethanolamine in which the piroxicam is deprotonated, with the hydrogen transferred to the amine group of ethanolamine (pKa = 9.5). The hydroxyl group of piroxicam has a pKa of 5.46 and the pyridine nitrogen has a pKa of 1.86 (conjugate acid). No studies have, however, been carried out to determine which functional group (and therefore which pKa value) should be considered when using the pKa rule (which states the approximation that $\Delta pKa = pKa[\text{protonated base}] - pKa[\text{acid}] \geq 3$ for salt formation) in predicting intermolecular hydrogen transfer in a potentially zwitterionic material such as piroxicam. In the solid state, pure piroxicam exists in the non-ionised form (with the exception of the metastable form IV - see Chapter 4). It has, however, been shown that the zwitterionic form is present in significant quantities[220,223] when piroxicam is dissolved in polar solvents such as acetonitrile or methanol. This makes it unclear if the hydrogen that is transferred should be considered as coming from the hydroxyl group or from the pyridine nitrogen. In the case of ethanolamine, the intermolecular hydrogen transfer is successfully predicted by application of the pKa rule for hydrogen transfer, regardless of which pKa value is considered. The pKa rule has been shown not always to be transferrable between systems[118], and in a zwitterionic system such as piroxicam the matter is further complicated. The piroxicam anion in the ethanolamine complex is formed despite the added competition for the proton, i.e. formation of the piroxicam zwitterion. As discussed extensively in Chapter 5, piroxicam is prone to adopting the zwitterionic tautomer when co-crystallised with weak acids and this also has to be considered when trying to predict hydrogen transfer.

In the work presented in this Chapter, a series of nitrogen heterocycles of varying basicity (Scheme 6-1) were co-crystallised with piroxicam to investigate the occurrence of hydrogen transfer from the piroxicam molecule to the basic nitrogen of the heterocycle and determine what effects the competition of intramolecular hydrogen-transfer may have. Application of the pKa rule will be investigated with regards to these systems and whether it is more suitable to consider the pKa value of the hydroxyl group or the pKa of the pyridine nitrogen when attempting to predict hydrogen transfer using the ΔpKa rule. The results will also be used to investigate further the occurrence of the zwitterionic tautomer of piroxicam and the conditions which give rise to its formation in the solid state. In addition to using basic N-heterocycles, piroxicam is also co-crystallised with the strong organic acids, chloranilic and bromanilic acid (also Scheme 6-1), to investigate the possibility of protonating the pyridine ring to form molecular salts where piroxicam is in a cationic form (PX^+). Co-crystallisation with the weaker acids used in Chapter 5 resulted in zwitterionic piroxicam complexes, so acids of a much lower pKa are required to attempt to protonate the piroxicam. Again, application of the ΔpKa rule will be investigated with regards to these complexes, as piroxicam in this case will behave as a base and this may affect if and how the pKa rule can be applied. All complexes will also be analysed from a crystal engineering perspective to ascertain if any robust synthons occur which may be utilised for future design of molecular complexes of piroxicam.

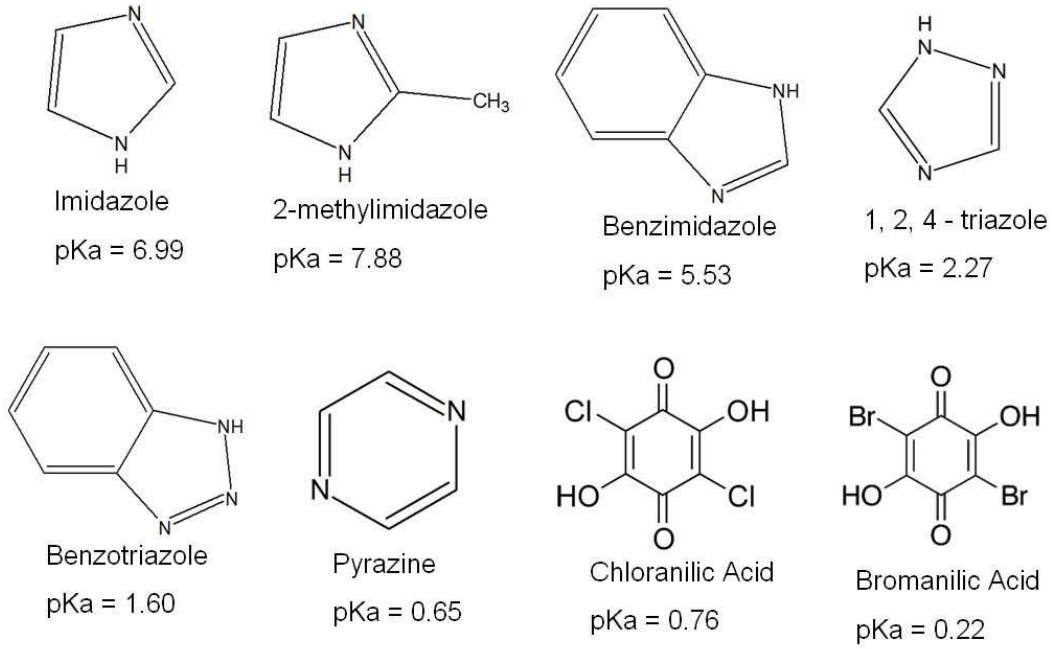

Scheme 6-1 The NHCs and organic acids used for co-crystallisation with piroxicam.

6.2 Crystallisation Conditions

Crystallisations were carried out according to the procedure outlined in Chapter 3. Table 6.1 below outlines the solvent and temperature systems under which each molecular complex described in this section was observed to crystallise. The piroxicam : pyrazine complex (marked *) did not crystallise from all experiments using the conditions described. In addition, it crystallised only in very small amounts, either concomitantly with piroxicam form IV, or concomitantly with form I, form II and/or the monohydrate.

Table 6.1 *Crystallisation conditions for molecular complexes of piroxicam with nitrogen heterocycles.*

Piroxicam Molecular Complex	Solvent	Temp (°C)
Imidazole hemihydrate	Methanol	RT
Imidazole acetonitrile Solvate (1:1:1)	Acetonitrile	RT
Imidazole acetonitrile Solvate (4:4:1)	Acetonitrile	50
2-methylimidazole	Acetonitrile	RT/40/50
Benzimidazole	Acetonitrile	50
1, 2, 4 - Triazole	Acetonitrile	40/50
Benzotriazole	Acetonitrile	RT/40
Pyrazine*	Acetonitrile	50
Chloranilic acid form I	Acetonitrile	RT
Chloranilic acid form II	Acetonitrile	40
Chloranilic acid acetonitrile solvate (2: 1: 2)	Acetonitrile	50
Bromanilic acid	Acetonitrile	RT/40/50

RT = Room Temperature

6.3 Crystal Structures of Piroxicam Molecular Complexes with Nitrogen-Heterocycles

Nine molecular complexes of piroxicam with nitrogen-heterocycles were produced in this study. Full refinement details for all complexes can be found in (Appendix A6 and Table A-6a).

6.3.1 Piroxicam : Imidazole Hemihydrate ($2(PX^{-}):2(IM^{+}).H_2O$)

The asymmetric unit of the piroxicam : imidazole hemihydrate features two symmetry independent piroxicam (PX) molecules, two symmetry independent imidazole (IM) molecules and a single water molecule. Deprotonation of the hydroxyl group occurs in

both PX molecules with the hydrogen transferred to the imidazole nitrogen atoms resulting in a salt of the PX enolate anion (PX^-) and the IM imidazolium cation (IM^+). PX^- molecules adopt a different conformation from that found in both the neutral and zwitterionic forms of piroxicam (Chapter 5), with a moderately strong intramolecular NH···O hydrogen bond formed (Figure 6.1, Table 6.2). One symmetry independent IM^+ molecule (B in Figure 6.2) has C-N bond lengths (between the two nitrogen atoms and the carbon in the 2-position) of 1.327(5) Å and 1.337(5) Å), whereas the other (B' in Figure 6.2) has C-N distances of 1.331(5)Å and 1.334(5)Å.

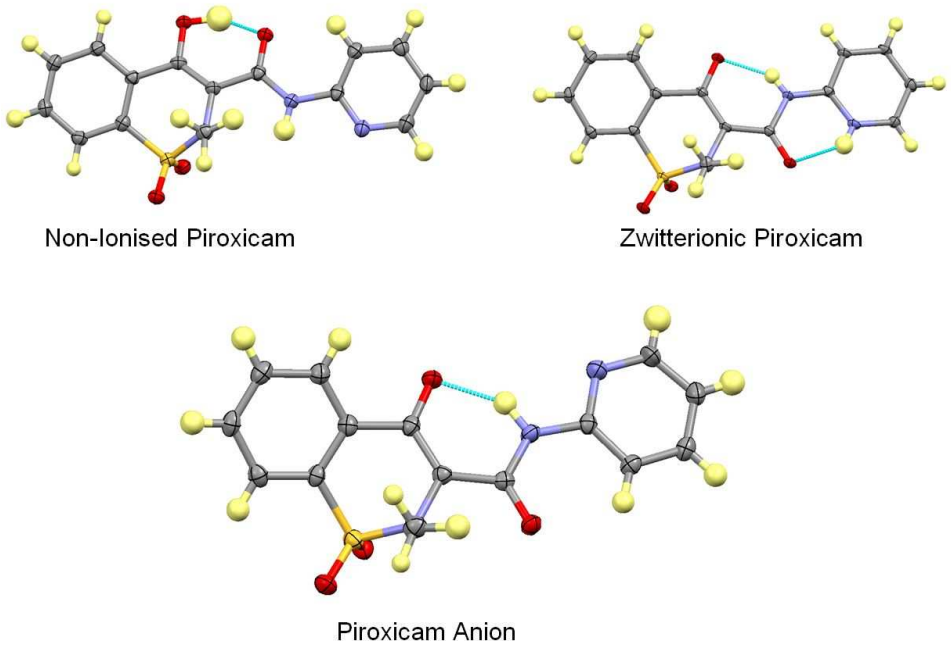

Figure 6.1 *Conformation of the deprotonated PX molecules (PX^-) in the piroxicam : imidazole hemihydrate complex (bottom). The conformations of non-ionised PX (top left) and zwitterionic PX (top right) are also shown.*

Non-equivalent PX^- molecules are linked by IM^+ molecules forming infinite chains of alternating PX^- and IM^+ molecules (Figure 6.2). The chains are arranged so that symmetry independent molecules also alternate, i.e. in an ABA'B' configuration (where A and A' indicate symmetry independent PX^- molecules). The symmetry independent IM^+ molecules link PX^- molecules via different interactions involving the NH groups. One IM^+ molecule (B in Figure 6.2) links two PX^- molecules by forming a moderately strong, charge-assisted $N^{\delta+}$-H···O^- hydrogen bond to the PX^- enolate oxygen atom of one (b in Figure 6.2) and an $N^{\delta+}$-H···N hydrogen bond to the pyridinal nitrogen atom of the other (a in Figure 6.2). Further weaker hydrogen bonds occur between an IM^+ CH group with the enolate O^- (e in Figure 6.2) as well as another IM^+ CH group with the pyridinal N atoms

which do not hydrogen bond to the NH groups (d in Figure 6.2). The second IM^+ molecule (B') links two PX molecules by forming two moderately strong $N^{\delta+}$-H···O hydrogen bonds to the PX^- carbonyl oxygen atoms (f and f' in Figure 6.2). Further weak hydrogen bonds are formed between the CH groups of IM^+ and the sulfonyl oxygen atoms of the PX^- molecules (g and g' in Figure 6.2). This IM^+ molecule also forms hydrogen bonds to the water molecule via a weak CH···O hydrogen bond (C···O = 3.214(5) Å) (Figure 6.3). All hydrogen bond lengths and angles in the chains can be found in Table 6.2.

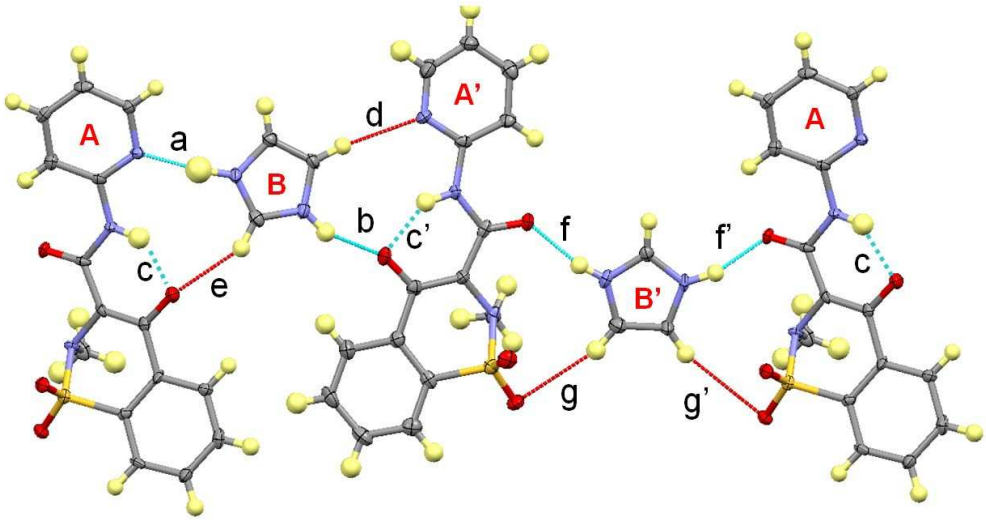

Figure 6.2 *The hydrogen bonding in the chains of PX^- and IM^+ in the piroxicam : imidazole hemihydrate complex (letters marked with ' indicate a symmetry independent molecule or interaction e.g. A and A'). One IM^+ molecule forms both NH···N and NH···O hydrogen bonds (blue dashed lines from B) and the other forms two NH···O hydrogen bonds (blue dashed lines from B'). Weaker hydrogen bonds involving CH donors are shown as red dashed lines.*

Table 6.2 *Hydrogen bond lengths and angles in the piroxicam : imidazole hemihydrate complex (refer to Figure 6.2 for key). Values which have no errors are due to hydrogen atoms being placed on calculated positions.*

Complex	H-Bond	D-H (Å)	H···A (Å)	D···A (Å)	∠ D-H···A (°)
$2(PX^-):2(IM^+).H_2O$	a	1.03(4)	1.76(4)	2.787(5)	173(4)
	b	0.89(4)	1.81(4)	2.661(5)	158(4)
	c	0.90(4)	1.85(4)	2.619(5)	143(4)
	c'	0.90(4)	1.86(4)	2.646(5)	144(4)
	d	0.93	2.45	3.371(5)	171
	e	0.93	2.32	3.161(5)	149
	f	0.82(4)	1.88(4)	2.685(5)	167(4)
	f'	0.91(4)	1.78(4)	2.663(5)	162(4)
	g	0.93	2.71	3.540(5)	150
	g'	0.93	2.53	3.333(5)	144

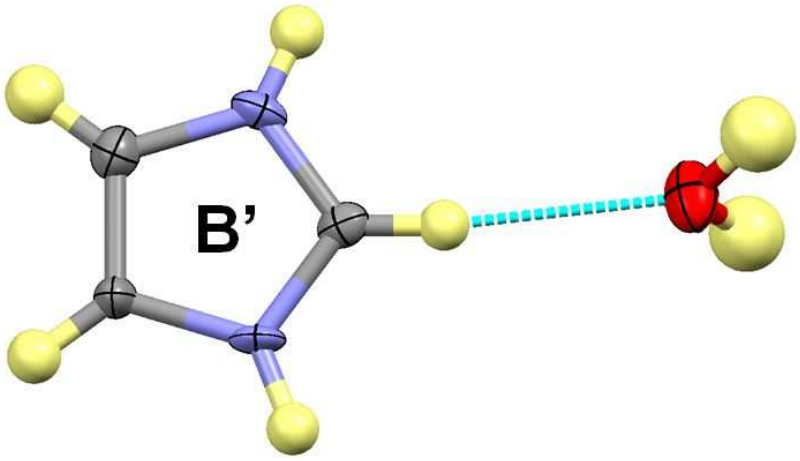

Figure 6.3 *CH···O hydrogen bond between IM^+ and the water molecule in the piroxicam : imidazole hemihydrate complex.*

The water molecule also links equivalent PX^- molecules in different chains above and below it via moderately strong OH···O hydrogen bonds with the amide carbonyl oxygen atoms (O···O = 3.068(4) Å and 2.841(4) Å) (Figure 6.4). The water molecules therefore link three chains together (Figure 6.5).

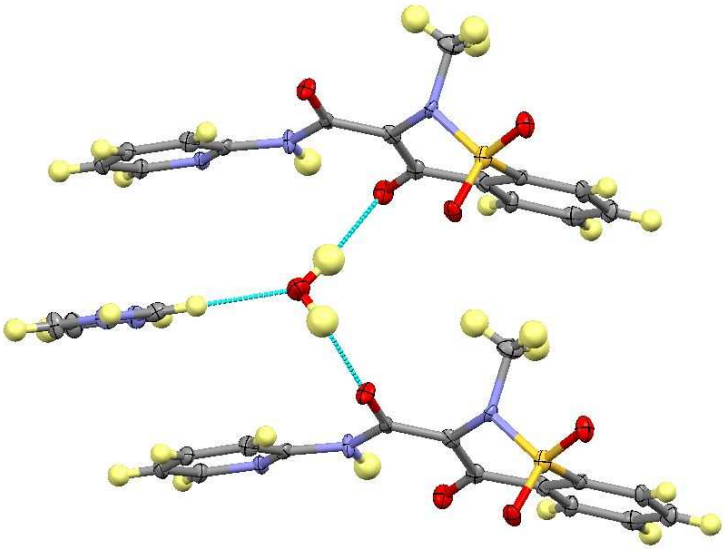

Figure 6.4 *Hydrogen bonds involving the water molecule linking three chains together in the piroxicam : imidazole hemihydrate complex. OH···O hydrogen bonds between the water molecule and PX^- molecules link the chain to a chain above and a chain below.*

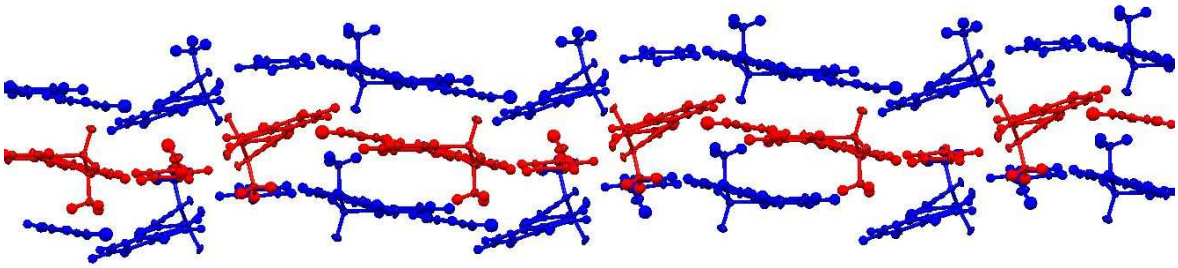

Figure 6.5 *The relative arrangement of three chains linked together by the water molecules in the piroxicam : imidazole hemihydrate complex. The water molecule in the red chain links to the blue chains above and below (via the hydrogen bonding in Figure 6.4).*

Various hydrogen bonds between chains are present involving the sulfonyl oxygen atoms of the PX^- molecules with each symmetry independent PX^- molecule forming different interactions. The sulfonyl oxygen of one PX^- molecule forms a moderately strong bifurcated hydrogen bond with two pyridine CH groups of the PX^- molecule below (C···O = 3.073(5) Å and 3.121(5) Å) as well as a CH···O hydrogen bond with the benzene ring CH of another PX^- molecule (C···O = 3.507(5) Å) (Figure 6.6a). The other sulfonyl oxygen of the same molecule forms further CH···O hydrogen bonds with the methyl group of the PX^- molecule above (C···O =2.873(5) Å) as well as an IM^+ CH group (C···O = 3.333(5) Å) (Figure 6.6b). One sulfonyl oxygen atom of the symmetry independent PX^- molecule forms similar interactions with an IM^+ CH group and a PX^- methyl group (C···O = 3.360(5) Å and 3.042(5) Å respectively) (Figure 6.6c), with the other sulfonyl oxygen forming a CH···O hydrogen bond with the CH of the PX^- benzene ring above (C···O = 3.361(5) Å) (also Figure 6.6c).

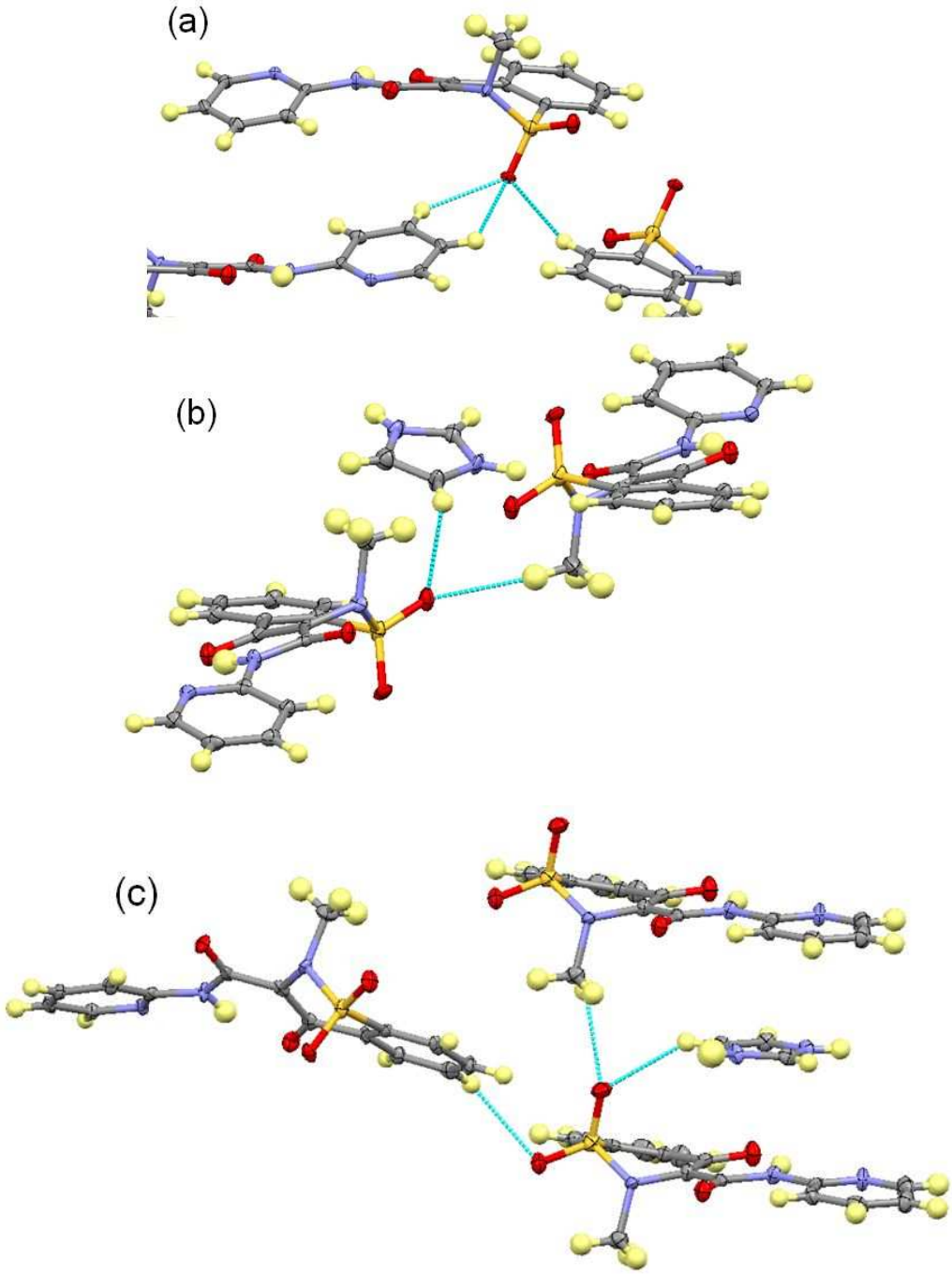

Figure 6.6 *Weak CH···O interactions involving the PX^- sulfonyl oxygen atoms in the piroxicam: imidazole hemihydrate complex.*

6.3.2 Piroxicam : Imidazole Acetonitrile Solvate (1:1:1) (PX^-:IM^+.ACN)

The PX molecules in the 1:1:1 piroxicam: imidazole acetonitrile solvate are again deprotonated to form the enolate oxygen with the hydrogen transferred to the IM molecule forming the imidazolium cation. The asymmetric unit for this complex features one of all three components with the PX^- molecule again adopting the conformation seen in the hemihydrate. The IM+ molecule has delocalisation of the charge, with C-N

distances of 1.332(3) Å and 1.328(3) Å between the carbon in the 2-position and the two nitrogen atoms.

Once again infinite chains with an ABAB configuration are formed featuring two of the interactions that are also found in the PX^-:IM^+ hemihydrate above. Each IM^+ molecule forms a moderately strong, charge-assisted NH···O^- hydrogen bond to the enolate oxygen of one PX^- molecule as well as a slightly weaker NH···O hydrogen bond to the amide carbonyl oxygen atom (Figure 6.7). No NH···N hydrogen bonds are present in this case involving the IM^+ NH and the pyridinal N of PX^-, with weak CH···N interactions occurring only (also Figure 6.7). Alternate PX^- molecules in the chains lie head-to-tail relative to each other, unlike the hemihydrate, in which alternate PX molecules lie head-to-head. Hydrogen bond lengths and angles in the chains can be found in Table 6.3.

The ACN molecule is linked into the chains via weak hydrogen bonds to the sulfonyl oxygen of PX^- via the methyl group (C···O = 3.407(4) Å) and weak CH···N hydrogen bonds from the IM^+ CH group to the ACN nitrogen (C···N = 3.355(4) Å) (Figure 6.8a). ACN molecules also dimerise via weak CH···N hydrogen bonds (C···N = 3.439(4) Å) (also shown in Figure 6.8a). The methyl group of ACN forms a further weak CH···O hydrogen bond to the sulfonyl oxygen of the PX^- molecule below (C···O = 3.570(4) Å) (Figure 6.8b).

Table 6.3 *Hydrogen bond lengths and angles in the 1:1:1 piroxicam : imidazole acetonitrile solvate complex (refer to Figure 6.7 for key). Values which have no errors are due to hydrogen atoms being placed on calculated positions.*

Complex	H-Bond	D-H (Å)	H···A (Å)	D···A (Å)	∠ D-H···A (°)
PX^-:IM^+.ACN	a	0.82(4)	1.89(4)	2.688(3)	164(4)
	b	0.92(3)	1.78(3)	2.659(3)	161(3)
	c	0.87(4)	1.91(4)	2.633(3)	141(3)
	d	0.93	2.79	3.679(3)	160

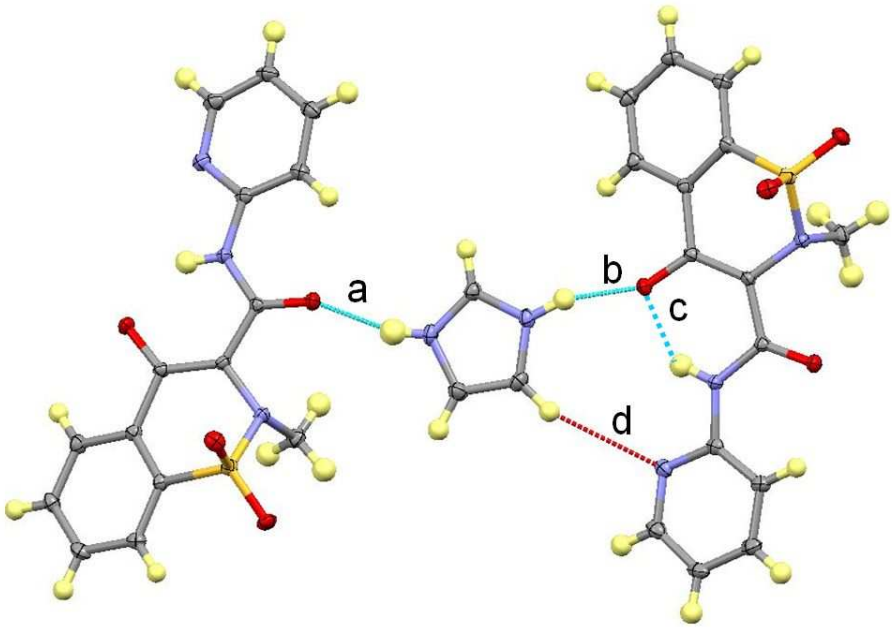

Figure 6.7 *Hydrogen bonding between PX^- and IM^+ in the 1:1:1 piroxicam : imidazole acetonitrile complex. NH···O hydrogen bonds are shown as blue dashed lines and the CH···N hydrogen bond is shown as a red dashed line.*

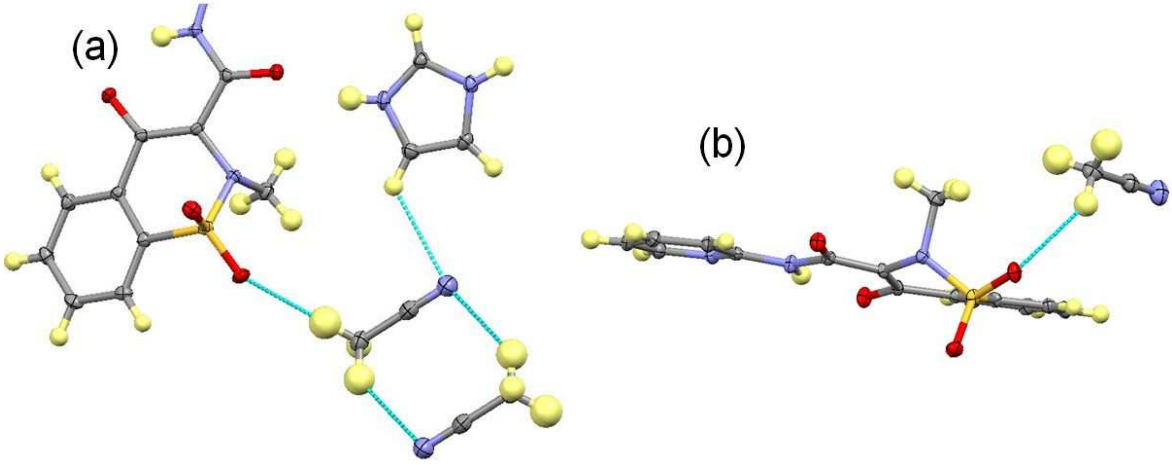

Figure 6.8 *Weak hydrogen bonds involving the ACN molecule in the 1:1:1 piroxicam : imidazole acetonitrile complex. (a) Weak CH···O and CH···N hydrogen bonds linking ACN molecules into the chains and weak CH···N hydrogen bonds resulting in ACN dimers. (b) The weak CH···O hydrogen bond between the ACN molecule and the PX molecule in the chain below.*

As well as forming the weak hydrogen bonds with the ACN molecules, one sulfonyl oxygen atom forms further weak CH···O hydrogen bonds with the CH groups of benzene rings and pyridine rings of neighbouring PX^- molecules (C···O = 3.194(3) Å and 3.598(3) Å) (Figure 6.9a). A weak hydrogen bond is formed to the other sulfonyl oxygen atom by the

CH group of the IM^+ molecule above (C···O = 3.297(3) Å) (Figure 6.9b). A moderately strong, bifurcated CH···N hydrogen bond is also formed between the methyl group of PX^- and the pyridinal N of the PX^- molecule below, with C···N = 3.187(3) Å (Figure 6.10).

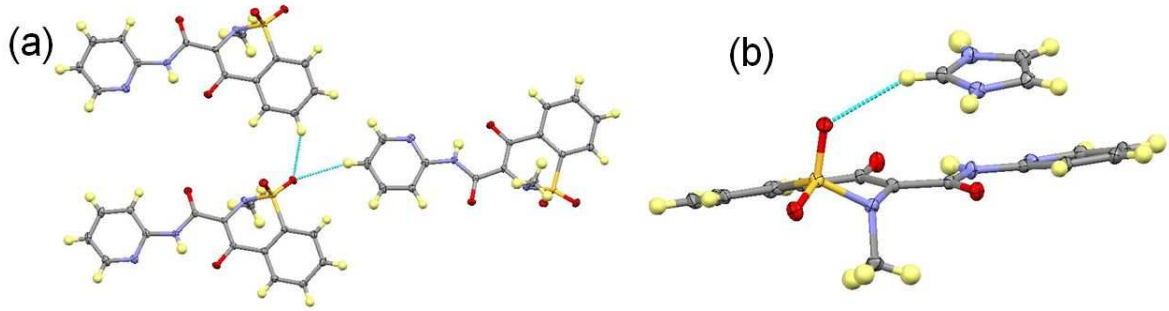

Figure 6.9 *CH···O hydrogen bonds in the 1:1:1 piroxicam: imidazole acetonitrile complex. (a) Weak CH···O hydrogen bonds involving the sulfonyl oxygen between PX^- molecules adjacent to each other and (b) Weak CH···O hydrogen bonds between the IM^+ CH and PX^- sulfonyl oxygen below.*

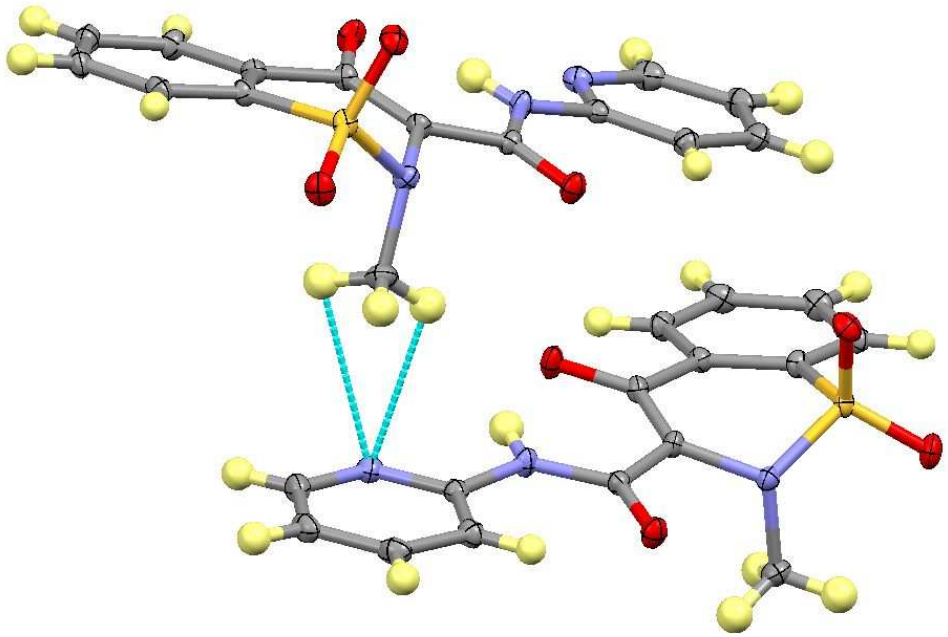

Figure 6.10 *Weak CH···N interactions between the PX^- methyl group and the pyridinal nitrogen in the 1:1:1 piroxicam: imidazole acetonitrile complex.*

6.3.3 Piroxicam : Imidazole Acetonitrile Solvate (4:4:1) (4(PX^-):4(IM^+).ACN)

The asymmetric unit of the 4:4:1 piroxicam : imidazole acetonitrile solvate has two symmetry independent PX^- molecules and IM^+ molecules and a single acetonitrile

molecule with 50% occupancy. It was crystallised from the same PX:IM component ratio (1:1) and solvent (ACN) as the 1:1:1 solvate but was found to crystallise only at 50°C (the 1:1:1 solvate crystallised at room temperature). As in the previous two complexes in this chapter, the PX^- hydroxyl is deprotonated with the hydrogen transferring to the IM nitrogen; the PX^- molecule therefore adopts the same conformation as is found in the previous two complexes. The C-N bond lengths between the 2-carbon and the nitrogen atoms of IM^+ are almost identical, indicating delocalisation of the charge across the two nitrogen atoms (C-N = 1.328(4) Å, 1.322(4) Å and 1.330(4) Å, 1.331(4) Å in the two independent molecules).

One PX^- molecule is disordered, with two positions of the pyridine ring (Figure 6.11). The two positions were refined to a 60/40 occupancy ratio. Fixing the two positions at 50/50 occupancy resulted in implausible thermal parameters. The disorder of the ring is related to the disorder of the ACN molecule which was refined at 50% occupancy across an inversion centre. Refinement of the ACN molecule at 100% occupancy resulted in abnormally large thermal parameters with the molecule lying unusually close to the minor position of the PX^- pyridine ring, with the central carbon of the ACN molecule lying approximately 2.046 Å from the nearest carbon. Refining the ACN molecule at 50% occupancy resulted in plausible thermal parameters and can be rationalised by consideration of the proximity to the two positions of the pyridine rings. The disordered pyridine rings of the PX^- molecules are arranged above and below the ACN molecules (Figure 6.12). In the model proposed, the ACN molecule favours one position across the inversion centre depending on which position the pyridine ring occupies. When the ring above occupies the major position, the ring below favours the minor position (Figure 6.12a). With the rings are in this configuration, one ACN molecule lies close to the bottom ring, with an implausible C···C distance between the two closest carbon atoms (see Table 6.4). The other position is therefore favoured in this case, where the C···C values between the carbon atoms are more plausible (also Table 6.4). When the pyridine rings occupy the reverse positions (minor above, major below), the other position of the ACN molecule is occupied (Figure 6.12b). There is a discrepancy, however, between the occupancy values of the disorder model, with the positions of the ring refined to a 60/40 occupancy ratio and the ACN molecules 50/50 disordered across the inversion centre. This suggests another possibility, where in some cases both ACN molecules related by the inversion centre are occupied and both of the neighbouring PX pyridine rings point away (i.e. both

rings occupy the major position). In other cases the rings would point inwards (i.e. occupy the minor position) and neither of the two ACN positions would be occupied.

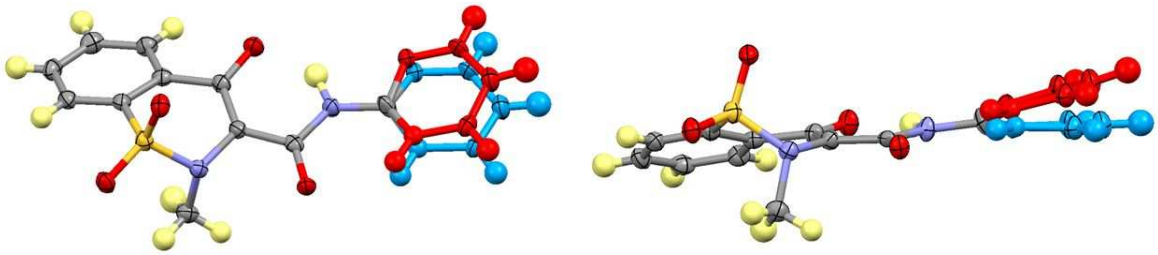

Figure 6.11 *The two positions of the disordered pyridine ring in the PX^- molecules of the 4:4:1 piroxicam : imidazole acetonitrile complex. The major position (60% occupancy) is shown in red, with the minor position (40%) in blue.*

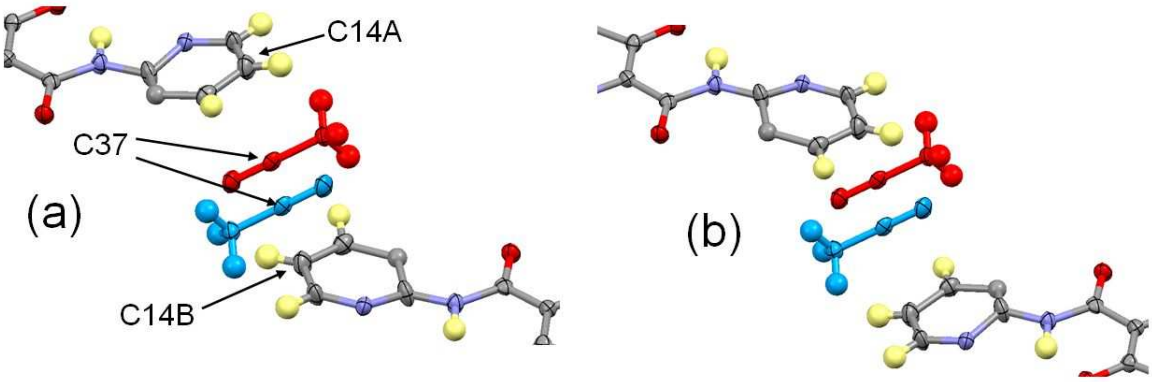

Figure 6.12 *Proposed disorder model of the 4:4:1 piroxicam : imidazole acetonitrile solvate complex. (a) The top pyridine ring is in the major position and the bottom ring in the minor position. The red position of the ACN molecule is occupied in this case. (b) The top pyridine ring is in the minor position and the bottom ring in the major position. The blue position of the ACN molecule is occupied in this case. Parts of the PX molecules are omitted.*

Table 6.4 *The distances between the closest PX^- pyridine and ACN carbon atoms in Figure 6.12a. The values show that the red ACN position is likely to be favoured in this case due to the implausible C···C distance with the blue ACN position (indicated with *).*

ACN Position	C14A···C37 (Å)	C14B···C37 (Å)
Red ACN (Figure 6.12a)	3.387(8)	3.097(10)
Blue ACN (Figure 6.12a)	3.794(8)	2.425(10)*

The structure consists of infinite chains similar to those observed in the 1:1:1 PX^-:IM^+.ACN complex, with the same NH···O hydrogen bonding present between PX^- and IM^+

molecules (Figure 6.13 and Table 6.5). The same weak CH···N hydrogen bond is also present between the IM^+ CH group and the PX^- pyridine N and is much stronger in this complex than in the 1:1:1 complex, although in general the interactions in this complex are slightly weaker. The chains are symmetry independent (i.e. an ABAB and an A'B'A'B' chain), with the IM^+ of only one chain interacting with the ACN molecule through a CH···N hydrogen bond (Also Figure 6.13). A difference is found when comparing the relative position of the ACN molecule, with the molecule lying along a different direction relative to the chain and no longer forming a CH···O hydrogen bond with the PX^- sulfonyl O as in the 1:1:1 complex. Hydrogen bond lengths and angles in the chains can be found in Table 6.5.

PX^- molecules are linked to neighbouring symmetry independent PX^- molecules in different chains by weak CH···O hydrogen bonds between the sulfonyl oxygen atoms and the CH groups of the pyridine (C···O = 3.404(6) Å) and benzene (C···O = 3.094(4) Å) rings (Figure 6.14a). The sulfonyl oxygen atoms also form further weak hydrogen bonds with the molecules below (Figure 6.14b). The sulfonyl oxygen atoms of both PX^- molecules form hydrogen bonds with the CH groups of IM+ molecules below (C···O = 3.197(3) Å and 3.178(4) Å) with one PX^- molecule also forming a hydrogen bond with the pyridine CH group of the PX^- molecule below (C···O = 3.291(4) Å).

Table 6.5 *Hydrogen bond lengths and angles in the 4:4:1 piroxicam : imidazole acetonitrile solvate complex (refer to Figure 6.13 for key). Equivalent values for the 1:1:1 solvate are also shown for comparison. Values which have no errors are due to hydrogen atoms being placed on calculated positions.*

Complex	H-Bond	D-H (Å)	H···A (Å)	D···A (Å)	∠ D-H···A (°)
4(PX^-):4(IM^+).ACN	a	0.98(4)	1.74(4)	2.690(3)	162(3)
	a'	0.97(4)	1.75(4)	2.710(3)	170(3)
	b	0.96(3)	1.77(3)	2.689(3)	161(3)
	b'	0.80(3)	1.92(3)	2.690(3)	160(3)
	c	1.03(3)	1.76(3)	2.636(3)	140(3)
	c'	0.93(3)	1.82(3)	2.626(3)	145(3)
	d	0.93	2.34	3.247(10)	167
	d'	0.93	2.43	3.322(4)	160
	e	0.93	2.55	3.403(6)	153
PX^-:IM^+.ACN	a	0.82(4)	1.89(4)	2.688(3)	164(4)
	b	0.92(3)	1.78(3)	2.659(3)	161(3)
	c	0.87(4)	1.91(4)	2.633(3)	141(3)
	d	0.93	2.79	3.679(3)	160
	e	0.93	2.73	3.355(4)	125.5

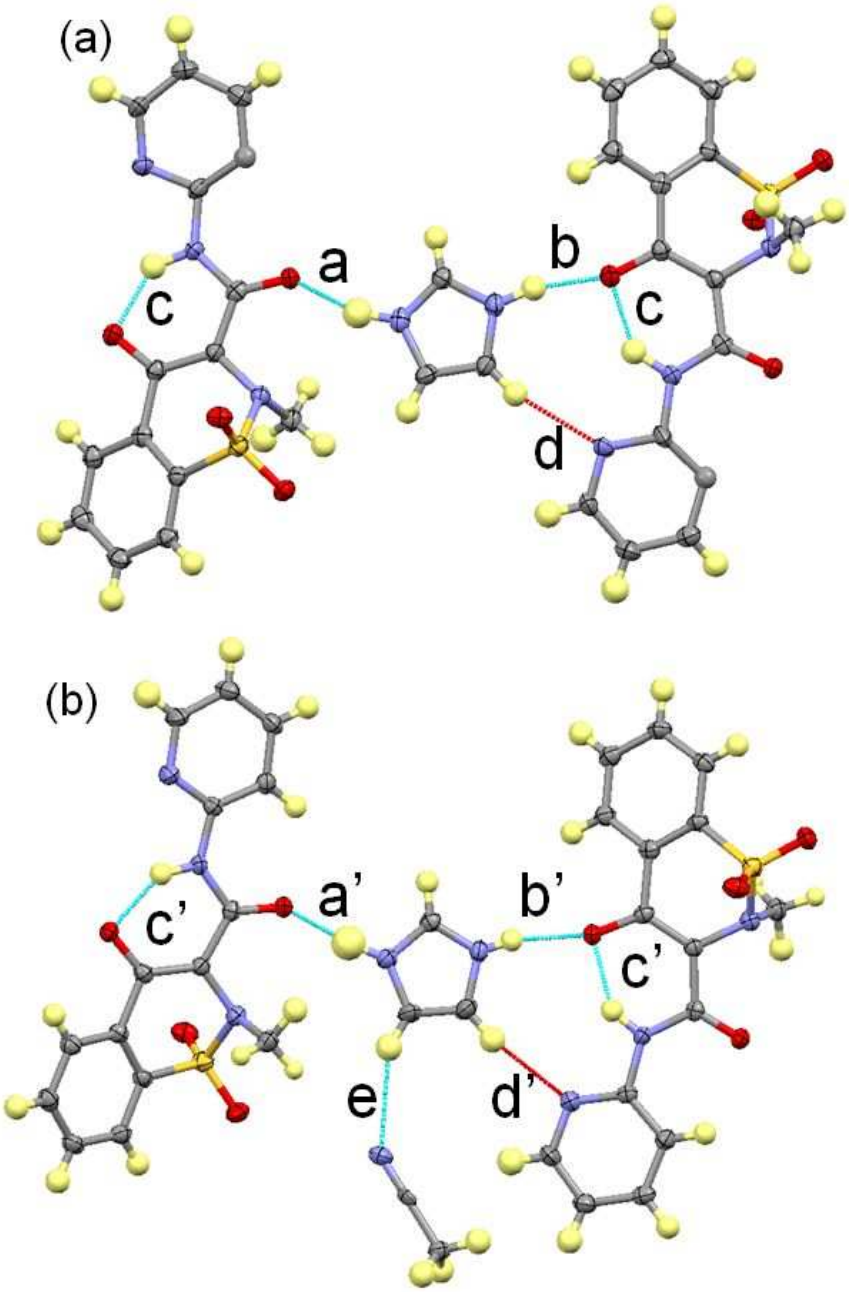

Figure 6.13 *Hydrogen bonding in the symmetry independent chains of PX^- and IM+ molecules in the 4:4:1 piroxicam : imidazole acetonitrile complex.*

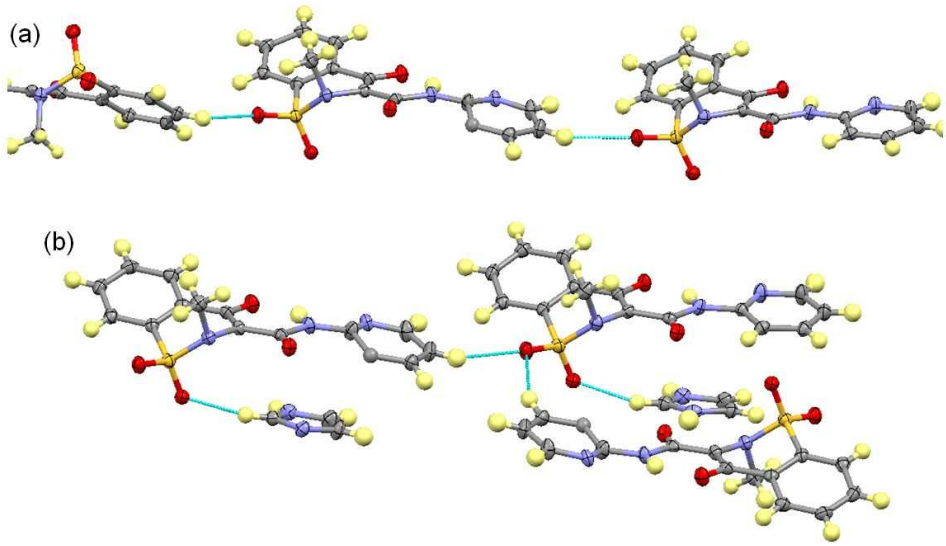

Figure 6.14 *Weak CH···O interactions involving the sulfonyl oxygen atoms with (a) neighbouring PX⁻ molecules and (b) PX⁻ and IM+ molecules below.*

6.3.4 Piroxicam : 2-methylimidazole (PX^-:$2MIM^+$)

The piroxicam : 2-methylimidazole molecular salt complex crystallises in a 1:1 ratio with the hydroxyl hydrogen of PX again having transferred to the 2MIM nitrogen forming a 2-methylimidazolium cation ($2MIM^+$). The piroxicam anion adopts the conformation found in the previous complexes in this chapter. The $2MIM^+$ molecules show delocalisation of the charge, evidenced by the bond lengths between the two nitrogen atoms and the 2-carbon (C-N = 1.317(3) Å and 1.326(3) Å).

ABAB chains of PX^- and $2MIM^+$ molecules are again formed and the structure directing NH···O^- and NH···O hydrogen bonds within the chains are the same as those seen in the PX^-:IM^+.ACN complex (Figure 6.15). The NH hydrogen bond to the carbonyl O is again the weaker of the two interactions (Table 6.6). The NH···O interactions are weaker than those in the 1:1:1 PX^-:IM^+.ACN although the NH interaction with the enolate oxygen is stronger than that seen in the 4:4:1 ACN solvate with the amide carbonyl interaction weaker. A key difference lies in the relative arrangement of alternate PX^- molecules, which are arranged in a head-to-head arrangement as opposed to head-to-tail as in the PX^-:IM^+.ACN complex. This difference means the weak CH···N hydrogen bond between the IM^+ and the PX^- pyridinal N is no longer present, although the absence of the solvent ACN molecule means a weak CH···O interaction to the sulfonyl oxygen atom is

formed as the PX^- molecule lies closer to the $2MIM^+$ molecule (also Figure 6.15). Hydrogen bond lengths and angles in the chains can be found in Table 6.6.

Adjacent chains are linked by moderately strong CH···O hydrogen bonds (C···O = 3.178(3) Å) between the CH of the pyridine ring and the sulfonyl oxygen which is hydrogen bonded to the $2MIM^+$ molecule (Figure 6.16). This holds the chains together in layers which are then stacked upon each other (Figure 6.17). Weak CH···O hydrogen bonds between the other sulfonyl oxygen atom and the CH groups of the pyridine and benzene rings of the PX molecules above help hold the layers together (C···O = 3.266(3) Å and 3.406(3) Å) (Figure 6.18).

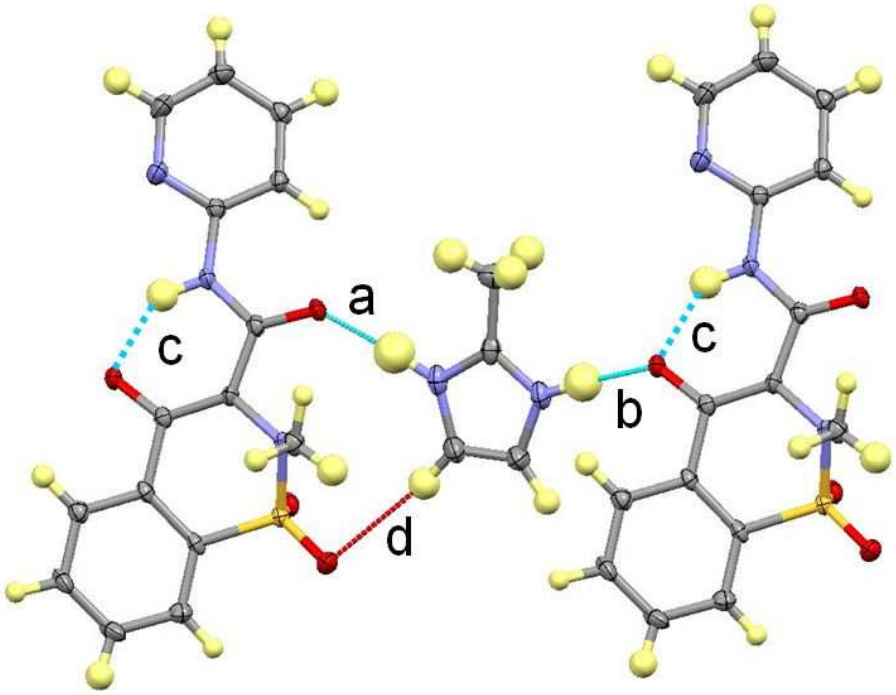

Figure 6.15 *NH···O⁻ and NH···O hydrogen bonds (blue dashed lines) between PX^- and $2MIM^+$ in the PX^-:$2MIM^+$ molecular salt complex and the weak CH···O hydrogen bond (red dashed line).*

Table 6.6 *Hydrogen bond lengths and angles in the piroxicam : 2-methylimidazole salt complex (refer to Figure 6.13 for key). Equivalent interactions in the PX^-:IM^+ 1:1:1 and 4:4:1 acetonitrile solvate complexes are also shown for comparison.*

Complex	H-Bond	D-H (Å)	H···A (Å)	D···A (Å)	∠ D-H···A (°)
PX^-:2MIM^+	a	1.02(4)	1.73(4)	2.746(3)	176(3)
	b	0.94(4)	1.74(4)	2.672(3)	171(3)
	c	0.93(3)	1.87(3)	2.656(3)	141(2)
	d	0.98(3)	2.51(3)	3.332(3)	142(2)
PX^-:IM^+.ACN	a	0.82(4)	1.89(4)	2.688(3)	164(4)
	b	0.92(3)	1.78(3)	2.659(3)	161(3)
	c	0.87(4)	1.91(4)	2.633(3)	141(3)
4(PX^-):4(IM^+).ACN	a	0.98(4)	1.74(4)	2.690(3)	162(3)
	a’	0.97(4)	1.75(4)	2.710(3)	170(3)
	b	0.96(3)	1.77(3)	2.689(3)	161(3)
	b’	0.80(3)	1.92(3)	2.690(3)	160(3)
	c	1.03(3)	1.76(3)	2.636(3)	140(3)
	c’	0.93(3)	1.82(3)	2.626(3)	145(3)

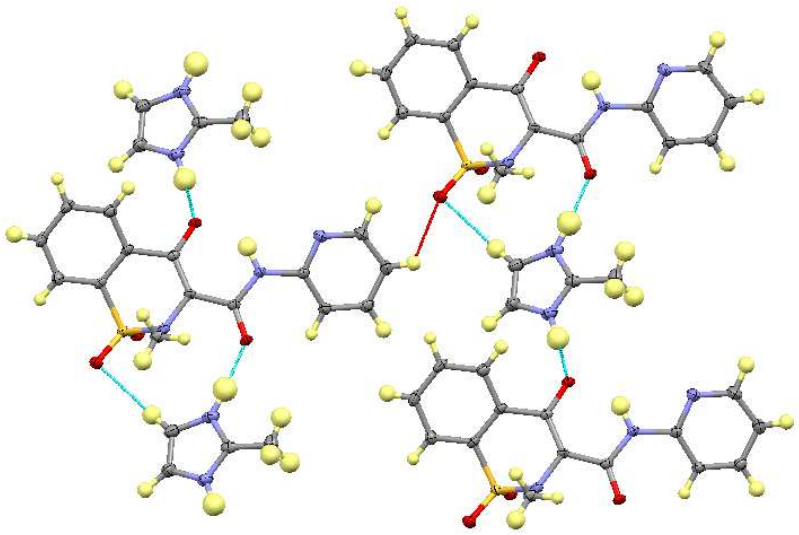

Figure 6.16 *The weak CH---O hydrogen bond (red dashed line) between the PX^- pyridine ring and the sulfonyl oxygen holding adjacent chains together in the piroxicam : 2-methylimidazole molecular salt complex.*

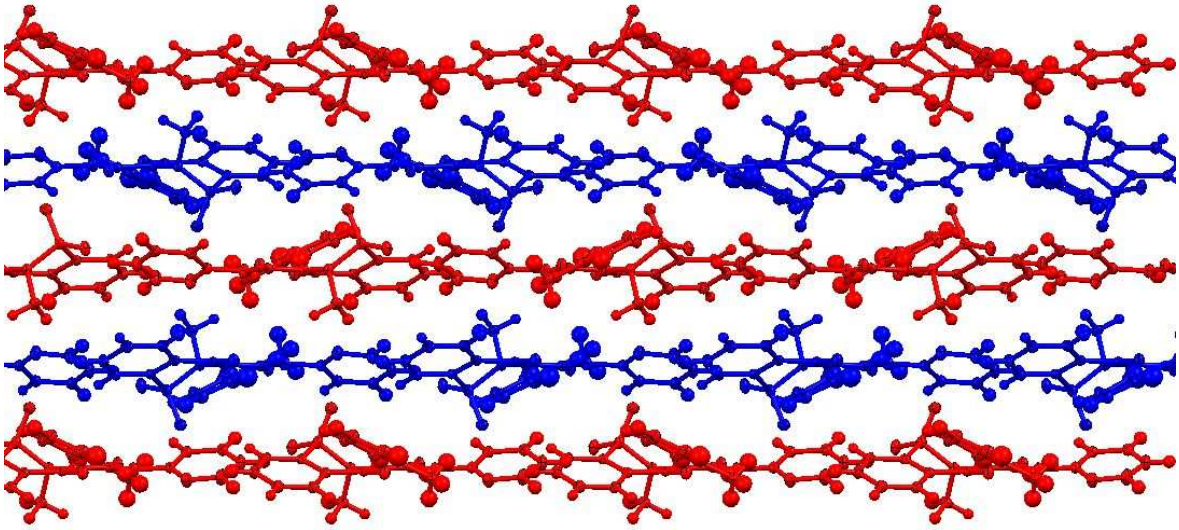

Figure 6.17 *Layered arrangement of chains in the piroxicam : 2-methylimidazole molecular salt complex with alternate chains in different colours.*

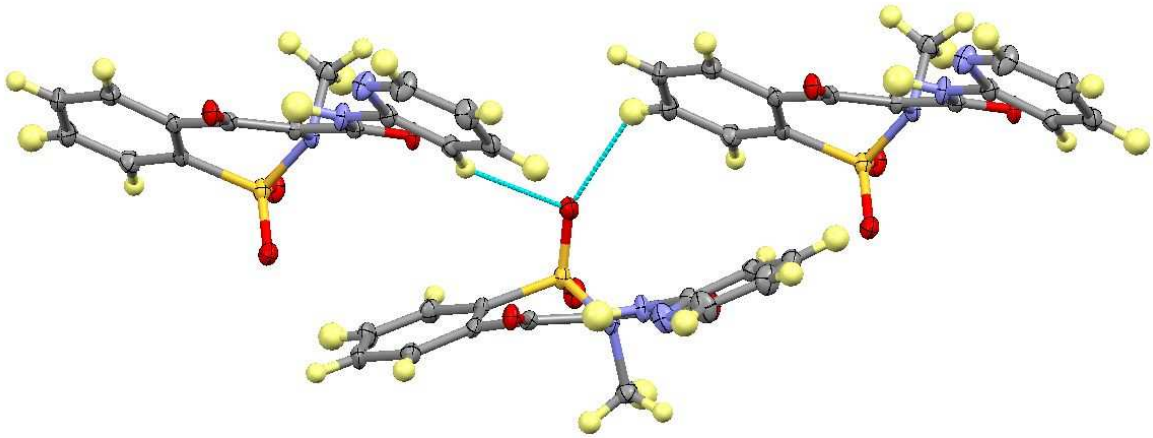

Figure 6.18 *CH···O interactions between the sulfonyl oxygen and the CH groups of the benzene ring and pyridine ring of the PX^- molecule above in the piroxicam : 2-methylimidazole molecular salt complex.*

Further weak hydrogen bonds are present between layers involving the methyl groups of both PX^- and $2MIM^+$. The methyl CH of PX^- forms very weak hydrogen bonds to the amide carbonyl oxygen of the PX^- molecule above/below (C···O = 3.653(3) Å) (Figure 6.19). The $2MIM^+$ methyl CH forms a stronger hydrogen bond to the enolate oxygen of the PX^- molecule above/below (C···O = 3.250(3) Å) (Figure 6.20).

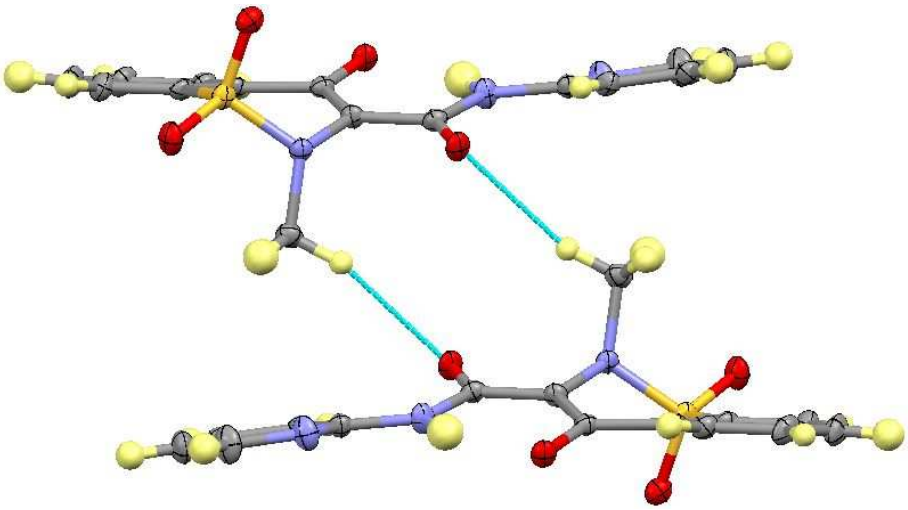

Figure 6.19 *Weak CH···O hydrogen bonds between the PX^- methyl group CH and the carbonyl oxygen atoms in the piroxicam : 2-methylimidazole molecular salt complex.*

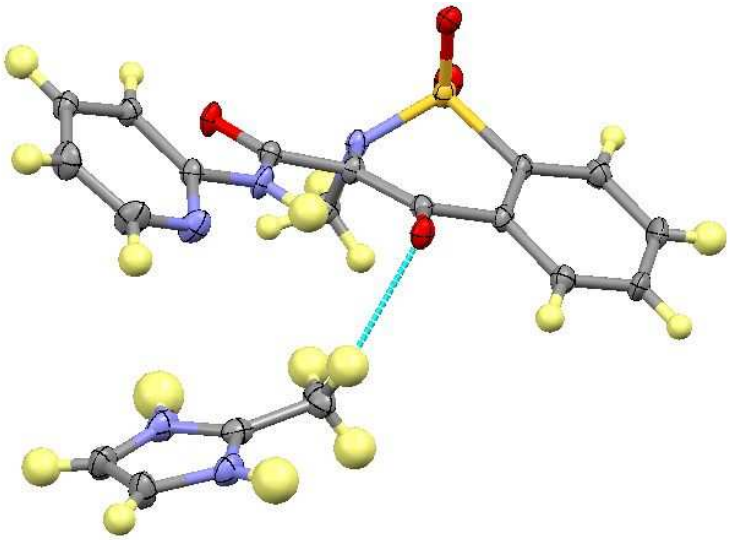

Figure 6.20 *Weak hydrogen bonds between the $2MIM^+$ methyl CH and the enolate oxygen of PX^- in the piroxicam : 2-methylimidazole molecular salt complex.*

6.3.5 Piroxicam : Benzimidazole (PX^-:BZ^+)

The piroxicam : benzimidazole molecular salt complex has four molecules (two symmetry independent molecules of both PX^- and BZ^+) in the asymmetric unit, with the PX hydroxyl hydrogen having transferred to the BZ nitrogen forming the benzimidazolium cation (BZ^+). PX^- molecules adopt the same conformation as the PX^- anions in the previously described molecular complexes in this chapter. The C···N distances to the carbon in the 2-position in the symmetry independent BZ^+ molecules are similar. One molecule (B in Figure 6.21) has

C-N distances of 1.333(6) Å and 1.317(6) Å and the other (B') has distances of 1.323(6) Å and 1.334(6) Å.

Once again the structure is primarily made up of chains of alternating PX^- and BZ^+ molecules with an ABA'B' arrangement. The structure directing NH···O^- and NH···O hydrogen bonds are arranged in the same way as in the PX^-:IM^+.ACN complex with alternate PX^- molecules lying head-to-tail relative to each other (Figure 6.21). The NH···O hydrogen bonds from one BZ^+ molecule (B' in Figure 6.21) are stronger than in any of the IM complexes or the 2MIM complex (Table 6.7). The NH···O interactions from the other BZ^+ molecule (B) are slightly weaker and more comparable with the 4:4:1 solvate complex. Weak hydrogen bonds are also present between the BZ^+ benzene ring CH groups and the sulfonyl oxygen atoms and pyridinal nitrogen atoms of the PX^- molecules (also Figure 6.21).

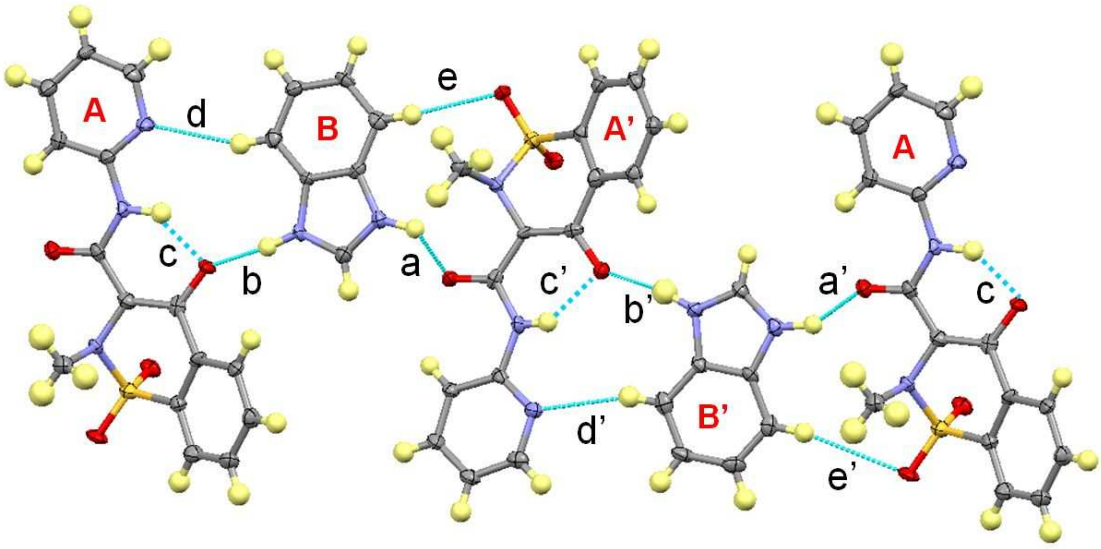

Figure 6.21 *Hydrogen bonding in the ABA'B' chains of the piroxicam : benzimidazole molecular salt complex.*

Table 6.7 *Hydrogen bond lengths and angles in the piroxicam: benzimidazole salt complex (refer to Figure 6.21 for key). Equivalent values for PX^-:2MIM^+, PX^-:IM^+.ACN and 4(PX^-):4(IM^+). ACN are shown for comparison. Values which have no errors are due to hydrogen atoms being placed on calculated positions.*

Complex	H-Bond	D-H (Å)	H···A (Å)	D···A (Å)	∠ D-H···A (°)
PX^-:BZ^+	a	1.01(4)	1.78(5)	2.696(6)	148(4)
	a'	1.00(4)	1.81(4)	2.656(5)	141(3)
	b	1.00(5)	1.72(5)	2.694(6)	163(5)
	b'	0.96(5)	1.69(4)	2.644(6)	174(4)
	c	0.81(6)	1.97(5)	2.651(6)	143(5)
	c'	1.00(5)	1.84(5)	2.662(6)	137(4)
	d	0.93	2.54	3.429(7)	161
	d'	0.93	2.51	3.378(7)	156
	e	0.93	2.91	3.817(6)	167
	e'	0.93	2.48	3.409(6)	174
PX^-:2MIM^+	a	1.02(4)	1.73(4)	2.746(3)	176(3)
	b	0.94(4)	1.74(4)	2.672(3)	171(3)
	c	0.93(3)	1.87(3)	2.656(3)	141(2)
PX^-:IM^+.ACN	a	0.82(4)	1.89(4)	2.688(3)	164(4)
	b	0.92(3)	1.78(3)	2.659(3)	161(3)
	c	0.87(4)	1.91(4)	2.633(3)	141(3)
4(PX^-):4(IM^+).ACN	a	0.98(4)	1.74(4)	2.690(3)	162(3)
	a'	0.97(4)	1.75(4)	2.710(3)	170(3)
	b	0.96(3)	1.77(3)	2.689(3)	161(3)
	b'	0.80(3)	1.92(3)	2.690(3)	160(3)
	c	1.03(3)	1.76(3)	2.636(3)	140(3)
	c'	0.93(3)	1.82(3)	2.626(3)	145(3)

Weak CH···O hydrogen bonds are formed to the sulfonyl oxygen atoms from CH groups of both the BZ^+ benzene ring (C···O = 3.556(6) Å) and the PX^- benzene ring (C···O = 3.167(7) Å), holding adjacent chains together in layers which stack on top of each other (Figure 6.22). Both symmetry independent PX^- molecules interact with BZ^+ molecules in the chain below with CH···O hydrogen bonds between the BZ^+ CH and the sulfonyl oxygen of PX^- (C···O = 3.207(7) Å and 3.189(7) Å) as well as π-π interactions (Figure 6.23) between the PX^- pyridine rings and the BZ^+ benzene rings. The π···π distances are approximately 3.331 Å and 3.374 Å (distance between centroids of the two closest π bonds).

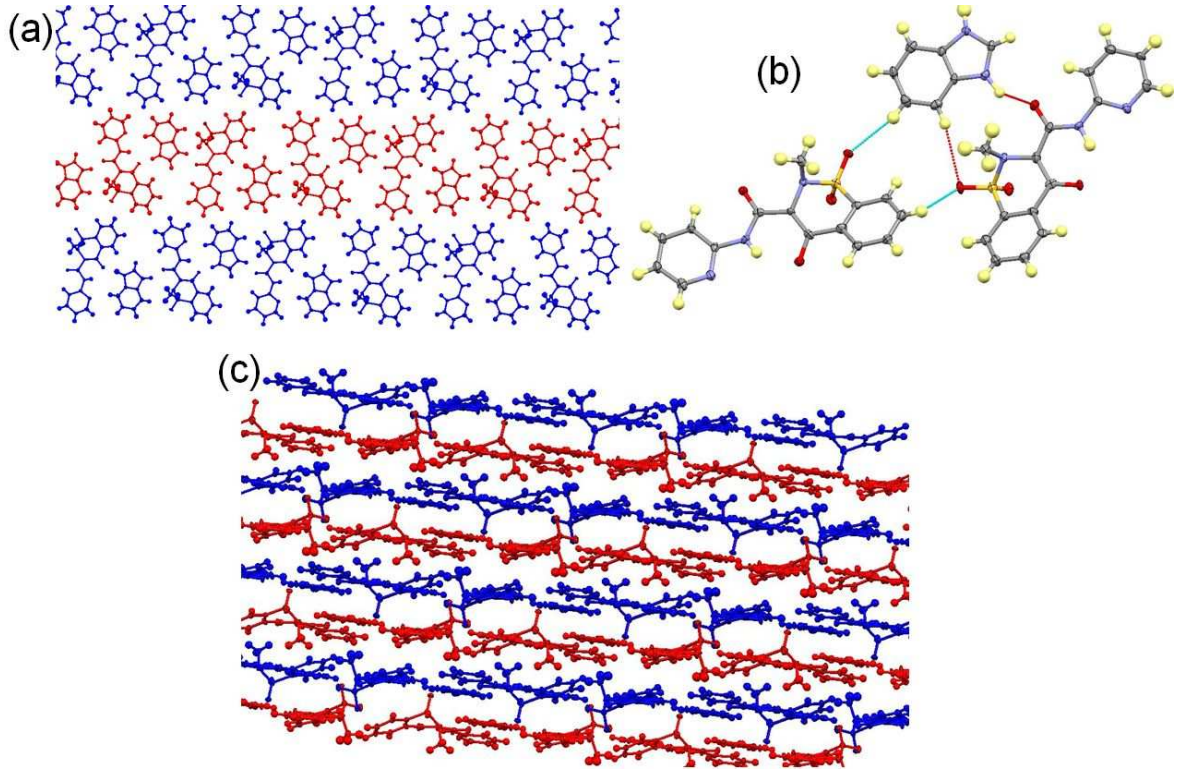

Figure *6.22* *The structure of the piroxicam : benzimidazole molecular salt complex. (a) Arrangement of chains within the layers, with alternate chains in different colours, (b) weak CH···O hydrogen bonds to the sulfonyl oxygen atoms formed by the PX^- and BZ^+ aromatic CH groups in neighbouring chains within layers (blue dashed lines). Interactions within the chains are shown as red dashed lines, (c) arrangement of layers relative to each other, with alternate layers in different colours. Note that neighbouring PX^- and BZ^+ molecules in the layers overlap slightly.*

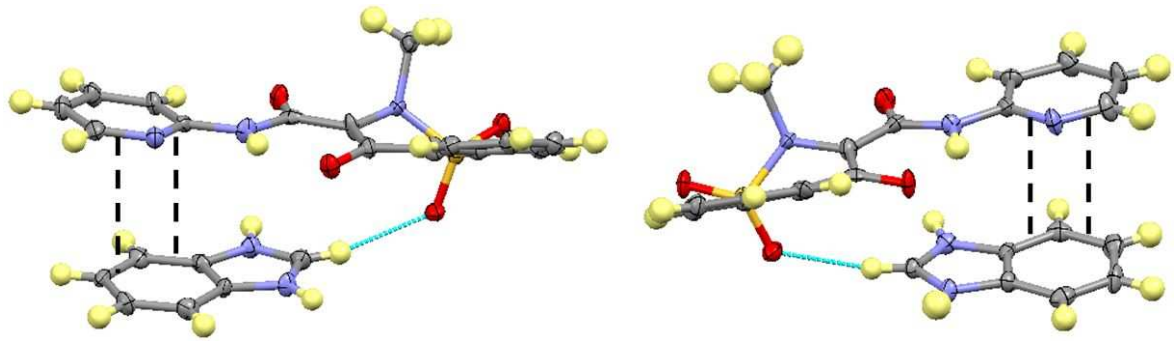

Figure 6.23 *CH···O hydrogen bonds and π···π interactions between PX^- and BZ^+ molecules above and below each other in the piroxicam : benzimidazole molecular salt complex (both non-equivalent interactions shown).*

6.3.6 Piroxicam : 1, 2, 4 - Triazole (2PXZ:TZ)

The piroxicam : triazole complex crystallises in a 2:1 ratio with no intermolecular hydrogen transfer occurring. Intramolecular hydrogen transfer does occur however, with PX molecules present in the zwitterionic tautomeric form and adopting the typical conformation found in this form (Figure 6.1). The asymmetric unit has two fully occupied PXZ molecules and two TZ molecules with 50% occupancy. Both symmetry independent TZ molecules are 50/50 disordered across an inversion centre resulting in two possible positions of the molecules (Figure 6.24).

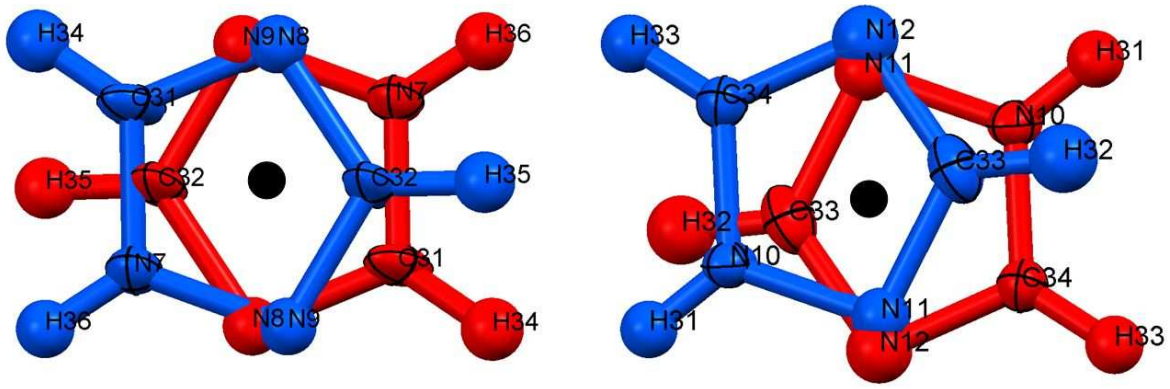

Figure 6.24 *Disorder of the triazole molecules in the piroxicam : triazole complex. The black circle indicates the inversion centre which relates two incomplete parts of each molecule.*

The PXZ molecules dimerise through the $R_2^2(12)$ ring (Figure 6.25) which is consistent with PXZ complexes with mono-substituted benzoic acids (see Chapter 5). Hydrogen bond lengths in the dimer can be found in Table 6.8. The TZ molecule links the dimers through moderately strong, charge-assisted NH···O$^-$ interactions with the PXZ enolate oxygen and weak CH···N interactions between the TZ N and the CH of the pyridine ring of the next PXZ molecule (Figure 6.26). A weak CH···O$^-$ hydrogen bond to the enolate oxygen of the next PX molecule is also formed (Also figure 6.26). When the TZ molecule lies in the second disordered position, the same interactions are formed in reverse (Figure 6.26b). The infinite chains created by these interactions have an TZZT configuration (where T = triazole and Z = zwitterionic piroxicam). Only symmetry equivalent PXZ and TZ molecules

are present in the same chain, i.e. chains of TZZT and T'Z'Z'T'. Hydrogen bond lengths and angles for both chains can be found in Table 6.8.

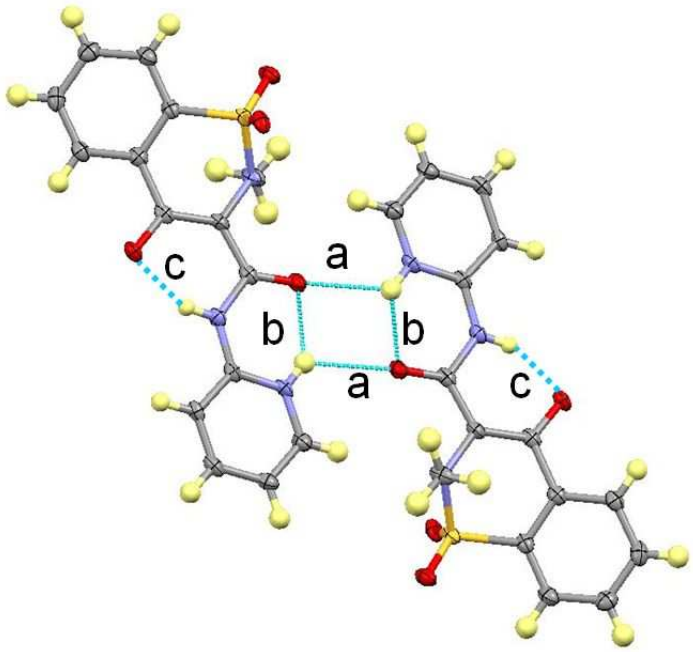

Figure 6.25 *The PXZ dimer in the piroxicam : triazole complex.*

Table 6.8 *Hydrogen bond lengths and angles in the piroxicam : triazole complex (refer to Figures 6.25 and 6.26 for key). Values which have no errors are due to hydrogen atoms being placed on calculated positions.*

Complex	H-Bond	D-H (Å)	H···A (Å)	D···A (Å)	∠ D-H···A (°)
2PXZ:TZ	a	0.80(3)	2.21(3)	2.804(3)	131(3)
	a'	0.84(4)	2.29(4)	2.852(3)	125(3)
	b	0.80(3)	2.05(3)	2.662(3)	133(3)
	b'	0.84(4)	1.97(3)	2.654(3)	138(4)
	c	0.80(3)	1.87(3)	2.569(3)	145(3)
	c'	0.82(3)	1.84(3)	2.575(3)	148(3)
	d	0.86	1.85	2.674(8)	160
	d'	0.86	1.93	2.749(7)	159
	e	0.93	2.35	3.280(10)	173
	e'	0.93	2.46	3.371(9)	166
	f	0.93	2.64	3.259(9)	125
	f'	0.93	2.91	3.398(10	114
	g	0.93	2.61	3.538(9)	175
	g'	0.93	2.35	3.275(9)	170

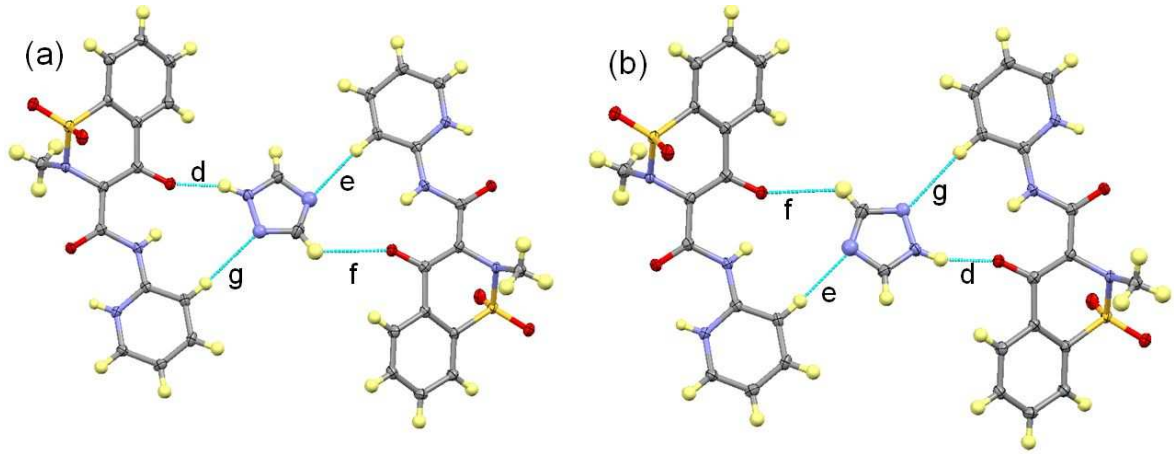

Figure 6.26 *(a) The hydrogen bonding between TZ molecules and PXZ molecules in the piroxicam : triazole complex with (b) showing the same interactions formed in reverse when the TZ molecule is in the second position.*

The symmetry independent chains are arranged alternately (Figure 6.27a) and this forms layers which are stacked upon each other in a wave-like fashion (Figure 6.27b). PXZ molecules in the alternate chains are linked by a moderately strong CH···O hydrogen bond between the aromatic CH of the pyridine ring and the sulfonyl oxygen atom which lies in the plane of the layer (C···O = 3.183(4) Å) (Figure 6.28a). The other sulfonyl oxygen bridges between layers and forms three CH···O hydrogen bonds of moderate to weak strength with molecules in the layers above (Figure 6.28b). The interactions are formed with the pyridine ring CH group of the PXZ molecule above (C···O = 3.249(4) Å), as well as the CH group of a TZ molecule (3.005(9) Å). A weak CH···O hydrogen bond is also formed to the methyl group of the PXZ molecule two layers above (3.203(4) Å). The symmetry independent PXZ molecule has one sulfonyl molecule in a similar environment, with the same three CH···O interactions formed (Figure 6.29a). The hydrogen bonds with the pyridine and methyl CH groups are similar to those in the other molecule, with C···O distances of 3.376(4) Å and 3.135(3) Å respectively. A large difference is seen in the TZ interaction however, which has a C···O distance of 3.461(6) Å in the second molecule. The CH···O interaction with PXZ molecules in the alternate chain is no longer present, replaced instead by a very weak CH···O hydrogen bond to a PXZ molecule above (C···O = 3.717(4) Å) (Figure 6.29b).

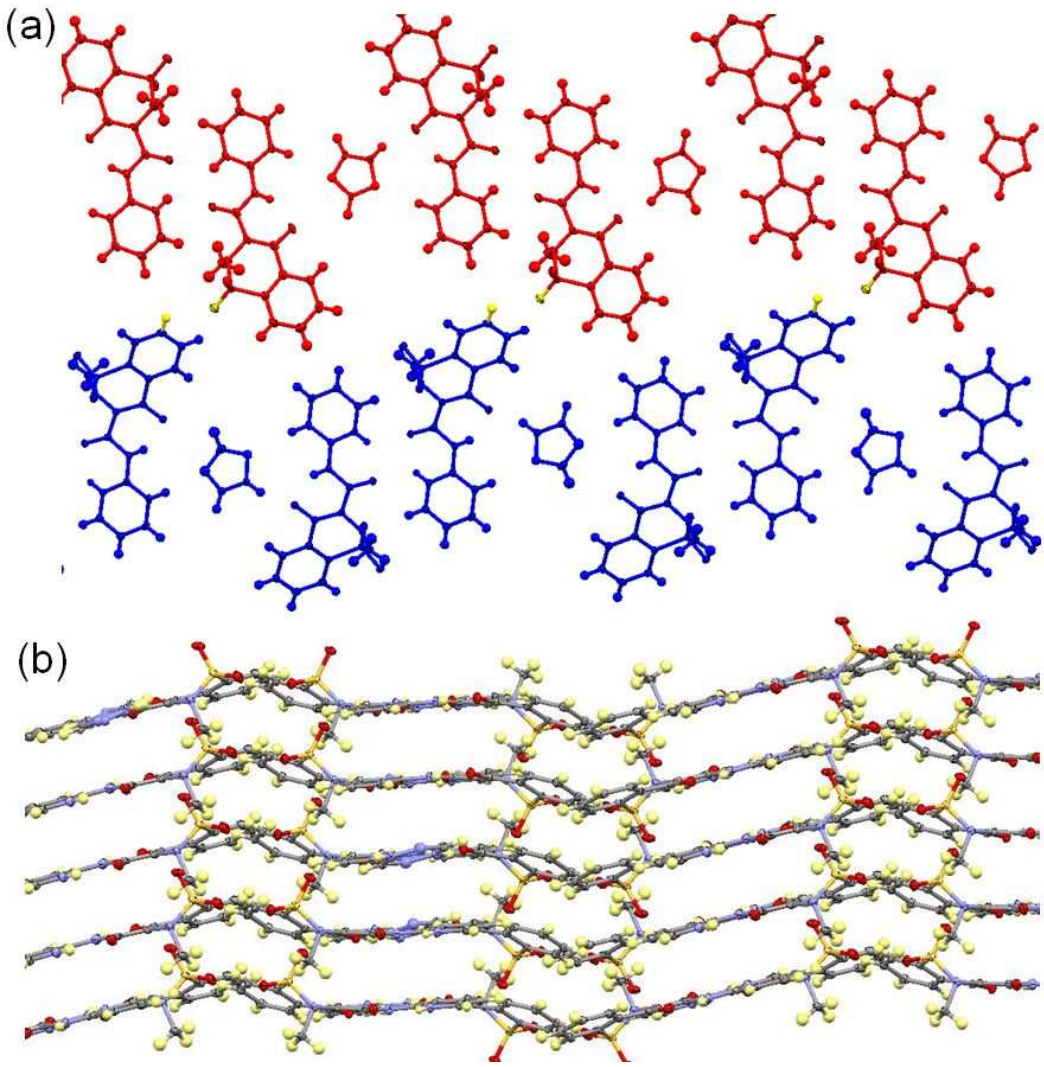

Figure 6.27 *Layers in the piroxicam : triazole complex. (a) The arrangement of alternate chains in a single layer, with symmetry independent chains shown in different colours. The aromatic H and sulfonyl O atoms that form moderately strong hydrogen bonds between chains are highlighted in yellow. Only one TZ orientation is shown for clarity. (b) Relative arrangement of layers in a wave like fashion with methyl groups and sulfonyl oxygen atoms bridging between layers.*

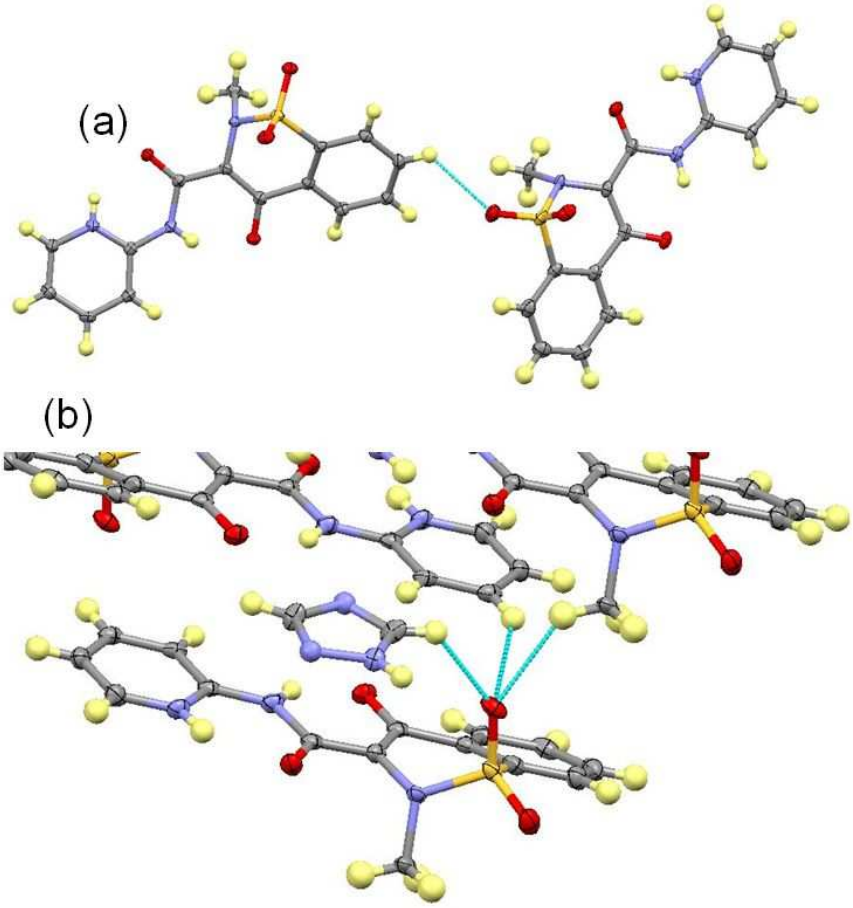

Figure 6.28 *Interactions of sulfonyl oxygen atoms in the piroxicam : triazole complex. (a) CH···O interactions between neighbouring chains in the layers. (b) CH···O interactions involving the sulfonyl oxygen atom bridging between layers. Only one TZ orientation is shown for clarity.*

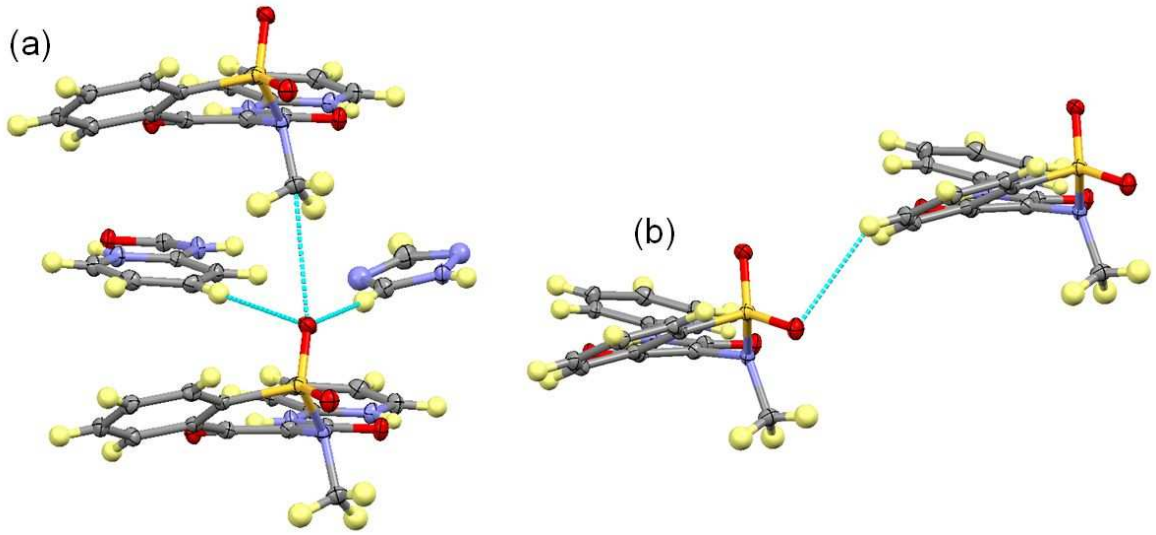

Figure 6.29 *Interactions of the PXZ sulfonyl oxygen atoms (symmetry independent of the PXZ molecule in Figure 6.28) in the piroxicam: triazole complex. Only one TZ orientation is shown for clarity. (a) CH···O hydrogen bonds to molecules in the layer(s) above. (b) CH···O interaction of the second sulfonyl oxygen atom (also to the layer above).*

6.3.7 Piroxicam : Benzotriazole (PXZ:BZT)

The piroxicam : benzotriazole 1:1 molecular complex again features PX molecules in the zwitterionic form with no intermolecular hydrogen transfer occurring. PXZ molecules again adopt the typical conformation of this tautomer. PXZ molecules again dimerise forming the $R_2^2(12)$ ring (Figure 6.30). The hydrogen bonding of the BZT molecule to the PXZ molecule is similar to that in the PXZ:TZ complex, with a moderately strong, charge-assisted NH···O$^-$ hydrogen bond to the enolate oxygen (also Figure 6.30). This forms a tetramer with a BZT:ZZ:BZT configuration, similar to the tetramers seen in the PXZ complexes with mono-substituted benzoic acids in Chapter 5. The hydrogen bond lengths and angles in the tetramer are presented in Table 6.9 along with the analogous hydrogen bonds in the PXZ:TZ complex (where applicable). All analogous bond lengths in the two complexes are similar despite the different arrangement of the nitrogen atoms and the presence of the six-membered ring.

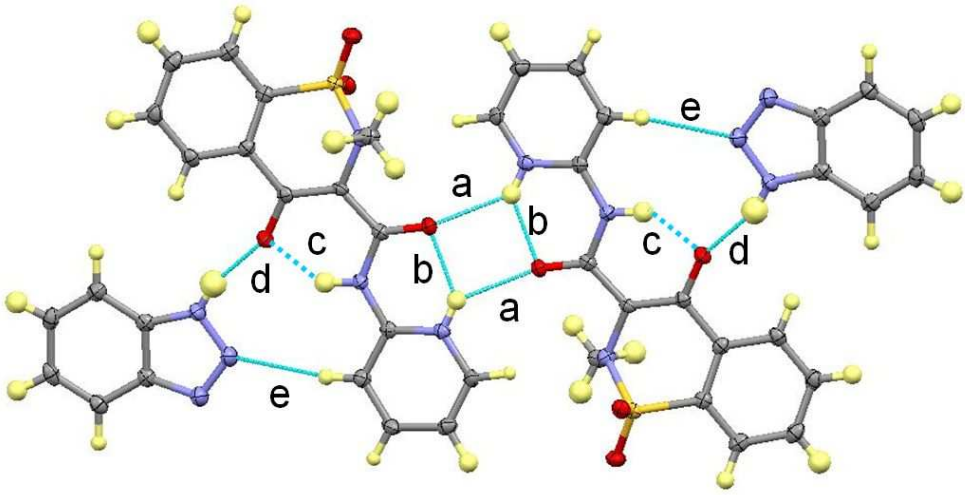

Figure 6.30 *Hydrogen bonding in the PXZ:BZT complex forming an ABBA tetramer.*

Table 6.9 *Hydrogen bond lengths and angles in the piroxicam : benzotriaozle complex (refer to Figure 6.30 for key). Analogous values for the piroxicam : triazole complex are also shown for comparison. Values which have no errors are due to hydrogen atoms being placed on calculated positions.*

Complex	H-Bond	D-H (Å)	H···A (Å)	D···A (Å)	∠ D-H···A (°)
PXZ:BZT	a	0.85(4)	2.19(4)	2.842(4)	133(4)
	b	0.85(4)	1.98(5)	2.644(4)	135(4)
	c	0.89(4)	1.81(5)	2.571(4)	142(4)
	d	0.85(5)	1.88(5)	2.697(4)	161(4)
	e	0.93(4)	2.59(4)	3.518(5)	171(3)
2PXZ:TZ	a	0.80(3)	2.21(3)	2.804(3)	131(3)
	a’	0.84(4)	2.29(4)	2.852(3)	125(3)
	b	0.80(3)	2.05(3)	2.662(3)	133(3)
	b’	0.84(4)	1.97(3)	2.654(3)	138(4)
	c	0.80(3)	1.87(3)	2.569(3)	145(3)
	c’	0.82(3)	1.84(3)	2.575(3)	148(3)
	d	0.86	1.85	2.674(8)	160
	d’	0.86	1.93	2.749(7)	159

The sulfonyl oxygen atoms again form a series of weak hydrogen bonds to molecules above and below (Figure 6.31). One sulfonyl oxygen atom forms three CH···O hydrogen bonds, with the pyridine CH of a PXZ molecule below (C···O = 3.440(4) Å), the methyl CH of another PXZ molecule (C···O 3.648(5) Å) below and the CH of a BZT molecule below (C···O = 3.489(5) Å). The other sulfonyl oxygen forms only weak hydrogen bonds to the methyl group of the PXZ molecule above with an inversion centre relating these two molecules so that an equivalent interaction goes both ways with C···O = 3.475(5) Å. PXZ molecules are further linked by weak CH···π interactions between the benzene rings with

an approximate C···π distance of 3.365 Å (Figure 6.32). The overall crystal packing has PXZ molecules arranged in a herringbone pattern (Figure 6.33a). BZT molecules are arranged parallel to each other, intersecting the herringbone arrangement of the PXZ molecules (Figure 6.33b).

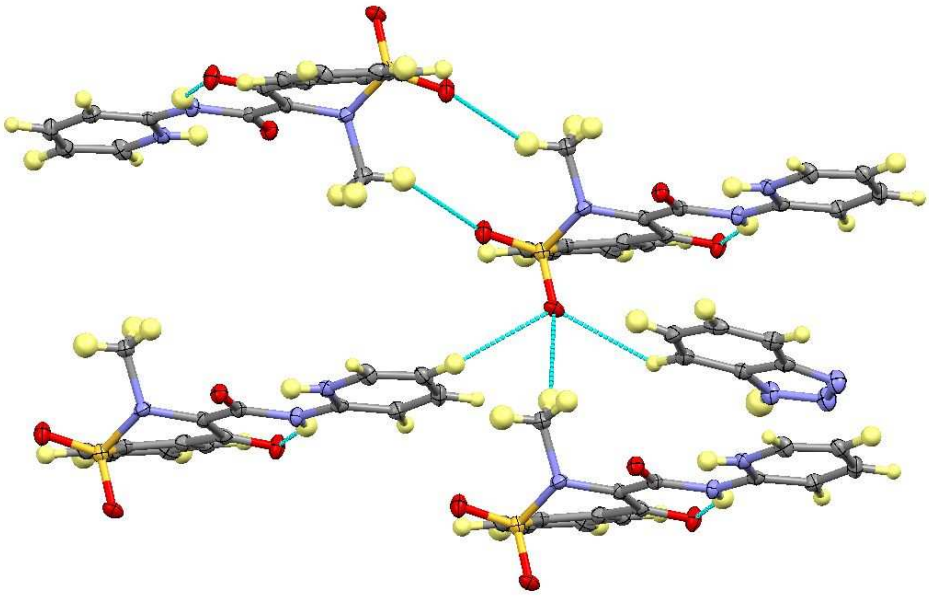

Figure 6.31 *CH···O hydrogen bonds involving the sulfonyl oxygen atoms in the piroxicam : benzotriazole complex.*

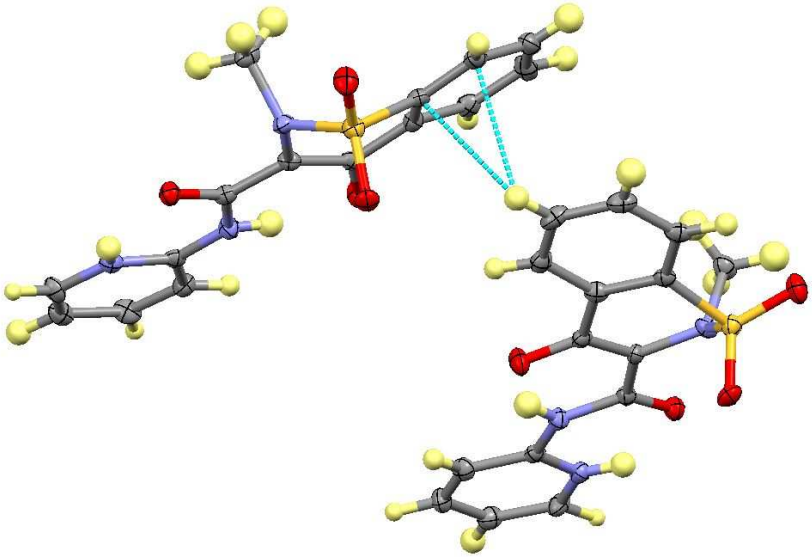

Figure 6.32 *CH···π interactions between PXZ molecules in the piroxicam : benzotriaozle complex.*

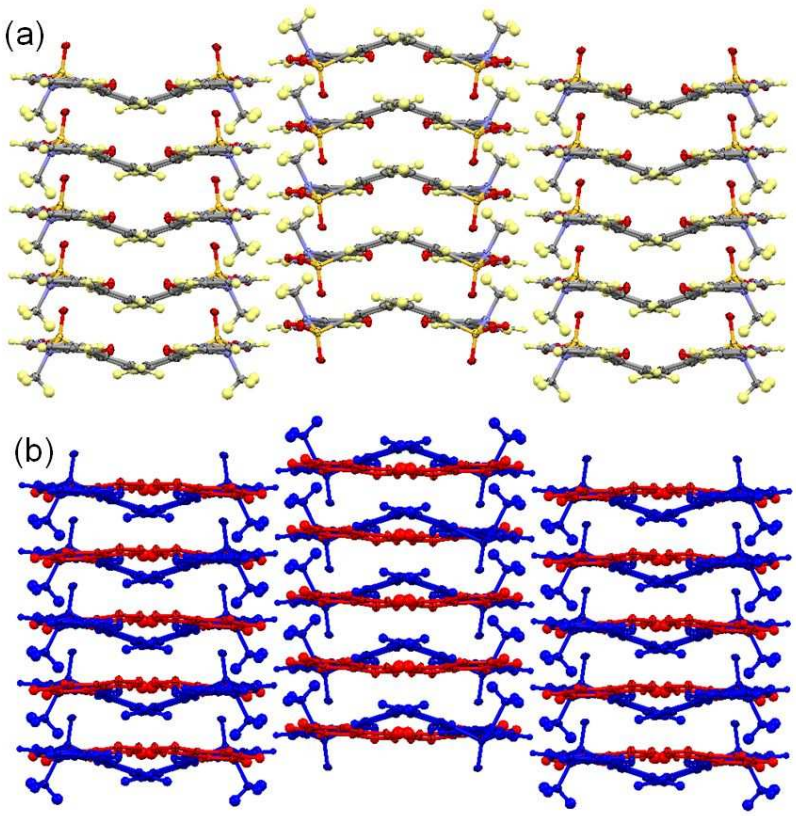

Figure 6.33 *Crystal packing in the piroxicam : benzotriazole complex. (a) The herringbone arrangement of the PXZ molecules (BZT molecules omitted) (b) the relative arrangement of the BZT molecules (red) with the PXZ molecules (blue).*

6.3.8 Piroxicam : Pyrazine (2PXZ:PZN)

The piroxicam : pyrazine complex crystallises in a 2:1 ratio with no intermolecular hydrogen transfer occurring. PX is in the zwitterionic tautomeric form with the typical conformation of this tautomer. There are two PXZ molecules in the asymmetric unit and two symmetry independent halves of PZN molecules lying on inversion centres. The PXZ molecules again form dimers via the typical $R_2^2(12)$ ring (Figure 6.34). The PZN molecules are linked to the PXZ molecules through moderately strong, charge-assisted CH···O^- hydrogen bonds with the enolate oxygen as well as weak CH···N hydrogen bonds from a PXZ pyridine CH group to the PZN nitrogen (also Figure 6.34). This forms infinite chains with a PZZPZZ configuration (where P = pyrazine and Z = zwitterionic piroxicam). The hydrogen bond lengths and angles in the chains are given in Table 6.10.

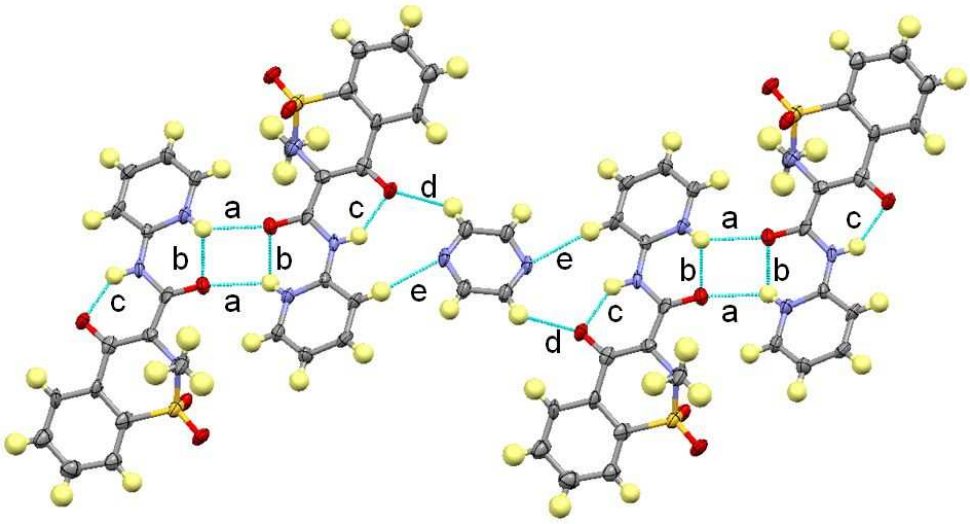

Figure 6.34 *Hydrogen bonding in the chains of PXZ and PZN in the piroxicam : pyrazine complex (only one symmetry independent chain shown).*

Table 6.10 *Hydrogen bond lengths and angles in the piroxicam : pyrazine complex (refer to Figure 6.34 for key; hydrogen bonds marked a and a' indicate identical hydrogen bonds in the symmetry independent chains). Values which have no errors are due to hydrogen atoms being placed on calculated positions.*

Complex	H-Bond	D-H (Å)	H···A (Å)	D···A (Å)	∠ D-H···A (°)
2PXZ:PZN	a	0.86	2.24	2.862(12)	129
	a'	0.86	2.22	2.845(12)	130
	b	0.86	2.02	2.675(12)	132
	b'	0.86	2.02	2.670(12)	132
	c	0.86	1.84	2.559(12)	140
	c'	0.86	1.80	2.524(13)	141
	d	0.93	2.33	3.087(14)	139
	d'	0.93	2.31	3.039(15)	135
	e	0.93	2.40	3.325(15)	172
	e'	0.93	2.45	3.378(15)	172

Symmetry independent chains are arranged alternately, linked by a weak to moderately strong CH···O hydrogen bond (C···O = 3.252(15) Å) between the PXZ benzene CH groups and the PXZ sulfonyl oxygen atoms to form layers (Figure 6.35). The layers are stacked upon each other (Figure 6.36a), linked by CH···O hydrogen bonds involving the sulfonyl oxygen atoms which bridge between the layers (Figure 6.36b). Both symmetry independent bridging sulfonyl oxygen atoms form similar interactions, with weak CH···O hydrogen bonds formed with the PXZ pyridine ring (C···O = 3.476(15) Å and 3.544(15) Å) and PZN (C···O = 3.575(14) Å and 3.457(15) Å) molecules in the layer below and a

moderately strong hydrogen bond formed to the methyl group of the PXZ molecules two layers away (C···O = 3.021(15) Å and 2.968(17) Å).

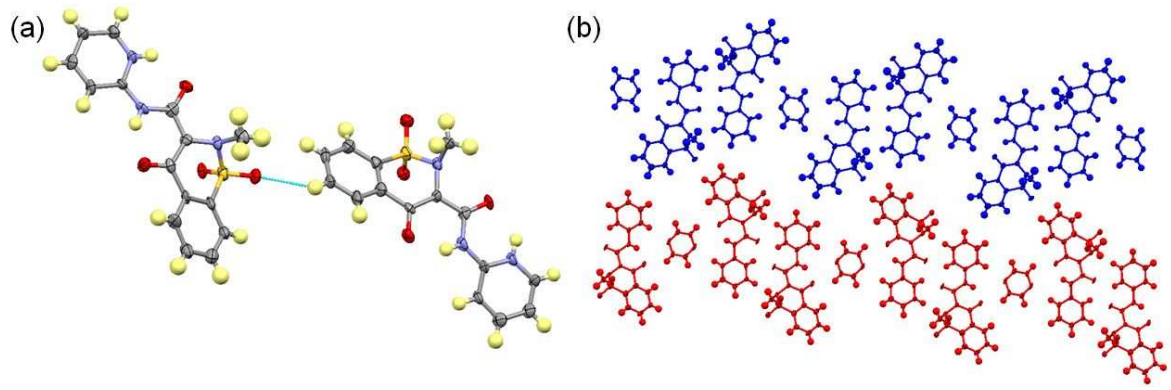

Figure 6.35 *Relative arrangement of symmetry independent chains showing (a) the CH···O hydrogen bond between PXZ molecules of neighbouring chains and (b) the relative arrangement of these chains which form layers (alternate symmetry independent chains linked by the interaction in (a) shown in different colours).*

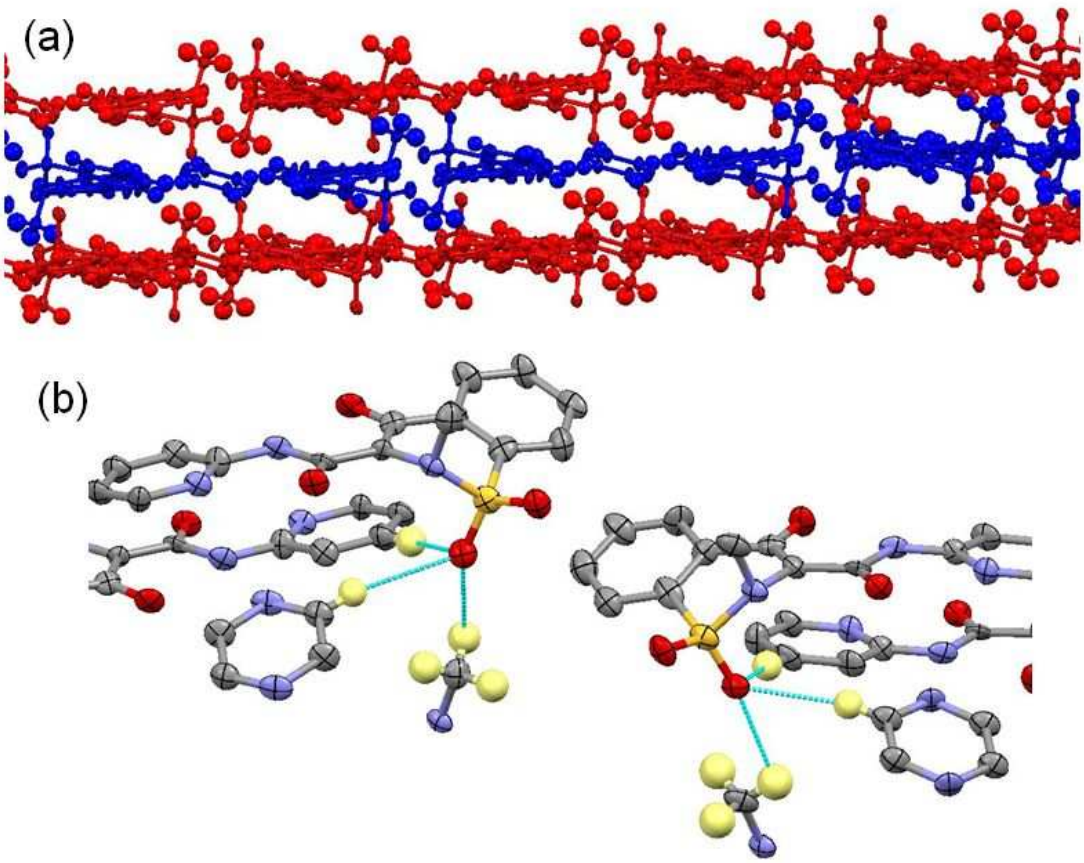

Figure 6.36 *(a) Relative arrangement of layers in the piroxicam : pyrazine complex. (b) CH···O hydrogen bonds involving the bridging sulfonyl oxygen atoms (bottom PXZ molecule and hydrogen atoms partially omitted for clarity).*

6.4 Crystal Structures of Molecular Complexes of Piroxicam with Strong Acids: Chloranilic Acid and Bromanilic Acid

To investigate the possibility of protonation of the PX pyridine ring to form a molecular salt containing a PX cation, chloranilic and bromanilic acid were chosen as co-molecules as they have low pKa values (chloranilic acid pKa1 = 0.76; bromanilic acid pKa1 = 0.22) and are known to readily give up at least one hydrogen atom when co-crystallised with bases that have pKa values in a similar range to the PX pyridine ring[224,225]. Four complexes were produced using these co-molecules. Full refinement details for all complexes can be found in (Appendix A6 and Table A-6b).

6.4.1 Piroxicam : Chloranilic Acid Form I (PX^+:CA^-) (Triclinic)

The 1:1 salt complex of piroxicam with chloranilic acid (CA) contains one molecule of each component in the asymmetric unit. An OH hydrogen from the CA molecule is transferred to the pyridinal nitrogen of PX, forming a positively charged PX ion (PX^+) and a CA anion (CA^-). This is the first time such an ion of PX has been isolated in the solid state. It adopts the same conformation as is seen in the non-ionised form of PX, with a short strong intramolecular OH···O hydrogen bond (Figure 6.37).

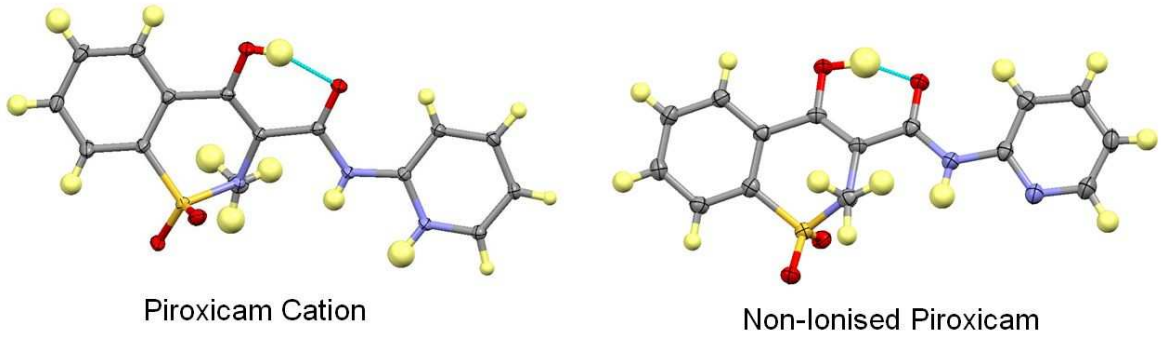

Figure 6.37 *Conformation of the protonated piroxicam molecules (PX^+) in the piroxicam : chloranilic acid form I complex. The conformation of non-ionised piroxicam is also shown for comparison.*

CA^- molecules dimerise through the OH groups and carbonyl groups forming moderately strong OH···O hydrogen bonds (d in Figure 6.38). The PX^+ molecules are then linked either side of the dimer to form relatively co-planar tetramers. They are linked via two

asymmetric, charge assisted, bifurcated NH···O hydrogen bonds to the deprotonated CA^- oxygen and the carbonyl oxygen (a, b and c in Figure 6.38). One bifurcated hydrogen bond has a DHAA configuration and the second a DDHHA configuration. The amide NH of PX^+ forms a moderately strong hydrogen bond with the deprotonated oxygen atom (longer C-O distance), which then forms hydrogen bonds to the pyridine NH through a slightly stronger interaction. The pyridine NH also forms another moderately strong - although weaker than the others - NH···O hydrogen bond to the carbonyl oxygen atom of CA^-. Hydrogen bond lengths and angles can be found in Table 6.11.

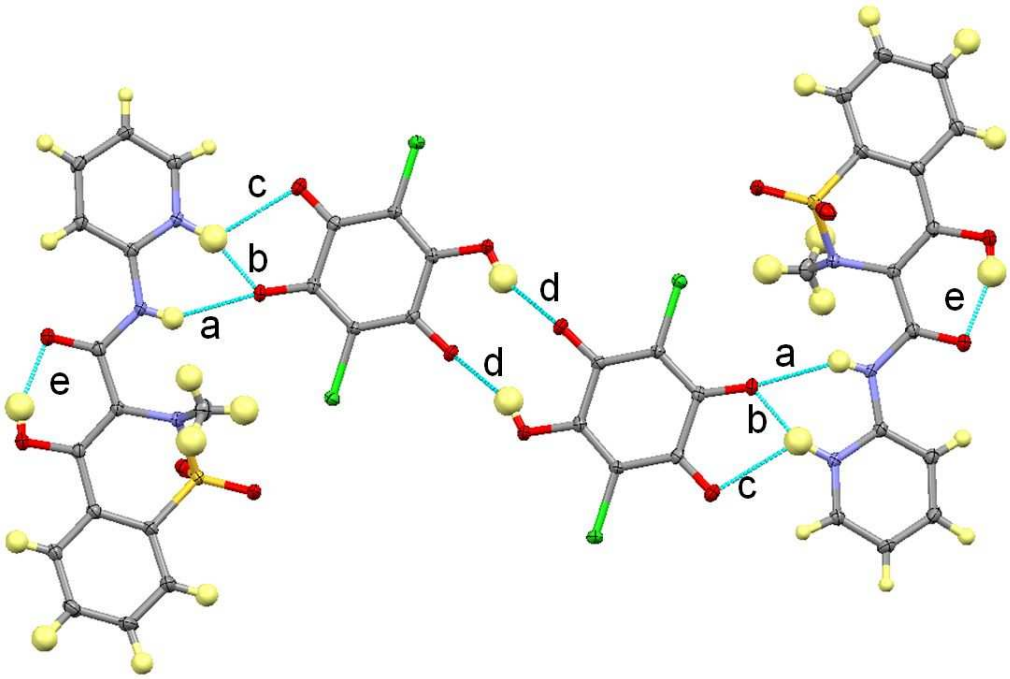

Figure 6.38 *Hydrogen bonded tetramers in the piroxicam : chloranilic acid 1:1 form I complex.*

Table 6.11 *Hydrogen bond lengths and angles in the piroxicam : chloranilic acid 1:1 form I complex (refer to Figure 6.38).*

Complex	H-Bond	D-H (Å)	H···A (Å)	D···A (Å)	∠ D-H···A (°)
$PX^+:CA^-$ (I)	a	0.79(2)	2.25(2)	2.942(2)	147(2)
	b	0.98(2)	1.70(2)	2.634(2)	158(3)
	c	0.98(2)	2.43(2)	3.065(2)	122(2)
	d	0.85(3)	1.98(2)	2.756(2)	153(3)
	e	0.81(3)	1.78(3)	2.533(2)	153(2)

Tetramers are linked by a series of weak hydrogen bonds involving the PX^+ aromatic CH groups to form layers (Figure 6.39a). The CH groups form hydrogen bonds with the CA^- hydroxyl oxygen atom (C···O = 3.548(2) Å) as well as the chlorine atom of the neighbouring CA^- (C···Cl = 3.882(2) Å) and the sulfonyl oxygen of the PX^+ molecule (C···O =

3.255(2) Å). The layers are stacked upon each other with the PX^+ methyl and sulfonyl oxygen bridging between layers (Figure 6.39b). The methyl group forms a weak hydrogen bond with an oxygen atom of the CA^- molecule below (C···O = 3.548(2) Å), as well as a weak hydrogen bond with the chlorine atom (C···Cl = 3.882(2) Å) (Figure 6.40). The bridging sulfonyl oxygen atom forms weak hydrogen bonds with the pyridine CH groups of two PX^+ molecules above (C···O = 2.951(2)Å and 3.122(2) Å).

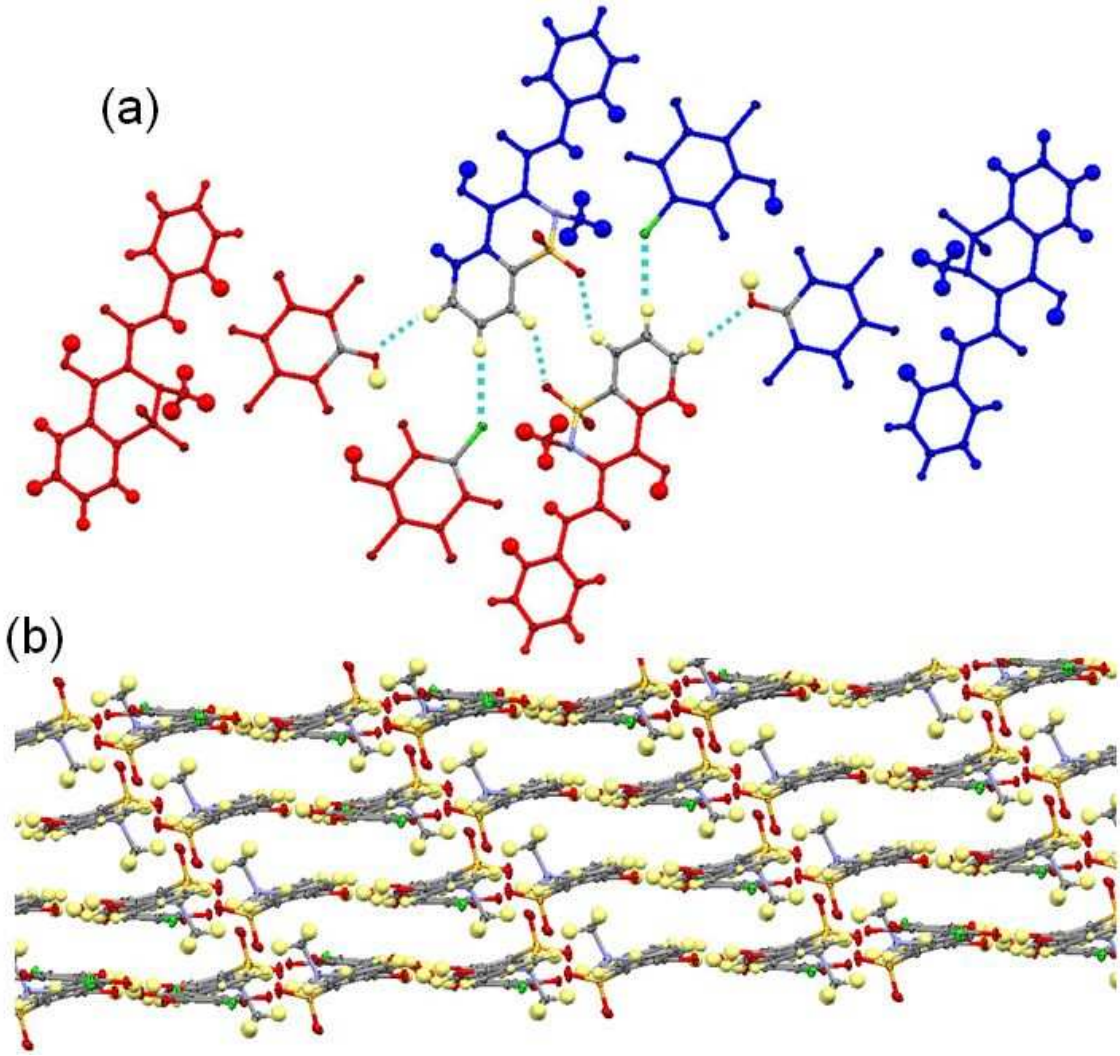

Figure 6.39 *Layers in the piroxicam : chloranilic form I salt complex. (a) The weak hydrogen bonds linking tetramers to form layers (different tetramers are coloured red and blue; donors and acceptors in the weak hydrogen bonds are coloured by atom). (b) The relative arrangement of the layers with the sulfonyl and methyl groups bridging.*

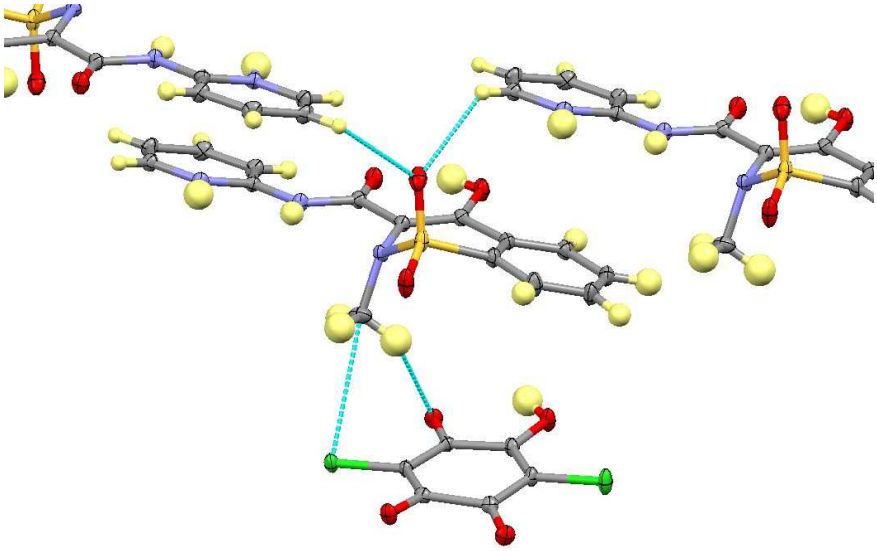

Figure 6.40 *Weak interactions between layers involving the methyl and sulfonyl groups in the piroxicam : chloranilic acid 1:1 salt complex.*

6.4.2 Piroxicam : Chloranilic Acid Form II (PX^+:CA^-) (Monoclinic)

The Form II polymorph of the piroxicam: chloranilic acid complex also has a single molecule of each in the asymmetric unit, with hydrogen transfer from the CA OH to the PX pyridinal N. The conformation of PX^+ is the same as that seen in form I. It was crystallised from a 1:1 ratio of the component materials in ACN at 40°C, whereas form I was crystallised from the same conditions at room temperature.

The CA^- molecules no longer dimerise, however, the main interactions between the CA^- and PX^+ molecules are similar to those in form I as they are linked through NH···O interactions involving the same groups (Figure 6.41). The chloranilic acid molecule, however, is twisted relative to the PX molecule (Figure 6.42), lying almost perpendicular to the plane of the pyridine ring as opposed to the co-planar arrangement in form I. The angle between the plane of the PX^+ pyridine ring and the plane of the CA^- six-membered ring is approximately 81°, whereas in form I the angle is approximately 21°. This changes the hydrogen bonding interactions slightly, leading to the formation of two DDHHA type bifurcated hydrogen bonds. The carbonyl oxygen atom now lies below the plane of the pyridine ring and forms an NH···O interaction with the amide oxygen (d in Figure 6.41), as well as a slightly stronger interaction with the pyridine NH - which is also observed in form I (see Table 6.12 for hydrogen bond lengths and angles). The two NH···O hydrogen bonds involving the deprotonated oxygen with the pyridine NH and the amide NH (a and

b in Figure 6.41) are both moderately strong, but with a slightly stronger amide interaction and slightly weaker pyridine interaction than in form I (also Table 6.12). The carbonyl lying below the plane of the pyridine ring also allows it to form a bifurcated, DDHHA, moderately strong CH···O hydrogen bond with the CH groups of the pyridine ring of the PX molecule below (C···O = 3.191(3) Å and 3.163(3) Å) (Figure 6.43). The two PX^+ molecules are also linked via weak CH···O hydrogen bonds of the pyridine CH with the sulfonyl oxygen (C···O = 3.318(3) Å).

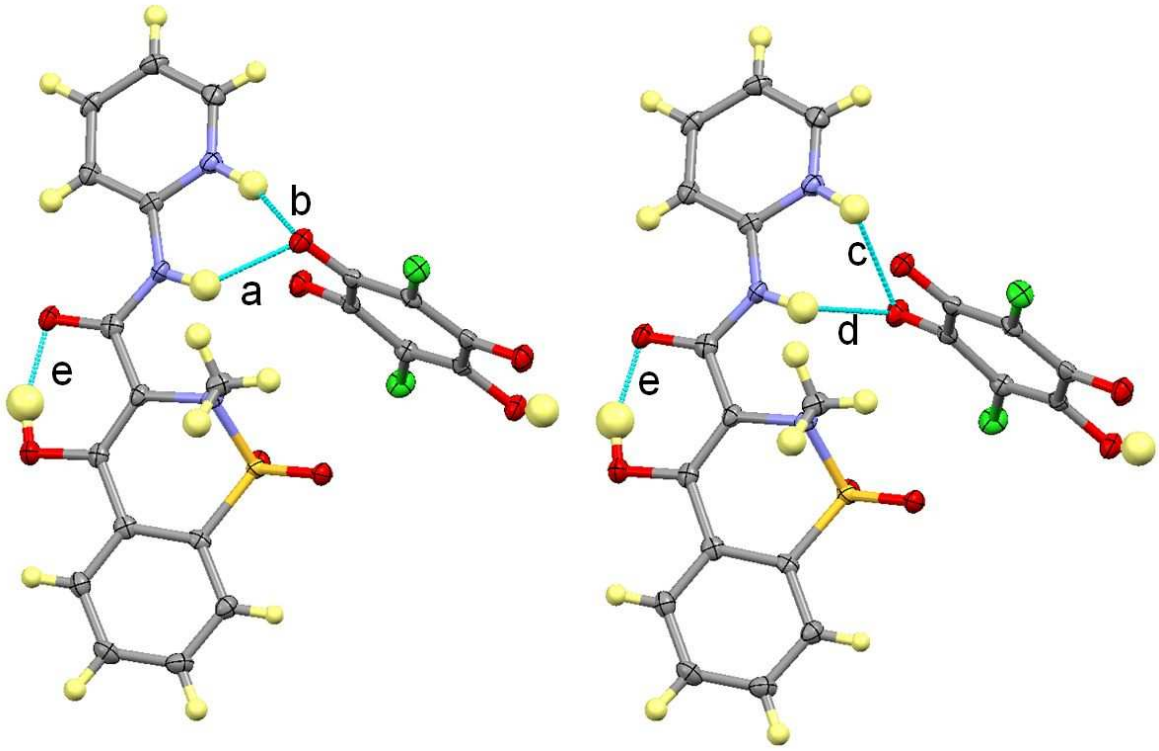

Figure 6.41 *Hydrogen bonding between* CA^- *and* PX^+ *molecules in the piroxicam : chloranilic acid form II salt complex. Hydrogen bonds involving the deprotonated oxygen are shown on the left and hydrogen bonds involving the carbonyl on the right.*

Table 6.12 *Hydrogen bond lengths and angles in the piroxicam : chloranilic acid 1:1 form II complex (refer to Figure 6.41 for key). Values for the analogous interactions in form I are also shown for comparison).*

Complex	H-Bond	D-H (Å)	H···A (Å)	D···A (Å)	∠ D-H···A (°)
$PX^+:CA^-$ (II)	a	0.90(2)	2.15(2)	2.891(2)	139(2)
	b	0.97(2)	1.74(2)	2.654(2)	157(2)
	c	0.97(2)	2.53(2)	3.028(2)	112(2)
	d	0.90(2)	2.48(3)	3.050(2)	121(2)
	e	0.95(3)	1.66(3)	2.560(2)	157(2)
$PX^+:CA^-$ (I)	a	0.79(2)	2.25(2)	2.942(2)	147(2)
	b	0.98(2)	1.70(2)	2.634(2)	158(3)
	c	0.98(2)	2.43(2)	3.065(2)	122(2)
	e	0.81(3)	1.78(3)	2.533(2)	153(2)

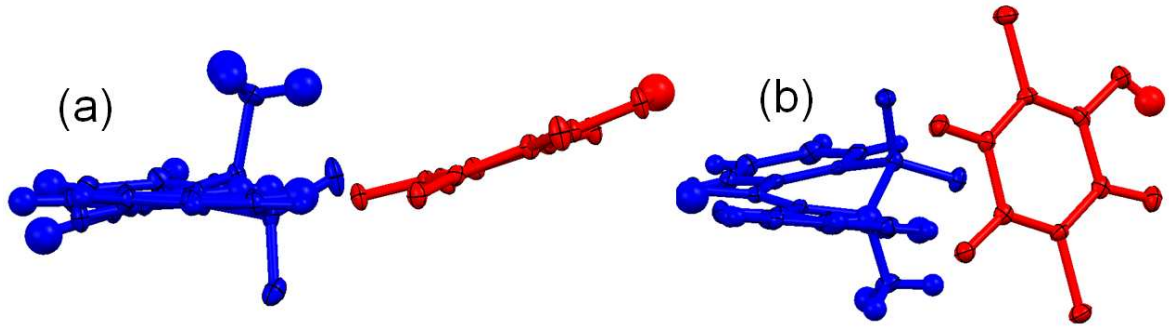

Figure 6.42 *Relative arrangements of the PX+ (blue) and CA⁻ (red) molecules in piroxicam : chloranilic acid (a) form I and (b) form II. Viewed along the plane of the pyridine ring.*

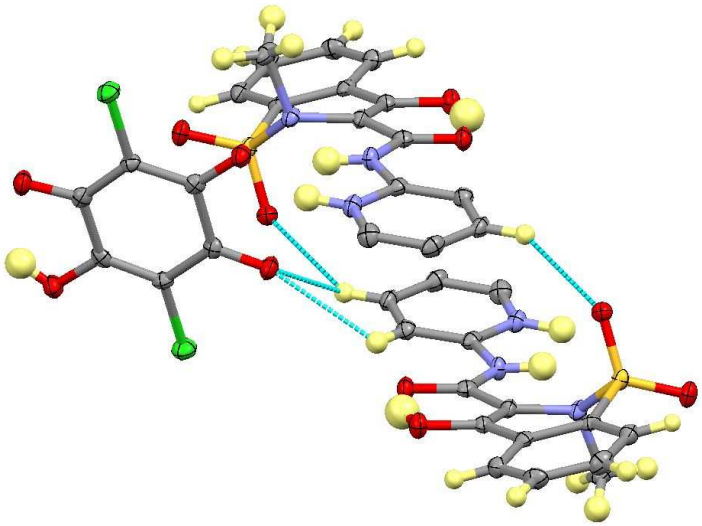

Figure 6.43 *The bifurcated CH···O hydrogen bonds between PX^+ and CA^- molecules and the CH···O=S interactions between PX^+ molecules in the piroxicam : chloranilic acid form II salt complex (some H atoms omitted for clarity).*

Unlike form I, CA^- molecules do not dimerise through the hydroxyl group, instead forming moderately strong OH···O interactions with the sulfonyl oxygen of another PX^+ molecule (Figure 6.44). The interaction is moderately strong (C···O = 2.799(2) Å, ∠ D-H···A = 124(2)°), with the hydroxyl oxygen also forming significant lone-pair···π interactions with the benzene ring of the PX^+ molecule, with a distance of approximately 2.970 Å between the oxygen and the centre of the π-bond (also Figure 6.44). Pyridine CH groups of a neighbouring PX^+ molecule form weak hydrogen bonds to both the hydroxyl oxygen and the sulfonyl oxygen (C···O = 3.221(3) Å an 3.318(3) Å). Further hydrogen bonds are formed involving the CA^- carbonyl and two neighbouring PX^+ molecules, with a moderately strong CH···O hydrogen bond formed with the pyridine CH of one (C···O = 3.164(3) Å) and a weak CH···O hydrogen bond with the benzene CH of another (C···O = 3.437(3) Å) (Figure 6.45).

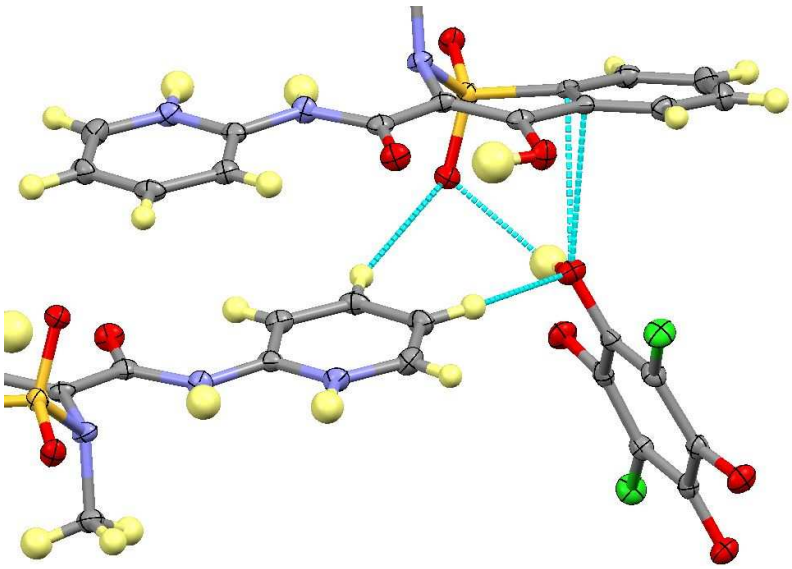

Figure 6.44 *Interactions of the CA^- hydroxyl with PX^+ molecules in the piroxicam : chloranilic acid form II salt complex.*

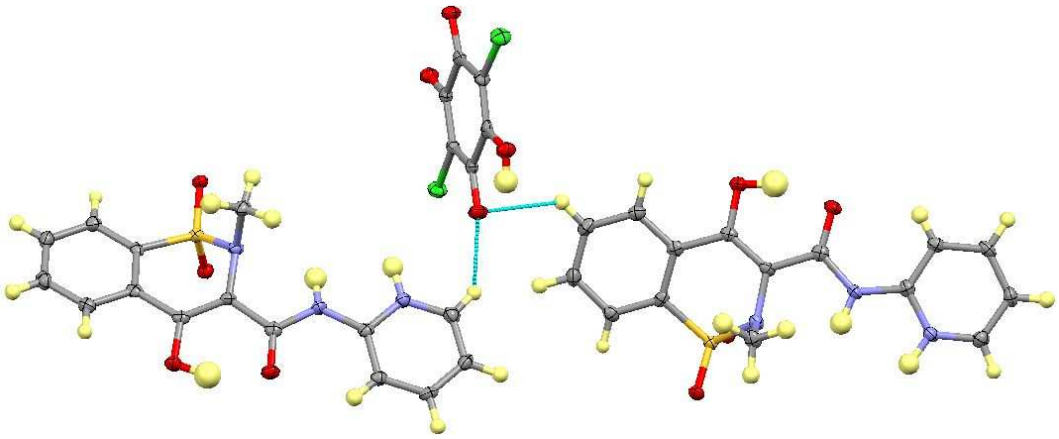

Figure 6.45 *Hydrogen bond interactions of the CA^- carbonyl oxygen with the aromatic CH groups of two PX^+ molecules in the piroxicam : chloranilic acid form II complex.*

PX^+ molecules all run in the same direction in a relatively layered arrangement, with CA^- molecules running across the layers interlocking the structure (Figure 6.46). The chlorine of the CA^- molecule again interacts with a PX^+ molecule through a weak hydrogen bond with the methyl group as in form I (C···Cl = 3.340(2) Å). The other Cl atom interacts with another PX^+ molecule via lone-pair···π interactions with the benzene ring (Figure 6.47). PX^+ molecules above and below each other interact with π···π interactions between the amide carbonyl double bonds with approximately 3.162 Å between the centroid of the bonds (Figure 6.48). Neighbouring PX molecules form moderately strong DDHHA bifurcated hydrogen bonds between the benzene ring CH groups and the sulfonyl oxygen (C···O = 3.136(3) Å and 3.236(3) Å) (Figure 6.48).

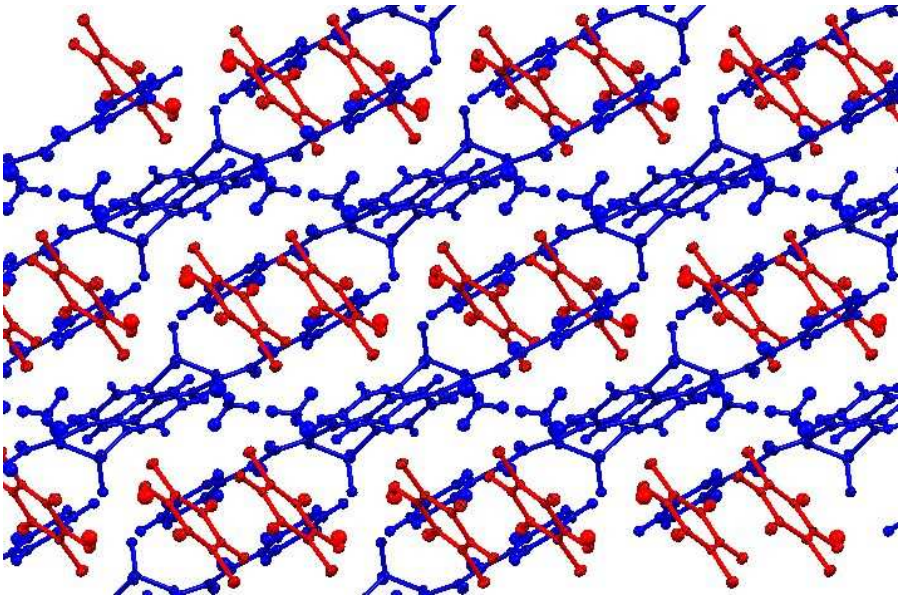

Figure 6.46 *Relative arrangement of PX^{+} and CA^{-} molecules in the piroxicam : chloranilic acid form II complex. PX molecules (blue) run from bottom left to top right with CA molecules (red) interlocking the structure.*

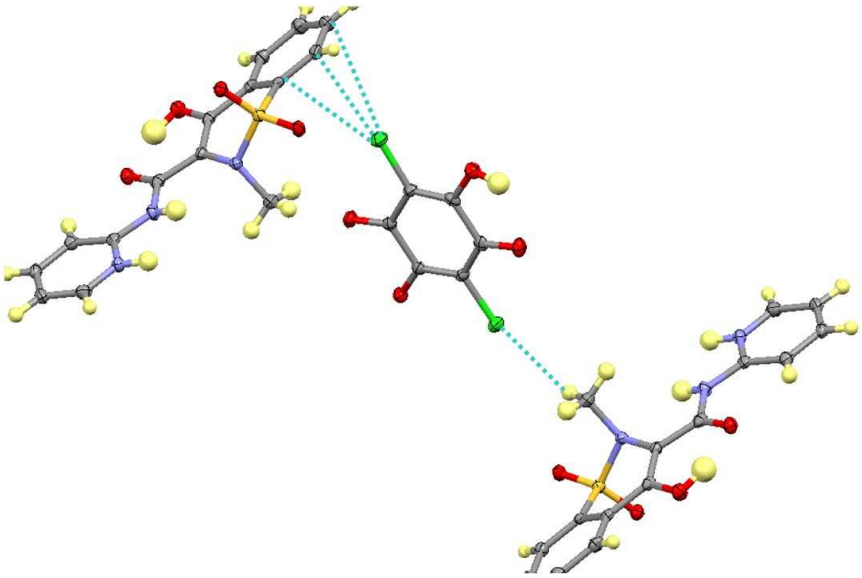

Figure 6.*47* *Interactions of the CA^{-} chlorine atoms in the piroxicam : chloranilic acid form II complex.*

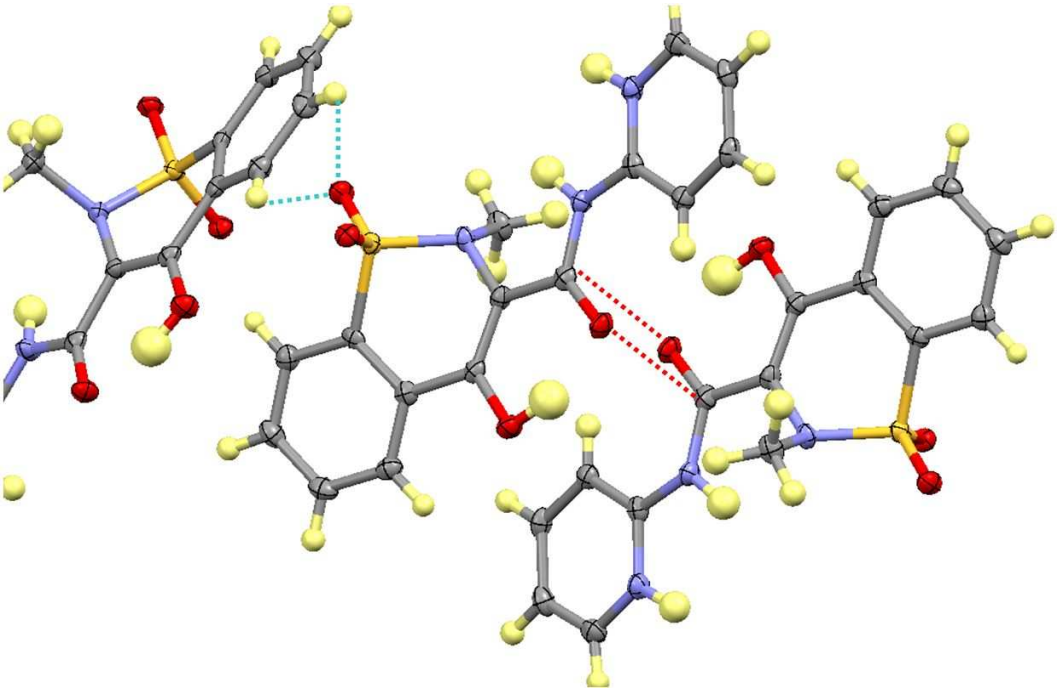

Figure 6.48 *Interactions between PX molecules, showing the π···π interactions between amide carbonyls (red dashed lines) as well as the bifurcated CH···O hydrogen bonds between the benzene ring and the sulfonyl oxygen (blue dashed) in the piroxicam : chloranilic acid form II complex.*

6.4.3 Piroxicam : Chloranilic Acid Acetonitrile Solvate (2(PX^+):CA^{2-}.2(ACN))

The piroxicam : chloranilic acid acetonitrile solvate (2:1:2) complex features a single PX^+ molecule in the asymmetric unit with one half of a doubly deprotonated CA molecule (CA^{2-}) lying on an inversion centre, as well as a single ACN molecule. It was crystallised from the same conditions as PX^+:CA^- forms I and II but at 50°C. The PX^+ molecule has the same conformation as is found in these two complexes.

The complex exhibits the same pattern of three hydrogen bonding interactions between co-planar CA^{2-} and PX^+ molecules (a bifurcated DDHHA arrangement and a bifurcated DHAA arrangement) as is found in form I of the 1:1 PX^+:CA^- complex (Figure 6.49). As the CA molecule is doubly deprotonated, this synthon occurs on both sides of the CA^{2-} molecule forming trimers. Analysis of C-O bond lengths in the CA^{2-} molecule indicates that the carbonyl (C=O = 1.239(4) Å) lies in the same position as it does in PX^+:CA^-, thus forming a single hydrogen bond with the pyridine NH group, with the deprotonated oxygen (C-O^- = 1.268(4) Å) forming bifurcated DDHHA hydrogen bonds with both the amide and pyridine NH groups. Table 6.13 shows that the hydrogen

bonding in the trimer is generally stronger than the corresponding hydrogen bonds in PX^+:CA^- forms I and II with the exception of the pyridine NH interaction with the deprotonated oxygen. An overlay of the structure with that of form I (Figure 6.50) shows this is due to a difference in the relative position of the CA^{2-} and CA^- molecules relative to the PX^+ pyridine ring. The PX^+ molecule also has a slight difference in conformation, with a stronger intramolecular hydrogen bond in the solvated complex (e in Table 6.13). The conformation of the PX^+ molecule also allows the methyl group to form a weak hydrogen bond with the CA^{2-} chlorine atom (C···Cl = 3.746(4) Å) (Figure 6.51).

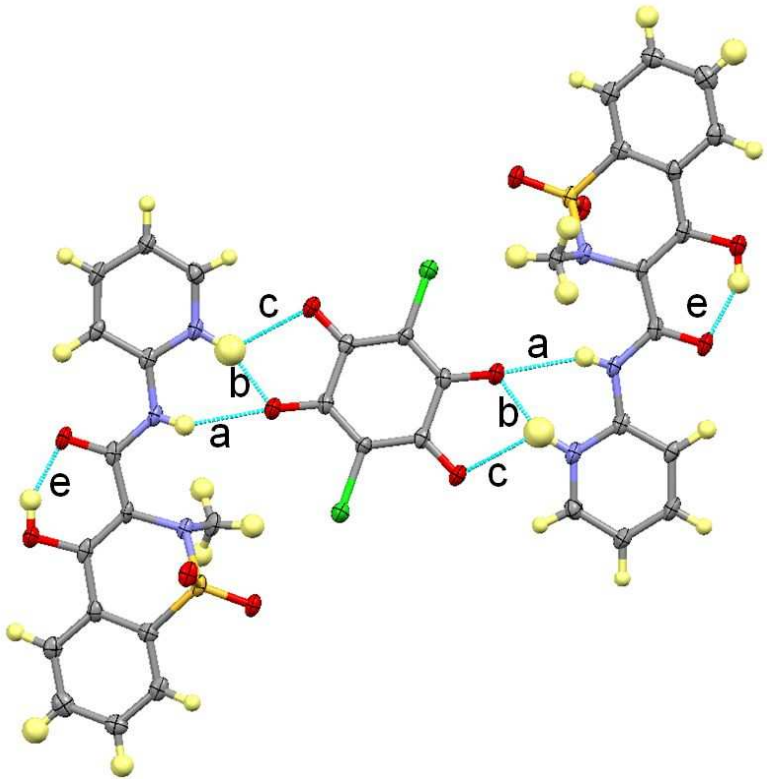

Figure 6.49 *Hydrogen bonding between CA^- and PX^+ molecules in the 2:1:2 piroxicam : chloranilic acid acetonitrile solvate complex.*

Table 6.13 *Hydrogen bond lengths and angles in the 2:1:2 piroxicam : chloranilic acid acetonitrile solvate complex (refer to Figure 6.49 for key). Values for the corresponding interactions in form I and II are also shown for comparison.*

Complex	H-Bond	D-H (Å)	H···A (Å)	D···A (Å)	∠ D-H···A (°)
2(PX^+):CA^{2-}.2(ACN)	a	0.75(4)	2.16(4)	2.834(4)	151(4)
	b	0.98(5)	1.74(5)	2.669(4)	156(4)
	c	0.98(5)	2.25(4)	2.885(4)	121(3)
	e	0.89(4)	1.69(4)	2.499(3)	159(3)
PX^+:CA^- (I)	a	0.79(2)	2.25(2)	2.942(2)	147(2)
	b	0.98(2)	1.70(2)	2.634(2)	158(3)
	c	0.98(2)	2.43(2)	3.065(2)	122(2)
	e	0.81(3)	1.78(3)	2.533(2)	153(2)
PX^+:CA^- (II)	a	0.90(2)	2.15(2)	2.891(2)	139(2)
	b	0.97(2)	1.74(2)	2.654(2)	157(2)
	c	0.97(2)	2.53(2)	3.028(2)	112(2)
	e	0.95(3)	1.66(3)	2.560(2)	157(2)

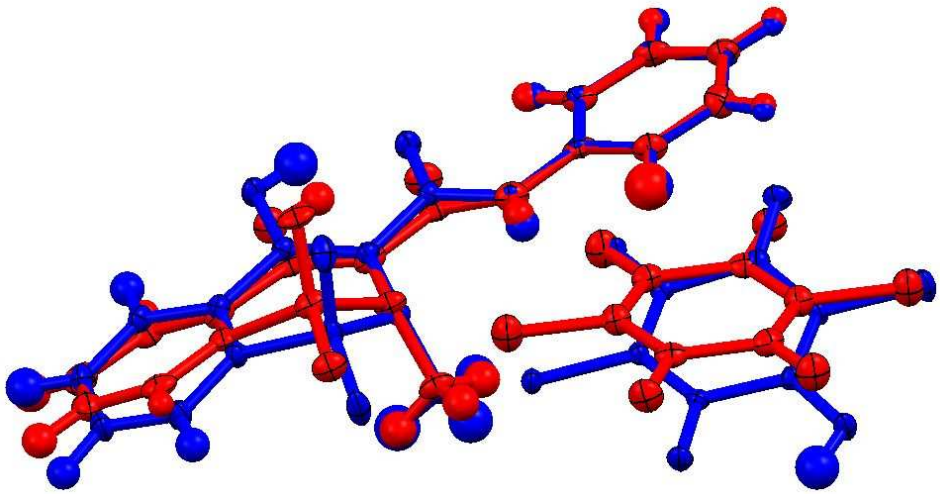

Figure 6.50 *Relative positions of the PX pyridine rings to the CA^- and CA^{2-} molecules in the piroxicam : chloranilic acid form I (blue) and piroxicam : chloranilic acid acetonitrile solvate (red) complexes.* Overlay is calculated for the pyridine rings and the neighbouring amide nitrogen.

Trimers are linked via further weak hydrogen bonding of the CA^{2-} molecule with the pyridine ring CH groups of other PX^+ molecules (Figure 6.51). The CH groups form weak hydrogen bonds to both the chlorine and carbonyl atoms of CA^{2-} with a C···Cl distance of 3.579(4) Å and a C···O distance of 3.418(4) Å. PX molecules are also linked by weak hydrogen bonding through the ACN molecules (Figure 6.52). Two CH groups of the PX benzene ring form hydrogen bonds to nitrogen atoms of two ACN molecules forming

$R_2^4(10)$ rings with C···O distances of 3.452(5) Å and 3.517(6) Å. The aforementioned interactions hold the molecules together in wave-like layers which are stacked upon each other with the methyl groups and sulfonyl oxygen atoms again bridging between layers (Figure 6.53) and forming weak CH···O hydrogen bonds (C···O = 3.267(4) Å and 3.469(4) Å) (Figure 6.54).

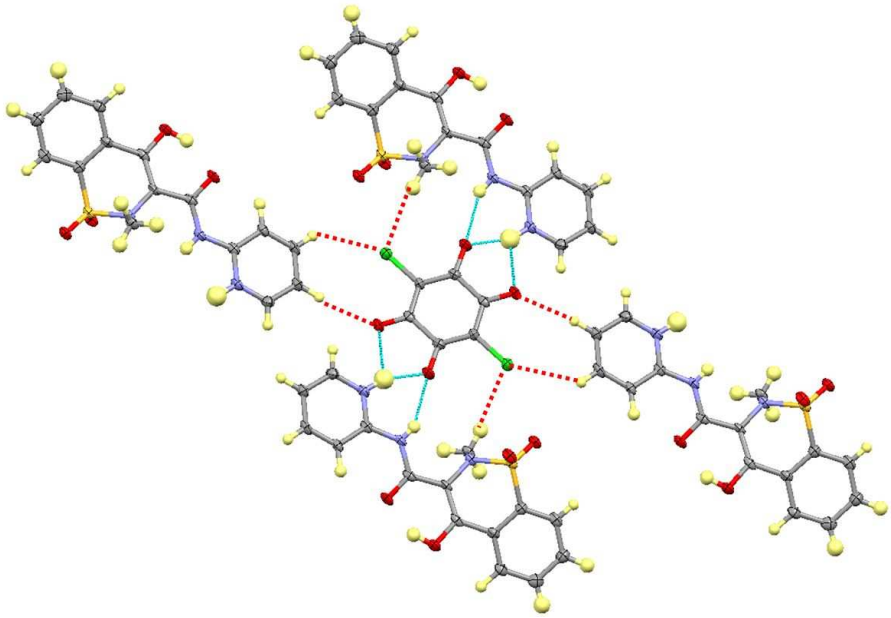

Figure 6.51 *Weak hydrogen bonds (red dashed lines) between PX^+ and CA^{2-} molecules in the piroxicam : chloranilic acid acetonitrile solvate complex.*

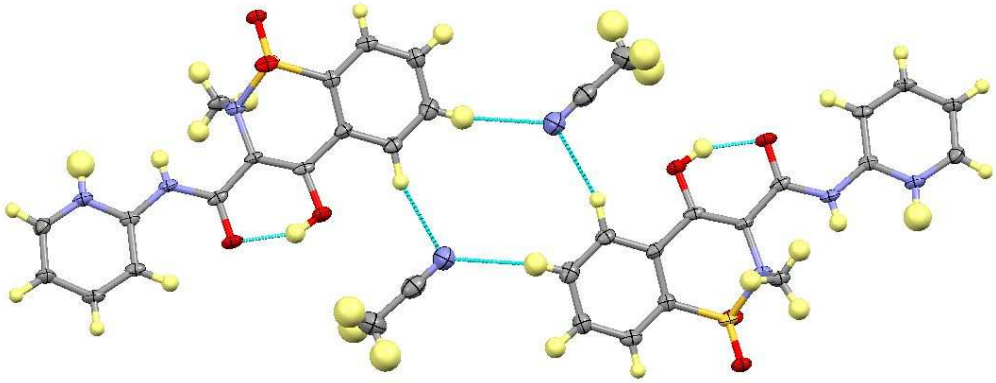

Figure 6.52 $R_2^4(10)$ *hydrogen bond ring formed by PX^+ and ACN molecules in the piroxicam : chloranilic acid acetonitrile solvate complex.*

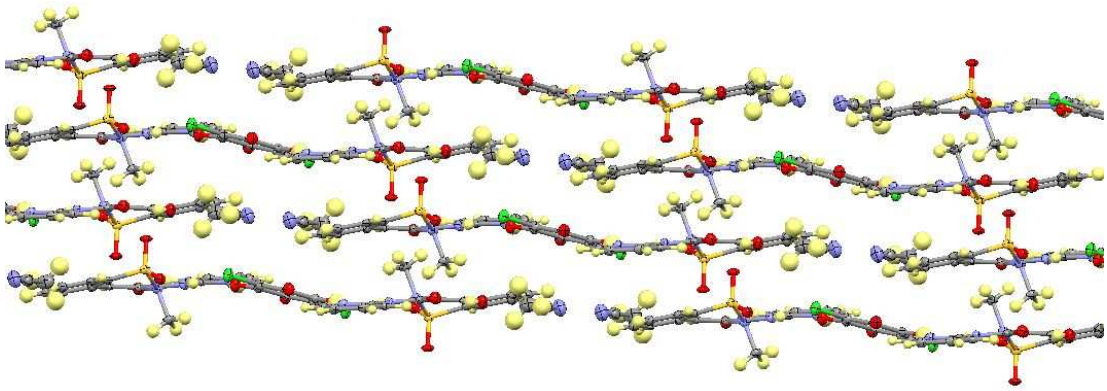

Figure 6.53 *Layered crystal packing in the piroxicam : chloranilic acid acetonitrile solvate complex.*

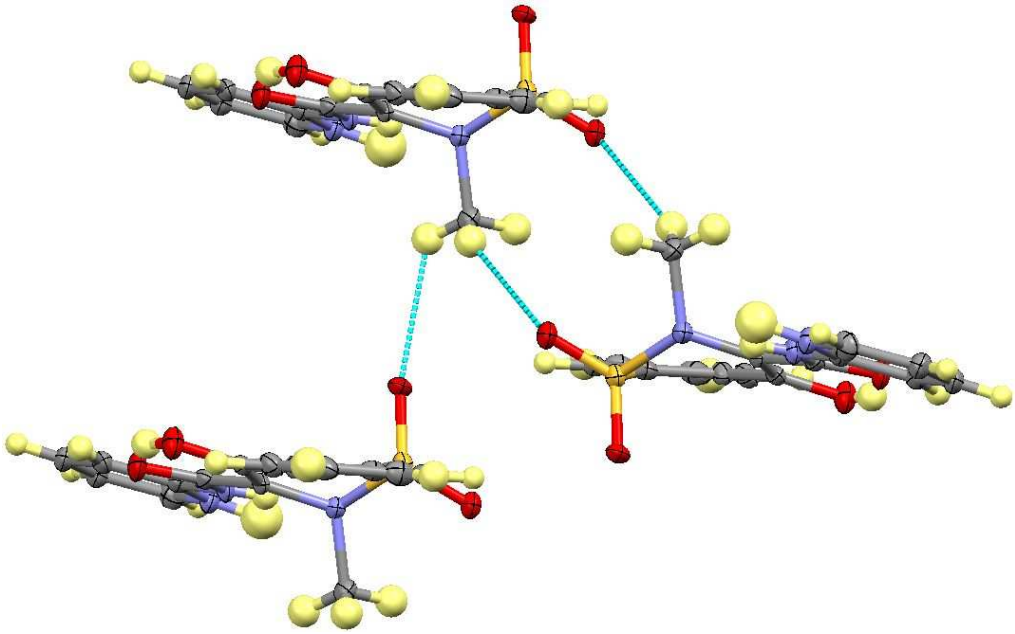

Figure 6.54 *Weak hydrogen bonds between layers involving the methyl groups and sulfonyl oxygen atoms of* PX^{+} *in the piroxicam : chloranilic acid acetonitrile solvate complex.*

6.4.4 Piroxicam : Bromanilic Acid (PX^{+}:BRA^{-})

The piroxicam : bromanilic acid salt complex is isomorphous to form II of the piroxicam : chloranilic acid complex. The structure directing hydrogen bonds in the complex (Figure 6.55) are similar in strength to those in PX^{+}:CA^{-} (II) (see Table 6.14 for hydrogen bond details). Unit cell parameters for this complex and PX^{+}:CA^{-} (II) are given in Table 6.15 for comparison.

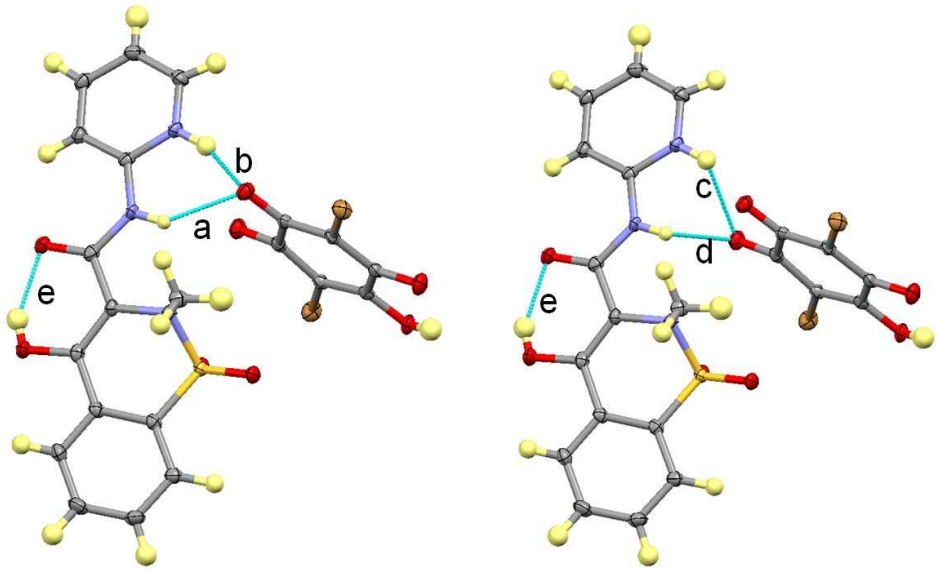

Figure 6.55 *Hydrogen bonding between BRA^- and PX^+ molecules in the piroxicam : chloranilic acid form II salt complex. Hydrogen bonds involving the deprotonated oxygen are shown on the left with hydrogen bonds involving the carbonyl on the right.*

Table 6.14 *Hydrogen bond lengths and angles in the piroxicam: bromanilic acid salt complex (refer to Figure 6.55 for key). Values for the corresponding interactions in piroxicam: chloranilic acid form II are also shown for comparison.*

Complex	H-Bond	D-H (Å)	H···A (Å)	D···A (Å)	∠ D-H···A (°)
PX^+: BRA^-	a	0.82(3)	2.22(3)	2.914(3)	144(3)
	b	0.89(3)	1.82(3)	2.660(3)	155(3)
	c	0.89(3)	2.54(3)	2.991(3)	112(2)
	d	0.82(3)	2.47(3)	3.000(3)	123(2)
	e	0.75(4)	1.90(4)	2.574(3)	151(4)
PX^+: CA^- (II)	a	0.90(2)	2.15(2)	2.891(2)	139(2)
	b	0.97(2)	1.74(2)	2.654(2)	157(2)
	c	0.97(2)	2.53(2)	3.028(2)	112(2)
	d	0.90(2)	2.48(3)	3.050(2)	121(2)
	e	0.95(3)	1.66(3)	2.560(2)	157(2)

Table 6.15 *Unit cell parameters of the isomorphous PX^+:BRA^- and PX^+:CA^- (II) complexes.*

Complex	Spc Grp	a (Å)	b (Å)	c (Å)	β (°)	V ($Å^3$)
PX^+: BRA^-	$P2_1/c$	8.842(2)	13.437(2)	19.242(4)	100.518(11)	2247.8(7)
PX^+: CA^- (II)	$P2_1/c$	8.5627(5)	13.3395(7)	19.396(1)	100.925(3)	2175.3(2)

6.5 Discussion

6.5.1 Supramolecular Synthons

Piroxicam Complexes with N-heterocycles

Of the eight PX complexes with N-heterocycles (NHCs), transfer of the PX hydroxyl hydrogen to the NHC to form PX^- occurs in five. Of the five complexes, three were solvated complexes with imidazole (IM), which all featured protonation of the IM despite varying the crystallisation conditions. The other three complexes feature intramolecular hydrogen transfer and form PXZ. No complexes crystallised with the non-ionised form of piroxicam. The conformation of PX^- seen in the complexes is distinct from the conformations of PXZ and PXN and is the same in all five complexes in which it occurs (Figure 6.1).

All five PX^- complexes feature chains of alternating PX^- and NHC, generally with an ABAB arrangement although some variations occur depending on the number of symmetry independent molecules in the asymmetric unit (i.e. ABA'B', A'B'A'B'). All also exhibit similar hydrogen bonding synthons, although with some noticeable differences from complex to complex. Four of the complexes feature NHC molecules sandwiched between two PX^- molecules and linked by NH···O=C hydrogen bonds to the PX^- amide oxygen and NH···O^- hydrogen bonds to the PX^- enolate oxygen. These interactions are to be expected as this arrangement matches the strongest hydrogen bond acceptors of PX^- with the strongest donors of IM^+. The $2(PX^-):2(IM^+).H_2O$ complex is the only exception to this, as neither of the two symmetry IM^+ molecules follow this hydrogen bonding pattern despite also having an ABAB arrangement (Figure 6.2). Instead, one chain features hydrogen bonds from the IM^+ NH groups to the PX^- pyridine nitrogen and enolate oxygen, and the other chain has both NH groups hydrogen bonding to the PX^- amide oxygen atoms. One enolate oxygen atom of PX^- is therefore not hydrogen bonded to the IM^+ NH groups and instead forms a hydrogen bond to the IM^+ CH in the 4/5 position, thus not satisfying the strongest donor/acceptor criterion. Other IM^+ CH groups in the 4 and 5 positions in the structure form hydrogen bonds with either the PX^- pyridine nitrogen or a sulfonyl oxygen atom. These interactions are also seen in the other PX^- structures, with the CH···N interactions occurring in the 1:1:1 and 4:4:1 PX:IM.ACN complexes, as well as with the analogous CH groups in the 5/8 positions of BZ^+ in the $PX^-:BZ^+$ complex (Figure

6.21). The PX^-:$2MIM^+$ complex does not have this interaction due to the alternate PX^- molecules lying head to head rather than head to tail which makes the pyridine nitrogen unavailable for hydrogen bonding to the $2MIM^+$ CH groups (Figure 6.15). The CH···O=S interaction does occur in the PX^-:$2MIM^+$ complex as well as the PX^-:BZ^+ complex (5/8 position) but does not occur in either of the PX:IM.ACN solvates. In the 1:1:1 ACN solvate it is compensated for by a CH hydrogen bond forming to the ACN nitrogen, with the ACN methyl group then forming a CH···O=S hydrogen bond to the PX^- molecule (Figure 6.8). A similar CH···N hydrogen bond to the ACN is formed in the 4:4:1 complex, although no CH···O=S interaction is formed between the ACN and PX^- as the ACN methyl group points away from the sulfonyl oxygen (Figure 6.13b).

It is interesting to note that despite exhibiting similar hydrogen bonding arrangements to the $2MIM^+$ and BZ^+ complexes, no 1:1 complex of PX and IM could be isolated, with instead two ACN solvates and a hydrate produced from varying the conditions. This is likely due to the small size of IM compared with BZ and 2MIM, as both have bulky groups attached to the imidazole group. To compensate for the void that would be left and to ensure efficient packing in the absence of these groups, a solvent molecule is incorporated into the PX^-:IM^+ complexes. This is reflected in the relative positions of the H_2O and ACN molecules in the complexes, as the H_2O molecule is hydrogen bonded to the CH group in the 2-position and the ACN molecules form hydrogen bonds to the CH in the 4/5 position. The solvent molecules therefore occupy equivalent positions to the methyl group and benzene ring in 2MIM and BZ respectively.

In the three complexes featuring PXZ with NHCs, the PXZ molecules dimerise, as is consistent with all known PXZ complexes. With the exception of the pyridinium nitrogen which is involved in hydrogen bonding to form the PXZ dimer, consistent hydrogen bonding is observed between the strongest NHC donors and the strongest free PXZ acceptors in all cases. Both the PXZ:TZ and PXZ:BZT complexes form NH···O^- hydrogen bonds between the TZ/BZT NH and the enolate oxygen. The PZN CH also forms hydrogen bonds to the enolate O^-. In all complexes a hydrogen bond is also formed from the same CH group of the PX^- pyridine nitrogen to a nitrogen atom of the heterocycle.

The PXZ:PZN complex is unusual as the only hydrogen bonds between PZN and PXZ molecules involve CH donors, as this is the only possible PZN donor and the pyridinium nitrogen is unavailable due to dimerisation of PXZ molecules. The fact that no conventional hydrogen bonds occur between the molecules may explain why crystallisation of this complex occurs so rarely and in such small quantities.

As PZN is symmetrical, the same interactions are formed on both sides of the molecule and it therefore forms chains with an ABBA configuration, with the PXZ dimers sandwiched by two PZN molecules resulting in a 2:1 complex (PXZ:PZN). In the PXZ:TZ complex, the disorder of the TZ molecule means it can effectively also form the same interactions on both sides and therefore also forms a 2:1 complex of PZZPZZ chains. The small size of the molecule allows it to occupy two possible positions without major disruption of the crystal packing. The PXZ:BZT complex, however, forms a 1:1 complex with tetramers of BZT:PXZ:PXZ:BZT, analogous to the common tetramer found in PXZ complexes with benzoic acids (see Chapter 5). Chains are not formed as there is no symmetry in the BZT molecule and only one sufficiently strong donor to form hydrogen bonds to the enolate O^-.

Piroxicam Complexes with Strong Acids: Chloranilic Acid and Bromanilic Acid

All PX complexes with CA and BRA resulted in intermolecular hydrogen transfer from the CA/BRA to the PX pyridine ring forming PX^+. The polymorphic PX^+:CA^- forms I and II both crystallise in a 1:1 ratio with similar hydrogen bonding patterns between the PX^+ and CA^- molecules. Form II has an extra NH···N hydrogen bond, however, due to the change in orientation of the CA^- molecule relative to the PX^+ molecule. Interestingly, increasing the temperature of crystallisation from RT to 40°C resulted in the formation of this second polymorph which has the CA^- molecule in a different orientation from form I. Increasing the crystallisation temperature to 50°C resulted in the ACN solvate complex with double deprotonation of the CA molecule. Deprotonation of both OH groups of the CA molecule is somewhat expected due to the decrease in pKa associated with increasing temperature. Unlike the PX:CA complexes, only a single PX^+:BRA^- phase was produced regardless of the temperature at which the crystallisation was carried out. In all complexes the strongest donor/strongest acceptor rule is satisfied, with charge-assisted hydrogen bonds formed between the protonated pyridine nitrogen of PX^+ and the deprotonated oxygen of CA^- (or CA^{2-}). In the case of the ACN solvate, this results in a 2:1 ratio as both CA OH groups are deprotonated.

6.5.2 Hydrogen Transfer and pKa

In total, five of the PX complexes with NHCs featured hydrogen transfer from the PX molecule to the basic nitrogen of the NHC. Table 6.16 shows that hydrogen transfer occurs in the complexes with the most basic three co-formers: all three IM complexes, the 2MIM complex and the BZ complex. The remaining three co-formers are poorly basic and resulted in complexes with the zwitterionic PX tautomer. Analysis of the ΔpKa values using the PX OH group or the N^+-H group as the acidic group show that the TZ, BZT and PZN complexes would not be expected to result in hydrogen transfer in either case, as the ΔpKa values are all negative or, in the case of TZ and N^+-H, very small.

Interpretation of the ΔpKa values of the complexes where hydrogen transfer occurs is slightly more complicated. Using the OH group as the acid, the ΔpKa values are all smaller than would be expected for complexes where hydrogen transfer occurs (all < 3), although all lie between 0 and 3 where hydrogen transfer may or may not occur. The ΔpKa for the 2MIM complex (2.42) is relatively close to the empirically significant value of 3, meaning hydrogen transfer is more likely to occur. The ΔpKa value for the PX complexes with IM is relatively low (1.53), despite hydrogen transfer occurring in all three complexes formed under different crystallisation conditions. Using the acid pKa value of the N^+-H produces far larger ΔpKa values and a clearer distinction of where hydrogen transfer will occur. This would also suggest it may be more appropriate, in the conditions studied at least, to describe the process as deprotonation of the pyridinium nitrogen rather than deprotonation of the hydroxyl, i.e. to consider PX as the zwitterionic form rather than the non-ionised form.

The ΔpKa values (where PX is a base) for the CA and BRA complexes follow a similar pattern to that found in the NHCs, in that the ΔpKa values suggest that it would perhaps be more appropriate to consider protonation of the enolate oxygen, rather than protonation of the pyridine nitrogen. The ΔpKa values using the N^+-H pKa value for the base are relatively small, and again smaller than may be expected in complexes where hydrogen transfer occurs. The fact they lie between 0 and 3 means hydrogen transfer may still occur. On the other hand, the ΔpKa values calculated when using the OH value again provide a much clearer distinction as to when hydrogen transfer occurs. Table 6.16 also includes the strongest acid used in Chapter 5 to form a molecular complex of piroxicam. Treating PX as the zwitterion and using the OH pKa value here results in a ΔpKa of 3.35 which would suggest intermolecular hydrogen transfer is likely to occur although

none is observed in the molecular complex formed. However, as previously stated, the ΔpKa rule is more of a guide and not always transferrable between systems and a slightly higher ΔpKa value may be required for hydrogen transfer to occur in this system.

Table 6.16 *ΔpKa values for the molecular complexes of piroxicam and the piroxicam ionisation state in each complex where ΔpKa = pKa[protonated base] – pKa[acid]. ΔpKa values using both the hydroxyl group and the N^+-H group of piroxicam as the acid/base are shown. pKa values for the NHC co-formers are quoted for the conjugate acid of the basic nitrogen. Note: pKa2 values for chloranilic and bromanilic acid were not considered.*

Co-Former	pKa_1	PX Form	ΔpKa OH (pKa = 5.46)	ΔpKa N^+-H (pKa = 1.86)
Bases				
Imidazole (3 complexes)	6.99	PX^-	1.53	5.13
2-Methylimidazole	7.88	PX^-	2.42	6.02
Benzimidazole	5.53	PX^-	0.07	3.67
1,2,4-Triazole	2.27	PXZ	-3.19	0.41
Benzotriazole	1.60	PXZ	-3.86	-0.26
Pyrazine	0.65	PXZ	-4.48	-1.15
Acids				
Chloranilic Acid (3 complexes)	0.76	PX^+	4.7	1.1
Bromanilic Acid	0.22	PX^+	5.24	1.64
2-Aminobenzoic Acid	2.11	PXZ	3.35	-0.25

6.5.4 Summary and Conclusions

6.5.4.1 N-Heterocycles as Co-formers

PX has been shown to form eight molecular complexes with NHCs. The three poorly basic NHCs (pKa = 0.65 - 2.27) resulted in complexes with the zwitterionic PXZ form, with no intermolecular hydrogen transfer. All exhibited the dimerisation of the PXZ molecules as seen in all known complexes featuring PXZ, with the strongest hydrogen bond donor of the NHC interacting with the enolate oxygen. In the case of PZN and TZ this forms infinite

chains due to the symmetry in PZN and the disorder of TZ which allow the same NH···O^- and CH···O^- interactions to form both sides of the molecules. In the case of BZT, discrete hydrogen bonded tetramers are formed as the NH donor of BZT only lies on one side. The BZT:PXZ:PXZ:BZT tetramers are analogous to the BZZB tetramers formed in the zwitterionic PXZ complexes with benzoic acids discussed in Chapter 5.

Tuning of the pKa values of the co-former allows complexes to be formed with the PX^- anion. Five complexes were crystallised featuring PX^- by using bases with pKa values in the range 5.33-6.99. All PX^- complexes exhibit consistent hydrogen bonding synthons, with interactions of the strongest donors and strongest acceptors (NH···O and NH···O^-) prevailing in all complexes except the anomalous $2(PX^-):2(IM^+).H_2O$ complex. All complexes resulted in chains with a general ABAB arrangement of the molecules.

Three complexes with $PX^-:IM^+$ were formed, with a hemihydrate as well as 1:1:1 and 4:4:1 ACN solvates. No 1:1 $PX^-:IM^+$ complex could be formed despite varying the crystallisation conditions. Selective crystallisation of the three $PX^-:IM^+$ solvates could be controlled by varying the crystallisation temperature.

Analysis of the ΔpKa values suggest that it may be more appropriate to consider PX as the zwitterionic form, with the N^+-H group as the acid, when attempting to predict hydrogen transfer using the ΔpKa rule. The resulting ΔpKa values give a clearer indication of whether or not hydrogen transfer will occur. Data on more complexes across a greater pKa range would be useful in quantifying the minimum ΔpKa at which hydrogen transfer should be expected for PX complexes with NHCs.

6.5.4.2 Acids as Co-formers

Molecular complexes of CA and BRA with PX resulted in salts where PX is present as a cation with both the hydroxyl and pyridine N protonated. This is the first time PX has been observed in the PX^+ form.

Polymorphism of the 1:1 complex can be induced by changing the crystallisation temperature. Both forms have the same basic hydrogen bonding motif, with the CA^- molecule in form II twisted relative to its position in form I and forming an extra hydrogen bond. A further increase in the crystallisation temperature resulted in the 2:1:2 ACN solvate which surprisingly reverts back to the motif seen in form I.

The ΔpKa values again indicate that PX should possibly be considered as the zwitterion when applying the ΔpKa rule. ΔpKa values using the OH pKa as the base value give a clear indication that hydrogen transfer will occur. The ΔpKa value of the PXZ:2ABA complex from Chapter 5 indicates that hydrogen transfer from acids does not necessarily occur at ΔpKa > 3, and stronger acids are required. Again, more complexes across a greater ΔpKa range are needed to adjust the predicted minimum ΔpKa value for hydrogen transfer to occur.

6.5.4.3 General Comments on Hydrogen Transfer in Molecular Complexes of Piroxicam

PX forms a range of different types of complexes with both acids and bases and adapts its ionisation state according to the co-former. The influence of pKa is apparent in these complexes and by tuning the pKa of the co-former, the piroxicam ionisation state can be tuned accordingly. Co-crystallisation with strong acids (pKa < 0.77) can be used to obtain the cationic PX^+ form of piroxicam whereas weaker benzoic acid derivatives can be used to obtain either the zwitterionic form or the non-ionised form depending on which side of the boundary regions (discussed in Chapter 5) the acids lie. Tautomeric polymorphs are also possible with the mono-substituted acids although predicting when they will occur is not possible from the data obtained so far. The use of strong bases (pKa > 5.52) can result in complexes with PX^- and weaker bases (pKa < 2.28) have been shown to result in complexes with PXZ.

The data presented in this chapter and in Chapter 5 however, suggest that more work is required with regards predicting which form of PX will be present in a given complex. When co-crystallising with the mono-substituted benzoic acids it is not yet clear why two boundary regions exist where PXZ and PXN are formed and until this is understood it cannot be considered a hard rule. It also does not account for the tautomeric polymorphism observed in four of the complexes. Also, it has been suggested in this chapter that it may be more appropriate to consider PX as the zwitterionic tautomer when calculating ΔpKa values for PX complexes. However, no definite ΔpKa value has yet been defined as a boundary at which intermolecular hydrogen transfer is expected to occur for either acids or bases.

7. Controlling Co-crystallisation Based Molecular Complex Formation of Paracetamol and its Derivatives

7.1 Introduction to Molecular Complexes of Paracetamol

As discussed in previous chapters, the solid form adopted by an API is an important consideration as it directly affects its physicochemical properties. When co-crystallising a particular API it is therefore useful to be able to predict, at least to a certain degree, the dominant interactions that will occur in the molecular complex formed, as these play an important role in controlling the structure and hence properties of the complex; this is tackled through the supramolecular synthon approach discussed in Chapter 1. As discussed in Chapter 4, the solid forms of paracetamol (PA) are the subject of much study, with much focus on improving physical properties through exploiting the polymorphism of the material. Co-crystallisation, however, is also seen as a potential route to optimising the properties of PA, via formation of molecular complexes with consequent altered physical properties, and it has previously been shown that the compression properties of PA can be improved through co-crystallisation[17]. Despite this, relatively few molecular complexes of PA exist, with only eighteen published in the Cambridge Structural Database (CSD)[65], five of which are hydrates or solvates. The range of co-formers used in these complexes show marked variations in nature and a recent study highlighted the variation in supramolecular synthons observed in these molecular complexes[226]. This study also highlights the tendency of PA to form molecular complexes with nitrogen heterocycle compounds (NHCs). Of the thirteen non-solvate complexes of PA reported in the CSD, five of these are with NHCs (excluding compounds with donors/acceptors other than NH/N). Of these NHCs, three are co-formers with only nitrogen hydrogen bond acceptors (4,4 -bipyridine[227], phenazine[17] and N, N -dimethylpiperazine[227]) and two are with piperazine (a 1:1 complex[227] and an ethanol solvate[228]) which has two NH hydrogen bond donors. An N-methylmorpholine complex is also known[227], which is useful for comparison to the complexes with N acceptors only, as the N-methylmorpholine molecule is disordered across an inversion centre with the nitrogen and oxygen occupying equivalent positions in the two disordered components.

In this chapter, the co-crystallisation of PA with a number of NHCs (Scheme 7-1) is investigated in an attempt to form molecular complexes. The co-formers used in this

investigation have been narrowed down to smaller subsets to facilitate a more relevant comparison between the supramolecular synthons formed in complexes with particular types of co-formers. One subset of co-formers chosen consists of imidazole (IM) and its derivatives, namely, 2-methylimidazole (2MIM), 4-methylimidazole (4MIM) and benzimidazole (BZ). These complexes will be compared only to each other as no other PA complexes with IM derivatives have previously been reported. The second subset consists of nitrogen heterocycles with only nitrogen acceptors, namely 2-picoline (2PIC), 3-picoline (3PIC), 4-picoline (4PIC). This subset is suitable for comparing to the other PA complexes in the CSD with NHCs that have only acceptor nitrogens, i.e. 4,4'-bipyridine (BP)[227], phenazine (PHEN)[17], N, N – dimethylpiperazine[227], as well as the N-methylmorpholine[227] complex.

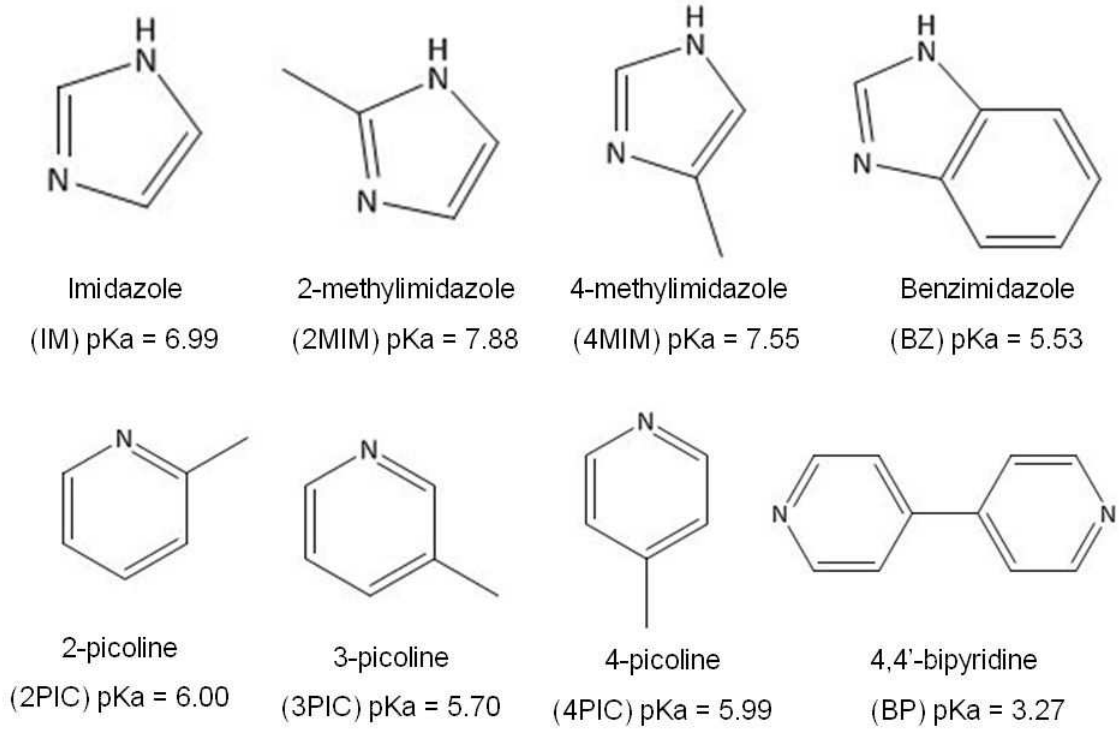

Scheme 7-1 *The nitrogen heterocycle co-formers used for co-crystallisation with paracetamol and 4-acetamidobenzoic acid.*

The co-crystallisation of these NHCs with the related API 4-acetamidobenzoic acid (4ABA), which is structurally similar to PA (Scheme 7-2), is also investigated in this chapter. 4ABA is a component of immunostimulant antiviral medications, of which no molecular complexes have previously been reported and only one polymorph is known[229]. Its molecular structure is similar to that of PA, with the exception of the presence of a carboxylic acid group replacing the PA phenolic hydroxyl. The molecular complexes produced will be compared to the PA complexes from a crystal engineering perspective to

determine if the structural similarity leads to the emergence of comparable, and therefore predictable, patterns in the structural motifs and packing in the molecular complexes formed with these small subsets of materials. 4ABA and PA have similar hydrogen bond donor/acceptor positions and are similar in size which could possibly allow them to co-crystallise with similar co-formers and lead to similar hydrogen bonding arrangements and crystal packing. The much lower pKa of the 4ABA carboxylic acid OH however, means it is a much better hydrogen bond donor and is more likely to be deprotonated should a co-former which is a strong enough base be used. The extra hydrogen bond acceptor in 4ABA (the carboxylic acid carbonyl) may also result in different hydrogen bonding arrangements from those in corresponding PA complexes. It is hoped, however, that a pattern might emerge from which the hydrogen bonding in a complex of one of the APIs will allow a reasonably accurate prediction of the hydrogen bonding present in a complex of the other API with the same co-former. The ultimate aim of such studies is eventually to be able to design molecular complexes of a material with specific properties based on the properties of molecular complexes of a similar material.

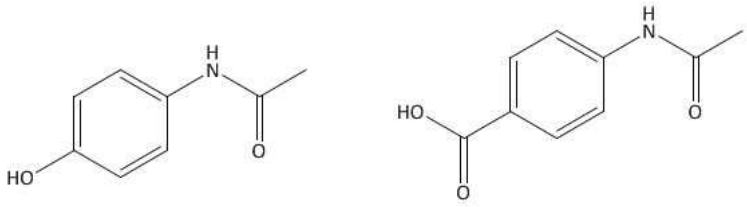

Scheme 7-2 *The molecular structures of paracetamol (left) and 4-acetamidobenzoic acid (right).*

7.2 Crystallisation Conditions

Crystallisations were carried out according to the procedure outlined in Chapter 3 unless otherwise stated. Table 7.1 below outlines the solvent and temperature systems under which each molecular complex described in this section was observed to crystallise. Further details for specific complexes are given below where relevant.

Table 7.1 Crystallisation conditions for molecular complexes of paracetamol and 4-acetamidobenzoic acid with nitrogen-heterocycles.

Molecular Complex	Solvent	Temp (°C)
PA:IM	Methanol/Ethanol/Isopropanol	RT (All solvents)
PA:2MIM (1:2)	Acetone	40
PA:4MIM	Methanol/Acetone	40 (both solvents)
4ABA:IM	Acetone	40/50
4ABA:2MIM (2:1)	Methanol/Acetone	RT/40/50
4ABA:4MIM	Methanol*/Acetone[#]	6*/6[#]/40[#]
4ABA:BZ	Methanol*/Acetone[#]	6*/RT[#]/40[#]/50[#]
4ABA:BP	Methanol	RT/40/50

RT = Room Temperature

Paracetamol: 2-methylimidazole (1:2)

This complex crystallised in a 1:2 molar ratio, despite a 1:1 molar ratio of the components being used in the co-crystallisation experiments. Unsuccessful attempts were made to alter the ratio of the molecular complex formed by co-crystallising in 2:1 molar ratios in methanol and acetone using the procedure outlined in Chapter 3.

4-acetamidobenzoic acid: 2-methylimidazole (2:1)

This complex crystallised in a 2:1 molar ratio, despite a 1:1 molar ratio of the components being used in the co-crystallisation experiments. Unsuccessful attempts were made to alter the ratio of the molecular complex formed by co-crystallising in 1:2 molar ratios in methanol and acetone using the procedure outlined in Chapter 3.

4-acetamidobenzoic acid: 2-picoline (1:1)

Crystallisation of this molecular complex was achieved by cooling crystallisation. This was carried out by dissolving 0.15g 4ABA in minimal 2PIC at 65°C to generate a supersaturated solution and allowing the solution to cool to 6°C. Attempts were made to generate a molecular complex using the general evaporation procedure outlined in Chapter 3 using molar quantities of 2PIC in various solvents. These resulted in amorphous material being formed.

4-acetamidobenzoic acid: 3-picoline (1:1)

Crystallisation of this molecular complex was achieved by cooling crystallisation. This was carried out by dissolving 0.15g 4ABA in minimal 3PIC at 50°C to generate a supersaturated solution and allowing the solution to cool to 6°C. Attempts were made to generate a molecular complex using the general evaporation procedure outlined in Chapter 3 using molar quantities of 3PIC in various solvents. These resulted in amorphous material being formed.

4-acetamidobenzoic acid: 4-picoline (1:1)

Crystallisation of this molecular complex was achieved by cooling crystallisation. This was carried out by 0.15g 4ABA in minimal 4PIC at 70°C to generate a supersaturated solution and allowing the solution to cool to 6°C. Attempts were made to generate a molecular complex using the general evaporation procedure outlined in Chapter 3, using molar quantities of 4PIC in various solvents. These resulted in amorphous material being formed.

7.2.1 Co-crystallisation of Paracetamol with Benzimidazole and Picolines

Unsuccessful attempts were made to co-crystallise paracetamol with benzimidazole using the procedure outlined in Chapter 3. The solvents used were methanol, ethanol, acetone and IPA. The molar ratios of the components were also varied between 1:1, 2:1 and 1:2 in attempts to induce molecular complex formation.

Unsuccessful attempts to co-crystallise PA with 2-, 3- and 4PIC were also carried out using the same procedure used in the co-crystallisations with 4ABA. Further unsuccessful attempts to co-crystallise PA with picolines were made by using the evaporation procedure outlined in Chapter 3. 1:1 molar ratios of PA and the picolines were dissolved in methanol, ethanol and acetone and the solvent evaporated at 6°C, ambient temperature, 40°C and 50°C. PA was also dissolved in excess quantities of the picolines as solvent and the picoline solvent evaporated at these temperatures.

7.2.2 Paracetamol: Imidazole Molecular Complex: Scale up for Continuous Crystallisation in an Oscillatory Baffled Crystalliser

The pharmaceutically acceptable co-former used in the PA:IM complex made it an ideal candidate for attempted scale-up to a continuous crystallisation process. Studies have also shown that the toxic effect of PA on the liver may be reduced by the presence of IM derivatives[230,231], meaning the complex also has potential pharmaceutical applications.

To facilitate co-crystallisation in a COBC, attempts were made to convert the evaporation co-crystallisation method employed in producing the complex to a cooling crystallisation method. 1:1 molar ratio solutions of various degrees of supersaturation were therefore generated through heating and the solutions crash cooled to either 4°C or ambient temperature to induce crystallisation. This, mainly resulted in crystallisation of the less soluble PA with the majority of IM remaining in solution and no molecular complex being formed. The relative molar ratios were varied to 1:2 (PA:IM) in an attempt to promote molecular complex formation. However, this was also unsuccessful. The solvents used were ethanol and IPA, chosen for their relatively low toxicity.

7.3 Crystal Structures of Multi-component Complexes of Paracetamol and Imidazoles

Three molecular complexes of PA with IM and its derivatives were produced in this study. Crystallographic data and full refinement details can be found in (Appendix A7, Table A-7a).

7.3.1 Paracetamol : Imidazole (PA:IM)

The 1:1 paracetamol : imidazole complex consists of one molecule of each component in the asymmetric unit with no hydrogen transfer occurring between the molecules. PA molecules form hydrogen bonds to each other through moderately strong interactions involving the amide NH of one with the hydroxyl oxygen of another (a in Figure 7.1). The hydroxyl group then forms a moderately strong OH···N hydrogen bond to the IM nitrogen atom, with the IM acting as a linker between PA molecules and forming further hydrogen bonding to another PA molecule through another moderately strong NH···O interaction with the amide carbonyl (b and c in Figure 7.1). These interactions form infinite chains,

with two chains branching off from each PA molecule. Hydrogen bond distances and angles can be found in Table 7.2. The two PA molecules linked by the IM molecules lie parallel to each other, while the two PA molecules linked directly to the first two through the NH···OH hydrogen bonds run parallel to each other, in intersecting planes with the first two, resulting in a staggered arrangement of PA molecules interlocking the structure (Figure 7.2). CH···π interactions are also present between the CH group of IM and the paracetamol benzene ring, with approximately 3.619 Å between the donor carbon and the centroid of the π bond (Figure 7.3). Slightly weaker CH···π interactions are present between the aromatic CH of the PA molecule and one of the IM double bonds with a distance of approximately 3.709 Å between the donor carbon and the centroid of the π bond (also Figure 7.3).

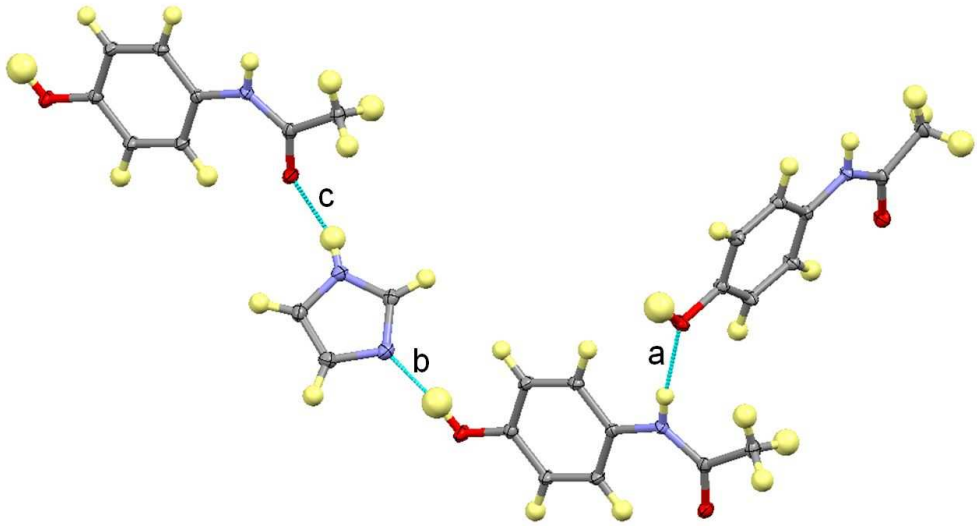

Figure 7.1 *Hydrogen-bonding in the paracetamol: imidazole molecular complex.*

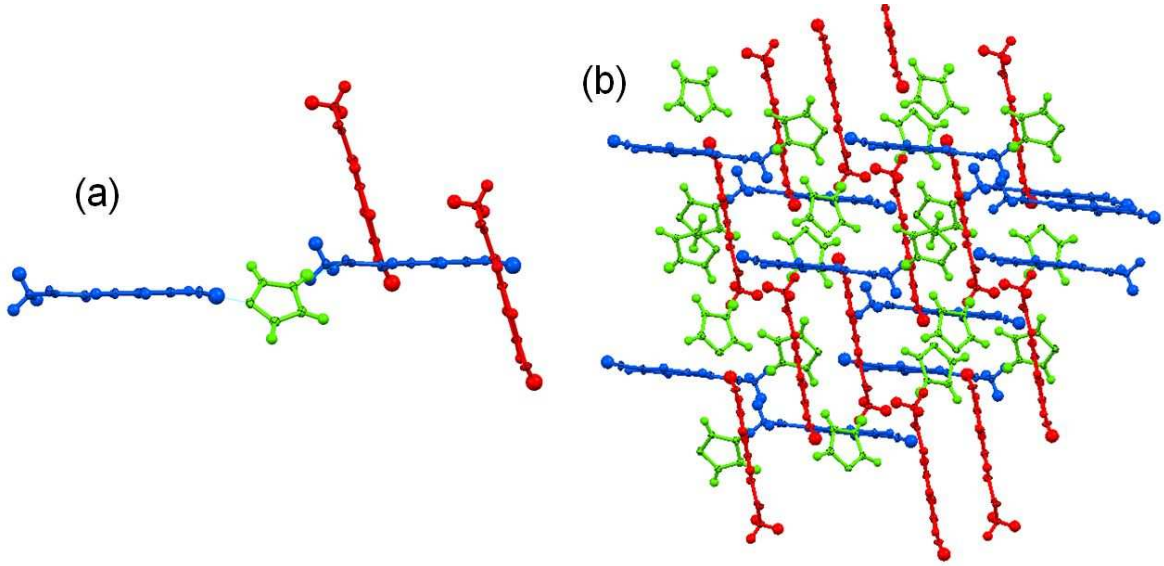

Figure 7.2 *The crystal packing in the paracetamol : imidazole complex. (a) PA molecules (blue) linked by IM molecules (green) lie parallel to each other. PA molecules (red) linked directly to the blue PA molecules run parallel to each other in planes intersecting the planes of the blue PA molecules. (b) The resulting interlocked crystal packing arrangement.*

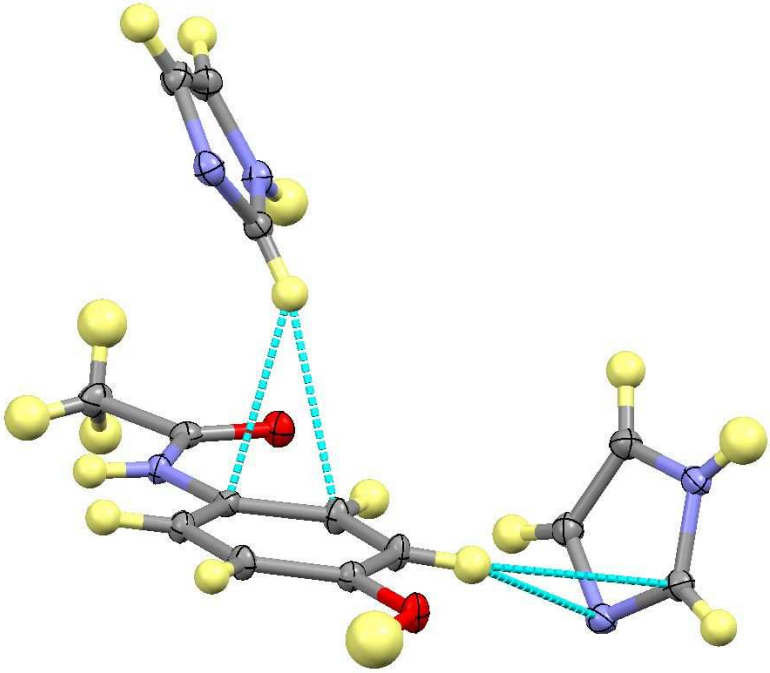

Figure 7.3 *CH···π interactions in the paracetamol : imidazole complex.*

7.3.2 Paracetamol : 2-methylimidazole (1:2) (PA:2MIM)

The 1:2 paracetamol: 2-methylimidazole complex consists of two 2MIM molecules and a single PA molecule in the asymmetric unit, forming a neutral complex with no hydrogen transfer occurring.

The paracetamol molecules are in the same hydrogen bonding environment as seen in the PA:IM complex (Figure 7.4). The hydrogen bonds are of similar strength to those in the PA:IM complex (Table 7.2), although with a slightly stronger OH···N interaction between the PA and 2MIM. The stronger OH···N interaction is reflective of the stronger basicity of 2MIM (pKa = 7.88 c.f. 6.99 for IM). A slightly weaker NH···O interaction occurs between the 2MIM NH and the PA amide oxygen. One major difference occurs in the hydrogen bonding arrangement of PX:2MIM, as the 2MIM molecule does not hydrogen bond directly to another PA molecule, instead forming a moderately strong NH···N hydrogen bond (N···N = 2.817(2) Å) to a symmetry independent 2MIM molecule, meaning that PA molecules are linked through two 2MIM molecules instead of one (Figure 7.5).

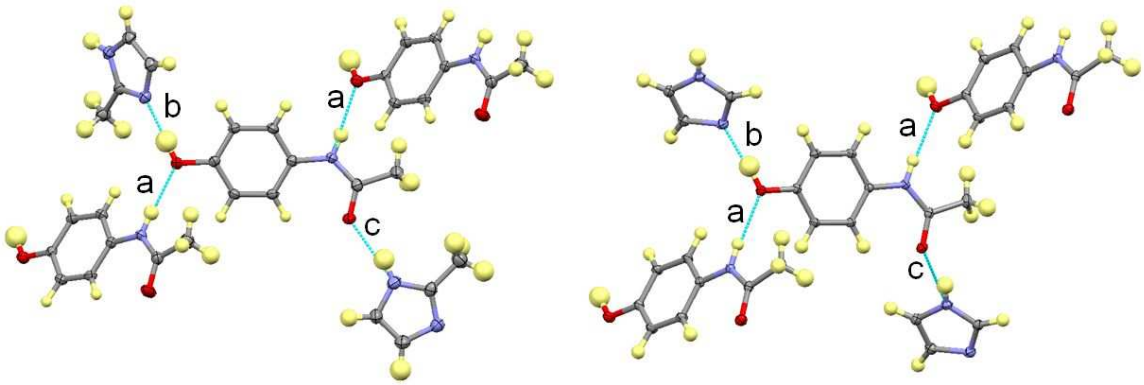

Figure 7.4 *Hydrogen bonding environment of the PA molecule in the paracetamol : 2-methylimidazole complex (left) and the paracetamol : imidazole complex (right).*

Table 7.2 *Hydrogen bond lengths and angles in the paracetamol : imidazole and paracetamol : 2-methylimidazole complexes (refer to Figure 7.4 for key).*

Complex	H-Bond	D-H (Å)	H···A (Å)	D···A (Å)	∠D-H···A (°)
PA:IM	a	0.89(2)	2.08(12)	2.9638(13)	173.7(15)
	b	0.89(2)	1.74(2)	2.6944(14)	173(2)
	c	0.96(2)	1.91(2)	2.7618(14)	160(2)
PA:2MIM	a	0.89 (2)	2.08(2)	2.959(2)	168(2)
	b	0.87(2)	1.78(2)	2.656(2)	177(2)
	c	0.92(2)	1.93(2)	2.820(2)	163(2)

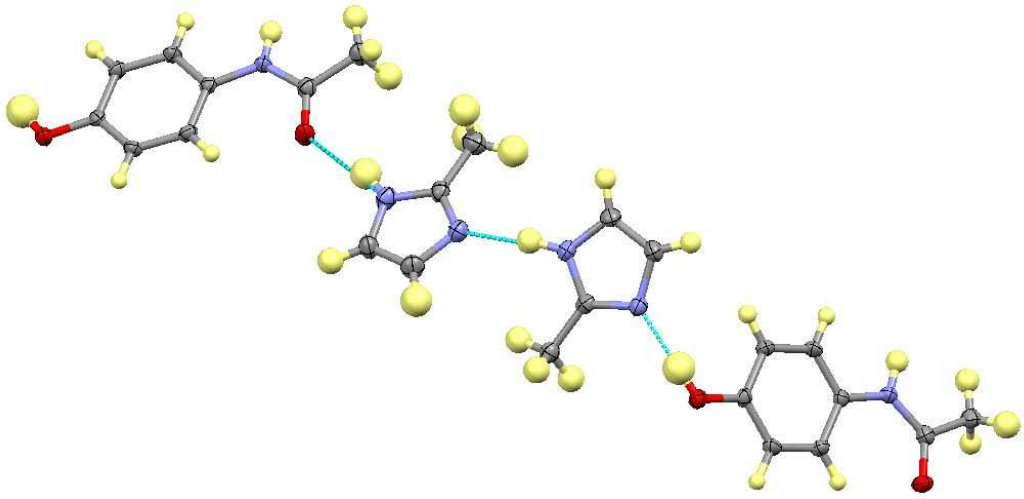

Figure 7.5 *PA molecules linked by two 2MIM molecules in the paracetamol : 2-methylimidazole complex.*

PA molecules again lie along planes running in two directions (Figure 7.6a). Parallel PA molecules are linked by a PA molecule lying along the second plane. This PA molecule links to another non-parallel PA molecule through the two hydrogen bonded 2MIM molecules. The planes of the PA molecules intersect, resulting in a herringbone arrangement of PA molecules (Figure 7.6b). Viewing the structure along the c-axis shows that the structure consists of domains of PA and 2MIM separated by domains of the symmetry independent 2MIM molecule (Figure 7.7). As in the PA:IM complex, there are again significant CH···π interactions (Figure 7.8). These involve the methyl CH of the IM interacting with the benzene ring of the PA molecule as well as the aromatic CH of the symmetry independent IM molecule (C···π(centroid) = approx. 3.511 Å and 3.661 Å).

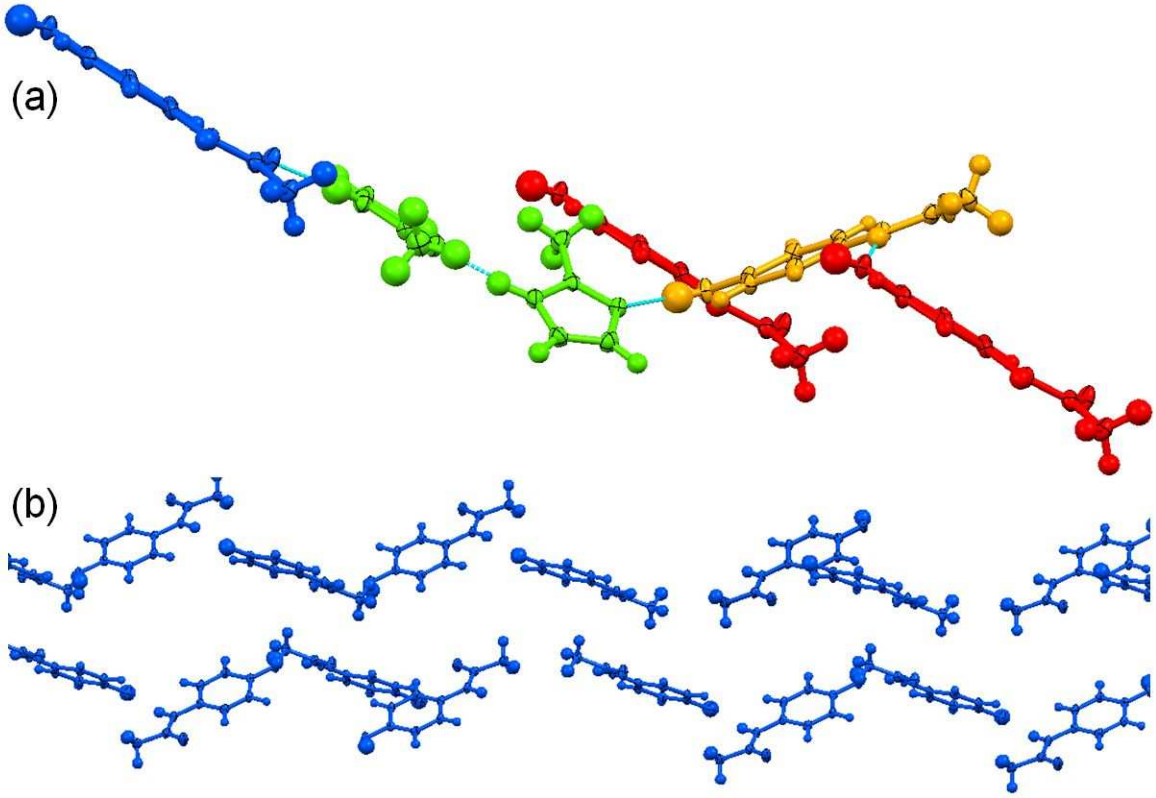

Figure 7.6 *Crystal packing in the paracetamol : 2MIM complex. (a) The relative planes of the paracetamol molecules. The red PA molecules are hydrogen bonded directly to the orange PA molecule and lie parallel with the blue PA molecule. The blue PA molecule links to the orange PA molecule through the two IM molecules (green). (b) The staggered herringbone arrangement of the PA molecules (with 2MIM omitted for clarity).*

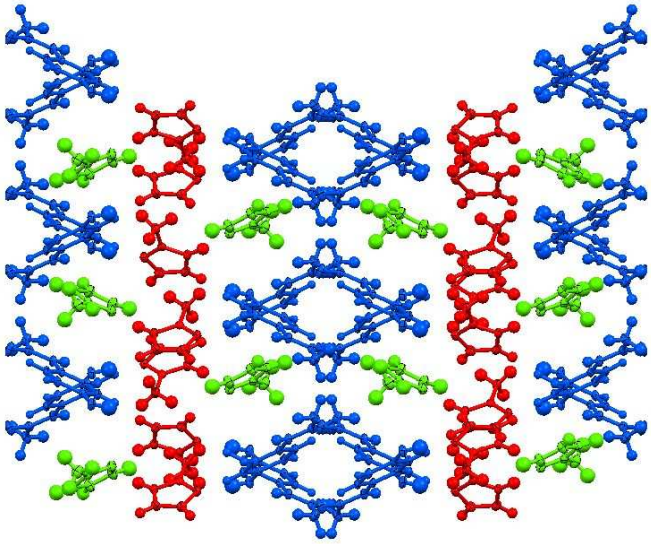

Figure 7.7 *View along the c-axis in the paracetamol : imidazole complex, showing domains of PA and 2MIM (blue and green, respectively) separated by domains of the symmetry independent 2MIM molecule (red).*

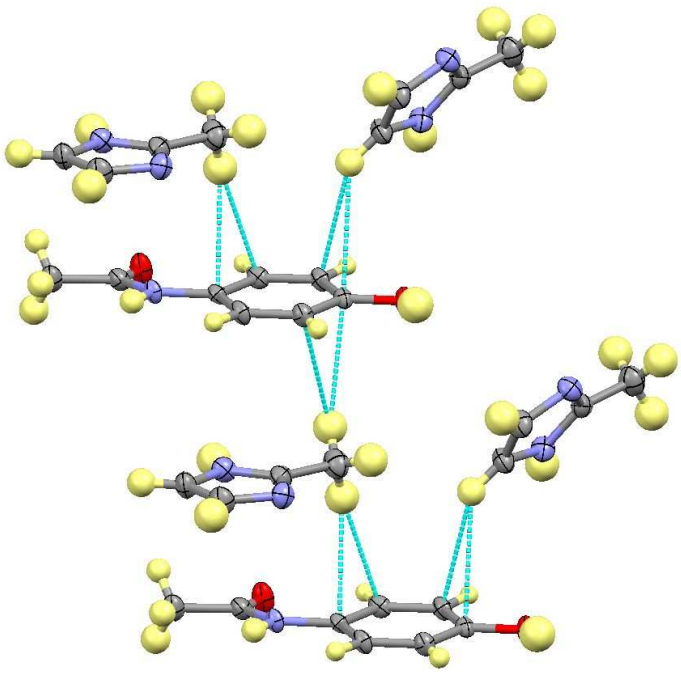

Figure 7.8 *CH···π interactions in the paracetamol : 2methylimidazole complex.*

7.3.3 Paracetamol : 4-methylimidazole (PA:4MIM)

The 1:1 paracetamol : 4-methylimidazole complex features one molecule of each component in the asymmetric unit. The PA molecule in the complex is twisted around the C-N bond so that the amide carbonyl and the methyl group lie out of plane with the benzene ring (Figure 7.9). The twisting is fairly pronounced, with a C5-C8-N3-C1 torsion angle of approximately 163.09°.

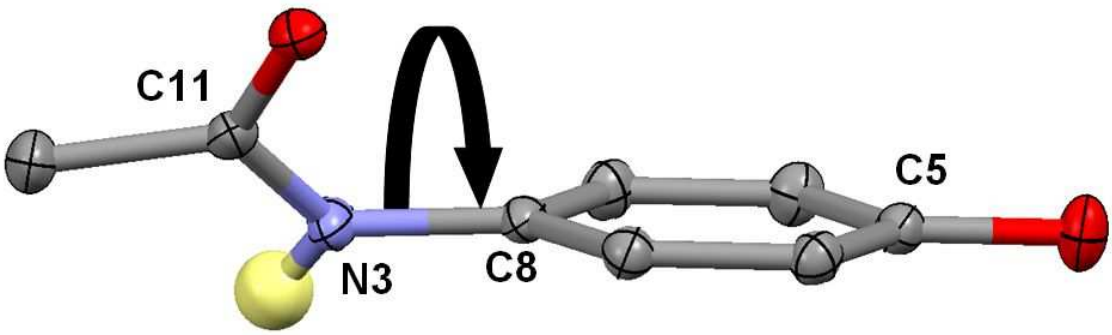

Figure 7.9 *Twisting around the C-N bond of the PA molecule in the paracetamol : 4-methylimidazole complex. H-atoms other than that on the amide nitrogen are omitted for clarity.*

A hydrogen bond is formed from the 4MIM NH to the PA carbonyl oxygen (c in Figure 7.10), as is also seen in the IM and 2MIM complexes. This interaction is similar in strength to that seen in the PA:2MIM complex (hydrogen bond distances and angles in Table 7.3). The twisting of the carbonyl oxygen means it is also able to form another moderately strong OH···O hydrogen bond with the hydroxyl of another paracetamol molecule as it is no longer limited sterically by the benzene ring (a in Figure 7.10). Other than the NH···O interaction, the hydrogen bonding in the complex is completely different to the IM and 2MIM complexes. Moderately strong NH···N interactions are formed between the PA amide NH and the 4MIM nitrogen (b in Figure 7.10) instead of the NH···O interactions between PA molecules found in the IM and 2MIM complexes.

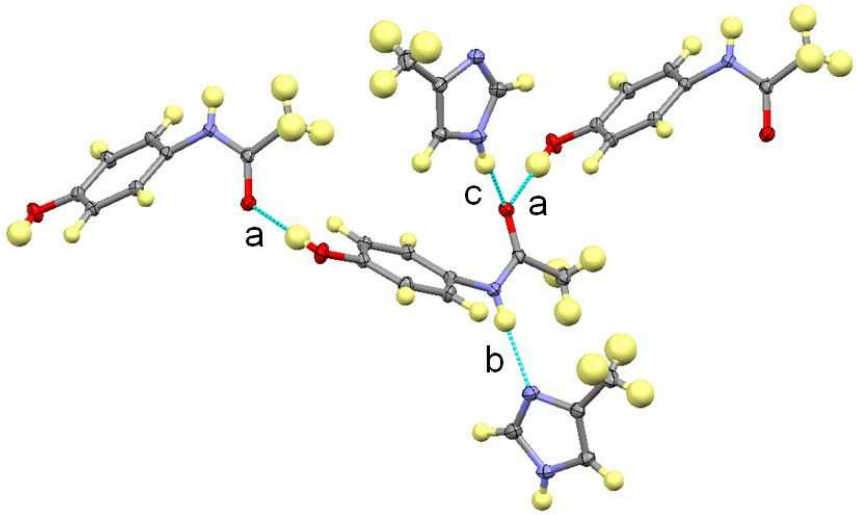

Figure 7.10 *Hydrogen bonding environment of the PA molecule in the paracetamol : 4-methylimidazole complex.*

Table 7.3 *Hydrogen bond lengths and angles in the paracetamol : 4-methylimidazole complex (refer to Figure 7.10 for key). Values for the equivalent NH···O interactions in the PA:IM and PA:2MIM complexes are also shown for comparison.*

Complex	H-Bond	D-H (Å)	H···A (Å)	D···A (Å)	∠D-H···A (°)
PA:4MIM	a	0.90(2)	1.81(2)	2.7099(11)	179(2)
	b	0.86(2)	2.01(2)	2.8712(13)	177 (2)
	c	0.89(2)	1.94(2)	2.8177(12)	167(2)
PA:IM	c	0.96(2)	1.91 (2)	2.7618(14)	160(2)
PA:2MIM	c	0.92(2)	1.93(2)	2.820(2)	163(2)

The PA forms hydrogen bonds with 4MIM (b and c in Figure 7.10), creating infinite chains of alternating PA and 4MIM (Figure 7.11a). The chains are then linked to adjacent chains

by the OH···O hydrogen bonds between PA molecules forming infinite PA chains in that direction. The PA molecules are arranged in a herringbone pattern and separated from the PA molecules below by the 4MIM molecules (Figure 7.11b). PA molecules are further linked to other PA molecules by weak CH···O hydrogen bonds (C···O = 3.5013(13) Å) between an aromatic CH and the hydroxyl oxygen (Figure 7.12). Weak CH···π interactions are also present between the 4MIM CH groups and the benzene rings of PA molecules, as well as between an aromatic CH group of the PA molecule and the aromatic 4MIM ring (Figure 7.13).

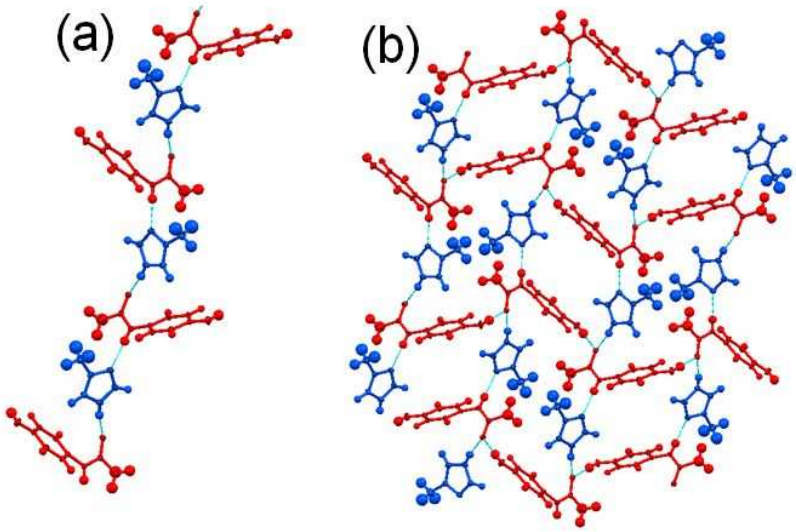

Figure 7.11 *Crystal packing in the paracetamol : 4-methylimidazole complex. (a) Infinite chains of alternating PA (red) and 4MIM (blue) linked by NH···O and NH···N interactions. (b) The herringbone arrangement of the PA molecules linked by OH···O hydrogen bonds, with 4MIM molecules separating PA molecules above and below each other.*

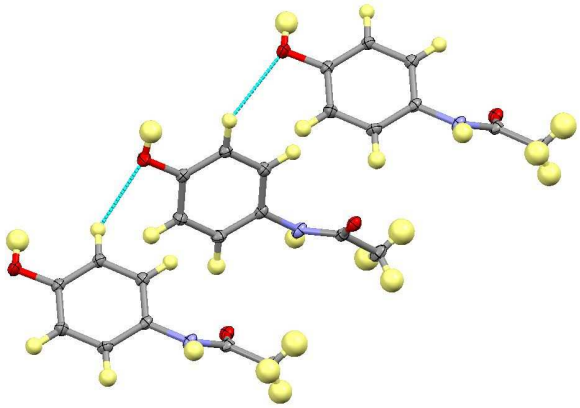

Figure 7.12 *Weak CH···O hydrogen between PA molecules in the paracetamol : 4-methylimidazole complex.*

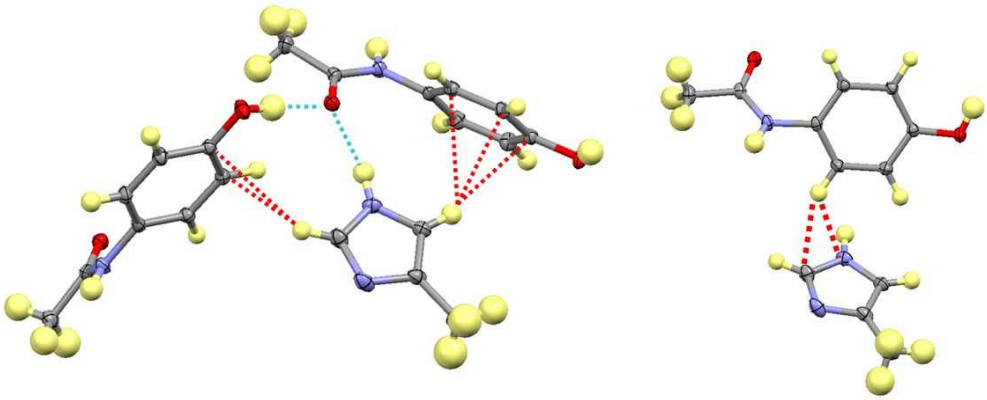

Figure 7.13 *CH···π interactions between the 4MIM CH groups and the PA benzene ring (red-dashed line, LHS) and between the PA CH group and the 4MIM ring (RHS).*

7.4 Crystal Structures of Multi-component Complexes of 4-Acetamidobenzoic Acid and Nitrogen-Heterocycles

Eight molecular complexes of 4ABA with NHCs were produced in this study. Crystallographic data and full refinement details can be found in (Appendix A7, Table A-7b).

7.4.1 4-Acetamidobenzoic acid : Imidazole ($4ABA^-$:IM^+)

The 1:1 4-acetamidobenzoic acid : imidazole complex features two symmetry independent molecules of each component in the asymmetric unit with the acidic hydrogen of both 4ABA molecules transferred to the basic nitrogen of the IM molecule forming a 4-acetamidobenzoate ($4ABA^-$) : imidazolium IM^+ salt. The C-N distances in the two IM^+ molecules between the carbon in the 2-position and the two nitrogen atoms suggest the charge is delocalised (C-N = 1.320(3) Å, 1.329(2) Å and 1.321(2) Å, 1.327(2) Å). $4ABA^-$, however, has a clear displacement of the negative charge onto one oxygen of the carboxylate group, evidenced in the C···O distances (1.237(2) Å, 1.290(2) Å and 1.244(2) Å, 1.277(2)Å). Lengthening of the C=O bond and shortening of the C-O bond does, however, still occur.

The hydrogen bonding of both symmetry independent $4ABA^-$ molecules is similar, although small differences do exist between them (Figure 7.14). Both the $4ABA^-$ molecules are linked to symmetry equivalent $4ABA^-$ molecules through NH···O hydrogen

bonding of the amide NH with a carboxylate oxygen in both cases, although in one case the hydrogen bond is charge assisted with the deprotonated oxygen (more δ^-) acting as acceptor (d in Figure 7.14, left), while in the other the carbonyl (less δ^-) is the acceptor (d' in Figure 7.14, right). Three IM^+ molecules are directly hydrogen bonded to each $4ABA^-$ molecule. The NH of one IM^+ forms a similar bifurcated DHAA hydrogen bond with the carboxylate oxygen atoms in each case, forming a stronger, charge assisted hydrogen bond with the deprotonated oxygen, as would be expected. One $4ABA^-$ molecule is linked to an IM^+ molecule through hydrogen bonds to its carboxylate carbonyl oxygen by the CH group in the 2-position (e in Figure 7.14) and to another IM^+ molecule through hydrogen bonds to its amide carbonyl through an NH···O interaction (c in Figure 7.14). The other $4ABA^-$ molecule (RHS in Figure 7.14) has IM^+ molecules forming hydrogen bonds to the same positions, but through different interactions: NH···O interactions with the deprotonated carboxylate oxygen (b in Figure 7.14), and CH···O interactions with the amide carbonyl oxygen (g in Figure 7.14). Hydrogen bond lengths and angles can be found in Table 7.4.

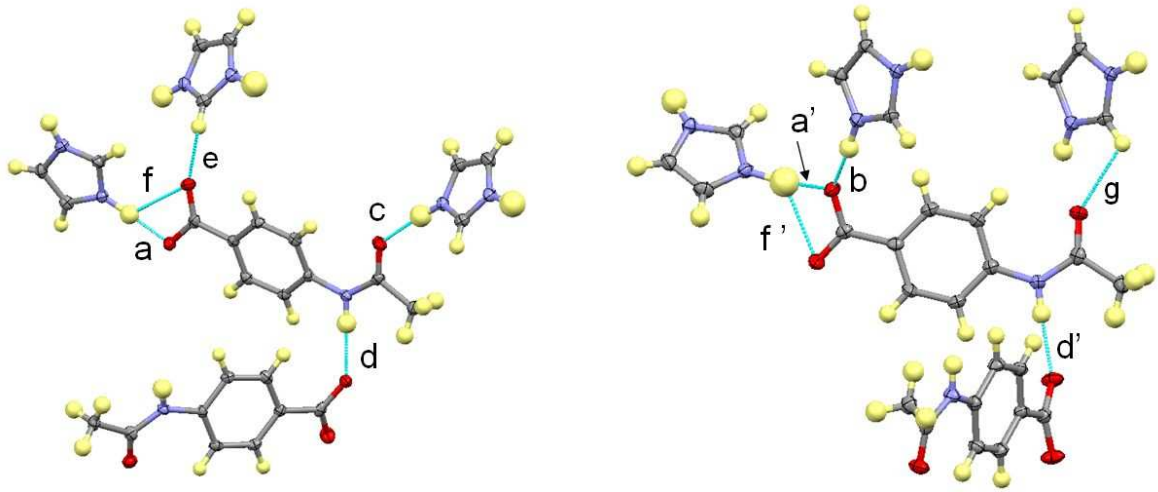

Figure 7.14 *Hydrogen bonding of the two symmetry independent $4ABA^-$ molecules in the 4-acetamidobenzoic acid : imidazole salt complex.*

Table 7.4 *Hydrogen bond lengths and angles in the 4-acetamidobenzoic acid : imidazole salt complex (refer to Figure 7.14 for key).*

Complex	H-Bond	D-H (Å)	H···A (Å)	D···A (Å)	∠D-H···A (°)
4ABA$^-$: IM$^+$	a	0.97(3)	1.72(3)	2.686(2)	175(3)
	a'	0.99(3)	1.63(3)	2.617(2)	171(3)
	b	0.94(2)	1.74(2)	2.657(2)	164(2)
	c	0.93(3)	1.82(3)	2.747(2)	173(3)
	d	0.90(2)	1.97(2)	2.866(2)	172(2)
	d'	0.89(2)	1.92(2)	2.809(2)	179(2)
	e	0.92(2)	2.25(2)	3.160(2)	174(2)
	f	0.97(3)	2.45(3)	3.034(2)	118(2)
	f'	1.00(3)	2.57(3)	3.297(2)	130(2)
	g	0.90(2)	2.37(2)	2.925(2)	120(2)

Symmetry equivalent 4ABA$^-$ molecules link to each other in infinite staggered chains (Figure 7.15a) through the NH···O interactions (d and d' in Figure 7.14), with IM$^+$ molecules linking each 4ABA$^-$ molecule in the chain to another 4ABA$^-$ chain (Figure 7.15b). Significant π···π interactions are also present between IM$^+$ and 4ABA$^-$ molecules with distances of approximately 3.325 Å and 3.281 Å between the centroids of the closest π systems (Figure 7.16).

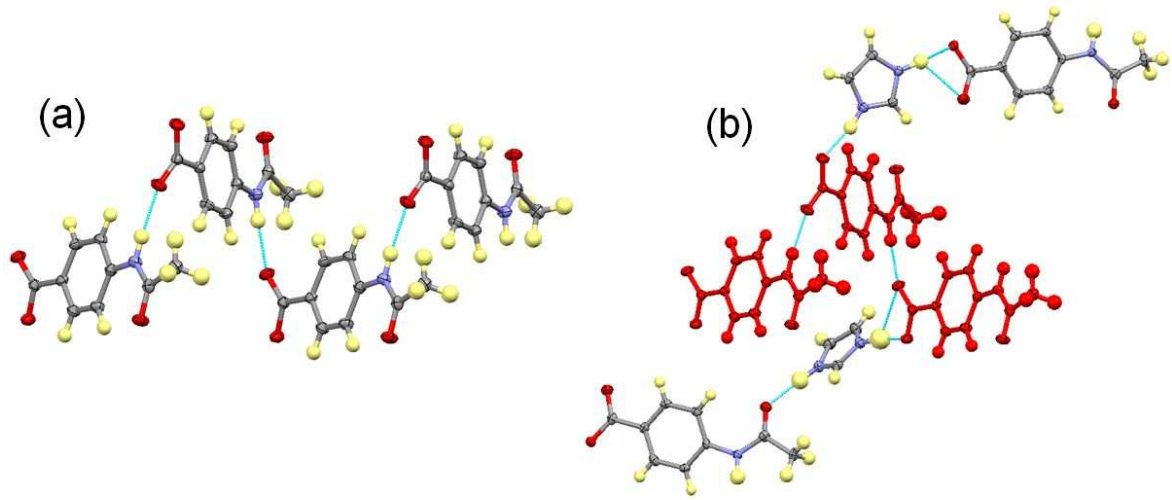

Figure 7.15 *(a) Chains of 4ABA$^-$ in the 4ABA$^-$:IM$^+$ complex (b) The IM$^+$ molecules linking the 4ABA$^-$ chain (red) to other ABA$^-$ molecules.*

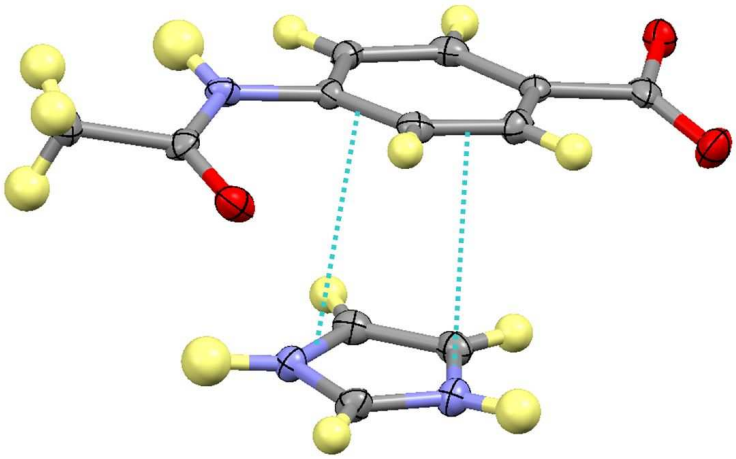

Figure 7.16 *π···π interactions between 4ABA⁻ and IM⁺ molecules in the 4-acetamidobenzoic acid : imidazole salt complex.*

7.4.2 4-Acetamidobenzoic acid : 2-methylimidazole (2:1) (4ABA:4ABA⁻:2MIM⁺)

The 2:1 4-acetamidobenzoic acid : 2-methylimidazole complex crystallises in a 2: 1 ratio, with the acidic hydrogen atom of one 4ABA molecule transferring to the 2MIM nitrogen, meaning the asymmetric unit consists of one neutral 4-acetamidobenzoic acid molecule (4ABA), one 4-acetamidobenzoate molecule ($4ABA^-$) and a 2-methylimidazolium molecule ($2MIM^+$). The $4ABA^-$ molecule has the delocalised charge displaced onto one oxygen of the carboxylate group, although with lengthening of the C=O bond and shortening of the C-O bond (C-O = 1.274(2) Å and 1.242(2) Å). The $2MIM^+$ molecule has a more delocalised charge with C-N lengths of 1.336(3) Å and 1.324(3) Å (carbon in the 2-position).

Chains of the neutral 4ABA molecules are formed through moderately strong NH···O hydrogen bonds involving the amide groups (d in Figure 7.17, Table 7.5 for hydrogen bond distances and angles). The $4ABA^-$ molecules form similar chains through the same type of interaction, with a slightly stronger NH···O interaction formed (d' in Figure 7.17). The chains are linked through a short, strong OH···O hydrogen bond between the carboxylic acid hydroxyl of 4ABA and the more δ^- oxygen (longer C-O bond) of the $4ABA^-$ carboxylate (c in Figure 7.17). The O-H distance in this hydrogen bond is significantly lengthened, suggesting the hydrogen is partially shared (Table 7.5). The chains are further linked through the $2MIM^+$ molecules, with NH···O hydrogen bonds formed between one $2MIM^+$ NH group and the carbonyl oxygen of 4ABA, with the other NH group forming an NH···O hydrogen bond with the other carboxylate oxygen of $4ABA^-$ (b and a in Figure 7.17 respectively). Both of these hydrogen bonds have long D-H

distances (Table 7.5) suggesting partial sharing of the hydrogen atom. Chains linked together in this way form layers that are stacked upon each other (Figure 7.18).

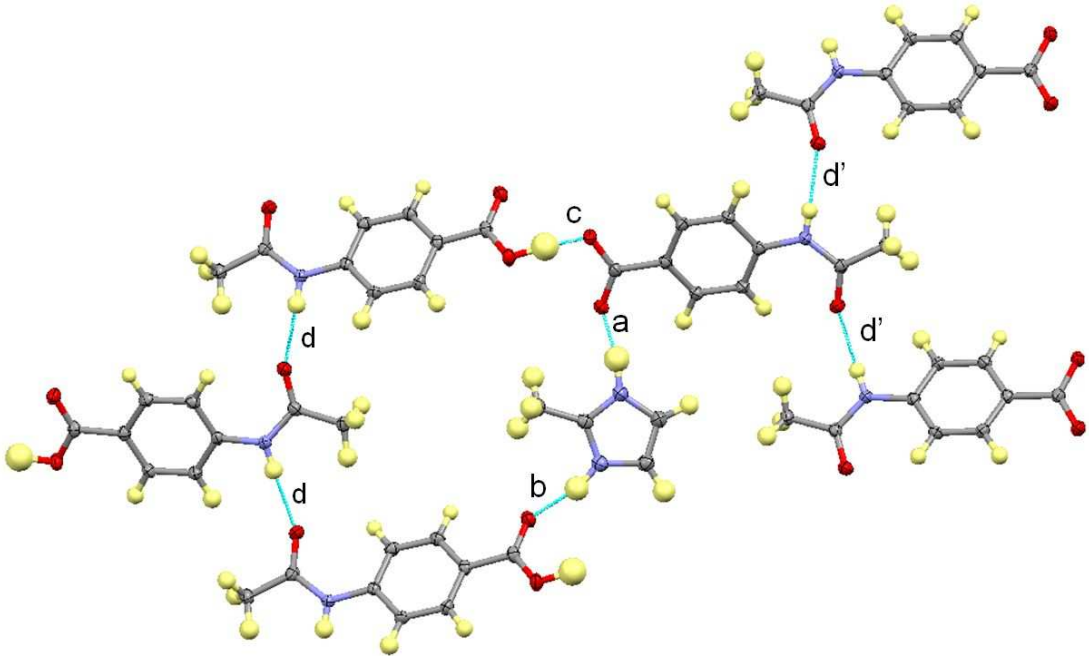

Figure 7.17 *Hydrogen bonding in the 4-acetamidobenzoic : 2-methylimidazole complex.*

Table 7.5 *Hydrogen bond lengths and angles in the 4-acetamidobenzoic acid : 2-methylimidazole complex (refer to Figure 7.17 for key).*

Complex	H-Bond	D-H (Å)	H···A (Å)	D···A (Å)	∠D-H···A (°)
4ABA:4ABA$^-$: **2MIM$^+$**	a	1.02(3)	1.61(3)	2.630(2)	169(3)
	b	1.01(3)	1.73(3)	2.701(2)	160(2)
	c	1.11(4)	1.37(3)	2.478(2)	175(4)
	d	0.87(3)	2.02(3)	2.887(2)	177(3)
	d'	0.84(3)	2.02(3)	2.851(2)	172(2)

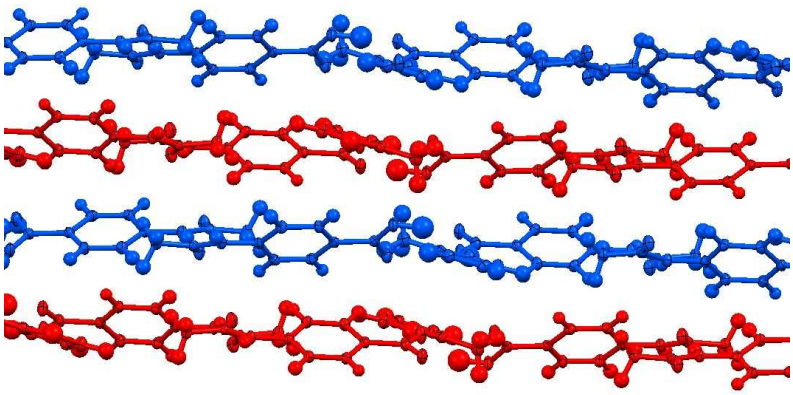

Figure 7.18 *Relative arrangement of the layers in the 2:1 4-acetamidobenzoic acid : 2-methylimidazole complex.*

Few significant interactions occur between layers, with only weak hydrogen bonds occurring (Figure 7.19). An aromatic CH group of the $2MIM^+$ forms hydrogen bonds to the carboxylic acid carbonyl oxygen (C···O = 3.216(3) Å) of the 4ABA below and the methyl group of $2MIM^+$ hydrogen bonds to the carboxylic acid hydroxyl oxygen of the 4ABA molecule above (C···O = 3.305(3) Å, ∠DHA = 123.2(1)°) (Figure 7.19a). CH···π hydrogen bonds also occur between $4ABA^-$ and 4ABA molecules with approximately 3.655 Å between the carbon and the centroid of the C=C bond (Figure 7.19b).

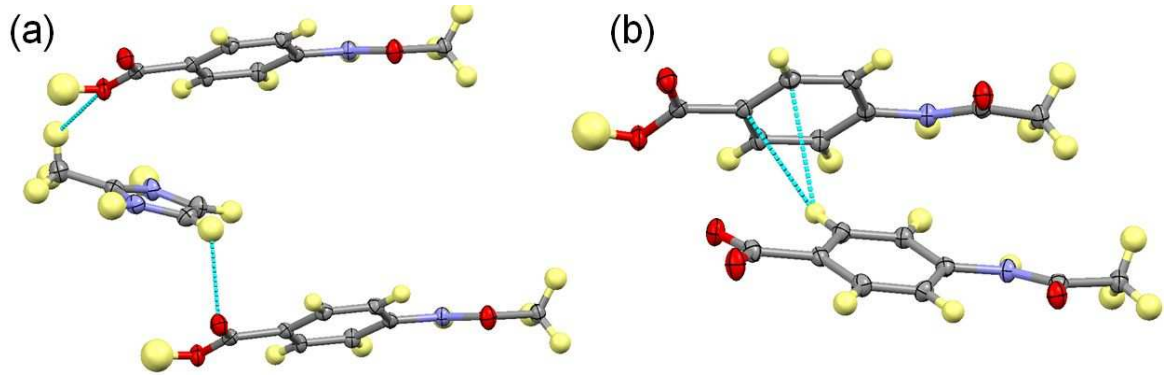

Figure 7.19 *Interactions between layers in the 2:1 4-acetamidobenzoic acid : 2-methylimidazole complex. (a) CH···O hydrogen bonds between the $2MIM^+$ molecule and the 4ABA molecules. (b) CH···π hydrogen bonds between $4ABA^-$ and 4ABA molecules.*

7.4.3 4-Acetamidobenzoic acid : 4-methylimidazole (4ABA:4MIM)

The 1:1 4-acetamidobenzoic acid: 4-methylimidazole complex crystallises in a 1:1 ratio with the acidic hydrogen of the 4ABA transferring to the 4MIM molecule. Delocalisation of the positive charge in the $4MIM^+$ molecule is evidenced by the N-C distances to the carbon in the 2-position (C-N = 1.324(2) Å and 1.326(2) Å). The C-O distances in the $4ABA^-$ indicate that the delocalised negative charge is displaced towards one oxygen (C-O = 1.245(2) Å and 1.284(2) Å), with the C=O again lengthened and the C-O shortened.

Interactions between $4ABA^-$ molecules are similar to those seen in the $4ABA:4ABA^-:2MIM^+$ complex, with chains of $4ABA^-$ formed through moderately strong NH···O hydrogen bonds involving the amide groups (d in Figure 7.20). These NH···O hydrogen bonds in this complex are, however, considerably weaker than those in the $4ABA:4ABA^-:2MIM^+$ complex (Table 7.6). The $4ABA^-$ chains in this complex are linked in a

different way to those in the $4ABA^-:2MIM^+$ complex, as no neutral 4ABA molecules are present. The chains are therefore linked solely through the two NH groups of $4MIM^+$ molecules forming NH···O hydrogen bonds with the carboxylate oxygen atoms of $4ABA^-$ molecules (a and b in Figure 7.20). The N-H bonds in these interactions are again relatively long (Table 7.6) The CH group in the 5-position of the $4MIM^+$ molecule also forms a weak hydrogen bond to the carboxylate oxygen of $4ABA^-$ which is slightly less δ^- in nature (e in Figure 7.20). These interactions again link the molecules into layers, although these layers are flatter than those in the $4ABA^-:2MIM^+$ complex (Figure 7.21).

The NH···O hydrogen bonds between the $4MIM^+$ and $4ABA^-$ in this complex (a and b in Figure 7.20) are both similar to the NH interaction with the carboxylic acid carbonyl oxygen in the $4ABA:4ABA^-:2MIM^+$ complex (b in Figure 7.17) - this despite both being charge assisted. The NH···O hydrogen bonds are, however, considerably weaker than the NH interaction with the carboxylate oxygen in the $4ABA:4ABA^-:2MIM^+$ complex (a in Figure 7.17).

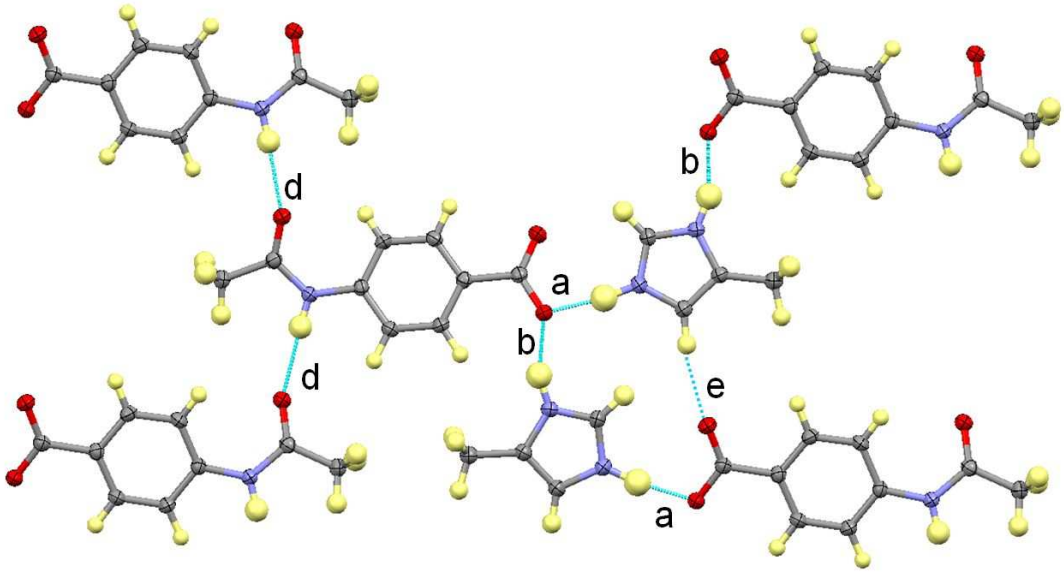

Figure 7.20 *Hydrogen bonded chains of $4ABA^-$ linked by $4MIM^+$ molecules in the 4-acetamidobenzoic acid: 4-methylimidazole complex.*

Table 7.6 *Hydrogen bond lengths and angles in the 4-acetamidobenzoic acid: 4-methylimidazole salt complex (refer to Figure 7.20 for key). Corresponding values for the 4-acetamidobenzoic acid: 2-methylimidazole complex are also shown for comparison.*

Complex	H-Bond	D-H (Å)	H···A (Å)	D···A (Å)	∠D-H···A (°)
4ABA$^-$:4MIM$^+$	a	1.03(2)	1.68(2)	2.696(2)	171(2)
	b	0.98(2)	1.76(2)	2.687(2)	157(2)
	d	0.92(2)	2.09(2)	2.998(2)	172.8(16)
	e	0.971(16)	2.277(16)	3.238(2)	169.9(14)
4ABA:4ABA$^-$: 2MIM$^+$	a	1.02(3)	1.61(3)	2.630(2)	169(3)
	b	1.01(3)	1.73(3)	2.701(2)	160(2)
	d	0.87(3)	2.02(3)	2.887(2)	177(3)
	d’	0.84(3)	2.02(3)	2.851(2)	172(2)

Note: a and b in the 4ABA$^-$: 4MIM$^+$ complex are both NH···O$^-$ interactions with the deprotonated oxygen, whereas a in the 4ABA:4ABA$^-$:2MIM$^+$ complex is an NH···O interaction with a carboxylate oxygen which is more of a carbonyl in nature and b is an NH···O interaction with a carboxylic acid carbonyl oxygen.

The layers are again held together by weak interactions (Figure 7.22). The methyl groups of both the 4MIM$^+$ and 4ABA$^-$ molecules form weak hydrogen bonds with the amide oxygen of the 4ABA$^-$ molecule below (C···O = 3.518(2) Å and 3.531(2) Å, respectively). Significant π···π interactions are also present between the 4ABA$^-$ and 4MIM$^+$ molecules, with approximately 3.267 Å and 3.425 Å between the two sets of closest C=C bonds (also Figure 7.22).

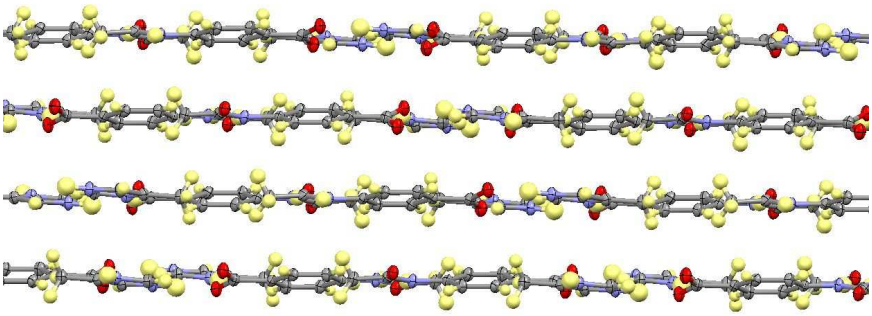

Figure 7.21 *Layers in the 4-acetamidobenzoic acid : 4-methylimidazole complex.*

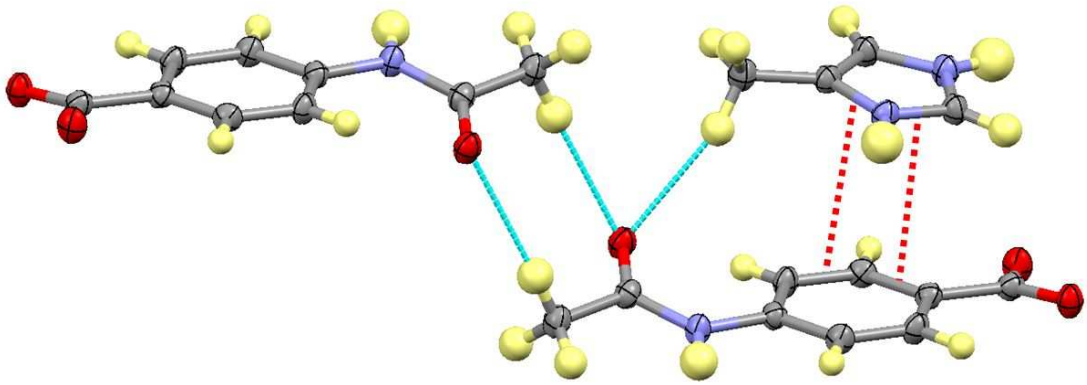

Figure 7.22 *The weak CH···O hydrogen bonds (blue dashed lines) and π···π interactions (red dashed lines) between layers in the 4-acetamidobenzoic acid : 4-methylimidazole complex.*

7.4.4 4-Acetamidobenzoic Acid : Benzimidazole Monohydrate ($ABA^-:BZ^+.H_2O$)

The 1:1 4-acetamidobenzoic acid : benzimidazole monohydrate complex features one molecule of each component in the asymmetric unit. The acidic hydrogen of 4ABA has transferred to the BZ nitrogen forming a benzimidazolium ion and a 4-acetamidobenzoate ion. The charge in both molecules is delocalised with the bond lengths indicating only slight displacement of the charge in both cases. The C-N bonds in BZ^+ between the nitrogen atoms and the 2-carbon have C-N distances of 1.321(3) Å and 1.334(3) Å. C-O distances in the carboxylate group of $4ABA^-$ are 1.262(3) Å and 1.278(3) Å.

The crystal structure consists of infinite ABAB chains of $4ABA^-$ and BZ^+ molecules linked by strong NH···O interactions (Figure 7.23). The slightly more δ^+ NH in the BZ^+ molecule forms hydrogen bonds to the slightly more δ^- carboxylate oxygen (a in Figure 7.23). The hydrogen in this interaction appears not to occupy fully the modelled position on the nitrogen. The Fourier difference synthesis shows the electron density to be significantly elongated in the direction of the acceptor oxygen atom (Figure 7.24). This suggests that the current model (with the hydrogen placed on the electron density maximum and bonded to BZ) may not be an accurate reflection of the true position. The N-H bond is also very long suggesting sharing of the hydrogen atom (Table 7.7). The bond lengths in $4ABA^-$ and BZ^+ suggest, however, that the charge is delocalised in both molecules, and therefore that BZ is protonated and 4ABA is deprotonated. No improvement upon the current model is possible without neutron diffraction data and therefore definite conclusions cannot be drawn. Hydrogen bond lengths and angles (a in

Table 7.7) are calculated for the hydrogen in the modelled position and may not be truly representative of the detailed, possibly disordered, location of this hydrogen atom. The second NH group of BZ forms a moderately strong hydrogen bond to the amide carbonyl of $4ABA^-$ to extend the chain (b in Figure 7.23).

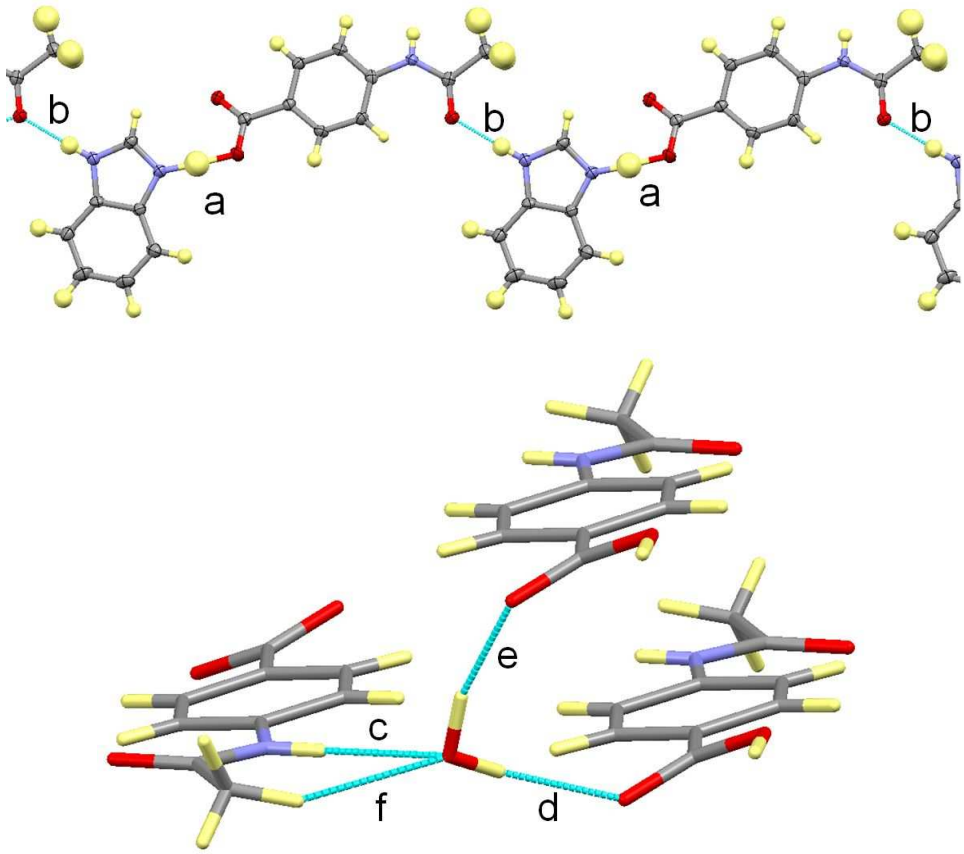

Figure 7.23 *Hydrogen bonding in the 4-acetamidobenzoic acid : benzimidazole monohydrate complex showing the infinite chains formed by NH···O hydrogen bonds (top) and the interactions of the water molecules (bottom).*

Table 7.7 *Hydrogen bond lengths and angles in the 4-acetamidobenzoic acid : benzimidazole monohydrate complex (refer to Figure 7.23 for key).*

Complex	H-Bond	D-H (Å)	H···A (Å)	D···A (Å)	∠D-H···A (°)
$4ABA^-$:BZ^+.H_2O	a	1.21(4)	1.34(4)	2.544(3)	178(4)
	b	0.87(3)	1.85(3)	2.725(3)	176(3)
	c	0.83(3)	2.06(3)	2.891(3)	176.2(16)
	d	0.89(4)	1.92(3)	2.778(3)	161(3)
	e	0.94(3)	1.86(3)	2.767(3)	164(3)
	f	1.02(4)	2.54(4)	3.394(4)	141(3)

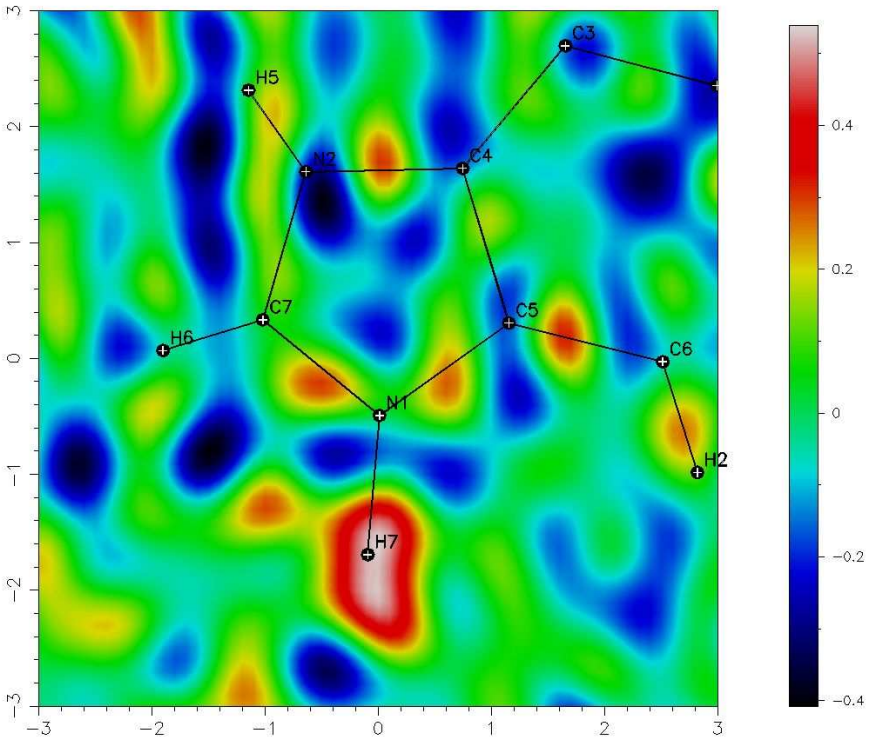

Figure 7.24 *Fourier difference map showing the electron density close to the modelled position of the hydrogen atom (H7) in the short, strong NH···O hydrogen bond between 4ABA⁻ and BZ⁺ in the 4-acetamidobenzoic acid : benzimidazole monohydrate complex. The map is calculated with the H atom (H7) removed from the model. The electron density is smeared out in the direction of the acceptor oxygen atom (not shown) suggesting the model is not a true reflection of the hydrogen position.*

Neighbouring chains are linked into bilayers through the water molecules, with the 4ABA⁻ amide NH group forming a moderately strong hydrogen bond to the water oxygen (c in Figure 7.23). The methyl group of 4ABA⁻ also forms a weak hydrogen bond to the water oxygen (f in Figure 7.23). The water OH then forms a moderately strong hydrogen bond to the 4ABA⁻ molecule in the next chain via the carboxylate oxygen which is not hydrogen bonded to BZ⁺ (d in Figure 7.23). The second water OH group forms another moderately strong hydrogen bond to the same carboxylate oxygen of a 4ABA⁻ molecule above (e in Figure 7.23) resulting in the bilayers stacking upon each other (Figure 7.25). Significant π···π stacking between BZ⁺ molecules is also present between the stacked bilayers with approximately 3.432 Å between the centroids of the two π bonds (Figure 7.26). Weak hydrogen bonds (Figure 7.27a) hold neighbouring bilayers together resulting in a herringbone arrangement of the bilayers. One is a weak, bifurcated, DDHHA hydrogen bond, formed between the CH groups of the BZ⁺ benzene ring and the carboxylate oxygen

of a $4ABA^-$ molecule (C···O = 3.439(4) Å and 3.446(4) Å). Another weak hydrogen bond is formed between an aromatic $4ABA^-$ CH group and the BZ^+ benzene ring (distance from C to centre of π bond = approximately 3.800 Å).

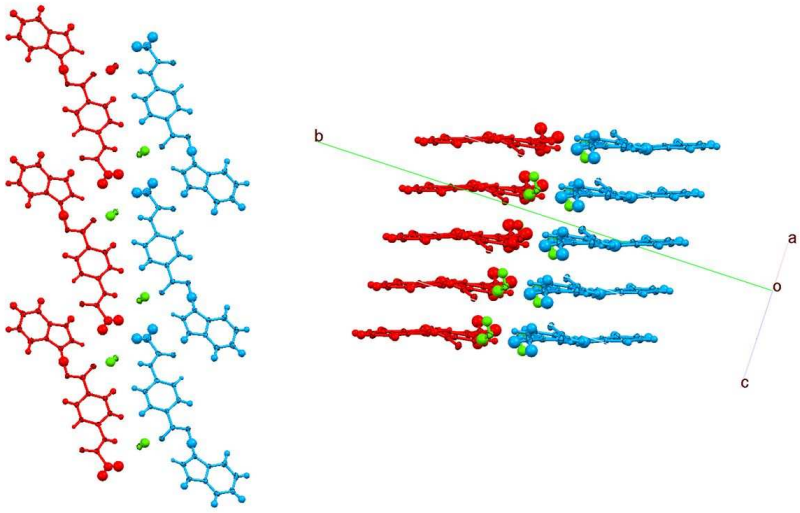

Figure 7.25 *Crystal packing in the 4-acetamidobenzoic acid : benzimidazole monohydrate complex. The view along the a-axis (LHS) shows the chains of $4ABA^-$ and BZ^+ are linked into bilayers by water molecules (green). The view along the ac diagonal (RHS) shows how the bilayers are stacked upon each other (Separate chains within the bilayers shown in red and blue).*

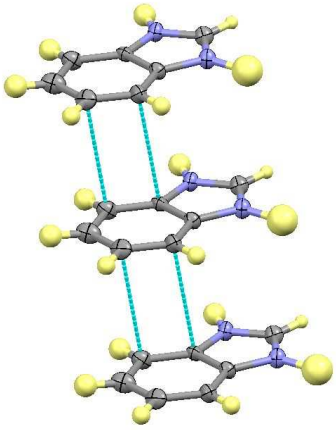

Figure 7.26 *π···π stacking of BZ^+ molecules in the 4-acetamidobenzoic acid : benzimidazole monohydrate complex.*

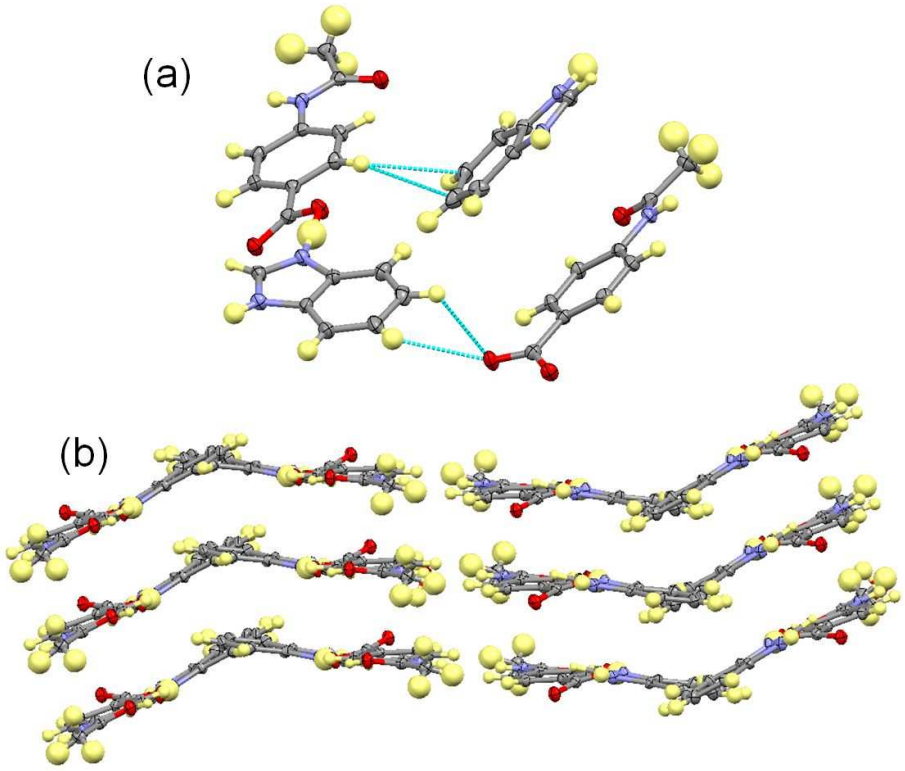

Figure 7.27 *Relative arrangement of bilayers in the 4-acetamidobenzoic acid : benzimidazole monohydrate complex. (a) Weak interactions between neighbouring bilayers. (b) Herringbone arrangement of the bilayers.*

7.4.5 4-Acetamidobenzoic acid : 4,4'-bipyridine (2:1) (ABA:BP)

The asymmetric unit of the 4-acetamidobenzoic acid : 4,4-bipyridine complex features one 4ABA molecule and half of a BP molecule, with the BP molecule lying on an inversion centre. No hydrogen transfer occurs in the complex. The crystal structure comprises chains of 4ABA molecules, linked through moderately strong NH···O hydrogen bonds between the amide groups (a in Figure 7.28, see Table 7.8 for hydrogen bond distances and angles). The chains are linked through moderately strong OH···N hydrogen bonds between the carboxylic OH group of 4ABA and the BP nitrogen (b in Figure 7.28). The O-H distance in this hydrogen bond is again relatively long. These interactions result in infinite hydrogen bonded units, with large gaps between the BP molecules in the units (Figure 7.29a). 4ABA molecules linked through the amide groups do not lie co-planar (Figure 7.29b), with the molecules running alternately in different planes, resulting in a zigzagging arrangement of the hydrogen bonded units (Figure 7.29c).

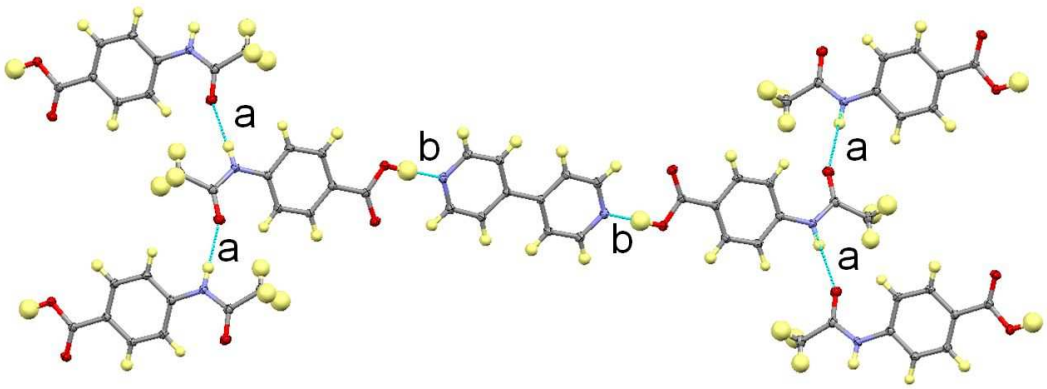

Figure 7.28 *The hydrogen bonded 4ABA chains linked by BP molecules in the 4-acetamidobenzoic acid : 4,4'-bipyridine complex.*

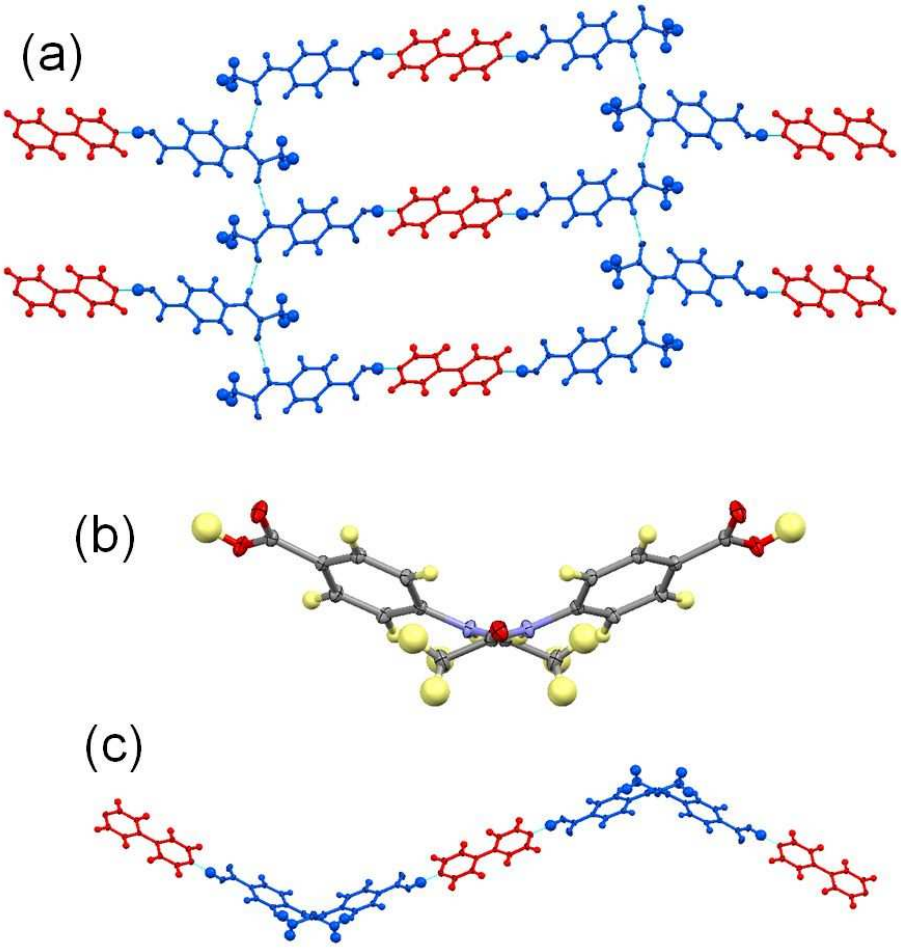

Figure 7.29 *Crystal packing in the 4-acetamidobenzoic acid : 4, 4' - bipyridine complex. (a) Infinite hydrogen bonded units formed by the interactions shown in Figure 7.28 (red = BP, blue = 4ABA). (b) The non co-planar arrangement of hydrogen bonded 4ABA molecules in the chains. (c) Rotation of (a) by 90° showing the zigzagging arrangement of the units.*

Table 7.8 *Hydrogen bond lengths and angles in the 4-acetamidobenzoic acid : 4,4'-bipyridine complex (refer to Figure 7.28 for key).*

Complex	H-Bond	D-H (Å)	H···A (Å)	D···A (Å)	∠D-H···A (°)
4ABA:BP (2:1)	a	0.893(14)	2.130(14)	3.0005(12)	164.7(13)
	b	1.02(2)	1.59(2)	2.6121(12)	179(2)

The 4ABA and BP molecules of other units pass through the gaps in the units, interlocking the structure (Figure 7.30). The 4ABA molecules passing through the gaps interact with the 4ABA molecules in the units via weak aromatic CH···O hydrogen bonds with the hydroxyl oxygen (C···O = 3.1878(14) Å) (Figure 7.31a). Further weak CH···O hydrogen bonds are formed by the aromatic CH groups of the BP molecules with the amide oxygen (C···O = 3.5338(15) Å) (also Figure 7.31a). BP molecules also interact with 4ABA molecules via a bifurcated DDHHA hydrogen bond to the carboxylic acid carbonyl oxygen (C···O = 3.4079(14) Å and 3.2651(14) Å) (Figure 7.31b). π···π stacking is also present between molecules passing through the gaps (Figure 7.32).

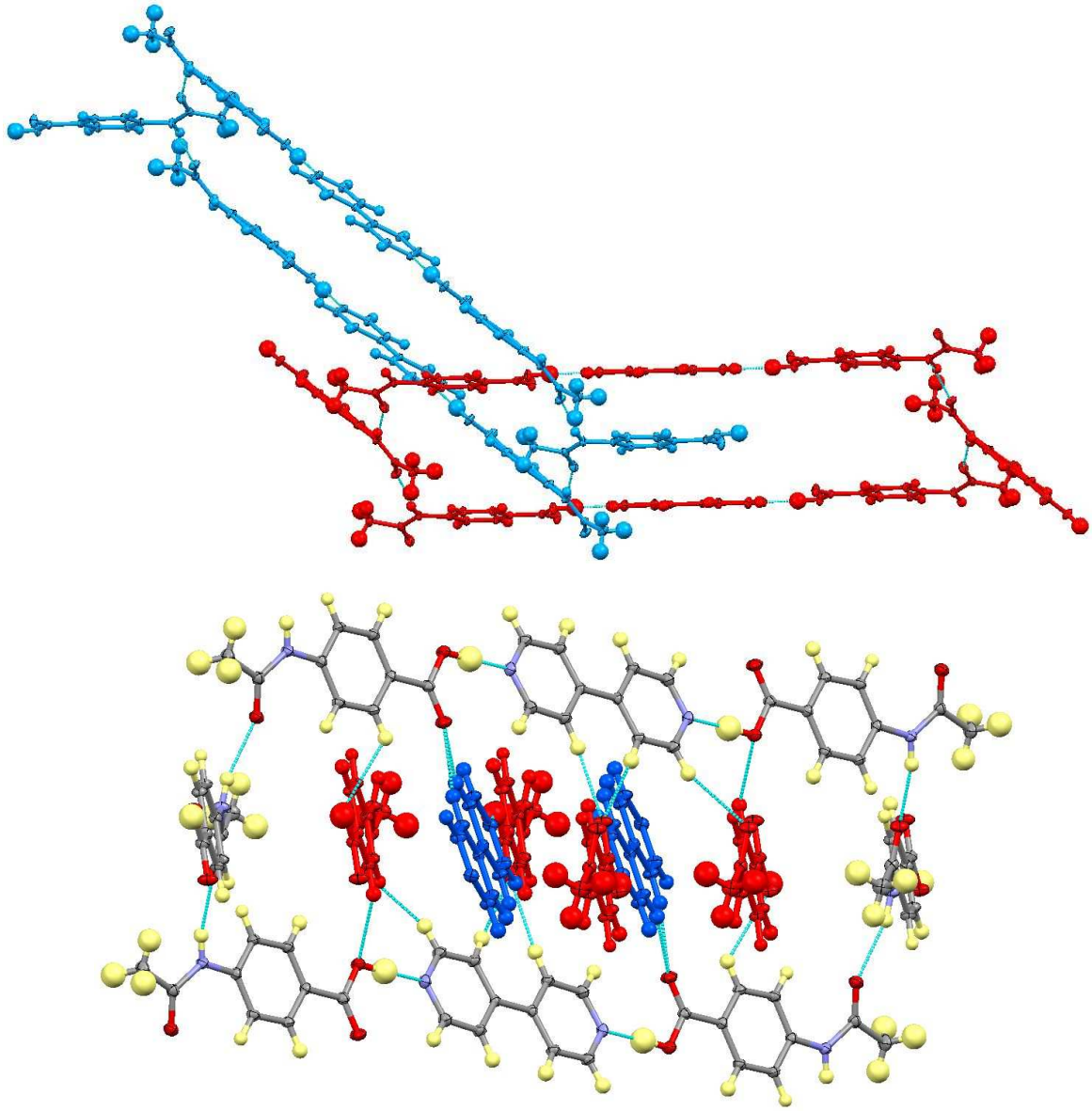

Figure 7.30 *Interpenetration of the primary hydrogen bonded units in the 4-acetamidobenzoic acid : 4,4-bipyridine complex. Two interpenetrating units with the different units coloured red and blue (top) and BP (blue) and 4ABA (red) molecules passing through the gaps in one of the hydrogen bonded units (bottom).*

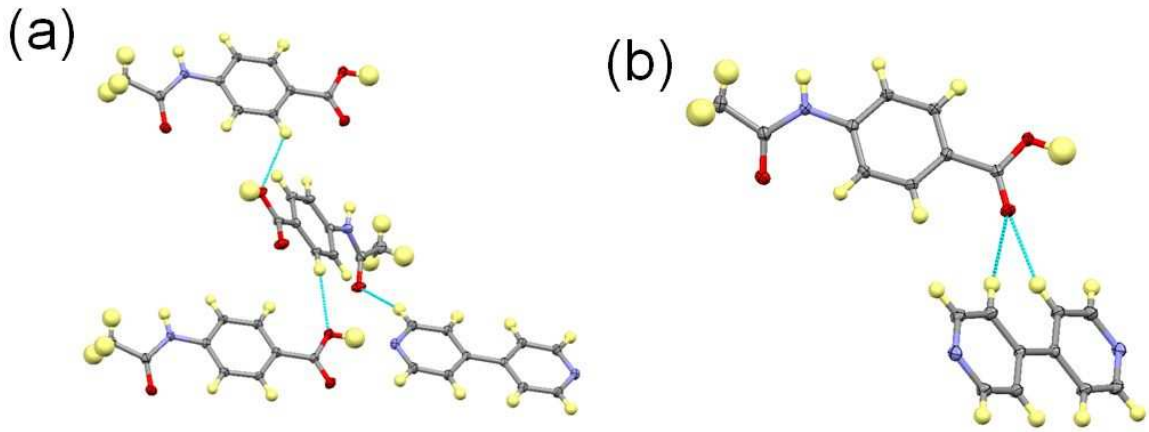

Figure 7.31 *Weak hydrogen bonding in the 4-acetamidobenzoic acid : 4,4-bipyridine complex. (a) Weak CH···O hydrogen bonds of 4ABA with other 4ABA molecules and BP molecules. (b) The weak bifurcated CH···O hydrogen bonding between 4ABA and BP molecules.*

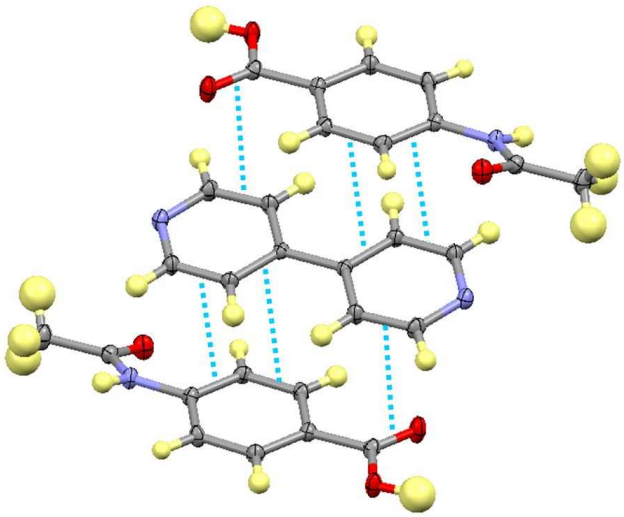

Figure 7.32 *π···π stacking between 4ABA and BP molecules in the 4-acetamidobenzoic acid : 4,4-bipyridine complex.*

7.4.6 4-Acetamidobenzoic acid : 2-picoline (4ABA:2PIC)

The 1:1 4-acetamidobenzoic acid : 2-picoline complex features one 4ABA and one 2PIC molecule in the asymmetric unit with no hydrogen transfer occurring. Chains of 4ABA are formed through moderately strong NH···O hydrogen bonds of the amide NH with the carbonyl oxygen atoms (a in Figure 7.33, see Table 7.9 for hydrogen bond lengths and angles). Stronger OH···N hydrogen bonds are then formed between the 4ABA carboxylic

OH and the 2PIC nitrogen (b in Figure 7.33). The O···N distance in this hydrogen bond is short and the O-H bond is lengthened significantly (Table 7.9). The 4ABA molecules in the chains are not co-planar (Figure 7.34a), instead lying alternately along two sets of parallel planes resulting in an interlocked structure (7.34b) with weak hydrogen bonds linking the chains.

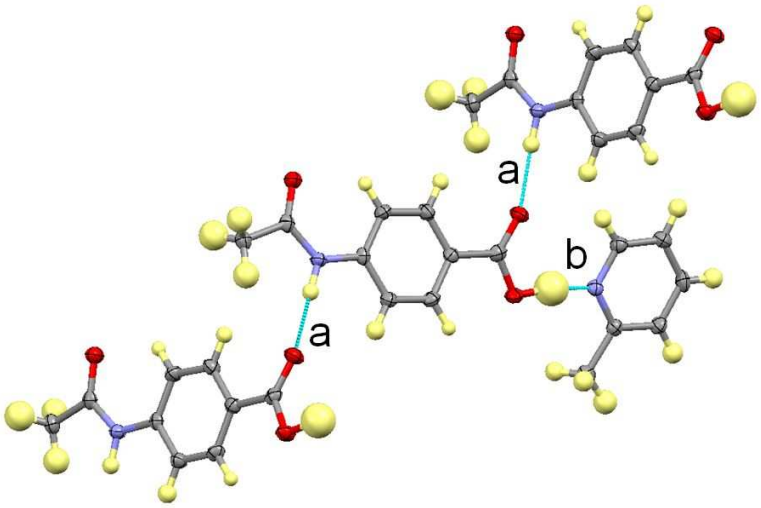

Figure 7.33 *Hydrogen bonding in the 4-acetamidobenzoic acid : 2-picoline complex showing moderately strong NH···O hydrogen bonds forming chains of 4ABA and the OH···N hydrogen bonds linking 2PIC molecules to the 4ABA molecules.*

Table 7.9 *Hydrogen bond lengths and angles in the 4-acetamidobenzoic acid : 2-picoline complex (refer to Figure 7.33 for key).*

Complex	H-Bond	D-H (Å)	H···A (Å)	D···A (Å)	∠D-H···A (°)
4ABA:2PIC	a	0.94(3)	1.99(3)	2.928(3)	172(2)
	b	1.18(4)	1.42(4)	2.587(3)	171(4)

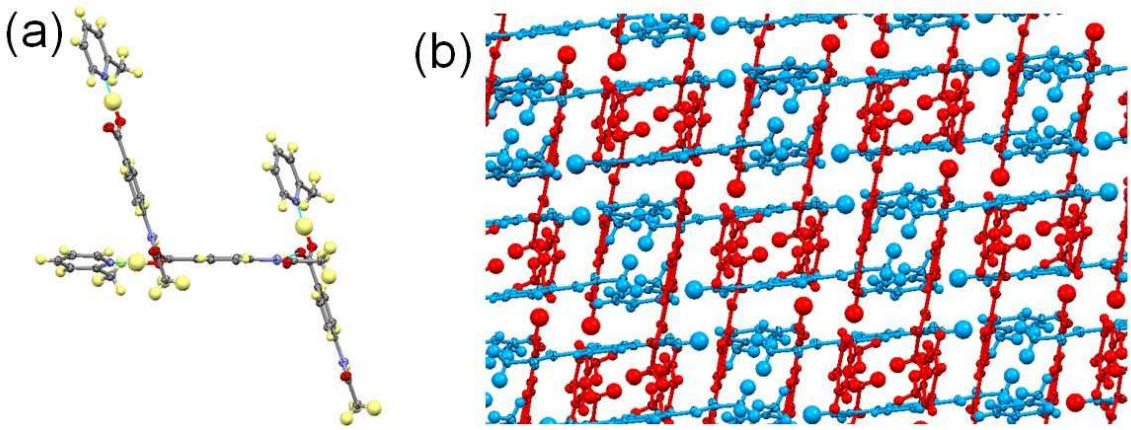

Figure 7.34 *Crystal packing in the 4-acetamidobenzoic acid : 2-picoline complex. (a) The relative arrangement of the 4ABA molecules (and the hydrogen bonded 2PIC molecules) in the chains showing the molecules running alternately in different directions. (b) The interlocked structure (molecules running in parallel planes are coloured accordingly).*

The 2PIC molecules link chains together through weak aromatic CH···O hydrogen bonds (C···O = 3.484(4) Å) to the 4ABA hydroxyl oxygen (Figure 7.35a) as well as weak CH···O hydrogen bonds (C···O = 3.518(4) Å and 3.510(5) Å) from the methyl CH to two 4ABA amide oxygen atoms (Figure 7.35b). A 4ABA methyl CH also forms a weak CH···π hydrogen bond (Figure 7.35c) with the aromatic ring of another 4ABA molecule (distance from methyl C to centroid of π bond = approximately 3.738 Å).

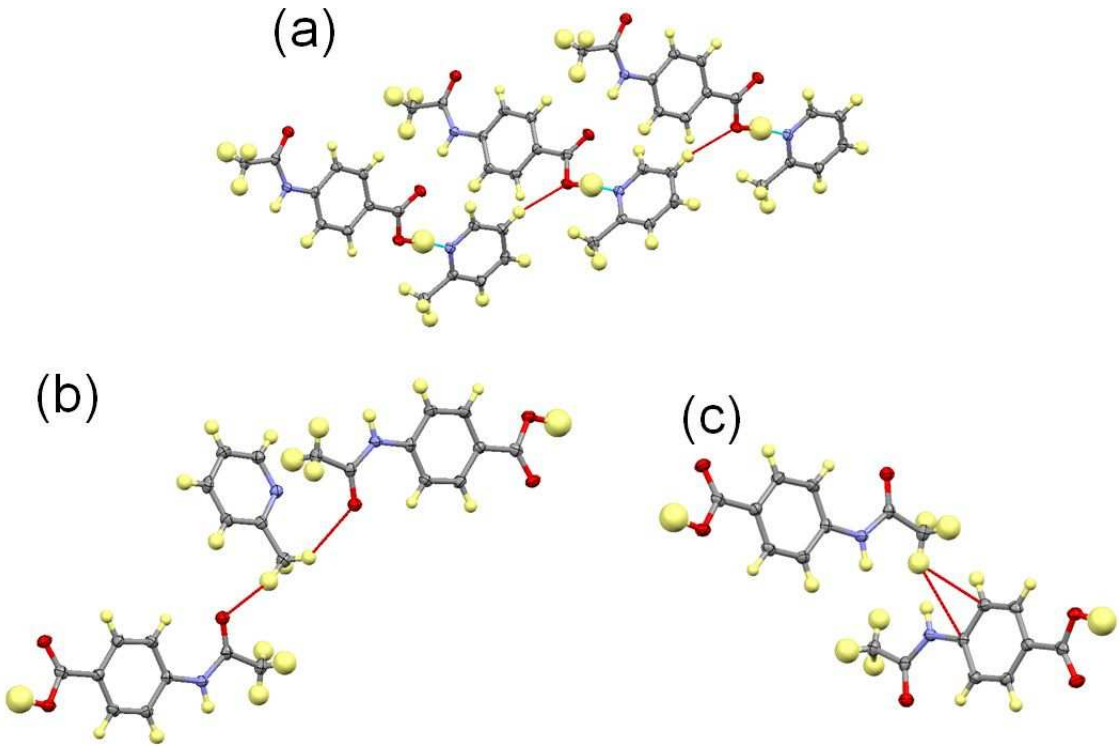

Figure 7.35 *Weak hydrogen bonds in the 4-acetamidobenzoic acid : 2-picoline complex (red dashed lines). (a) CH···O hydrogen between the 2PIC aromatic CH group and 4ABA hydroxyl oxygen. (b) CH···O hydrogen bonds between the 2PIC methyl CH groups and the 4ABA amide oxygen atoms. (c) Methyl CH···π hydrogen bonds between 4ABA molecules.*

7.4.7 4-Acetamidobenzoic acid : 3-picoline (4ABA:3PIC)

The 4-acetamidobenzoic acid : 3-picoline complex features one 4ABA and one 3PIC molecule in the asymmetric unit with no hydrogen transfer occurring. As in the 4ABA: 2PIC complex, the 3PIC molecule forms hydrogen bonds to the 4ABA carboxylic acid hydroxyl via an OH···N bond (Figure 7.36a). Chains of 4ABA are formed through moderately strong NH···O hydrogen bonds involving the NH and carbonyl of the amide groups (Figure 7.36a). The hydrogen bonding in these chains is slightly stronger than that seen in the NH···O hydrogen bonds between the amide NH and the carboxylic acid carbonyl in the 4ABA:2PIC complex (Table 7.10). The 4ABA molecules in the chains do not lie co-planar and are slightly staggered relative to each other (Figure 7.36b).

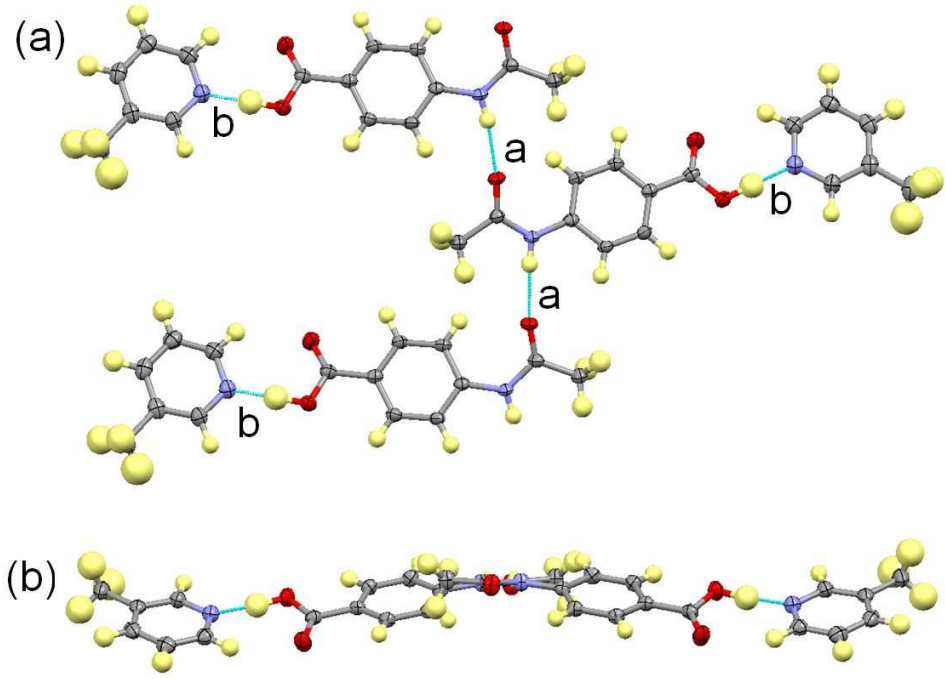

Figure 7.36 *The hydrogen bonded chains in the 4-acetamidobenzoic acid : 3-picoline complex. (a) Hydrogen bonding in the chains. (b) 90° rotation of (a) showing the slightly staggered arrangement of the 4ABA molecules relative to each other.*

Neighbouring chains are linked by weak CH···O hydrogen bonds between the aromatic CH groups of 3PIC with the 4ABA carboxylic acid hydroxyl oxygen (C···O = 3.190(2) Å, ∠DHA = 100.5(12) Å) as well as between the 3PIC methyl CH and the 4ABA carboxylic acid carbonyl oxygen (C···O = 3.527(3) Å) (Figure 7.37a). This creates non co-planar layers which are arranged in a wave-like fashion (Figure 7.37b). The interactions between these layers are weak with two types of methyl CH···O hydrogen bonding occurring between 4ABA molecules (Figure 7.38a). The first weak hydrogen bond occurs between the methyl group and the carboxylic acid hydroxyl oxygen with a C···O distance of 3.412(2) Å. The second hydrogen bond is slightly weaker with a C···O distance of 3.516(2) Å and involves the carboxylic acid carbonyl oxygen as the acceptor. Significant π···π interactions are also present between the aromatic rings of 4ABA and 3PIC molecules in different layers with distances of approximately 3.360 Å and 3.415 Å between the two sets of closest π bonds (Figure 7.38b).

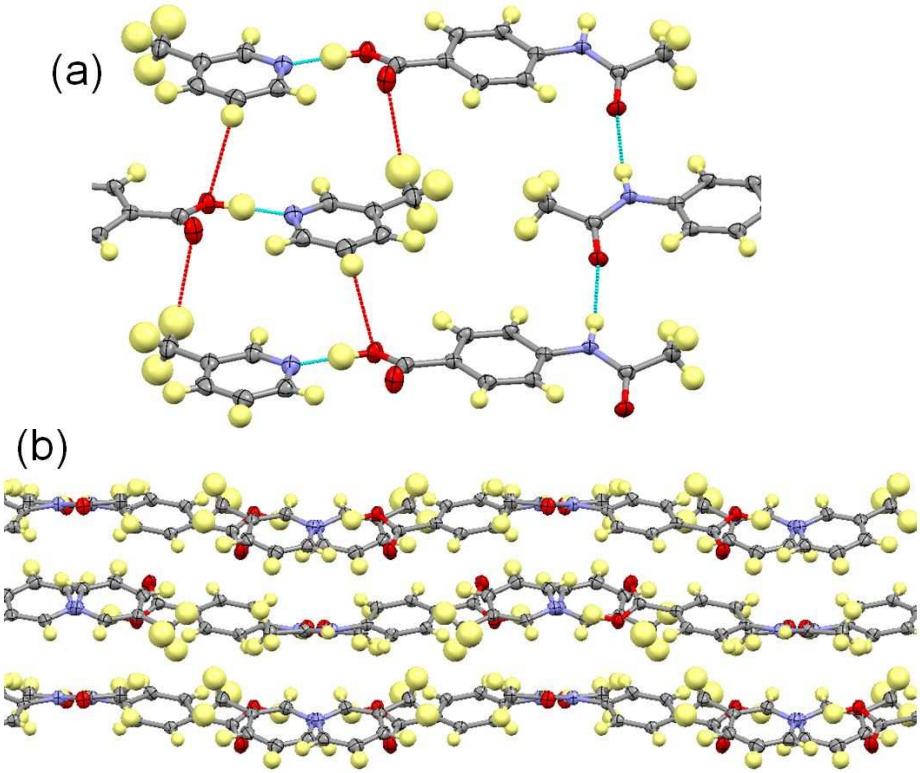

Figure 7.37 *The non-coplanar layers in the 4-acetamidobenzoic acid : 3-picoline complex. (a) The weak CH···O interactions (red dashed lines) holding chains together in layers. (b) The relative arrangement of three of the layers.*

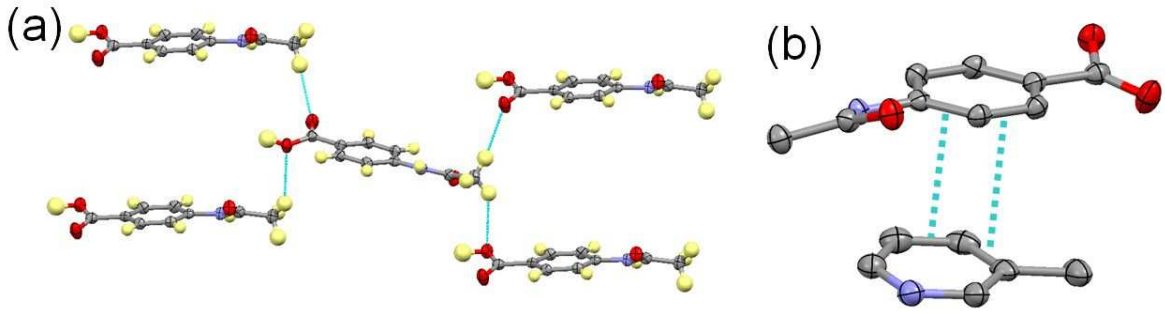

Figure 7.38 *The weak interactions between layers in the 4-acetamidobenzoic acid : 3-picoline complex. (a) The weak methyl CH hydrogen bonds with the carboxylic acid oxygen atoms. (b) π···π interactions between 4ABA and 3PIC molecules (H-atoms omitted for clarity).*

7.4.8 4-Acetamidobenzoic Acid : 4-picoline (4ABA:4PIC)

The 1:1 4-acetamidobenzoic acid : 4-picoline complex features one 4ABA and one 4PIC molecule in the asymmetric unit with no hydrogen transfer occurring**.** The structure-

directing hydrogen bonds in the complex are similar to those in the 4ABA:3PIC complex with NH···O interactions of the amide groups linking the 4ABA molecules into infinite chains and the carboxylic acid OH forming hydrogen bonds to the 4PIC nitrogen atom (Figure 7.39). Once again the O-H distance in this hydrogen bond is lengthened (Table 7.10). Both the hydrogen bonds in this complex, however, are slightly stronger than those in the 3PIC complex (Table 7.10). The relative orientation of alternate 4ABA molecules in the chains is significantly different from that found in the ABA:3PIC complex (Figure 7.40), with the planes of the benzene rings almost at right angles (approximately 87.40°) to each other, whereas the planes of alternate 4ABA molecules in the 4ABA:3PIC complex lie much closer to parallel (approximately 10.31° between the planes of the benzene rings).

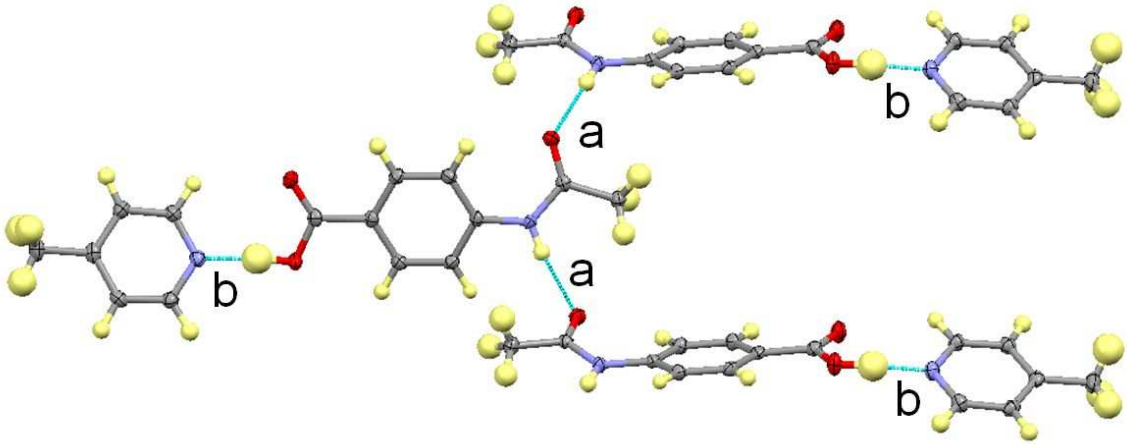

Figure 7.39 *The hydrogen bonded chains in the 4-acetamidobenzoic acid : 4-picoline complex.*

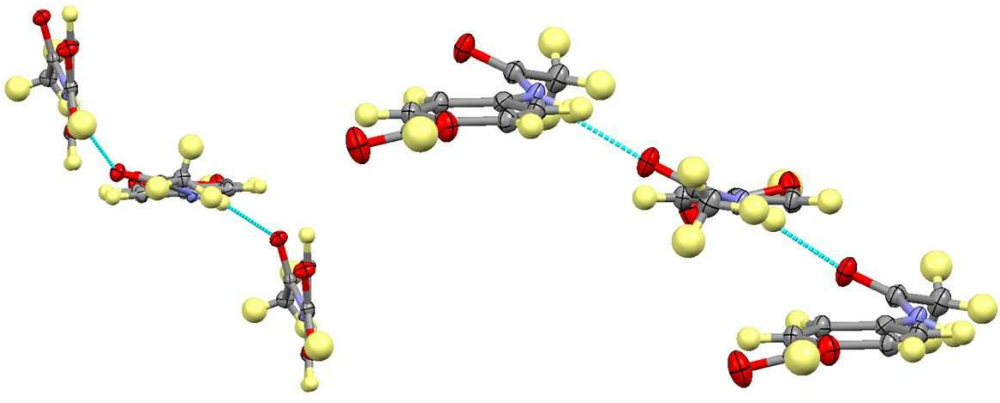

Figure 7.40 *Relative arrangement of 4ABA chains in the molecular complexes with 4-picoline (left) and 3-picoline (right) as viewed along the plane of the benzene ring.*

Table 7.10 *Hydrogen bond lengths and angles in the 4-acetamidobenzoic acid complexes with 3- and 4-picoline (refer to Figure 7.36 and Figure 7.39 for key). The corresponding values for the 4ABA:2PIC and 4ABA:BP complexes are also shown for comparison.*

Complex	H-Bond	D-H (Å)	H···A (Å)	D···A (Å)	∠D-H···A (°)
4ABA:4PIC	a	0.861(16)	2.036(16)	2.8696(16)	162.8(16)
	b	1.02(2)	1.58(2)	2.6067(14)	176.5(16)
4ABA:3PIC	a	0.88(2)	2.02(2)	2.8931(15)	168.3(15)
	b	1.06(2)	1.57(2)	2.627(2)	176(2)
4ABA:2PIC	a*	0.94(3)	1.99(3)	2.928(3)	172(2)
	b	1.18(4)	1.42(4)	2.587(3)	171(4)
4ABA:BP (2:1)	a	0.893(14)	2.130(14)	3.0005(12)	164.7(13)
	b	1.02(2)	1.59(2)	2.6121(12)	179(2)

Note: NH···O hydrogen bonds in the 4ABA:2PIC complex (marked a) involve the carboxylic carbonyl of 4ABA; values for hydrogen bond a in the other complexes refer to NH···O interactions with the amide carbonyl.*

The aromatic CH groups of 4ABA form hydrogen bonds to both the carbonyl oxygen of the amide group (C···O = 3.533(2) Å) and the carbonyl oxygen of the carboxylic acid group (C···O = 3.270(2) Å) (Figure 7.41). The CH forms hydrogen bonds with the carboxylic acid carbonyl oxygen, linking the 4ABA molecules in a herringbone arrangement (Figure 7.42), while the NH···O chains (in Figure 7.39) link these herringbone units into layers. The 4PIC molecules then intersect these layers (also Figure 7.42).

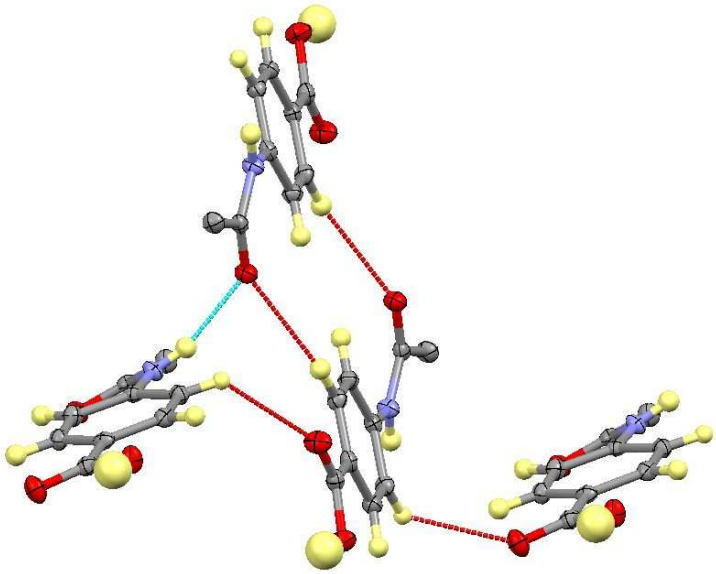

Figure 7.41 *Weak hydrogen bonds (red dashed lines) between 4ABA molecules in the 4-acetamidobenzoic acid : 4-picoline complex (methyl H-atoms omitted for clarity).*

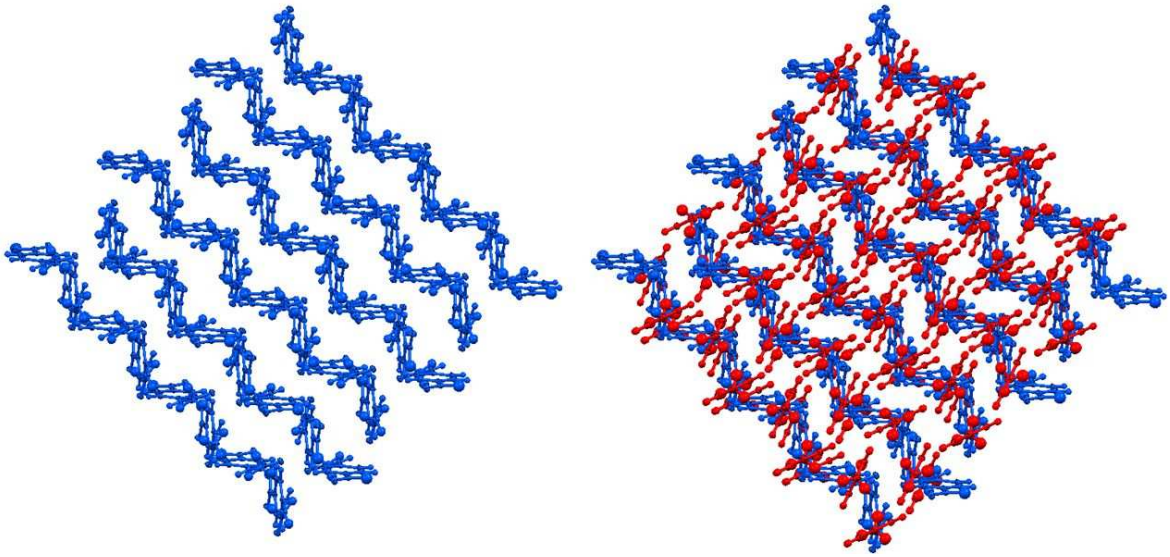

Figure 7.42 *Crystal packing in the 4-acetamidobenzoic acid : 4-picoline complex showing the herringbone arrangement of 4ABA molecules (blue, left) and the relative positions of the 4PIC molecules (red, right).*

Further weak interactions are present involving the 4PIC molecules (Figure 7.43). Weak CH···π hydrogen bonds are formed between an aromatic CH group of 4PIC and the 4ABA benzene ring (distance from C to centroid of π bond = approximately 3.542 Å). Another aromatic CH group forms a weak hydrogen bond to the carboxylic acid carbonyl oxygen of another 4ABA molecule (C···O = 3.226(2) Å). A 4ABA methyl group also forms another CH···π hydrogen bond to the 4PIC benzene ring (distance from C to centroid of π bond = approximately 3.588 Å).

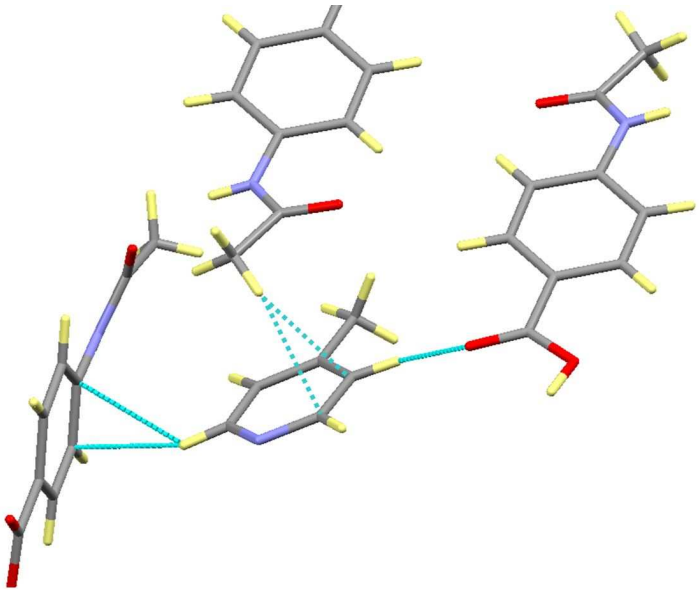

Figure 7.43 *Weak CH···π and CH···O hydrogen bonds involving the 4PIC molecule in the 4-acetamidobenzoic acid : 4-picoline complex.*

7.5 Discussion

In total three molecular complexes of paracetamol (PA) were synthesised in the co-crystallisation experiments. The co-formers used (imidazole (IM), 2-methylimidazole (2MIM) and 4-methylimidazole (4MIM)) were also successfully co-crystallised with 4-acetamidobenzoic acid (4ABA). 4ABA was also successfully co-crystallised with 4,4-bipyridine, for which a molecular complex with PA can be found in the CSD[227]. In addition, four other molecular complexes of 4ABA were synthesised; the co-formers used (benzimidazole (BZ), 2-picoline (2PIC), 3-picoline (3PIC) and 4-picoline (4PIC)) could not, however, be co-crystallised with PA under the conditions studied.

7.5.1 Supramolecular Synthons

Molecular Complexes of Paracetamol with Imidazole and Derivatives

Of the three complexes of PA with IMs, two exhibited very similar hydrogen bonding synthons. These were the PA:IM complex and the PA:2MIM complex (see Figure 7.4). Both complexes exhibit the same hydrogen bonding between PA molecules with the amide NH forming a hydrogen bond to the hydroxyl oxygen. The PA molecules also form hydrogen bonds to the IM and 2MIM molecules via the same interactions, with NH···O hydrogen bonds from the IM/2MIM to the PA amide carbonyl and OH···N hydrogen bonds from the PA OH to the IM/2MIM nitrogen. The major difference in the 2MIM complex is the presence of two 2MIM molecules separating the PA molecules, linked to each other through an NH···N hydrogen bond, resulting in the 1:2 (PA:2MIM) ratio of the complex. The PA:2MIM complex is unable to adopt an isostructural structure to that of PA:IM, as the IM CH in the 2-position forms significant CH···π interactions with a PA benzene ring (Figure 7.3) which is not possible with the bulkier methyl group in the 2-position. Rearrangement of the weak interactions alone is not sufficient to stabilise an equivalent structure in the 2MIM complex, as the hydrogen bonding involving PA molecules either side of the methyl group in the 2-position would presumably also be unfavourable in that case. The PA:IM complex has very little space either side of the 2-position of IM and could not accommodate a methyl group in this position (Figure 7.44). The 2MIM molecules in the PA:2MIM complex lie head to tail allowing sufficient space for the methyl groups (also Figure 7.44). The different arrangement results in the NH of one IM molecule forming a

hydrogen bond to the nitrogen of the second IM molecule, a weaker acceptor than the amide oxygen.

The PA:4MIM complex shares little in common with the other two complexes in terms of hydrogen bonding although it is the only complex to exhibit hydrogen bonding between the strongest donor and strongest acceptor, the OH···O hydrogen bond from the PA hydroxyl to a PA amide carbonyl oxygen. The only hydrogen bond to feature in all three complexes is the NH···O hydrogen bond from the IM NH to the same amide carbonyl oxygen (Figure 7.10). The amide group of PA in the PA:4MIM complex is twisted out of the plane of the benzene ring (Figure 7.9), which allows two hydrogen bonds to be formed to the carbonyl oxygen. No such twisting occurs in the other two complexes, preventing a second hydrogen bond being formed as the benzene ring sterically limits access to the position. Significant CH···π interactions also occur in all three complexes although they vary in nature from system to system.

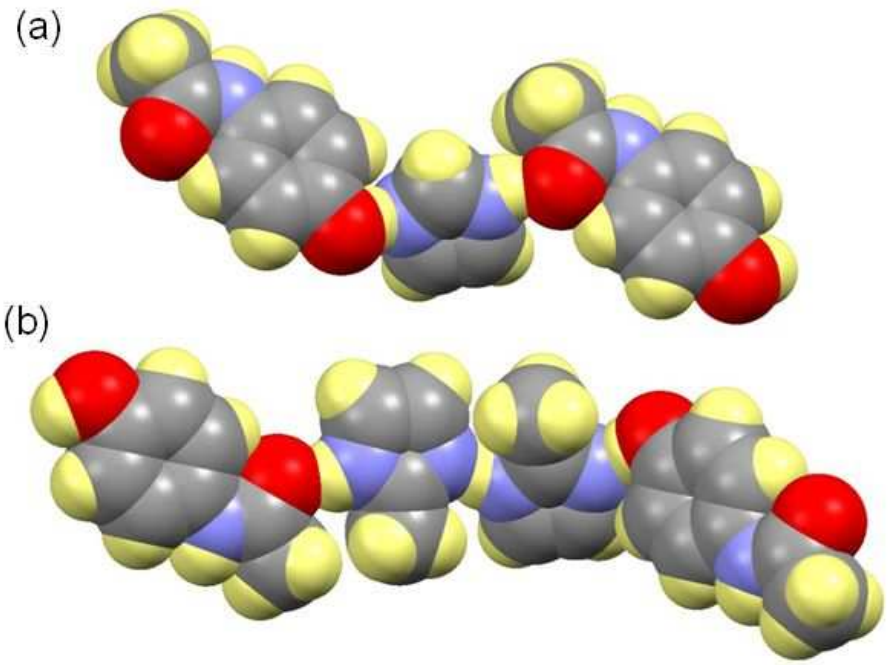

Figure 7.44 *Spacefill diagram showing the relative positions of the IM and 2MIM molecules in the (a) PA:IM and (b) PA:2MIM complexes. The 2-position of IM is too crowded to accommodate a bulky methyl group whereas the packing in the PA:2MIM complex allows sufficient space for the methyl groups.*

All four complexes of 4ABA with imidazole and its derivatives resulted in complexes with intermolecular hydrogen transfer between the carboxylic acid group of 4ABA and the basic nitrogen of the IM ring. The 4ABA:4ABA$^-$:2MIM$^+$ complex is a partial exception to this, having one 4ABA molecule neutral and the other deprotonated. In all cases a charge assisted hydrogen bond is formed between the NH of the imidazolium ring and a carboxylate oxygen. In the 4ABA$^-$:IM$^+$ complex this occurs between both symmetry independent pairs of 4ABA$^-$ and IM$^+$ molecules, while one IM$^+$ molecule also forms a second NH···O interaction of this kind through the other NH group. Two of these interactions are also formed in the 4ABA$^-$:4MIM$^+$ complex. The 4ABA$^-$:BZ$^+$.H_2O complex possesses the strongest of these hydrogen bonds (Table 7.11), as may be expected given BZ is the least basic co-former and therefore produces the strongest conjugate acid (pKa = 5.53). The Fourier difference map showing elongation of the hydrogen position in the hydrogen bond (Figure 7.24), as well as the long N-H bond which suggests sharing of the hydrogen atom, is also explained by the weak basicity of BZ. The next strongest of these hydrogen bonds occurs in the 4ABA$^-$:IM$^+$ complex; this is also expected as IM is the second weakest of the bases (pKa = 6.99). Both hydrogen bonds in the 4MIM complex are weaker than the hydrogen bond in the 2MIM complex, which is unexpected as 4MIM has a lower pKa than 2MIM (4MIM pKa = 7.5 c.f. 7.88 in 2MIM).

Table 7.11 *Hydrogen bond lengths and angles between the NH groups of the imidazolium rings and 4ABA carboxylate oxygen in the 4ABA complexes with IM, 2MIM, 4MIM and BZ.*

Complex	H-Bond	D-H (Å)	H···A (Å)	D···A (Å)	∠D-H···A (°)
4ABA$^-$:IM$^+$	a	0.97(3)	1.72(3)	2.686(2)	175(3)
	a’	0.99(3)	1.63(3)	2.617(2)	171(3)
	b	0.94(2)	1.74(2)	2.657(2)	164(2)
4ABA:4ABA$^-$: 2MIM$^+$	a	1.02(3)	1.61(3)	2.630(2)	169(3)
4ABA$^-$:4MIM$^+$	a	1.03(2)	1.68(2)	2.696(2)	171(2)
	b	0.98(2)	1.76(2)	2.687(2)	157(2)
4ABA$^-$:BZ$^+$.H_2O	a	1.21(4)	1.34(4)	2.544(3)	178(4)

In cases where the second NH group of the imidazolium ring does not also form a hydrogen bond to the carboxylate oxygen, hydrogen bonds are formed to carbonyl oxygen atoms of 4ABA/4ABA$^-$. In the 4ABA$^-$:IM$^+$ complex the second IM$^+$ molecule forms

a hydrogen bond with the amide carbonyl oxygen which is also the case in the $4ABA^-:BZ^+.H_2O$ complex. In the $4ABA:4ABA^-:2MIM^+$ complex, on the other hand, the second NH···O hydrogen bond is with the carboxylic acid carbonyl oxygen of the neutral 4ABA molecule.

The $2MIM^+$ and $4MIM^+$ complexes share the same hydrogen bonding between $4ABA^-$ molecules (Figures 7.17 and 7.20), with chains of $4ABA^-$ formed in both complexes through NH···O hydrogen bonding of the amide groups. The neutral 4ABA molecules in the 2MIM complex also form chains through this synthon. This synthon does not occur in the complexes with IM^+ or BZ^+. The amide NH of $4ABA^-$ molecules in the $4ABA^-:IM^+$ complex is hydrogen bonded to the carboxylate oxygen atom to form a similar type of chain. In the $4ABA^-:BZ^+.H_2O$ complex, the amide NH is hydrogen bonded to the water molecule which then in turn is hydrogen bonded to the carboxylate oxygen through an OH···O interaction.

The $4ABA:4ABA^-:2MIM^+$ complex is the only complex that does not crystallise in a 1:1 ratio, forming a complex with a 2:1 ratio with both neutral and deprotonated 4ABA molecules in the asymmetric unit (for completeness, this could also be termed a 1:1:1 complex if the neutral and deprotonated ABA molecules are regarded as distinct species). This ratio of components in the product complex is found despite being crystallised from a 1:1 molar ratio of the components. The presence of the neutral 4ABA molecule increases competition for hydrogen bonding to the carboxylate site of the deprotonated $4ABA^-$. With the OH···O hydrogen bond formed between 4ABA and $4ABA^-$ molecules, only one $2MIM^+$ molecule can form a hydrogen bond to the site resulting in the 2:1 ratio (Figure 7.17). In the $4ABA^-:4MIM$ complex, which shares the same amide NH···O hydrogen bonding between $4ABA^-$ molecules, two $4MIM^+$ molecules form hydrogen bonds to the carboxylate site, resulting in a 1:1 ratio of components in the product complex (Figure 7.20). The different position of the methyl in the $2MIM^+$ complex would prevent the formation of the same hydrogen bonding arrangement as found in the $4MIM^+$ complex.

Molecular Complexes of 4-Acetamidobenzoic Acid with Aprotic N-Heterocycles

Four complexes of 4ABA with aprotic nitrogen heterocycles (aNHCs) were synthesised, and no hydrogen transfer was found to occur in any of the complexes formed. In all four

complexes a common synthon is formed between the 4ABA and the aNHC, with the carboxylic acid OH forming a hydrogen bond to the nitrogen atom in all cases. In the case of the 4ABA:BP complex, this results in a 2:1 molar ratio as there are two acceptor nitrogen atoms present.

Three of the four complexes feature the same 4ABA chains seen in the $4ABA^-$ complexes with $2MIM^+$ and $4MIM^+$, formed through NH···O hydrogen bonds between the amide groups. The exception to this is the 4ABA:2PIC complex, where similar chains are formed but with the NH···O=C interaction involving the carboxylic acid carbonyl as the acceptor. This carbonyl oxygen forms only weak CH···O hydrogen bonds in the other three complexes.

Comparison of Molecular Complexes of Paracetamol and 4-Acetamidobenzoic acid with Imidazole and Derivatives

Comparing the synthons present in these structures is complicated by the fact that hydrogen transfer occurs in the 4ABA complexes which alters the hierarchy of the hydrogen bonding strengths of the donors and acceptors available. In spite of this, patterns do emerge. A common synthon is the NH···O hydrogen bond between the imidazole/imidazolium NH and the amide carbonyl of PA/4ABA. This occurs in all three PA complexes as well as the $4ABA^-$ complexes with IM^+ and BZ^+. The interactions of the $4ABA^-$ carboxylate and the PA carboxylic acid can also be considered interchangeable to a certain degree. With the exception of the PA:4MIM complex, the OH···N interaction between PA and the imidazole nitrogen is interchangeable with the charge assisted NH···O interaction between the imidazolium NH and the 4ABA carboxylate oxygen. The combination of these interactions results in a 1:1 complex in four of the five cases in which it occurs; the PA:2MIM complex is the exception, due to the steric affect of the methyl in the 2-position. The amide chains occurring in the 4ABA complexes with $2MIM^+$ and $4MIM^+$ are not seen in any of these PA complexes.

Comparison of Molecular Complexes of Paracetamol and 4-Acetamidobenzoic acid with Aprotic Nitrogen Heterocycles

Of the aNHCs successfully co-crystallised with 4ABA, only BP has also been co-crystallised with PA[227]. Three other complexes of PA with aNHCs can be found in the CSD, however, which are suitable for comparison to the 4ABA complexes reported here. These are the complexes with phenazine[17], N,N-dimethylpiperazine[227] and N-methylmorpholine[227]. The N-methylmorpholine molecule in the PA : N-methylmorpholine complex is disordered across an inversion centre, with the effective equivalence of the nitrogen and oxygen atom resulting in it being isostructural with the PA : N,N-dimethylpiperazine complex. The lack of hydrogen transfer in the 4ABA complexes here makes the comparison more relevant than in the complexes with imidazole and its derivatives.

As discussed above, the four complexes of 4ABA exhibit persistent patterns of hydrogen bonding with only one (4ABA:2PIC) showing slight variation. Analysis of the PA : N,N-dimethylpiperazine complex and the isostructural PA : N-methylmorpholine complex shows that these two complexes share comparable hydrogen bonding synthons to those found in the 4ABA complexes with BP, 3PIC and 4PIC (Figure 7.45). All feature chains of 4ABA or PA formed through NH···O hydrogen bonds of the amide groups. NH···O hydrogen bonds are also formed in both between the aNHC and either the carboxylic acid or hydroxyl OH group. As in the 4ABA complex with BP, the presence of two nitrogen atoms in the aNHC results in 2:1 PA:aNHC complexes being formed in both of these complexes.

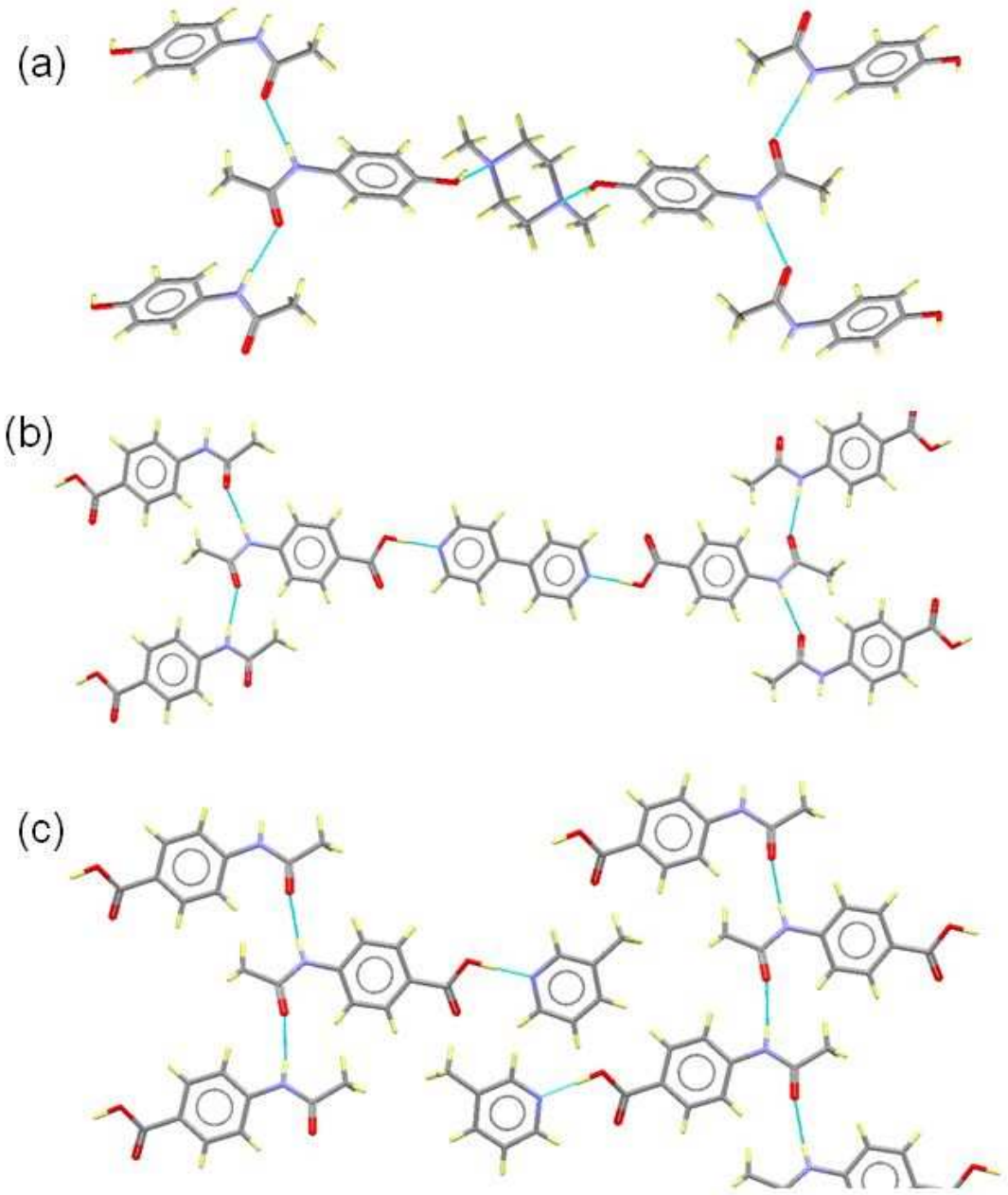

Figure 7.45 *Hydrogen bonding in (a) the PA : N,N-dimethylpiperazine complex[227], (b) the PA:BP complex[227] and (c) the 4ABA:4PIC complex. The PA : N,N-dimethylpiperazine complex is isostructural to the PA : N-methylmorpholine complex[227].*

Comparison of the 4ABA and PA complexes with BP shows very different hydrogen bonding arrangements (Figure 7.46). The PA complex features chains of PA formed through OH···O hydrogen bonds between the hydroxyl and the amide carbonyl, whereas the 4ABA complex features 4ABA chains formed through NH···O hydrogen bonding of the amide groups. BP molecules are hydrogen bonded to each PA molecule through NH···N interactions of the amide NH with the second BP nitrogen, forming only weak hydrogen bonds with the aromatic CH groups of PA. This results in a 1:1 ratio of the components in

the molecular complex as opposed to the 2:1 ratio found in the 4ABA complex due to the two OH···N interactions formed.

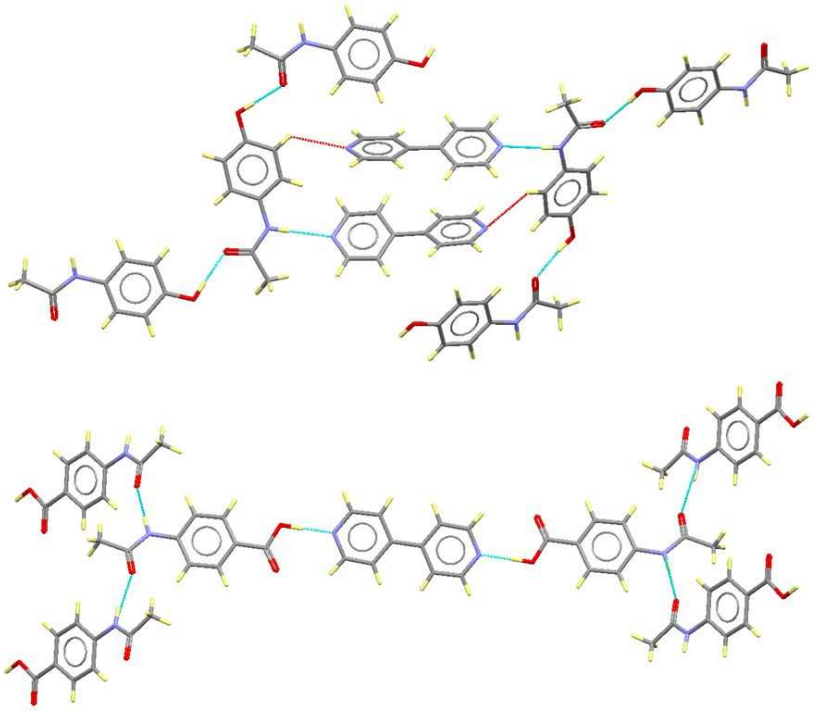

Figure 7.46 *The hydrogen bonding arrangement in the 1:1 PA:BP complex (top) and the 2:1 4ABA:BP complex (bottom). The conventional hydrogen bonds are shown as blue dashed lines with the CH···N hydrogen bonds between PA and BP shown as red dashed lines.*

The PA complex with phenazine (PHEN)[17] again shows a different hydrogen bonding arrangement to any of the 4ABA complexes or other PA complexes (Figure 7.47). The complex crystallises in a 1:2 ratio (PA:PHEN) with PA molecules forming both OH···N and NH···N hydrogen bonds to the PHEN nitrogen atoms, with further weak aromatic CH···N hydrogen bonds also present, along with aromatic CH···O hydrogen bonds to the amide oxygen of other PA molecules.

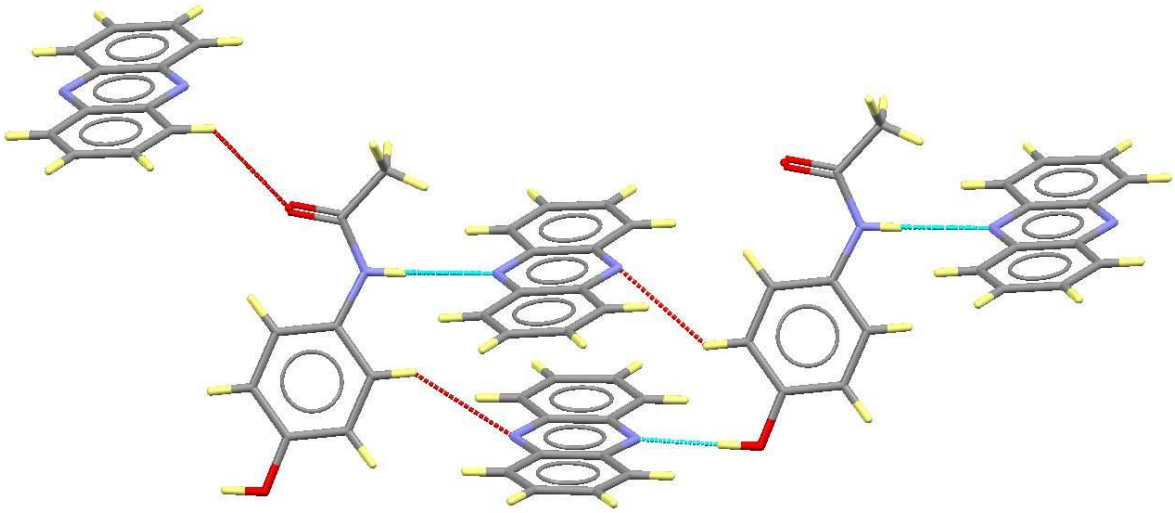

Figure 7.47 *Hydrogen bonding in the PA:PHEN complex[17]. Conventional OH···O and NH···N hydrogen bonds are shown as blues dashed lines, whilst weak CH···N and CH···O hydrogen bonds are shown as red dashed lines.*

7.5.2 Hydrogen Transfer and ΔpKa

No hydrogen transfer occurs in any of the PA complexes and this can be rationalised by consideration of the ΔpKa values for these complexes (Table 7.12). The hydroxyl group of PA is weakly acidic (pKa = 9.5) and as a result all ΔpKa values for the complexes are negative.

Hydrogen transfer behaviour in the majority of the 4ABA complexes can similarly be rationalised by application of the ΔpKa rule (also Table 7.12). Use of the co-formers with the highest ΔpKa values (IM, 2MIM and 4MIM) results in complexes exhibiting hydrogen transfer, whereas in the majority of complexes with weaker bases (2PIC, 3-PIC, 4PIC and BP) no hydrogen transfer occurs. The $4ABA^{-}:BZ^{+}.H_2O$ complex is anomalous as the ΔpKa value is below that of the PIC complexes yet hydrogen transfer appears to occur, as indicated by the bond distances in both the component $4ABA^{-}$ and BZ^{+} molecules; as discussed above, however, the hydrogen position determined from the single crystal X-ray diffraction data is poorly defined. This highlights the difficulty in predicting hydrogen transfer when the ΔpKa lies between 1 and 3.

The $4ABA:4ABA^{-}:2MIM^{+}$ complex may also be classed as an anomaly due to the presence of both neutral and deprotonated 4ABA molecules. In this case the ΔpKa is greater than 3 and so hydrogen transfer is expected. Complexes such as these highlight

one of the flaws in attempting to predict hydrogen transfer via the pKa rule, in this case the fact that it does not account for the 2:1 molar ratio in the complex.

The inability to obtain molecular complexes through the co-crystallisation of PA with BZ, 2PIC, 3PIC or 4PIC can also be partly rationalised by inspection of the ΔpKa values. The majority of co-formers for which large negative ΔpKa values are obtained using the PA acidity value (ΔpKa ≤ –3.50 - red in Table 7.12) could not be co-crystallised to form molecular complexes under the conditions studied. The PA : BP complex is the exception to this, with the poor basicity of BP and poor acidity of PA reflected in the ΔpKa value. This explains the lack of OH···N hydrogen bonds, with the low affinity causing the OH group to favour the much stronger amide acceptor of another PA molecule in this complex. In contrast, for 4ABA, all co-formers used yield ΔpKa values ≥ –1 and hence molecular complexes are formed successfully in these cases.

Table 7.12 *ΔpKa values for the molecular complexes of 4ABA and PA with NHCs, where ΔpKa = pKa[base] – pKa[acid]. pKa values for the NHC co-formers are quoted for the conjugate acid of the basic nitrogen. Complexes where hydrogen transfer occurs are highlighted in blue. Boxes highlighted in red indicate co-formers which did not co-crystallise with PA to form molecular complexes.*

Co-Former, pKa1	**ΔpKa PA (pKa = 9.50)**	**ΔpKa 4ABA (pKa = 4.27)**
2-Methylimidazole, 7.88	-1.62	3.61*
4-Methylimidazole, 7.55	-1.95	3.28
Imidazole, 6.99	-2.51	2.27
2-Picoline, 6.00	-3.50	1.73
4-Picoline, 5.99	-3.51	1.72
3-Picoline, 5.70	-3.80	1.43
Benzimidazole, 5.53	-3.97	1.26
4, 4 - Bipyridine, 3.27	-6.23	-1.00

** The 2:1 4-acetamidobenzoic acid : 2-methylimidazole complex features one deprotonated 4ABA⁻ and one neutral 4ABA.*

7.5.3 Scale Up of the Paracetamol : Imidazole Co-crystallisation for Continuous Crystallisation in an OBC

The inability to convert the evaporative process used for the co-crystallisation of this complex to a cooling crystallisation process meant that scale up for trials in the batch OBC was not possible. The different solubilities of the two components resulted in the PA crystallising out of solution with the majority of IM remaining in solution and not crystallising. This highlights the need to carry out extensive investigations of the solvent system and relative concentrations required to convert an evaporative process to a cooling process, as the conditions used in each process are not necessarily interchangeable. PXRD analysis (Appendix B7a) shows that the co-crystallisation from evaporation produced a mixture of the molecular complex and the two starting components. The difference in solubility between components of a molecular complex has also, of course, wider reaching implications when considering the potential use of even molecular complexes with favourable properties in industries such as pharmaceuticals; the inability to scale up efficiently in non-evaporative continuous crystallisation environments would make such materials non-viable. Following on from the preliminary investigations reported here, further studies are ongoing in this area within a larger collaborative project as part of the EPSRC National Centre in Continuous Crystallisation and Manufacturing[232]; these include the examination of other important variables such as the cooling rate, which was not controlled in the trials carried out, and/or seeding of the supersaturated solution.

7.5.4 Summary and Conclusions

All co-formers which formed molecular complexes with PA also formed molecular complexes with 4ABA although the reverse was not true as BZ, 2PIC, 3PIC or 4PIC could not be co-crystallised with PA to form molecular complexes under the conditions studied, yet all co-crystallised readily with 4ABA. The increased flexibility of 4ABA to form molecular complexes readily with weak bases such as BZ, 2PIC, 3PIC and 4PIC is likely due to the stronger hydrogen bond donating carboxylic acid present in 4ABA, as illustrated by the relatively large negative ΔpKa values between PA and these co-formers compared with the ΔpKa values for 4ABA and the same co-formers.

No hydrogen transfer occurred in any of the PA complexes, which is to be expected given the negative ΔpKa values for these complexes. The hydrogen transfer observed in the 4ABA complexes is relatively predictable based on ΔpKa values, with the exception of the $4ABA^-:BZ^+.H_2O$ complex.

The formation of PA complexes with IM and 2MIM resulted in structures with similar supramolecular synthons, despite a 1: 1 component ratio being formed in the complex with IM and a 1:2 (PA:2MIM) complex being formed in the complex with 2MIM. The PA:4MIM complex, on the other hand, resulted in a very different hydrogen bonding arrangement due to twisting of the PA molecule allowing two hydrogen bonds to be formed to the amide oxygen. The NH···O interaction of the imidazole ring with the amide oxygen is the only common synthon to be found in all three complexes. This synthon is also found in the $4ABA^-$ complexes with BZ^+ and IM^+ (in the latter case the synthon formation involves one symmetry independent IM^+ only). The synthon is not as persistent in the 4ABA complexes with imidazoles however, as the carboxylate group provides extra competition for hydrogen bond acceptors. NH···O hydrogen bonds to the carboxylate oxygens are found in all 4ABA complexes with imidazole derivatives, with both imidazolium NH groups forming hydrogen bonds to the carboxylate in some cases.

The 4ABA complexes with aNHCs, where no hydrogen transfer occurs, show reproducible supramolecular synthons in three of the four complexes produced; these comprise OH···N hydrogen bonds between the carboxylic acid OH and the aNHC nitrogen as well as chains of 4ABA formed through NH···O hydrogen bonding between amide groups. Analogous synthons are seen in the PA complexes with N,N-dimethylpiperazine[227] and N-methylmorpholine[227]. The presence of these synthons allows prediction of the relative ratio of the components based on the number of acceptors in the aNHC, as 2:1 PA/4ABA:aNHC complexes are formed when there are two acceptors sites for the OH···N hydrogen bond. These synthons are formed less reliably in the PA complexes, with completely different interactions formed between PA molecules and the aNHCs in the complexes with phenazine[17] and BP[227]. Although the 4ABA:2PIC complex deviates from the hydrogen bonding seen in the other three 4ABA:aNHC complexes, the OH···N hydrogen bond still persists and the only change is the acceptor group in the NH···O=C hydrogen bonds between 4ABA molecules. In this case the carboxylic acid carbonyl replaces the amide carbonyl as the hydrogen bond acceptor.

For the small subsets of materials studied, the ability to predict the hydrogen bonding arrangement in complexes of PA from analysis of complexes of 4ABA (or *vice*

versa) is found not to be reliable in complexes where hydrogen transfer occurs from the 4ABA to the imidazole co-former. Complexes of 4ABA where no hydrogen transfer occurs show more promise for comparison to PA complexes. There is possible potential to predict the ratio of components based on the number of acceptors in the aNHC. The completely different hydrogen bonding in the PA and 4ABA complexes with BP shows that prediction of both hydrogen bonding and molar ratios is still relatively unreliable.

The ability to predict which co-formers will readily co-crystallise to form molecular complexes with PA, based on those which co-crystallise with 4ABA, is also unreliable, although in the experiments carried out all co-formers that formed complexes with PA could also be co-crystallised with 4ABA, indicating that 4ABA is more predisposed to molecular complex formation with the small subsets of materials studied.

To investigate the potential for scaling up the co-crystallisation of paracetamol with imidazole into a continuous crystallisation environment, a thorough exploration of possible conditions is required to achieve a non-evaporative process in which the molecular complex is produced. Investigation of variables such as solvent, relative molar ratios of the components, cooling rates and seeding may lead to a viable process. Studies such as this may give clues to the potential of molecular complexes with favourable physical properties to be used in real world applications.

8. Additional Molecular Complexes of APIs

The co-crystallisation screening of APIs carried out in this study resulted in a number of other molecular complexes being synthesised. The molecular complexes of paracetamol (PA) with maleic acid (MA) and citraconic acid (CCA) were produced as part of the PA co-crystallisation screen with carboxylic acid containing co-molecules described in Chapter 4. The molecular complex of piracetam (PTM) with gallic acid (GA) is also discussed here. This complex is also mentioned in Chapter 4, as it often crystallised concomitantly with the porous phase of gallic acid monohydrate. Three other molecular complexes of PTM are also discussed. The discussion will focus mainly on the primary hydrogen bonding synthons observed in the complexes and comparison made to complexes with similar co-formers in the Cambridge Structural Database (CSD)[65].

8.1 Molecular Complexes of Paracetamol with Co-Formers Containing Multiple Carboxylic Acid groups

As discussed in Chapter 7, there is a marked variation in the types of co-formers found to co-crystallise with paracetamol in terms of the functional groups present and the synthons formed. Only two complexes of paracetamol (PA) with carboxylic acids are known, one of which is with the dicarboxylic acid, oxalic acid[17] and the other with the tricarboxylic acid, citric acid[233] (Scheme 8-1). No molecular complexes of paracetamol with monocarboxylic acids are known. As discussed in Chapter 4, monocarboxylic acids tend not to form molecular complexes with paracetamol and instead have been found often to direct the formation of paracetamol form II in co-crystallisation experiments. The preparation and crystal structures of two further molecular complexes of PA with dicarboxylic acids, maleic acid and citraconic acid (also Scheme 8-1), are described below. Full refinement details for all structures can be found in (Appendix A-8).

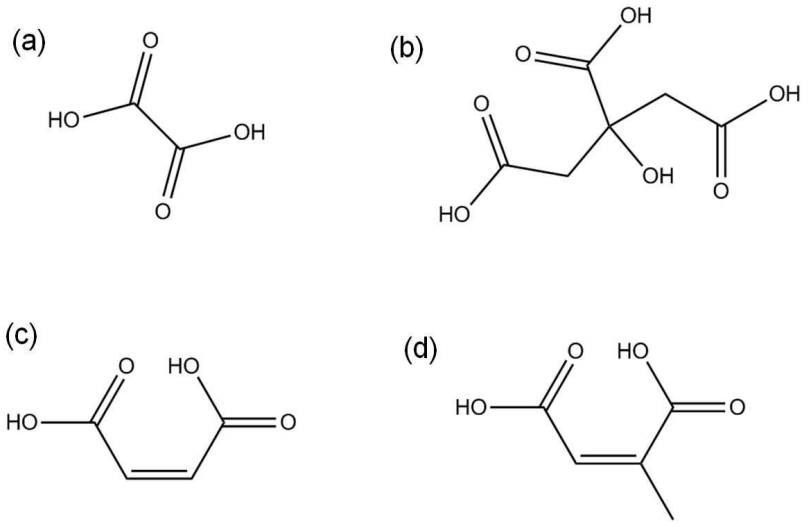

Scheme 8-1 *The structures of the co-molecules with multiple carboxylic acid groups that form molecular complexes with paracetamol. (a) oxalic acid; (b) citric acid; (c) maleic acid; (d) citraconic acid.*

8.2 Crystallisation Conditions

8.2.1 Paracetamol : Maleic Acid

The paracetamol maleic acid molecular complex could be crystallised using the general co-crystallisation procedure outlined in Chapter 3, from methanol, ethanol, isopropanol or acetonitrile at room temperature.

8.2.1.1 Paracetamol : Maleic Acid Molecular Complex: Scale up for Continuous Crystallisation in an Oscillatory Baffled Crystalliser

The PA : MA molecular complex was considered a good candidate for scale up to cooling crystallisation in the COBC as MA is a pharmaceutically acceptable co-former and maleate salts are commonly used in the pharmaceutical industry[234].

To facilitate co-crystallisation in a COBC, a similar screen of cooling conditions to that carried out for the PA:IM complex was used (see Chapter 7). Attempts were made to convert the evaporation co-crystallisation method employed in producing the complex to a cooling crystallisation method. 1:1 molar ratio solutions of various degrees of supersaturation were therefore generated through heating and the solutions cooled to

either 4°C or ambient temperature to induce crystallisation. The samples were left to cool to the relevant temperature with no control exercised over the cooling rate. This mainly resulted in crystallisation of the less soluble PA, with the majority of MA remaining in solution and no molecular complex being formed. The relative molar ratios were varied to 1:2 (PA:MA) in an attempt to promote molecular complex formation. However, this was also unsuccessful. The solvents originally used were ethanol, IPA and acetone, chosen for their relatively low toxicity. Due to the failure to yield the molecular complex from cooling co-crystallisation, anti-solvent addition was also investigated using IPA as the solvent and one of hexane, diisopropyl ether or ethyl acetate as the anti-solvent. This, however, also failed to yield the PA:MA molecular complex.

8.2.3 Paracetamol : Citraconic Acid

The paracetamol : citraconic acid molecular complex was crystallised from methanol at room temperature, using the general co-crystallisation procedure outlined in Chapter 3.

8.3 Crystal Structures of Multi-Component Complexes of Paracetamol and Dicarboxylic Acids

8.3.1 Paracetamol : Maleic Acid (PA:MA)

The asymmetric unit of the PA:MA complex consists of two PA molecules and two MA molecules. The structure comprises infinite chains of alternating PA and MA molecules held together by OH···O hydrogen bonds (Figure 8.1). The moderately strong OH···O hydrogen bonds are formed between the PA hydroxyl and an MA carbonyl (a and a' in Figure 8.1) and a stronger OH···O hydrogen bond is formed between an MA hydroxyl and the PA carbonyl (b and b' in Figure 8.1). A short, strong intramolecular OH···O hydrogen bond is also formed in the MA molecule (d and d' in Figure 8.1). Neighbouring symmetry independent chains are linked into two-chain ribbons via NH···O hydrogen bonds between the PA and the oxygen atom of the maleic acid hydroxyl which is involved in the intramolecular hydrogen bond (c and c' in Figure 8.1). Hydrogen bond distances and angles are shown in Table 8.1. The methyl groups of the PA molecules also form weak

hydrogen bonds to neighbouring MA oxygen atoms in the same chain (C···O = 3.1759(14) Å, and 3.1743(14) Å) as well as significantly weaker hydrogen bonds to MA oxygen atoms in the neighbouring chain (C···O = 3.496(2) Å and 3.501(2) Å) (red dashed lines in Figure 8.1).

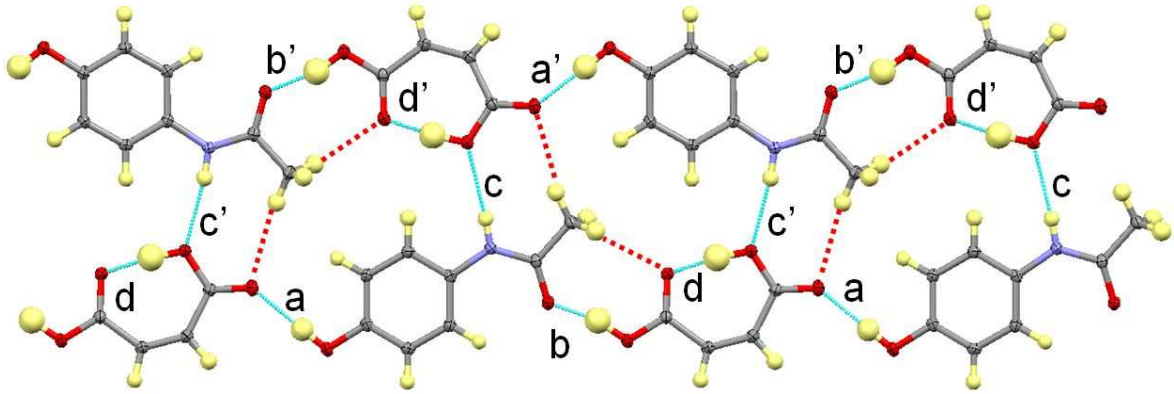

Figure 8.1 *Hydrogen bonded chains in the paracetamol : maleic acid molecular complex. Conventional hydrogen bonds are shown as blue dashed lines whereas weak CH···O hydrogen bonds involving the PA methyl group are shown as red dashed lines.*

Table 8.1 *Hydrogen bond lengths and angles in the paracetamol : maleic acid and paracetamol : citraconic acid complexes (refer to Figure 8.1 for key).*

Complex	H-Bond	D-H (Å)	H···A (Å)	D···A (Å)	∠D-H···A (°)
PA:MA	a	0.90(2)	1.86(2)	2.7623(12)	176.7(14)
	a'	0.90(2)	1.82(2)	2.7222(12)	178(2)
	b	1.02(2)	1.50(2)	2.5089(11)	165(2)
	b'	0.97(2)	1.58(2)	2.5327(11)	167(2)
	c	0.86(2)	2.26(2)	3.1210(13)	176.2(13)
	c'	0.88(2)	2.177(15)	3.0500(13)	173.1(14)
	d	1.00(2)	1.49(2)	2.4851(11)	173(2)
	d'	1.02(2)	1.47(2)	2.4772(11)	173(2)
PA:CCA	a	0.87(3)	1.89(3)	2.757(3)	172(3)
	b	1.06(3)	1.57(3)	2.534(3)	149(3)
	c	0.89(2)	2.20(2)	3.073(4)	170(2)
	d	0.93(3)	1.54(3)	2.466(3)	173(3)

The hydrogen bonded ribbons are linked into sheets by weak bifurcated CH···O hydrogen bonds (C···O = 3.2011(15) Å and 3.2138(15) Å) involving the CH groups of one of the MA molecules and the PA hydroxyl oxygen atom (Figure 8.2). The hydroxyl oxygen of this MA molecule is also linked to the neighbouring ribbon through a weaker CH···O hydrogen

bond with the CH group of the symmetry independent MA molecule (C···O = 3.4710(14) Å).

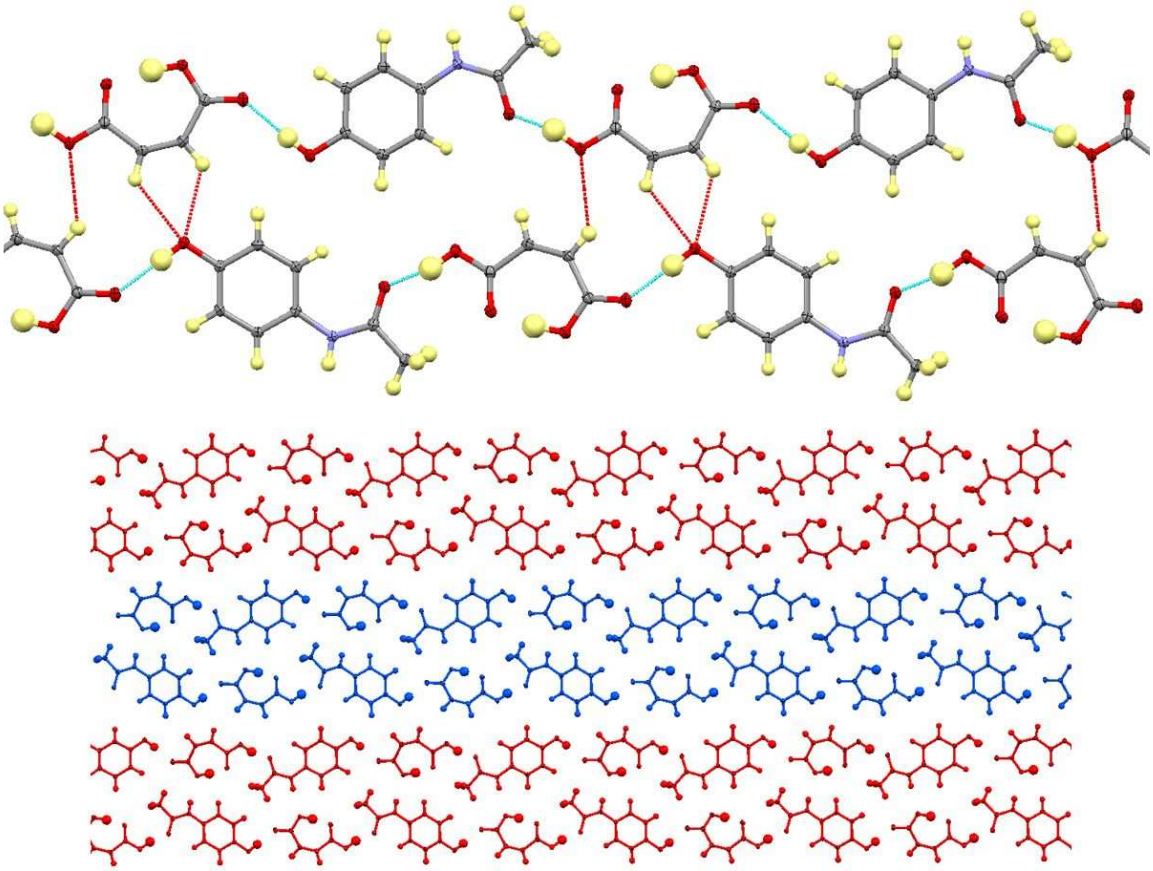

Figure 8.2 *The weak CH···O hydrogen bonds between ribbons (red-dashed lines) in the PA:MA complex (top) and the sheets formed by these ribbons (bottom, alternate ribbons coloured red and blue).*

The sheets are stacked upon each other to form a layered structure (Figure 8.3a). Layers are linked by π···π interactions between the PA aromatic rings and the MA double bonds with approximately 3.375 Å and 3.430 Å between the planes of the aromatic rings and the centroids of the MA double bonds (Figure 8.3b). The layers are further linked via weak hydrogen bonds between the methyl groups of PA with the carboxylic acid oxygen atoms of MA (C···O = 3.4684(14) Å and 3.7561(14) Å), as well as with the nitrogen atom of another PA molecule (C···N = 3.5450(15) Å) (Figure 8.3c).

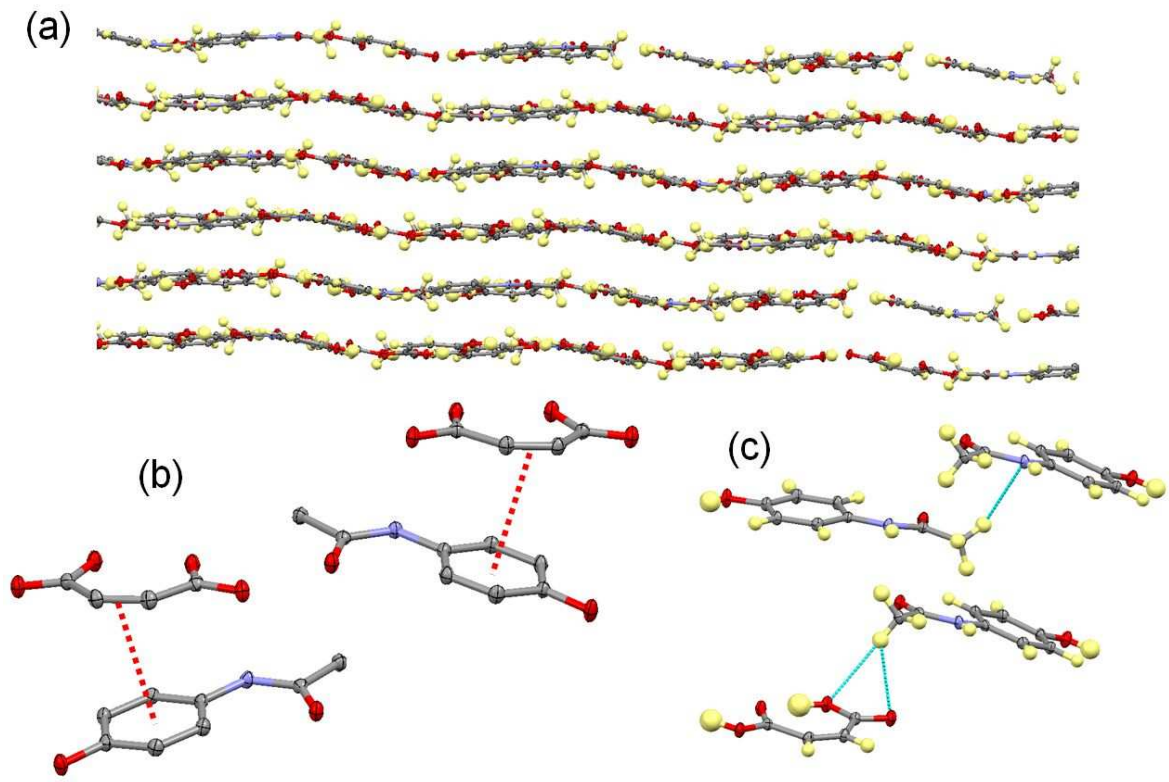

Figure 8.3 *Packing in the PA:MA complex. (a) The layered arrangement of the sheets; (b) π···π interactions between layers; (c) weak hydrogen bonds between layers involving the methyl groups.*

8.3.2 Paracetamol : Citraconic Acid (PA:CCA)

The PA:CCA complex features the same hydrogen bonded ribbons as the PA:MA complex (Figure 8.4), with similar hydrogen bond strengths (Table 8.1). The asymmetric unit in PA:CCA contains only one occurrence of each molecule as opposed to two formula units in the PA:MA complex. The ribbons are again arranged into sheets, although neighbouring ribbons are displaced relative to each other due to the presence of the methyl group; interactions between ribbons are therefore significantly different (Figure 8.4b). The bifurcated CH···O hydrogen bonds between the MA CH groups and the PA hydroxyl oxygen are no longer present. Instead, an aromatic CH group of another PA molecule forms a hydrogen bond to this PA hydroxyl oxygen (C···O = (3.414(4) Å) (Figure 8.4b). The CCA CH group then forms hydrogen bonds to the hydroxyl oxygen of another MA molecule (C···O = 3.567(3) Å).

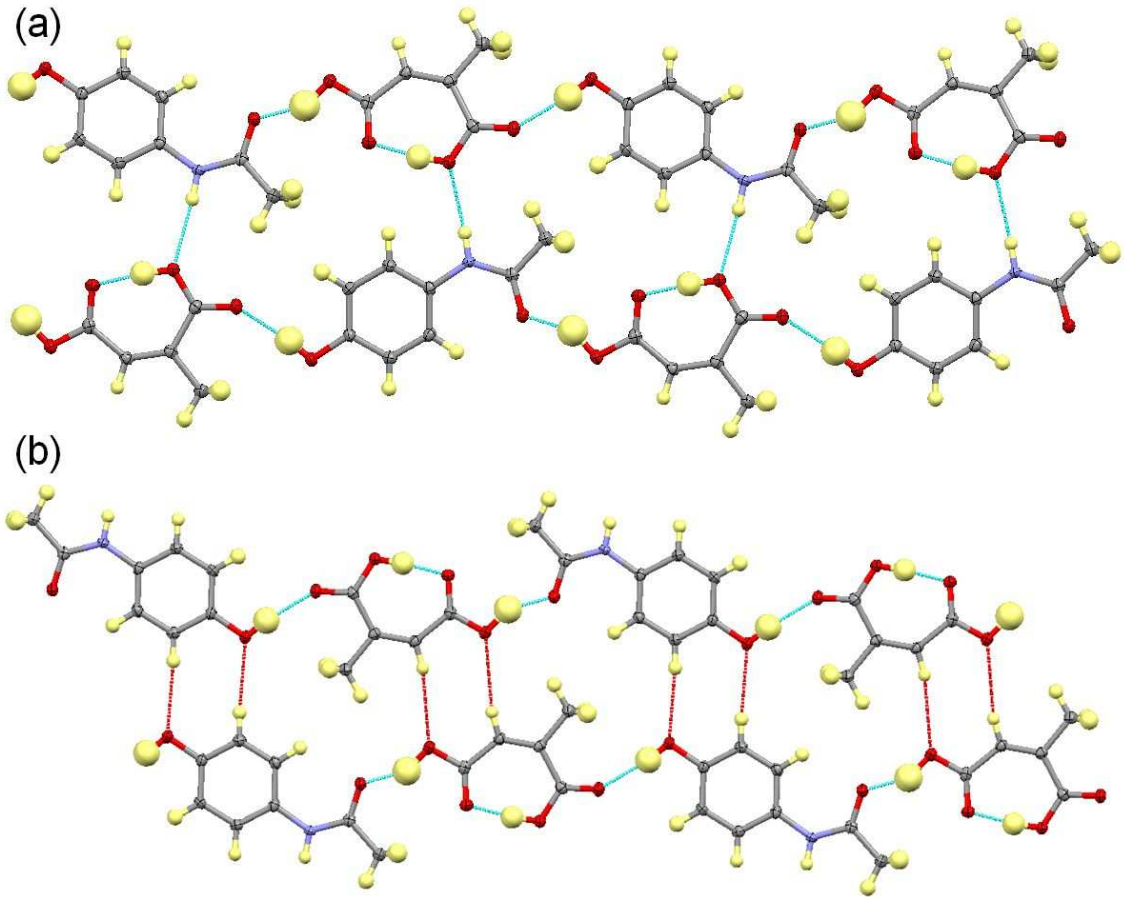

Figure 8.4 *(a) The two-chain hydrogen bonded ribbons in the PA:CCA complex; (b) the weak CH···O hydrogen bonds linking ribbons.*

The sheets have a layered arrangement (Figure 8.5a), with π···π interactions linking layers between the PA aromatic ring and the carbonyl double bonds of the MA molecules (Figure 8.5b). The π···π interactions have distances of approximately 3.413 Å and 3.446 Å between the centroid of the carbonyl and the closest bond in the aromatic ring.

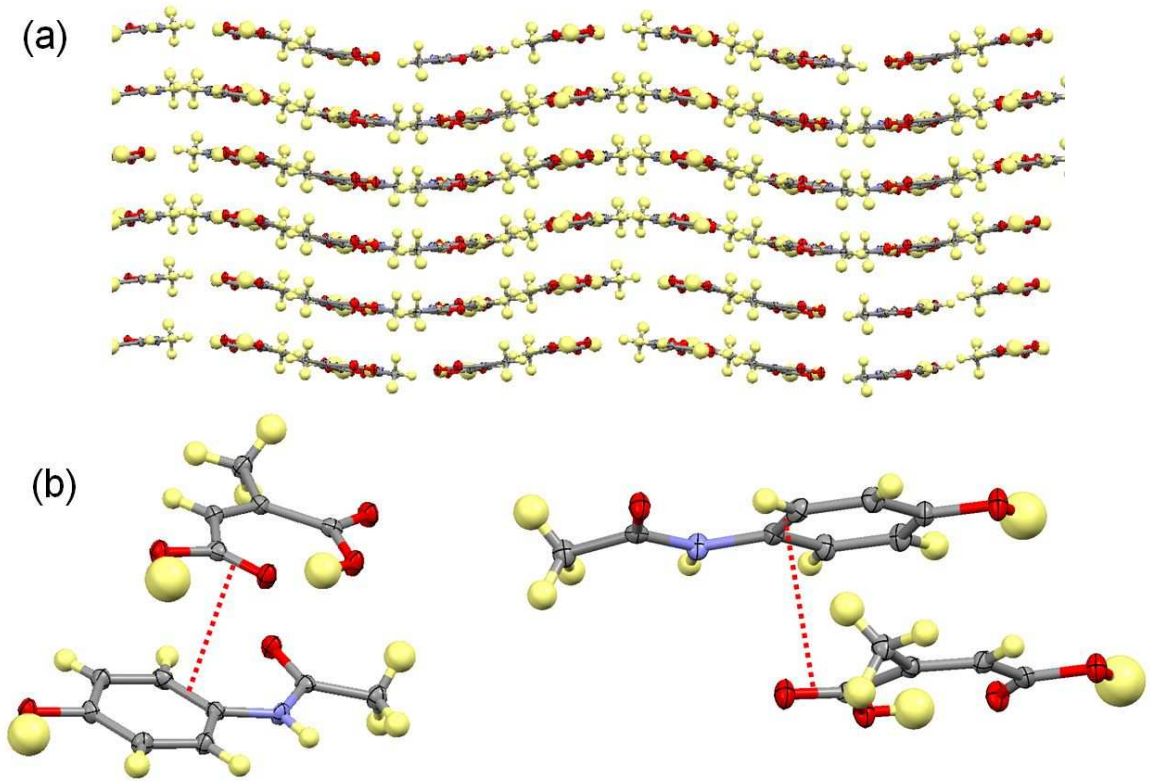

Figure 8.5 *Crystal packing in the PA:CCA complex. (a) The layered arrangement of the sheets; (b) the π···π interactions between PA and CCA molecules.*

8.4 Discussion of Paracetamol Molecular Complexes

8.4.1 Supramolecular Synthons in Paracetamol Molecular Complexes with Co-formers Comprising Multiple Carboxylic Acid Groups

The molecular complexes of PA with MA and CCA have identical primary hydrogen bonding motifs. Both form infinite hydrogen bonded chains of alternating PA and MA/CCA molecules linked by OH···O hydrogen bonds and NH···O hydrogen bonds linking two layers into ribbons. The structures differ in the extended packing due to the presence of the methyl group in the CCA complex preventing the formation of the bifurcated CH···O hydrogen bonds between the MA CH groups and the PA hydroxyl. Both complexes feature a layered packing arrangement.

The hydrogen bonding in the PA complexes with MA and CCA is difficult to compare to that in the oxalic acid[17] and citric acid[233] complexes, as the intramolecular

hydrogen bond in MA/CCA makes one hydroxyl hydrogen unavailable for hydrogen bonding. The citric acid (CTA) complex forms a 2:1 (PA:CTA) complex and two of the CTA carboxylic acid groups dimerise while the other forms an OH···O hydrogen bond to the hydroxyl oxygen of another CTA molecule (Figure 8.6a). This means the only strong interactions between PA and CTA are OH···O hydrogen bonds involving the PA hydroxyl with a carboxylic acid carbonyl on the CTA and the CTA hydroxyl with the PA hydroxyl oxygen (Figure 8.6b). The remaining hydrogen bonding sites in PA form hydrogen bonds with other PA molecules. The PA hydroxyl OH interaction with the CTA carboxylic acid carbonyl is present in the MA/CCA complexes (shown in Figure 8.6d) but other than this the structures have very different hydrogen bonding due to homomeric interactions dominating in the PA:CTA complex.

The PA : oxalic acid (OA) complex shares more similarities with the MA/CCA complexes. Just as in the MA/CCA complexes, the PA hydroxyl forms hydrogen bonds to the OA carboxylic acid carbonyl and the OA hydroxyl forms hydrogen bonds to the PA carbonyl oxygen (Figure 8.6c). The PA NH also forms hydrogen bonds to a carboxylic acid carbonyl in all three complexes. The lack of an intramolecular hydrogen bond in OA results in some differences however, as the hydroxyl hydrogen is free to form a hydrogen bond to the PA hydroxyl oxygen. This replaces the weak CH···O hydrogen bonding involving the PA hydroxyl oxygen that occurs in the MA/CCA complexes. Nevertheless all three structures consist of infinite chains of alternating PA and MA/CCA/OA molecules which are arranged into layered sheets.

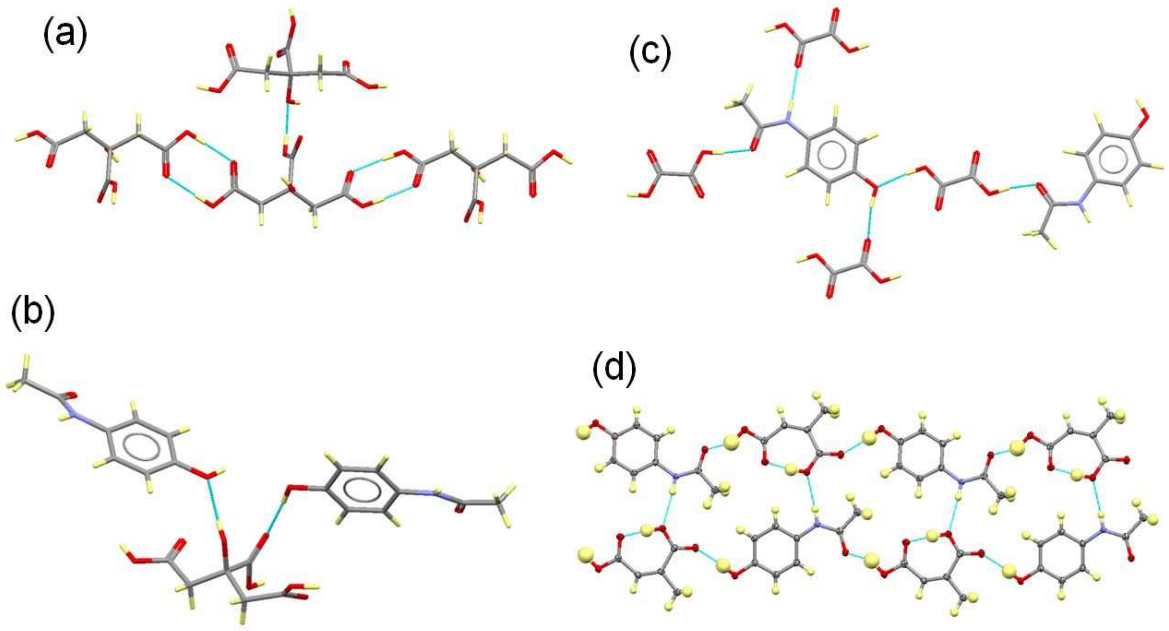

Figure 8.6 *Hydrogen bonding in the paracetamol molecular complexes with carboxylic acids. (a) Carboxylic acid dimers in the PA : citric acid complex*[233]*; (b) hydrogen bonding between PA molecules and the citric acid molecule in the PA : citric acid complex; (c) hydrogen bonding between PA and oxalic acid molecules in the PA : oxalic acid complex*[17]*; (d) hydrogen bonding in the PA:CCA complex.*

8.4.2 Scale up of the Paracetamol : Maleic Acid Molecular Complex

The failure to convert the PA:MA co-crystallisation from an evaporation process to a cooling process once again shows the difficulty in transferring these systems and suggests a more careful consideration of the solvent used and component solubilities is required. The PA:MA complex represents an ideal candidate for scale up due to the pharmaceutically acceptable co-former used. The crystal structure of this complex is also layered with possible slip layers, which suggests investigation of its compaction properties for tabletting. As discussed in Chapter 4, this is seen as one of the main advantages that would be provided by using PA II instead of PA I as the marketed form and the use of a pharmaceutically acceptable molecular complex such as that reported here may provide a viable alternative without the stability issues of PA II. Tests on the physical properties of this molecular complex have yet to be carried out.

8.4.3 Conclusions

In total, four molecular complexes of paracetamol with co-formers containing multiple carboxylic acid groups have been synthesised; two were produced as part of this study and two were previously known[17, 233]. One complex was formed with the tricarboxylic acid, citric acid, and three with dicarboxylic acids: maleic acid, citraconic acid and oxalic acid. Formation of complexes with the three dicarboxylic acids all resulted in similar hydrogen bonding motifs. The MA and CCA complexes show identical arrangement of the primary hydrogen bonds with the added methyl group of CCA causing differences in the extended packing. The PA:OA complex features one major difference in its hydrogen bonding arrangement, which is the OH···O hydrogen bond formed to the PA hydroxyl, made possible as neither hydroxyl of OA is involved in an intramolecular hydrogen bond as is the case in the MA/CCA complexes. The extra carboxylic acid group and hydroxyl group of citric acid contributes to a very different hydrogen bonding arrangement as well as a 2:1 stoichiometric ratio.

There are no known molecular complexes of PA with monocarboxylic acids and this study suggests potential for further PA molecular complexes with co-formers containing multiple carboxylic acid groups. This work also suggests that dicarboxylic acids in particular may be of interest due to the relatively consistent hydrogen bonding motifs observed. The layered arrangement of all three PA : dicarboxylic acid complexes also suggests there may be scope for investigating the compaction properties of these complexes - the pharmaceutically acceptable complex with maleic acid being of particular interest in this respect. Attempts to convert the evaporation crystallisation process employed in the synthesis of the latter complex to a cooling or anti-solvent process viable for scale-up have so far been unsuccessful. Further work is required to find a suitable solvent system and greater consideration of solubility is required, possibly by utilising ternary phase diagrams.

8.5 Molecular Complexes of Piracetam

As discussed in Chapter 4, the co-crystallisation of the nootropic API piracetam (PTM) with gallic acid (GA) resulted in the crystallisation of a porous form of gallic acid monohydrate (PGAM), mostly concomitantly with a molecular complex of PTM:GA.

Analysis of the CSD shows that PTM has only been found to form molecular complexes with five different co-formers[40, 92], all of which contain carboxylic acid groups. This section will discuss the primary hydrogen bonding synthons in the PTM:GA complex, with comparison to the known molecular complexes of PTM and another new molecular complex, formed with the dicarboxylic acid citraconic acid (CCA). In particular, the occurrence of the amide-carboxylic acid $R^2_2(8)$ heterodimer is investigated in the PTM : carboxylic acid complexes. A previous study[92] found this synthon to be unreliable in predicting the hydrogen bond motifs in PTM complexes. Two other new PTM complexes with chloranilic acid (CA) and bromanilic acid (BRA) are also described and discussed in terms of the primary hydrogen bonding motifs observed. The occurrence of an $R^2_2(9)$ heterodimer with chloranilic/bromanilic acid (Scheme 8-2) is investigated, as this is analogous to the amide-carboxylic acid heterodimer in terms of hydrogen bond donors/acceptors. Full refinement details for all structures presented in this section can be found in (Appendix A-8).

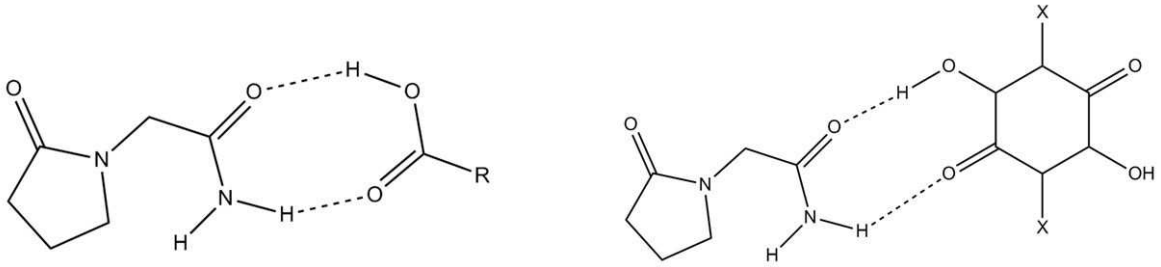

Scheme 8-2 *The piracetam-carboxylic acid $R^2_2(8)$ dimer (LHS) and the analogous $R^2_2(9)$ dimer formed by piracetam with chloranilic or bromanilic acid (RHS, X = Br or Cl).*

8.6 Crystallisation Conditions

Piracetam : Gallic Acid

As described in Chapter 7, the PTM: GA molecular complex was obtained in powder form from evaporation crystallisation experiments using methanol or ethanol (concomitant with PGAM) and single crystals could be obtained from ethyl acetate with a single drop of water from a pipette.

Other Complexes

Table 8.2 below summarises the crystallisation conditions under which single crystals of the remaining three complexes discussed in this section were isolated. All co-crystallisations were carried out at room temperature following the general evaporation procedure outlined in Chapter 3.

Table 8.2 *Crystallisation conditions for the synthesis of molecular complexes of PTM with citraconic acid, chloranilic acid and bromanilic acid.*

Complex	Molar Ratio (in solution)	Solvent
PTM:CCA	1:1	Acetone
PTM:CA	1:1	Acetonitrile
PTM:BRA	1:1	Acetone

8.7 Crystal Structures of Multi-Component Complexes of Piracetam

8.7.1 Piracetam : Gallic Acid (PTM:GA)

The PTM:GA complex contains one molecule of each component in the asymmetric unit. The PTM and GA molecules dimerise, although the dimer is not of the amide-carboxylic acid type as might have been expected. Instead, the dimer is formed through the amide group forming hydrogen bonds with the neighbouring hydroxyl groups in the 3- and 4-positions, with one OH group acting as a hydrogen bond donor to the amide carbonyl and the oxygen of the other as an acceptor for the amide NH group. This forms a hydrogen bonded $R^2_2(9)$ ring (a and b in Figure 8.7). Both hydrogen bonds in the dimer are moderately strong (see Table 8.3). The second amide NH also forms a moderately strong NH···O hydrogen bond with the GA hydroxyl in the 5-position (c in Figure 8.7). This hydroxyl group also forms an OH···O hydrogen bond to the carboxylic acid carbonyl of another GA molecule (e in Figure 8.7). The GA molecules form two moderately strong OH···O hydrogen bonds to the pyrrolidone carbonyl of PTM through the hydroxyl in the 3-position and the carboxylic acid hydroxyl (d and f in Figure 8.7).

Molecules in the structure are stacked in two directions (Figure 8.8a), with weak interactions holding the stacks together (Figure 8.8b). The molecules are stacked in pairs

of PTM molecules followed by pairs of GA molecules. PTM molecules in the stacks are linked by weak CH···O hydrogen bonds between the CH groups in the pyrrolidone rings and the amide oxygen atoms (C···O = 3.224(4) Å). An acetamide CH group of PTM forms CH···π interactions with the aromatic ring of GA (approx. 3.345 Å between the carbon and the plane of the ring). The aromatic rings of GA molecules are then stacked upon each other via π···π interactions (approx. 3.386 Å between the plane of the rings).

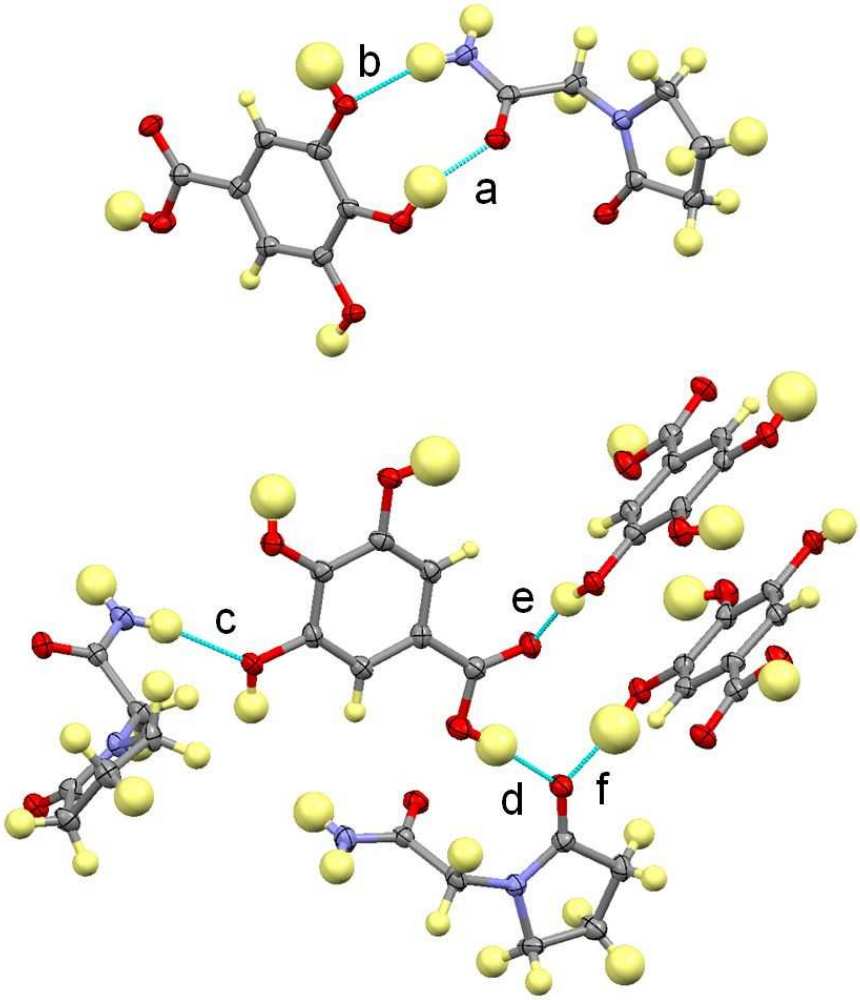

Figure 8.7 *The heterodimer formed by PTM and GA molecules in the PTM:GA complex (top) and the remaining NH···O and OH···O hydrogen bonds that occur between PTM and GA molecules (bottom).*

Table 8.3 *Hydrogen bond lengths and angles in the piracetam : gallic acid complex (refer to Figure 8.7 for key).*

Complex	H-Bond	D-H (Å)	H···A (Å)	D···A (Å)	∠D-H···A (°)
PTM:GA	A	0.95(5)	1.84(5)	2.726(4)	156(5)
	b	0.91(5)	2.07(5)	2.954(4)	164(4)
	c	0.96(4)	2.01(4)	2.950(4)	167(4)
	d	0.94(5)	1.72(5)	2.662(3)	173(3)
	e	0.99(4)	1.73(4)	2.707(3)	167(3)
	f	0.99(5)	1.69(5)	2.675(3)	170(5)

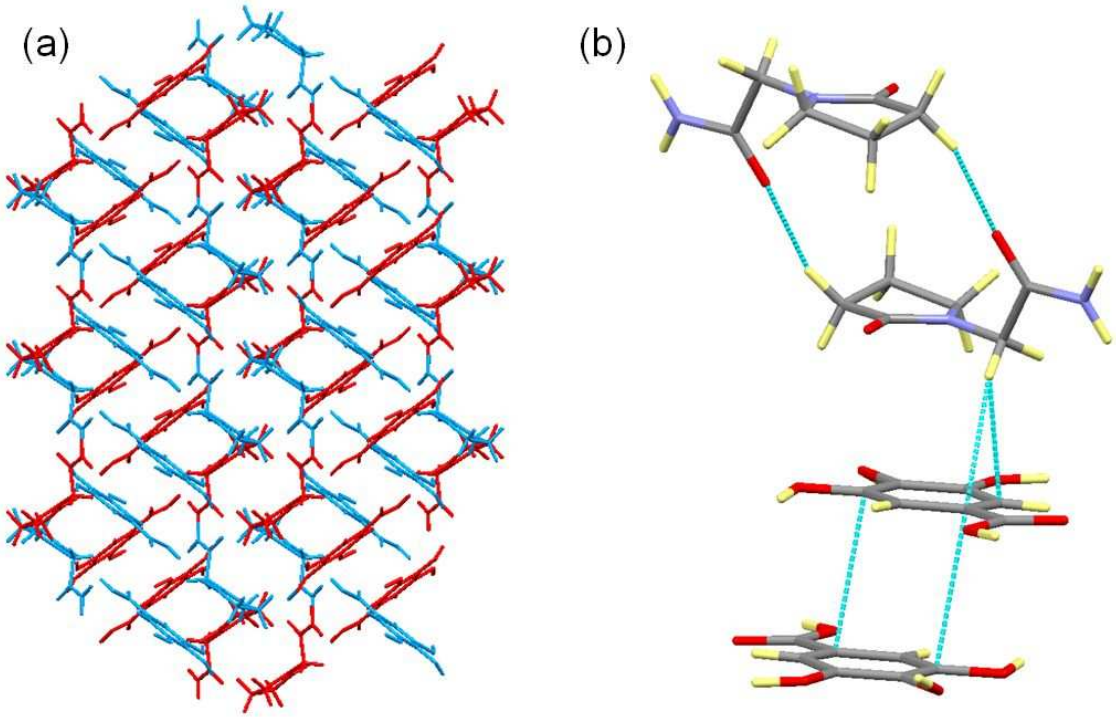

Figure 8.8 *Crystal packing in the PTM:GA complex. (a) The molecules arranged in stacks running in two directions (the different parallel stacks are coloured red and blue); (b) the interactions between stacked molecules.*

8.7.2 Piracetam : Citraconic Acid (PTM:CCA)

The PTM:CCA complex features one occurrence of each molecule in the asymmetric unit. PTM molecules in the complex form homodimers through the amide groups and CCA molecules also form carboxylic acid homodimers (a and b in Figure 8.9). Both the NH···O hydrogen bonds in the amide dimers and the OH···O hydrogen bonds in the carboxylic acids group are moderately strong (Table 8.4). Another moderately strong NH···O

hydrogen bond links the PTM amide group to the GA carboxylic acid carbonyl (c in Figure 8.9). The dimers are further linked by a moderately strong OH···O hydrogen bond involving the second carboxylic acid hydroxyl of CCA and the pyrrolidone carbonyl oxygen (d in Figure 8.9). This links the molecules into infinite hydrogen bonded chains of alternating homodimers.

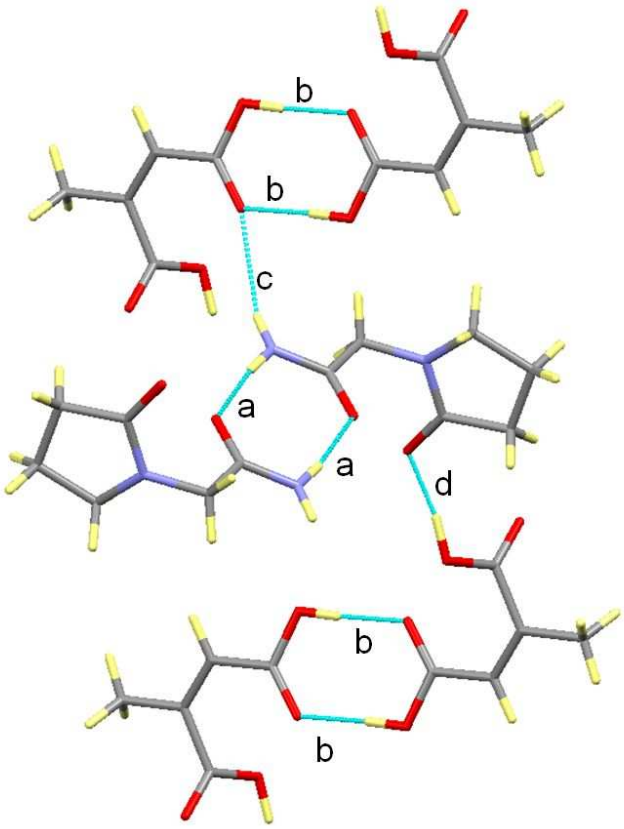

Figure 8.9 *The homodimers in the PTM:CCA complex, linked into chains by OH···O and NH···O hydrogen bonds between PTM and CCA molecules.*

Table 8.4 *Hydrogen bond lengths and angles in the piracetam : citraconic acid complex (refer to Figure 8.9 for key).*

Complex	H-Bond	D-H (Å)	H···A (Å)	D···A (Å)	∠D-H···A (°)
PTM:CCA	a	0.894(15)	2.029(15)	2.9160(13)	171.6(13)
	b	0.922(15)	1.727(16)	2.6486(12)	176.9(16)
	c	0.883(14)	2.349(14)	3.1108(12)	144.6(12)
	d	0.94(2)	1.63(2)	2.5564(11)	169.5(15)

The PTM molecules and the CCA molecules are arranged in linear three molecule units, with the PTM amide groups pointing outwards (Figure 8.10a). The PTM amide groups interrupt these three molecule units, forming the homodimers described above (also Figure 8.10a). This forms a layered structure, with the amide groups bridging between layers (Figure 8.10b). The CCA carboxylic acid dimers lie along the plane of these layers. The pyrrolidone CH groups form weak hydrogen bonds between layers to both the carboxylic acid carbonyl oxygen of CCA (C···O = 3.3542(14) Å) and the pyrrolidone carbonyl of another PTM molecule (C···O = 3.5276(14) Å) (Figure 8.11a). The layers are further linked by weak hydrogen bonds involving the CCA CH groups. The methyl CH group of CCA forms a weak CH···O hydrogen bond to the carboxylic acid hydroxyl oxygen of the CCA molecule in the next layer (C···O = 3.3406(15) Å) (Figure 8.11b). The CH group of CCA also forms a weak CH···O hydrogen bond to the bridging amide carbonyl (C···O = 3.3826(13) Å) (also Figure 8.11b).

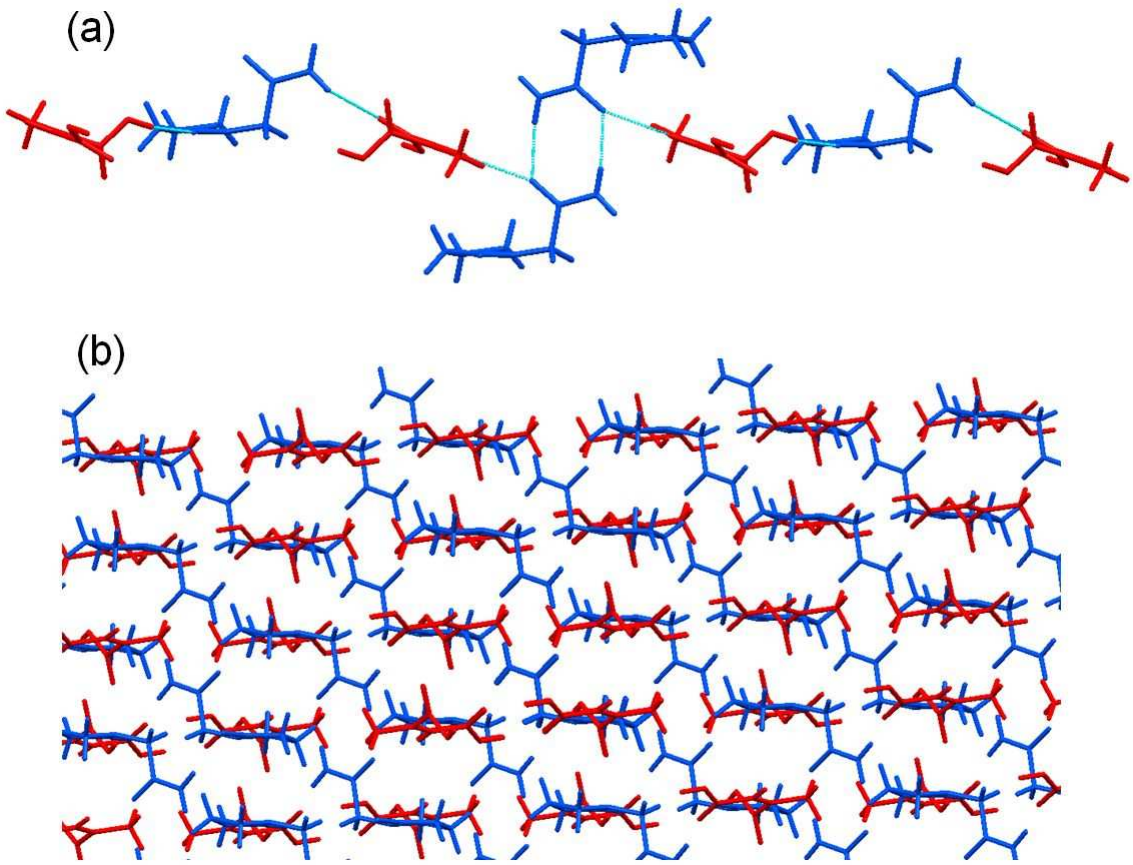

Figure 8.10 *Crystal packing in the PTM:CCA complex. (a) Arrangement of the CCA molecules and PTM pyrrolidone rings along the plane with the PTM amide group pointing outwards and forming the amide homodimer; (b) the resultant layered arrangement of the structure with amide groups bridging between layers.*

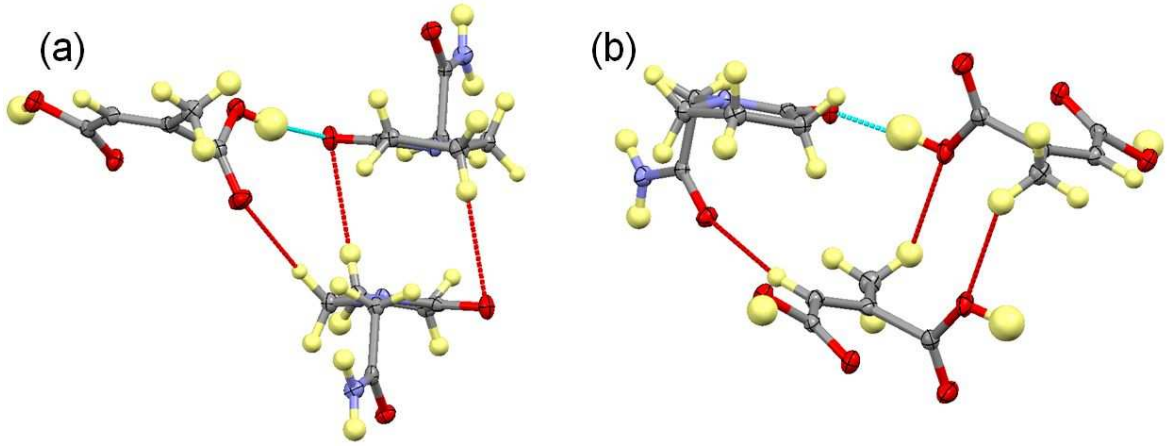

Figure 8.11 *Weak CH···O hydrogen bonds (red dashed lines) in the PTM:CCA complex. (a) Weak CH···O hydrogen bonds involving the pyrrolidone CH groups; (b) weak CH···O hydrogen bonds involving the CCA CH groups.*

8.7.3 Piracetam : Chloranilic Acid (PTM:CA)

The PTM:CA complex crystallises in a 1:1 ratio. The asymmetric unit features a single PTM molecule with two unconnected halves of CA molecules. The two half CA molecules lie on inversion centres and thus two symmetry independent CA molecules are present in the complex. One CA molecule is linked to the pyrrolidone oxygen of PTM through a moderately strong OH···O hydrogen bond, with another PTM molecule linked to the carbonyl of the CA molecule through an amide NH···O hydrogen bond (Figure 8.12a). This results in chains being formed with CA molecules linked by two PTM molecules (also Figure 8.12a). The PTM molecules are linked to the second symmetry independent CA molecule through moderately strong NH···O and OH···O hydrogen bonds involving the amide group to form an $R^2_2(9)$ ring (Figure 8.12b) This forms PTM:CA:PTM trimers which link the chains forming a 2D network (Figure 8.12c). Hydrogen bond distances and angles are shown in Table 8.5.

The pyrrolidone rings of PTM molecules in neighbouring chains lie in the gaps of the 2D network, forming weak hydrogen bonds that link the networks in the third dimension (Figure 8.13). Weak CH···O hydrogen bonds are formed to the molecules in the chains between the pyrrolidone CH groups and the amide carbonyl of PTM (C···O = 3.373(4) Å), as well as the hydroxyl oxygen of CA (C···O = 3.519(5) Å) (e and f, respectively in Figure 8.13). A further weak hydrogen bond is present between a pyrrolidone CH group

and the chlorine atom of the chain-linking CA molecule (C···Cl = 3.472(4) Å) (g in Figure 8.13).

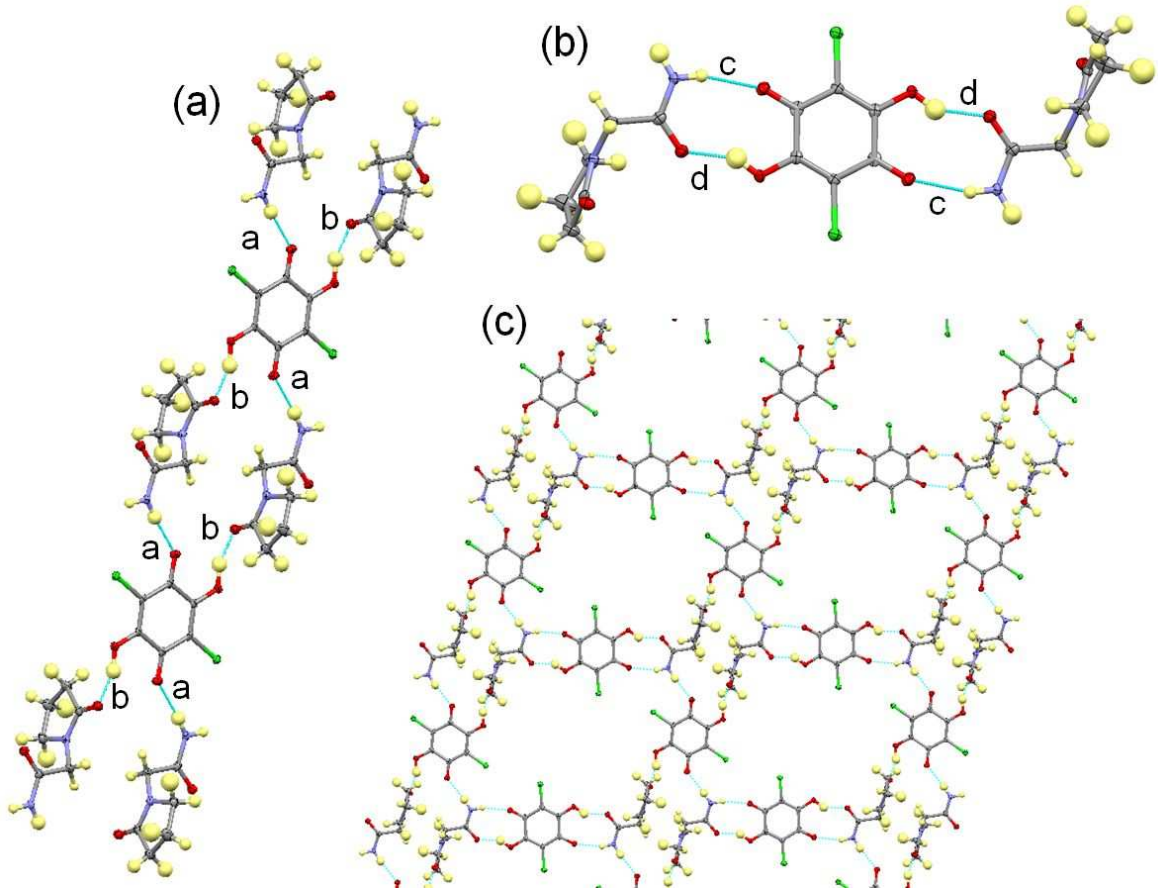

Figure 8.12 *Hydrogen bonding in the PTM:CA complex. (a) The chains formed by OH···O and NH···O hydrogen bonds between PTM and CA molecules; (b) the trimers formed by the CA molecule with two PTM molecules through the* $R^2_2(9)$ *ring formed with the amide group; (c) the hydrogen bonded chains in (a) linked by the hydrogen bonding motif in (b).*

Table 8.5 *Hydrogen bond lengths and angles in the piracetam : chloranilic acid complex (refer to Figure 8.12 for key).*

Complex	H-Bond	D-H (Å)	H···A (Å)	D···A (Å)	∠D-H···A (°)
PTM:CA	a	0.91(4)	1.99(4)	2.897(4)	175(4)
	b	1.02(4)	1.58(4)	2.554(3)	159(3)
	c	0.87(4)	2.02(3)	2.860(4)	163(3)
	d	0.90(4)	1.74(4)	2.551(3)	149(3)

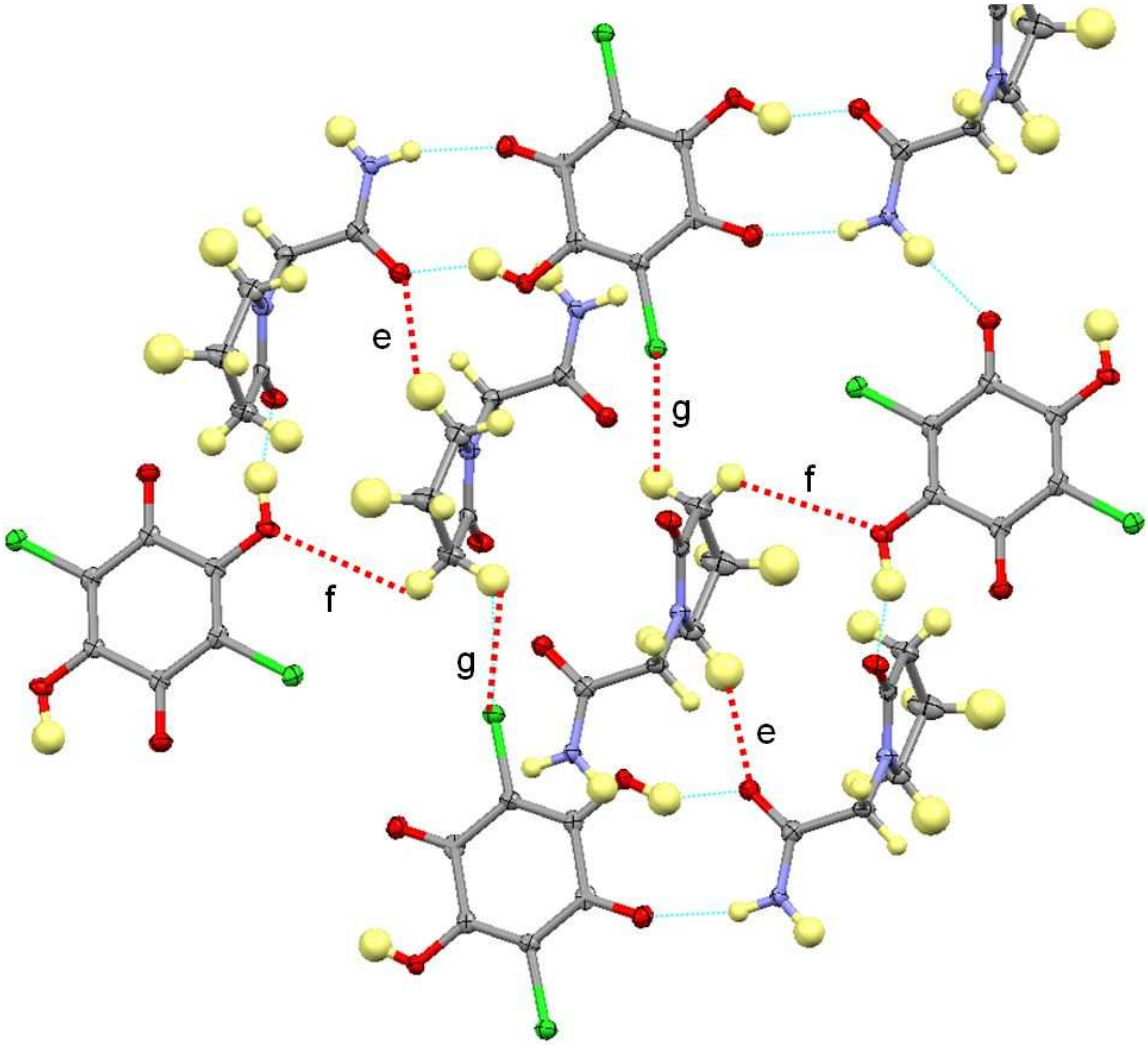

Figure 8.13 *The two PTM molecules lying in the gaps of the 2D hydrogen bonded network of PTM:CA (shown in Figure 8.12c) and the weak hydrogen bonds between them and the surrounding molecules (red dashed lines).*

8.7.4 Piracetam : Bromanilic Acid (PTM:BRA)

The PTM:BRA complex crystallises in a 1:1 ratio; unlike the PTM:CA complex, it features one full BRA molecule in the asymmetric unit with a single PTM molecule. The complex displays the same two primary hydrogen bonding motifs as the PTM:CA complex (Figure 8.14). As all BRA molecules are symmetry equivalent, however, each is therefore linked to PTM molecules by both the $R^2_2(9)$ ring seen in the PTM:CA:PTM trimers (c and d in Figure 8.14) and by the NH···O and OH···O hydrogen bonds in the PTM:CA chains (a and b in Figure 8.14). In the PTM:CA complex, CA is linked to two PTM molecules in the trimers and four PTM molecules in the chains. As the hydrogen bonding of BRA in the PTM:BRA

complex is a combination of both hydrogen bonded units, it is therefore linked to three PTM molecules (the average of the two CA molecules). The hydrogen bond strengths are generally similar in both complexes (Table 8.6).

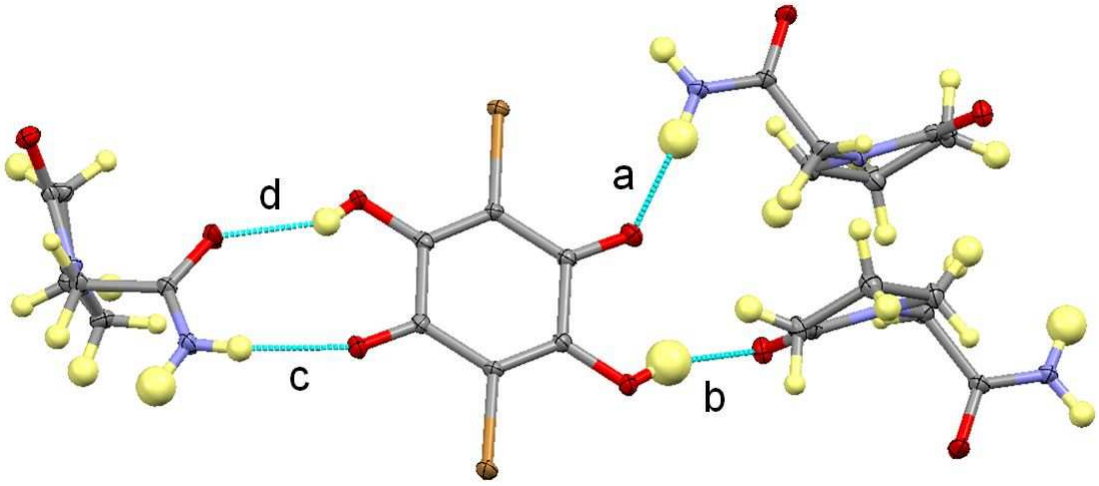

Figure 8.14 *The primary hydrogen bonding motifs between PTM molecules and BRA molecules in the PTM:BRA complex.*

Table 8.6 *Hydrogen bond lengths and angles in the piracetam : bromanilic acid complex (refer to Figure 8.14 for key). Equivalent values for the PTM:CA complex are provided for comparison.*

Note: The single BRA molecule in the PTM:BRA complex forms hydrogen bonds a-d to PTM molecules, while in the PTM:CA complex one CA molecule forms two sets of hydrogen bonds a and b only, while a symmetry independent molecule forms two sets of c and d only.

Complex	H-Bond	D-H (Å)	H···A (Å)	D···A (Å)	∠D-H···A (°)
PTM:BRA	a	0.91(4)	1.97(4)	2.879(3)	173(3)
	b	0.96(5)	1.68(5)	2.590(2)	158(4)
	c	0.92(3)	1.98(3)	2.846(3)	156(3)
	d	0.71(4)	1.92(4)	2.521(2)	142(40
PTM:CA	a	0.91(4)	1.99(4)	2.897(4)	175(4)
	b	1.02(4)	1.58(4)	2.554(3)	159(3)
	c	0.87(4)	2.02(3)	2.860(4)	163(3)
	d	0.90(4)	1.74(4)	2.551(3)	149(3)

The structure is made of regions of zigzagging PTM molecules separated by regions of zigzagging BRA molecules (Figure 8.15). The neighbouring PTM molecules are linked via weak CH···O hydrogen bonds between the acetamide CH and the pyrrolidone oxygen

(C···O = 3.311(3) Å) (highlighted in Figure 8.15). Weak hydrogen bonds are also present between the PTM NH and the BRA bromine (C···Br = 3.430(2) Å) (also highlighted in Figure 8.15).

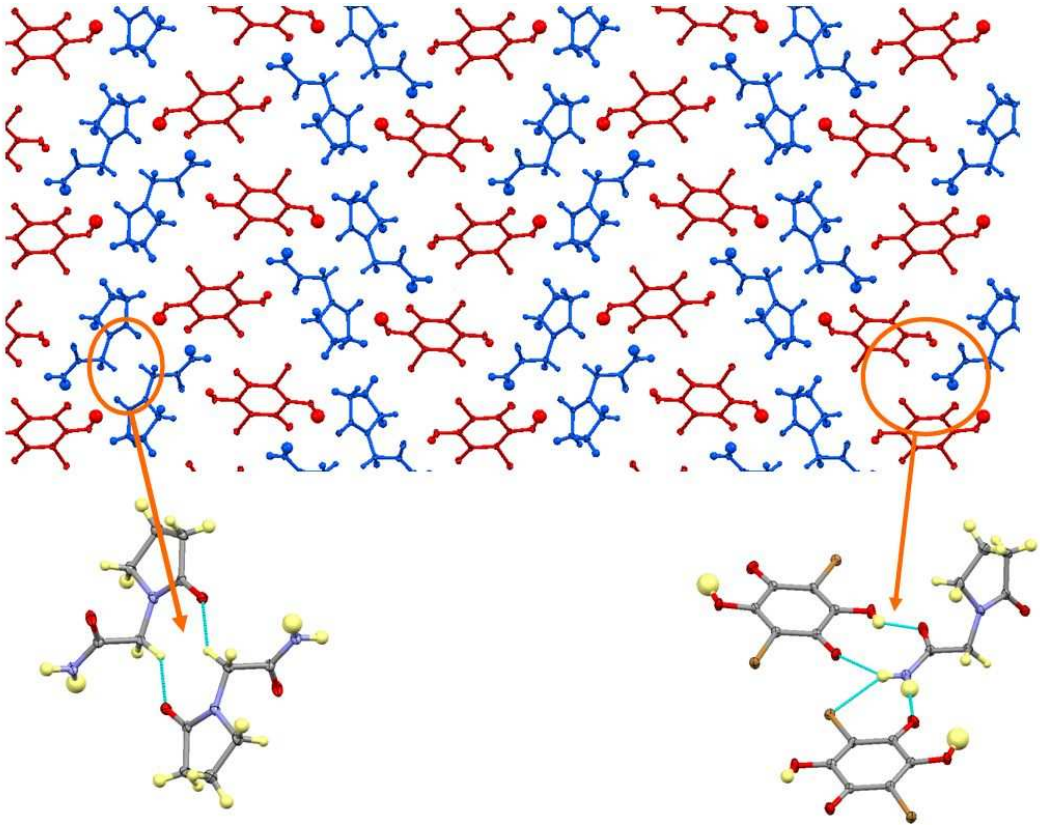

Figure 8.15 *The crystal packing of the PTM:BRA complex showing the zigzagging regions of PTM (blue) separated by zigzagging regions of BRA molecules (red) (top). A weak CH···O hydrogen bond between PTM molecules is highlighted (bottom left), as is a region where the NH···Br hydrogen bond occurs, with the relative positions of the $R^2_2(9)$ ring and NH···O hydrogen bonds also shown (bottom right).*

8.8 Discussion of Piracetam Molecular Complexes

8.8.1 Supramolecular Synthons in Piracetam Molecular Complexes

Four new 1:1 molecular complexes of PTM have been produced in this study, with the co-formers gallic acid (GA), citraconic acid (CCA), chloranilic acid (CA) and bromanilic acid (BRA). The PTM:CCA complex did not result in the formation of the amide-carboxylic acid heterodimer despite the presence of two carboxylic acid groups, with amide-amide and carboxylic acid-carboxylic acid homodimers formed instead. The PTM:GA complex also

failed to yield the amide-carboxylic acid dimer, although a heterodimer was formed through an $R^2_2(9)$ ring involving the PTM amide group and two GA hydroxyl groups. This dimer is analogous to the $R^2_2(9)$ ring found in the PTM complexes with CA and BRA, with the hydroxyl oxygen of GA acting as an acceptor instead of the CA/BRA carbonyl oxygen.

The inability to obtain the amide-carboxylic acid dimer is consistent with the known complexes of PTM. There are currently seven PTM : carboxylic acid molecular complexes in the CSD, utilising five different co-formers (complexes with both racemic mandelic acid and L-mandelic acid are known[92], although both are treated as a single co-former for the purpose of this discussion due to the identical functional groups present). In these seven complexes, the amide-carboxylic acid dimer is observed in only three; the co-formers used were 2,5-dicarboxylic acid[40], 4-hydroxybenzoic acid[40] and citric acid (3:2 complex)[92]. In addition only one of the three symmetry independent PTM molecules in the 3:2 citric acid complex forms the heterodimer, with another PTM molecule forming amide-amide homodimers and the other forming neither dimer. The amide-amide homodimer also occurs in both mandelic acid complexes as well as in the PTM:CCA complex presented above, therefore occurring in four of nine complexes in total. Analysis of the interactions of the carboxylic acid in all nine PTM complexes (both those described here and those found in the CSD) shows that the carboxylic acid has a far greater tendency to form an OH···O hydrogen bond to the pyrrolidone carbonyl oxygen; this interaction is found in seven of the nine PTM complexes, including the GA and CCA complexes described above (see Figures 8.7 and 8.9).

The PTM complexes with BRA and CA both exhibit two identical primary hydrogen bonding synthons. One synthon is the expected $R^2_2(9)$ ring which is analogous to the amide-carboxylic acid heterodimer. The second is made up of both the amide NH···O interaction with the CA/BRA carbonyl and the CA/BRA hydroxyl OH···O interaction with the PTM pyrrolidone carbonyl. Interestingly, in the CA complex each symmetry independent CA molecule participates in only one type of synthon while in the PTM:BRA complex all BRA molecules are equivalent and participate in both.

8.8.2 Conclusions

Although carboxylic acids appear to be useful co-formers for co-crystallisation with PTM, the evidence of these structures suggests that the amide-carboxylic acid dimer is not a

suitable supramolecular synthon target for these systems and the competition from other interactions needs to be considered. The amide-carboxylic acid dimer was found to occur in only three of nine PTM : carboxylic acid complexes in total. The carboxylic acid group appears to be far more likely to form OH···O hydrogen bonds to the pyrrolidone carbonyl oxygen with this occurring in seven of the nine complexes. The amide-amide homodimer was also found to occur more frequently than the amide carboxylic acid-heterodimer - although only slightly, with four complexes exhibiting this synthon. When co-crystallising PTM with carboxylic acids, it may therefore be appropriate to anticipate the formation of the carboxylic acid-pyrrolidone OH···O hydrogen bond, rather than a carboxylic acid-amide heterodimer.

The occurrence of the OH···O hydrogen bonds involving the pyrrolidone carbonyl in the PTM complexes with CA and BRA, again suggests it may be appropriate to anticipate that the strongest hydrogen bond donor of the co-former will interact with the pyrrolidone carbonyl oxygen. In these complexes, however, the occurrence of the $R^2_2(9)$ hydrogen bonded ring is equally prevalent. A similar $R^2_2(9)$ heterodimer is seen in the PTM:GA complex (Figure 8.7). It may be of interest to investigate the occurrence of this $R^2_2(9)$ heterodimer, by selection of suitable co-formers, to determine if it is more prevalent than the amide-carboxylic acid heterodimer. If so, it may be useful in the crystal engineering of PTM molecular complexes.

9. Conclusions and Forward Look

9.1 Multi-Component Crystallisation as a Route to New and Elusive Polymorphs

9.1.1 Paracetamol Form II

Co-crystallisation methodology has been demonstrated as a method of producing new and elusive polymorphs (and solvates) of a variety of materials with pharmaceutical properties. The metastable and pharmaceutically relevant paracetamol form II (PA II) could be produced from simple evaporation co-crystallisation with a variety of mono-substituted benzoic acids and the yield obtained has been shown to be dependent on the substituent and substitution position as well as the solvent used for crystallisation. It was shown to be possible to obtain 100% yields of PA II and the use of 4-substitued benzoic acids as co-former was found to be particularly consistent in obtaining this. Other co-formers containing carboxylic acid groups could also be used, namely, nicotinic acid, fumaric acid, succinic acid and creatine. This led to the investigation of a carboxylic acid as a solvent, with recrystallisation of PA from excess acetic acid found to be a route to producing PA II with yields close to 100%. Several other co-molecules not containing carboxylic acid groups were also found to encourage the crystallisation of PA II under certain conditions, including the three nitrogen heterocycles (NHCs), pyrazole, 3,5-dimethylpyrazole and pyrazine.

The co-crystallisation method of producing PA II consistently resulted in large (> 1 mm^3) crystals being produced. This enabled the first variable temperature single crystal neutron diffraction study of PA II to be carried out. A comparison of the hydrogen bond parameters was made between the neutron and X-ray data. Good agreement was found between the donor and acceptor atom distances at corresponding temperatures, as expected. The neutron data, however, showed a general increase in H···A distances with temperature as well as a decrease in D-H distances between 200 K and 300 K; this evolution of the hydrogen parameters was not observed in the X-ray data. The neutron data also showed that there is a significant increase in librational motion of the methyl hydrogen atoms with temperature - similar to that seen in neutron diffraction studies of PA I.

The simplicity of the co-crystallisation method to produce PA II, as well as the flexibility in terms of the co-molecules and solvents that can be used, made it a good candidate for scaled-up crystallisation in the OBC. Problems were encountered, however, in converting the evaporation co-crystallisation process to a cooling co-crystallisation process - with no PA II produced under the conditions investigated. Problems were encountered with some of the more reliable co-molecules (in the evaporation experiments) due to the poor solubility of the co-molecules used (4-chlorobenozic acid, 4-bromobenzoic acid, succinic acid), as they mainly crashed out preferentially from the solution, leaving the PA remaining in solution. Using more soluble co-molecules resulted in only PA I crystallising. A more thorough investigation of the cooling crystallisation parameters is therefore required to assess the viability of using this co-crystallisation method to produce PA II on a large scale in non-evaporative environments. This should involve trying different co-molecules from those that have been investigated here, as well as different solvents. More careful control over the cooling rate may be required and the effect of altering the cooling rate should also be investigated.

9.1.2 New Crystal Forms of Piroxicam

Co-crystallisation was used to obtain a new polymorph of PX - PX form IV - as well as a new PX : methanol solvate. Both of these new phases featured a mixture of both the zwitterionic and non-ionised PX tautomers. A simple evaporative co-crystallisation route to the known PX III polymorph was also discovered, which enabled the first full crystal structure determination to be carried out on this polymorph. All three phases were obtained using NHCs as the structure-directing co-molecules at elevated temperatures. PX III was produced by co-crystallisation with an excess quantity of pyrazole or 3,5-dimethylpyrazole at 40°C/50°C; PX IV could be obtained from co-crystallisation with excess pyrazine at 40°C/50°C and the PX : methanol solvate was produced by co-crystallisation with indazole at 60°C.

Problems were encountered in obtaining 100% yields of PX III, while the reproducibility of PX IV was poor. DSC measurements of all polymorphs were carried out to rationalise this. The stability of the polymorphs was found to be I>III>II>IV. The crystallisation of PX IV is likely to be highly sensitive to perturbations of the crystallisation environment due to its poor stability relative to the other three polymorphs. The poor yield of PX III, despite being the second most stable form, is possibly due to this

polymorph lying in an energy minimum close to that of PX I, which may mitigate against its formation. This is supported by the fact that both feature the same primary hydrogen bonding motifs between PX molecules.

Future work should involve optimisation of the co-crystallisation process to obtain consistent 100% yields of PX III and IV. This may involve experimenting with different crystallisation temperatures between 40°C and 60°C in smaller increments to find the optimal temperature for producing each form. The effect of different solvents should also be investigated as well as the ratio of PX to co-molecule that is used. Obtaining large yields of these polymorphs would facilitate a thorough investigation of the properties of each form to assess what advantages they may have over the more stable forms. In particular, it may be of interest to investigate the properties of PX IV and the methanol solvate to investigate what effects the mixed tautomers present in these phases may have.

9.1.3 A New Porous Form of Gallic Acid Monohydrate

A new porous form of gallic acid monohydrate (PGAM) was obtained from co-crystallisation with piracetam (PTM). PXRD of the co-crystallisation products from methanol or ethanol solution indicated that a gallic acid (GA) : PTM molecular complex may crystallise concomitantly with PGAM, although it was not observed in unit cell screens of single crystals of the sample. This suggests the molecular complex may have formed during the grinding of the sample in preparation for PXRD. This could be resolved by repeating the co-crystallisation experiments and using PXRD analysis without grinding the sample.

The disordered solvent in the pores of PGAM could not be resolved from the single crystal X-ray diffraction data collected. Analysis using TGA may give clues as to the nature of the solvent in the pores. It remains to be seen whether the solvent can be removed from the pores with the structure remaining intact and TGA may also be used to determine if this is possible. If the solvent can be removed, PGAM may have potential for use as an organic lightweight gas storage material.

9.1.4 Piracetam Form I

The elusive metastable form I of PTM was initially crystallised from a co-crystallisation experiment with pyrazole at 50°C using methanol as the solvent. Subsequent experiments under the same conditions without pyrazole also resulted in the formation of PTM I. It remains unclear whether the initial co-crystallisation experiment that resulted in crystallisation of PTM I has resulted in subsequent seeding of the laboratory with this form. To clarify this it must be independently verified in another laboratory - first by crystallisation of PTM in methanol at 50°C to observe which polymorph is obtained. If PTM I is not obtained this should be followed by a repeat of the initial co-crystallisation experiment outlined here.

9.1.5 Understanding the Mechanism

The mechanism by which the co-molecules used direct the formation of metastable phases remains unclear. The evidence from the investigations presented here suggests that the mechanism is solution-based rather than epitaxial in nature. The fact that NHCs can be used to direct the formation of three different forms of PX is possibly indicative of a related mechanism, as is the fact that three of these NHCs have also been observed to direct the formation of PA II.

Future work to investigate this mechanism should involve co-crystallising the co-formers which have been observed to direct the formation of metastable forms with a variety of other materials to observe what effect they have on the polymorph obtained (assuming a molecular complex is not formed). Any structural or property relationships between the target molecules of which metastable forms are obtained could give clues about the nature of the mechanism. Similarly, structural or property relationships between the co-molecules which are found to direct the formation of a metastable form of a material may also provide clues as to the mechanism.

9.1.6 The Utility of Co-Crystallisation for Polymorph Screening

Co-crystallisation as a route to polymorph screening has been shown to be useful in accessing crystal forms which are otherwise difficult to obtain, such as PA II and PX III. It

has also been shown to be useful in obtaining forms with otherwise unobtainable structural features such as PX IV, the PX : methanol solvate and PGAM. This highlights the potential importance of co-crystallisation as a route to polymorph selection. Its viability as a common method of polymorph screening, however, remains questionable. Some co-molecules direct polymorph formation in some materials and not others and there is thus an almost infinite number of possible co-molecules that could be screened. The range could be narrowed down by using only a select few co-molecules or a select class of co-molecules which are known to direct polymorph formation in a number of materials (possibly materials such as the NHCs used in this work). Issues would remain, however, as there are an infinite number of conditions under which these co-crystallisations could be carried out. Elevated temperatures may or may not be required and the co-molecule may also need to be used in excess, as in the case of the co-crystallisation experiments that resulted in the formation PX III and PX IV. Ultimately, a better understanding of the mechanism involved could allow prediction of the type of co-molecule required and the conditions that may give rise to the formation of a certain polymorph.

9.2 Tautomerisation and Polymorphism in Molecular Complexes of Piroxicam with Mono-Substituted Benzoic Acids

PX was found to readily form molecular complexes with monosubtituted benzoic acids (BAs). Twenty complexes in total were synthesised in this study - twelve incorporating the zwitterionic form of PX (PXZ) and eight incorporating the non-ionised form (PXN). This adds to the known complexes of PXZ with 4-hydroxybenzoic acid (4HBA) and benzoic acid as well as the known complex of PXN with 4HBA[27]. All PX complexes with fluorobenzoic acids were found to exhibit the rare phenomenon of tautomeric polymorphism. Both the PXZ and PXN complexes were found to have a tendency to form four-molecule hydrogen bonded supramolecular units. These units were comprised of a PX dimer flanked by two BA molecules. This BZZB tetramer unit in the PXZ complexes was found to be highly robust, with all twenty complexes synthesised exhibiting the same type of hydrogen bonding, as well as the known complex with benzoic acid. The PXN complexes were less predictable with two recurring PXN dimer synthons observed as well as two complexes exhibiting unique hydrogen bonding between PXN molecules (PXN:4FBA and PXN:4HBA[27]). The hydrogen bonding motif between the PXN molecules and the BA

molecules was found to be much more robust with the same $R_2^2(8)$ ring found in all PXN structures with the exception of the PXN:4HBA complex[27].

DSC analysis of the tautomeric polymorphs showed that their relative stability was not dependent on the tautomer present in the complex. One might expect the PXZ polymorphs to be more stable due to the presence of charge-assisted hydrogen bonds, however, the PXN:2FBA complex was found to be more stable than the PXZ:2FBA complex. Studies of these tautomeric polymorphs may offer insight into other physical properties that may be inferred by the presence of different PX tautomers.

An empirical relationship was found between the PX tautomer present in the molecular complexes and the pKa of the BA co-formers in the complexes. The data gathered suggests a region of co-former pKa values is present within which the non-ionised PXN tautomer is favoured in molecular complex formation. Co-formers with pKa values above or below the boundaries of this region favour the formation of complexes incorporating the zwitterionic PXZ tautomer. Using this as a guide allows a reasonable prediction to be made regarding which tautomer will be present in a PX complex with BAs, which in turn means a reasonable prediction of the hydrogen bonding motifs can also be made based on the supramolecular synthons observed in this work. It is unclear, however, why BA co-formers with relatively high and relatively low pKa values would favour molecular complex formation with PXZ while a middle region would favour molecular complex formation with PXN. Further investigation of this is required by expanding the number of BA co-formers in this series. It would also be of interest to investigate other tautomeric materials via similar systematic co-crystallisation studies to determine if such an empirical observation can be made. This may lead to a rationale as to why such a boundary region exists. Ultimately, through empirical deduction, this could lead to guidelines for predicting intramolecular hydrogen transfer in molecular complexes - similar to the pKa rule that is already in use for predicting intermolecular hydrogen transfer in molecular complexes.

9.3 Intermolecular Hydrogen Transfer in Multi-Component Complexes of Piroxicam

Eight molecular complexes of PX with NHCs were synthesised. Three of the complexes were solvated complexes with imidazole (IM). Hydrogen transfer occurred from the PX

molecule to the basic nitrogen in all three IM complexes as well as in the 2-methylimidazole (2MIM) and benzimidazole (BZ) complexes. No intermolecular hydrogen transfer occurred in the PX complexes with triazole (TZ), benzotriazole (BZT) or pyrazine (PZN). In these three complexes, PX was found to exist in the zwitterionic tautomer.

All five of the PX^{-}:NHC complexes feature infinite chains of alternating PX^{-} and NHC in an ABABA configuration. Four of the complexes feature the same primary hydrogen bonding motifs between the PX^{-} molecule and the NHC molecule. These involve the NHC molecule forming two NH···O hydrogen bonds to the PX molecule; one is formed to the amide carbonyl oxygen and the second to the PX enolate oxygen. The only PX^{-}:NHC complex not to exhibit this hydrogen bonding pattern is the PX:IM hemihydrate. The hydrogen bonding in this complex is unusual as it features a CH···O hydrogen bond to the PX^{-} enolate oxygen whereas the other four complexes satisfy the strongest donor-strongest acceptor hydrogen bonding arrangement. No 1:1 PX^{-}:IM^{+} complex was found, despite the two PX^{-}:IM^{+} acetonitrile solvates exhibiting the same hydrogen bonding pattern as the 2MIM and BZ complexes. This was rationalised by the fact that 2MIM and BZ have large bulky groups attached to the imidazole ring. In the absence of the solvent molecules a large void would be left if it were to form this hydrogen bonding pattern. Other than this one exception it would appear that the hydrogen bonding in PX complexes with co-molecules possessing the imidazole ring is reasonably predictable.

The three PXZ:NHC complexes featured the PXZ dimer that is found in all PXZ complexes. The PXZ:TZ and PXZ:BZT complexes both featured the TZ/BZT molecules being hydrogen bonded to both PXZ molecules in the dimer through NH···O hydrogen bonds to the enolate oxygen atoms. In the case of the PXZ:TZ complex, this results in infinite chains, whereas in the PXZ:BZT complex discrete tetramers are formed. The PXZ:PZN complex was found to feature only weak CH···O and CH···N hydrogen bonds between PXZ and PXN molecules which explains why it crystallised rarely and in small quantities.

Co-crystallisation of PX with the strong acids, chloranilic acid (CA) and bromanilic acid (BRA), resulted in hydrogen transfer occurring from the acid to the PX molecule in all four complexes. Form I and form II of the PX^{+}:CA^{-} complex feature similar hydrogen bonding involving the same groups, with form II possessing an extra NH···O hydrogen bond due to the a different orientation of the CA^{-} molecule. The PX^{+}:CA^{2-}.ACN 2:1:2 solvate possesses the same hydrogen bonding motif as is seen in PX^{+}:CA^{-} form I, which results in a 2:1 ratio as the CA is doubly deprotonated. Only one form of the PX^{+}:BRA^{-}

complex was found, which was isomorphous to form II of the PX^{+}:CA^{-} complex. This form was produced even when PX and BRA were co-crystallised under the same conditions as those that resulted in form I of the PX^{+}:CA^{-} complex and the 2:1:2 PX^{+}:CA^{2-}.ACN solvate.

The ΔpKa values for the complexes formed in this study suggest that, at least under certain conditions, it may be more appropriate to consider PX as the zwitterionic form when predicting intermolecular hydrogen transfer using the pKa rule. By considering the N^{+}-H group as the acidic group and the enolate O^{-} as the basic group, a clear indication is given of which complexes will result in hydrogen transfer. This is further supported by the study which has shown that a significant proportion of PX is in the zwitterionic form in polar solvents[223]. Within this analysis, none of the complexes which do not undergo intermolecular hydrogen transfer have a ΔpKa greater than (or even close to) the empirically significant value of 3. The study presented here is relatively small and more molecular complexes using co-formers with a range of pKa values is required to assess how useful the pKa rule is in predicting hydrogen transfer in molecular complexes of PX. This would assist in determining whether the pKa values used in the pKa rule equation should be derived from the zwitterionic tautomer or the non-ionised tautomer of PX.

9.4 General Comments on Hydrogen Transfer in Molecular Complexes of Piroxicam

It has been shown that piroxicam forms molecular complexes with a range of different acids and bases. The pKa of these co-formers has been shown to have a major influence on the ionisation state of PX in the resultant complex. The work presented here has provided a tentative route to predicting which PX form will be present in a particular molecular complex based on the pKa of the co-former used – with the non-ionised form, the zwitterionic form, the anionic form and the cationic form all obtainable. Challenges remain in rationalising the presence of a pKa boundary region in which the non-ionised form of PX is found to crystallise with BAs; this boundary region also does not account for the existence of the tautomeric polymorphism observed in the PX complexes with fluorobenzoic acids. The use of the pKa rule also requires further investigation as to which pKa values are most appropriate for use in the pKa equation. Similar systematic studies using other tautomeric materials would also be useful to determine to what extent, if any, the empirical observations made in this study can be applied to other materials.

9.5 Molecular Complexes of Paracetamol and 4-Acetamidobenzoic Acid

PA was found to co-crystallise with imidazole (IM), 2-methylimidazole (2MIM) and 4-methylimidazole (4MIM) to form molecular complexes. Attempts to form a molecular complex with benzimidazole (BZ) were unsuccessful. The PA:IM and PA:2MIM complexes exhibited similar primary hydrogen bonding patterns. Steric effects, caused by the presence of the methyl group in 2MIM, meant slight differences were observed and this resulted in a 1:2 PA:2MIM complex forming as opposed to the 1:1 ratio found in PA:IM. The 4MIM complex crystallised in a 1:1 ratio but exhibited a completely different hydrogen bonding pattern from that found in the IM and 2MIM complexes. This was found to be due to a pronounced twisting of the PA molecule which resulted in the amide group lying out of the plane of the aromatic ring; the PA molecule in the PA:IM and PA:2MIM complexes was relatively planar. The only common synthon to all three complexes was the NH···O hydrogen bond between the IM NH group and the PA carbonyl.

4ABA was found to form molecular complexes with IM, 2MIM, 4MIM and BZ (co-crystallisation with BZ formed a 1:1:1 hydrated complex). The carboxylate hydrogen transfers to the basic nitrogen of the imidazole ring in all four complexes. The 4ABA:2MIM complex was a partial exception to this as it possessed one neutral 4ABA and one deprotonated $4ABA^{-}$. The presence of a neutral 4ABA molecule increased competition for hydrogen bonding to the carboxylate of $4ABA^{-}$, meaning that only one 2MIM molecule could form hydrogen bonding links to it. This resulted in a 2:1 (4ABA: 2MIM) ratio (which could also be classed as a 1:1:1 $4ABA:4ABA^{-}:2MIM^{+}$ ratio). The IM, 4MIM and BZ complexes all featured two $IM^{+}/4MIM^{+}/BZ^{+}$ molecules forming hydrogen bonds to the carboxylate group of $4ABA^{-}$, resulting in the different ratio to that found in the $4ABA^{-}:2MIM^{+}$ complex.

Comparison of the PA and 4ABA complexes formed with imidazole derivatives was made difficult due to hydrogen transfer occurring in the 4ABA complexes but not in the PA complexes. This altered the hierarchy of the hydrogen bond acceptor strengths in the 4ABA molecule. The lack of robust transferrable synthons in either series of complexes also made it difficult to compare them. The NH···O hydrogen bond between the imidazole ring NH and the amide carbonyl oxygen was found to occur in all three PA complexes but only in two of the 4ABA complexes (4ABA:IM and $4ABA:BZ.H_2O$). In summary, no robust hydrogen bonded synthons are present in either series that would facilitate the

prediction of the hydrogen bonding that will occur in molecular complexes with other imidazole derivatives. The hydrogen transfer that occurs in the 4ABA complexes also precludes prediction of the hydrogen bond interactions of one based on those formed by the other with the same imidazole co-former.

Four molecular complexes of 4ABA were synthesised with aprotic nitrogen heterocycles (aNHCs), 2-picoline (2PIC), 3-picoline (3PIC), 4-picoline (4PIC) and 4,4-bipyridine (BP). No hydrogen transfer occurred in any of these complexes. All four complexes showed consistent OH···N hydrogen bonding between the carboxylic acid group and the nitrogen of the aNHC. The 4ABA molecules in three of the complexes also featured chains of 4ABA molecules formed by NH···O hydrogen bonds between the amide groups. The exception was the 4ABA:2PIC complex which had a slight variation, instead forming 4ABA chains through hydrogen bonds between the amide NH and the carboxylic acid carbonyl oxygen. The consistent hydrogen bonding seen suggests that the relative ratio of components can be predicted based on the number of nitrogen acceptor atoms in the aNHC, as illustrated by the 4ABA:BP complex where a 2:1 ratio is found. It should be noted, however, that this conclusion is based on a relatively small subset of co-formers and considerably more work is required to determine how valid is this conclusion.

A complex of PA with BP was previously known[227], however PA was not found to form molecular complexes with 2-, 3- or 4-picoline under the conditions investigated. The 4ABA complexes with aNHCs were therefore compared to the four known structures[17, 227] of PA with aNHCs. The phenolic OH···N hydrogen bond to the aNHC nitrogen was found to be less persistent than the corresponding OH···N interaction in the 4ABA complexes and only found in two of the four complexes. This can be rationalised by the fact that the phenolic hydroxyl group is a weaker donor than the carboxylic acid hydroxyl and so synthons involving this group are more susceptible to competition from other donors. Again, however, this is based on a relatively small subset of co-formers and expanding the number of molecular complexes of 4ABA and PA with aNHCs is desirable, to allow more definite conclusions to be drawn on how predictable, and comparable, the interactions are in both series of complexes.

Using the ΔpKa values to predict hydrogen transfer was investigated for all 4ABA and PA complexes with imidazole derivatives and aNHCs. For PA, no hydrogen transfer occurred as expected, as all ΔpKa values were negative. The 4ABA complexes with IM, 2MIM and 4MIM all resulted in hydrogen transfer as may be expected given the co-formers were the most basic of those used. No hydrogen transfer occurred in the

4ABA:BP complex, which was also to be expected as it has a negative ΔpKa value. The 4ABA:BZ complex was anomalous; hydrogen transfer occurred in this complex despite no hydrogen transfer occurring in the 4ABA complexes with 2-, 3- and 4PIC - all of which had higher ΔpKa values than the aforementioned complex. These results highlight the difficulty in using pKa values to predict hydrogen transfer in molecular complexes - especially when the ΔpKa value lies between 0 and 3.

9.6 Molecular Complexes of Paracetamol with Co-Formers with Multiple Carboxylic Acid Groups

Two new molecular complexes of PA were synthesised and characterised, using maleic acid (MA) and citraconic acid (CCA) as co-formers. This adds to the known molecular complexes of PA with citric acid (CTA)[233] and oxalic acid (OA)[17] which also contain multiple carboxylic acid groups (three and two carboxylic acid groups respectively). The PA complexes with MA and CCA feature identical arrangements of the primary hydrogen bonding motifs, with differences in the extended packing caused by the presence of the methyl group in CCA. The lack of intramolecular hydrogen bonding of the carboxylic acid groups in the PA complexes with CTA and OA meant that it was difficult to compare the primary hydrogen bonding motifs to those in the MA/CCA complexes. CTA molecules in the PA:CTA complex were found to prefer forming hydrogen bonds to other CTA molecules. The PA:OA complex was found to share more similarities to the MA/CCA complexes in terms of the hydrogen bonding motifs. All three complexes were found to form chains of alternating PA and OA/MA/CCA and all form layered structures. This work suggests that co-formers with multiple carboxylic acid groups may be useful in synthesising molecular complexes of PA.

9.7 General Comments on the Scale-Up Crystallisation of Paracetamol Molecular Complexes for Crystallisation in a COBC

Attempts were made in this study to scale up the co-crystallisation of molecular complexes of PA with IM and MA for continuous crystallisation in an OBC. None of the experiments progressed past the initial stage of converting the evaporation crystallisation method, employed in the initial synthesis of the molecular complex, to a cooling

crystallisation process. In both cases, the co-former was often found to crash out preferentially from solution upon cooling, leaving the PA in solution. This work has highlighted the need to investigate extensively the solvent used and the relative solubility of the components, as well as the relative concentrations required to convert an evaporative process to a cooling process, as the conditions used in each process are not necessarily interchangeable. If molecular complexes, such as those presented in this work, are to be used on an industrial scale, then ability to scale up crystallisation efficiently in a non-evaporative environment is crucial. Future work should involve crystallising with a controlled cooling rate as opposed to the crash-cooled crystallisation carried out as part of this work. A more in-depth investigation of other parameters such as the effect of cooling rate and seeding of the solution should also be carried out. Following on from the preliminary investigations reported here, further studies are ongoing in this area within a larger collaborative project as part of the EPSRC National Centre in Continuous Crystallisation and Manufacturing[232].

9.8 Molecular Complexes of Piracetam

Four new molecular complexes of piracetam (PTM) were synthesised in this work, with the co-formers gallic acid (GA), citraconic acid (CCA), chloranilic acid (CA) and bromanilic acid (BRA). The two PTM complexes with carboxylic acids (GA and CCA) failed to yield the amide-carboxylic acid $R^2_2(9)$ heterosynthon. This was found to be consistent with known complexes of PTM and this synthon was only found to occur in three of the nine known complexes (both in this work and in structures reported in the CSD) of PTM. It was found that the carboxylic acid was far more likely to form an OH···O hydrogen bond to the pyrrolidone carbonyl oxygen, with this occurring in seven of the nine complexes. In the molecular complexes of PTM with CA and BRA, the hydroxyl group of CA/BRA was also found to form a hydrogen bond to the pyrrolidone oxygen. The evidence of these structures suggests that when co-crystallising PTM, it may be appropriate to anticipate the strongest hydrogen bond donor interacting with pyrrolidone oxygen. The PTM complexes with CA and BRA also exhibit an $R^2_2(9)$ ring involving the CA/BRA hydroxyl and carbonyl groups forming hydrogen bonds to the PTM amide group. This hydrogen bonding motif is analogous to the $R^2_2(9)$ ring found in the PTM:GA complex involving two of the GA hydroxyl groups, with one hydroxyl acting as a hydrogen bond donor (to the CA/BRA carbonyl oxygen) and one an acceptor (to the CA/BRA hydroxyl). It may be of

interest to investigate the occurrence of this synthon, by suitable selection of co-formers, to determine if it is useful in the crystal engineering of molecular complexes of PTM.

9.9 Concluding Remarks

Although predicting the crystal structure of a material from a defined set of conditions remains a huge challenge in crystal engineering, insight is provided by empirical observations of related materials crystallised under related conditions. In this work, such insight has enabled the production and sometimes selective crystallisation of new and elusive crystalline phases of materials. It has also facilitated reasonable prediction of which ionisation state a material will adopt when co-crystallised with another material to form a molecular complex. Challenges remain, however, in rationalising such predictions and determining how and when empirically derived “rules” can be applied. This is especially relevant with regards to crystal engineering, as it has been shown in this work (as well as elsewhere) that hydrogen bonding does not always follow the expected pattern as defined by the supramolecular synthon approach.

10. APPENDIX

APPENDIX A: Crystallographic Data and Refinement Details

For all structures reported, hydrogen atoms were located using a Fourier difference synthesis unless stated otherwise. In cases where hydrogen atoms were placed on calculated positions, methyl and hydroxyl hydrogen atoms were located initially using a Fourier difference synthesis and the bond distances and angles constrained to take standard values unless otherwise stated.

APPENDIX A4. Chapter 4 - Multi-Component Crystallisation Routes to New and Elusive Polymorphs

Refinement details for all structures can be found in Table A-4.

Paracetamol Form II (X-ray Diffraction Data)

Single crystal X-ray diffraction data were collected on a Bruker-Nonius Kappa CCD diffractometer at 100K.

Paracetamol (Neutron Diffraction Data)

Single crystal neutron diffraction data were collected using the VIVALDI instrument at the Institute Laue Langevin (ILL).

The data were processed in the standard space group, Pbca, as opposed to Pcab as the software used does not allow processing in non-standard settings. As unit cell parameters cannot be calculated accurately using Laue diffraction, unit cell parameters were taken from X-ray structure determinations at the corresponding temperatures. Unit cell parameters for the 100K neutron data were taken from the 100K single crystal X-ray re-determination carried out as part of this work. Unit cell parameters for the 200K and 300K neutron data were taken from X-ray diffraction data found in the CSD at the corresponding temperatures[205]. Structure determination using X-rays at 30K has yet to be carried out; the unit cell parameters were therefore extrapolated from the difference between 200K and 100K unit cell parameters and may not be accurate.

Piroxicam form III

Single crystal X-ray diffraction data for this complex were collected on a Bruker AXS Apex II CCD diffractometer at 100K.

Piroxicam Form IV

Single crystal X-ray diffraction data were collected on a Rigaku R-AXIS RAPID Image Plate diffractometer at 100K. Single crystals were small and of poor quality and did not diffract well. Several attempts at data collection were carried out, including data collection at the I19 beamline at Diamond; the data presented is the best which could be obtained from the poor quality crystals.

Anisotropic refinement caused the thermal parameters of one carbon atom (C75) to become abnormally elongated along one axis; its thermal parameters were therefore fixed to be equal to those of C72 to obtain a plausible approximation. Data were weak and of poor resolution with a high Rint (0.106), meaning H-atoms could not be accurately located using the Fourier difference synthesis. All hydrogen atoms were therefore placed on calculated positions and refined as riding on the atoms to which they were bonded. The piroxicam tautomer present was inferred by the conformation of the molecules and the hydrogen bonding interactions. The yellow colour of the crystals further evidenced the presence of the zwitterionic tautomer.

Piroxicam: Methanol Solvate

Single crystal X-ray diffraction data were collected on a Rigaku R-AXIS RAPID Image Plate diffractometer at 100K. Single crystals were small and of extremely poor quality and did not diffract well. Several attempts at data collection were carried out, including data collection at the I19 beamline at Diamond; the data presented is the best which could be obtained from the poor quality crystals.

Anisotropic refinement of the heavy atoms resulted in implausible thermal parameters of a number of atoms. Heavy atoms were therefore refined isotropically in the final refinement cycles. To locate the hydroxyl hydrogen (H44) of the methanol molecule, anisotropic refinement of the heavy atoms was first carried out. H44 was then located and the O-H distance constrained to 0.9Å and the thermal parameter refined as riding on the oxygen to which it is bonded. All other hydrogen atoms were then placed on calculated positions and refined as riding on the atoms to which they were bonded. The piroxicam tautomer present was inferred by the conformation of the molecules and the

hydrogen bonding interactions. The yellow colour of the crystals further evidenced the presence of the zwitterionic tautomer.

Gallic Acid Monohydrate (Porous Form)

Single crystal X-ray diffraction data for this complex were collected on a Bruker AXS Apex II CCD diffractometer at 100K. The crystals were thin needles and diffracted poorly resulting in weak data.

The water oxygen (O6) has elongated thermal parameters suggesting it may be disordered across two or more positions although this disorder could not be modelled from the available data. The water hydrogen atoms could not be located - likely a result of the disorder of the molecule.

All H-atoms were identified from the Fourier difference synthesis. The positions of the hydrogen atoms were allowed to freely refine but the size of the thermal parameters were constrained to be proportional to the atom to which they were bonded.

An excess of electron density was present in the channels, indicating the presence of disordered solvent molecules. The disordered solvent molecules could not be resolved and the electron density was therefore removed from the final refinement cycle using the SQUEEZE procedure[216] and the number of electrons estimated. The estimate of 69 electrons in the unit cell could correspond to approximately ten water molecules or four methanol molecules although a definite conclusion has not been reached.

Table A-4a Crystallographic data for paracetamol form II from both X-ray and neutron diffraction.

Radiation Source	**X-ray**	**Neutron**	**Neutron**	**Neutron**	**Neutron**
Formula	C8 H9 N1 O2	C8 H9 N1 O2	C8 H9 N1 O2	C8 H9 N1 O2	C8 H9 N1 O2
M/g mol^{-1}	151.17	151.17	151.17	151.17	151.17
T/K	100	30	100	200	300
Space Group	Pcab	Pbca*	Pbca*	Pbca*	Pbca*
a/Å	7.2028(2)	17.167	17.168	17.169	17.162
b/Å	11.7764(3)	11.756	11.776	11.806	11.837
c/Å	17.1677(5)	7.143	7.203	7.293	7.406
A	90	90	90	90	90
B	90	90	90	90	90
Γ	90	90	90	90	90
V/$Å^3$	1456.22(7)	1441.57	1456.23	1478.27	1504.50
Z	8	8	8	8	8
ρ_{cal}/ g cm^{-3}	1.379	1.391	1.377	1.357	1.333
μ/mm^{-1}	0.100	N/A	N/A	N/A	N/A
θ Range/°	2.37 - 27.50	N/A	N/A	N/A	N/A
Ref (meas. / ind.)	96660 / 1660	17996 / 2298	28761 / 2097	14274 / 1649	14083 / 1116
Observed>2σ	1363	1900	1727	1255	842
Rint	0.0667	N/A	N/A	N/A	N/A
Completeness %	99.6	N/A	N/A	N/A	N/A
Parameters	136	182	182	182	182
GooF	1.206	1.294	1.279	1.156	1.202
R_1 (obs)	0.0471	0.0402	0.0376	0.0397	0.0324
R_1 (all)	0.0593	0.0603	0.0600	0.0689	0.0580
wR2 (all)	0.1394	0.0705	0.0665	0.0671	0.0641
$\rho_{max,min}$/e $Å^{-3}$/fm A^{-3}	0.422, -0.480	0.074, -0.076	0.056, -0.064	0.042, -0.084	0.035, -0.038

*Neutron data were solved in the standard space group setting (Pbca) as the software used for processing the data does not allow for non-standard settings to be used. Unit cell parameters for neutron data were also fixed to the X-ray values at the corresponding temperature (see above).

Table A-4b Crystallographic data for new and elusive phases of piroxicam and gallic acid monohydrate produced by co-crystallisation methods.

	PX III	**PX IV**	**PX : MeOH**	**PGAM**
Formula	C15 H13 N3 O4 S1	C15 H13 N3 O4 S1	3(C15 H13 N3 O4 S1), (C1 H4 O1)	(C7 H6 O5), (H2O)
M/g mol^{-1}	331.35	331.35	1026.09	188.13
T/K	100	100	100	100
Space Group	P-1	P-1	P-1	$P2_1/n$
a/Å	7.8557(3)	12.6899(9)	7.037(2)	3.6803(3)
b/Å	10.1043(4)	14.6928(9)	12.917(4)	27.724(2)
c/Å	10.4713(5)	20.5097(16)	25.467(8)	9.3579(7)
α	80.602(2)	84.866(2)	84.077(7)	90
β	68.952(2)	74.669(3)	89.174(7)	94.397(3)
γ	69.742(2)	84.683(2)	83.327(6)	90
V/$Å^3$	727.01(5)	3663.7(4)	2287.0(12)	952.00(12)
Z	2	10	2	4
ρ_{cal}/ g cm^{-3}	1.514	1.502	1.443	1.299
μ/mm^{-1}	0.248	0.246	0.236	0.117
θ Range/°	2.09 - 30.52	3.04 - 24.71	3.02 - 20.82	1.47 - 28.09
Ref (meas. / ind.)	16541 / 4375	40126 / 11817	14992 / 4731	12141 / 2115
Observed>2σ	3102	6294	2059	929
Rint	0.0746	0.1060	0.2357	0.0676
Completeness %	98.6	94.7	99.4	91.8
Parameters	260	1039	292	136
GooF	0.968	1.011	1.440	0.907
R_1 (obs)	0.0407	0.0803	0.2271	0.0568
R_1 (all)	0.0678	0.1562	0.3371	0.1327
wR2 (all)	0.1011	0.2812	0.5325	0.1636
$\rho_{max,min}$/e $Å^{-3}$	0.536, -0.468	1.161, -0.790	1.498, -1.383	0.323, -0.205

APPENDIX A5. Chapter 5 - Multi-Component Complexes of Piroxicam with Mono-substituted Benzoic Acids

Refinement details for all structures can be found in Table A-5.

Piroxicam: 2-Fluorobenzoic Acid (PXZ: 2FBA and PXN: 2FBA)

Single crystal X-ray diffraction data for the PXN: 2FBA complex were collected on a Bruker AXS Apex II CCD diffractometer.

Single crystal X-ray diffraction data for the PXZ: 2FBA complex were collected on a Bruker-Nonius Kappa CCD diffractometer. The disordered benzene ring of the 2-fluorobenzoic acid molecule has two possible positions which could be identified from the Fourier difference map. The two positions are too close to each other to allow a well-behaved anisotropic refinement. The isotropic thermal parameters of the corresponding carbon atoms of each benzene carbon were therefore constrained to be equal and the two sites allowed to refine freely against each other to an approximate 60: 40 occupancy. Attempts to model two positions of the carboxylic acid group on the 2-fluorobenzoic acid resulted in an increased R-factor when compared to the reported model and so a single site was retained for this group. This was further supported by the plausible thermal parameters of the carboxylic group. Hydrogen atoms not involved in hydrogen bonds were placed on calculated positions and refined as riding on the atoms to which they were bonded. The H-atoms involved in hydrogen bonds were then identified using Fourier difference synthesis.

Piroxicam: 3-Fluorobenzoic Acid (PXZ: 3FBA and PXN: 3FBA)

Single crystal X-ray diffraction data for the PXN: 3FBA complex were collected on a Bruker AXS Apex II CCD diffractometer.

Crystals of PXZ: 3FBA were particularly small and of poor quality and data were therefore collected using beamline I19 (EH1) at Diamond Light Source. Hydrogen atoms not involved in hydrogen bonds were placed on calculated positions and refined as riding on the atoms to which they were bonded. The H-atoms involved in hydrogen bonds were then identified using Fourier difference synthesis and allowed to freely refine but with the size of the thermal parameter constrained to be proportional to the atom to which it was bonded.

Piroxicam: 4-Fluorobenzoic Acid (PXZ: 4FBA and PXN: 4FBA)

Single crystal X-ray diffraction data for PXN: 4FBA were collected on a Bruker-Nonius Kappa CCD diffractometer and data for the PXZ: 4FBA complex collected on a Bruker AXS Apex II CCD diffractometer.

Piroxicam: 2-Chlorobenzoic Acid (Zwitterionic) (PXZ: 2CLBA)

Crystals of PXZ: 2CLBA were particularly small and of poor quality and data were therefore collected using beamline I19 (EH1) at Diamond Light Source.

Hydrogen atoms not involved in hydrogen bonds were placed on calculated positions and refined as riding on the atoms to which they were bonded. The H-atoms involved in hydrogen bonds were then identified using the Fourier synthesis.

Piroxicam: 3-Chlorobenzoic Acid (Non-Ionised) (PXN: 3CLBA)

Single crystal X-ray diffraction data for PXN: 3CLBA were collected on a Bruker AXS Apex II CCD diffractometer.

Piroxicam: 2-Bromobenzoic Acid (Zwitterionic) (PXZ: 2BRBA)

Single crystal X-ray diffraction data for PXN: 2BRBA were collected on a Bruker AXS Apex II CCD diffractometer.

Hydrogen atoms not involved in hydrogen bonds were placed on calculated positions and refined as riding on the atoms to which they were bonded. The H-atoms involved in hydrogen bonds were then identified using the Fourier difference synthesis.

Piroxicam: 3-Bromobenzoic Acid (Non-Ionised) (PXN: 3BRBA)

Single crystal X-ray diffraction data for PXN: 3BRBA were collected on a Bruker AXS Apex II CCD diffractometer.

Piroxicam: 2-Hydroxybenzoic Acid (Zwitterionic) (PXZ: 2HBA)

Single crystal X-ray diffraction data for PXZ: 2HBA were collected on a Bruker-Nonius Kappa CCD diffractometer.

Piroxicam: 3-Hydroxybenzoic Acid Monohydrate (Zwitterionic) (PXZ: 3HBA.H_2O)

Single crystal X-ray diffraction data for PXZ: 3HBA.H_2O were collected on a Bruker AXS Apex II CCD diffractometer.

Hydrogen atoms not involved in hydrogen bonds were placed on calculated positions and refined as riding on the atoms to which they were bonded. The H-atoms involved in hydrogen bonds were then identified using the Fourier synthesis.

The positions of H21 and H22 (water hydrogen atoms) were allowed to freely refine but the size of the thermal parameter was constrained to be proportional to the atom to which it was bonded.

Piroxicam: 2- Nitrobenzoic Acid (PXZ: 2NBA)

Single crystal X-ray diffraction data for PXZ: 2NBA were collected on a Bruker AXS Apex II CCD diffractometer.

Piroxicam: 3-Nitrobenzoic Acid (Non-Ionised) (PXN: 3NBA)

Single crystal X-ray diffraction data for PXZ: 3NBA were collected on a Bruker AXS Apex II CCD diffractometer.

Piroxicam: 4-Nitrobenzoic Acid Hydrate (Non-Ionised) (PXN: 4NBA.H_2O)

Single crystal X-ray diffraction data for PXZ:4NBA.H_2O were collected on a Bruker-Nonius Kappa CCD diffractometer.

Aromatic hydrogen atoms were placed on calculated positions and refined as riding on the atoms to which they were bonded. All other hydrogen atoms were located using the Fourier difference map and allowed to refine freely. The water molecule resides in a void with a large degree of freedom which makes modelling of it difficult. Estimation of the electron density (before assignment of the water oxygen atom) using the SQUEEZE procedure indicated 16 electrons were present in the unit cell (representing less than half a water molecule per asymmetric unit). The oxygen atom was refined at 30% to obtain plausible anisotropic thermal parameters. This position is likely to be the major position occupied by the water molecule. The water hydrogen atoms could not be located using Fourier difference synthesis.

Piroxicam: 2-Methylbenzoic Acid (Non-Ionised) (PXN: 2MBA)

Single crystal X-ray diffraction data for PXZ: 2MBA were collected on a Bruker AXS Apex II CCD diffractometer.

Piroxicam: 3-Methylbenzoic Acid (Zwitterionic) (PXZ: 3MBA)

Single crystal X-ray diffraction data for PXZ: 3MBA were collected on a Bruker-Nonius Kappa CCD diffractometer.

The methyl hydrogen atoms of the methylbenzoic acid molecule were placed in calculated positions and refined as riding on the carbon atom to which they were bonded to obtain plausible thermal parameters.

Piroxicam: 3-Methylbenzoic Acid Acetonitrile Solvate (Zwitterionic) (PXZ: 3MBA.ACN)

Single crystal X-ray diffraction data for PXZ: 3MBA.ACN were collected on a Bruker-Nonius Kappa CCD diffractometer.

Disordered complex PXZ: 3MBA.ACN was refined with 50: 50 occupancy of the two positions for the 3-methylbenzoic acid and acetonitrile molecules across an inversion centre. Due to overlapping regions of electron density, the thermal parameters of similar atoms were constrained to be equal to ensure a well-behaved refinement. This allowed anisotropic refinement of all non-hydrogen atoms.

H-atoms were identified using Fourier synthesis for the non-disordered PX molecule and the remaining disordered H-atoms placed in calculated positions with the exception of the carboxylic acid H24 which was found using Fourier difference synthesis and allowed to freely refine at 50% occupancy.

Piroxicam: 4-Methylbenzoic Acid (Zwitterionic) (PXZ: 4MBA)

Single crystal X-ray diffraction data for PXZ: 4MBA were collected using a Rigaku R-axis/RAPID image plate diffractometer.

The methyl hydrogen atoms of the methylbenzoic acid molecule were located initially using the Fourier difference synthesis and the bond distances and angles constrained to take standard values. The thermal parameters of the methyl hydrogen atoms were then refined as riding on the carbon atom to which they are bonded.

Piroxicam: 2-Aminobenzoic Acid (Zwitterionic) (PXZ: 2ABA)

Single crystal X-ray diffraction data for PXZ: 2ABA were collected on a Bruker-Nonius Kappa CCD diffractometer.

Table A-5 Crystallographic data for molecular complexes of piroxicam with mono-substituted benzoic acids

	PXZ:2FBA	**PXZ:3FBA**	**PXZ:4FBA**	**PXN:2FBA**	**PXN:3FBA**	**PXN:4FBA**	**PXZ:2CLBA**	**PXN:3CLBA**
Formula	(C15 H13 N3 O4 S), (C7 H5 F O2)	(C15 H13 N3 O4 S), (C7 H5 F O2)	(C15 H13 N3 O4 S), (C7 H5 F O2)	(C15 H13 N3 O4 S), (C7 H5 F O2)	(C15 H13 N3 O4 S), (C7 H5 F O2)	(C15 H13 N3 O4 S), (C7 H5 F O2)	(C15 H13 N3 O4 S), (C7 H5 Cl O2)	(C15 H13 N3 O4 S), (C7 H5 Cl O2)
M/g mol^{-1}	471.46	471.46	471.46	471.46	471.46	471.46	487.90	487.90
T/K	100	100	100	100	100	100	100	100
Space Group	$P2_1/c$	$P2_1/c$	P-1	P-1	P-1	$P4_2/n$	$P2_1/c$	P-1
a/Å	10.8016(3)	10.415(11)	6.7753(3)	8.4319(13)	8.4670(6)	24.4459(3)	19.768(17)	8.2160(5)
b/Å	20.9659(6)	21.17(2)	11.4738(4)	11.4199(18)	11.1895(9)	24.4459(3)	6.917(6)	10.9570(7)
c/Å	9.2105(2)	9.557(10)	13.7702(6)	12.3466(19)	12.2950(9)	6.9701(1)	31.56(3)	13.7261(9)
A	90	90	80.079(2)	115.410(6)	114.729(4)	90	90	67.227(4)
B	95.787(2)	100.053(13)	81.802(2)	95.966(7)	96.555(4)	90	100.693(12)	74.686(4)
Γ	90	90	76.925(2)	100.016(7)	98.491(4)	90	90	68.598(4)
V/$Å^3$	2075.23(9)	2075(4)	1021.12(7)	1036.0(3)	1026.17(13)	4165.4(4)	4240(7)	1049.85(12)
Z	4	4	2	2	2	8	8	2
ρ_{cal}/ g cm^{-3}	1.509	1.509	1.533	1.511	1.526	1.504	1.529	1.543
μ/mm^{-1}	0.212	0.212	0.216	0.213	0.215	0.212	0.251	0.329
θ Range/°	1.89- 25.36	1.90- 26.7	1.51-29.4	1.86-28.66	1.86-29.50	1.67-27.49	1.77-26.68	1.63-35.98
Ref. (meas. / ind.)	26715 / 3776	18646 / 4796	33567 / 5628	29514 / 5252	27127 / 5635	37056 / 4762	36761 / 9709	27036 /9418
Observed>2σ	2649	2932	4357	3808	2967	2886	5087	5619
Rint	0.0959	0.0934	0.068	0.1120	0.0883	0.1405	0.1402	0.0786
Completeness %	99.5	99.7	99.9	98.5	98.5	99.9	98.8%	94.8
Parameters	286	308	370	370	370	370	613	370
GooF	1.067	1.044	0.989	0.9610	0.947	0.956	1.094	0.8710
R_1 (obs)	0.0568	0.0952	0.0358	0.0441	0.0417	0.0440	0.1103	0.0454
R_1 (all)	0.0927	0.1437	0.0498	0.0683	0.0682	0.0998	0.1874	0.0851
wR2 (all)	0.1325	0.2938	0.0985	0.1062	0.1025	0.1058	0.2803	0.1014
$\rho_{max,min}$/e $Å^{-3}$	0.575, -0.486	1.224, -0.811	0.486, -0.367	0.473, -0.474	0.624, -0.461	0.250, -0.367	0.758, -0.688	0.694, -0.441

Table A-5 Crystallographic data for molecular complexes of piroxicam with mono-substituted benzoic acids continued.

	PXZ:2BRBA	**PXN:3BRBA**	**PXZ:2HBA**	**PXZ:3HBA.H_20**	**PXZ:2NBA**	**PXN:3NBA**	**PXN:4NBA.xH_2O**
Formula	(C15 H13 N3 O4 S), (C7 H5 Br O2)	(C15 H13 N3 O4 S), (C7 H5 Br O2)	(C15 H13 N3 O4 S), (C7 H6 O3)	(C15 H13 N3 O4 S), (C7 H6 O3), (H2O)	(C15 H13 N3 O4 S), (C7 H5 N O4)	(C15 H13 N3 O4 S), (C7 H5 N O4)	2(C15 H13 N3 O4 S), 2(C7 H5 N O4), 0.3(H2O)
M/g mol^{-1}	532.36	532.36	469.47	487.49	498.46	498.46	503.86
T/K	100	100	100	100	100	100	100
Space Group	P-1	P-1	$P2_1/n$	P-1	P-1	P-1	$P2_1/n$
a/Å	8.8280(5)	8.2526(8)	11.5454(5)	9.1121(11)	8.0433(7)	8.2304(4)	6.9031(2)
b/Å	10.9297(6)	11.0759(10)	9.2118(4)	9.9763(13)	11.0546(8)	10.8476(6)	36.7155(10)
c/Å	12.2953(11)	13.7895(18)	19.8419(9)	11.9501(16)	13.8361(11)	13.7358(7)	17.2917(5)
α	105.494(4)	101.575(5)	90	78.512(5)	99.646(4)	68.267(3)	90
β	98.381(4)	105.505(6)	102.438(2)	86.201(4)	106.649(4)	75.086(3)	100.571(1)
γ	105.396(3)	111.738(4)	90	88.375(5)	107.631(4)	69.107(3)	90
V/$Å^3$	1071.81(13)	1063.1(2)	2060.73(16)	1062.1(2)	1078.84(15)	1053.11(9)	4308.21
Z	2	2	4	2	2	2	4
ρ_{cal}/ g cm^{-3}	1.650	1.663	1.513	1.524	1.534	1.572	1.429
μ/mm^{-1}	2.062	2.079	0.210	0.210	0.210	0.215	0.107
θ Range/°	1.77-28.29	1.63-26.32	1.88-27.82	1.74-24.54	1.60-29.51	1.61-27.67	1.32-27.57
Ref (meas. / ind.)	26796 / 5269	26239 / 4328	20087 / 4853	19534 / 3477	25857 / 5764	27710 / 4908	58925 / 9869
Observed>2σ	4373	3370	2639	2050	4101	3448	5322
Rint	0.1107	0.0958	0.1531	0.1149	0.0895	0.0850	0.1440
Completeness %	98.8	99.9	99.1	97.9	95.9	99.6	99.3
Parameters	322	370	374	337	388	388	688
GooF	1.028	0.959	0.956	0.908	1.020	0.875	0.908
R_1 (obs)	0.0369	0.0305	0.0506	0.0471	0.0519	0.0380	0.460
R_1 (all)	0.0481	0.0470	0.1301	0.1032	0.0834	0.0620	0.1177
wR2 (all)	0.0969	0.0666	0.1044	0.1070	0.1251	0.0928	0.1005
$\rho_{max,min}$/e $Å^{-3}$	1.196, -0.577	0.625, -0.418	0.286, -0.399	0.351, -0.456	0.560, -0.416	0.490, -0.375	0.310, -0.440

Table A-5 Crystallographic data for molecular complexes of piroxicam with mono-substituted benzoic acids continued.

	PXN:2MBA	**PXZ:3MBA**	**PXZ:3MBA.MeCN**	**PXZ:4MBA**	**PXZ:2ABA**
Formula	(C15 H13 N3 O4 S), (C8 H8 O2)	(C15 H13 N3 O4 S), (C8 H8 O2)	2(C15 H13 N3 O4 S), (C8, H8, O2), (C2, H3, N)	(C15 H13 N3 O4 S), (C8 H8 O2)	(C15 H13 N3 O4 S), (C7 H7 N O2)
M/g mol^{-1}	467.5	467.5	839.91	467.5	468.48
T/K	100	100	100	100	100
Space Group	P-1	$P2_1/c$	P-1	P-1	P-1
a/Å	8.512(3)	9.4317(2)	8.4985(2)	9.5744(12)	6.8637(6)
b/Å	9.602(3)	11.3940(3)	9.8813(2)	10.4949(16)	11.6363(11)
c/Å	14.260(5)	20.4344(4)	12.5408(3)	12.5497(16)	13.8047(12)
α	82.134(23)	90	93.6020(10)	66.362(5)	83.313(4)
β	75.238(22)	99.9790(10)	104.0920(10)	73.077(4)	79.158(5)
γ	73.081(22)	90	112.1530(10)	75.292(5)	73.738(5)
V/$Å^3$	1075.7(6)	2162.76(8)	931.91(4)	1091.6(3)	1037.17(16)
Z	2	4	1	2	2
ρ_{cal}/ g cm^{-3}	1.443	1.436	1.497	1.422	1.500
μ/mm^{-1}	0.198	0.197	0.216	0.195	0.207
θ Range/°	1.48-28.22	2.02-25.35	1.00-27.10	3.18-27.48	1.83-26.03
Ref (meas. / ind.)	27724 / 5281	33953 / 3961	19882 / 4108	11677 / 4676	17744 / 4095
Observed>2σ	3924	2830	2874	2837	3035
Rint	0.0790	0.1275	0.1337	0.0829	0.0825
Completeness %	99.2	100	99.7	93.3	99.7
Parameters	382	371	341	371	378
GooF	1.032	0.994	1.071	1.033	1.051
R_1 (obs)	0.0410	0.0520	0.0929	0.1177	0.0770
R_1 (all)	0.0651	0.0881	0.0562	0.0651	0.0476
wR2 (all)	0.1010	0.1255	0.1493	0.1605	0.1137
$\rho_{max,min}$/e $Å^{-3}$	0.424, -0406	0.305, -0.428	0.535, -0.397	0.362, -0.600	0.216, -0.435

APPENDIX A6. Chapter 6 - Intermolecular Hydrogen Transfer in Multi-Component Complexes of Piroxicam

Refinement details for all structures can be found in Table A-6.

Piroxicam: Imidazole Hemihydrate (2(PX^-): 2(IM^+).H2O)

Single crystal X-ray diffraction data for this complex were collected on a Bruker AXS Apex II CCD diffractometer at 100K.

Hydrogen atoms not involved in conventional hydrogen bonds were placed on calculated positions and refined as riding on the atoms to which they were bonded. The hydrogen atoms involved in hydrogen bonds were then identified using the Fourier difference synthesis.

The positions of H33 and H34 (water hydrogen atoms) were allowed to freely refine but the size of the thermal parameter was constrained to be proportional to the atom to which it was bonded. Imidazole (B') NH hydrogen atoms (H35 and H36) were also treated in this way.

Piroxicam: Imidazole Acetonitrile Solvate (1:1:1) (PX^-: IM^+.ACN)

Single crystal X-ray diffraction data for this complex were collected on a Bruker AXS Apex II CCD diffractometer at 100K.

All hydrogen atoms were placed on calculated positions and refined as riding on the atoms to which they were bonded, with the exception of the hydrogen atoms on the IM+ nitrogens (H13 and H16), the PX^- amide nitrogen (H5), and the ACN methyl hydrogen atoms (H18, H19 and H20), which were located using the Fourier difference map and allowed to freely refine.

Piroxicam: Imidazole Acetonitrile Solvate (4:4:1) (4(PX^-): 4(IM^+).ACN)

Single crystal X-ray diffraction data for this complex were collected on a Bruker-Nonius Kappa CCD diffractometer at 100K.

Two positions of the disordered pyridine ring were modelled and refined against each other, with the thermal parameters of equivalent atoms constrained to be equal. The two positions refined to a 60: 40 occupancy ratio. Carbons C12A and C12B could not be modelled anisotropically as their relative positions are too close.

The ACN molecule was refined at 50% occupancy, and assumed to be disordered across the inversion centre with its position at least partially dependent on that of the PX^- pyridine ring (see Chapter 6: 6.2.3 for further details). The Fourier difference synthesis when reducing the occupancy of the ACN molecule did not indicate a second position within the asymmetric unit.

Hydrogen atoms not involved in conventional hydrogen bonds were placed on calculated positions and refined as riding on the atoms to which they were bonded. The hydrogen atoms involved in hydrogen bonds were then identified using the Fourier difference synthesis.

Piroxicam: 2-methylimidazole (PX^-: $2MIM^+$)

Single crystal X-ray diffraction data for this complex were collected on a Bruker AXS Apex II CCD diffractometer at 100K.

The $2MIM^+$ methyl group hydrogen atoms (H5A, H5B and H5C) were located initially using the Fourier difference synthesis and the bond distances and angles constrained to take standard values.

Piroxicam: Benzimidazole (PX^-: BZ^+)

Single crystal X-ray diffraction data for this complex complex were collected on a Bruker AXS Apex II CCD diffractometer at 100K.

Hydrogen atoms not involved in conventional hydrogen bonds were placed on calculated positions and refined as riding on the atoms to which they were bonded. The hydrogen atoms involved in conventional hydrogen bonds were then identified using a Fourier difference synthesis. Hydrogen atoms on the PX^- amide nitrogen atoms (H24 and H5) were allowed to freely refine but the size of the thermal parameter was constrained to be proportional to the atom to which it was bonded.

Piroxicam: 1, 2, 4 - Triazole (2PXZ: TZ)

Single crystal X-ray diffraction data for this complex were collected on a Bruker AXS Apex II CCD diffractometer at 100K.

The disordered TZ molecules were modelled with 50% occupancy across the inversion centre. The positions of the nitrogen atoms in the TZ molecules (N8 and N9, N11 and N12) lie too close to each other to allow a meaningful anisotropic refinement.

All hydrogen atoms on the TZ molecules were placed on calculated positions and refined as riding on the atoms to which they were bonded. Hydrogen atoms on the PXZ molecules that are not involved in conventional hydrogen bonds were placed on calculated positions and refined as riding on the atoms to which they were bonded. The hydrogen atoms involved in conventional hydrogen bonds were then identified using the Fourier difference synthesis.

Piroxicam: Benzotriazole (PXZ: BZT)

Single crystal X-ray diffraction data for this complex were collected on a Bruker-Nonius Kappa CCD diffractometer at 100K.

Piroxicam: Pyrazine (2PXZ: PZN)

Crystals of 2PXZ: PZN were particularly small and of poor quality and data were therefore collected using beamline I19 (EH1) at Diamond Light Source at 100K. Despite being collected using the synchrotron, the data was still weak and of poor quality. Significant data were missing along the z-axis, resulting in slight elongation of the thermal ellipsoids along this direction.

The tautomer of PX was inferred from the conformation of the molecule and the hydrogen bonding within the structure. The thermal parameters of pyrazine carbons C33 and C34 were constrained to be equal to allow a well behaved anisotropic refinement as the elongation was particularly pronounced in this molecule. All hydrogen atoms were placed on calculated positions and refined as riding on the atoms to which they were bonded.

Piroxicam: Chloranilic Acid Form I (PX^+: CA^-) (Triclinic)

Single crystal X-ray diffraction data for the PXN: 2FBA complex were collected on a Bruker AXS Apex II CCD diffractometer at 100K.

Piroxicam: Chloranilic Acid Form II (PX^+: CA^-) (monoclinic)

Single crystal X-ray diffraction data for the PXN: 2FBA complex were collected on a Bruker AXS Apex II CCD diffractometer at 100K.

Piroxicam: Chloranilic Acid Acetonitrile Solvate (2(PX^+): CA^{2-}.2(ACN))

Single crystal X-ray diffraction data for the PXN: 2FBA complex were collected on a Bruker AXS Apex II CCD diffractometer at 100K.

All hydrogen atoms were located using the Fourier difference synthesis with the exception of the methyl group hydrogen atoms of PX^+ and ACN which were located initially using the Fourier difference synthesis and the bond distances and angles constrained to take standard values.

Piroxicam: Bromanilic Acid (PX^+: BRA^-)

Single crystal X-ray diffraction data for the PXN: 2FBA complex were collected on a Bruker AXS Apex II CCD diffractometer at 100K.

The hydrogen of the BRA hydroxyl was located initially using the Fourier difference synthesis and the O-H bond distance constrained to take a standard value. The bond angle was constrained to be equal to that of the equivalent O-H bond in the isomorphous PX^+:CA^- II complex. All other hydrogen atoms were located using the Fourier difference map. The thermal parameters of the PX^+ aromatic hydrogen atoms were refined as riding on the atoms to which they were bonded.

Table A-6a Crystallographic data for molecular complexes of piroxicam with N-heterocycles.

	$2(PX^-):2(IM^+).H2O$	**$PX^-:IM^+.ACN$**	**$4(PX^-):4(IM^+).ACN$**	**$PX^-:2MIM^+$**
Formula	2(C15 H12 N3 O4 S), 2(C3 H5 N2), H2O	(C15 H12 N3 O4 S), (C3 H5 N2), (C2 H3 N)	4(C15 H12 N3 O4 S), 4(C3 H5 N2), (C2 H3 N)	(C15 H12 N3 O4 S), (C4 H7 N2)
M/g mol^{-1}	816.89	440.48	1638.78	413.46
T/K	100	100	100	100
Space Group	P-1	$P2_1/c$	$P2_1/n$	$P2_1/n$
a/Å	6.8019(4)	8.1510(5)	6.9103(1)	10.9928(8)
b/Å	14.4384 (8)	26.5997(17)	22.1444(5)	15.3135(15)
c/Å	19.8727(12)	10.1579(7)	25.1813(5)	12.551(1)
α	90.460(2)	90	90	90
β	99.276(2)	113.394(3)	97.068(1)	112.039(4)
γ	101.460(2)	90	90	90
$V/Å^3$	1886.1(2)	2021.3(2)	3824.07(13)	1958.4(3)
Z	2	4	2	4
ρ_{cal}/ g cm^{-3}	1.438	1.447	1.423	1.402
μ/mm^{-1}	0.211	0.202	0.207	0.202
θ Range/°	1.44 - 23.51	1.53 - 29.61	1.63 - 27.08	2.11 - 28.31
Ref. (meas. / ind.)	39268/ 5468	31622/ 5639	56462/ 8406	22807/ 4828
Observed>2σ	2890	4387	4565	3085
Rint	0.1704	0.1084	0.1572	0.1100
Completeness %	97.6	99.0	99.9	99.1
Parameters	544	305	592	327
GooF	0.950	1.127	0.978	0.985
R_1 (obs)	0.0565	0.0601	0.0572	0.0567
R_1 (all)	0.1541	0.0797	0.1322	0.1021
wR2 (all)	0.0989	0.1699	0.1456	0.1309
$\rho_{max,min}$/e $Å^{-3}$	0.337, -0.323	0.594, -0.597	0.327, -0.389	0.519, -0.373

Table A-6a Crystallographic data for molecular complexes of piroxicam with N-heterocycles continued.

	PX^-: BZ^+	**2PXZ: TZ**	**PXZ: BZT**	**2PXZ: PZN**
Formula	(C15 H12 N3 O4 S), (C7 H7 N2)	2(C15 H13 N3 O4 S), (C2 H3 N3)	(C15 H13 N3 O4 S), (C6 H5 N3)	2(C15 H13 N3 O4 S), (C4 H4 N2)
M/g mol^{-1}	449.48	731.76	450.47	742.80
T/K	100	100	100	100
Space Group	P-1	P-1	$P2_1/c$	P-1
a/Å	12.005(3)	6.9267(2)	11.6101(6)	6.792(11)
b/Å	13.789(3)	8.3356(3)	26.2908(15)	8.646(15)
c/Å	13.810(4)	28.8177(10)	6.7710(3)	29.66(5)
α	72.186(7)	86.485(2)	90	94.159(11)
β	68.682(7)	84.209(2)	103.480(3)	90.51(2)
γ	80.962(7)	76.271(1)	90	104.78(4)
V/$Å^3$	2024.8(8)	1606.89(9)	2009.8(2)	1679(5)
Z	4	2	4	2
ρ_{cal}/ g cm^{-3}	1.474	1.512	1.489	1.469
μ/mm^{-1}	0.202	0.235	0.205	0.225
θ Range/°	1.55 - 23.90	0.71 - 28.26	1.96 - 25.35	2.00 - 25.93
Ref. (meas. / ind.)	23716/ 6114	35311/ 7358	22167/ 2942	17445/ 6529
Observed>2σ	2700	5437	2320	2898
Rint	0.1716	0.0857	0.0444	0.2110
Completeness %	97.2	92.6	80.2	90.8
Parameters	598	503	361	387
GooF	0.882	1.096	1.085	1.246
R_1 (obs)	0.0617	0.0616	0.0542	0.1767
R_1 (all)	0.1856	0.0916	0.0716	0.2680
wR2 (all)	0.1045	0.1457	0.1512	0.4928
$\rho_{max,min}$/e $Å^{-3}$	0.328, -0.342	0.544, -0.457	0.852, -0.373	0.956, -0.723

Table A-6b Crystallographic data for molecular complexes of piroxicam with strong acids.

	PX^+: CA^- (I)	**PX^+: CA^- (II)**	**2(PX^+): CA^{2-}.2(ACN)**	**PX^+: BRA^-**
Formula	(C15 H14 N3 O4 S), (C6 H Cl2 O4)	(C15 H14 N3 O4 S), (C6 H Cl2 O4)	2(C15 H14 N3 O4 S), (C6 Cl2 O4), 2(C2 H3 N)	(C15 H14 N3 O4 S), (C6 H Br2 O4)
M/g mol^{-1}	540.32	540.32	476.89	629.24
T/K	100	100	100	100
Space Group	P-1	$P2_1/c$	P-1	$P2_1/c$
a/Å	9.1504(4)	8.5627(5)	7.0616(8)	8.842(2)
b/Å	10.9678(4)	13.3395(7)	11.6031(13)	13.437(2)
c/Å	11.7747(5)	19.3963(12)	13.2994(17)	19.242(4)
α	89.228(2)	90	71.351(5)	90
β	75.765(2)	100.925(3)	84.932(5)	100.518(11)
γ	70.977(2)	90	78.919(5)	90
V/$Å^3$	1080.00(8)	2175.3(2)	1012.8(2)	2247.8(7)
Z	2	4	1	4
ρ_{cal}/ g cm^{-3}	1.662	1.650	1.564	1.859
μ/mm^{-1}	0.455	0.452	0.340	3.755
θ Range/°	1.79 - 30.56	1.86 - 27.72	1.62 - 24.95	1.86 - 27.83
Ref (meas. / ind.)	30881/ 6607	39751/ 5083	14653/ 2948	64513/ 5309
Observed>2σ	4819	3284	1959	3938
Rint	0.0665	0.0920	0.1007	0.0952
Completeness %	99.8	99.4	82.9	99.4
Parameters	376	376	335	366
GooF	0.945	0.922	0.981	0.917
R_1 (obs)	0.0376	0.0397	0.0447	0.0320
R_1 (all)	0.0586	0.0797	0.0895	0.0492
wR2 (all)	0.0909	0.0762	0.1058	0.0793
$\rho_{max,min}$/e $Å^{-3}$	0.524, -0.320	0.474, -0.458	0.400, -0.366	1.092, -0.556

APPENDIX A7. Chapter 7 - Controlling Molecular Complex Formation of Paracetamol and its Derivatives

Refinement details for all structures can be found in Table A-7.

Paracetamol: Imidazole (PA: IM)

Single crystal X-ray diffraction data for this complex were collected on a Bruker AXS Apex II CCD diffractometer at 100K.

Paracetamol: 2-methylimidazole (1:2) (PA: 2MIM)

Single crystal X-ray diffraction data for this complex were collected on a Bruker AXS Apex II CCD diffractometer at 100K.

All H-atoms were identified using a Fourier difference synthesis with the exception of the methyl group hydrogen atoms on the 2MIM molecules (H4, H5, H6 and H10, H11, H12) which were located initially using a Fourier difference synthesis and the bond distances and angles constrained to take standard values.

Piroxicam: 4-methylImidazole (PA: 4MIM)

Single crystal X-ray diffraction data for this complex were collected on a Bruker AXS Apex II CCD diffractometer at 100K.

4-acetamidobenzoic acid: Imidazole ($4ABA^-$: IM^+)

Single crystal X-ray diffraction data for this complex were collected on a Rigaku R-AXIS RAPID Image Plate diffractometer at 100K.

The absolute structure was not determined in the analysis as it was not required for the purpose of this work.

4-acetamidobenzoic acid: 2-methylimidazole (2:1) ($4ABA^-$: $2MIM^+$)

Single crystal X-ray diffraction data for this complex were collected on a Bruker-Nonius Kappa CCD diffractometer at 100K.

All H-atoms were identified from a Fourier difference synthesis with the exception of the methyl group hydrogen atoms on the $2MIM^+$ molecule (H1, H2 and H3) and the $4ABA^-$ molecule (H20, H21 and H22) which were located initially using the Fourier difference synthesis and the bond distances and angles constrained to take standard values.

4-acetamidobenzoic acid: 4-methylimidazole ($4ABA^-$: $4MIM^+$)

Single crystal X-ray diffraction data for this complex were collected on a Bruker-Nonius Kappa CCD diffractometer at 100K.

4-acetamidobenzoic acid: benzimidazole monohydrate ($4ABA^-$: BZ^+. H2O)

Single crystal X-ray diffraction data for this complex were collected on a Bruker AXS Apex II CCD diffractometer at 100K.

One hydrogen atom of the BZ^+ molecule (H7) shows significant elongation of its electron density towards the acceptor oxygen atom to which it is hydrogen bonded. The hydrogen has been placed on the electron density maximum bonded to the BZ molecule. Analysis of the bond lengths in both molecules indicate that the BZ molecule is indeed protonated and the 4ABA molecule is deprotonated suggesting this is the most accurate model possible with X-ray data. This is discussed further in Chapter 7.

4-acetamidobenzoic acid: 4, 4 - bipyridine (2:1) (4ABA: BP)

Single crystal X-ray diffraction data for this complex were collected on a Bruker-Nonius Kappa CCD diffractometer at 100K.

4-acetamidobenzoic acid: 2-picoline (4ABA: 2PIC)

Single crystal X-ray diffraction data for this complex were collected on a Bruker AXS Apex II CCD diffractometer at 100K.

4-acetamidobenzoic acid: 3-picoline (4ABA: 3PIC)

Single crystal X-ray diffraction data for this complex were collected on a Bruker-Nonius Kappa CCD diffractometer at 100K.

4-acetamidobenzoic acid: 4-picoline (4ABA: 4PIC)

Single crystal X-ray diffraction data for this complex were collected on a Bruker AXS Apex II CCD diffractometer at 100K.

Table A-7a Crystallographic data for molecular complexes of paracetamol with N-heterocycles.

	PA: IM	**PA: 2MIM (1:2)**	**PA: 4MIM**
Formula	(C8 H9 N O2), (C3 H4 N2)	(C8 H9 N O2), 2(C4 H6 N2)	(C8 H9 N O2), (C4 H6 N2)
M/g mol^{-1}	219.24	315.38	233.27
T/K	100	100	100
Space Group	$P2_1/c$	C2/c	Pbca
a/Å	9.770(2)	30.940(2)	9.9578(6)
b/Å	8.661(2)	7.7357(6)	13.7235(7)
c/Å	13.545(3)	13.9295(9)	18.1220(10)
α	90	90	90
β	108.331(11)	91.046(4)	90
γ	90	90	90
V/$Å^3$	1088.1(4)	3333.3(4)	2476.5(2)
Z	4	8	8
ρ_{cal}/ g cm^{-3}	1.338	1.257	1.251
μ/mm^{-1}	0.095	0.086	0.088
θ Range/°	2.20 - 31.10	1.32 - 26.79	2.25 - 33.38
Ref. (meas. / ind.)	31131 / 3485	26420 / 3536	47349 / 4802
Observed>2σ	2803	2007	3257
Rint	0.0446	0.1157	0.1278
Completeness %	99.6	99.2	99.9
Parameters	197	270	214
GooF	1.032	0.900	0.959
R_1 (obs)	0.0421	0.0465	0.0477
R_1 (all)	0.0549	0.1053	0.0768
wR2 (all)	0.1173	0.0977	0.1349
$\rho_{max,min}$/e $Å^{-3}$	0.498, -0.189	0.249, -0.193	0.488, -0.224

Table A-7b Crystallographic data for molecular complexes of 4-acetamidobenzoic acid with N-heterocycles.

	$4ABA^-$: IM^+	**4ABA: $4ABA^-$: $2MIM^+$**	**$4ABA^-$: $4MIM^+$**	**$4ABA^-$: BZ^+. H2O**
Formula	(C9 H8 N O3), (C3 H5 N2)	(C9 H9 N1 O3), (C9 H8 N1 O3), (C4 H7 N2)	(C9 H8 N O3), (C4 H7 N2)	(C9 H8 N O3), (C7 H7 N2), (H2O)
M/g mol^{-1}	247.25	440.45	261.28	315.33
T/K	100	100	100	100
Space Group	P 2_1 2_1 2_1	$P2_1/n$	$P2_1/c$	$P2_1/c$
a/Å	6.90430(10)	7.35450(10)	13.4181(7)	4.0287(3)
b/Å	8.7161(2)	9.6675(2)	10.0408(6)	32.217(2)
c/Å	39.8192(7)	31.1406(5)	9.4283(6)	11.7052(9)
A	90	90	90	90
B	90	96.0140(10)	107.342(3)	92.541(4)
Γ	90	90	90	90
V/$Å^3$	2396.26(8)	2201.90(6)	1212.52(12)	1517.8(2)
Z	8	4	4	4
ρ_{cal}/ g cm^{-3}	1.371	1.329	1.431	1.380
μ/mm^{-1}	0.101	0.098	0.104	0.101
θ Range/°	3.07 - 27.47	2.21 - 27.88	1.59 - 27.48	1.26 - 25.260
Ref (meas. / ind.)	10048 / 5411	41495 / 5229	94055 / 2759	17870 / 2742
Observed>2σ	5083	4183	1814	1748
Rint	0.0145	0.0811	0.0903	0.1093
Completeness %	99.0	99.7	99.4	99.8
Parameters	429	363	232	276
GooF	1.150	1.129	1.022	0.989
R_1 (obs)	0.0293	0.0543	0.0440	0.0513
R_1 (all)	0.0339	0.0709	0.0864	0.1002
Wr2 (all)	0.0978	0.1433	0.1034	0.1197
$\rho_{max,min}$/e $Å^{-3}$	0.289, -0.231	0.478, -0.323	0.254, -0.209	0.275, -0.214

Table A-7b Crystallographic data for molecular complexes of 4-acetamidobenzoic acid with N-heterocycles continued.

	4ABA: Bipy (2:1)	**4ABA: 2PIC**	**4ABA: 3PIC**	**4ABA: 4PIC**
Formula	(C9 H9 N O3), 0.5(C10 H8 N2)	(C9 H9 N O3), (C6 H7 N1)	(C9 H9 N O3), (C6 H7 N)	(C9 H9 N O3), (C6 H7 N)
M/g mol^{-1}	257.26	272.30	272.30	272.30
T/K	100	100	100	100
Space Group	$P2_1/c$	$P2_1/c$	$P2_1/c$	$P2_1/n$
a/Å	12.8097(11)	11.392(2)	7.6215(2)	12.3881(16)
b/Å	9.7699(7)	8.7690(13)	18.7544(7)	8.9244(14)
c/Å	10.1260(8)	14.476(3)	9.8712(3)	13.780 (2)
A	90	90	90	90
B	98.212(5)	108.381(8)	97.363(2)	114.754(7)
Γ	90	90	90	90
V/$Å^3$	1254.3(2)	1372.3(4)	1399.32(8)	1383.5(3)
Z	4	4	4	4
ρ_{cal}/ g cm^{-3}	1.362	1.318	1.293	1.307
μ/mm^{-1}	0.10	0.093	0.091	0.092
θ Range/°	1.61 - 31.580	1.88 - 22.67	2.17 - 27.13	1.86 - 27.43
Ref (meas. / ind.)	37929 / 4201	14193 / 1839	19804 / 3079	19020 / 3145
Observed>2σ	2873	1190	2355	2339
Rint	0.0848	0.1292	0.0483	0.0928
Completeness %	99.9	99.9	99.7	99.6
Parameters	224	245	245	245
GooF	0.952	1.073	1.058	0.941
R_1 (obs)	0.0440	0.0498	0.0428	0.0383
R_1 (all)	0.0710	0.0972	0.0648	0.0529
wR2 (all)	0.1178	0.0972	0.1019	0.0973
$\rho_{max,min}$/e $Å^{-3}$	0.449, -0.190	0.202, -0.191	0.204, -0.195	0.267, -0.203

APPENDIX A8. Chapter 8 - Additional Molecular Complexes of APIs

Refinement details for all structures can be found in Table A-8.

Paracetamol : Maleic Acid (PA:MA)

Single crystal X-ray diffraction data for this complex were collected on a Bruker-Nonius Kappa CCD diffractometer at 100K.

Paracetamol : Citraconic Acid (PA:CCA)

Single crystal X-ray diffraction data for this complex were collected on a Bruker AXS Apex II CCD diffractometer at 100K.

Piracetam : Gallic Acid (PTM:GA)

Single crystal X-ray diffraction data for this complex were collected on a Rigaku R-AXIS RAPID Image Plate diffractometer at 100K.

Piracetam : Citraconic Acid (PTM:CCA)

Single crystal X-ray diffraction data for this complex were collected on a Bruker AXS Apex II CCD diffractometer at 100K.

Piracetam : Chloranilic Acid (PTM:CA)

Single crystal X-ray diffraction data for this complex were collected on a Bruker AXS Apex II CCD diffractometer at 100K.

Piracetam : Bromanilic Acid (PTM:BRA)

Single crystal X-ray diffraction data for this complex were collected on a Bruker AXS Apex II CCD diffractometer at 100K.

Four large electron density peaks were remaining on the Fourier difference map after full assignment of the structure, of size 1.39 - 1.65 $e^-/Å^3$. The proximity of these peaks to the Br atoms suggests they are not missing atoms (all peaks lie approximately 0.85Å from Br atoms).

Table A-8a Crystallographic data for molecular complexes of paracetamol with maleic acid and citraconic acid.

	PA:MA	**PA:CCA**
Formula	C8 H9 N O2, C4 H4 O4	C8 H9 N O2, C5 H6 O4
M/g mol^{-1}	267.13	281.26
T/K	100	100
Space Group	P-1	$P2_1/c$
a/Å	7.24700(10)	7.061(1)
b/Å	11.13330(10)	23.607(3)
c/Å	15.7616(2)	7.677(1)
α	71.6440(6)	90
β	84.0490(7)	92.930(8)
γ	80.4430(6)	90
V/$Å^3$	1188.44(2)	1278.1(4)
Z	4	4
ρ_{cal}/ g cm^{-3}	1.493	1.462
μ/mm^{-1}	0.121	0.117
θ Range/°	1.36 - 27.49	1.73 - 26.36
Ref. (meas. / ind.)	45715 / 5436	16355 / 2614
Observed>2σ	4695	1318
Rint	0.0328	0.1304
Completeness %	99.5	99.7
Parameters	447	241
GooF	1.036	0.917
R_1 (obs)	0.0314	0.0450
R_1 (all)	0.0390	0.1322
wR2 (all)	0.0829	0.0822
$\rho_{max,min}$/e $Å^{-3}$	0.305, -0.229	0.233, -0.218

Table A-8b Crystallographic data for molecular complexes of piracetam with gallic acid, citraconic acid, chloranilic acid and bromanilic acid.

	PTM:GA	**PTM:CCA**	**PTM:CA**	**PTM:BRA**
Formula	C6 H10 N2 O2, C7 H6 O5	C6 H10 N2 O2, C5 H6 O4	C6 H10 N2 O2, C6 H2 O4 Cl2	C6 H10 N2 O2, C6 H2 O4 Br2
M/g mol^{-1}	312.28	272.26	351.14	440.04
T/K	100	100	100	100
Space Group	$P2_1/c$	P-1	P-1	$P2_1/n$
a/Å	12.554(2)	7.2737(4)	5.3052(4)	5.2279(2)
b/Å	8.8499(15)	8.9268(5)	11.2111(9)	25.1285(11)
c/Å	12.6253(17)	10.6101(6)	12.3555(12)	11.3404(5)
A	90	95.793(3)	100.689(4)	90
B	103.988(5)	105.310(3)	91.025(4)	103.168(2)
Γ	90	100.116(3)	96.568(4)	90
V/$Å^3$	1361.1(4)	646.22(6)	716.80(11)	1450.61(11)
Z	4	2	2	4
ρ_{cal}/ g cm^{-3}	1.524	1.399	1.627	2.015
μ/mm^{-1}	0.125	0.115	0.484	5.620
θ Range/°	3.08 - 27.48	2.01 - 31.95	1.68 - 25.90	1.62 - 30.03
Ref (meas. / ind.)	10236 / 3044	22460 / 4071	11710 / 2789	34033 / 4231
Observed>2σ	1684	2905	1762	3565
Rint	0.0958	0.0550	0.1113	0.0989
Completeness %	97.5	100	99.7	99.8
Parameters	263	236	247	247
GooF	1.056	0.930	0.928	1.001
R_1 (obs)	0.0562	0.0374	0.0457	0.0317
R_1 (all)	0.1209	0.0576	0.0910	0.0397
wR2 (all)	0.1633	0.0898	0.1020	0.0790
$\rho_{max,min}$/e $Å^{-3}$	0.355, -0.427	0.460, -0.205	0.395, -0.345	1.646, -0.640

APPENDIX B: Powder X-ray Diffraction

Appendix B4a - Powder X-ray Diffraction of Paracetamol Form II from Multi-Component Crystallisations (Section 4.2)

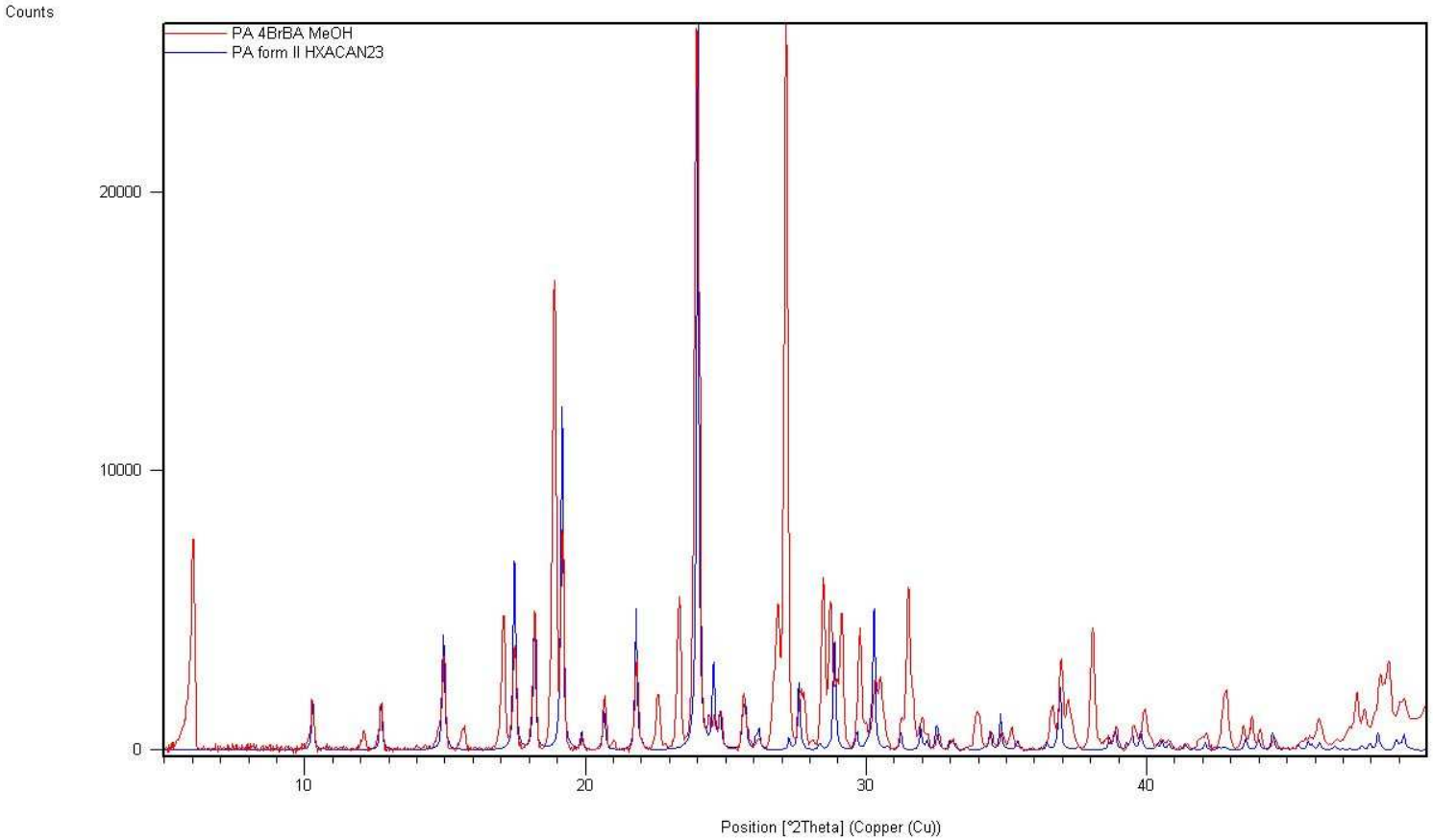

Appendix B4a-1 PXRD analysis of the co-crystallisation of paracetamol and 4-bromobenzoic acid in methanol (red) overlaid with the calculated PXRD pattern of paracetamol form II (blue). The pattern shows unambiguously the presence of paracetamol form II in approximately 100% quantities.

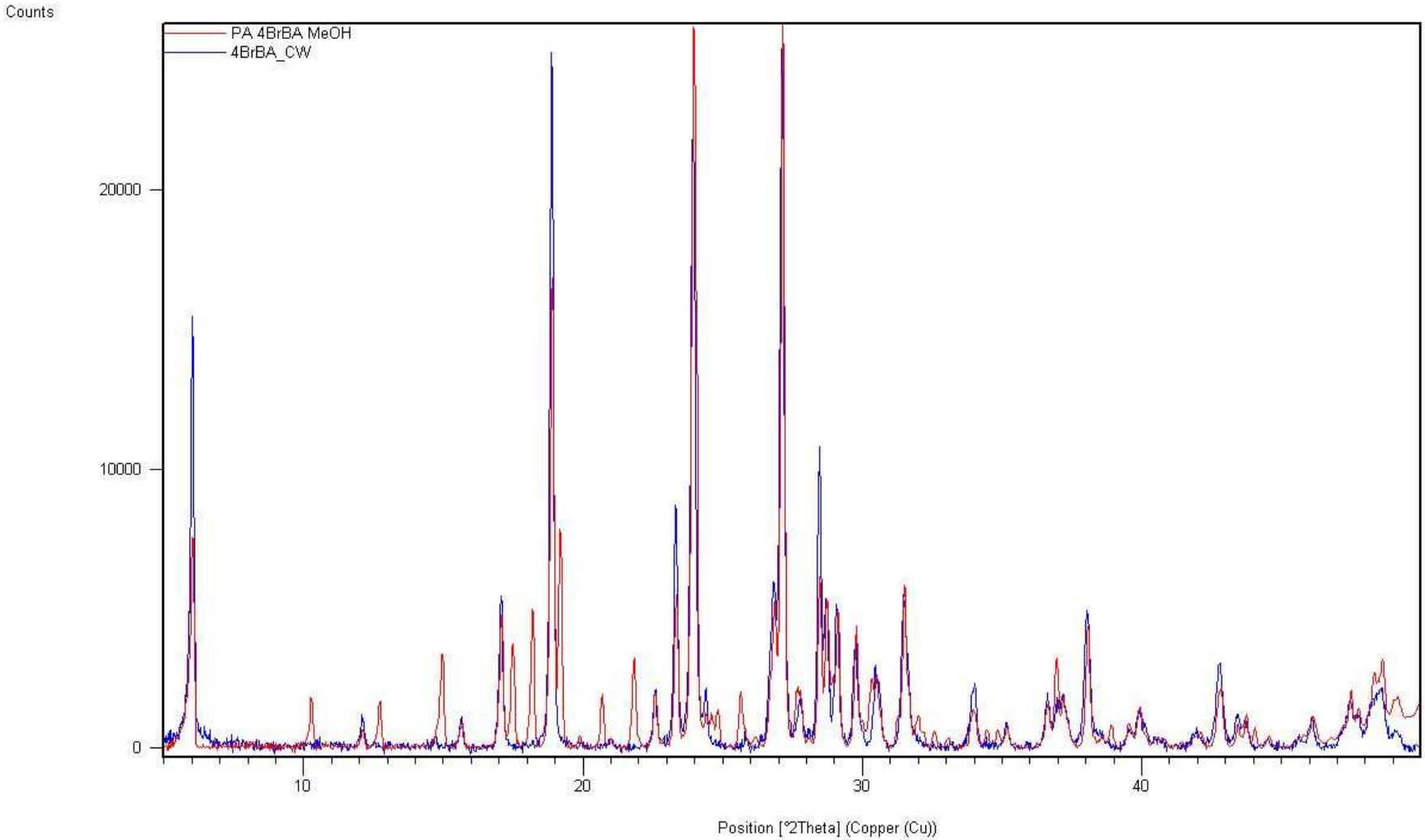

Appendix B4a-1 PXRD analysis of the co-crystallisation of paracetamol and 4-bromobenzoic acid in methanol (red) overlaid with the experimental PXRD pattern of 4-bromobenzoic acid (blue). The pattern shows that all peaks not corresponding to paracetamol form II correspond to 4-bromobenzoic acid.

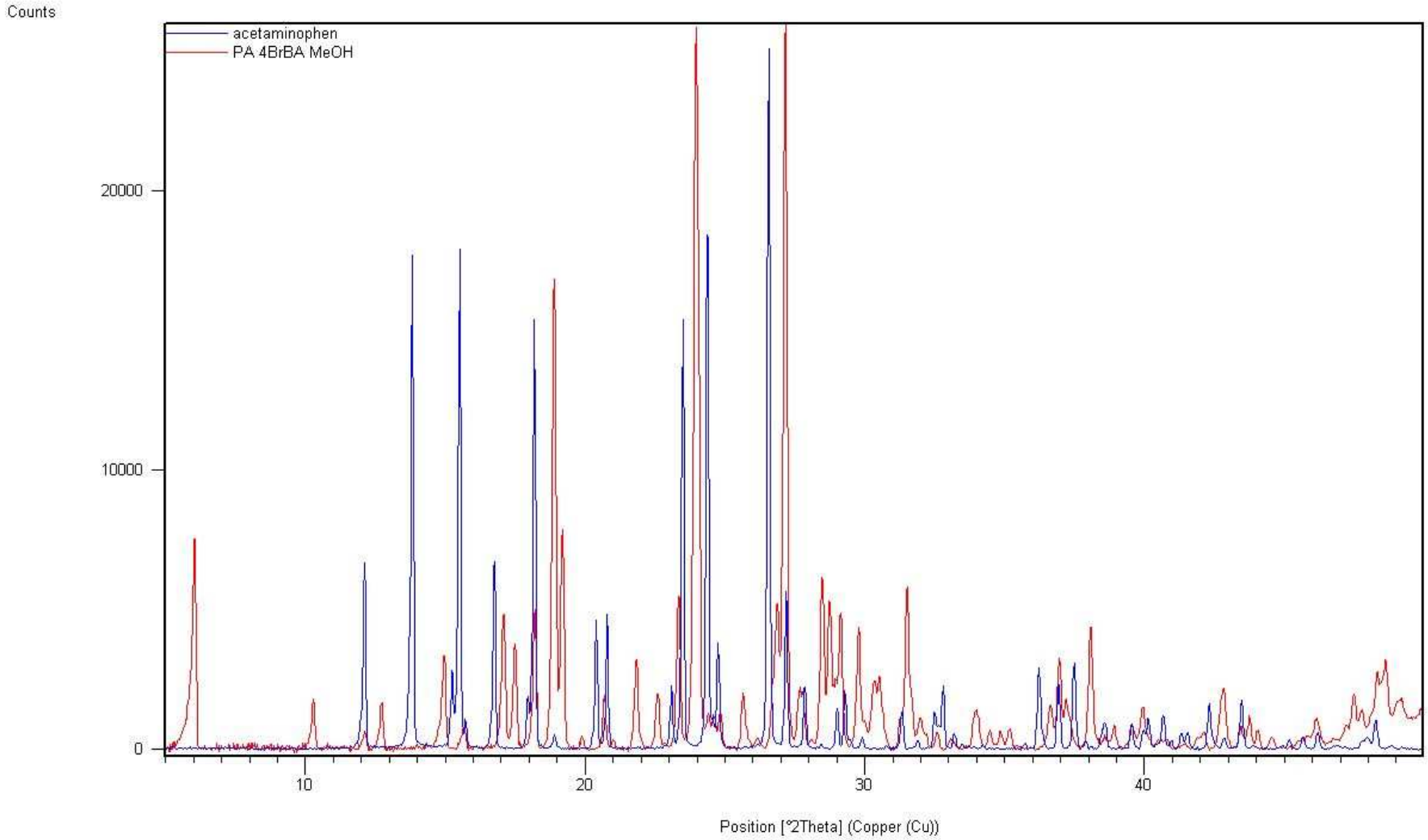

Appendix B4a-1 PXRD analysis of the co-crystallisation of paracetamol and 4-bromobenzoic acid in methanol (red) overlaid with the experimental PXRD pattern of paracetamol form I (blue). The pattern shows that no paracetamol form I is present in the sample.

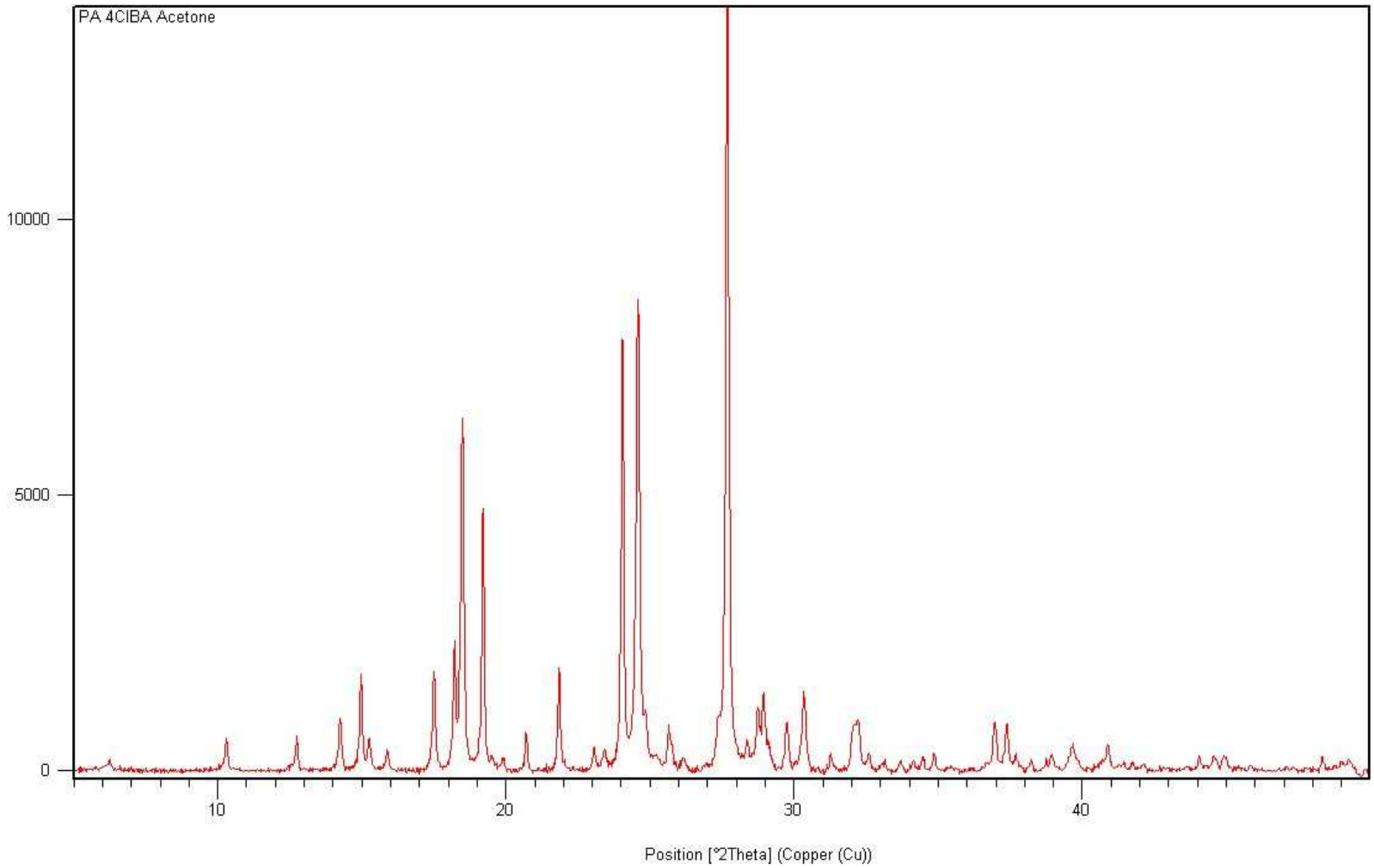

Appendix B4a-2 PXRD of the co-crystallisation of paracetamol with 4-chlorobenzoic acid in acetone. The pattern shows a mixture of 4ClBA and PA II in 100% yield.

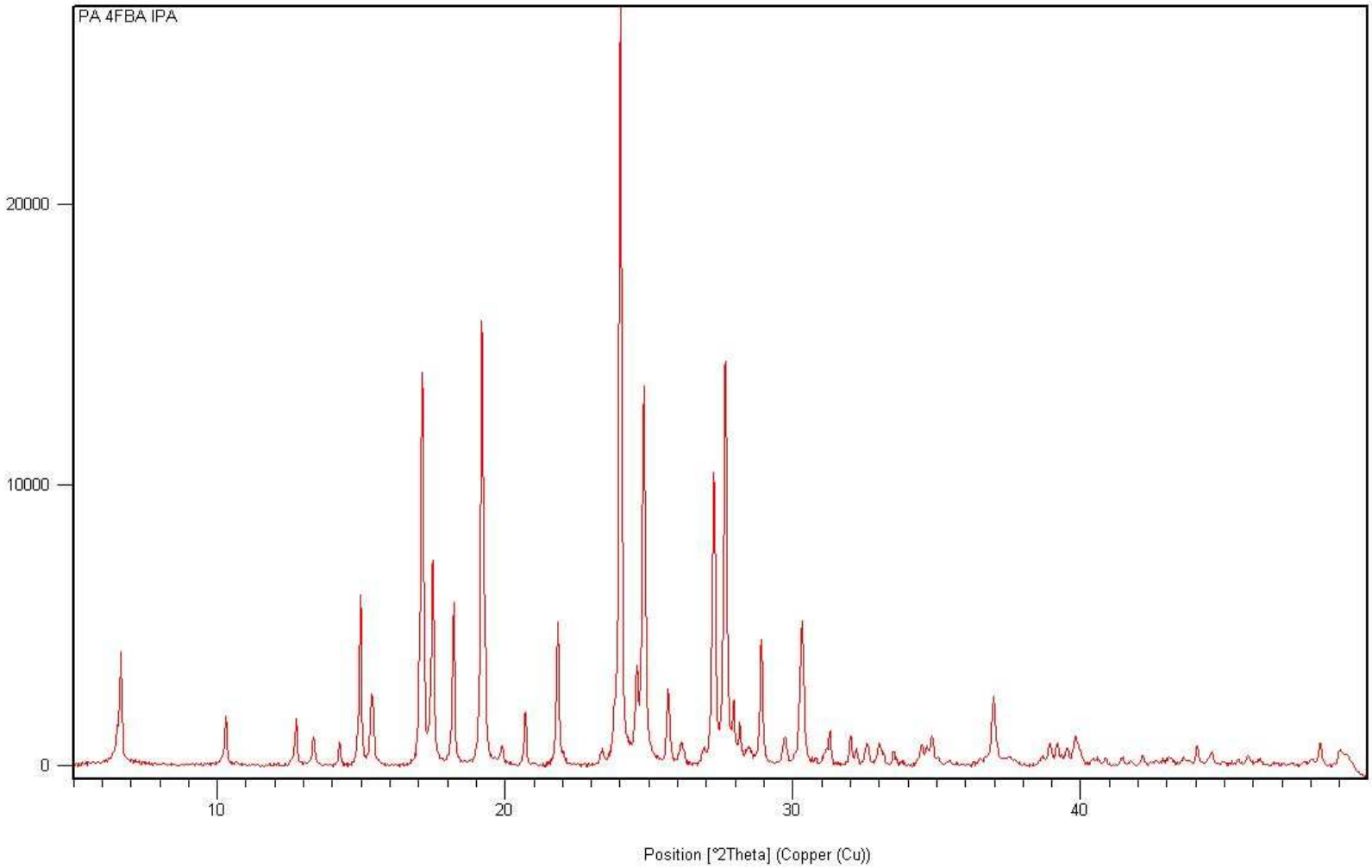

Appendix B4a-3 PXRD of the co-crystallisation of paracetamol with 4-fluorobenzoic acid in IPA. The pattern shows a mixture of 4FBA and PA II in 100% yield.

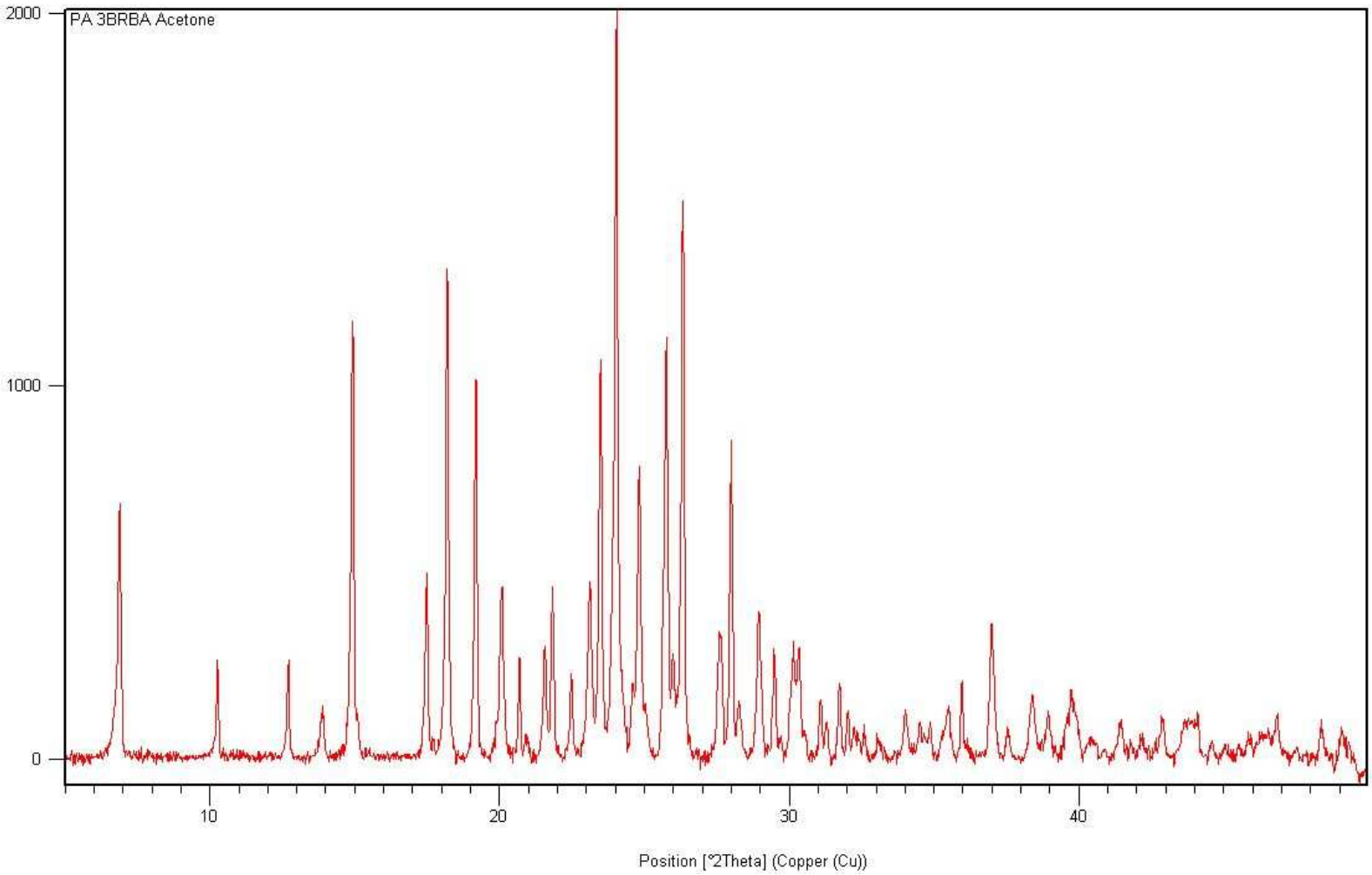

Appendix B4a-4 PXRD of the co-crystallisation of paracetamol with 3-bromobenzoic acid in acetone. The pattern shows a mixture of 3BRBA and PA II in 100% yield.

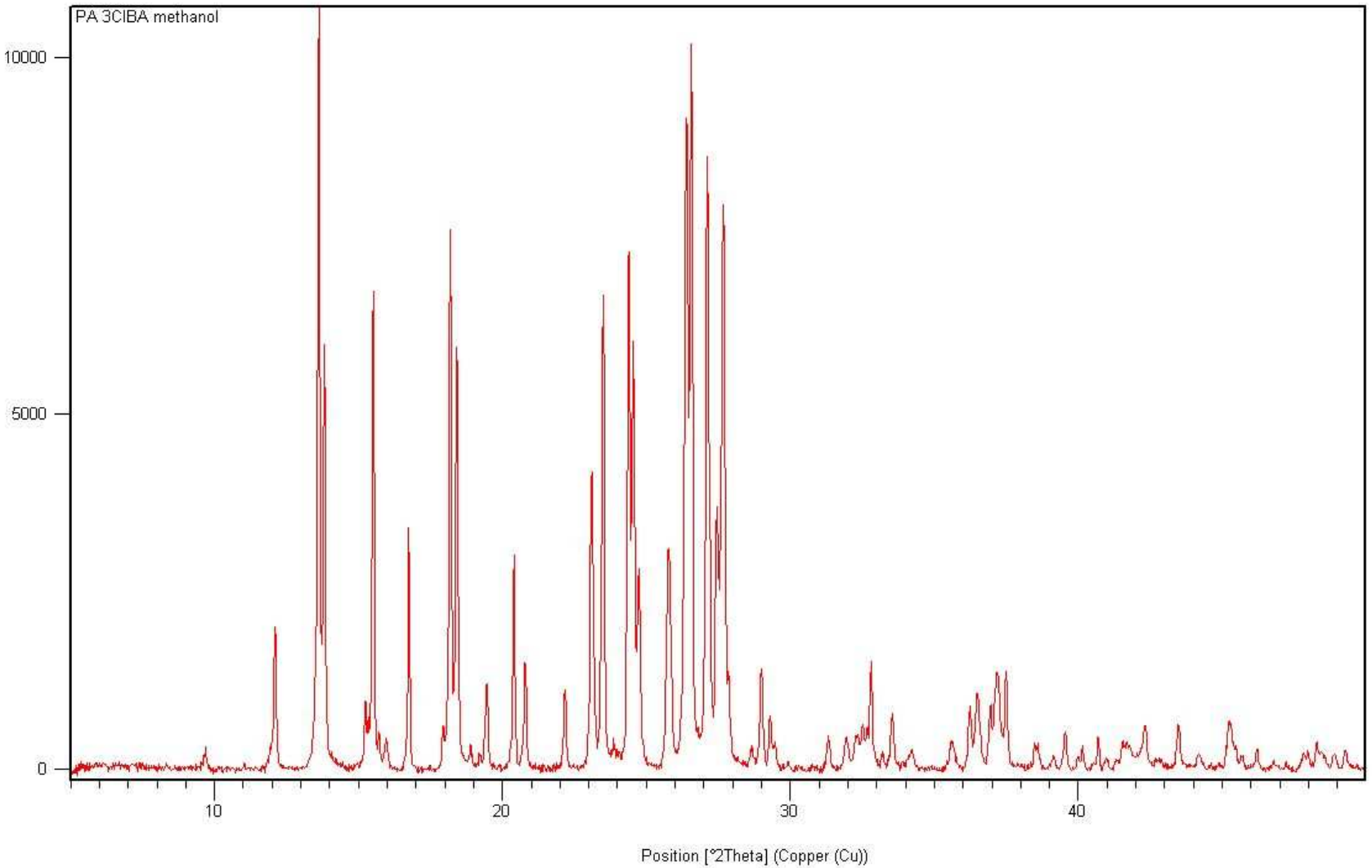

Appendix B4a-5 PXRD of the co-crystallisation of paracetamol with 3-chlorobenzoic acid in methanol. The pattern shows a mixture of 3ClBA and PA I in 100% yield. No PA II was found to be present in the co-crystallisation with 3ClBA that were analysed.

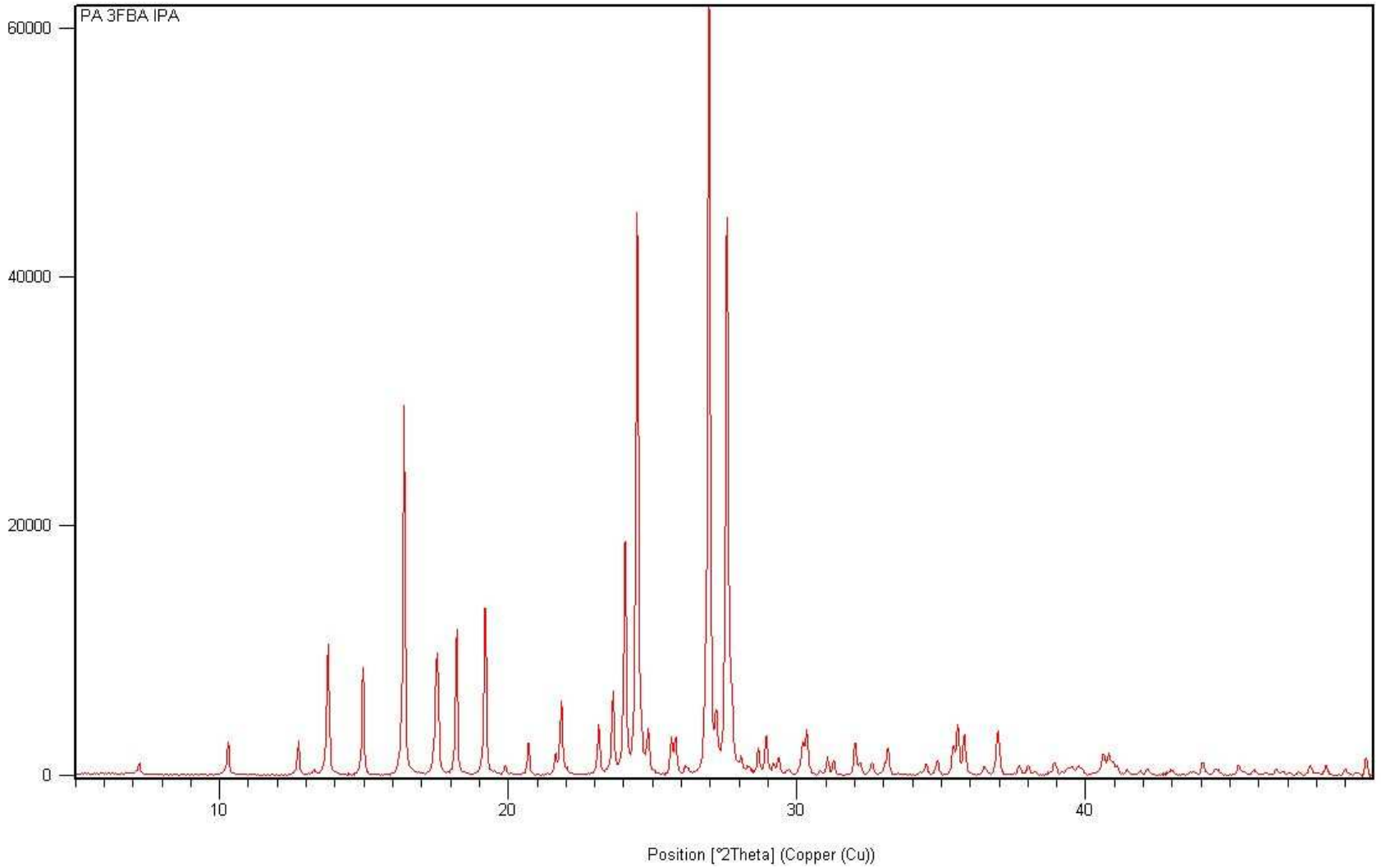

Appendix B4a-6 PXRD of the co-crystallisation of paracetamol with 3-fluorobenzoic acid in isopropanol. The pattern shows a mixture of 3FBA and PA II in 100% yield.

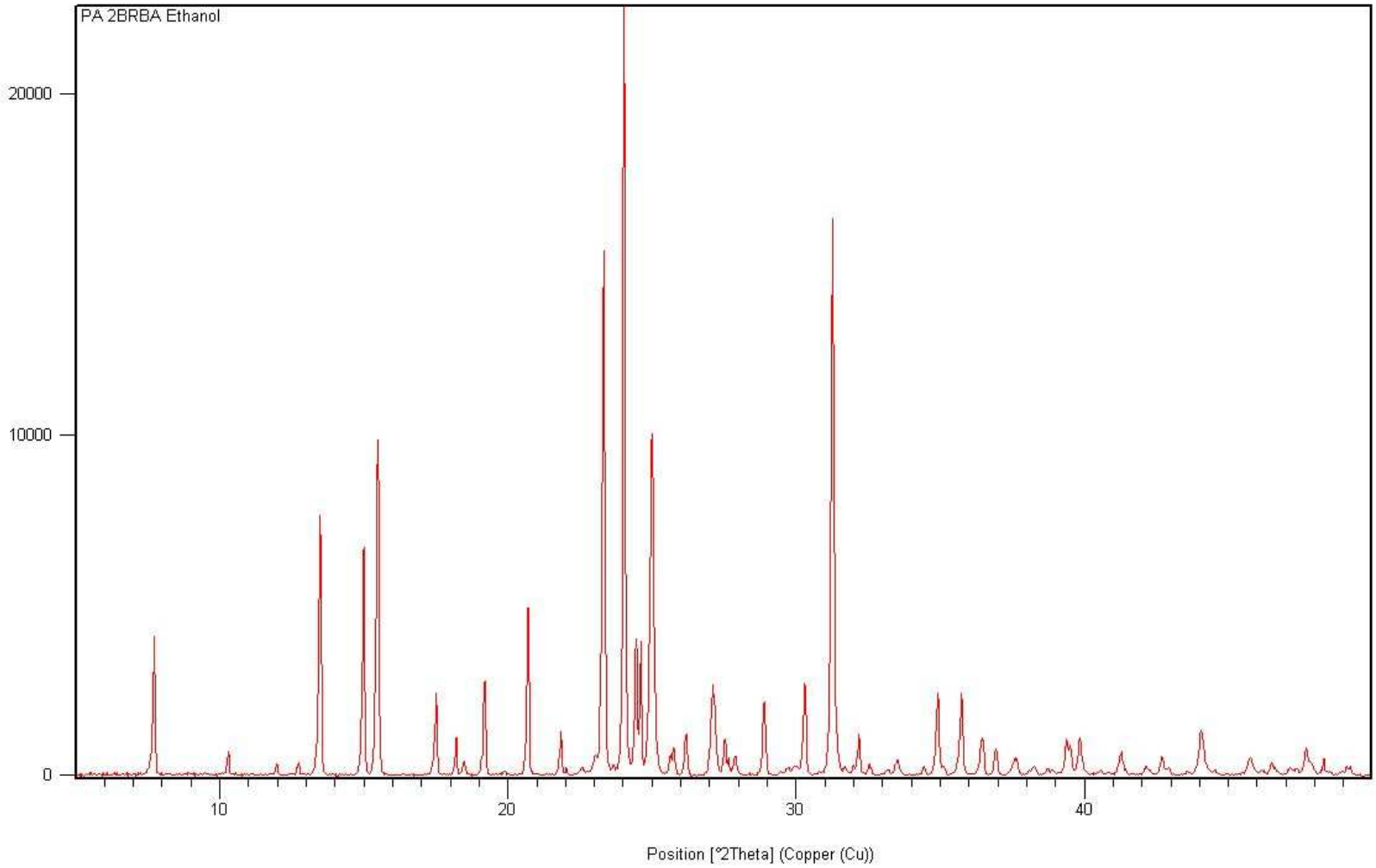

Appendix B4a-7 PXRD of the co-crystallisation of paracetamol with 2-bromobenzoic acid in ethanol. The pattern shows a mixture of 2BRBA and PA II in 100% yield.

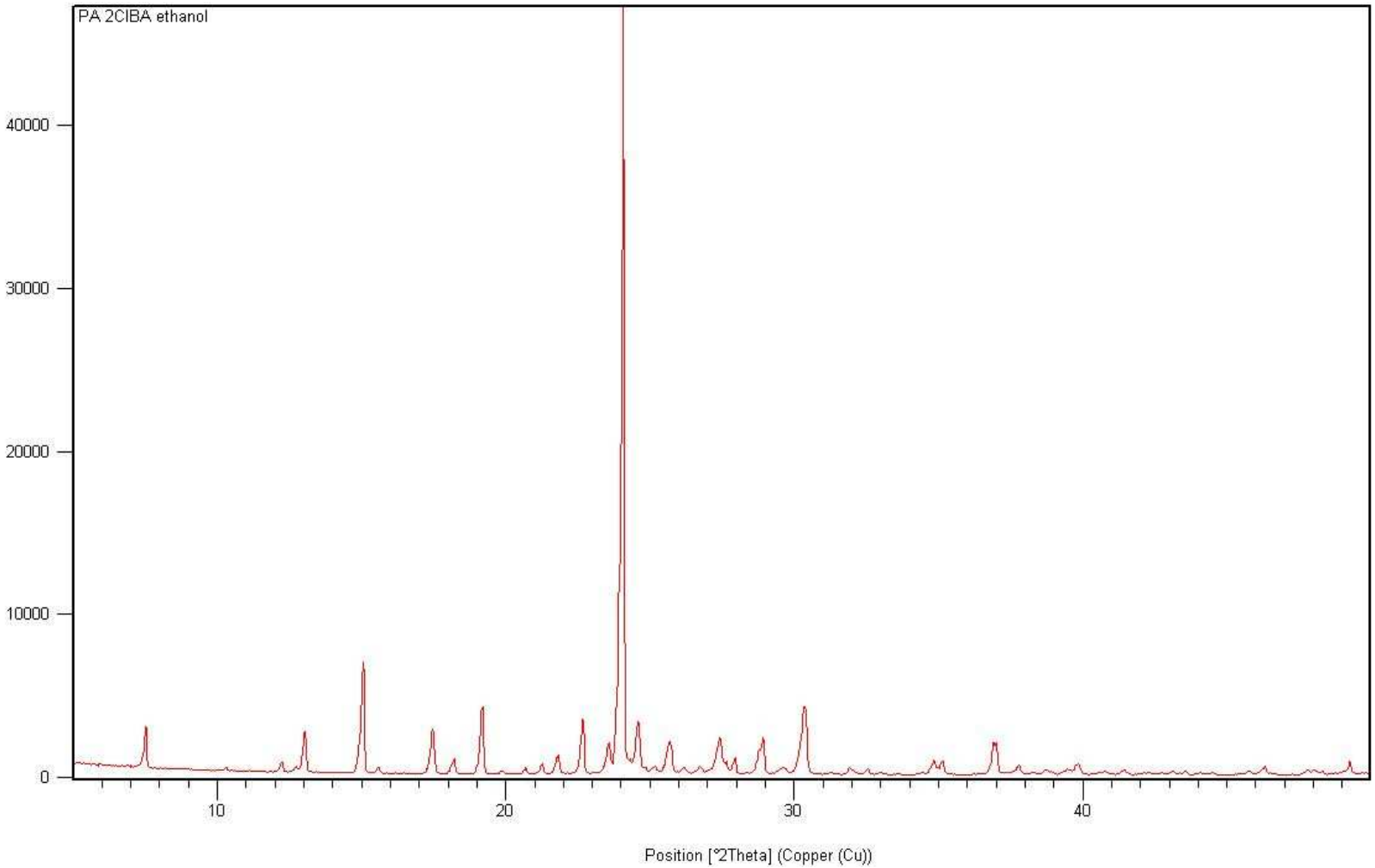

Appendix B4a-8 PXRD of the co-crystallisation of paracetamol with 2-chlorobenzoic acid in ethanol. The pattern shows a mixture of 2ClBA and PA II in 100% yield.

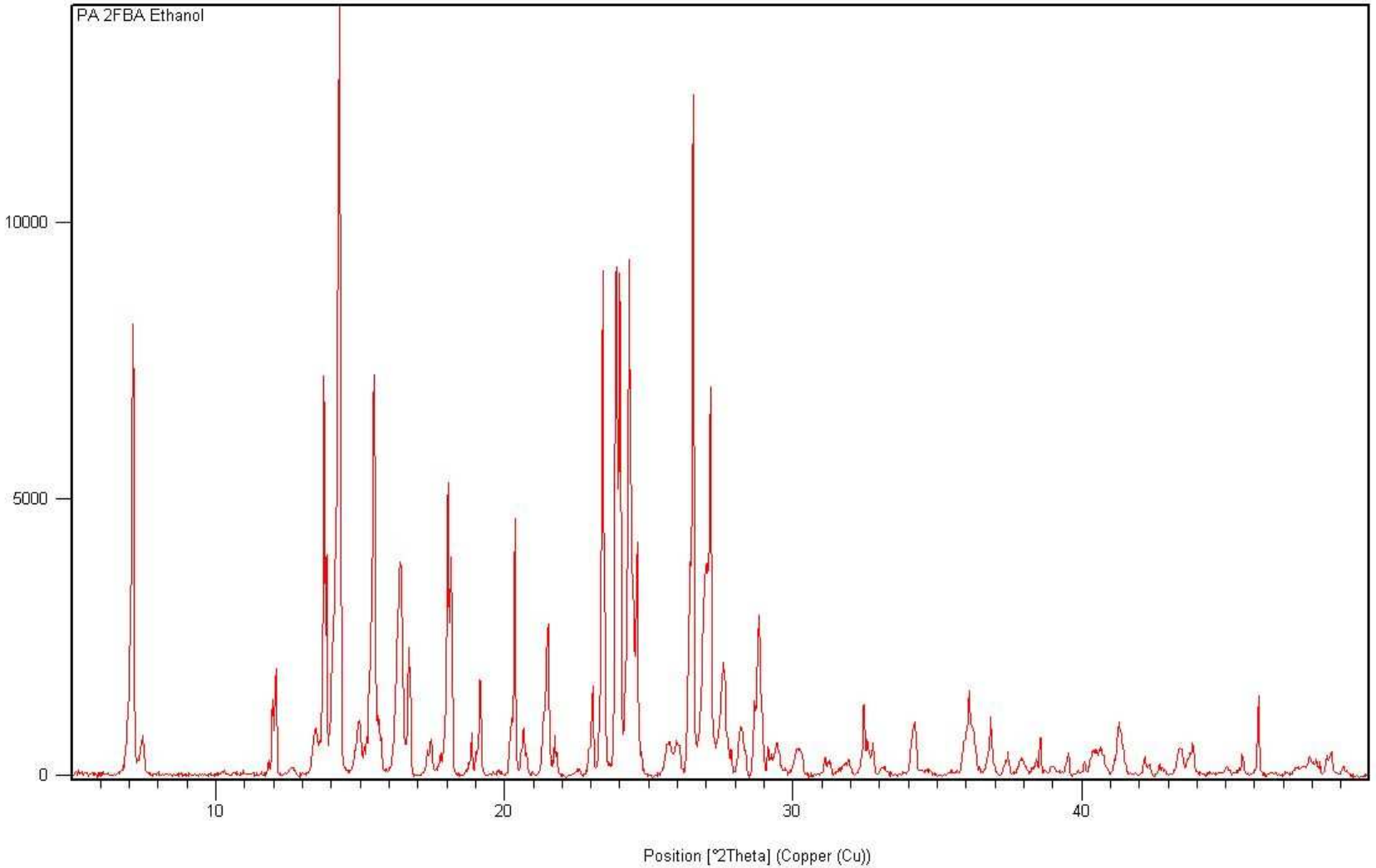

Appendix B4a-9 PXRD of the co-crystallisation of paracetamol with 2-fluorobenzoic acid in ethanol. The pattern shows a mixture of 2FBA with both PA I and PA II. 100% PA II was not achieved under the conditions studied using 2FBA as the co-molecule.

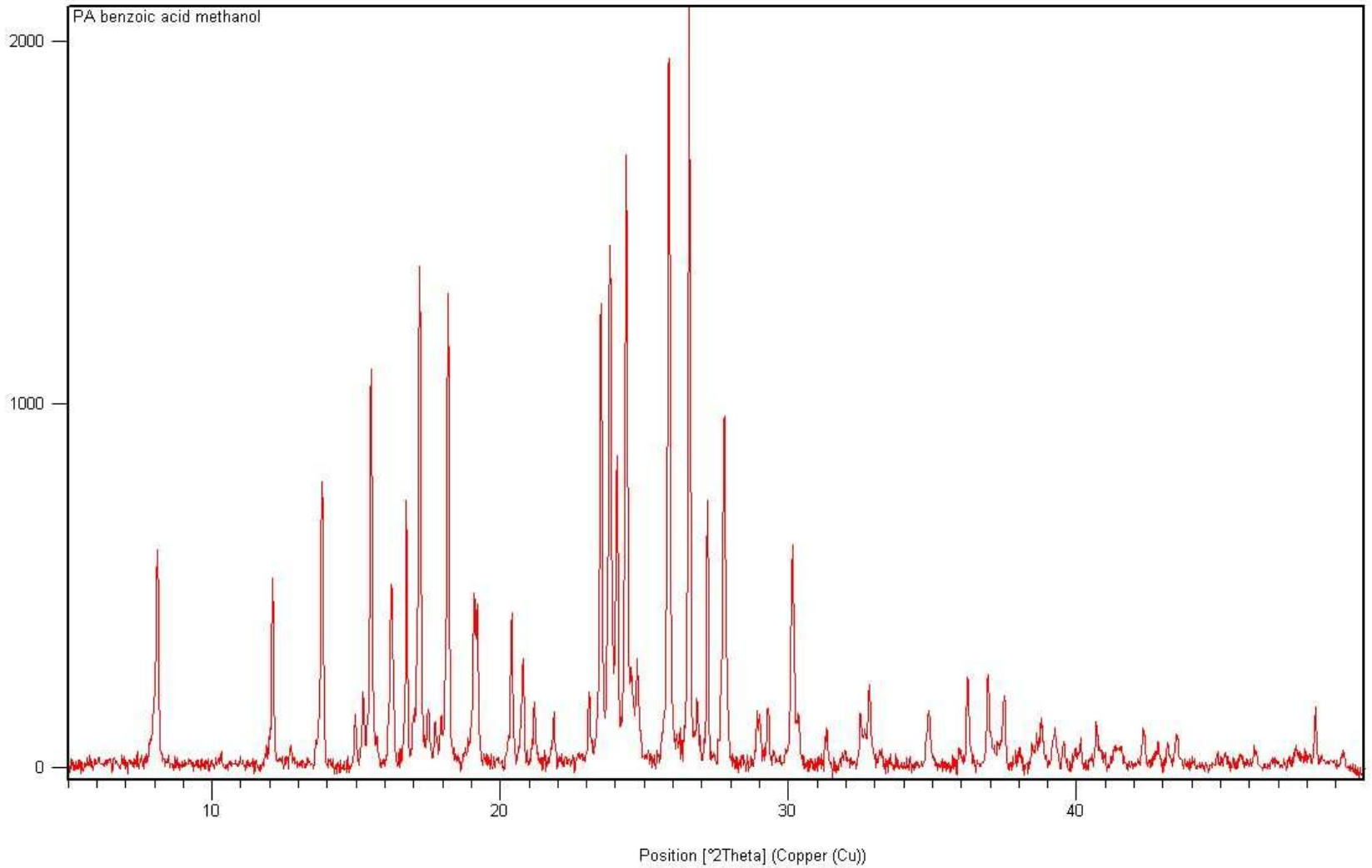

Appendix B4a-10 PXRD of the co-crystallisation of paracetamol with benzoic acid in methanol. The pattern shows a mixture of BA with both PA I and PA II. 100% PA II was not achieved under the conditions studied using BA as the co-molecule.

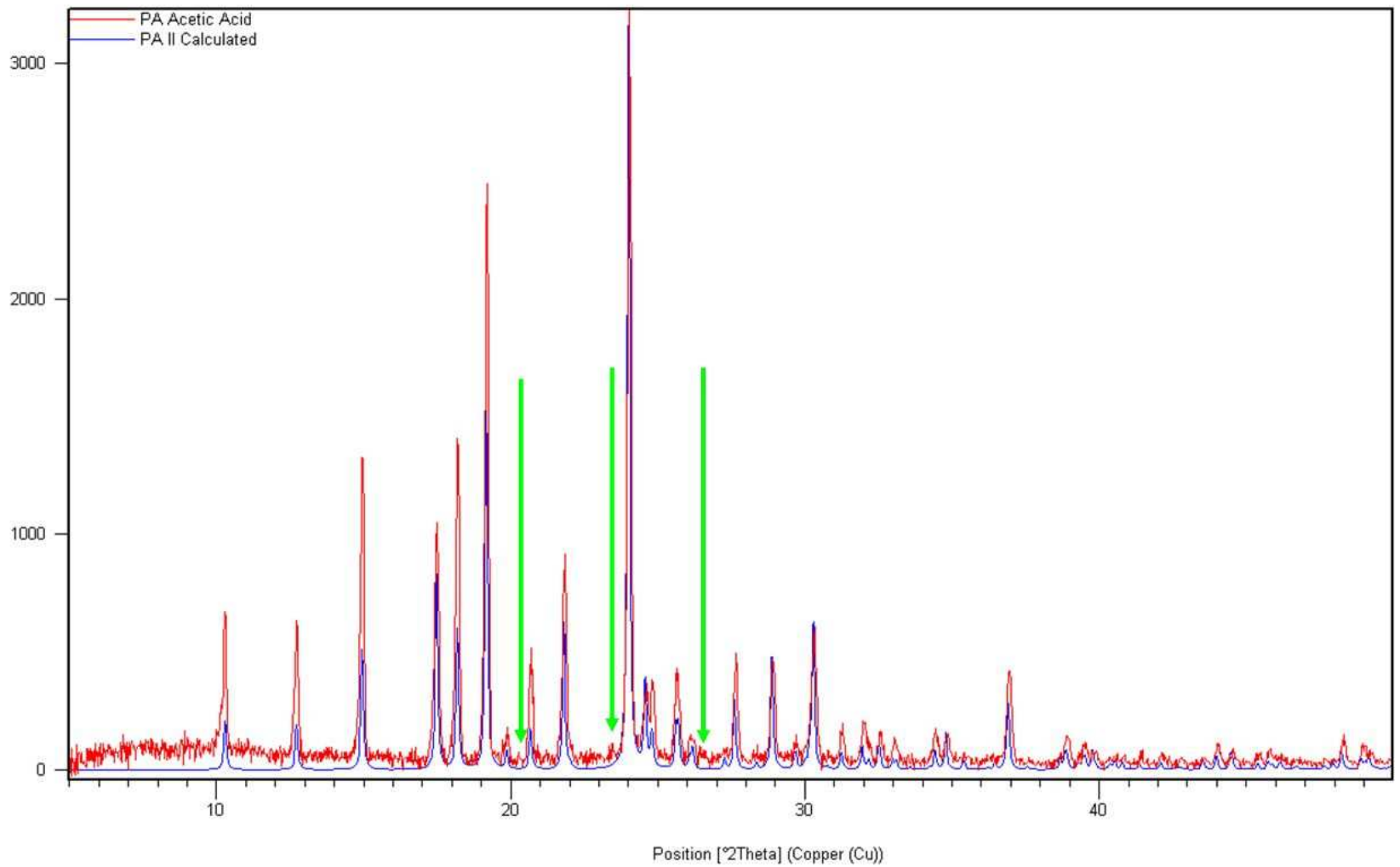

Appendix B4a-11 PXRD of the recrystallisation of paracetamol from excess acetic acid. The pattern shows almost 100% PA II. Small peaks corresponding to PA I are highlighted with green arrows.

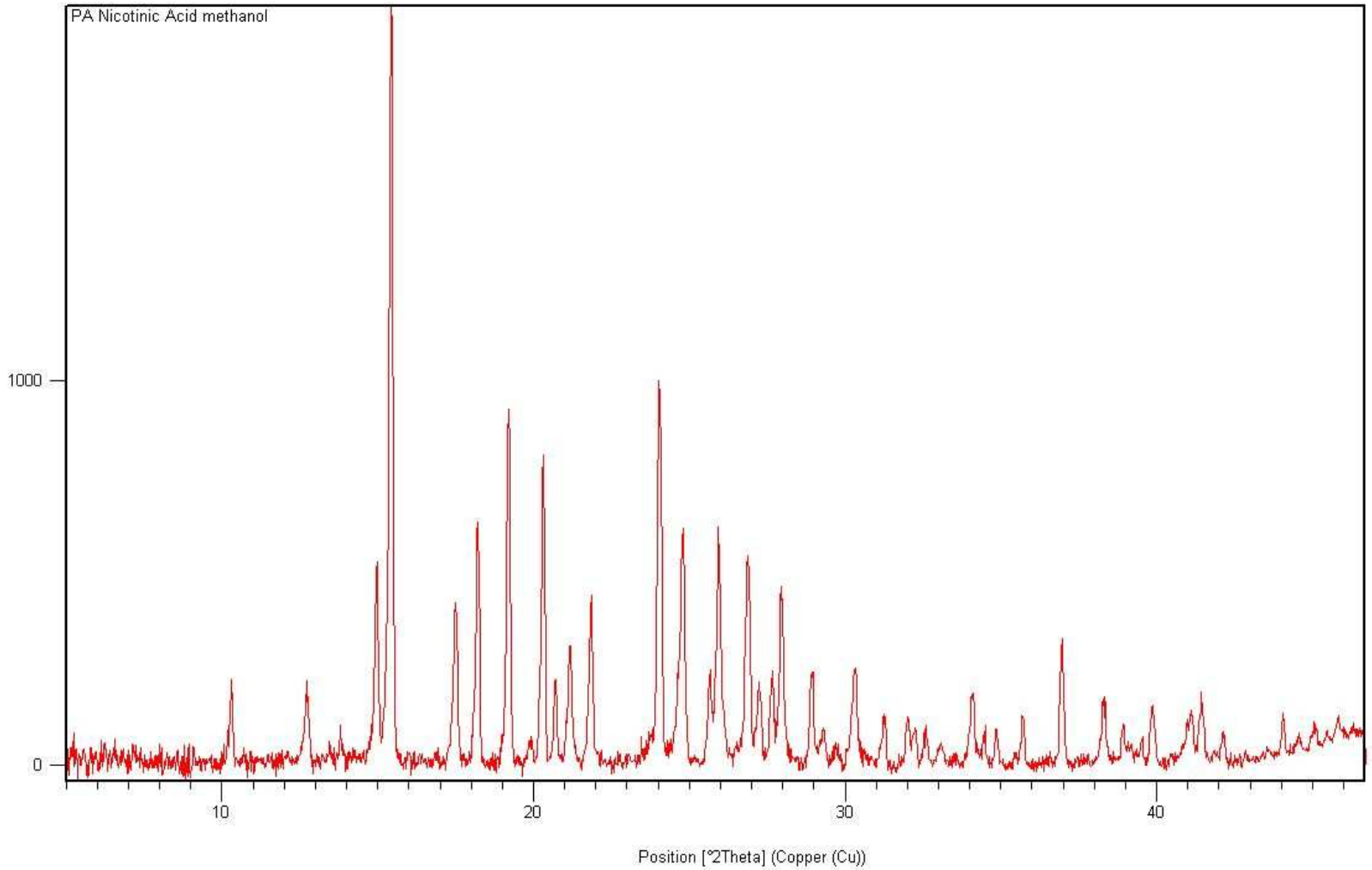

Appendix B4a-12 PXRD of the co-crystallisation of paracetamol with nicotinic acid in ethanol. The pattern shows a mixture of nicotinic acid with both PA I and PA II (PA II in the majority).

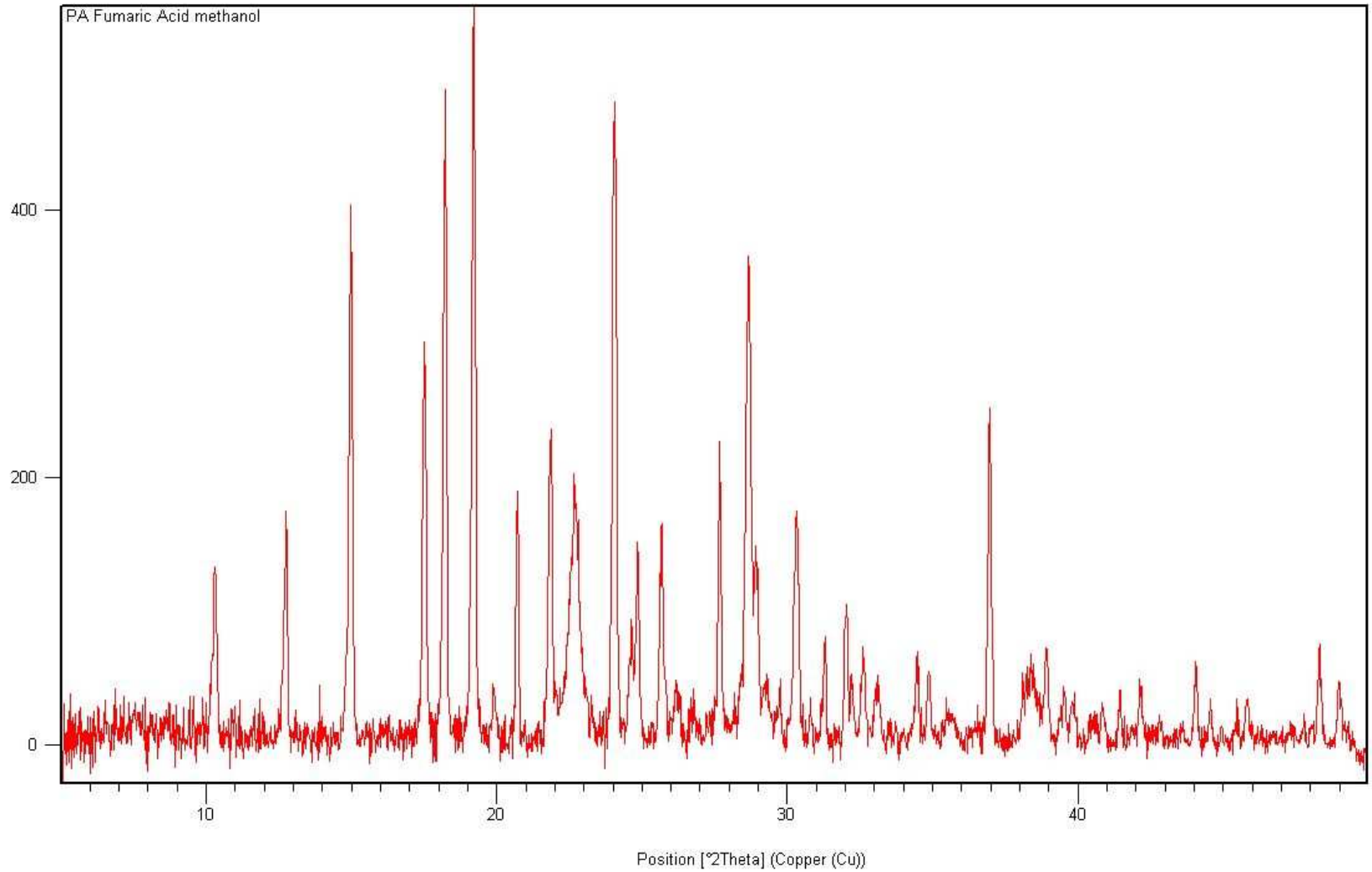

Appendix B4a-13 PXRD of the co-crystallisation of paracetamol with fumaric acid in methanol. The pattern shows a mixture of fumaric acid with PA II in 100% yield.

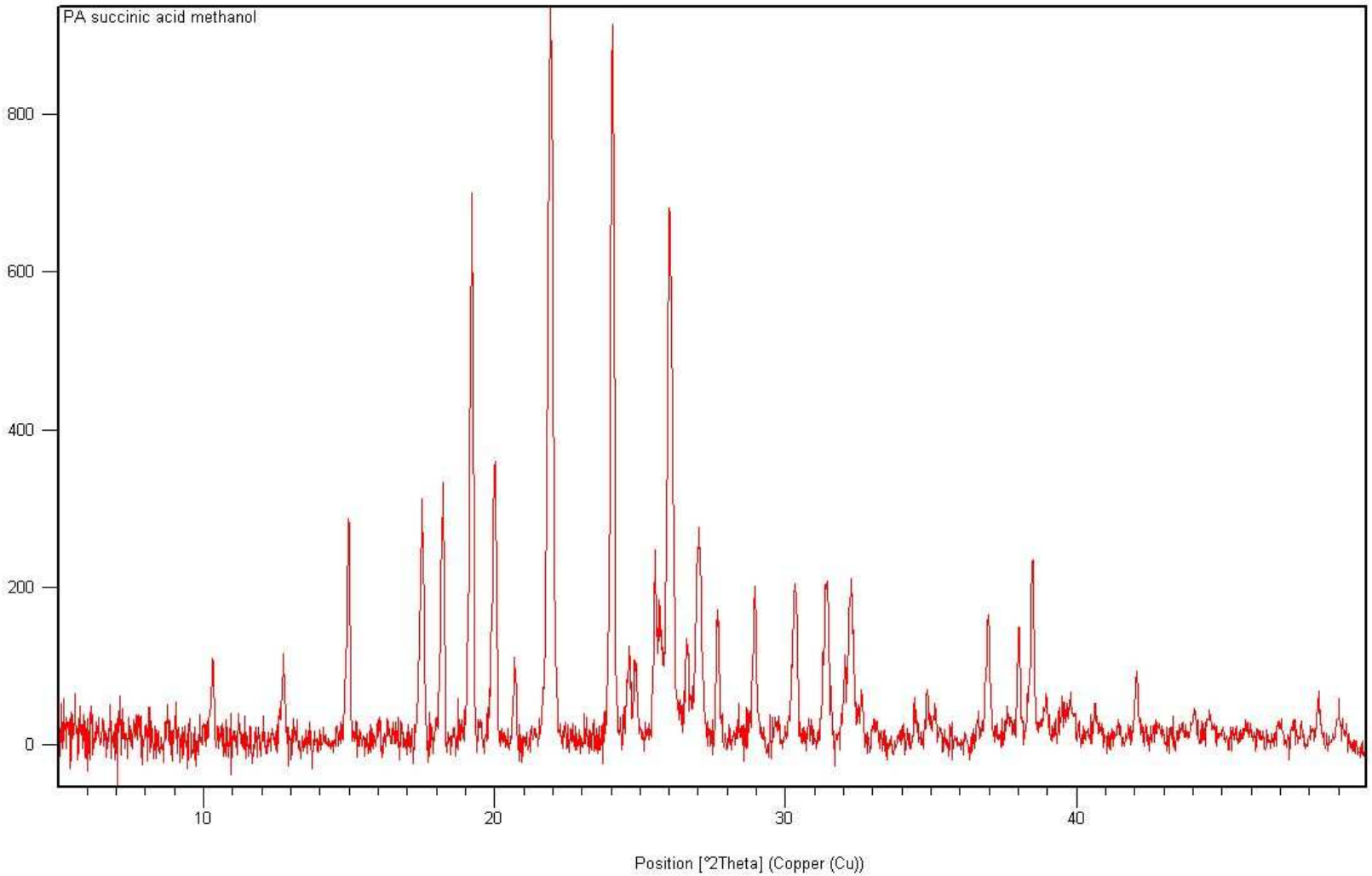

Appendix B4a-14 PXRD of the co-crystallisation of paracetamol with succinic acid in methanol. The pattern shows a mixture of succinic acid (alpha and beta forms) with PA II in 100% yield.

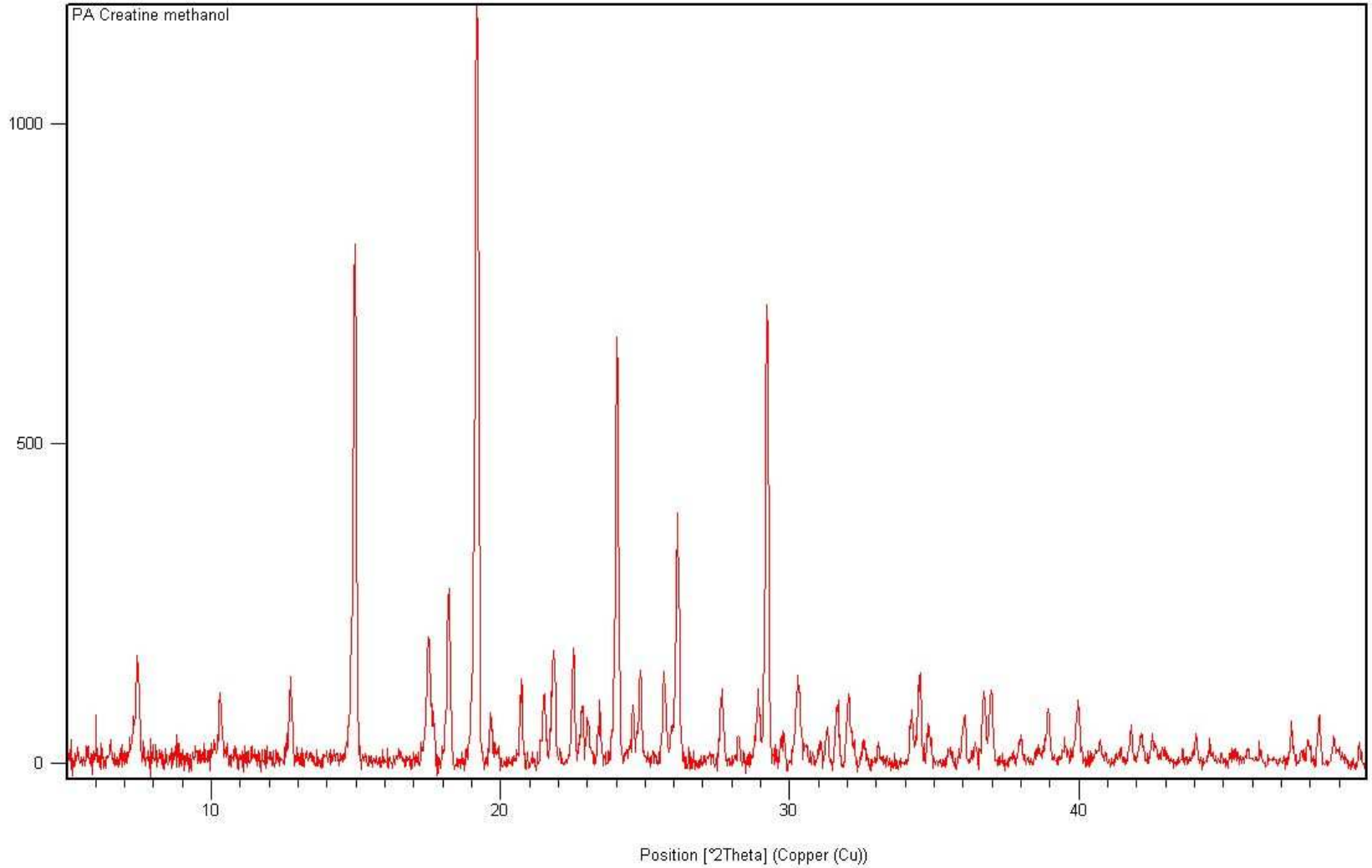

Appendix B4a-15 PXRD of the co-crystallisation of paracetamol with creatine in methanol. The pattern shows a mixture of creatine monohydrate with PA II in 100% yield.

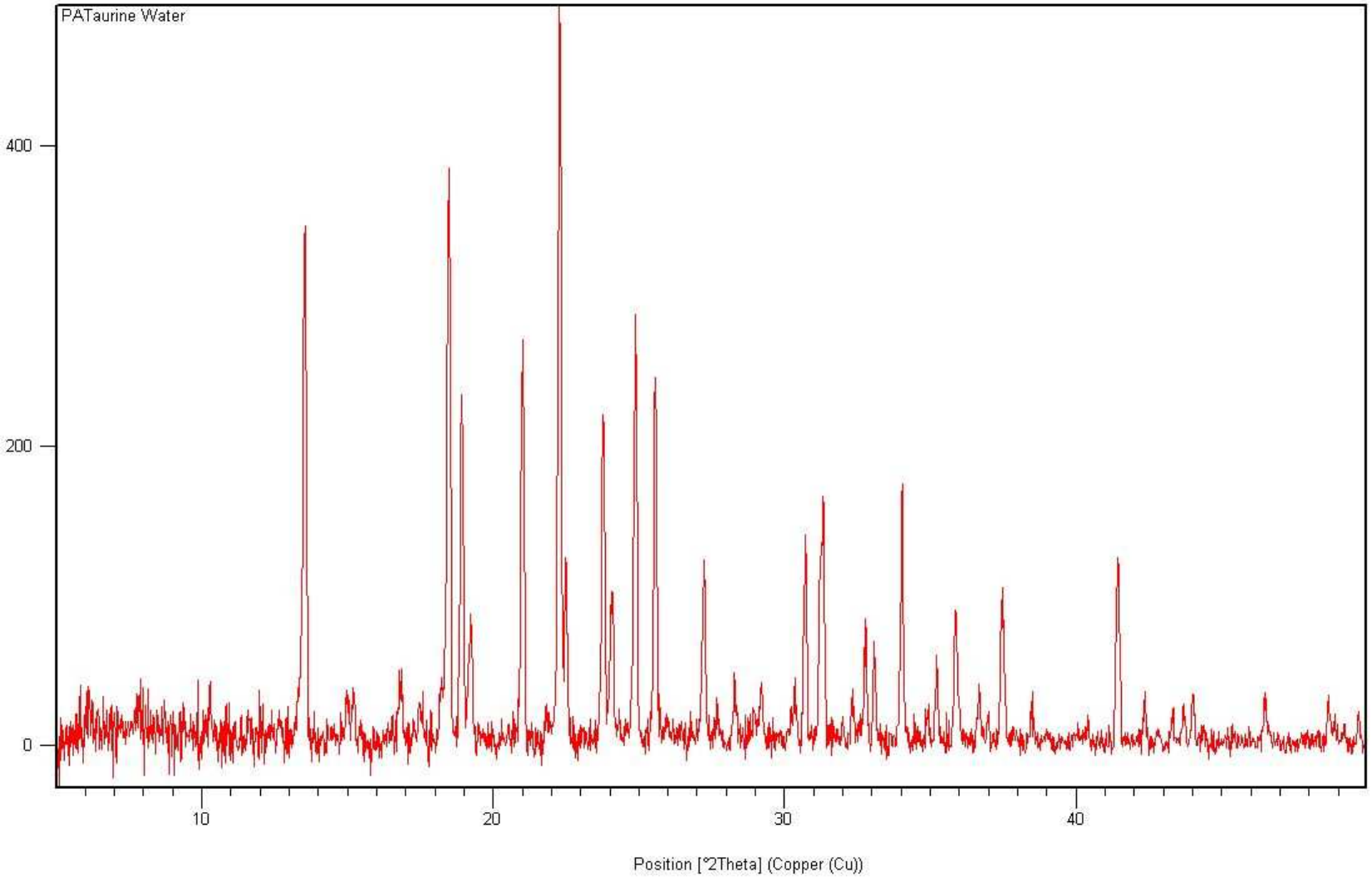

Appendix B4a-16 PXRD of the co-crystallisation of paracetamol with taurine in water at 30°C. The pattern shows a mixture of taurine with PA II in 100% yield.

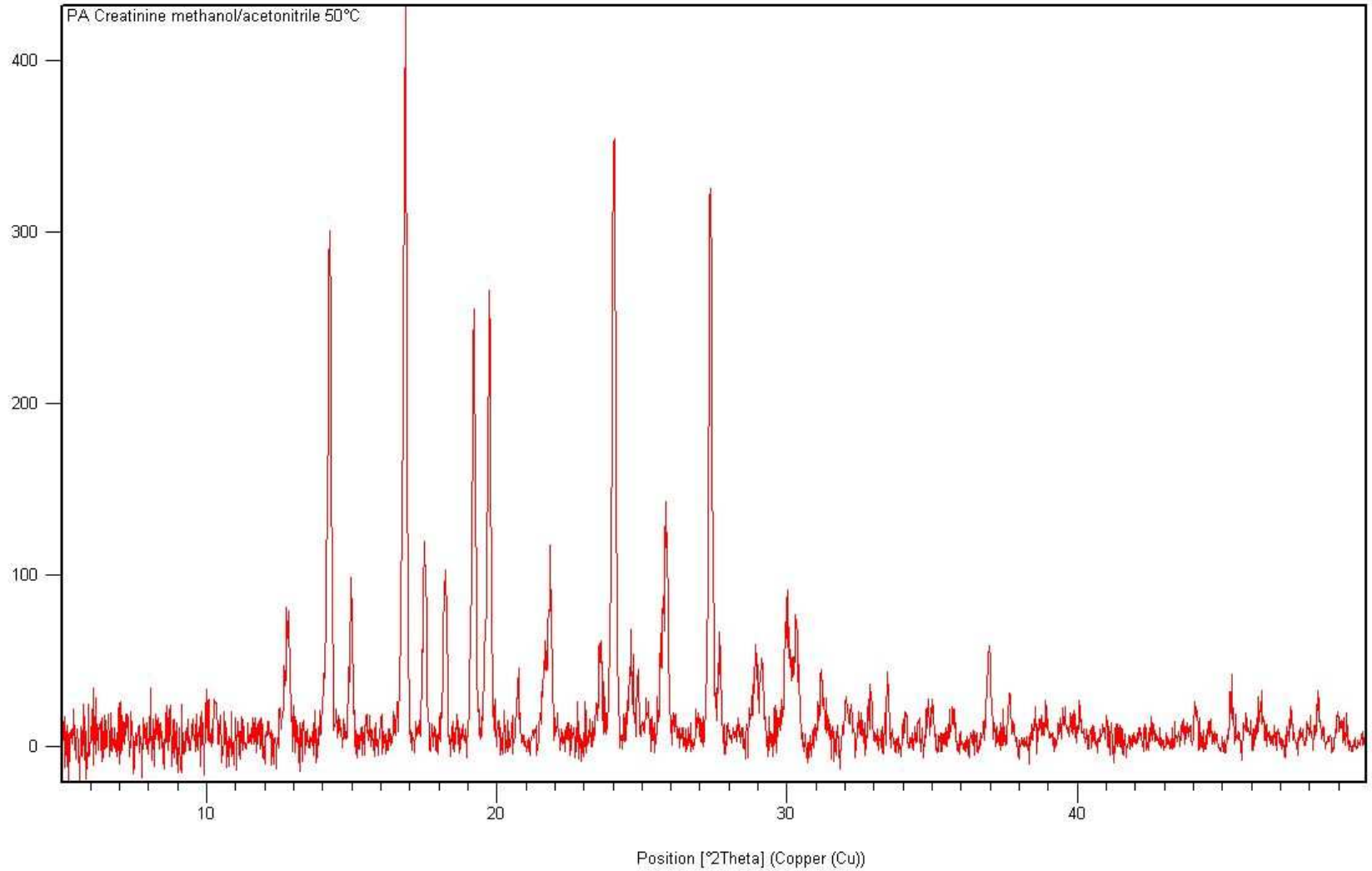

Appendix B4a-17 PXRD of the co-crystallisation of paracetamol with creatinine in a methanol/acetonitrile 50/50 (V/V) mixture at 30°C. The pattern shows a mixture of creatinine with PA II in 100% yield.

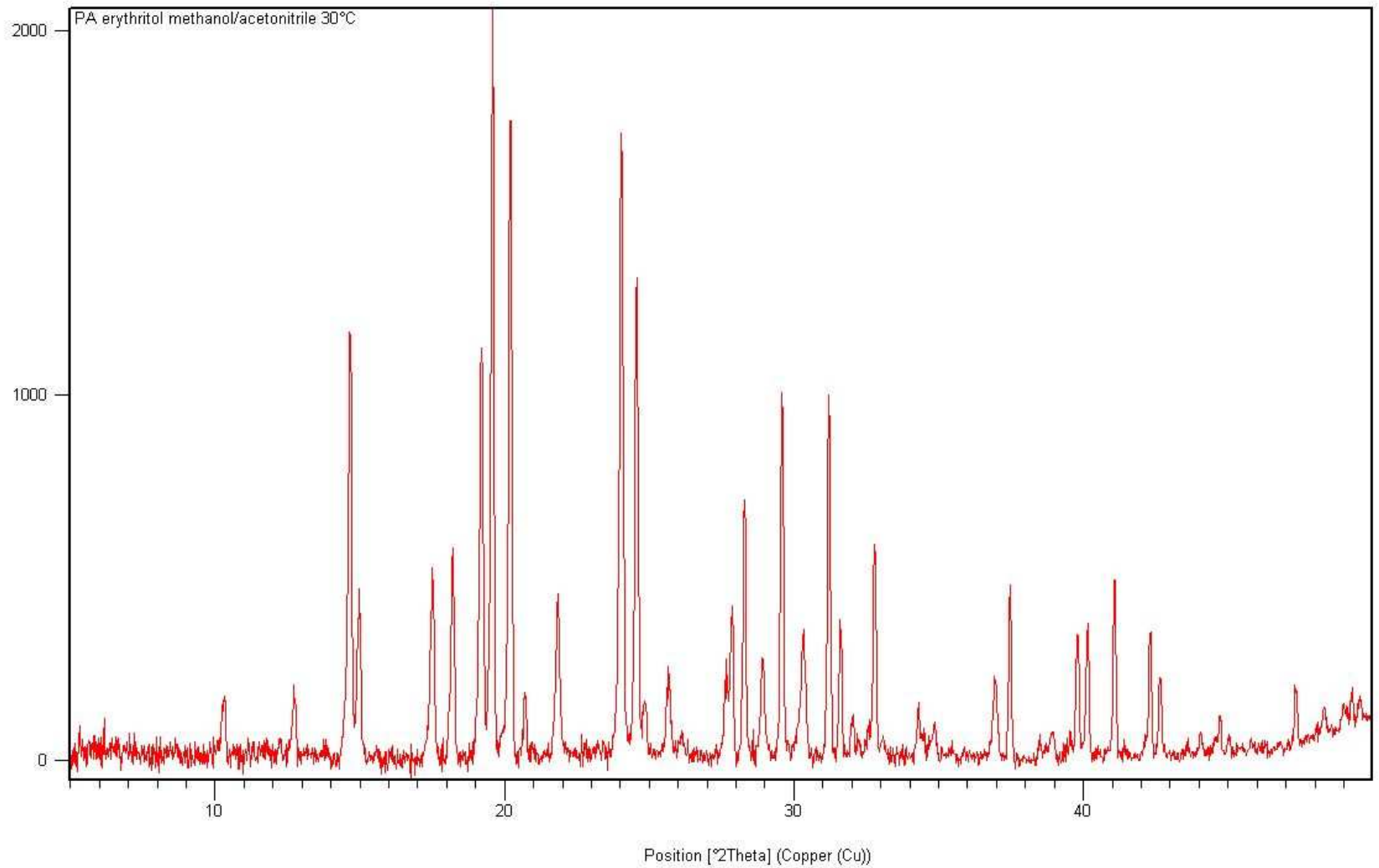

Appendix B4a-18 PXRD of the co-crystallisation of paracetamol with erythritol in a methanol/acetonitrile 50/50 (V/V) mixture at 30°C. The pattern shows a mixture of erythritol with PA II in 100% yield.

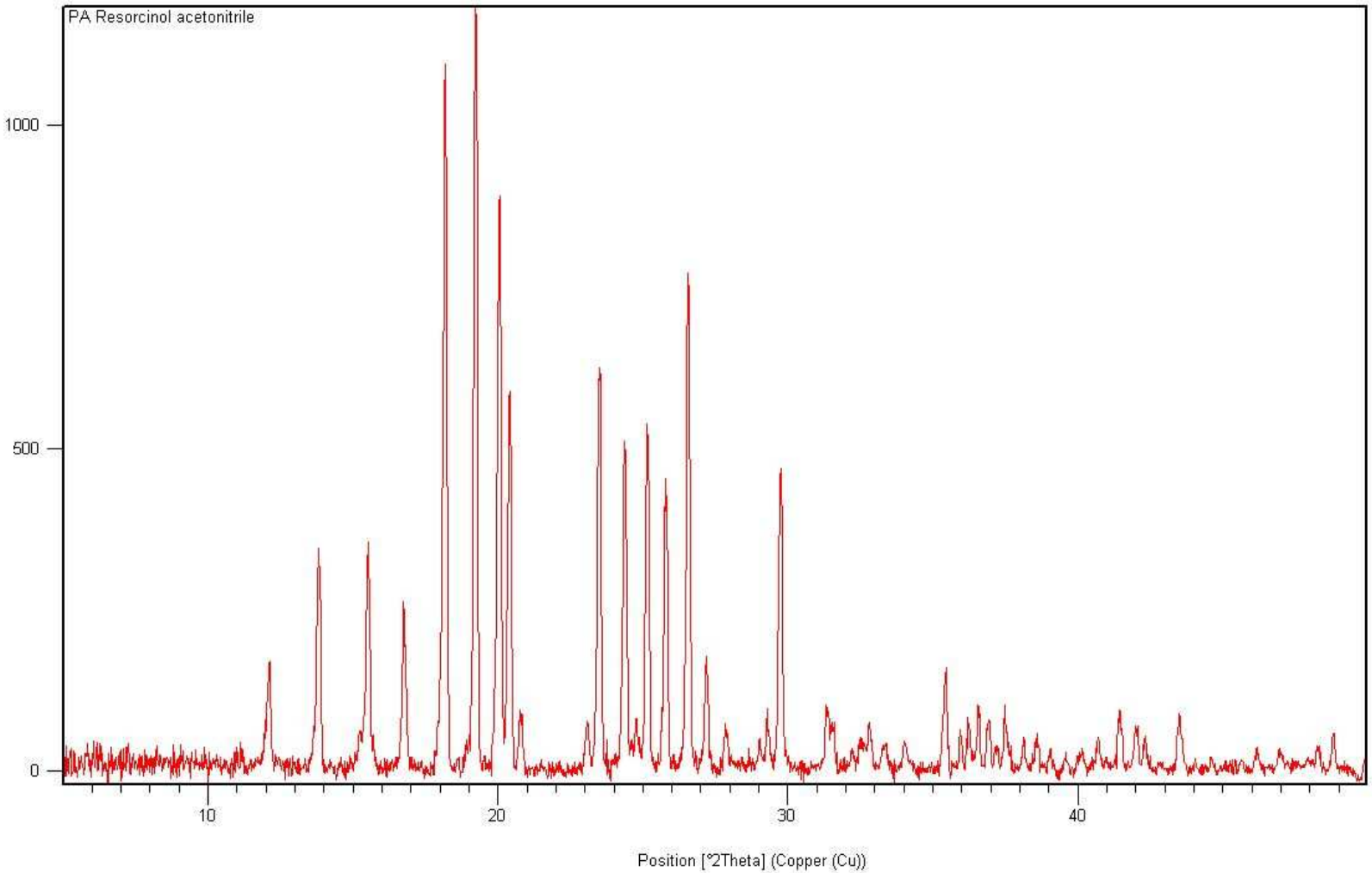

Appendix B4a-19 PXRD of the co-crystallisation of paracetamol with resorcinol in acetonitrile. The pattern shows a mixture of resorcinol with both PA I and PA II (PA I in the majority).

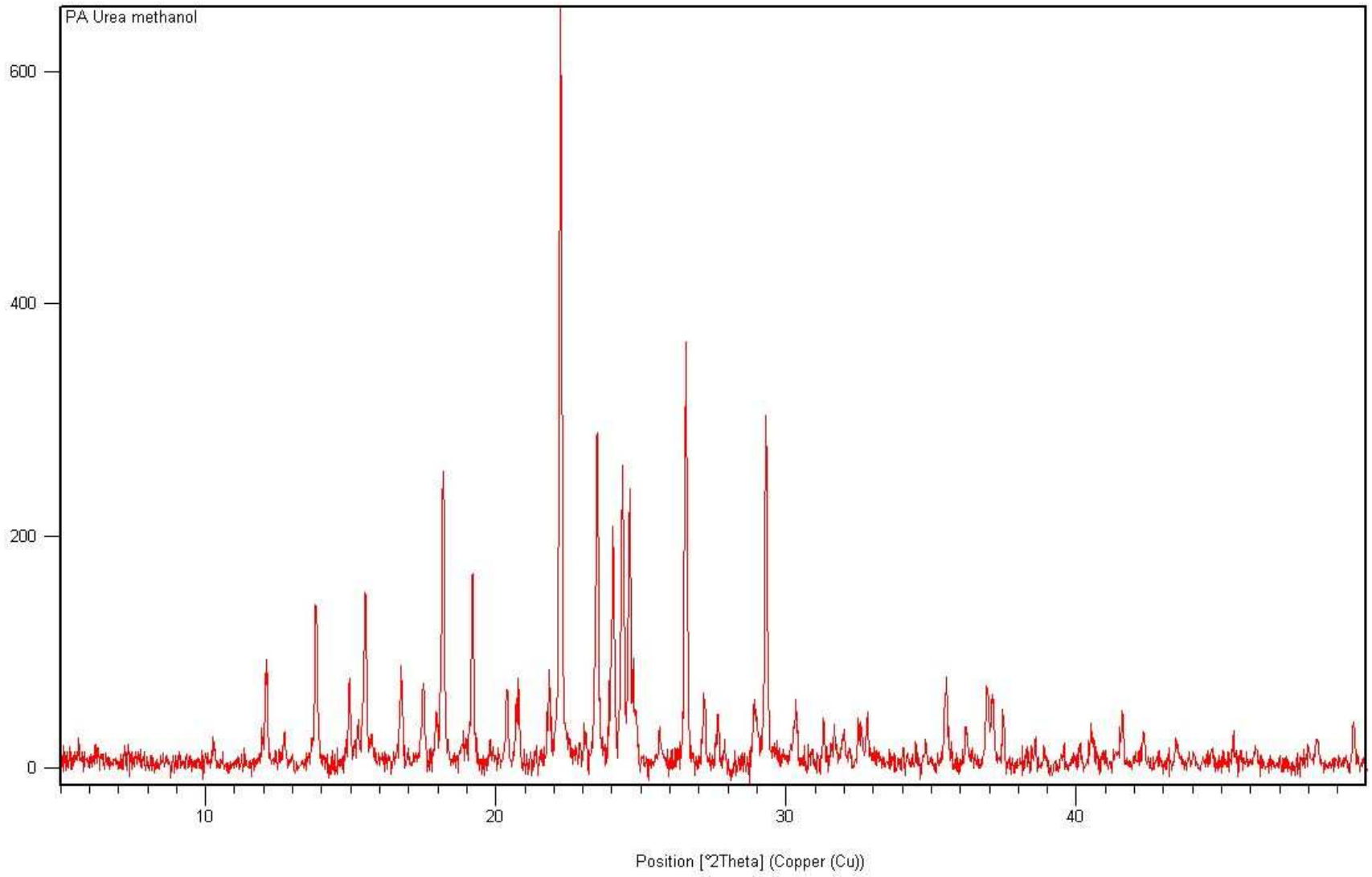

Appendix B4a-20 PXRD of the co-crystallisation of paracetamol with urea in methanol. The pattern shows a mixture of urea with both PA I and PA II.

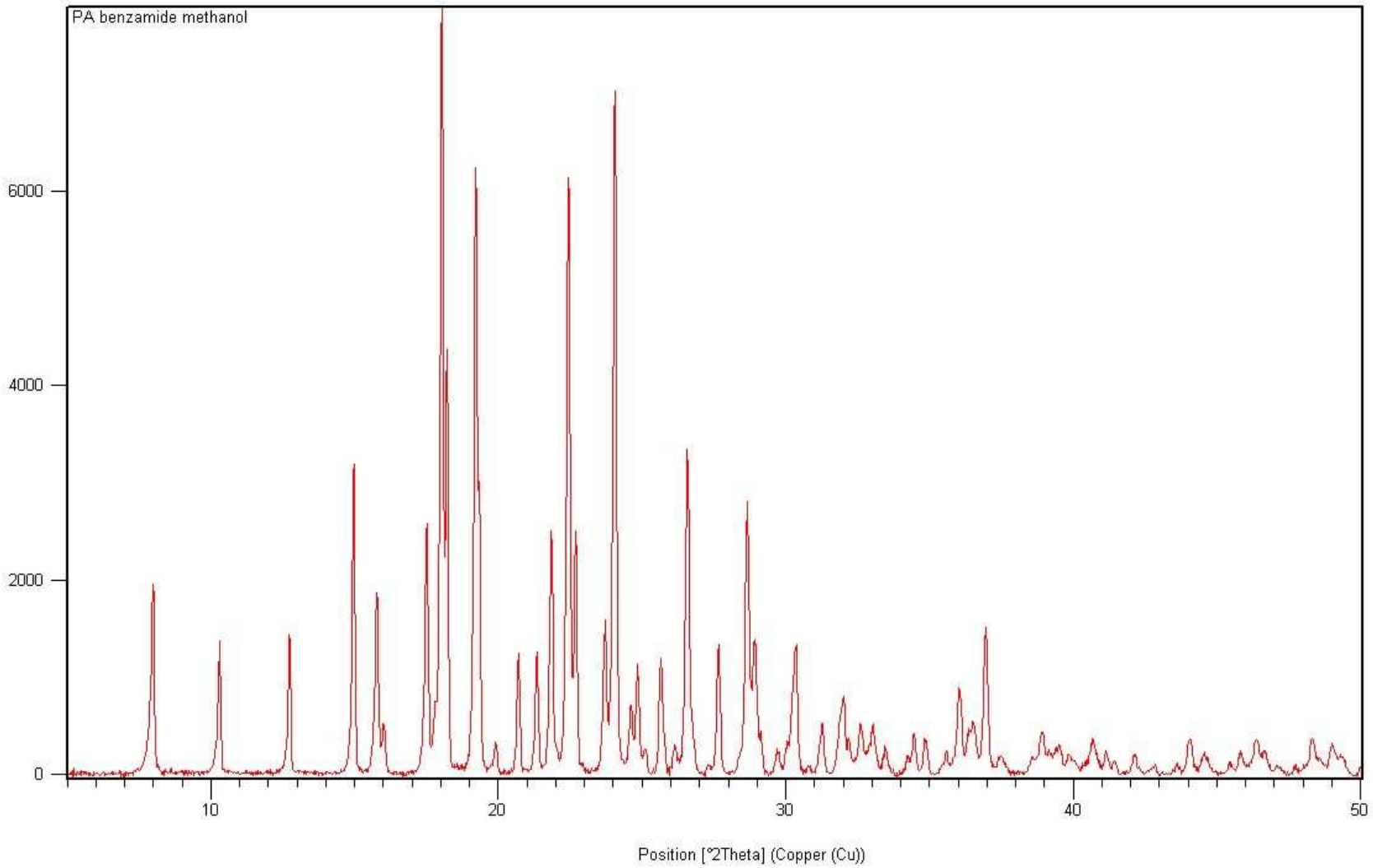

Appendix B4a-21 PXRD of the co-crystallisation of paracetamol with benzamide in methanol. The pattern shows a mixture of benzamide with PA II in 100% yield.

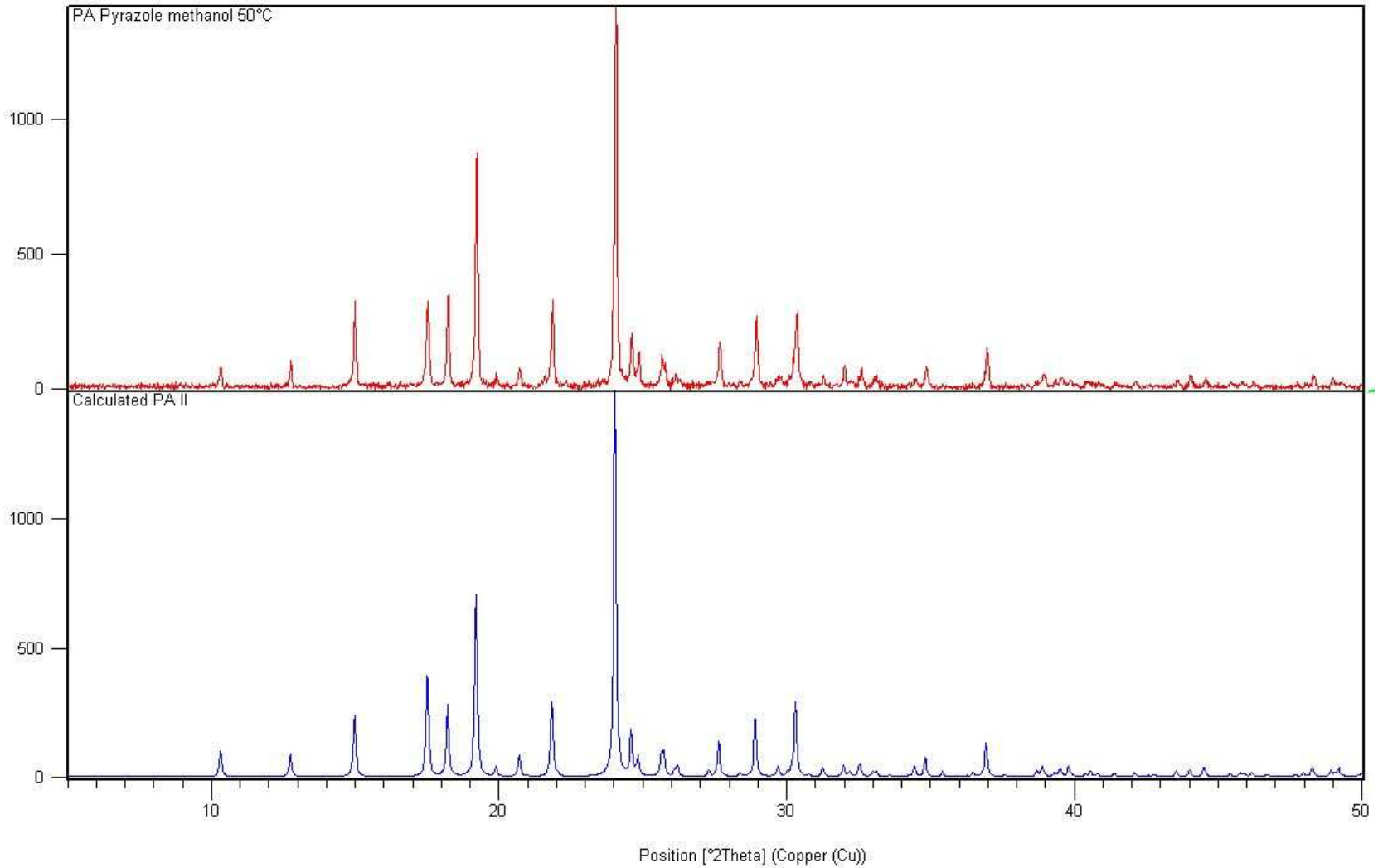

Appendix B4a-22 PXRD of the co-crystallisation of paracetamol with pyrazole in methanol at 50°C (top, red). The pattern shows PA II in 100% yield (calculate PA II shown below in blue). The pattern indicates no pyrazole is present.

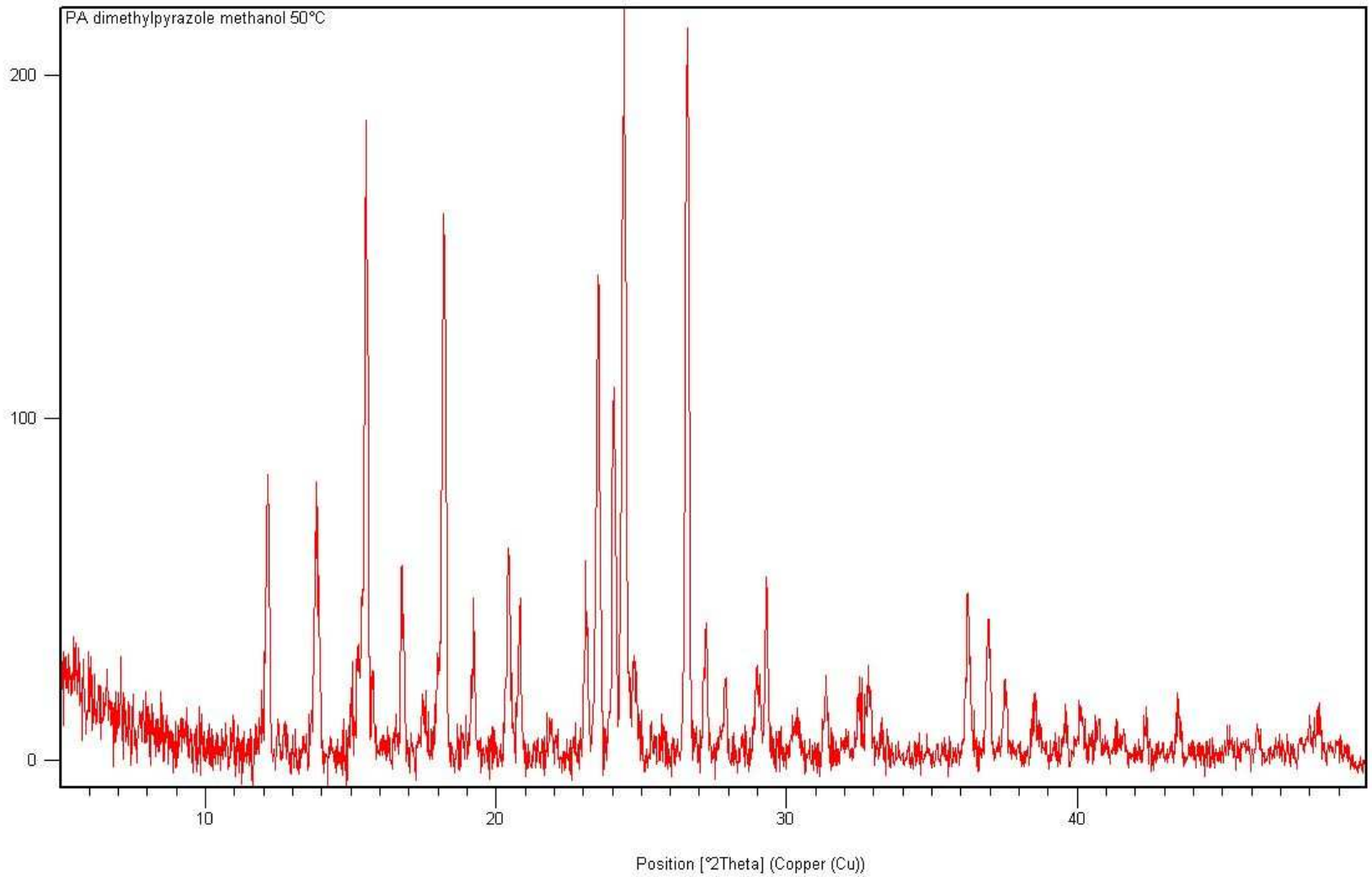

Appendix B4a-23 PXRD of the co-crystallisation of paracetamol with 3,5-dimethylpyrazole in methanol at 50°C. The pattern shows a mixture of PA I and PA II with only small quantities of 3,5-dimethylpyrazole detected.

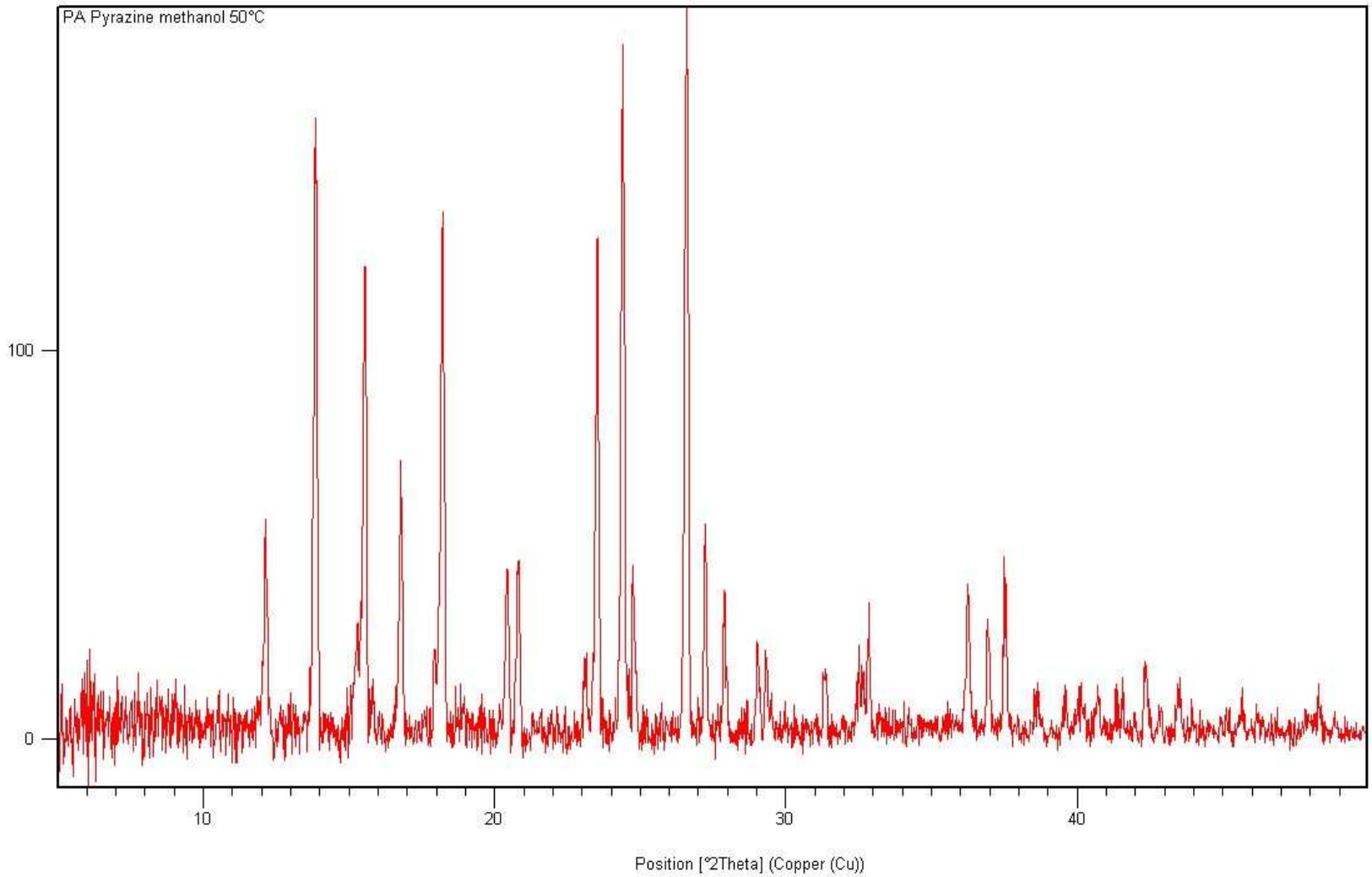

Appendix B4a-24 PXRD of the co-crystallisation of paracetamol with pyrazine in methanol at 50°C. The pattern shows PA II in 100% yield. The majority of the pyrazine appears to have sublimed during the evaporation process.

Appendix B4b - Powder X-ray Diffraction of New and Elusive Polymorphs of Piroxicam from Multi-Component Crystallisations (Section 4.4)

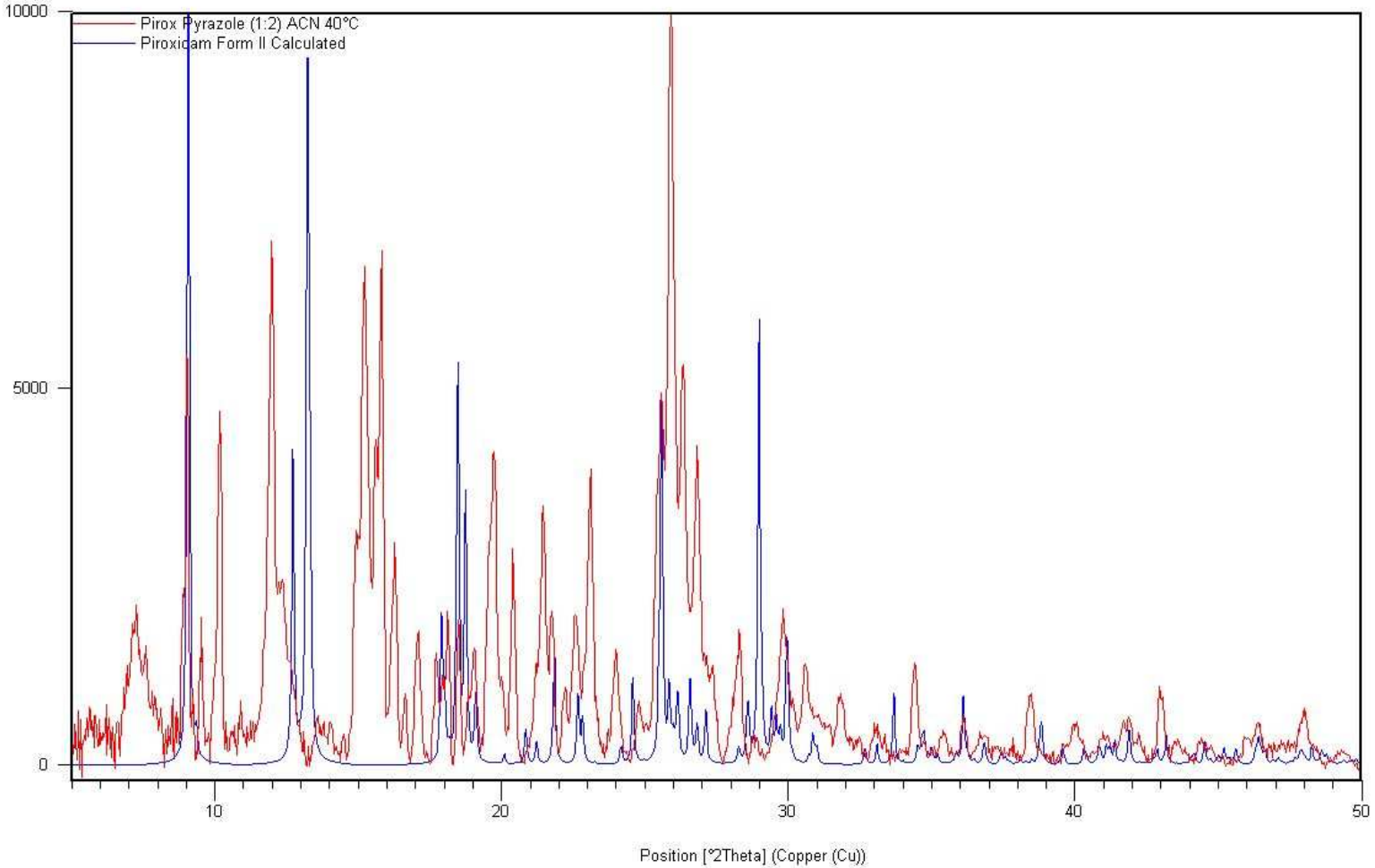

Appendix B4b-1 PXRD of the co-crystallisation of piroxicam with pyrazole (1:2 mass ratio) in acetonitrile at 40°C (red). The pattern shows a poor match with the calculated PX III pattern (blue) despite its presence being confirmed by unit cell screening of single crystals. The peaks instead correspond to a mixture of PX II and PX monohydrate.

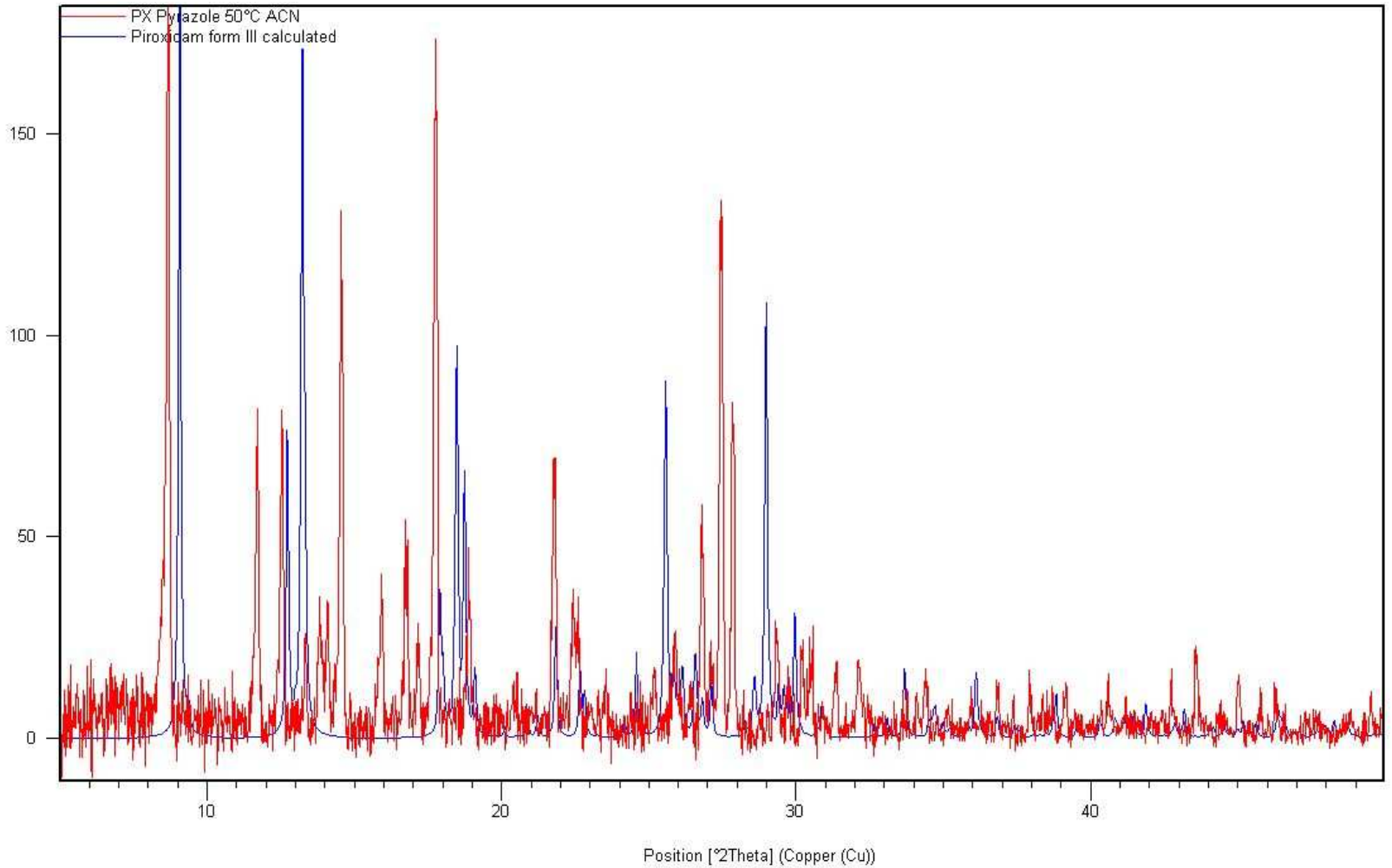

Appendix B4b-2 PXRD of the co-crystallisation of piroxicam with pyrazole (1:2 mass ratio) in acetonitrile at 50°C (red). The pattern shows a poor match with the calculated PX III pattern (blue) despite its presence being confirmed by unit cell screening of single crystals. The peaks instead correspond to PX I.

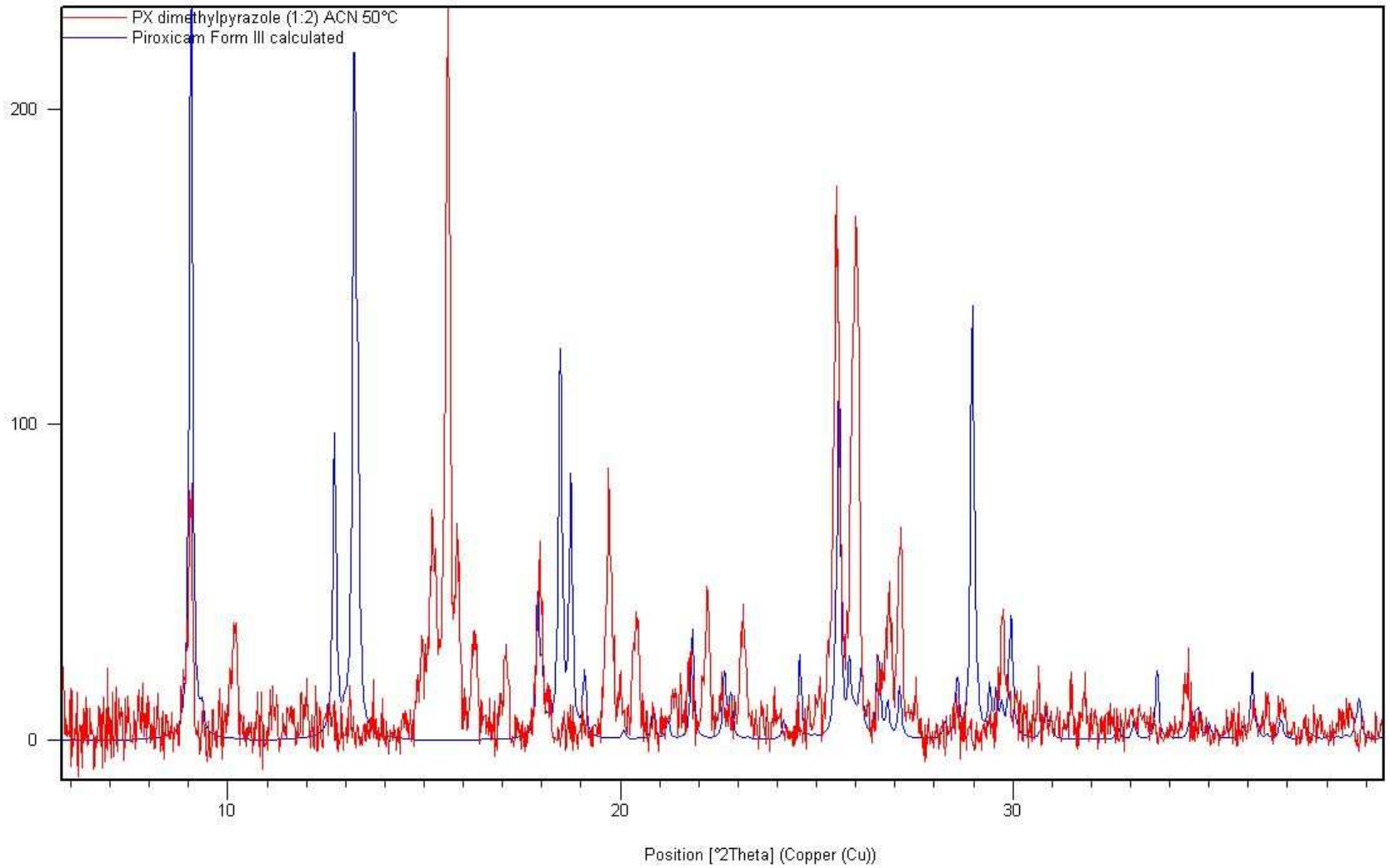

Appendix B4b-3 PXRD of the co-crystallisation of piroxicam with 3,5-dimethylpyrazole (1:2 mass ratio) in acetonitrile at 50°C (red). The pattern shows the presence of PX III (blue) although the majority is PX I.

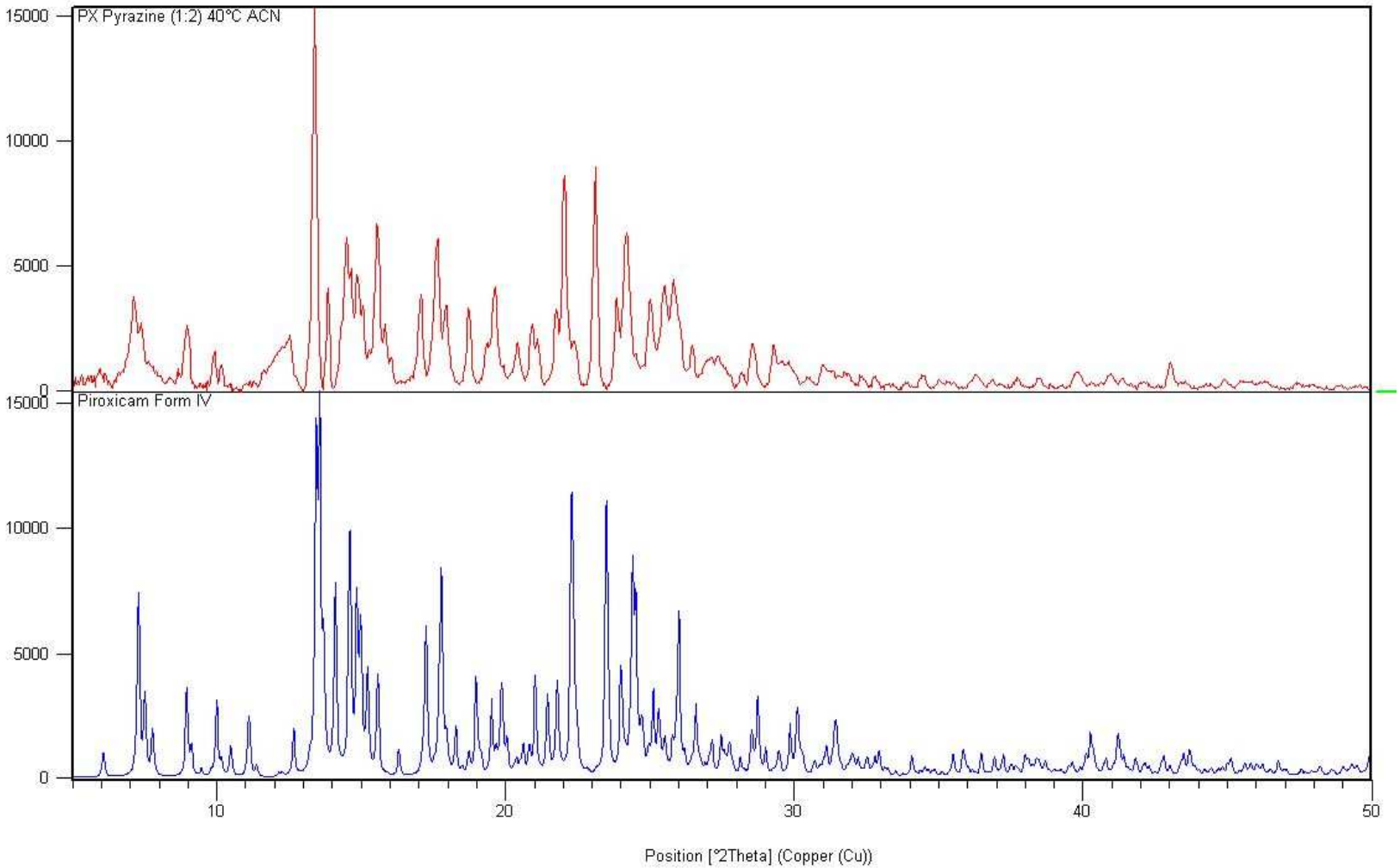

Appendix B4b-4 PXRD of the co-crystallisation of piroxicam with pyrazine (1:2 mass ratio) in acetonitrile at 40°C (red). The pattern shows a high yield of PX IV (blue) with PX II also present. The PX IV pattern is calculated from 100K data while the experimental PXRD was carried out at room temperature; a slight x-shift may therefore be required for some of the peaks.

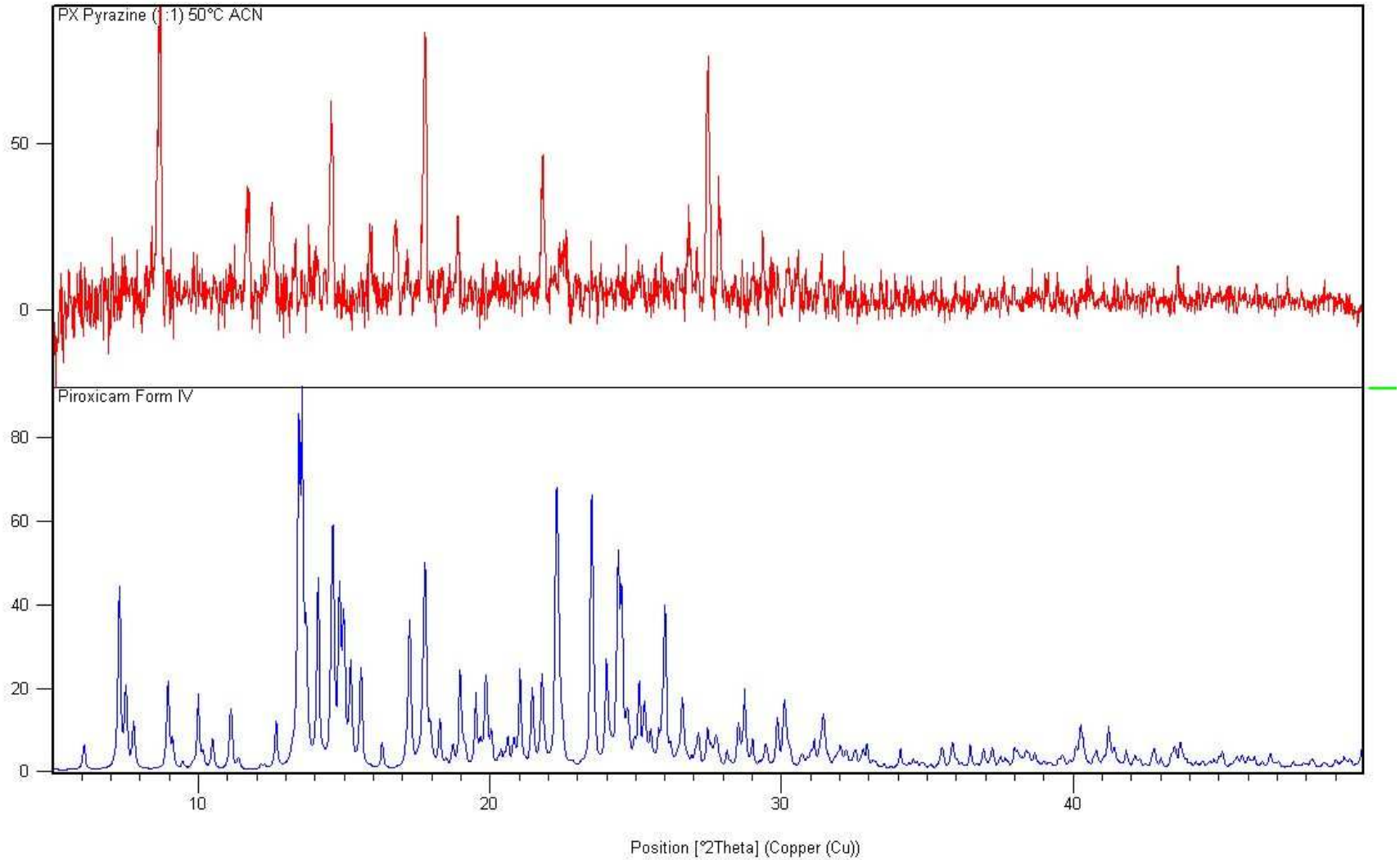

Appendix B4b-5 PXRD of the co-crystallisation of piroxicam with pyrazine (1:1 mass ratio) in acetonitrile at 50°C (red). The pattern shows a poor match with PX IV (blue) and shows approximately 100% PX II.

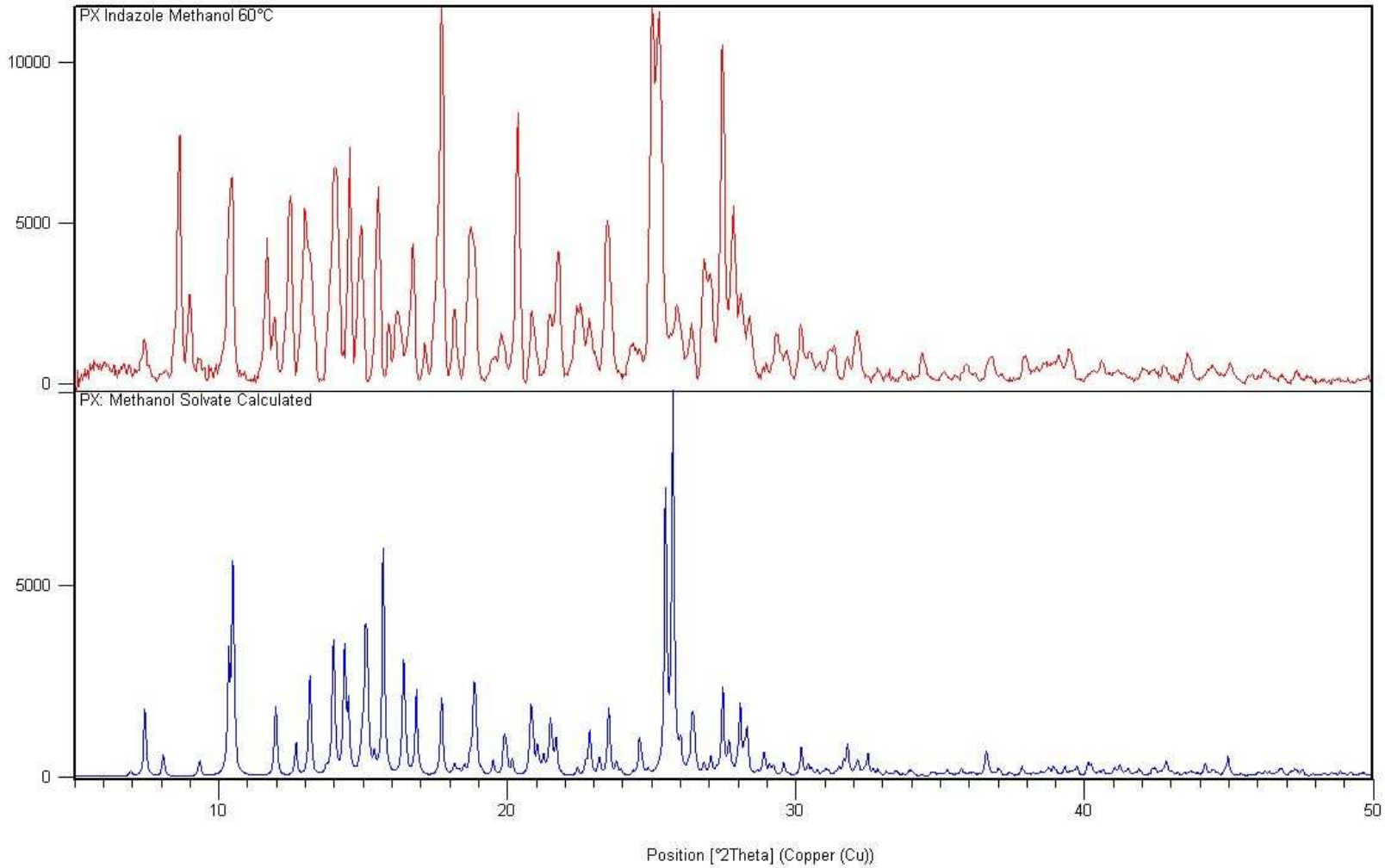

Appendix B4b-6 PXRD of the co-crystallisation of piroxicam with indazole in methanol at 60°C (red). The pattern shows a significant quantity of the PX : methanol solvate (blue) with PX I also present. The PXRD pattern for the PX : methanol solvate was calculated from 100K data while the experimental PXRD was carried out at room temperature; an x-shift is therefore required to match the peaks.

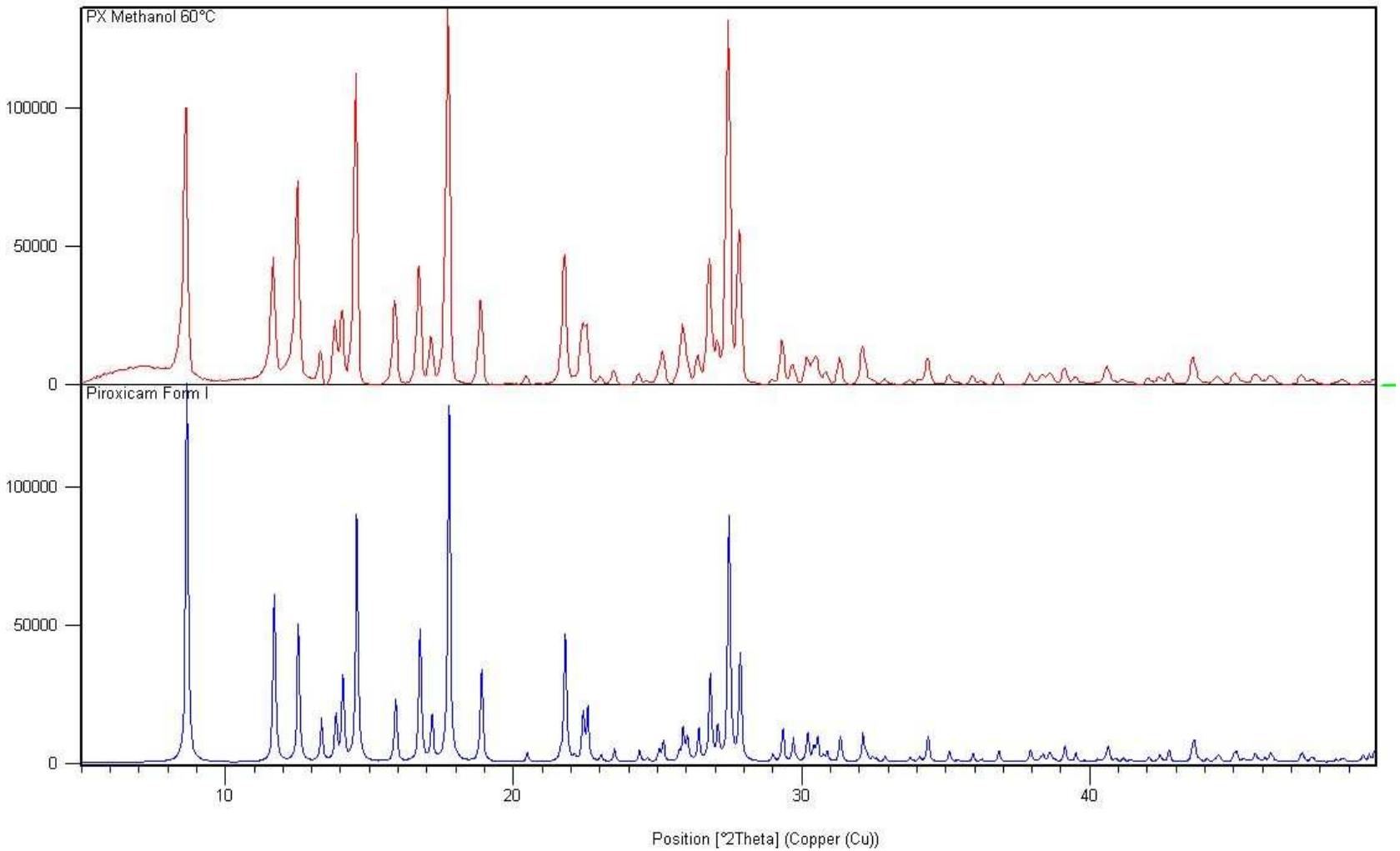

Appendix B4b-7 PXRD of the recrystallisation of piroxicam from methanol at 60°C (red). The pattern shows 100% form I (blue) with no PX : methanol solvate present.

Appendix B4c - Powder X-ray Diffraction of the Porous Gallic Acid Monohydrate from Multi-Component Crystallisations (Section 4.6)

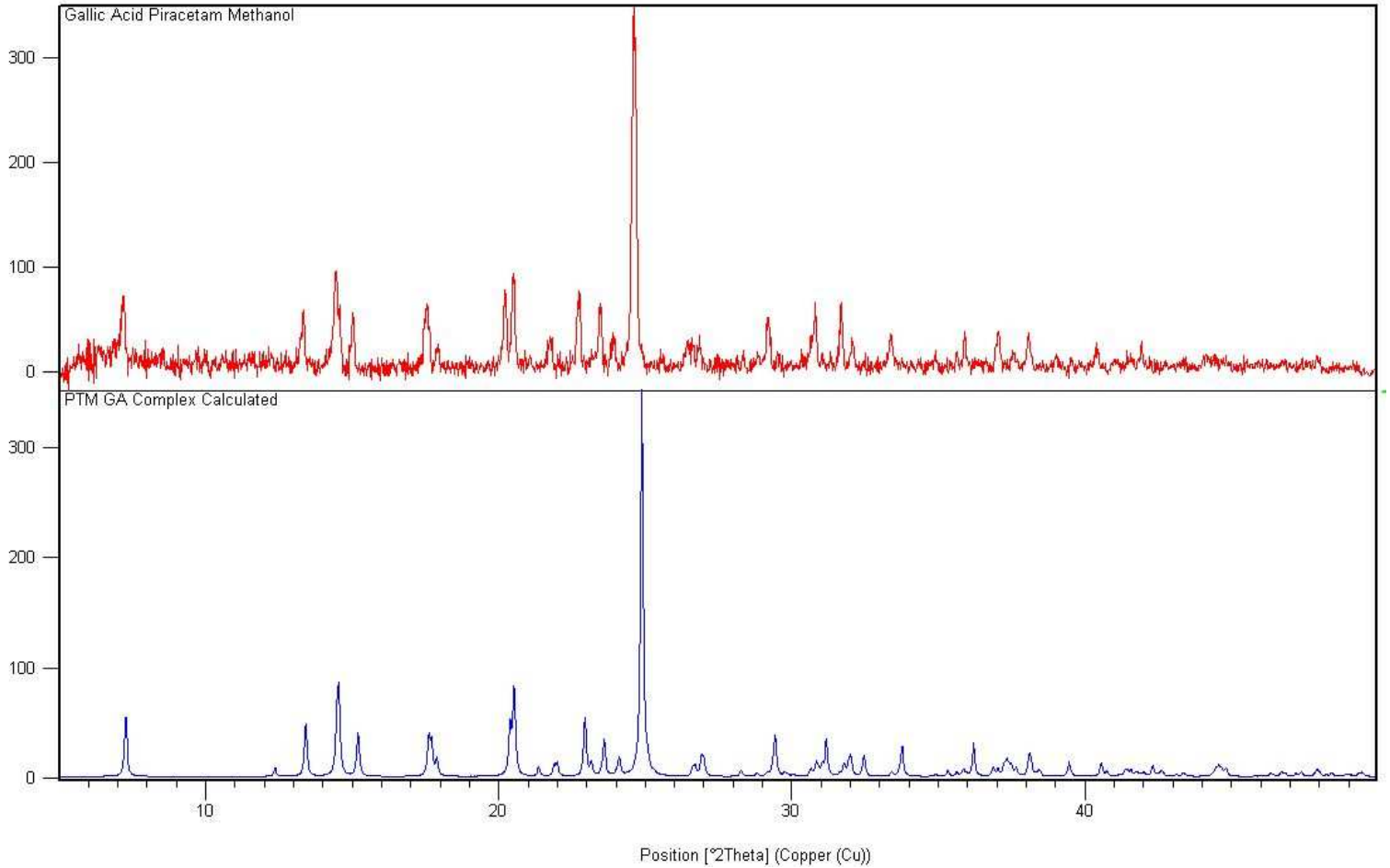

Appendix B4c-1 PXRD of the co-crystallisation of gallic acid with piracetam from methanol (red, room temperature). The patterns shows 100% of the gallic acid : piracetam molecular complex (blue, calculated at 100K) and none of the porous gallic acid monohydrate, despite its presence being confirmed by single crystal XRD. An x-shift is required due to the different experimental temperatures.

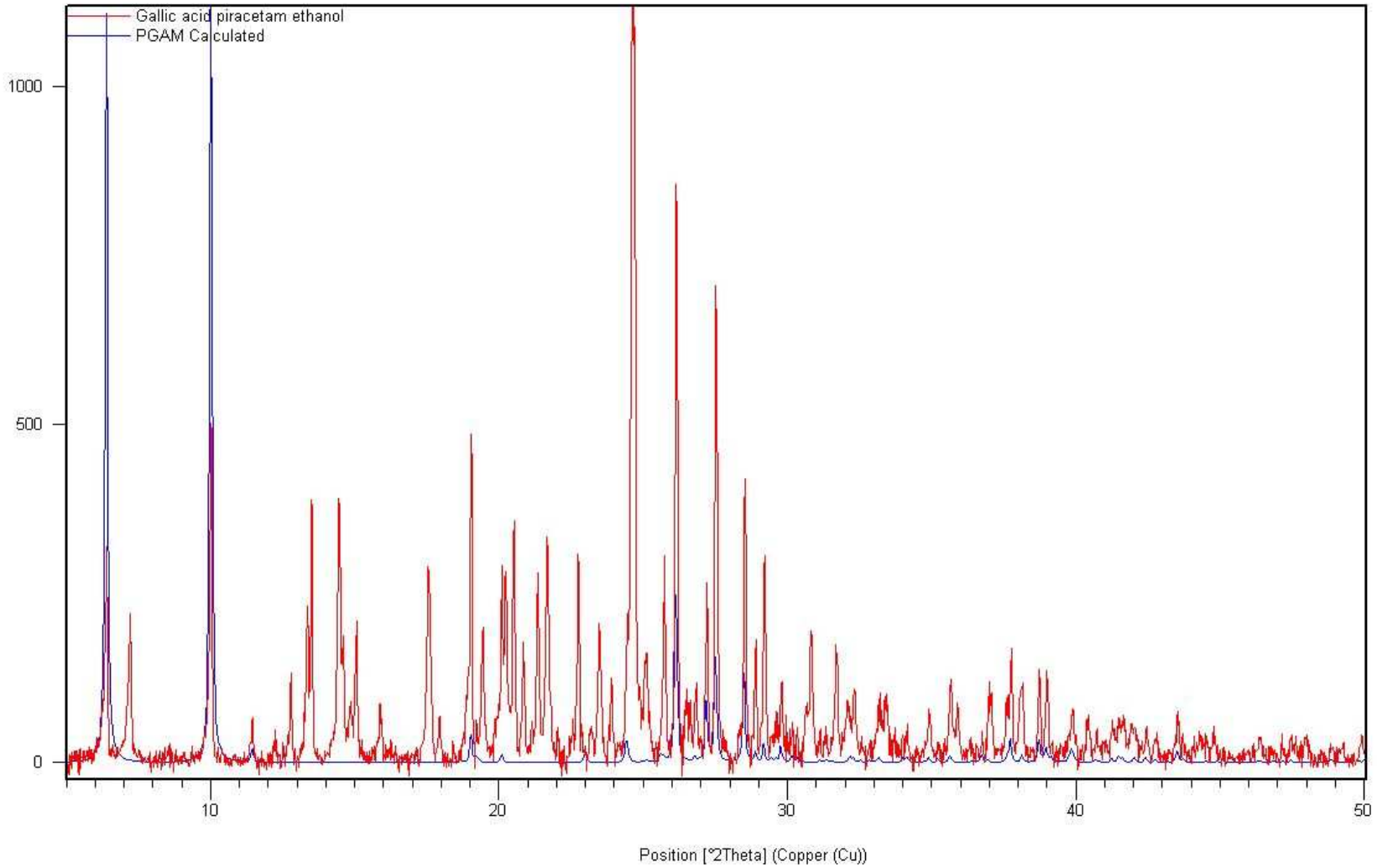

Appendix B4c-2 PXRD of the co-crystallisation of gallic acid with piracetam from ethanol (red). The pattern shows the presence of the porous gallic acid monohydrate (blue). The other peaks correspond to the GA : PTM molecular complex as well as PTM III and GAM I.

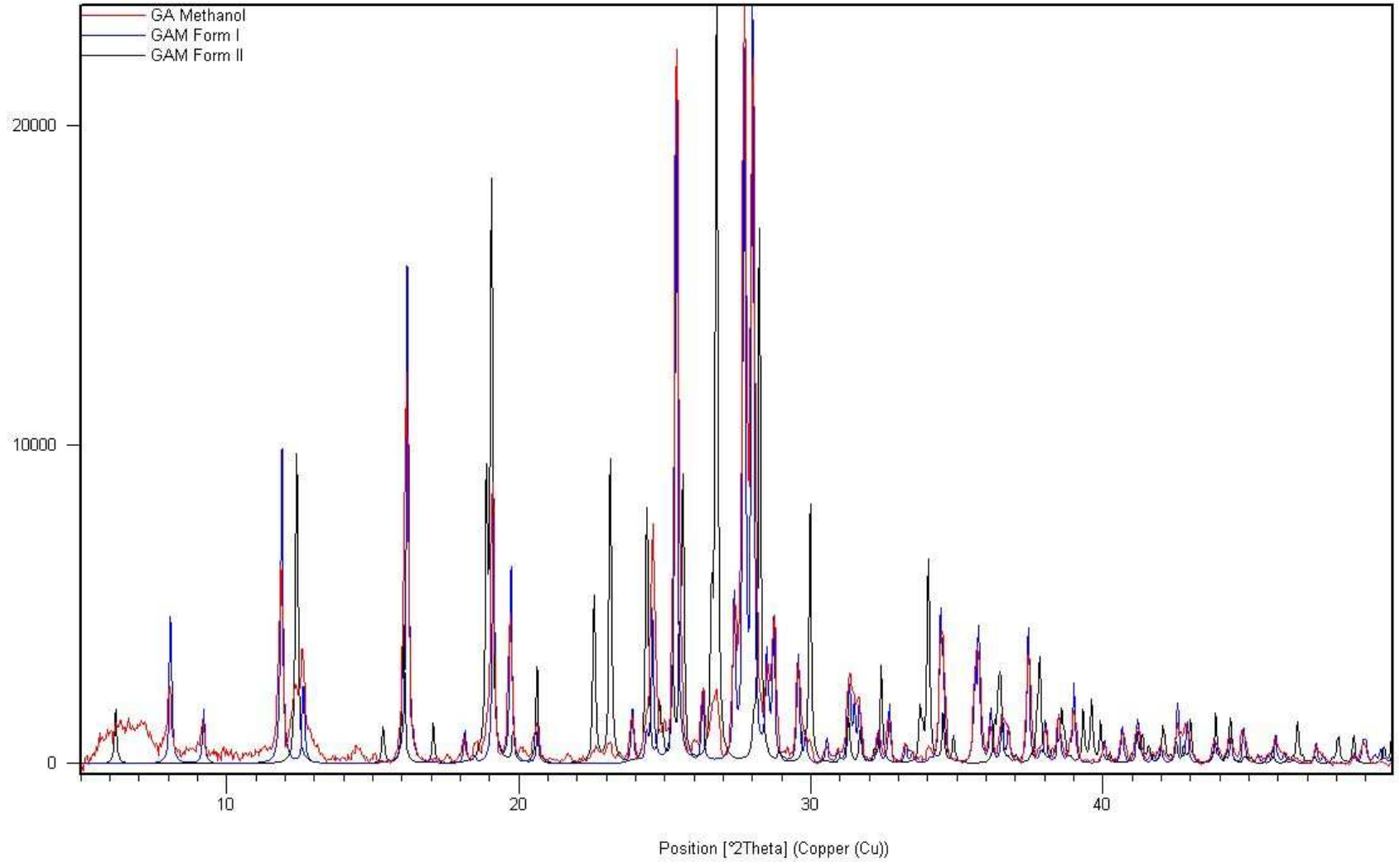

Appendix B4c-3 PXRD of the recrystallisation of gallic acid from methanol with no co-molecule (red). The pattern shows only GAM I and GAM II (blue and black).

Appendix B4d - Powder X-ray Diffraction of the Piracetam Form I from Multi-Component Crystallisations (Section 4.8)

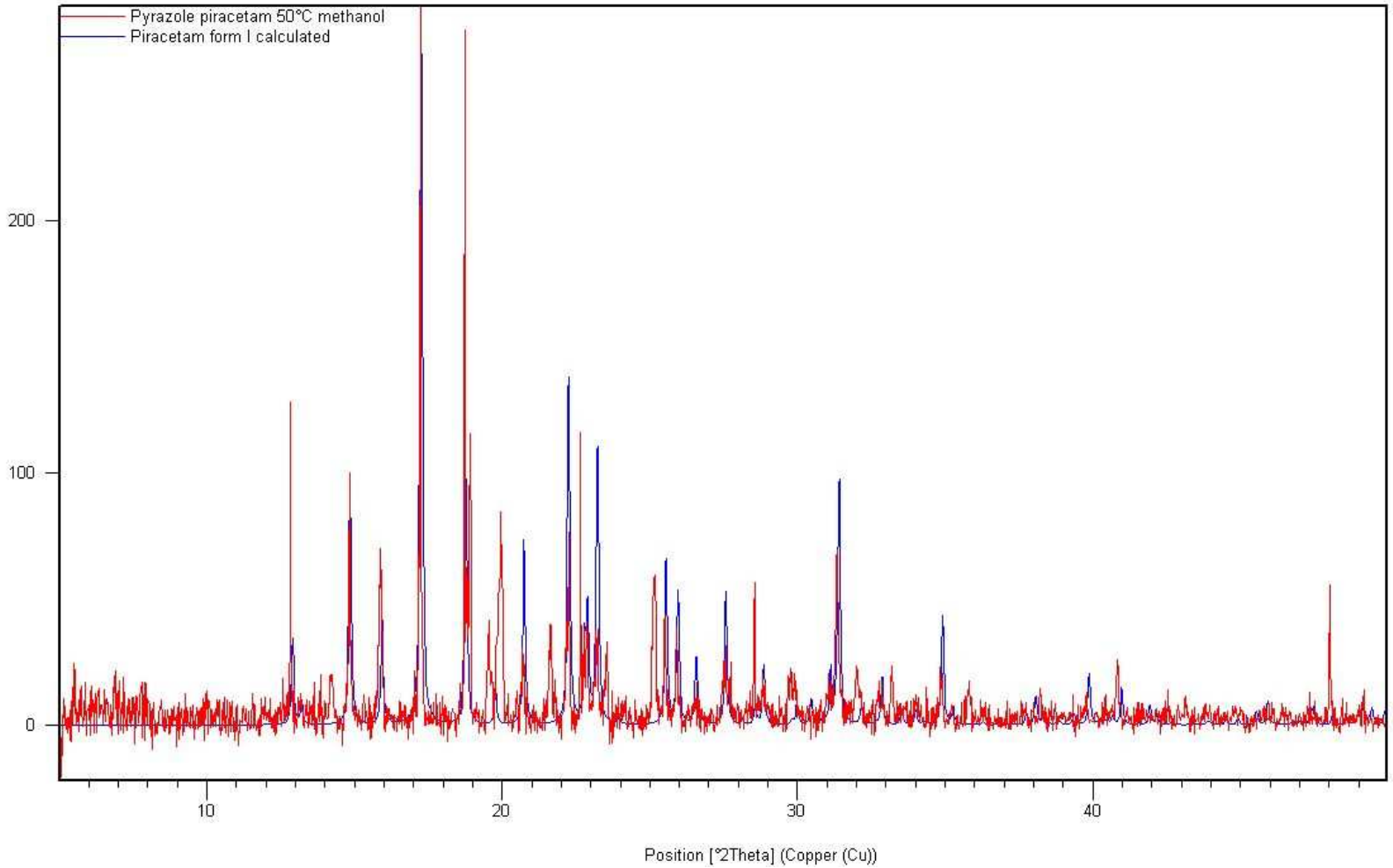

Appendix B4d-1 PXRD of the co-crystallisation of piracetam with pyrazole (1:2 mass ratio) in methanol at 50°C (red). The patterns shows a mixture of piracetam from I (blue) and form II (remaining peaks).

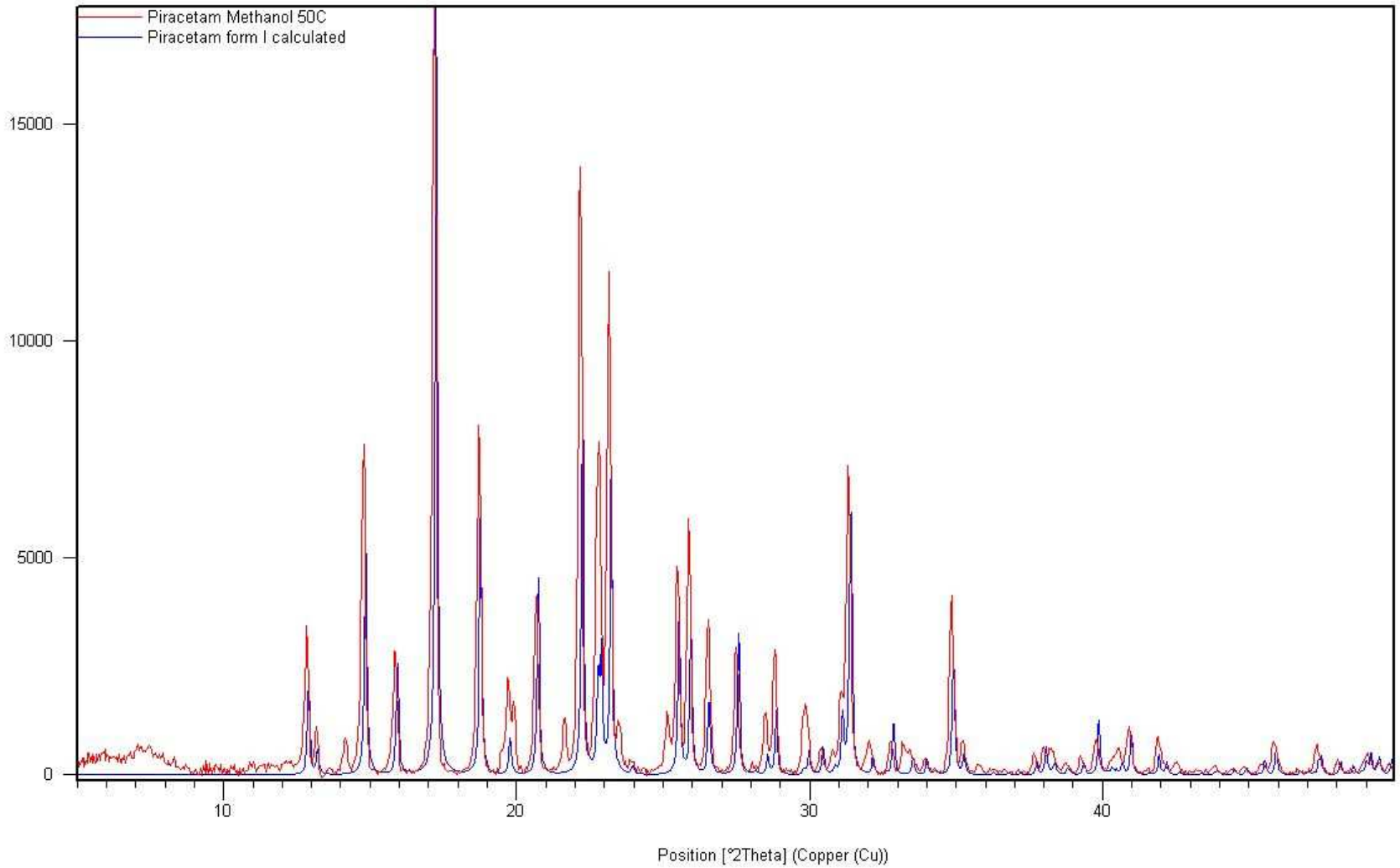

Appendix B4d-2 PXRD of the recrystallisation of piracetam in methanol at 50°C (red). The pattern shows a mixture of piracetam from I (blue) and form II (remaining peaks).

Appendix B - Powder X-Ray Diffraction for Molecular Complexes of Piroxicam with Mono-Substituted Benzoic Acids

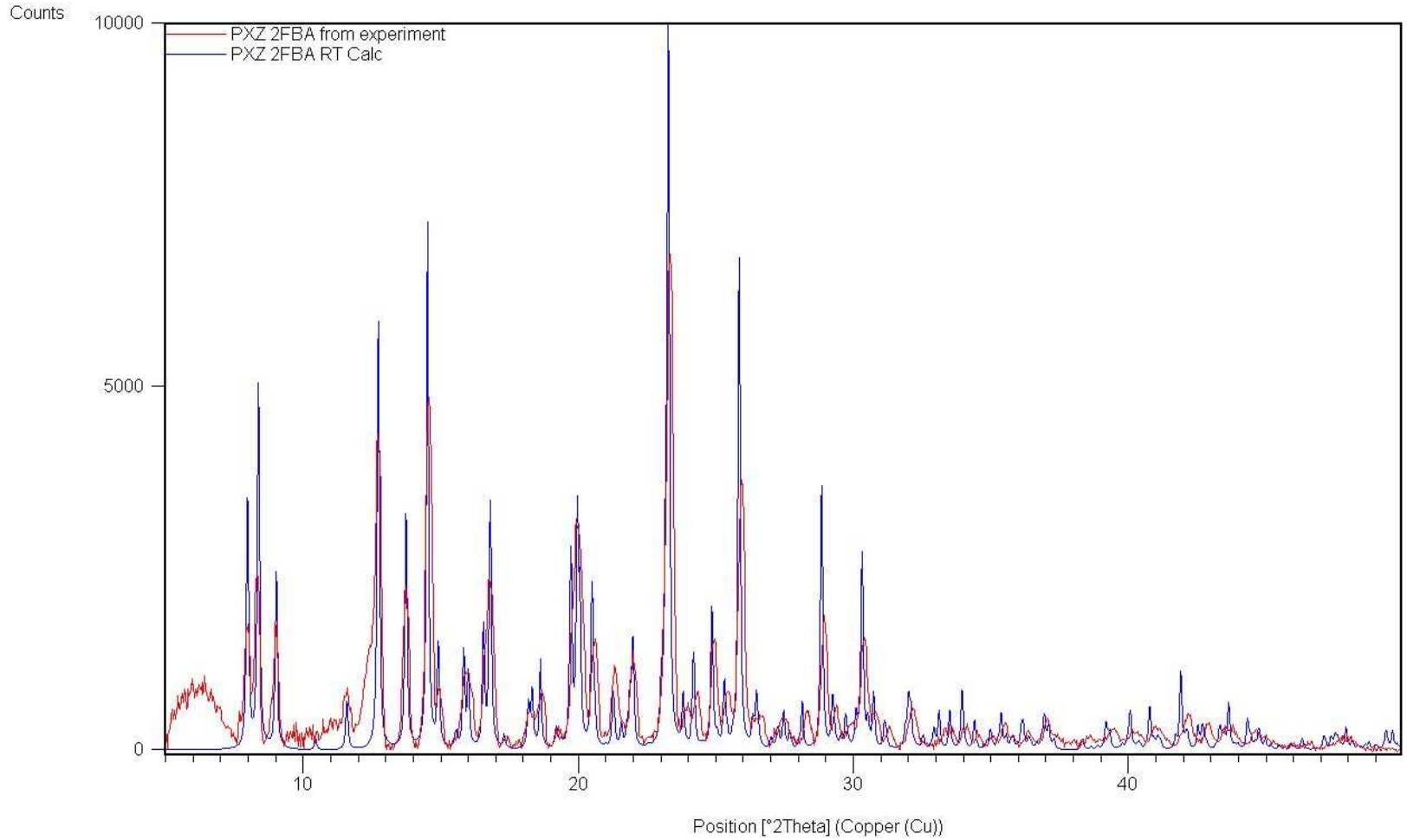

Figure B5-1 PXRD of the PXZ : 2FBA complex from co-crystallisation experiment (red) (prior to heating regime) shows an almost perfect match with PXRD calculated directly from the crystal structure of PXZ : 2FBA (Blue).

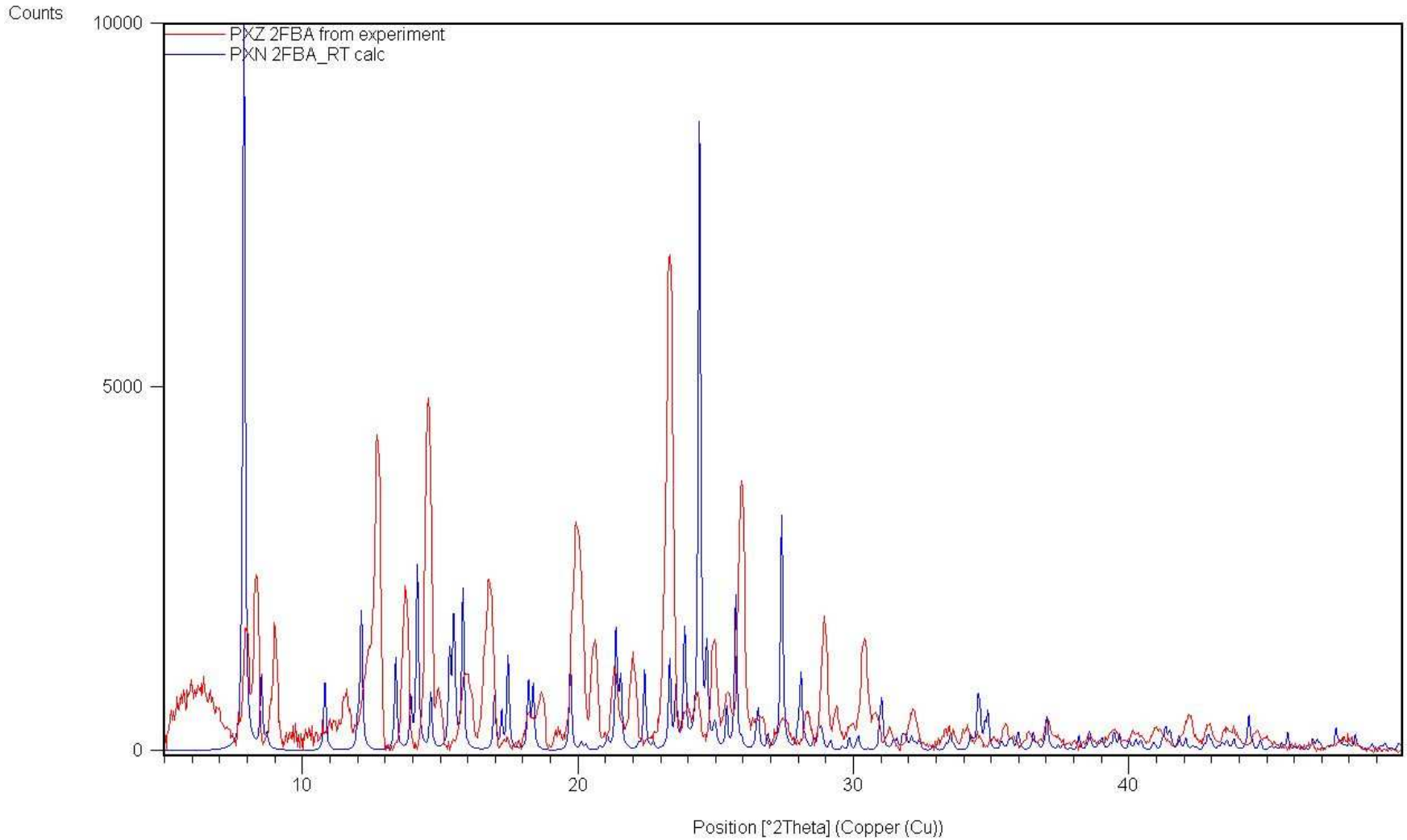

Figure B5-2 PXRD of the PXZ : 2FBA complex from crystallisation experiment (red) (prior to heating regime) shows a poor match with PXRD calculated directly from the crystal structure of PXN : 2FBA (Blue).

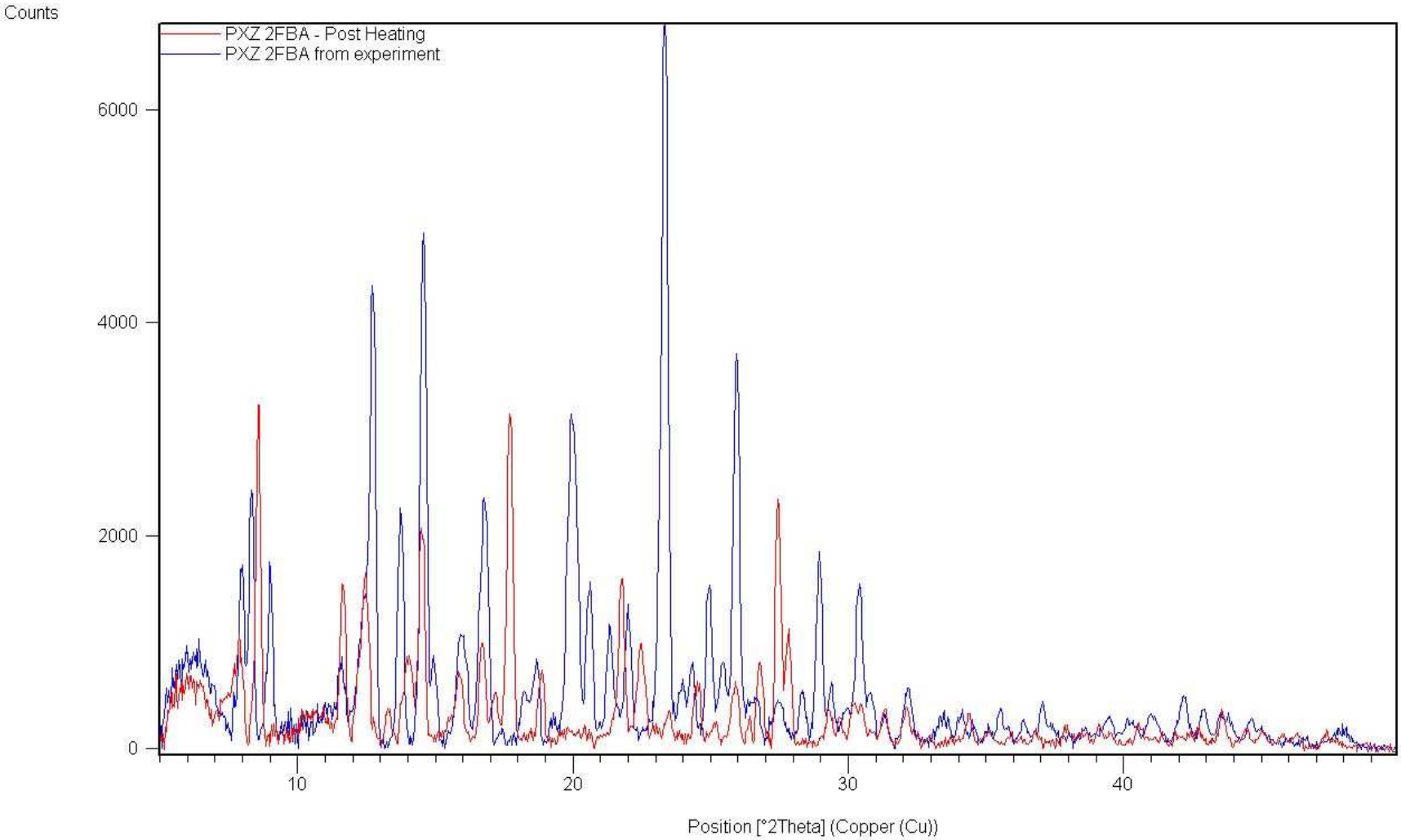

Figure B5-3 PXRD of PXZ : 2FBA sample, after annealing at 140°C for twenty minutes (red), shows a distinct change in the crystal structure when compared with the PXRD of the PXZ : 2FBA complex before heating (blue).

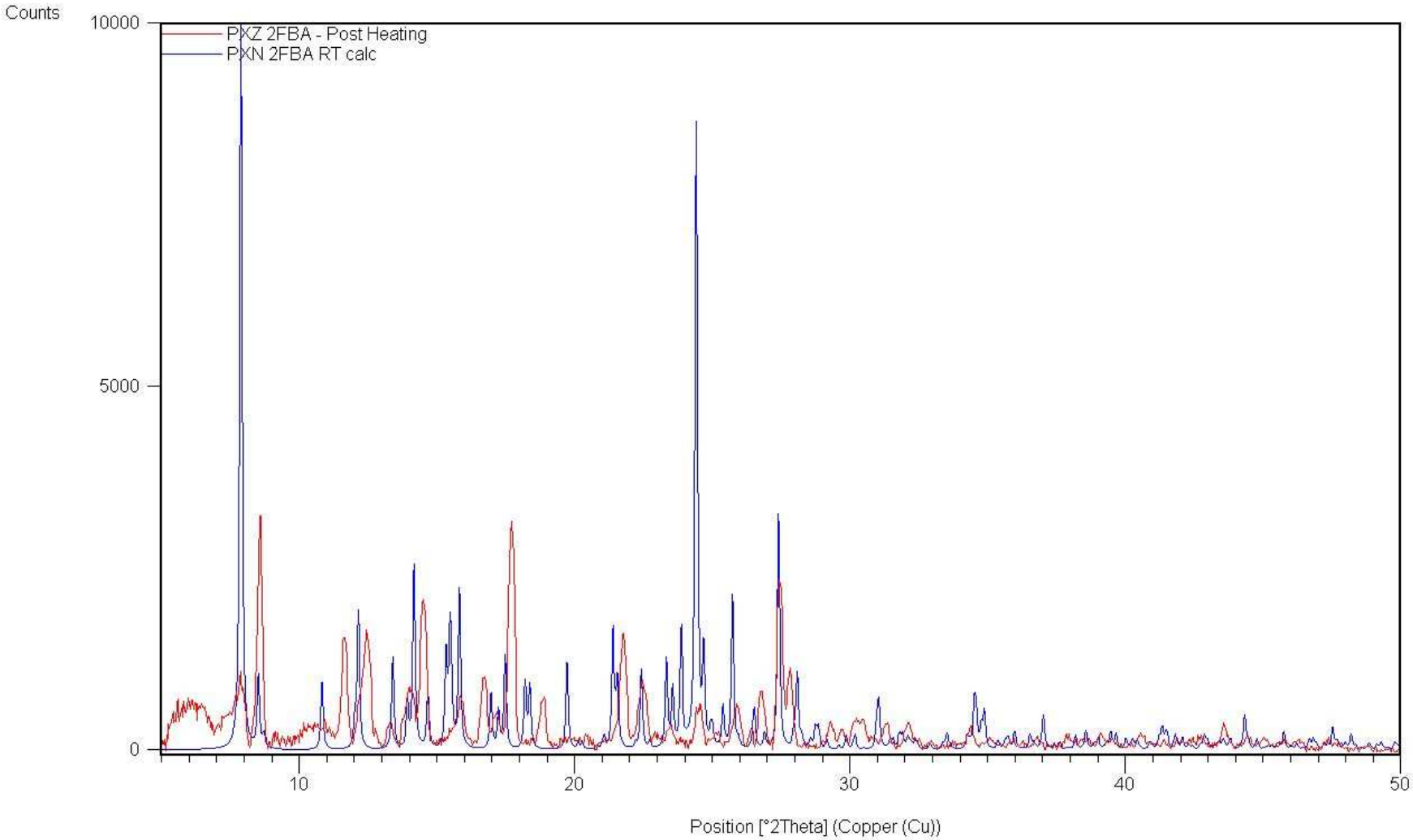

Figure B5-4 PXRD of PXZ : 2FBA sample post annealing (red) shows a closer match with the calculated PXRD from the PXN : 2FBA crystal structure (blue). Note: complete solid - solid phase transition is not achieved resulting in some remaining PXZ : 2FBA.

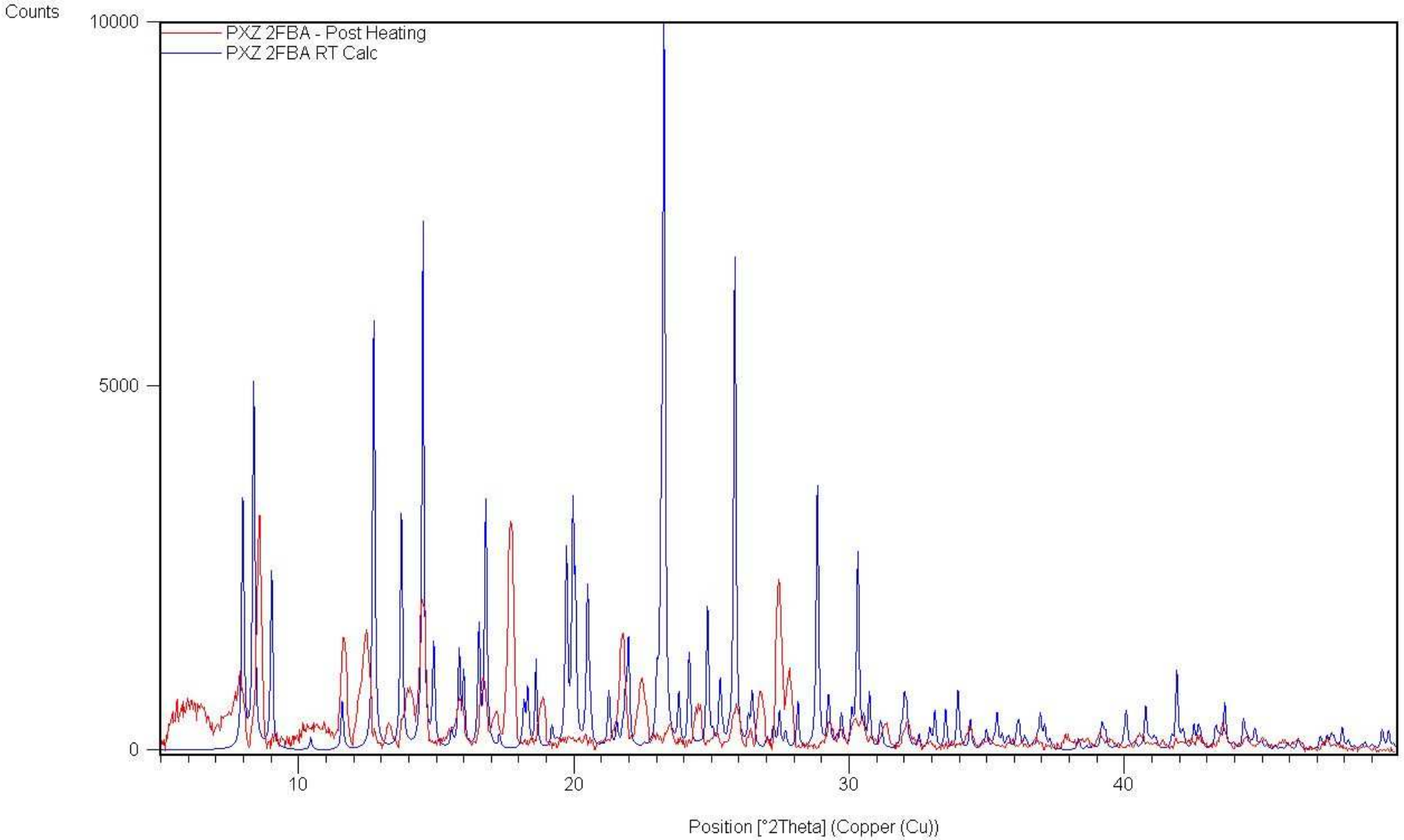

Figure B5-5 PXRD of PXZ : 2FBA sample post annealing (red) is no longer a match with the calculated PXRD of the PXZ : 2FBA complex (blue).

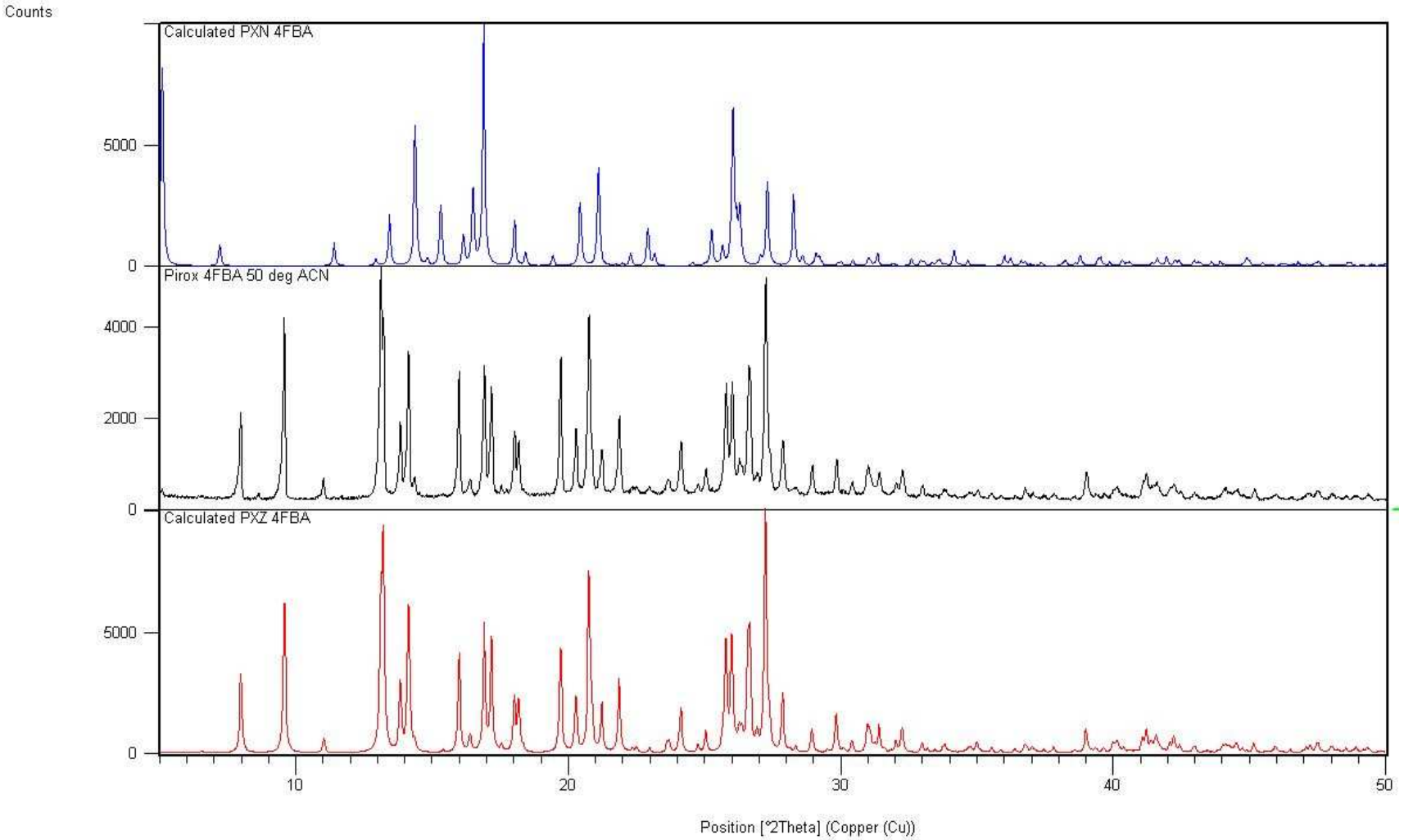

Figure B5-6 PXRD profile of initial crystallisation of PXZ: 4FBA from acetonitrile at 50°C showing 100% yield was obtained (Calculated profile for both tautomeric polymorphs shown for comparison).

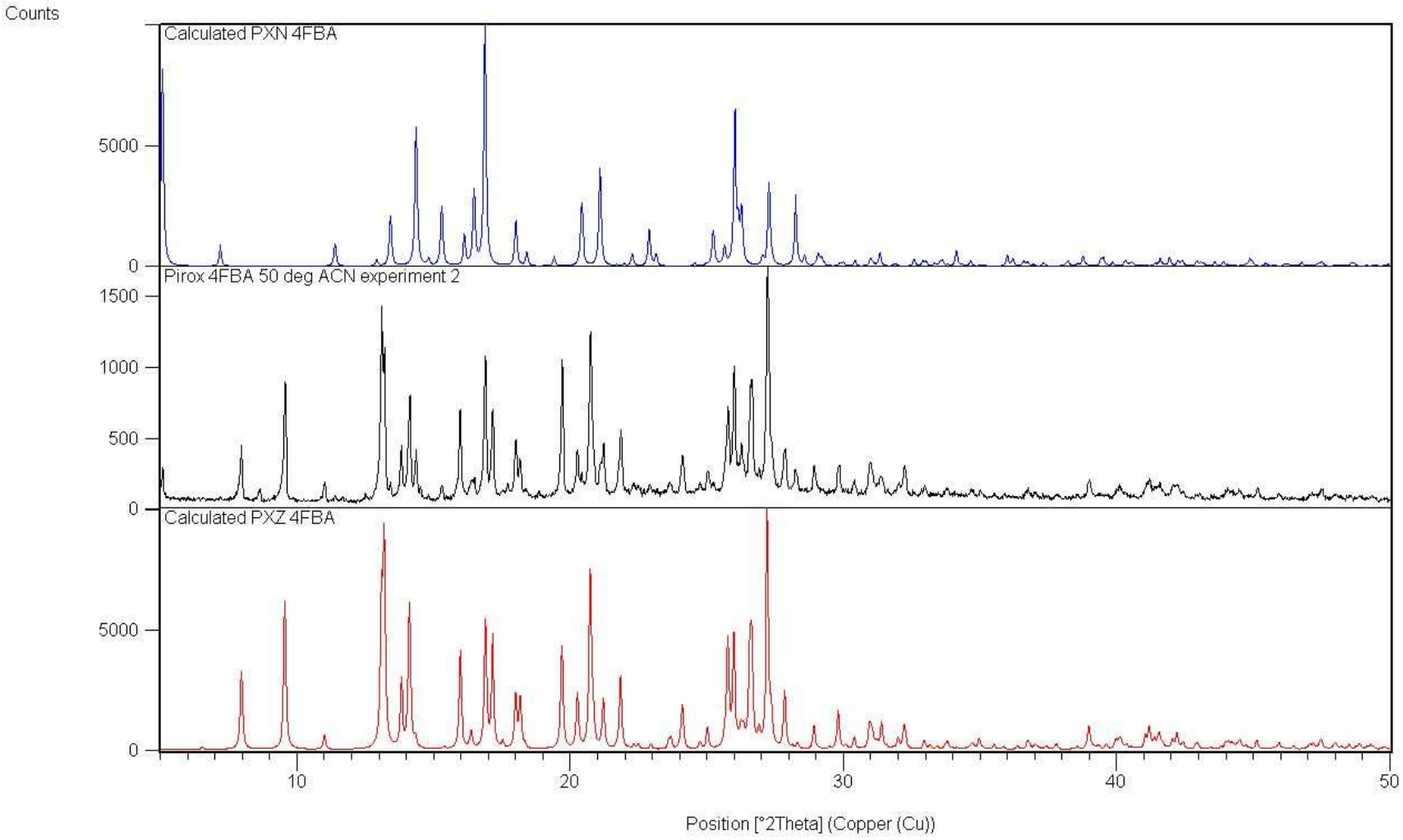

Figure B5-7 PXRD profile of repeat crystallisation of PX and 4FBA from acetonitrile at 50°C showing a mixture of PXZ: 4FBA and PXN: 4FBA was obtained (majority PXZ: 4FBA).

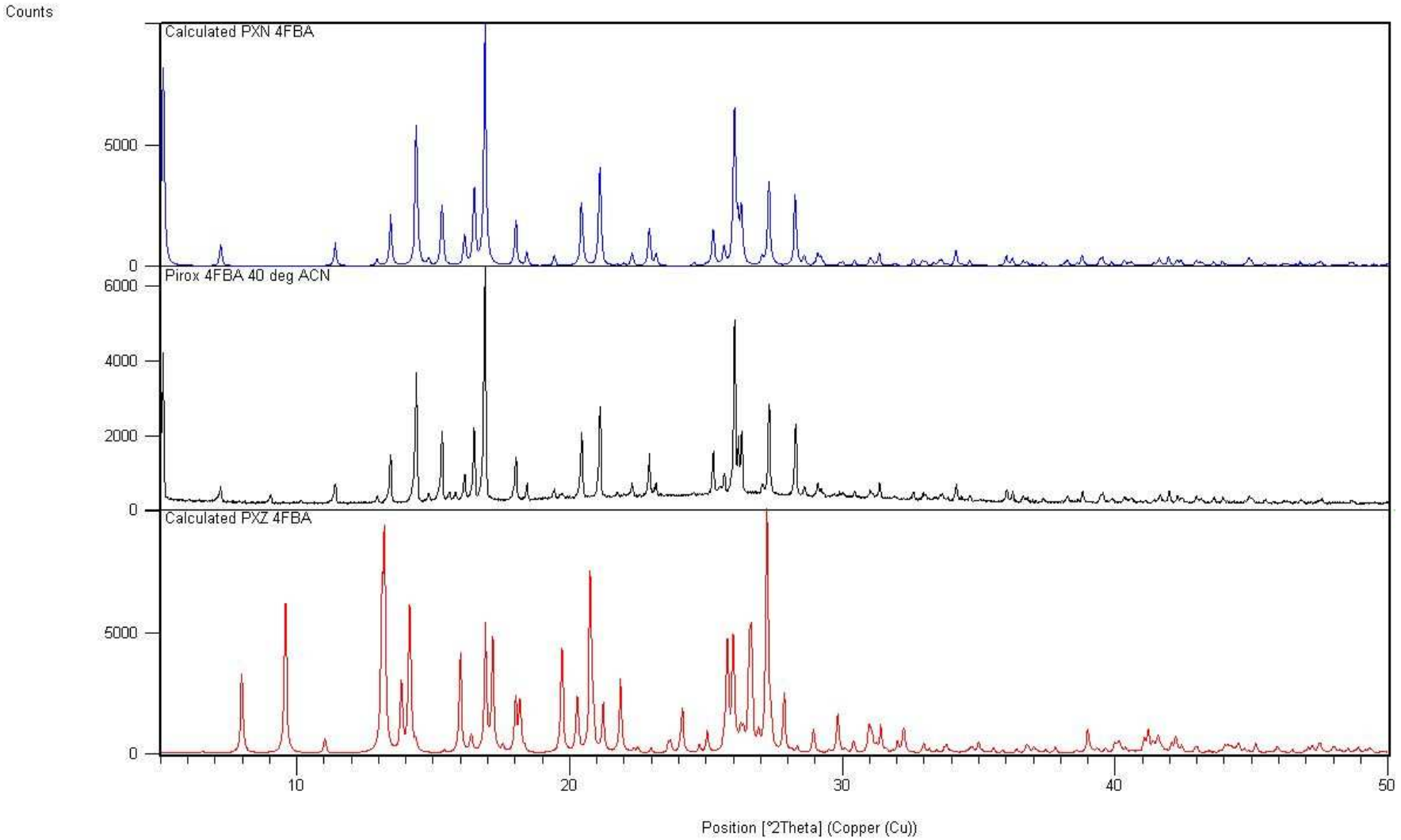

Figure B5-8 PXRD profile of initial crystallisation of PXN: 4FBA from acetonitrile at 40°C showing 100% yield was obtained.

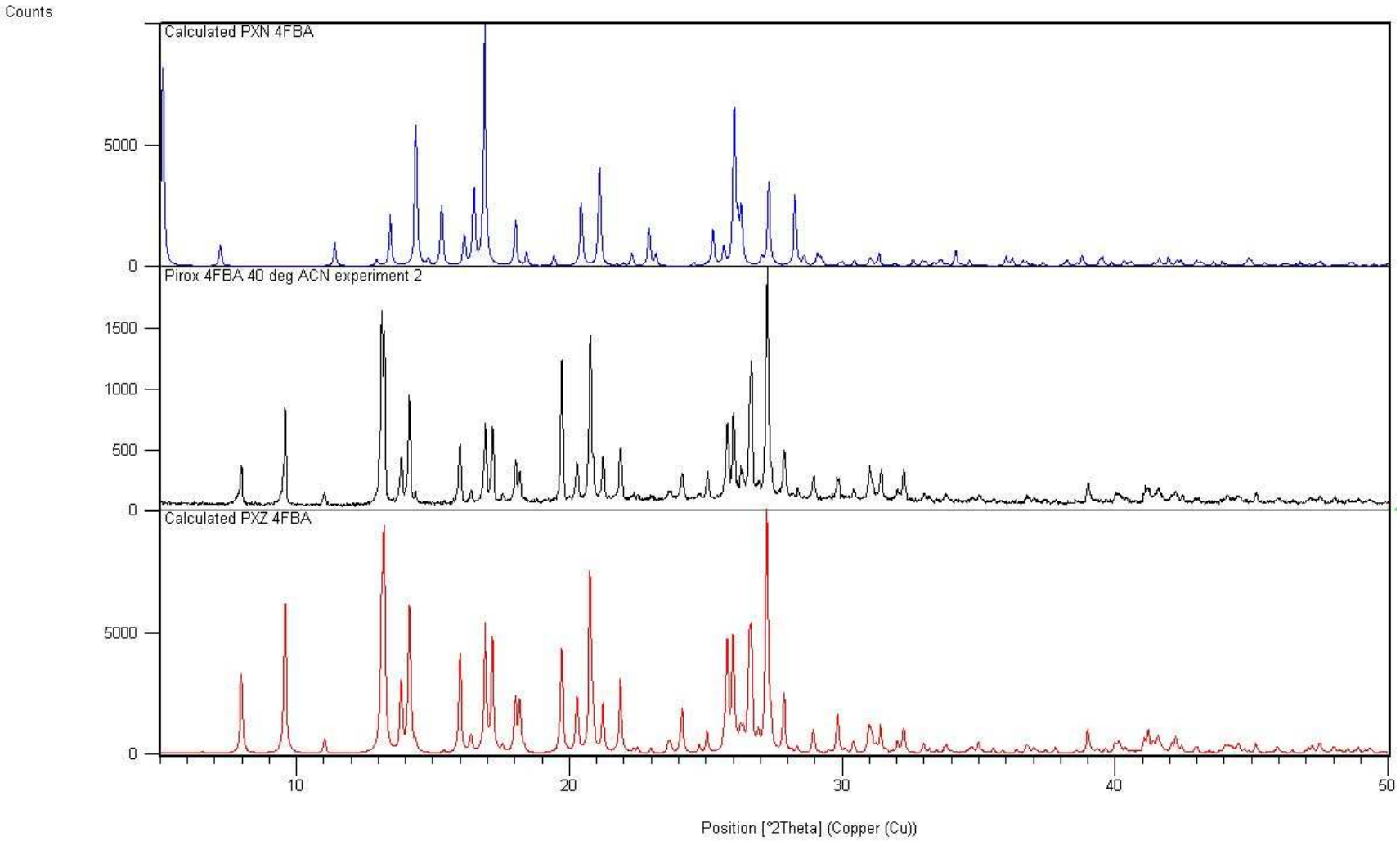

Figure B5-9 PXRD profile of repeat crystallisation of PX and 4FBA from acetonitrile at 40°C showing 100% yield of PXZ: 4FBA was obtained.

Appendix B7 - Powder X-ray Diffraction of the Molecular Complex of Paracetamol with Imidazole

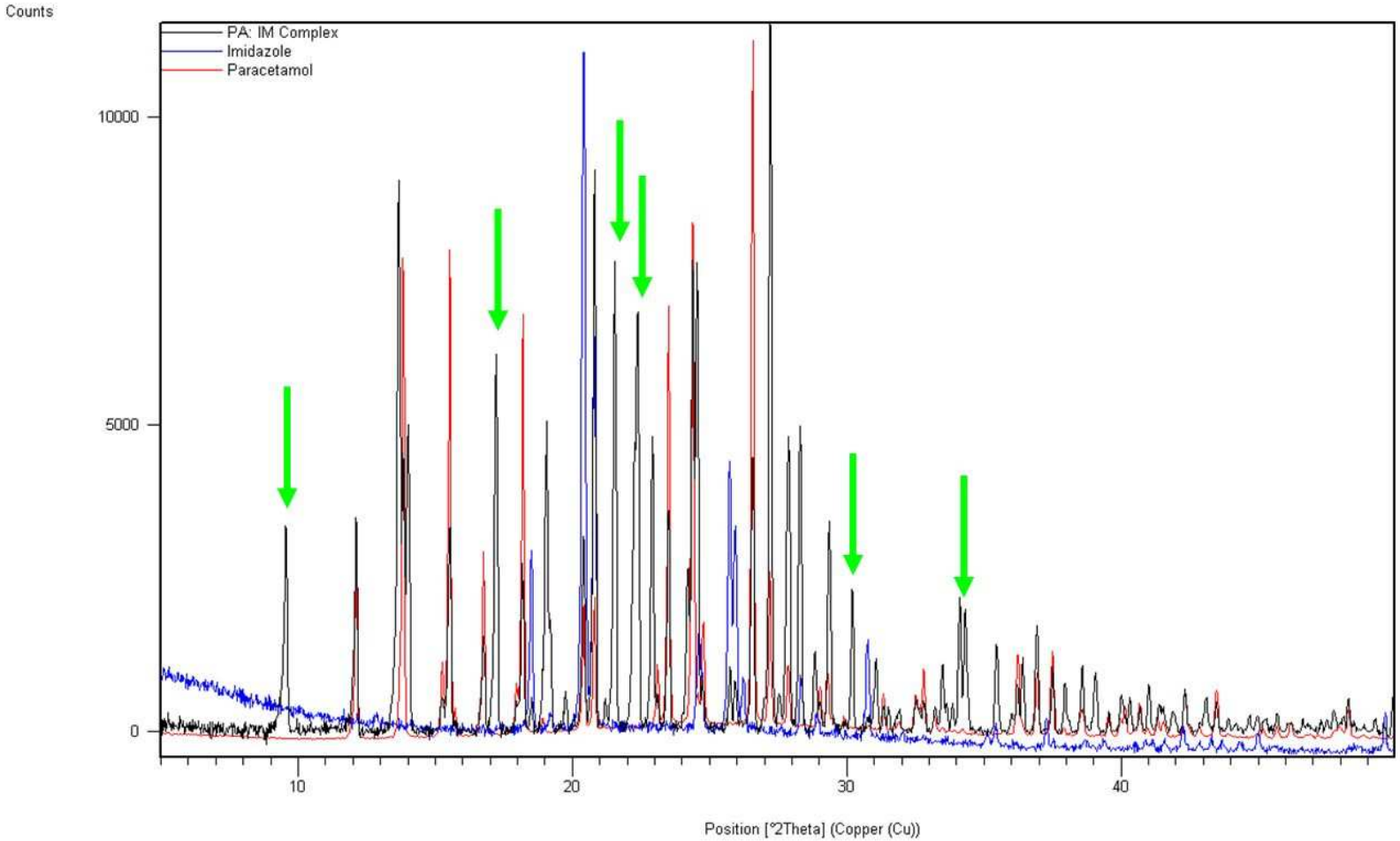

Figure B-7a Powder X-ray diffraction pattern of the paracetamol: imidazole co-crystallisation (black). The pattern shows a mixture of paracetamol (red), imidazole (blue) and the co-crystal (major unique peaks highlighted with a green arrow).

APPENDIX C: Thermal Analysis

Appendix C4 - DSC Analysis of Piroxicam Polymorphs

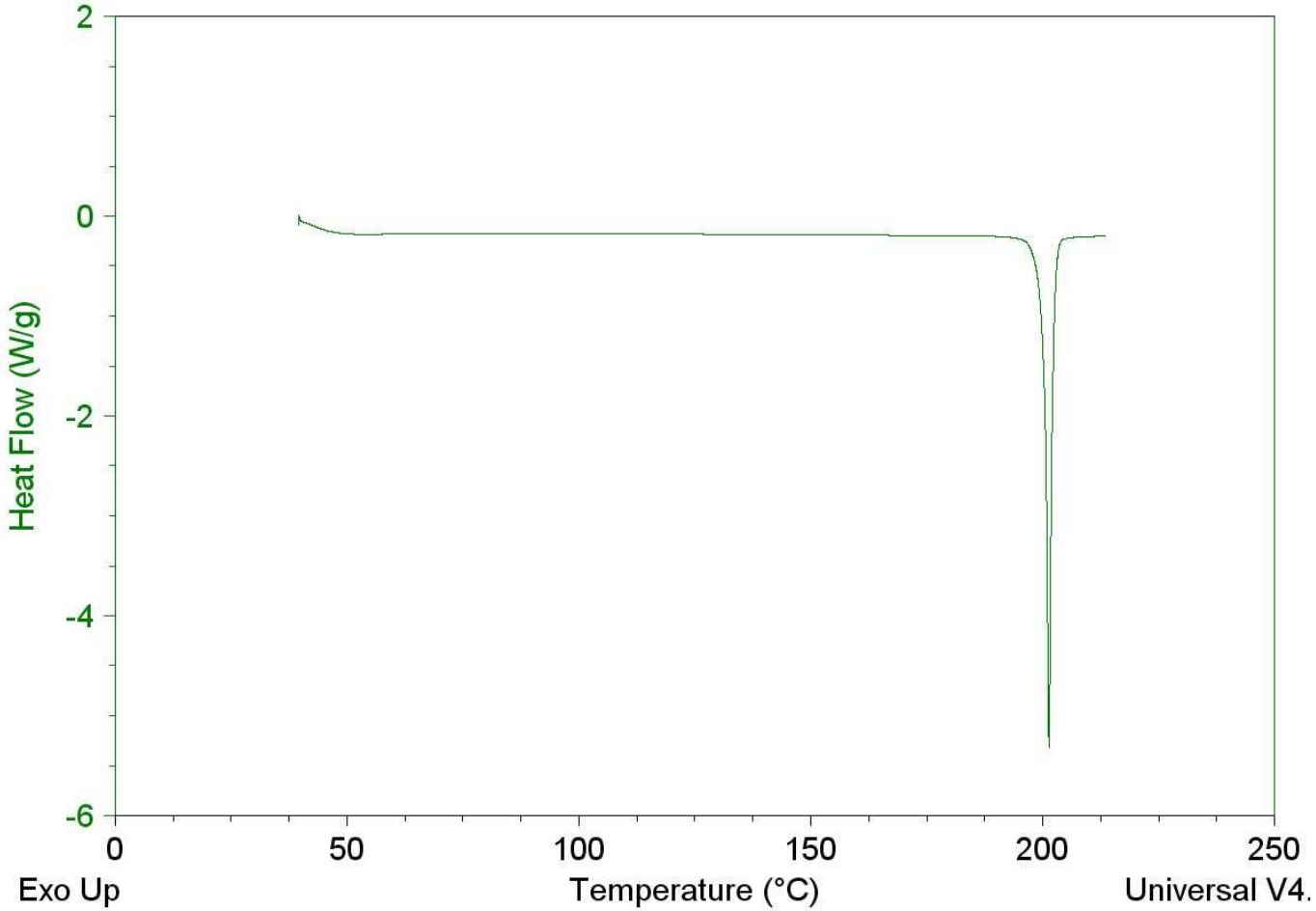

Figure C4-1 DSC of piroxicam form I.

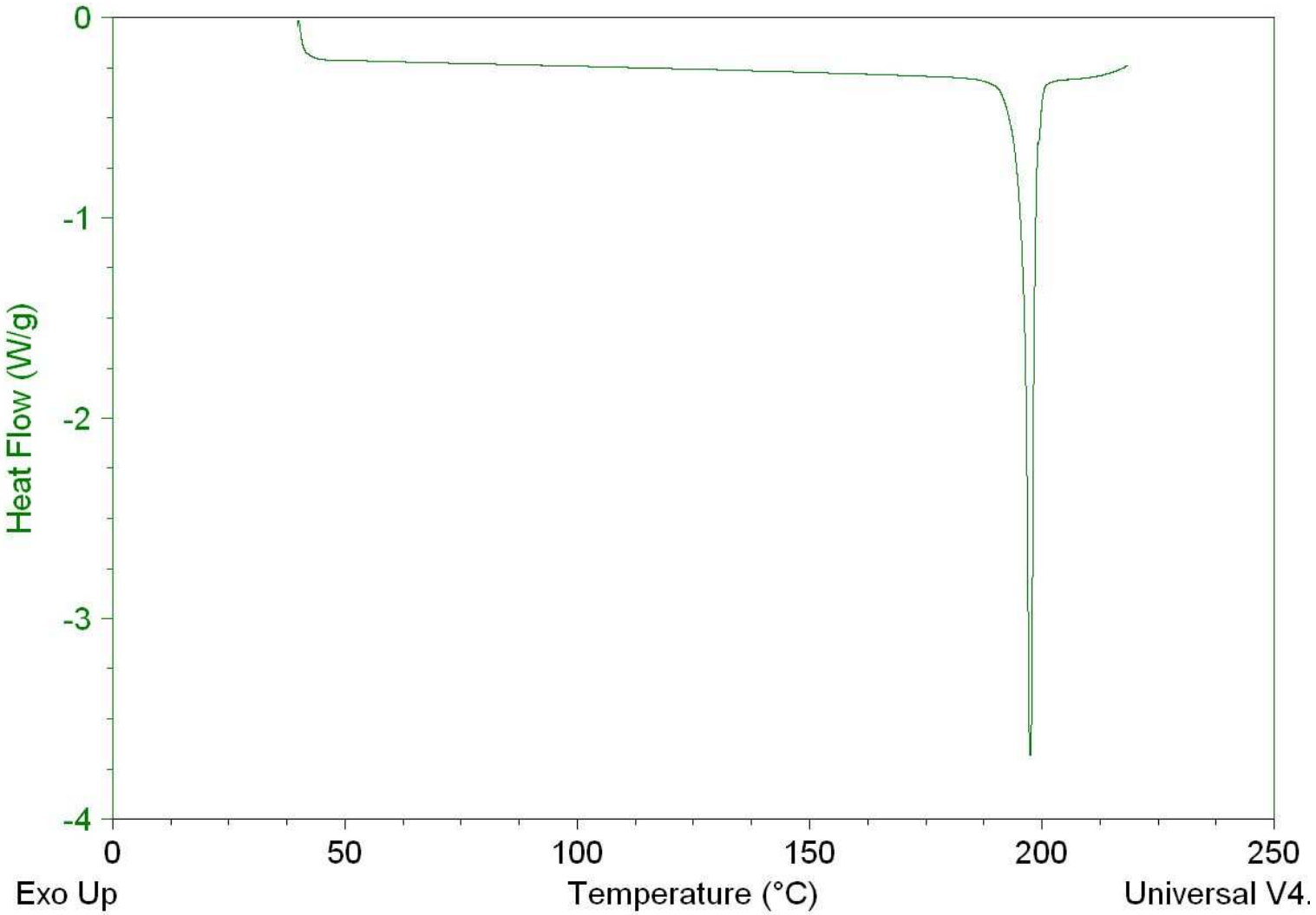

Figure C4-2 DSC of piroxicam form II.

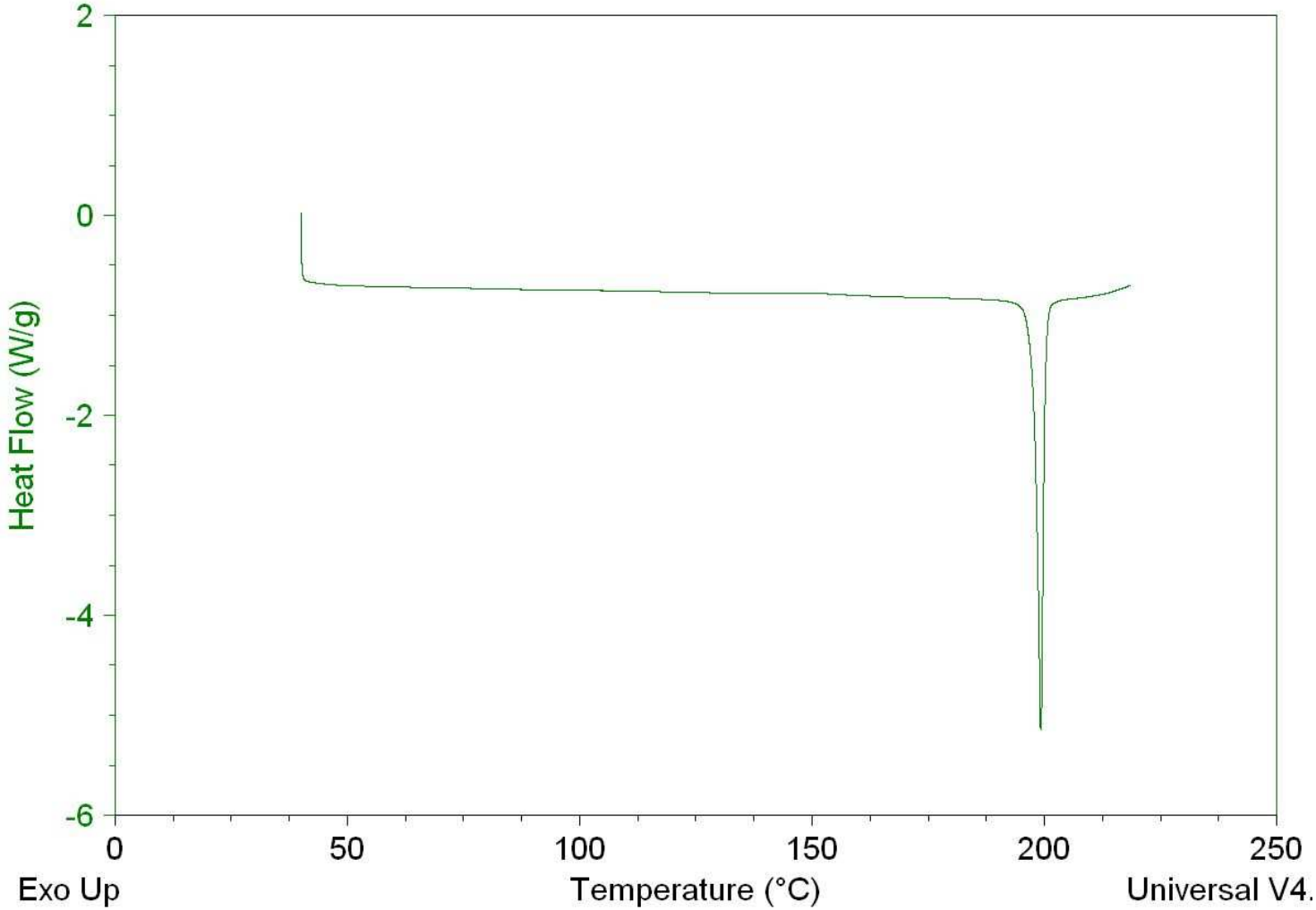

Figure C4-3 DSC of piroxicam form III.

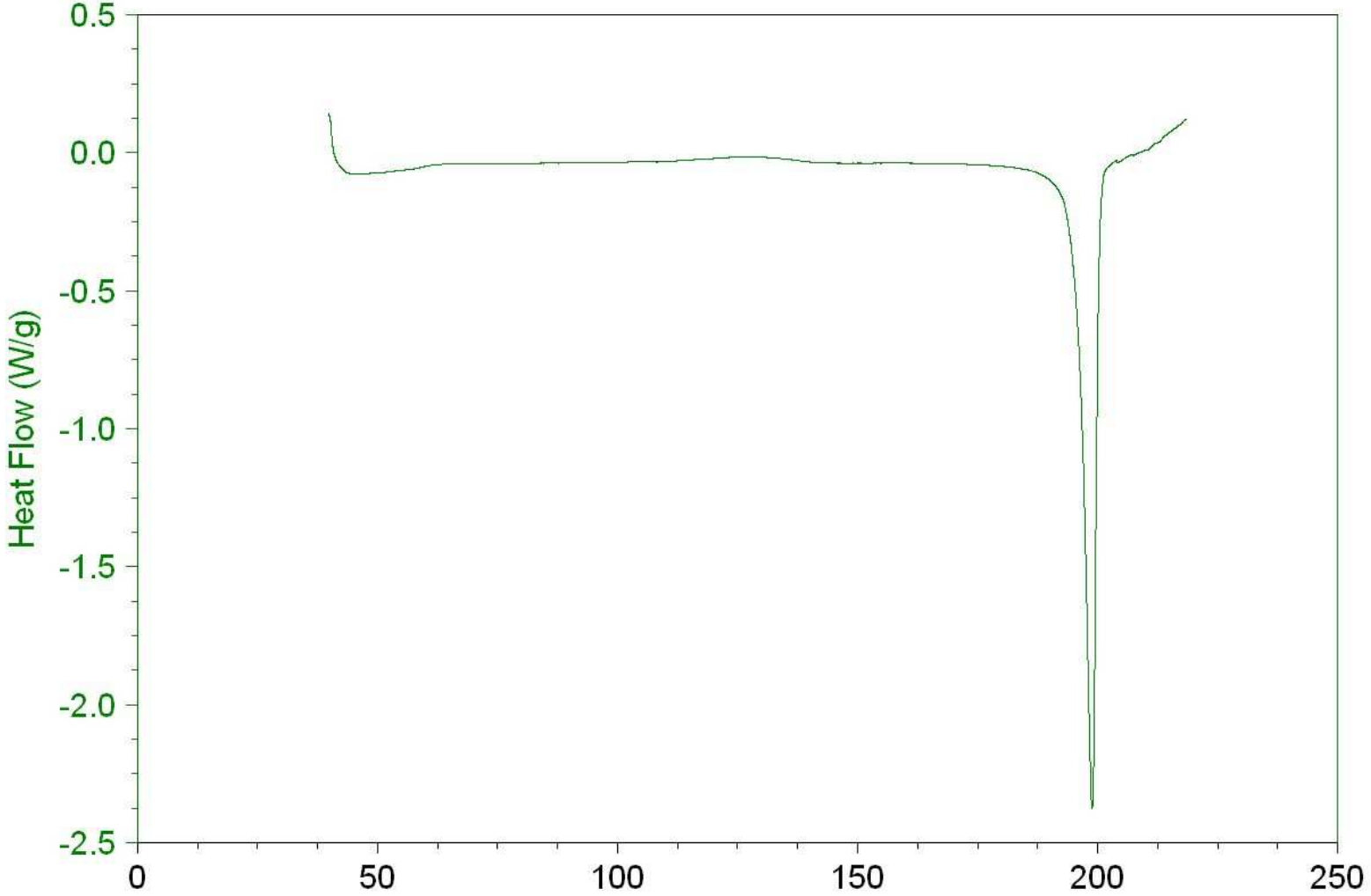

Figure C4-4 DSC of piroxicam form IV.

Appendix C5 - Thermal Analysis of Piroxicam Molecular Complexes with Mono-Substituted Benzoic Acids

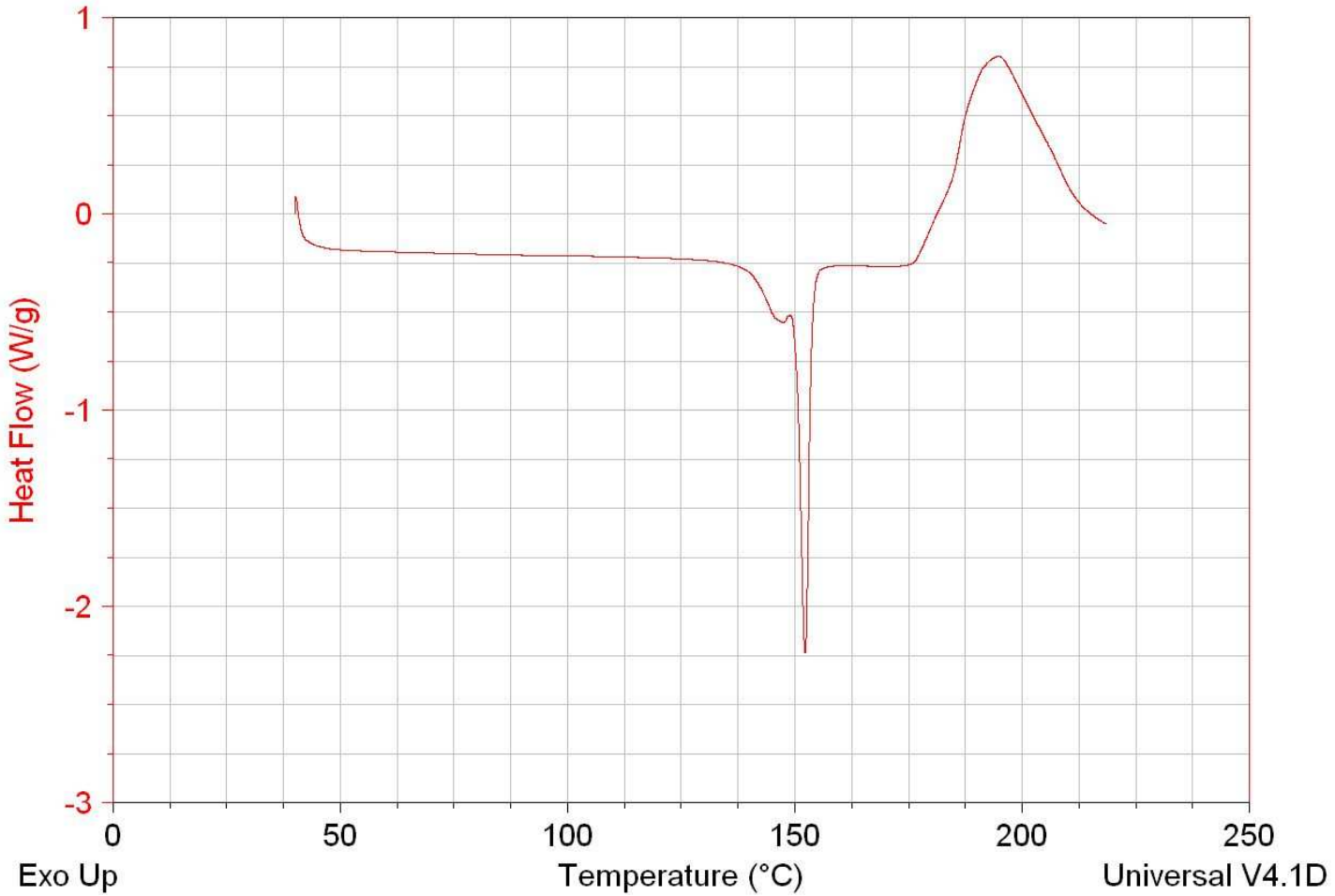

Figure C5-1 DSC trace of PXZ: 2FBA.

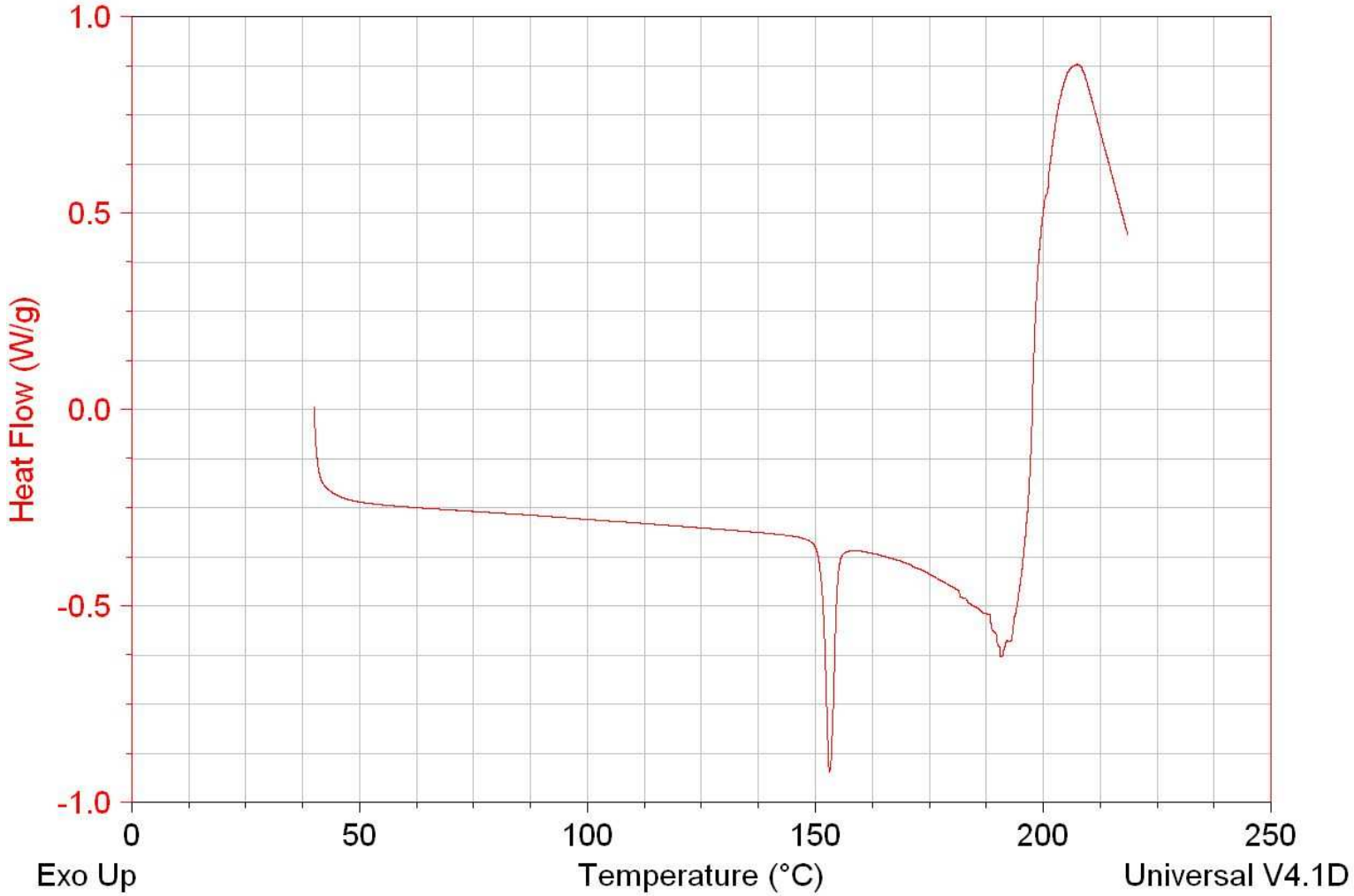

Figure C5-2 DSC trace of PXN: 2FBA.

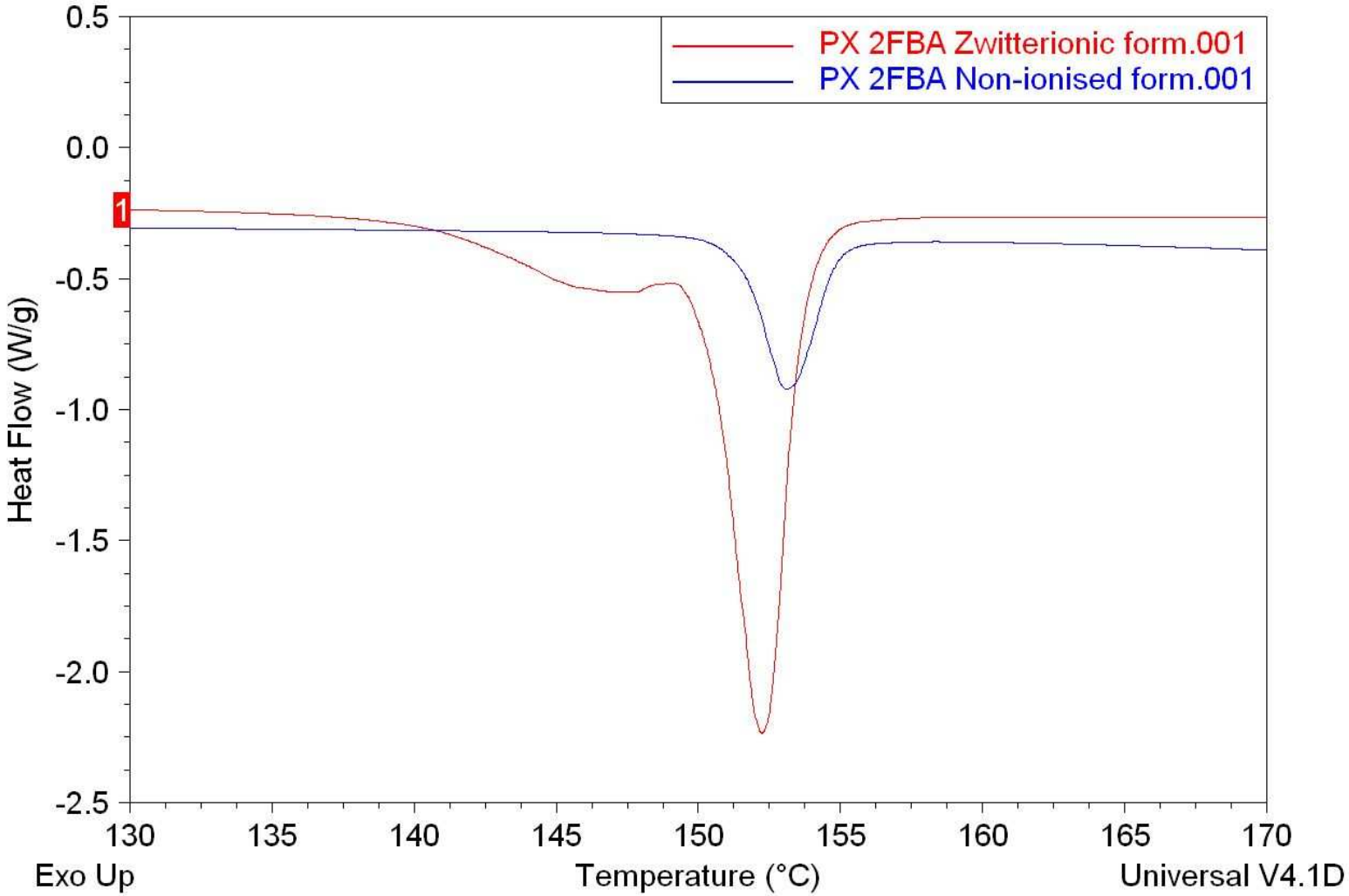

Figure C5-3 Overlay of PXZ: 2FBA and PXN: 2FBA DSC traces.

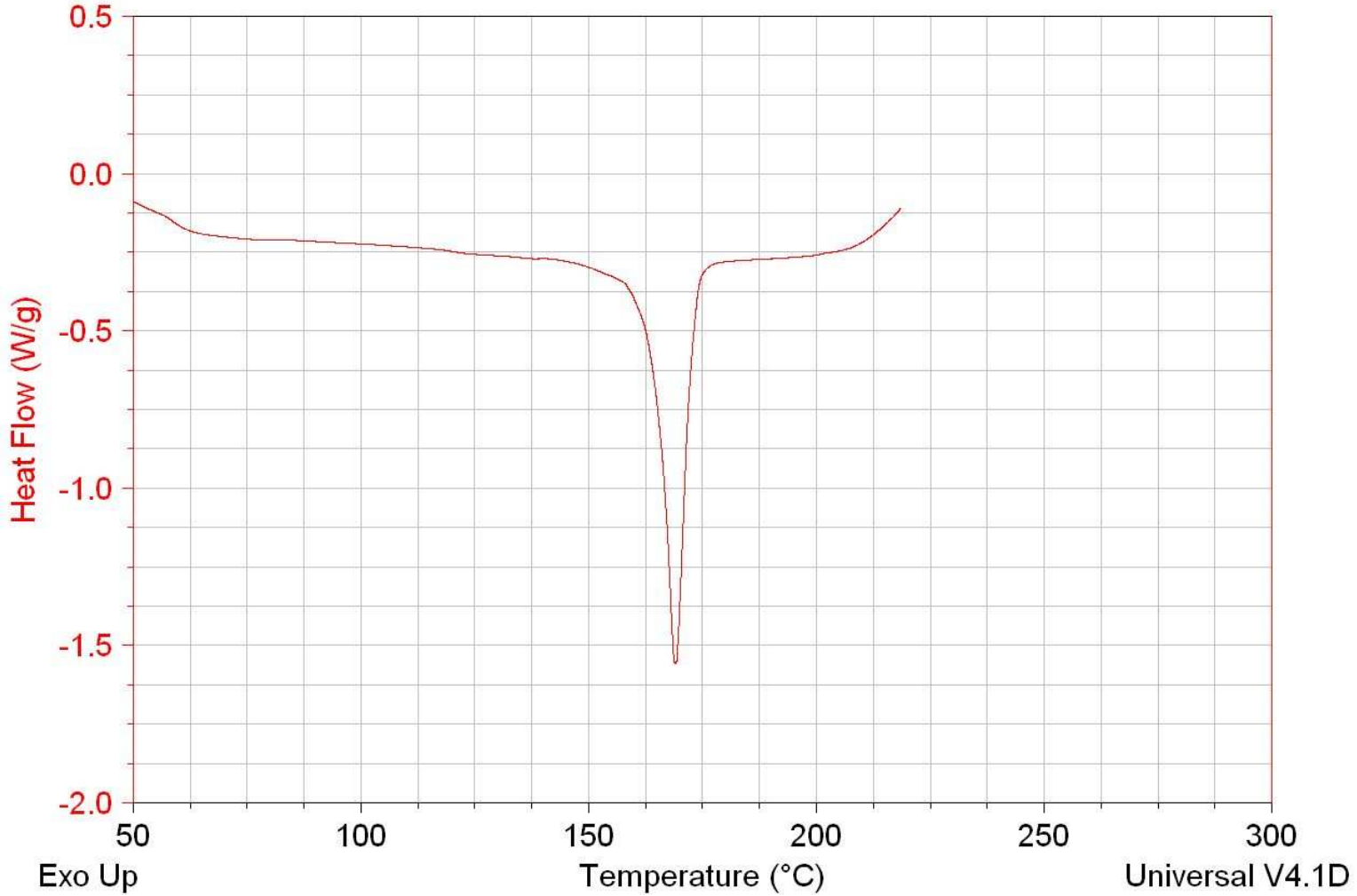

Figure C5-4 DSC trace of PXZ: 3FBA.

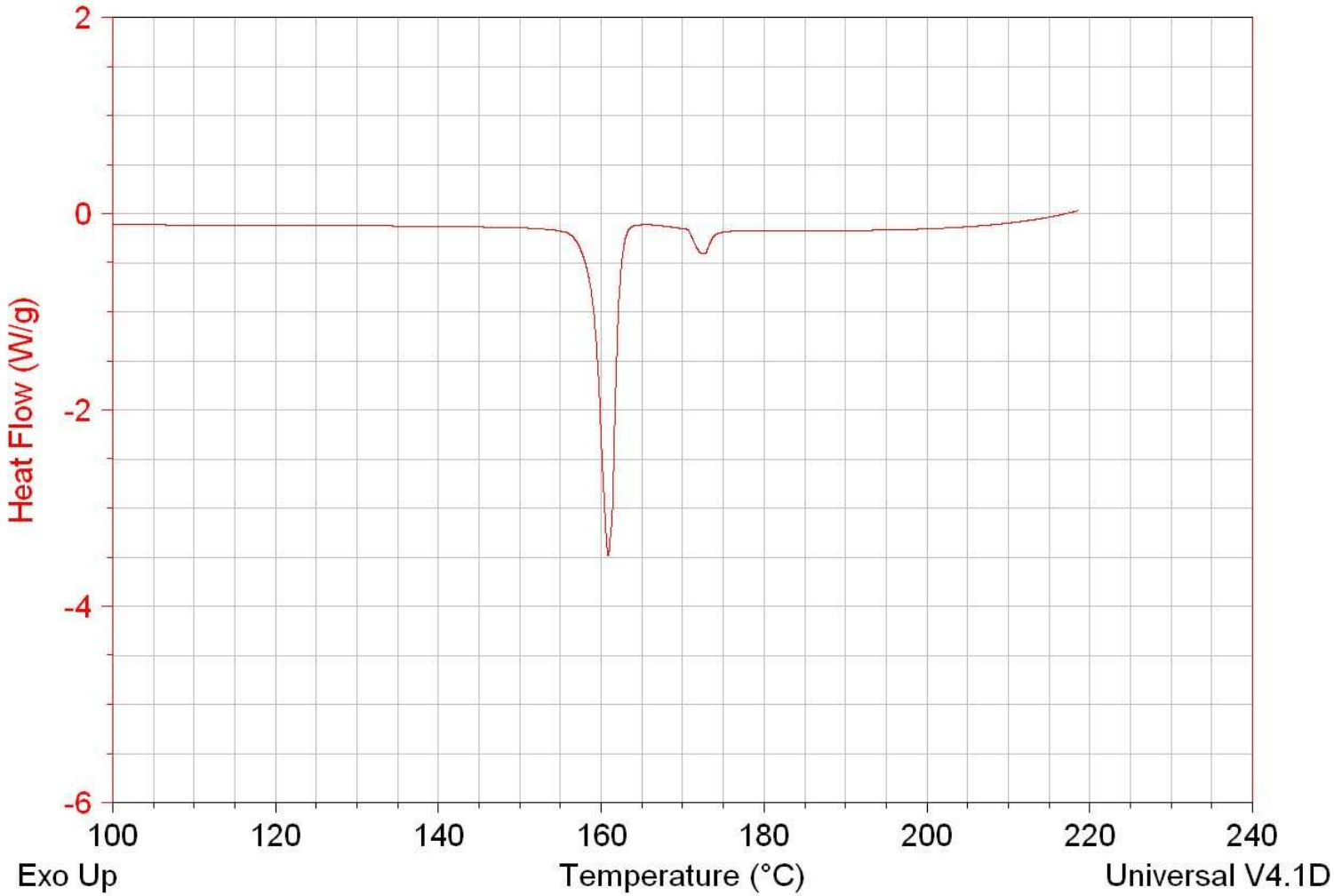

Figure C5-5 DSC trace of PXN: 3FBA.

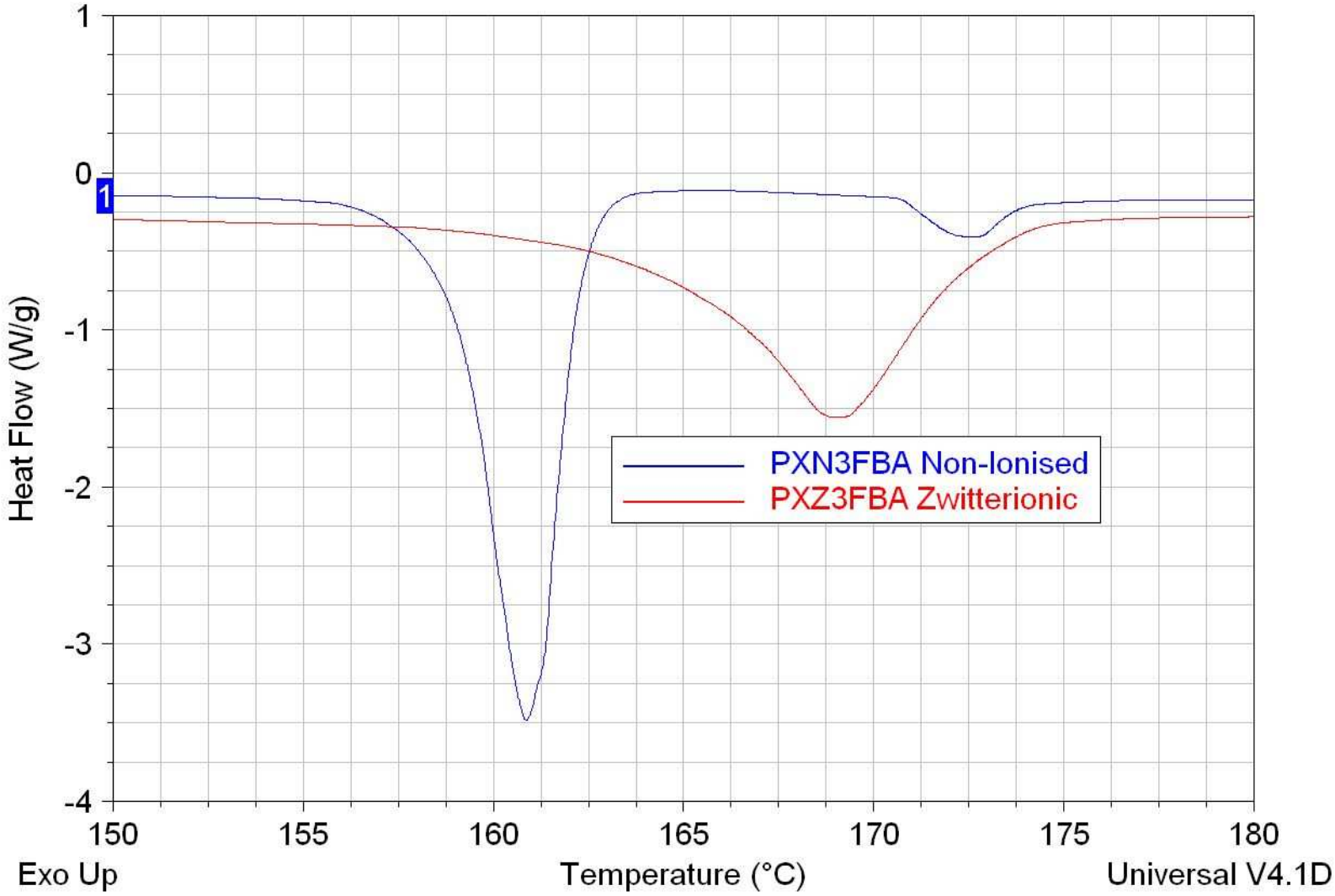

Figure C5-6 Overlay of PXZ: 3FBA and PXN: 3FBA DSC traces.

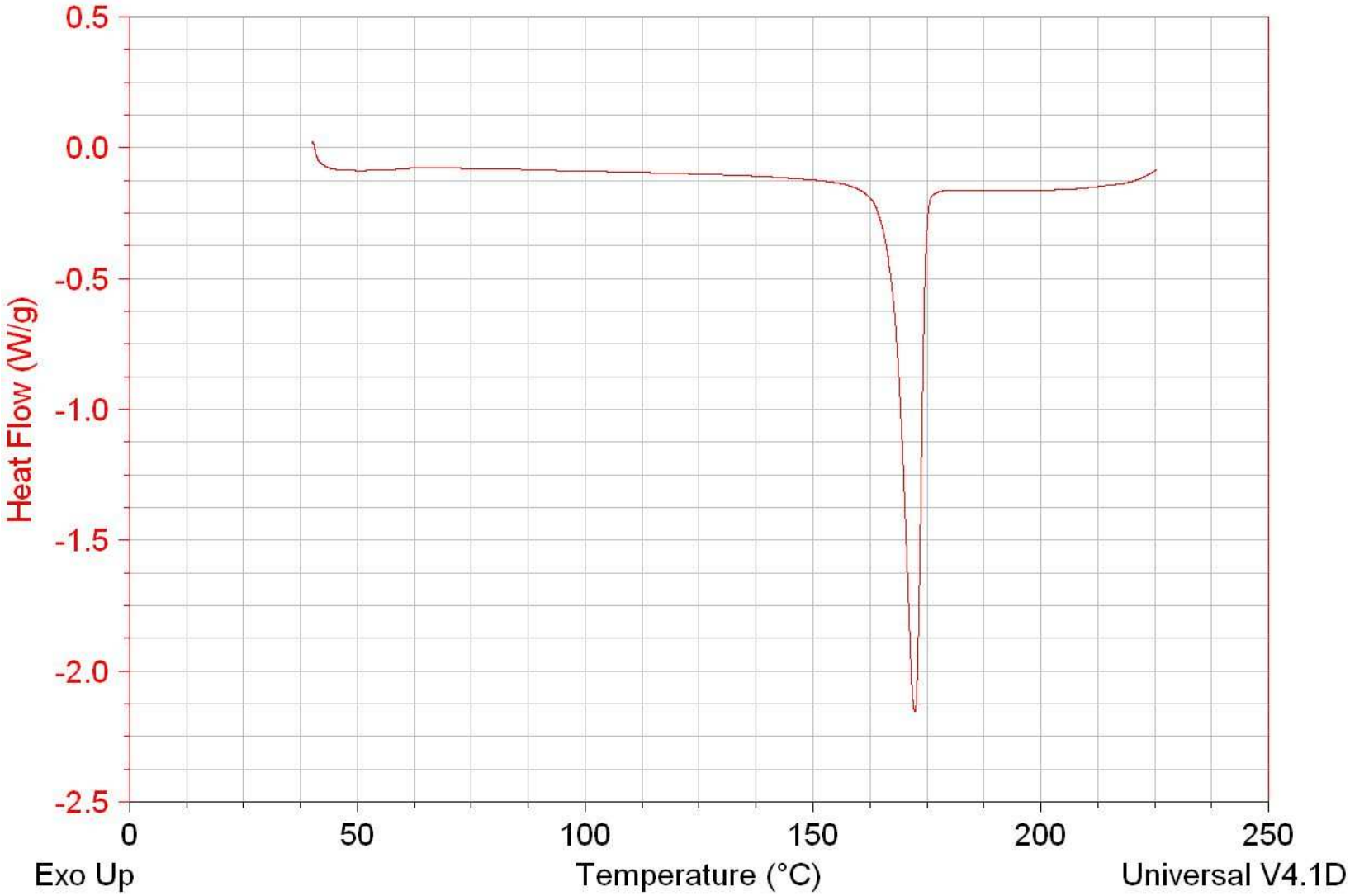

Figure C5-7 DSC trace of PXZ: 4FBA.

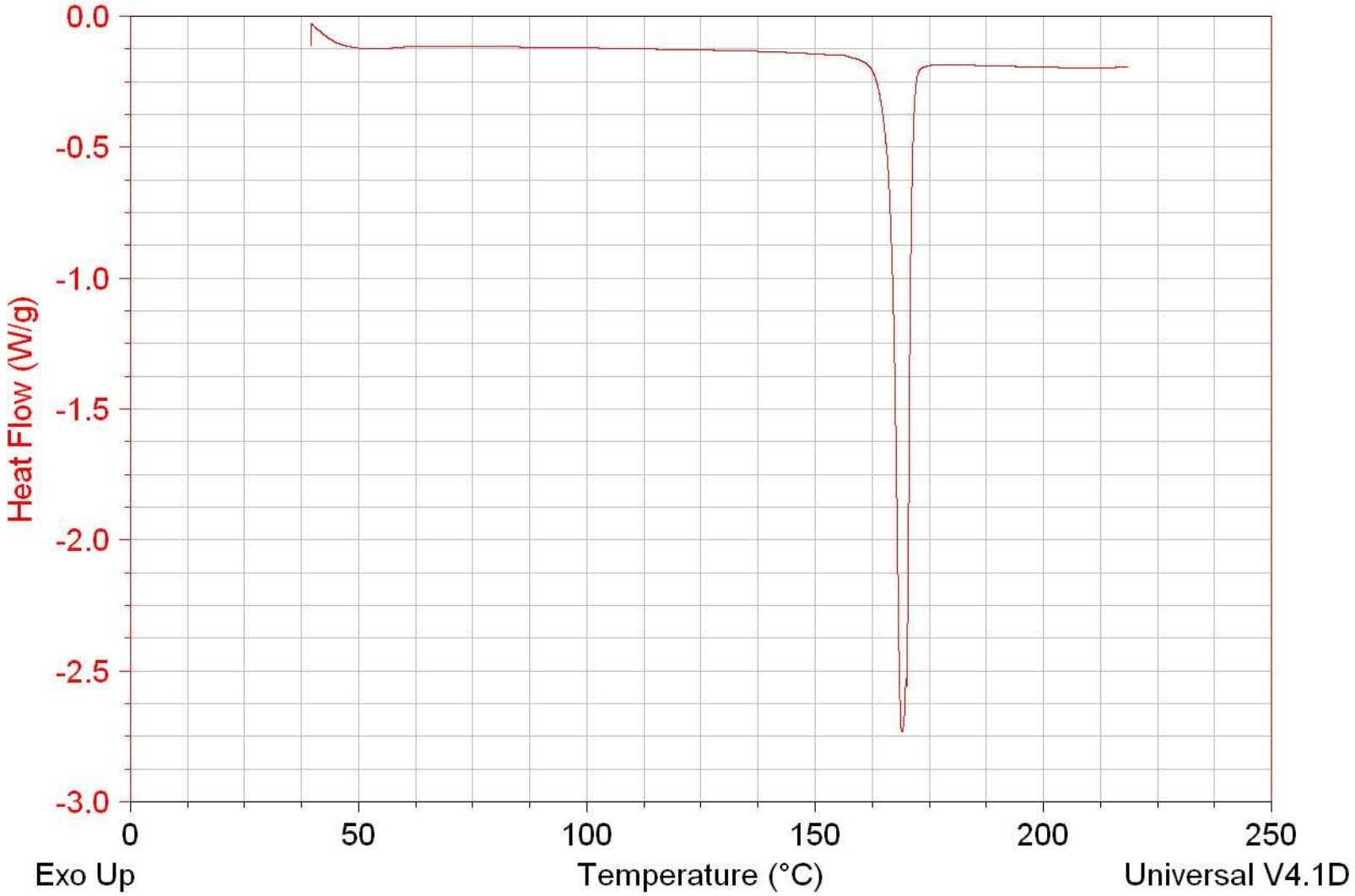

Figure C5-8 DSC trace of PXN: 4FBA.

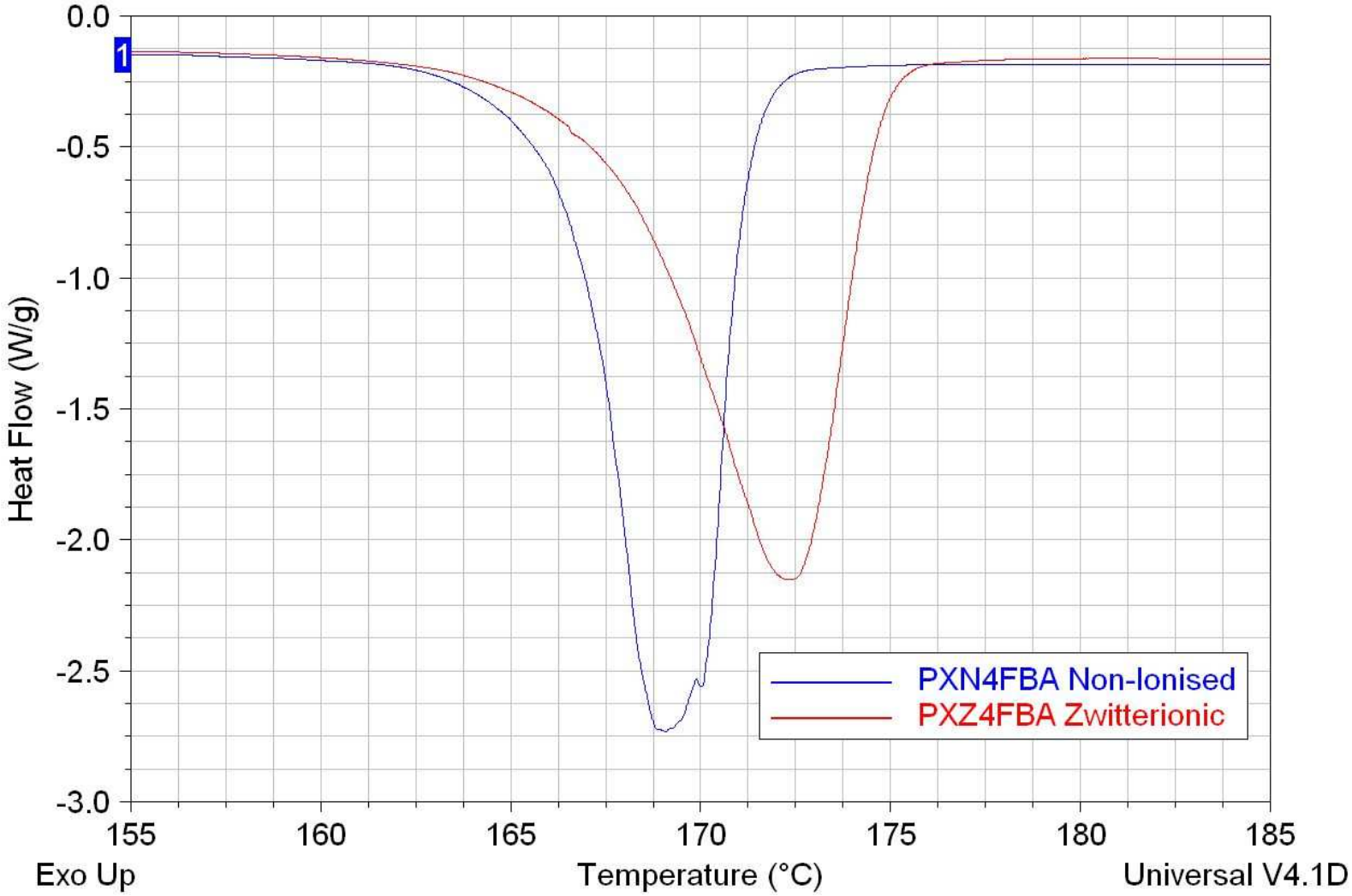

Figure C5-9 Overlay of PXZ: 4FBA and PXN: 4FBA DSC traces.

References

1. C. B. Aakeroy, D. J. Salmon, *CrystEngComm* **7** (72), p439-448 (2005).
2. G. R. Desiraju, *CrystEngComm* **5** (82), p466-467 (2003).
3. J. D. Dunitz, *CrystEngComm* **5** (91), p506 (2003).
4. A. D. Bond, *CrystEngComm* **9**, p833-834 (2007).
5. A. Parkin, C. J. Gilmore, C. C. Wilson, *Z. Kristallogr.* **223**, p430 (2008).
6. S. Aitipamula, R. Banerjee, A. K. Bansal, K. Biradha, M. L. Cheney, A. R. Choudhury, G. R. Desiraju, A. G. Dikundwar, R. Dubey, N. Duggirala, P. P. Ghogale, S. Ghosh , P. K. Goswami, N. Rajesh Goud, R. R. K. R. Jetti, P. Karpinski, P. Kaushik, D. Kumar, V. Kumar, B. Moulton, A. Mukherjee, G. Mukherjee, A. S. Myerson, V. Puri, A. Ramanan, T. Rajamannar, C. M. Reddy, N. Rodriguez-Hornedo, R. D. Rogers, T. N. G. Row, P. Sanphui, N. Shan, G. Shete, A. Singh, C. C. Sun, J. A. Swift, R. Thaimattam, T. S. Thakur, R. K. Thaper, S. P. Thomas, S. Tothadi, V. R. Vangala, N. Variankaval, P. Vishweshwar, D. R. Weyna, M. J. Zaworotko, *Cryst. Growth Des.* **12** (5), p2147-2152 (2012).
7. J. Bernstein, *J. Phys D: Appl. Phys* **26**, pB66-B76 (1993).
8. A. V. Trask, *Mol. Pharmaceutics* **4** (3), p301-309 (2007).
9. N. Schultheiss, A. Newman, *Cryst. Growth Des.* **9** (6), p2950-2967 (2009).
10. P. Vishweshwar, J. A. Mcmahon, J.A. Bis, M. J. Zaworotko, *J. Pharm. Sci.* **95** (3), p499-516 (2006).
11. W. Jones, W. D. S. Motherwell, A. V. Trask, *MRS Bull.* **31**, p875-879 (2006).
12. S. Tothadi, B. R. Bhogala, A. R. Gorantla, T. S. Thakur, R. K. R. Jetti, G. R. Desiraju, *Chem. Asian J.* **7** (2), p330-342 (2011).
13. A. S. Cannon, J. C. Warner, *Cryst. Growth Des.* **2** (4), p255-257 (2002).
14. M. Bavin, *Chem. Ind.* **21**, p527-529 (1989).
15. D. P. McNamara, S. L. Childs, J. Giordano, A. Larriccio, J. Cassidy, M. S. Shet, R. Mannion, E. O'Donnell, A. Park, *Pharm. Res.* **23**, p1888-1897 (2006).
16. S. Basavoju, D. Bostrom, S. P. Velaga, , *Pharm. Res.* **25**, p530-541 (2008).
17. S. Karki, T. Friščić, L. Fábián, P. R. Laity, G. M. Day, W. Jones, *Adv. Mater* **21**, p3905–3909 (2009).
18. C. C. Sun, H. Hou, *Cryst. Growth Des.* **8** (5), p1575-1579 (2008).
19. J. F. Remenar, S. L. Morisette, M. L. Peterson, B. Moulton, J. M. Macphee, H. R. Guzman, O. J. Almarsson, *J. Am. Chem. Soc.* **125** (28), p8456–8457 (2003).

20. C. B. Aakeroy, S. Forbes, J. Desper, *J. Am. Chem. Soc.* **131** (47), p17048-17049 (2009).
21. S. L. Childs, L. J. Chyall, J. T. Dunlap, V. N. Smolenskaya, B. C. Stahly, G. P. Stahly, *J. Am. Chem. Soc.* **126** (41), p13335-13342 (2004).
22. K. Shiraki, N. Takata, R. Takano, Y. Hayashi, K. Terada, *Pharm. Res.* **25** (11), p2581-2592 (2008).
23. A. Bak, A. Gore, E. Yanez, M. Stanton, S. Tufekcic, R. Syed, A. Akrami, M. Rose, S. Surapaneni, T. Bostick, A. King, S. Neervannan, D. Ostovic, A. Koparkar, *J. Pharm. Sci.* **97** (9), p3942-3956 (2008).
24. D. Braga, F. Grepioni, L. Maini, D. Capucci, S. Nanna, J. Wouters, L. Aerts. L. Quéré, *Chem. Commun.* (48), p8219-8221 (2012).
25. S. Aitipamula, P. S. Chow, R. B. H. Tan, *CrystEngComm* **11**, p1823-1827 (2009).
26. P. Kavuru, D. Aboarayes, K. K. Arora, H. D. Clarke, A. Kennedy, L. Marshall, T. T. Ong, J. Perman, T. Pujari, L. Wojtas, M. J. Zaworotko, *Cryst. Growth Des.* **10** (8), p3568–3584 (2010).
27. S. L. Childs, K. I. Hardcastle, *Cryst. Growth Des.* **7** (7), p1291-1304 (2007).
28. S. Ghosh, P. P. Bag, C. M. Reddy, *Cryst. Growth Des.* **11** (8), p3489–3503 (2011).
29. C. Puigjaner, R. Barbas, A. Portell, M. Font-Bardia, X. Alcobe, R. Prohens, *Cryst. Growth Des.* **10** (7), p2948-2953 (2010).
30. E. Nauha, M. Nissinen, *J. Mol. Struct.* **1066**, p566-569 (2011).
31. J. R. G. Sander, D. K. Bučar, R. F. Henry, J. Baltrusaitis, G. G. Z. Zhang, L. R. MacGillivray, *J. Pharm. Sci.* **99** (9), p3676-3683 (2010).
32. R. Kuroda, Y. Imai, N. Tajima, *Chem. Commun.* (23), p2848-2849 (2002).
33. M. C. Etter, G. M. Frankenbach, *Chem. Mater.* **1**, p12-14 (1989).
34. M. S. Wong, C. Bosshard, P. Gunter, *Adv. Mater.* **9** (10), p837-842 (1997).
35. T. V. Timofeeva, V. N. Nesterov, R. D. Clark, B. Penn, D. Frazer, M. Y. Antipin, *J. Mol. Struc.* **647**, p181-202 (2003).
36. K. Raatikainen, J. Huuskonena, M. Lahtinenb, P. Metrangolo, K. Rissanen, *Chem. Commun.* (16), p2160-2162 (2009).
37. J. T. A. Jones, T. Hasell, X. Wu, J. Bacsa, K. E. Jelfs, M. Schmidtmann, S. Y. Chong, D. J. Adams, A. Trewin, F. Schiffman, F. Cora, B. Slater, A. Steiner, G. M. Day, A. I. Cooper, *Nature* **474**, p367-371 (2011).
38. D. Braga, J. Bernstein, *Making Crystals by Design*. D. Braga, F. Grepioni Ed., (WILEY-VCH Verlag GmbH & Co. KGaA, Weinheim, 2007), vol. 1, Section 3.3.

39. J. Haleblian, W. McCrone, *J. Pharm. Sci.* **8** (58), p911-929 (1969a).

40. P. Vishweshwar, J. A. McMahon, M. L. Peterson, M. B. Hickey, T. R. Shattock, M. J. Zaworotko, *Chem. Commun.* (36), p4601-4603 (2005).

41. A. F. Findlay, *The phase rule and its applications*. A. N. Campbell, N. O. Smith, Ed., (Dover Publications, New York, 1951), pp7-19.

42. W.C. McCrone, *Physics and Chemistry of the Solid State*. D. Fox, M.M. Labes, A. Weissberger Ed., (Interscience, New York, 1965), vol. 2, pp725-767.

43. J. Bernstein, *Polymorphism in Molecular Crystals*. A. A. Chernov, P. Coppens, G. R. Desiraju, J. Drenth, A. M. Glazer, J. P. Glusker, J. R. Helliwell, Ed., IUCR Monographs of Crystallography (Oxford Science Publications, Oxford, 2002).

44. W. W. Porter, S. C. Elie, A. J. Matzger, *Cryst. Growth Des.* **8** (1), p14-16 (2008).

45. S. L. Childs, K. I. Hardcastle, *CrystEngComm.* **9** (5), p364-367 (2007).

46. J. M. Miller, B. M. Collman, L. R. Greene, D. J.W. Grant, A. C. Blackburn, *Pharmaceut. Dev. Tech.* **10** (2), p291-297 (2005).

47. M. Haisa, S. Kashino, H. Maeda, *Acta Cryst.* **B30**, p2510-2512 (1974).

48. Y.T. Sohn, *J. Korean Pharm. Sci.* **20**, p97–104 (1990).

49. P. Di Martino, A-M. Guyot-Hermann, P. Conflant, M. Drache, J-C. Guyot, *Int. J. Pharm.* **128**, p1-8 (1996).

50. G. Nichols, C. S. Frampton, *J. Pharm. Sci.* **87** (6), p684-693 (1998).

51. S. R. Chemburkar, J. Bauer, K. Deming, H.Spiwek, K. Patel, J. Morris, R. Henry, S. Spanton, W. Dziki, W. Porter, J. Quick, P. Bauer, J. Donaubauer, B. A. Narayanan, M. Soldani, D. Riley, K. McFarland, *Org. Proc. Res. Dev.* **4** (5), p413–417 (2000).

52. J. Bauer, S. Spanton, R. Henry, J. Quick, W. Dziki, W. Porter, J. Morris, *Pharm. Res.* **18** (6), p859-866 (2001).

53. G. D. Woddard, W. C. McCrone, *J. Appl. Cryst* **8**, p342 (1975).

54. J. D. Dunitz, J. Bernstein, *Acc. Chem. Res* **28**, p193-200 (1995).

55. J. M. Rubin-Perminger, J. Bernstein, *Cryst. Growth Des.* **5** (4), p1343–1349 (2005).

56. R. W. Lancaster, P. G. Karamertzanis, A. T. Hulme, D. A. Tocher, T. C. Lewis, S. L. Price, *J. Pharm. Sci.* **96** (12), p3419-3431 (2007).

57. V. W. Jacewicz, J. H. C. Nayler, *J. Appl. Cryst* **12**, p396-397 (1979).

58. T. Tozawa, J. T. A. Jones, S. I. Swamy, S. Jiang, D. J. Adams, S. Shakespeare, R. Clowes, D. Bradshaw, T. Hasell, S. Y. Chong, C. Tang, S. Thompson, J. Parker, A. Trewin, J. Bacsa, A. M. Z. Slawin, A. Steiner, A. I. Cooper, *Nature* **8**, p973-978 (2007).

59. Y. Wang, W. Tam, S.H. Stevenson, R.A. Clement, J. Calabrese, *Chem. Phys. Lett* **148**, p136-141 (1988).
60. T. Kinuta , T. Sato , N. Tajima , Y. Matsubara , M. Miyazawa, Y. Imai *CrystEngComm* **14**, p1016-1020 (2012).
61. José Elguero, *Cryst. Growth Des.* **11** (11), (2011).
62. A. J. Cruz-Cabeza, C. R. Groom, *CrystEngComm* **13**, p93-98 (2011).
63. G. R. Desiraju, *Cryst. Growth Des.* **8** (1), p3–5 (2008).
64. S. P. Delaney, E. M. Witko, T. M. Smith, T. M. Korter, *J. Phys. Chem.* **116** (30), p8051–8057 (2012).
65. F. H. Allen, *Acta Cryst.* **B58**, p380-388 (2002).
66. N. K. Nath, S. S. Kumar, A. Nangia, *Cryst. Growth Des.* **11** (10), p4594–4605 (2011).
67. M. E. Garcia-Rubino, D. Choquesillo-Lazarte, M. C. Nunez, J. M. Campos, *Acta Cryst.* **C67**, p484-486 (2011).
68. G. R. Desiraju, *Angew. Chem. Int. Ed. Engl.* **34**, p2311-2327 (1995).
69. M. C. Etter, D. A. Adsmond, *J. Chem. Soc., Chem. Commun.*, p589-591 (1990).
70. R. D. B. Walsh, M. W. Bradner, S. Fleischman, L. A. Morales, B. Moulton, N. Rodriguez-Hornedo, M. J. Zaworotko, *Chem. Commun.* (2), p186-187 (2002).
71. C. A. Hunter, K, R. Lawson, J. Perkins, C. J. Urch, *J. Chem. Soc., Perkin Trans.* **2** (651-669), (2001).
72. H. R. Khavasi, M. A. Fard, *Cryst. Growth Des.* **10**, p1892-1896 (2012).
73. M. Nishio, *CrystEngComm* **6**, p130-158 (2004).
74. M. Nishio, Y. Umezawa, K. Honda , S. Tsuboyama, H. Suezawa *CrystEngComm* **11**, p1757-1788 (2009).
75. L. Brammer, G. Mínguez Espallargas, S. Libri, *CrystEngComm* **10**, p1712-1727 (2008).
76. K. Rissanen, *CrystEngComm* **10**, p1107-1113 (2008).
77. P. Metrangolo, H. Neukirch, T. Pilati, G. Resnati, *Acc. Chem. Res.* **38**, p386-395 (2005).
78. K. Raatikainen, K. Rissanen, *CrystEngComm* **11**, p750–752 (2009).
79. O. Almarsson, M. J. Zaworotko, *Chem. Commun.* (50), p1889-1896 (2004).
80. M. C. Etter, *J. Am. Chem. Soc.* **23** (4), p120-126 (1990).
81. L. Leiserowitz, *Acta Cryst.* **B32**, p775-802 (1976).
82. F. H. Allen, W. D. S. Motherwell, P. R. Raithby, G. P. Shields, R. Taylor, *New J. Chem.* **23**, p25-34 (1999).

83. F. H. Allen, P. R. Raithby, G. P Shields, R. Taylor, *Chem. Commun.* (9), p1043-1044 (1998).
84. L. Fabian, *Cryst. Growth Des.* **9** (3), p1436-1443 (2009).
85. J. A. Mcmahon, P. Vishweshwar, J.A. Bis, T. R. Shattock, O. L. McLaughlin, M. J. Zaworotko, *Z. Kristallogr.* **220**, p340-350 (2005).
86. T. R. Shattock, K. K. Arora, P. Vishweshwar, M. J. Zaworotko, *Cryst. Growth Des.* **8** (12), p4533-4545 (2008).
87. P. Fernandes, J. Bardin, A. Johnston, A. J. Florence, C. K. Leech, W. I. F. David, K. Shankland, *Acta Cryst.* **E63**, p4269 (2007).
88. S. L. Childs, P. A. Wood, N. Rodriguez-Hernedo, L. S. Reddy, K. I. Hardcastle, *Cryst. Growth Des.* **9** (4), p1869-1888 (2009).
89. G. Smith, K. E. Baldry, K. A. Byriel, C. H. L. Kennard, *Aust. J. Chem.* **50**, p727-736 (1997).
90. C. B. Aakeröy, A. M. Beatty, B. A. Helfrich, *Angew. Chem. Int. Ed.* **40** (17), p3240-3242 (2001).
91. C. B. Aakeroy, J. Desper, B. A. Helfrich, *CrystEngComm* **6** (5), p19-24 (2004).
92. M. Viertelhaus, R. Hilfiker, F. Blatter, *Cryst. Growth Des.* **9** (5), p2220-2228 (2009).
93. H. D. Clarke, K. K. Arora , H. Bass, P. Kavuru, T. T. Ong, T. Pujari, L. Wojtas, M. J. Zaworotko, *Cryst. Growth Des.* **10**, p2152-2167 (2010).
94. M. Polito, E. D'Oria, L. Maini, P. G. Karamertzanis, F. Grepioni, D. Braga, S. L. Price,, *CrystEngComm* **10**, p1848-1854 (2008).
95. A. Gavezzotti, *Acc. Chem. Res* **27**, p309-314 (1994).
96. C. B. Aakeröy, N. Schultheiss, *Making Crystals by Design*. D. Braga, F. Grepioni, Ed., (WILEY-VCH Verlag GmbH & Co. KGaA, Weinheim, 2007), vol. 1, Section 2.5.
97. G. M. J. Schmidt, *Pure Appl. Chem.* **27**, p647 (1971).
98. C. B. Aakeröy, N. R. Champness, C. Janiak, *CrystEngComm* **12**, p22-43 (2010).
99. L. R. MacGillivray, *CrystEngComm* **6**, p77-78 (2004).
100. G. Desiraju, *Nature Materials* **1**, p77-79 (2002).
101. P. G. Karamertzanis, A. V. Kazantsev, N. Issa, G. W.A. Welch, C. S. Adjiman, C. C. Pantelides, S. L. Price, *J. Chem. Theory Comput.* **5** (5), p1432–1448 (2009).
102. T. S. Thakur, G. Desiraju, *Cryst. Growth Des.* **8** (11), p4031–4044 (2008).
103. G. M. Day, T. G. Cooper, A. J. Cruz-Cabeza, K. E. Hejczyk, H. L. Ammon, S. X. M. Boerrigter, J. S. Tan, R. G. Della Valle, E. Venuti, J. Jose, S. R. Gadre, G. R. Desiraju, T. S. Thakur, B. P. van Eijck, J. C. Facelli, V. E. Bazterra, M. B. Ferraro, D. W. M.

Hofmann, M. A. Neumann, F. J. J. Leusen, J. Kendrick, S. L. Price, A. J. Misquitta, P. G. Karamertzanis, G. W. A. Welch, H. A. Scheraga, Y. A. Arnautova, M. U. Schmidt, J. van de Streek, A. K. Wolf, B. Schweizer, *Acta Cryst.* **B65**, p107-125 (2009).

104. D. A. Bardwell, C. S. Adjiman, Y. A. Arnautova, E. Bartashevich, S. X. M. Boerrigter, D. E. Braun, A. J. Cruz-Cabeza, G. M. Day, R. G. Della Valle, G. R. Desiraju, B. P. van Eijck, J. C. Facelli, M. B. Ferraro, D. Grillo, M. Habgood, D. W. M. Hofmann, F. Hofmann, K. V. J. Jose, P. G. Karamertzanis, A. V. Kazantsev, J. Kendrick, L. N. Kuleshova, F. J. J. Leusen, A. V. Maleev, A. J. Misquitta, S. Mohamed, R. J. Needs, M. A. Neumann, D. Nikylov, A. M. Orendt, R. Pal, C. C. Pantelides, C. J. Pickard, L. S. Price, S. L. Price, H. A. Scheraga, J. van de Streek, T. S. Thakur, S. Tiwari, E. Venuti, I. K. Zhitkov, *Acta Cryst.* **B67**, p535-551 (2011).
105. M. Bhatt, Y. Azim, T.S. Thakur, G. R. Desiraju, *Cryst. Growth Des.* **9** (2), p951-957 (2009).
106. A. Mukherjee, P. Grobelny, T. S. Thakur , G. R. Desiraju, *Cryst. Growth Des.* **11** (6), p2637-2653 (2011).
107. R. A. Chiarella, R. J. Davey, M. L. Peterson, *Cryst. Growth Des.* **7** (7), p1223-1226 (2007).
108. J. H. Horst, M. A. Deij, P. W. Cairns, *Cryst. Growth Des.* **9** (3), p1531-1537 (2009).
109. M. A. Mohammad, A. Alhalaweha, S. P. Velaga, *Int. J. Pharm.* **407** (1-2), p63-71 (2011).
110. N. Issa, P. G. Karamertzanis, G. W. A. Welch, S. L. Price, *Cryst. Growth Des.* **9** (1), p442-453 (2009).
111. S. L. Johnson, K. A. Rumon, *J. Phys. Chem.* **69** (1), p74-86 (1965).
112. B. R. Bhogala, S. Basavoju, A. Nangia, *CrystEngComm* **7**, p551-562 (2005).
113. S. L. Childs, G. P. Stahly, A. Park, *Mol. Pharmaceutics* **4** (3), p323-338 (2007).
114. C. B. Aakeröy, M. E. Fasulo, J. Desper, *Mol. Pharmaceutics* **4** (4), p317-322 (2007).
115. S. Mohamed, D. A. Tocher, M. Vickers, P. G. Karamertzanis, S. L. Price, *Cryst. Growth Des.* **9** (6), p2881-2889 (2009).
116. M. K. Stanton, A. Bak, *Cryst. Growth Des.* **8** (10), p3856-3862 (2008).
117. D. A. Haynes, W. Jones, W. D. S. Motherwell, *CrystEngComm* **8**, p830-840 (2006).
118. M. Schmidtmann, C. C. Wilson, *CrystEngComm* **10**, p177-183 (2008).
119. G. P. Stahly, *Cryst. Growth Des.* **7** (6), p1007-1026 (2007).
120. T. Steiner, I. Majerz, C. C. Wilson, *Angew. Chem. Int. Ed.* **40** (14), p2651-2654 (2001).

121. A. Parkin, S. M. Harte, A. E. Goeta, C. C. Wilson, *New J. Chem.* **8**, p718-721 (2004).

122. D. A. Haynes, L. K. Pietersen, *CrystEngComm* **10**, p518-524 (2008).

123. W. Ostwald, *Z. Phys. Chem.* **22**, p289 (1897).

124. T. Threlfall, *Org. Proc. Res. Dev.* **7** (6), p1017–1027 (2003).

125. J. C. Burley, M. J. Duer, R. S. Stein, R. M. Vrcelj, *Eur. J. Pharm. Sci.* **31** (5), p271-276 (2007).

126. C. Stoica, P. Tinnemans, H. Meekes, E. Vlieg, *Cryst. Growth Des.* **5** (3), p975-981 (2003).

127. I. Halasz, *Cryst. Growth Des.* **10**, p2817-2823 (2010).

128. A. Dawson, D. R. Allan, S. A. Belmonte, S. J. Clark, W. I. F. David, P. A. Macgregor, S. Parson, C. R. Pulham, L. Sawyer, *Cryst. Growth Des.* **5** (4), p1415-1427 (2005).

129. H. Y. Ye, J. Z. Ge, F. Chen, R. G. Xiong, *CrystEngComm* **12**, p1705-1708 (2010).

130. F. P. A. Fabbiani, D. R. Allan, W. I. F. David, A. J. Davidson, A. R. Lennie, S. Parsons, C. R. Pulham, J. E. Warren, *Cryst. Growth Des.* **7** (6), p1115-1124 (2007).

131. S. Long, S. Parkin, M.A. Siegler, A. Cammers, T. Li, *Cryst. Growth Des.* **8** (11), p4006-4013 (2008).

132. M. Rafilovich, J. Bernstein, *J. Am. Chem. Soc.* (128), p12185-12191 (2006).

133. G.G. Z. Zhang, R. F. Henry, T. B. Borchardt, X. Lou, *J. Pharm. Sci.* **96** (5), p990-995 (2007).

134. G. Di Profio, S. Tucci, E. Curcio, E. Drioli, *Cryst. Growth Des.* **7** (3), p526-530 (2006).

135. M. M. Parmar, O. Khan, L. Secton, J. L. Ford, *Cryst. Growth Des.* **7** (9), p1635-1642 (2007).

136. S. Gracin, A. C. Rasmuson, *Cryst. Growth Des.* **4** (5), p1013-1023 (2004).

137. F. P. A. Fabbiani, D. R. Allan, W. I. F. David, S. A. Moggach, S. Parsons, C. R. Pulham, *CrystEngComm* **6** (82), p504-511 (2004).

138. P. A. McGregor, D. R. Allan, S. Parsons, C. R. Pulham, *J. Pharm. Sci.* **91** (5), p1308-1311 (2002).

139. F. P. A. Fabbiani, D. R. Allan, A. Dawson, W. I. F. David, P. A. McGregor, I. D. H. Oswald, S. Parsons, C. R. Pulham, *Chem. Commun.* (24), p3004-3005 (2003).

140. D. R. Weyna, T. Shattock, P. Vishweshwar, M. J. Zaworotko, *Cryst. Growth Des.* **9** (2), p1106-1123 (2009).

141. K. Chadwick, R. Davey, W. Cross, *CrystEngComm* **9** (9), p732-734 (2007).

142. N. Shan, W. Jones, *Green Chem.* **5** (6), p728-730 (2003).

143. A. V. Trask, J. v. d. Streek, W. D. S. Motherwell, W. Jones, *Cryst. Growth Des.* **5** (6), p2233-2241 (2005).

144. E.V. Boldyreva, V. A. Drebushchak, I. E. Paukov, Y. A. Kovalevskaya, E. S. Shutova, *J. Anal. Calorim.* **73** (2), p409-418 (2003).

145. S. Chen, H. Xi, L. Yu, *J. Am. Chem. Soc.* **127** (49), p17439-17444 (2005).

146. A. D. Bond, K. A. Solanko, S. Parsons, S. Redderc, R. Boese, *CrystEngComm* **13**, p399–401 (2011).

147. N. K. Nath, A. Nangia, *CrystEngComm* **13**, p47–51 (2011).

148. K. Chadwick, A. Myerson, B. Trout, *CrystEngComm* **13**, p6626-6627 (2011).

149. K. Chadwick, J. Chen, A. S. Myerson, B. L. Trout, *Cryst. Growth Des.* **12** (3), p1159–1166 (2012).

150. C. C. Seaton, A. Parkin, C. C. Wilson, N. Blagden, *Cryst. Growth Des.* **8** (2), p363-368 (2008).

151. R. J. Davey, N. Blagden, *J. Am. Chem. Soc.* **119** (7), p1767–1772 (1997).

152. G. M. Day, A. V. Trask, W. D. S. Motherwell, W. Jones, *Chem. Commun.* (1), p54-56 (2006).

153. B. Lou, D. Bostrom, S. P. Velaga, *Cryst. Growth Des.* **9** (3), p1254-1257 (2009).

154. L. Cronin, P. J. Kitson, C. C. Wilson, *Process Understanding For Scale-Up and Manufacturing of Active Ingredients*. Ian Houson, Ed., (Wiley-VCH Verlag GmbH & Co. KgaA, Weinheim, 2011).

155. S. Lawton, G. Steele, P.Shering, *Org. Process Res. Dev.* **13** (6), p1357–1363 (2009).

156. C. M. Chew, R. I. Ristic, R. D. Dennehy, J. J. De Yoreo, *Cryst. Growth Des.* **4** (5), p1045-1052 (2004).

157. X. Ni, A. Liao, *Cryst. Growth Des.* **8** (8), p2875-2881 (2008).

158. X. Ni, A. Valentine, A. Liao, S. B. C. Sermage, G. B. Thomson, K. J. Roberts, *Cryst. Growth Des.* **4** (6), p1129-1135 (2004).

159. Image available from: http://en.wikipedia.org/wiki/User:Nitech2008/Oscillatory_baffled_reactor (Last accessed 06-09-2012)

160. T. Steiner, *Angew. Chem. Int. Ed.* **41**, p48-76 (2002).

161. G. Desiraju, *Angew. Chem. Int. Ed.* **50**, p52-59 (2011).

162. A. I. Kitajgorodskij, *Acta Cryst.* **18**, p585 (1961).

163. E. Arunan, G. R. Desiraju, R. A. Klein, J. Sadlej, S. Scheiner, I. Alkorta, D. C. Clary, R. H. Crabtree, J. J. Dannenberg, P. Hobza, H. G. Kjaergaard, A. C. Legon, B. Mennucci, D. J. Nesbitt, *Pure Appl. Chem.* **83** (8), p1637–1641 (2011).

164. G. A. Jeffrey, *An Introduction to Hydrogen Bonding*. D. G. Truhlar, Ed., (Oxford University Press, 1997).

165. R. Bertani, P. Metrangolo, A. Moiana, E. Perez, T. Pilati, G. Resnati, I. Rico-Lattes, A. Sassi, *Adv. Mater* **14** (17), p1197–1201 (2002).

166. V. Amico, S. V. Meille, E. Corradi, M. T. Messina, G. Resnati, *J. Am. Chem. Soc.* **120** (32), p8261–8262 (1998).

167. W. Clegg, *Crystal Structure Determination*. J. Evans, Ed., Oxford Chemistry Primers (Oxford University Press, Oxford, 1998), 5.

168. BCA/CCG, *BCA/CCG Intensive Teaching School in X-ray Structure Analysis*. (2005).

169. Image available from: http://www.infosteel.net/images/s61-1.jpg (Last accessed 29-08-2012)

170. W. Massa, *Crystal Structure Determination*. (Springer-Verlag, Berlin Heidelberg New York, ed. 2, 2004).

171. H. M. Rietveld, *J. Appl. Cryst.* **2**, p65-71 (1969).

172. D. L. Bish, S. A. Howard, *J. Appl. Cryst.* **21**, p86-91 (1988).

173. C. Wilson, *Single Crystal Neutron Diffraction from Molecular Materials*. Series on Neutron Techniques and Applications (World Scientific, 2000), 22, 23, 77.

174. L. H. Thomas, N. Blagden, M. J. Gutmann, A. A. Kallay, A. Parkin, C. C. Seaton, C. C. Wilson, *Crystal Growth & Design* **10** (6), p2770-2774 (2010).

175. C. C. Wilson, *Journal of Molecular Structure* **405**, p207-217 (1997).

176. J. B. Parise, *RiMG* **63** (1), p1-25 (2006).

177. J. Bernstein, *Polymorphism in Molecular Crystals*. (Oxford University Press, Oxford, 2002).

178. H. G. McAdie, P. D. Garn, O. Menis, *Selection of differential thermal analysis temperature standards through a cooperative study (SRM 758, 759, 760)*. (U.S. National Bureau of Standards, 1972).

179. Image available from: http://www.anasys.co.uk/library/dsc1.htm (Last accessed 29-08-2012)

180. Image adapted from http://www.npl.co.uk/science-technology/thermal-performance/areas/thermal-analysis/differential-scanning-calorimetry (Last accessed 29-08-12)

181. L. H. Thomas, E. Cheung, A. O. F. Jones, A. A. Kallay, M. H. Lemée-Cailleau, G. J. McIntyre, C. C. Wilson, *Cryst. Growth Des.* **12** (4), p1746-1751 (2012).
182. R.H. Blessing, *Acta Crystallogr.* **A51**, p33-38 (1995).
183. G. M. Sheldrick, *Acta Cryst.* **A64**, p112-122 (2008).
184. A. Altomare, G. Cascarano, C. Giacovazzo, A. Guagliardi, M. C. Burla, G. Polidori, M. Camalli, *J. Appl. Cryst* **27**, p435-436 (2004).
185. L. J. Farrugia, *J. Appl. Crystallogr.* **32**, p837-838 (1999).
186. Apex (2009), Bruker AXS Inc., Madison, Wisconsin, USA
187. G. M. Sheldrick, *SADABS. Programme for Empirical Absorption Correction of Area Detector Data*, University of Gottingen, Germany (1996)
188. Collect (1998), Nonius BV, Delft, The Netherlands
189. Z. Otwinowski, W. Minor *Methods in Enzymology*. C. W. Carter, R. M. Sweet, Ed., Macromolecular Crystallography (Academic Press, New York, 1997), vol. 276.
190. CRYSTALCLEAR v1.4.0 (2009), Rigaku Americas Corporation, 9009 New Trails Drive, The Woodlands, Texas, USA
191. T. Higashi, *ABSCOR,* (1995), Rigaku Corporation, Tokyo, Japan
192. CrystalClear-SM Expert 2.0 r5 (2010), Rigaku Americas Corporation, 9009 New Trails Drive, The Woodlands, Texas, USA
193. Image adapted from: http://www.diamond.ac.uk/Home/About/Facts.html (Last accessed 20-09-2012)
194. C. Wilkinson, J. A. Cowan, D. A. A. Myles, F. Cipriani, G. J. McIntyre, *Neutron News* **13** (1), p37-41 (2002).
195. G. Barr, W. Dong, C. J. Gilmore, *J. Appl. Cryst.* **42**, p965-974 (2009).
196. C. J. Gilmore, G. Barr, J. Paisley, *J. Appl. Cryst* **37**, p231-242 (2004).
197. I. D. H. Oswald, I. Chataigner, S. Elphick, F. P. A. Fabbiani, A. R. Lennie, J. Maddaluno, W. G. Marshall, C. R. Pulham, T. J. Prior, R. I. Smith, *CrystEngComm* **11**, p359-366 (2008).
198. M. Haisa, S. Kashino, R. Kawai, H. Maeda, *Acta Cryst.* **B32**, p1283-1285 (1976).
199. C. C. Wilson, *Z. Kristallogr.* **215**, p693-701 (2000).
200. M. A. Perrin, M. A. Neumann, H. Elmaleh, L. Zaske, *Chem. Commun.* (22), p3181-3183 (2009).
201. M. A. Mikhailenko, *Journal of Crystal Growth* **265** (3-4), p616-618 (2004).
202. C. P. Price, A. L. Grzesiak, A. J. Matzger, *J. Am. Chem. Soc.* **127** (15), p5512-5517 (2004).

203. G. Di Profio, S. Tucci, E. Curcio, E. Drioli, *Chem. Mater* **19** (10), p2386-2388 (2007).

204. L. H. Thomas, C. Wales, L. Zhao, C. C. Wilson, *Cryst. Growth Des.* **11** (5), p1450-1452 (2011).

205. T. N. Drebushchak, E. V. Boldyreva, *Z. Kristallogr.* **219**, p506-512 (2004).

206. B. Kojic-Prodic, Z. Ruzic-Toros *Acta Cryst.* **B38** (11), p2948-2951 (1982).

207. F. Vrecer, S. Srcic, J. Smid-Korbar, *Int. J. Pharm.* **68** (1-3), p35-41 (1991).

208. F. Vrecer, M. Vrbinc, A. Meden, *Int. J. Pharm.* **256**, p3-15 (2003).

209. A. R. Sheth, S. Bates, F. X. Muller, D. J. W. Grant, *Cryst. Growth Des.* **4** (6), p1091-1098 (2004).

210. A. R. Sheth, S. Bates, F. X. Muller, D. J. W. Grant, *Cryst. Growth Des.* **5** (2), p571–578 (2005).

211. J. Bordner, J. A. Richards, P Weeks, E. B. Whipple, *Acta Cryst.* **C40**, p989-990 (1984).

212. H. A. Cheong, H. K. Choi *Pharm. Res.* **19** (9), p1375 - 1380 (2002).

213. M. Inoue, R. Suzuki, N. Sakaguchi, Z. Li, T. Takeda, Y. Ogihara, B. Y. Jiang, Y. Chen *Biol. Pharm. Bull.* **18** (11), p1526-1530 (1995).

214. J. Zhao, I. A. Khan, F. R. Fronczek, *Acta Cryst.* **E67**, p316-317 (2011).

215. H. D. Clarke, K. K. Arora, Ł.Wojtas,M. J. Zaworotko, *Cryst. Growth Des.* **11** (4), p964-966 (2011).

216. P. v.d. Sluis, A.L. Spek, *Acta Cryst.* **A46**, p194-201 (1990).

217. F. P. A. Fabbiani, D. R. Allan, S. Parsons, C. R. Pulham, *CrystEngComm* **7**, p179-186 (2005).

218. G. Admiraal, J. C. Eikelenboom, A. Vos, *Acta Cryst.* **B38** (10), p2600-2605 (1982).

219. D. Louer, M. Louer, *Acta Cryst.* **B51**, p182-187 (1995).

220. J. Bordner, P. D. Hammen, E. B. Whipple, *J. Am. Chem. Soc.* **111**, p6572–6578 (1989).

221. P. M. Bhatt, N. V. Ravindra, R. Banerjee, G. R. Desiraju, *Chem. Commun.* (8), p1073-1075 (2005).

222. C. Wales, L. H. Thomas, C. C. Wilson, *CrystEngComm* (Advance Article; DOI: 10.1039/C2CE26069G), (2012).

223. J. M. Geckle, D. M. Rescek, E. B. Whipple, *Magn. Reson. Chem.* **27** (2), p150-154 (1989).

224. M. S. Adam, A. Parkin, L. H. Thomas, C. C. Wilson, *CrystEngComm* **12**, p917-924 (2009).

225. K. Molcanov, B. Kojic-Prodij, *CrystEngComm* **12**, p 925-939 (2010).

226. V. André, M. F. M. da Piedade, M. T. Duarte *CrystEngComm* **14**, p5005-5014 (2012).

227. I. D. H. Oswald, D. R. Allan, P. A. McGregor, W. D. S. Motherwell, S. Parsons, C. R. Pulham, *Acta Cryst.* **B58**, p1057-1066 (2002).

228. I. D. H. Oswald, C. R. Pulham *CrystEngComm* **10**, p1114-1116 (2008).

229. S. L. Huth, T. L. Threlfall, M. B. Hursthouse, in *Crystal Structure Report Archive*. (University of Southampton, 2008).

230. F. Guarner, N. K. Boughton-Smith, G. J. Blackwell, S. Moncada, *Hepatology* **8** (2), p248-253 (1988).

231. M. C. Mitchell, S. Schenker, K. V. Speeg, *J Clin Invest.* **73** (2), p383–391 (1984).

232. EPSRC National Centre in Continuous Crystallisation and Manufacturing: http://www.cmac.ac.uk/ (Last accessed 24-09-2012)

233. M. A. Elbagerma, H. G. M. Edwards, T. Munshi, I. J. Scowen, *CrystEngComm* **13**, p1877-1884 (2011).

234. S. Lee, C. Hoff, *Handbook of Pharmaceutical Salts*. P. H. Stahl, C. G. Wermuth, Ed., (Wiley-VCH Verlag GmbH & Co. KgaA, Weinheim, 2008), 213.